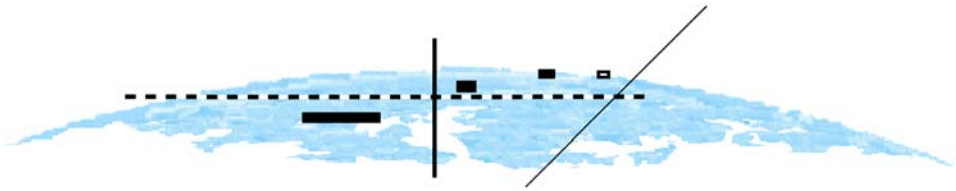

GeoForschungsZentrum Potsdam

STIFTUNG DES ÖFFENTLICHEN RECHTS

Scientific Technical Report

ISSN 1610-0956

Scientific Technical Report STR 98/05
DOI: 10.2312/GFZ.b103-98055

GeoForschungsZentrum Potsdam
STIFTUNG DES OFFENTLICHEN RECHTS

Peter Bormann

Regional International
Training Course 1997 on

Seismology and Seismic Hazard Assessment

Lecture and exercise notes

Complementary volume

Scientific Technical Report STR98/05

Scientific Technical Report STR 98/05
DOI: 10.2312/GFZ.b103-98055

Imprint

Edited by:

Peter Bormann
GeoForschungsZentrum Potsdam
Telegrafenberg
D-14473 Potsdam, Germany

Printed in Potsdam, Germany
March 1998

The Regional International Training Course on „Seismology and Seismic Hazard Assessment" was held in Nairobi, Kenya
05 October to 08 November, 1997

It was sponsored by:

- GeoForschungsZentrum Potsdam (GFZ)
- University of Nairobi, Department of Geology
- Federal Foreign Office (AA), Bonn
- Federal Ministry of Economical Co-Operation and Development (BMZ), Bonn
- Carl Duisberg Gesellschaft (CDG), Regional Office of the State of Brandenburg in Berlin
- United Nations Department of Humanitarian Affairs (DHA), Geneva
- United Nations Educational, Scientific and Cultural Organization (UNESCO), Paris
- Canadian International Development Agency (CIDA), Ottawa
- Incorporated Research Institutions for Seismology (IRIS), Seattle, USA

Scientific Technical Report STR 98/05
DOI: 10.2312/GFZ.b103-98055

Lecture and exercise notes
Complementary Volume

Regional International Training Course 1997 on

Seismology and Seismic Hazard Assessment

Nairobi, Kenya, 05 October to 08 November 1997

---

organized by
GeoForschungsZentrum Potsdam (GFZ)

in cooperation with

University of Nairobi, Department of Geology
Carl Duisberg Gesellschaft (CDG)

co-sponsored by
AA (Bonn), BMZ (Bonn), CDG (Berlin), DHA (Geneva),
UNESCO (Paris), CIDA (Ottawa), IRIS (Seattle)

Peter Bormann
Editor

Scientific Technical Report STR98/05

Scientific Technical Report STR 98/05
DOI: 10.2312/GFZ.b103-98055

GeoForschungsZentrum Potsdam

CONTENTS

Scientific Technical Report STR 98/05
DOI: 10.2312/GFZ.b103-98055

2. Regional geology and investigation of the Earth´s crust in Africa

3. Seismic hazard assessment in Africa

Scientific Technical Report STR 98/05
DOI: 10.2312/GFZ.b103-98055

Foreword by the editor

The 1997 international regional training course on „Seimology and Seismic Hazard Assessment" was held in Nairobi, Kenya, between 05 October and 08 November. It had been jointly organized by the Division of Solid Earth Physics and Disaster Research of the GeoForschungsZentrum Potsdam (GFZ) and by the Department of Geology of the University of Nairobi. Most of the organizational expenses were covered by the GFZ.

18 participants from twelve African countries attended the course.This was made possible through fellowships and travel grants provided by the German Federal Foreign Office (AA), the Federal Ministry of Economic Co-operation and Development, the Regional Office of the Carl Duisberg Gesellschaft (CDG) in the State of Brandenburg, the United Nations Department of Humanitarian Affairs (DHA, Geneva), the United Nations Educational, Scientific and Cultural Organization (UNESCO, Paris), and the Canadian International Development Agency (CIDA, Ottawa). Additionally, the AA allocated funds for international texbooks and software and the Incorporated Research Institution for Seismology (IRIS, Seattle, USA) provided- at ist own cost - the services of two instructors. Lectures, exercises, demonstrations and excursions were shared by an international team of 20 instructors from nine countries from Africa, Europe and North America, the majority of which were from the GFZ (7) and the University of Nairobi (4).

Course participants received lecture and exercise notes which had been compiled and printed by the GFZ. Additionally, in the case of regional training courses, the regular, methodologically structured printed material for the „Potsdam standard course" is being supplemented by a „complementary course volume" which introduces in the peculiarities of seismotectonics, seismicity and seismic hazard assessment in the host country or region, summarizes the local and/or regional state-of-the-art pertaining to seismological data acquisition and analysis and provides write-ups of new or up-dated lectures and exercises pertaining to the standard course.

Last year´s appeal to lecturers to submit relevant new material of high standard for printing in the series of Scientific Technical Reports (STR) of the GFZ, which would allow the publication of the Nairobi complementary course volume as an internationally quotable source of reference, was very well received. A total of 361 manuscript pages reached the course chairman by February 1998 and was carefully compiled and edited. Thus the Nairobi complementary course volume now represents a comprehensive and authoritative review report of seismicity, seismic hazard assessment and seismological practice in Africa as well as on the complex investigation of the Earth´s crust in the Kenyan rift system (by D. Benouar, D. Dindi, D.J. Hlatywayo, D. Hollnack, E. Jonathan, F. Kebede, A. Kijko, J. Mechie, O. Novak, I.O. Nyambok;189 pages in total).

Besides this, the volume contains an extensive contribution by A. Trnkoczy (51 pages) on „Getting the right seismic system". It dwells on the rich experience from many case studies in different parts of the world and will surely become a fundamental guide for all developing countries which embark on the planning, site and instrument selection, installation and organization of seismic monitoring networks. Only by strictly observing the general criteria and ways of reasoning and questioning, outlined in this paper, can the cost-effectiveness of seismic systems be assured and their pre-defined primary goals be achieved. Other contributions deals with the acquisition of high-quality data from IRIS/USGS broad-band

Scientific Technical Report STR 98/05
DOI: 10.2312/GFZ.b103-98055

stations through international data links (S. McLafferty), the use of one of the most advanced and versatile seismological data analysis programs currently available (SEISAN; by J. Havskov) and about the goals and merits of recent international projects for international data exchange and cooperation in seismology (ISOP and GARNET; by E. Bergman). Finally, the complementary Nairobi course volume presents more than 70 pages of new lecture and exercise notes related to the acquisition and analysis of seismic signals and noise as well as on the analysis and interpretation of seismic core phases and earthquake source mechanisms (M. Baumbach, P. Bormann, S. Wendt).

The editor notes with great satisfaction that in the Nairobi training course several lectures and exercises had been presented by four former participants of the Potsdam seismology training course, namely Dr. Fekadu Kebede from Ethopia (participant in 1983), Dr. D. John Hlatywayo from Zimbabwe (participant in 1986), Dr. Djillali Benouar from Algeria (participant in 1987) and Dr. Edwin Dindi from Kenya (participant in 1992). All of them have meanwhile matured to specialists with internationally acknowledged reputation.Furthermore, Drs. Dindi, Hlatywayo and Kebede have, under the chairmanship of Mr. G. Turyomurugyendo from Uganda (who was another course participant in 1991) and in close collaboration with many others (amongst them participants in the Nairobi training course) done an excellent job in initiating and running (under the Swedish International Program in the Physical Sciences - IPPS) the reknowned „Eastern and Southern Africa Regional Seismological Working Group" (ESARSWG). The latter has done an excellent job in training personnel from seismological stations in Africa, in bringing together annually all available records and data from seismic stations in eastern and southern Africa, in jointly re-analysing them, in significantly increasing the number of identified and relocated seismic events, and thus, in producing more complete, reliable and homogeneous data sets (catalogues) for seismic hazard assessment. Prof. Isaac O. Nyambok, the host and co-chairman of the Nairobi training course and Head of the Global Seismic Hazard Assessment Project (GSHAP) Regional Centre in Nairobi, knows best how valuable and indispensable this careful „grass-roots" work of seismological station operators is for achieving the ambitous goals of GSHAP.

I am looking forward to the prospect that the experience and enthusiasm of former course participants from Africa, together with the efforts of other members of the international team of lecturers from France, Germany, Kenya, Norway, Poland, South Africa, Switzerland, and the United States, will bear rich fruits in future. A first indication which justifies this hope is the „Letter of Understanding" adopted by the participants at the end of the course. Therein they express their dedication to strive for the establishment of two more regional seismological working groups for Western and Northern Africa along the lines which have proved to be so successful in case of ESARSWG. The long-term goal envisaged in this „Letter of Understanding" is the foundation of an African Seismological Society under the umbrella of the International Association of Seismology and Physics of the Earth Interior (IASPEI). If the Nairobi training course has stimulated such a drive it has, indeed, not been in vain.

Potsdam, 20 March 1998

Prof. Dr. Peter Bormann
Chairman of the training course

GETTING THE RIGHT SEISMIC SYSTEM

Amadej Trnkoczy

Kinemetrics SA, Z.I.Le Tresi 3, 1028 Preverenges, Switzerland
Fax: 41-21-803-28-95, e-mail:amadej.trnkoczy@quantum.si

1. INTRODUCTION: HOW TO GET THE RIGHT SEISMIC SYSTEM

In the last two decades of the 20th Century, several developing countries have set numerous seismological projects into motion. Unfortunately, viewing all of them from the latter half of the 1990s, we honestly must rank many as unsuccessful.

Of all the seismometric equipment installed in developing countries in the last 20 years, probably less than 50 percent is working properly today. An even smaller percentage operates at full technical capacity. And quite a few projects have yet to contribute seismic information of any significant use.

Reasons for this distressing situation is probably the shortage of knowledge in seismometry among the developing countries that launched these projects. The great majority had little or no education or experience in this field. Yet such specialized knowhow is an indispensable precondition for establishing and operating a truly beneficial seismic network. Sadly, given the narrowness of the seismometry field, such specialized training is difficult to get. Among developing nations who have purchased seismic equipment, basic misunderstandings and unrealistic expectations, combined with factors intrinsic to the small size of the seismic instrumentation market, have led many to disappointments.

Seismometry newcomers who join the field early and "grow" along with the gradual development of the system usually have enough time to gain the required knowledge and develop proper procedures to continue that work. However, someone trying to establish a new seismic network from the ground up does not have that same time luxury. Too often in developing countries - most often right after major strong earthquakes - governments will decide to establish a seismic network. However, those suddenly given responsibility for establishing this network must spend the allotted amount of government funds within a relatively short time. Yet added to the worldwide scarcity of expertise, this politically-forced lack of time greatly increases the tendency towards vague goals, and selection of a seismic system grossly inappropriate to that country's seismic and socio-economic conditions.

Because of these problems, below there are outlined:

- *Proper procedures* for how to establish a seismic network,
- *Criteria* for how to allocate best the available funds among the various essential tasks to establishing and operating a successful seismic network,
- *Conceptual or technical aspects* of seismic system selection that several less experienced purchasers have neglected - or even ignored - resulting, at best, in inefficient use of the purchased equipment, and at worst, in serious system failures.

The main conclusion is:

> Purchasing seismic equipment is neither the first nor the last step necessary to establish an effective seismic network.

2. PLANNING AND FEASIBILITY STUDY

2.1. First step to success: Goal-setting and feasibility study

The most needed first step towards establishing a successful seismic network is to figure out and set the network's goals. Because

> Just as each country has unique seismicity, seismo-tectonical and geological formations, so every seismological project has unique contextual combinations that must be considered to find the optimal system design for that project.One will not have an optimal system until one clearly defines the project's unique goals

To begin goal-setting, one needs to address:

- *The interest*, in ranked order, in *local* seismology (epicentral distances < 140 km), *regional* seismology (epicentral distances between 140 and 2.000 km); and/or *global* seismology (epicentral distances > 2.000 km)
- *The main purpose* of the planned network: Is it aimed at a) monitoring a region's general seismicity; or b) special studies such as monitoring of special seismo-tectonic features, nuclear explosions, induced seismicity, engineering purposes etc.

- *How urgent* the data are required, e.g., has the network alarm functions, for civil or governmental defense purposes; or are the data collected mainly for seismological research aimed at either long-term mitigation of the country's seismic risk or improved knowledge of the Earth's deep structure

- *The relative importance* of observing weak-motions, strong-motions or both.

When countries, having little or no seismic equipment, first consider buying a system to monitor the region's general seismicity, they typically hope that over the long term the new system will help mitigate that region's seismic risk. Nevertheless, even for a project of such narrow scope, several questions must be answered beforehand:

- How big is the country or region to be monitored ?
- What is the seismicity level in the intended country or region ?
- How developed is the country's infrastructure, particularly in telecommunications ?
- What is the country's existing level of seismometry knowledge, and practically, considering the country's financial and academic realities, what are its resources for increasing that knowledge?
- How much is the country willing to pay, per year, to operate the system, to maintain and service the system, and to support research work using its data ?
- How much is the country willing to pay to establish the system ?

Having clarified your goals - this is always a trade off between desires and reality - and quantified the above facts, you can then begin shopping for a seismic system that meets those criteria and needs and thus holds promise to operate successfully in the existing environment.

• ***Goal-setting recommendations:***

o If your country has only few or no seismology experts, you should get help from independent consultants in the international academic world. In this early phase, focus considerations on your country's specific socio-economic and seismic-awareness needs, and do not worry too much about specific equipment.

o In the later phases of goal-setting for your new system, contact sales engineers from various seismic-equipment manufacturers. However, for your initial goal-setting, these engineers usually lack seismological knowledge of your specific country and, of course, might be biased towards their own products.

2.2. Second step to success: Realistic awareness of finances

Even when developing countries' governments have been motivated to establish seismic networks, they normally do not know how to allocate the funds best so that the network can gain optimal effectiveness. Often they spent most of their seismic network funds purely on buying equipment, even though, identically important, one has to provide or procure beforehand the conditions needed for proper installation and operation of this equipment. To make sure you have correctly prepared for the purchase of seismic network equipment, your budget must include money for:

- *A feasibility study* that examines both the selection of potential sites and of potential seismic systems

- *Preparation* of a remote station and a central *recording site*

- *Purchase of equipment*

- *Purchase of* manufacturer's *services* such as installation, training, maintenance agreements, and long term support

- *New personnel* for network operation and data analysis and their training

- *Network operation cost*

- *Servicing and maintenance cost.*

The six figures on the following pages show examples of cost allocation among several different seismic network projects. The numbers in the figures give the amounts allocated to different tasks (normalized per single station) both in thousands of US dollars and as percentage of the project's total cost.

Figure 1 shows an approximate cost distribution (per station) for establishing and operating a global seismic network (GSN) station for five (5) years, according to IRIS plan 1990-1996. Not only did this network use the most advanced and expensive equipment available, it often demanded site preparations (mostly bore-holes) and worldwide maintenance that made it extremely costly per station. Despite of the unusually high cost for IRIS GSN's, this figure seems to indicate the same thing as the others below, namely, that the percentages of total cost needed for each task remain similar from network to network, although the network's size or complexity may change the percentage to some extent.

Figure 2 and Figure 3 show the average cost per station of establishing the IRIS GSN system (not including any operation costs). Since IRIS constructed most of the sites as deep (thus expensive) bore-hole installations, its cost percentages for site preparation are especially high.

Figure 3 shows an approximate average cost distribution for establishing an IRIS GSN station in a surface seismic vault. Although the vaults are cheaper than bore hole sites, IRIS still allocated substantial funds for the vaults and to tasks other than equipment-buying.

Scientific Technical Report STR 98/05
DOI: 10.2312/GFZ.b103-98055

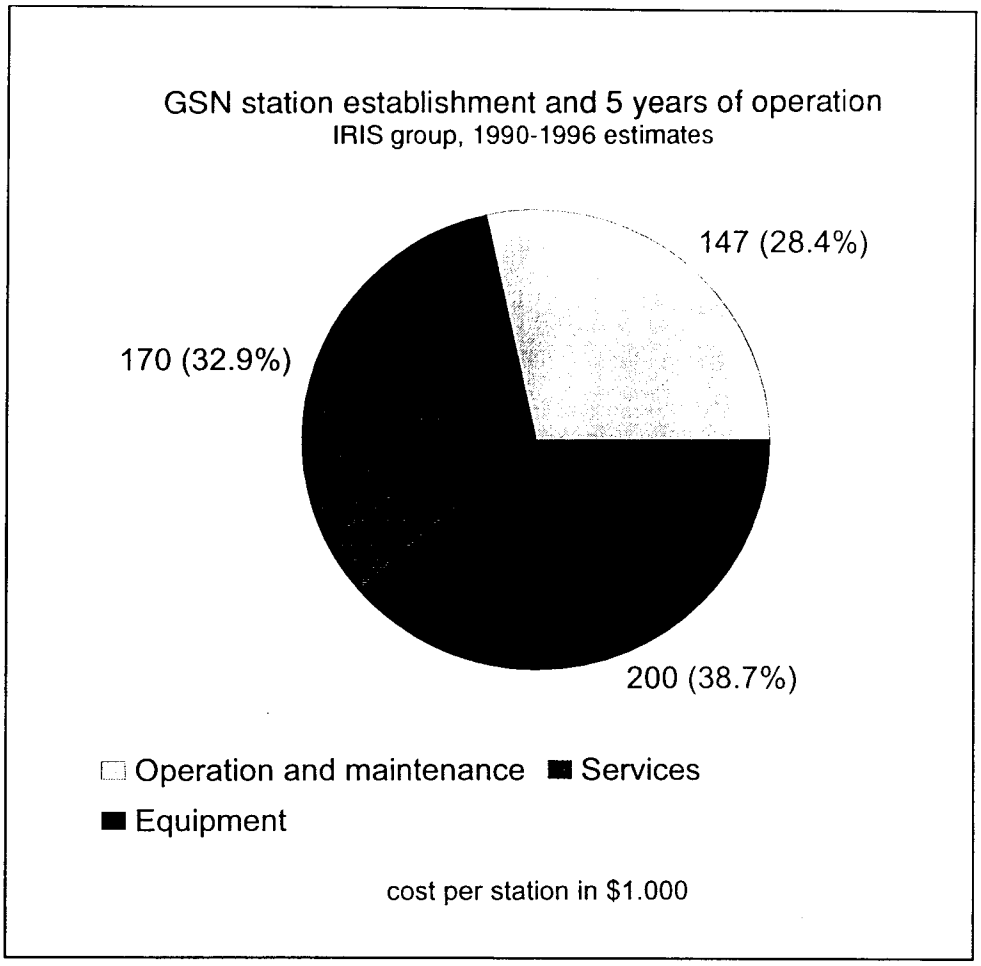

Fig.1: Average cost of establishment and 5 years of operation of a GSN station (in total: 517.000 US$).

Figure 4 shows a distribution of the money spent by a developing country on the establishment of a reasonably large seismic network that uses analog telemetry. The country's significant investment in services (21.6%) paid for site selection, extensive training at the factory and during installation, as well as one year of the manufacturer's full-time engineer support - all of which led to the successful, ongoing operation of this network today.

Figure 5 shows a poor choice example of cost distribution, for a small, yet technologically demanding seismic network. Note the small amount invested in tasks other than equipment-buying, particularly the site preparation works; 4.0% is surely inadequate, making it difficult to believe that these sites could provide ample working conditions for such demanding sensors as very broadband (VBB) and and broadband (BB) seismometers as STS-1 and STS-2. The relatively high amounts going for services (9.8% for installation and 2.4% for training) came mostly because the purchasers insisted on a turn-key type of system. Since that particular country could claim no one with seismometry experience, the chances of using the installed equipment efficiently seem to be small.

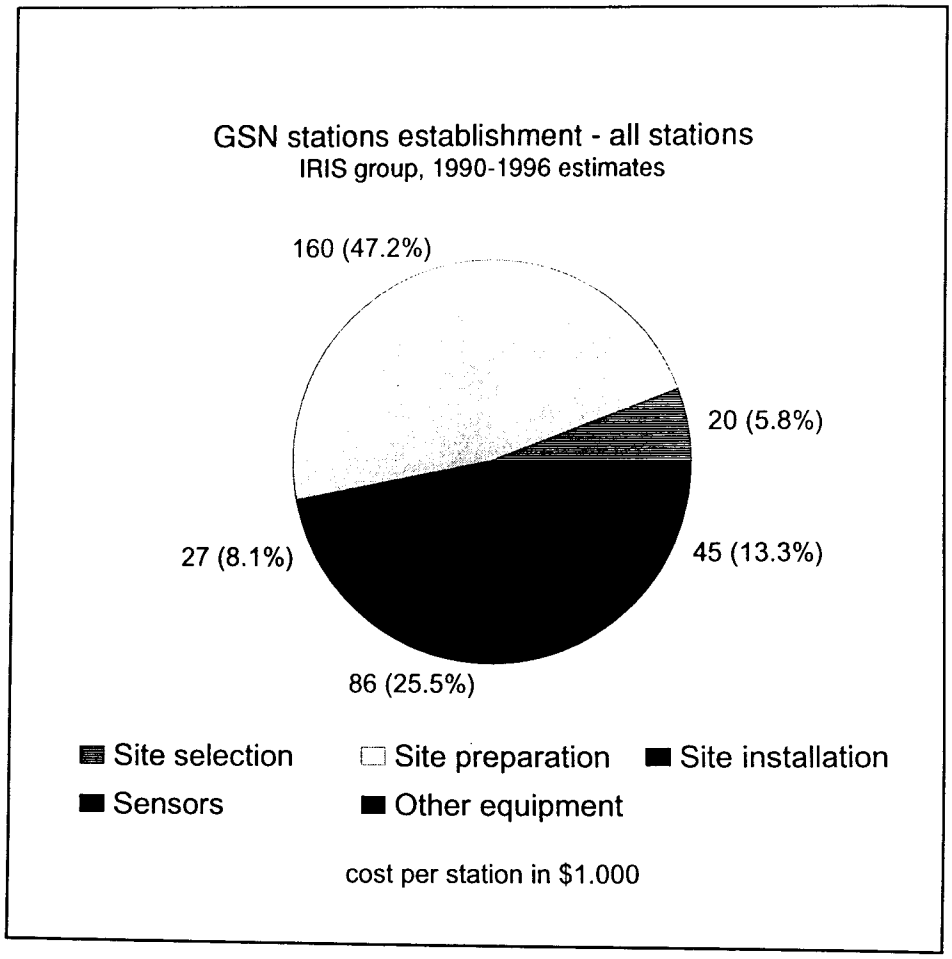

Fig.2: Average cost of establishment of a GSN station without operational cost (total: 338.000 US$).

Figure 6 shows another example of a large seismic network - a national, high-end technology, duplex-digital telemetry system installed in a large country. But again, despite the network's size, the country only invested about one-half of its total project funds in the equipment. The other half went for follow-up services, including a great deal of training and two years of full-time engineer support provided by the equipment's manufacturer.

The funding distributions shown in the figures 1 through 6 are approximate, and for illustration purposes only. Actual conditions (including the type of network, the level of existing technical knowledge, labor prices, and the type of site preparation necessary) will change substantially from country to country. This will influence both the total funds required as well as their most appropriate allocation to the various items and tasks involved. Regardless, the main message of these figures stays the same:

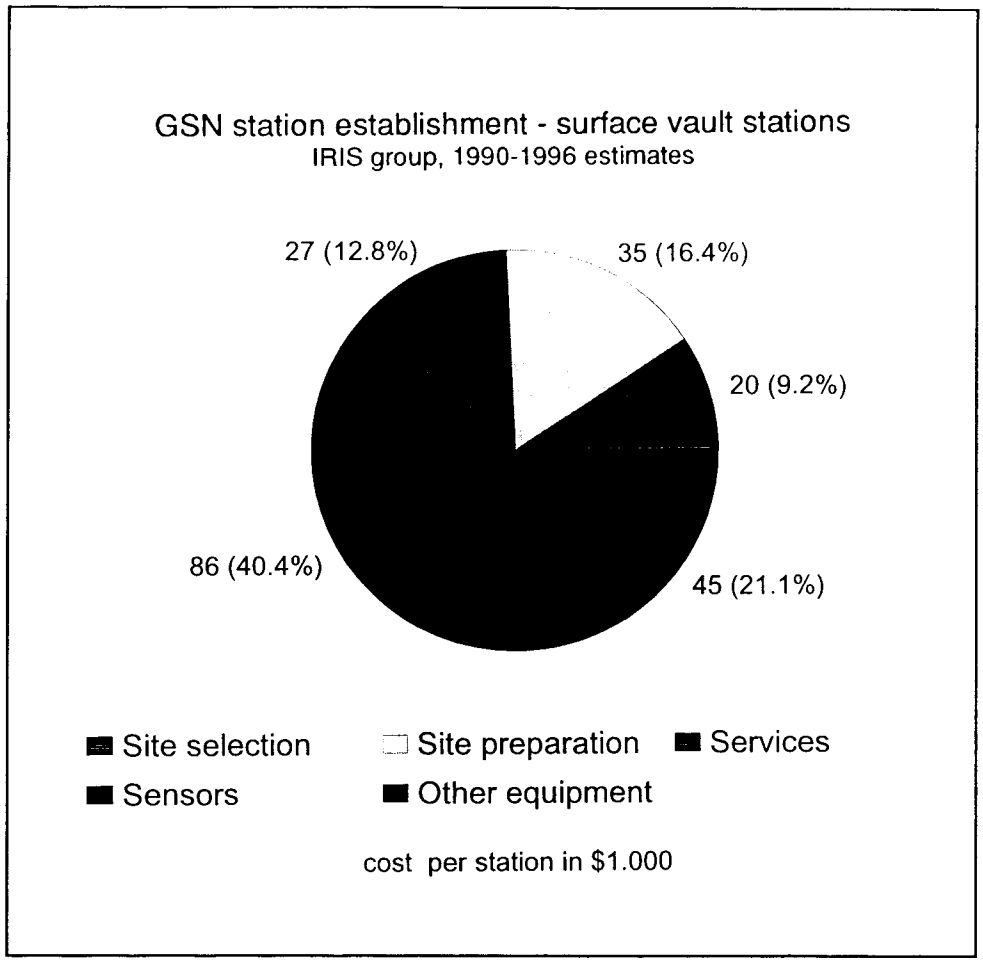

Fig.3: Average cost of establishment of a GSN surface vault station (total: 213.000 US$).

Do not plan to spend nearly all of your allocated funds on buying equipment; save at least one-third to one-half of the moneys for research that moves you towards purchasing the 'right' network, establishing of the proper working conditions, and gaining seismic expertise necessary to use the equipment properly.

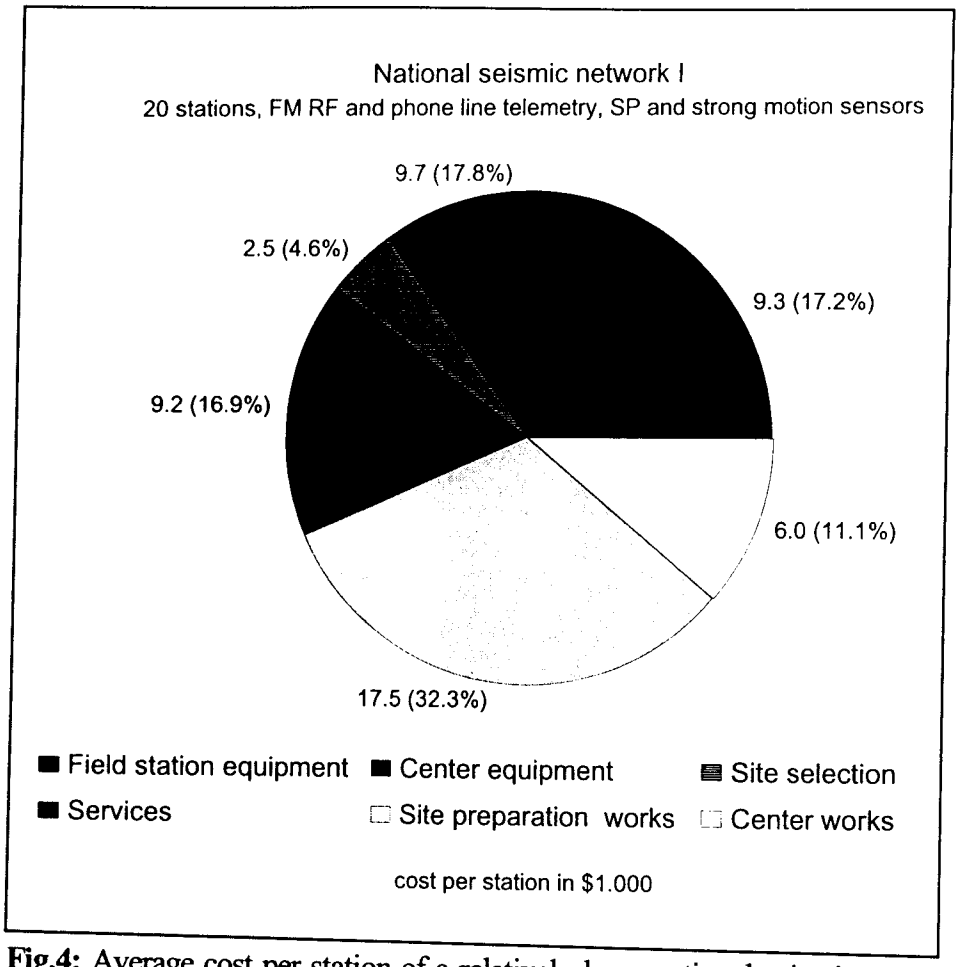

Fig.4: Average cost per station of a relatively large national seismic network with 20 stations and analogue FM telemetry (total: 54.200 US$).

• ***Financing recommendations:***

o Before purchasing anything, try to make sure you have procured long-term financing for the network's operational costs, technical support, maintenance, spare parts, and consumables. All too often planners overlook these (inevitable) costs, which over time will inevitably downgrade the quality of the seismic network's operation if there is no money available to cover them.

o Around the globe, experience has shown (unfortunately) that funding for seismology projects is hard to find until a strong destructive earthquake strikes. Then the money suddenly pops up everywhere. But also note that after a strong event, the public's concern about seismic risk lasts a surprisingly short time. Therefore, you should have your system's plan ready to present while the people do still care.

2.3. Third step to success: Clarifying reasonable expectations

There is still at least one more major and multifaceted task to be completed in order to assure that the proper equipment is ordered, namely, clarifying all interrelated seismological and technological aspects of your project. Thereby one should pay attention to the following points:

- The kind of seismic events to be monitored (e.g. local, regional and/or global events? Preferably micro-earthquakes or mainly recording of strong events or both?), what for (mainly investigation of seismicity, source mechanisms, engineering seismological parameters and/or Earth structure?) and the required accuracy for event parameters, structural parameters or wave form data

- What is the distribution and level of seismicity to be monitored and consequently the kind and amount of data one has to deal with?

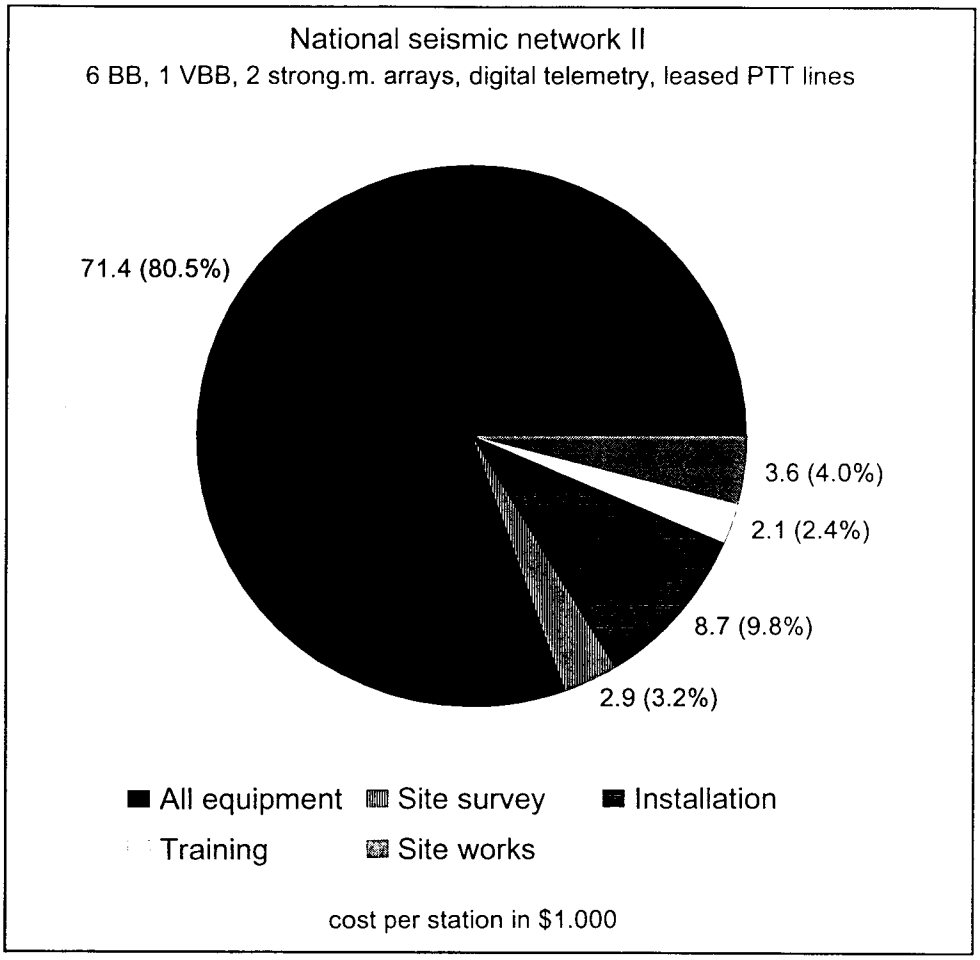

Fig. 5: Average cost per station of a small, technologically demanding seismic network with inappropriate allocation of funds (total: 88.700 US$)

The answers to the above questions will determine:

- The required *type of sensors* (e.g. partitioning between sensors for weak and/or strong-motion recordings, narrow-band or (very)broad-band sensors)
- Their required *resolution and dynamic range* and thus whether still analog technique will do or digital technique is a must
- Accordingly to the above, the *type of recorders/data loggers* needed
- The required number and siting of stations (i.e. *network size and layout*), data links and related infrastructure and services to run such a network
- The needed *equipment for data transmission and* for assuring the required real-time and/or off-line *processing* capabilities at the central site

- Whether the system should acquire seismic data in *continuous or triggered mode*, and in case of the latter, what type of *trigger algorithm* is most suitable
- The *type of archiving system* required

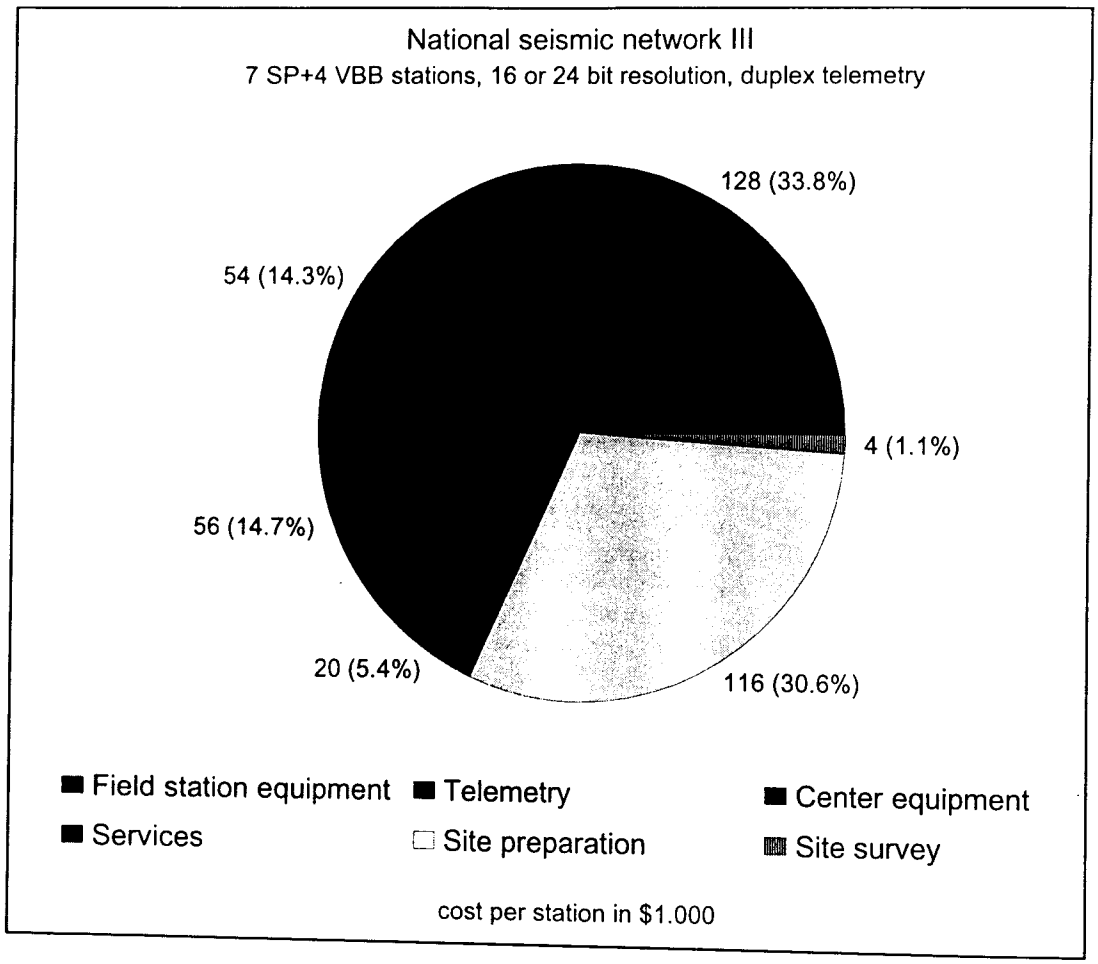

Fig. 6: Average cost per station of a large national, high-end technology, duplex digital telemetry system (total: 378.000 US$)

- The amount of *technical reliability* you expect from the system; this will affect the type of data transmission links you choose, as well as how much hardware-system redundancy one can afford or has to provide by auto-duplicating memory drives, double computers, etc.)
- The *robustness* you desire from the system in terms of how well it will function *during damaging earthquakes*; this will influence the choice of data-transmission links, power back-up utilities for the remote stations and the central recording site, and of civil-engineering designs for the central processing site

Once all these aspects have been considered and decisions been made in compliance with your unique situation, only then you can choose a system engineering approach and begin selecting equipment with the following in mind: Try to find an on-the-market seismic system which, within reason, matches best your idealized needs. And be aware that you will almost certainly have to make compromises.

Avoid pushing a manufacturer to develop something completely new for your particular situation. Such a system would then be unique, will surely cost more, most probably be only minimally tested, and be more difficult to support for many years into the future. Therefore, try to keep to a system and components that are functioning successfully elsewhere, and which have already been tested under real-life conditions.

2.4. Determining the network layout

Determining a successful layout for your seismic network will require two stages:

- Stage 1: Articulating your preferrences with respect to the number of stations and their approximate positions, and
- Stage 2: Determining the exact final station sites for actual installation.

The first stage is closely related to the goals of the network, therefore, the main user of the network should carry it out, decide how many stations he wants to have and can afford, and where he prefers to locate them. The second stage typically requires knowledge of seismometry, seismo-geology, data transmission technology (if applicable), and of equipment capabilities and limitations. Therefore, if you do not avail of the required expertise yourself, you may want to have it performed by the manufacturer's expert staff of whatever seismic system you choose. But even then you should insist on getting involved and to have on-the-job training provided to your staff members who will later be responsible for running and maintaining your network.

2.4.1. Number of network stations

During stage 1, base your decision with respect to the number of seismic stations you want on goals for the network, the size of the region to be studied, and (because this is real life) on the amount of funding available. In short, the following general points have to be considered at this stage:

A minimum of three to four stations with reasonably good records of a seismic event are required to determine its location. More precise locations with better credibility for practical decisions and later scientific use of the data can be expected when good-quality records from about 6 or more stations are availabe. About 10-15 stations would provide already an acceptable basis for more-sophisticated studies of the earthquake's source parameters and mechanism.

Larger countries or regions will require a greater number of stations, of course, unless their interest is only in the strongest earthquakes. Note that seismic researchers do not care much about the total number of stations in a network. What counts is the number of stations in the network that successfully record a given event ('event record' meaning that triggered - or continous - data acquisition occured with large-enough signal-to-noise ratio). In large regions, long epicentral distances often prevent the triggering of distant stations and signals get buried in seismic noise. Thus the total information available for a given event, unless very large, typically comes from only a portion of the total network. Note also that the higher seismic noise you have at the sites, the poorer recording you will get.

2.4.2. Distribution of the network stations

Although the station distribution in a seismic network is very significant to the network's capabilities this topic can only be briefed here and some general recommendations be given.

First on should on a map subdivide the region to be monitored into a series of reasonably regular and approximately even-sided triangles with about equal areas. Avoid narrow and long triangles and thinking in rigid patterns of straight lines, perfect triangles, or circles (seismic arrays are not discussed in this paper). Such rigidity may cause "blind spots", i.e. regions with poor event-location capability. Once you have marked the triangular areas determine the approximate latitude and longitude for every triangle corner. These are the rough, tentative locations where you will try to put your stations, provided that these locations prove to be suitable after site inspection and noise measurements. However, before placing stations definitely, take into account any existing seismic stations in neighboring countries or regions as well. If there are none, push some of your outlying stations as close as possible to the borders of the region being monitored.

• ***Network layout recommendations:***

o Have realistic expectations with respect to depth determination of local earthquakes. To define how reliable your network's event-depth determinations (based on phase readings) will be, there is a rule of thumb: For reliable depth determination, first, one needs to estimate how deep, in the average, earthquakes are in the area covered by your network. Then make sure that the average distance between stations in the network is not bigger than approximately twice that average event depth. The latter condition is admittedly a tough requirement, especially for monitoring large regions with typically shallow events! Only a few small countries or regions can afford such dense networks, and almost none of the larger countries can.

o Alternatively, one could make the network more dense in places, temporarily, if one additionally buys a few portable seismic stations and installs them in any sub-region of particular interest, e.g. right after a strong event in its epicentral region for studying aftershocks. At least for a time, this will increase the network's density drastically in that area of interest, allowing more detailed investigation that may include determination of event depths, source mechanisms etc.

o Also, have realistic expectations with respect to the accuracy of your system's earthquake epicenter determinations. For events outside your seismic network errors will be large (up to several 10 km)! Do not expect reliable determinations for such events unless the "seismic gap" (i.e. the largest of all the angles among the lines connecting a potential epicenter with all the stations in the network) is 200^0 or less. Thus to increase the accuracy of your epicenter determinations, especially for events outside of your seismic network, you need, as much as possible, to:

> Include data in the analysis from seismic stations in neighboring countries, as well as from any other international sources. Acquiring this wider database is nearly a must for determining any event location outside your network.

3. SELECTING THE RIGHT SYSTEM

3.1. Choosing the right seismic sensor

The four most important factors to be considered in selecting sensors for your applications are:

- Type of the sensors
- Number of sensor components per station site
- Sensitivity, and
- Frequency range of operation.

3.1.1. The right choice - seismometers and/or accelerometers?

First you have to decide whether weak-motion sensors - seismometers, or strong-motion sensors - accelerometers, or a combination of both types of instruments, is best suited to meet your needs. Note that in seismic high-risk countries and for networks aimed mainly at seismic risk mitigation studies, strong-motion instrumentation plays a very important role because during the most damaging earthquakes, weak motion records are usually clipped near the event epicenter. For large regional or national projects, a portion of your budget should, therefore, be set aside for strong-motion equipment.

Strong-motion seismic networks generate far less data than weak-motion networks. Therefore, their technical designs differ significantly. For example, seismic data transmission links that are acceptable for strong-motion data may be totally inadequate for weak-motion data. Nevertheless, in many cases, both types of sensors are integrated into a single system. Six-channel data loggers for recording both three weak and three strong-motion sensors are very common choice today.

The relative merits of these systems, however, are not addressed in this article.

3.1.2. Choosing between one-component and three-component seismic stations

Historically, many seismic stations and networks used only one component sensor(s) - usually vertical seismometers. Many still do use only one component. This has been the case because the equipment was analog and required paper-recording for seismic data. If three components were used, then three times more equipment was necessary but three times more valuable information was not gathered. Also, it was very difficult, if not impossible, to generate a vector of ground motion from three separate paper seismograms.

Today, in the era of digital recording and processing of seismic data, the situation is different. The price/performance ratio is much more favorable for three-component stations. Most data recorders and data transmission links are set up to accept at least three channels. Upgrading the central processing facilities for an increased number of channels, including three-component systems, require relatively small extra cost and generating true vector-of-ground-motion is easy now with computers. Given the advanced technology available today, there is virtually no good reason to purchase one component stations any more.

The fact that ground motion is essentially a vector containing all seismic information, which in principle requires three-component data acquisition, and being aware that many modern

seismological analysis methods require this vector as input information, one component stations are no longer a sensible choice for new installations. In any event, a one component station can serve only a limited purpose.

3.1.3. Sensitivity of seismic sensors

Strong-motion accelerometers are relatively insensitive. They are designed to record, close to the epicenter, the ground motion of very strong events with maximal acceleration measured in g-s. They are not suitable for micro-earthquake recording, but they will also give very valuable data from events within the epicentral region where sensitive seismometer records are usually clipped. Accelerometers with 0.25, 0.5, 1, 2, and 4 g full scale sensitivity are available on the market. Be sure you order full scale sensitivity suitable to the maximal expected acceleration at your sites.

Weak motion seismometers can be orders of magnitude more sensitive. They can record weak events which produce ground motion amplitudes comparable to natural seismic noise. Some seismometers can measure ground motion smaller than the amplitudes of the lowest natural seismic noise found anywhere in the world, i.e. amplitudes in the range of the diameter of molecules or even atoms ($< 1\ A^0 = 10^{-10}$ m). If you plan to purchase such sensitive sensors be sure you are willing and able to find the appropriate low seismic noise sites. If your sites are not appropriately chosen and have high seismic noise, natural or man made, this very high sensitivity is of little use.

3.1.4. Frequency range of seismic sensors

Today's sensors are divided into three basic categories:

- Short-period (SP) seismometers measuring signals from approximately 0.1 to 100 Hz (a typical example is Kinemetric's SS-1 sensor).
- Broad-band sensors (BB) measuring seismic signals from approximately 0.01 to 50 Hz (typical examples are the Guralp CMG 40T and the Streckeisen STS-2 seismometer).
- Very broad-band seismometers (VBB) measuring frequencies from below 0.001 Hz to approximately 5-10 Hz (a typical example is the Streckeisen STS-1 seismometer).

Strong-motion sensors (accelerometers) measure seismic signals between DC to up to 100 Hz. However, their output voltage is proportional to ground acceleration and not to ground velocity as is usual for weak motion seismometers.

3.1.4.1. Short-period seismometers

Short-period seismometers (SP) (also called "narrow-band" sensors) were historically developed as 'filters' to mitigate the disturbance by the dominant natural noise peak between about 0.13 and 0.3 Hz. However, with today's digital and high resolution data recording, this 'hardware' filtering can be easily replaced by computer processing, so there is no need for sensors that filter seismic signals by themselves. Nevertheless, SP seismometers are still, and will remain in the future, a valid choice for many seismological applications, particularly for local seismology and microearthquake studies where high frequencies dominate.

Nearly all SP seismometers are passive sensors and are, therefore, easy to install and operate.

They require no power, which allows the use of smaller back-up batteries at remote station sites. They are relatively stable in a broad range of temperatures, and thus require less exacting (and expensive) vault design and environmental shielding. The electronic drift and mass position instability usually associated with active sensors are not a problem. They are, in short, a very practical solution for all applications where seismic signals are not expected to contain significant low-frequency components below 0.1 Hz.

3.1.4.2. Broad-band seismometers

Today, broad-band (BB) sensors are a very popular choice. They provide complete seismic information from around 0.01Hz to 50 Hz and therefore allow for a much broader range of studies than do SP records. I cite Prof. Kanamori (Very Broad Band Study of a Local Earthquake Asperities and Stress Drop, IRIS 1990-1996, GSN proposal):

> "... a single high performance BB seismic station can determine as much, if not more information than a conventional network measuring arrival time and first motion."

However, BB seismometers are more demanding and expensive to install and operate than SP seismometers. They are active feed-back sensors and require a stable power supply. They also require very careful site-selection in a seismo-geological sense, a better controlled environment in seismic vaults, tunnels or mines, careful thermal shielding and they are sometimes a bit tricky to install.

Their output signal contains much more seismic noise than the signals of a SP seismometer. Often, useful signals are buried in seismic noise and can be analyzed only after digital processing. In principle, their raw signals are not viewed directly but must be pre-processed and filtered in order to reveal their content. Even a simple phase reading from the raw signals is far more difficult than from SP or long-period (LP) traces.

BB seismometry requires a higher level of expertise with regard to both instrumentation and analysis methods. Nevertheless, it is a frequent choice in today's market and a must for more sophisticated and comprehensive, research-oriented seismic data analysis.

3.1.4.3. Very broad band seismometers

Very broad band (VBB) sensors are utilized in global seismology studies. Their primary function is for research of the deep interior of the earth. Their only, however important, advantage, compared to BB seismometers, is in their ability to record very low frequencies around and below 0.001 Hz. They are very expensive, require very elaborate and expensive vaults, and are, as a rule, difficult to install. Therefore they are price-wise ineffective for seismic-risk mitigation goals and some also lack frequency response high enough for local/regional seismology.

However, data from a VBB station is extremely useful to the international seismological research community and for educational purposes. For a large national project, it is recommended, therefore, to include, if affordable, also one VBB station (or perhaps 2 or 3 in a large country). Such stations can also serve as important "contact points" with seismologists from developed countries thus promote the transfer of expertise and knowledge to you.

Site selection and preparation for a VBB station requires extensive study and often expensive civil engineering work. The cost of a single good VBB site preparation works can sometime exceed $100,000.

3.1.4.4. Long period passive seismometers

Long-period (LP) passive sensors are not a good choice for new installations. These sensors are clearly inferior to BB equivalents are of interest only in terms of "historical" value.

• ***Critical Observation:***

Because nobody wants to purchase "old fashioned" equipment, developing nations sometimes err in the other extreme and try to buy exclusively BB or even VBB seismic networks. There has been a case a few years ago when a developing country requested for a system of 64 (V)BB stations, up-gradable to 200. It is highly questionable whether such a demanding and expensive system would be worth its cost to a nation whose technological expertise and financial resources are scarce. VBB sensors are definitely not the only good choice under all circumstances and for all seismological goals.

3.2. Seismic data acquisition

The three most important decisions to be made with respect to data acquisition are :

- Digital versus analog data acquisition
- Continuous versus triggered mode of operation, and
- Choice of data transmission method from remote stations to the central recording site.

3.2.1. Digital data acquisition versus analog data acquisition

With respect to data acquisition and transmission technology there are three primary options:

- Analog,
- Mixed, and
- Fully digital.

3.2.1.1. Analog seismic systems

Analog seismic systems include analog sensors, analog signal conditioning, (in most cases) frequency modulated (FM) telemetry through radio frequency (RF) or phone lines, analog demultiplexers, and analog drum recorders. The final product of analog systems is paper seismograms. The two primary drawbacks of such systems are:

(1) Low dynamic range and resolution (about 40-45 dB with single and about 60-65 dB with double, low- and high-gain data transmission channels for each station). This results in many missed events since they are of too small in amplitude to be resolved on paper records while others are too large and therefore distorted or even clipped. Consequently, only a small portion of the full dynamic range of earthquakes that interest seismologists (about 120 to 160 dB) can actually be recorded usefully in an analog manner.

(2) Incompatibility of paper records with computer analysis. This is the most important drawback because modern seismic analysis is almost entirely based on computer processing.

For these reasons, such systems are no longer built although they are still in use in many countries.

3.2.1.2. Mixed analog/digital seismic systems

Mixed systems, frequently and erroneously called digital, have analog sensors, analog signal conditioning, FM telemetry, analog demultiplexers, but digital data acquisition in the central recording site, digital processing, and digital data archiving.

Such systems also have low dynamic range and resolution (FM links are the limiting factor) and therefore, the same disadvantage as pure analog systems. However, they are able to accommodate computer analysis. You may use most modern analysis methods, except those which require very high resolution data. Such systems are still useful for some limited applications when dynamic range is not of prime importance and the purpose of the seismic network is limited to a specific goal such as comprehensive recording and localization of (much more frequent) microearthquakes.

3.2.1.3. Digital seismic systems

In digital systems, only the seismometers are analog. Dynamic range and resolution is much higher than that of analog and mixed type systems and depends mainly - but not only - on the number of bits of analog-to-digital (A/D) converters used in the digitizers. With 12 to 24 bit A/D converters available, the obtainable dynamic range is approximately 72 to 140 dB. In practice, however, the dynamic range and resolution of data acquisition is usually less than the number of bits in A/D converters would theoretically allow. This is always true for the high-end, 24-bit digitizers.

There are two design principles that can further increase dynamic range and/or resolution of seismic data recording.

The gain ranging method automatically adjusts the gain of the system according to the amplitude of the signal and thus prevents clipping of many strong events. In this way, dynamic range of data acquisition is significantly increased. However, even modern electronics is imperfect and this method increases difficult-to-control gain ranging errors in the data. Therefore, actual data acquisition resolution of gain-ranged recording is decreased. For this reason, many seismologists don't like to use the gain ranging systems. They have been mostly replaced by straightforward, multi-bit A/D conversion which nowadays allows nearly as wide a dynamic range.

The over-sampling principle is another approach which helps to improve dynamic range and

resolution of digital data acquisition. The data are sampled at a much higher rate than needed for seismology and then the value of each sample of the final (lower sampling rate) output data stream is calculated using a statistical model. The increase of resolution is significant. However, the efficiency of over-sampling depends on the ratio between the over-sampling frequency and the final sampling rate of the seismic data. The higher the final sampling rate used, the less benefit is gained from over-sampling. Therefore, for local seismology which requires a 100 or 200 Hz sampling rate, the benefit of over-sampling is sometimes quite modest.

- ***Recommendation:***

The buyers of digital seismic networks from developing countries often ask for additional paper drum recorders because they wish to continuously monitor incoming signals on paper and/or believe they will serve as an excellent educational tool. However, there are a number of drawbacks with paper drum recorders. "Hardware-wise" they are incompatible with digital systems (which requires additional digital-to-analog converters). Being mechanical devices, they are and will continue to be expensive and require extensive maintenance. All modern digital observatory seismic systems allow for continuous observation of incoming signals in (near) real time and some even simulate the traditional appearance of paper seismograms because of their advantages for seismic phase identification, especially in teleseismic records. But experience shows that once the user becomes familiar with a digital system, paper drum recorders soon prove to be of little or no use. The desire for paper records stems mostly from the long tradition in analog seismology.

3.2.3. Continuous versus triggered mode of data acquisition

Continuous digitally acquired seismic signals, by their very nature, provide a huge amount of data. Therefore, most of us end up with a data storage problem. For example, a reasonably sized digital weak motion seismic network operating in continuous mode will produce a volume of data so big that most would find it impossible to store for any length of time. Yet, only a small portion of that data contains in fact useful information, i.e. seismic signals above the noise level.

This storage problem has frequently led seismic network users to operate their systems on a "triggered" basis (particularly those local and regional seismic networks that require a high frequency of sampling). Such systems typically do continuous, real-time acquisition and processing of seismic signals, but for trigger purposes only. They begin storing those signals only if the system's trigger algorithm recognizes that a seismic event is occurring. Such systems do not generate continuous time histories of seismic signals, but rather produce "event files."

However, those inexperienced in the purchase of seismic networks often do not sufficiently understand the data-producing limits of the triggered mode of operation, and many have felt disappointed at the results. Note that a decision between continuous or triggered mode of operation usually means a decision between high network event-detectability and reduced detectability by approximately one magnitude unit. The difference between detectability easily becomes dramatic if man-made seismic noise at the remote stations is high (due to poorly selected station sites). Note that:

Continuous data recording in a seismic network provides the most complete data, but storing and processing all that data can become difficult and expensive. Obviously, systems operating in triggered mode will lose the weaker events and produce some false triggers. However, the quality of data recorded is high in both types of systems.

3.2.3.1. Trigger algorithm types

Triggered seismic systems can have various types of trigger algorithm:

- The amplitude threshold trigger simply looks for any signal amplitude exceeding a pre-set threshold value. This algorithm is normally used in strong motion seismic instruments, in systems where high sensitivity is not important, and where man-made and natural seismic noise is not a critical issue because the sensitivity of these instruments is in most cases intentionally low and the trigger threshold well above the noise level.

- The RMS threshold trigger is similar to the amplitude threshold algorithm except that the RMS values of the amplitude are used instead of peak values. Accordingly, it is less sensitive to spike-like man-made seismic noise.

- The short-time average through long-time average trigger (STA/LTA) is most often used in weak-motion seismology. The algorithm calculates the average values of the absolute amplitude of a seismic signal in two consecutive moving-time windows. The short time window (STA) detects seismic events while the long time window (LTA) provides information about temporal amplitudes of seismic noise at the site. When the ratio of both exceeds a pre-set value (usually set to between 4 and 8) an event is "declared" and data 'archiving' in a file begins. The STA/LTA trigger algorithm is well-suited to cope with fluctuations of natural seismic noise which are slow in nature. It is much less effective in situations where man-made seismic noise of a bursting or spiky nature is present. At sites with high, irregular man-made seismic noise, the STA/LTA trigger usually doesn't work well. It is also not very efficient to detect tele-seismic events.

- There are several more sophisticated and theoretically more effective trigger algorithms but they are rarely used in the seismic equipment currently on the market. The sophisticated adjustments of operational parameters to actual signal and noise conditions at each seismic site that these triggers require has proven unwieldy and subject to error.

3.2.4. Stand alone, coincidence triggered, and ring buffered systems

Trigger algorithms are generally implemented in two ways. In seismic networks with stand-alone triggered stations, each remote station has its own independent trigger. In such

networks, data are transferred to the central recording site on request-only or collected in-person. These networks have the lowest effectiveness of triggering and consequently the smallest detectability and the highest rate of falsely triggered records. The completeness of data is low because not all stations in the network trigger simultaneously for each event. This approach also requires a lot of routine maintenance work to "clear" numerous false records if trigger thresholds are set low (alternatively, the network has lower detectability). Remote stations frequently encounter "memory full" errors because they evidently have a limited local memory. They absolutely require a careful selection of station sites with low man-made seismic noise amplitudes. If low-noise is not assured, such networks may become very insensitive and may frequently be considered a serious project failure (from observatory seismology view point).

Seismic networks that use a coincidence trigger algorithm are much better at detectability and completeness of data. In these systems, data is transmitted continuously from all remote stations to the central recording site where a complex trigger algorithm discriminates between seismic events and excessive seismic noise. The coincidence trigger takes into account not only signal amplitudes in all incoming channels but also the number of simultaneously 'activated' stations and potentially their spatial distribution. A much more robust-to-false-triggers algorithm results. Thus, the trigger threshold level can be lowered which results in better detectability by the whole network. Each station's signals are recorded for every trigger which greatly improves completeness of data.

An even better solution is provided by systems that keep continuous signals in their memory (ring buffers) for a given period of time, from several hours to several days. After the specified time, these systems erase the old data replacing them by the new incoming data. However, during the designated time a seismologist can detect and extract events far better than any automatic trigger algorithm. While this method requires prompt analysis of seismic signals, excellent completeness of data and detectability is obtained. In addition, for the most interesting periods, like aftershock sequences, the data can be stored in a continuous manner, thus keeping all information contained in the signals. Such systems may still have an automatic trigger algorithm working simultaneously which enables automatic processing and a short reaction time in the case of large events. Modern high capacity and very affordable hard disks enable relatively inexpensive systems to use the ring buffer approach. Probably this approach is currently the best compromise between a triggered and continuous seismic system.

• **Suggestion:**

Be sure your triggered system has an adjustable band-pass filter in front of the trigger algorithm. This is particularly important in BB seismometry where small signals are often completely buried in the dominant marine seismic noise between 0.13-0.3 Hz. The adjustable pass-band filter allows the trigger algorithm to be most sensitive to the frequency band of your greatest interest. Events buried in seismic noise may still be resolved and acquired. Not all systems on the market are flexible enough in this respect.

3.3. General considerations about seismic data transmission from remote stations to the central processing site

While data transmission may seem like a minor part of a seismic network, poorly designed or selected data transmission links are the most frequent cause of disappointments and

technical failures. The quality of network operation rests largely on the reliability and efficiency of data transmission.

Another important but frequently over-looked consideration is the cost of data transmission. Don't forget to factor in these costs when determining the budget for long-term seismic network operation. Many seismic networks all over the world (also in some very developed countries) have been forced to change data transmission links to cheaper solutions after some years of operation due to the very high cost of data transmission links. Note that

> Technical considerations, reliability, initial price, and operational costs of data transmission vary widely from country to country. It is the responsibility of a seismic system buyer to find the optimal solution for a given country.

The right decision about which data transmission method to use is not an easy one. Key technical parameters in this decision are: Baud rate required, desired reliability (acceptable error-rate), and the distances data must be transmitted..

3.3.1. Types of data transmission links used in seismology and their choice

There are several varieties of data transmission links used in seismology:

- *Wire lines*, which are cheap, reliable, but useful for very short distances only.
- *Leased phone lines*, which are reliable, but usually very expensive in the long-run.
- *Dial-up PTT lines*, which are effective only in low seismicity countries; experience shows that their throughput is limited and that they never work after stronger earthquakes with macroseismic effects; an exception is seismic equipment which grabs telephone lines automatically at the moment of triggering to large event.
- *Radio-frequency links* on a VHF or UHF band, which have limited low dynamic range of data acquisition for analog FM telemetry, are often difficult to obtain; they are robust for strong events, and are relatively inexpensive once they are established.
- *RF spread spectrum links*, which are useful for relative short distances, are relatively cheap, easy to obtain, modern and promising.
- *Microwave links*, which are expensive, appropriate for long distances, and useful for analog and digital data transmission.

- *Computer networks (X25, Internet)* with different level protocols, which may be unavailable at remote seismic stations sites, but when available, are very powerful and not too expensive.

- *Satellite links*, which are very expensive, appropriate only for extremely remote sites or very large national seismic networks, and thus still rarely used.

Data transmission links may be of two different basic types: the simplex type in which information is transmitted one-way only - from remote stations to the center - or the duplex type where data can flow in both ways. The duplex type allows for remote control of seismic stations from central facilities and significantly increases reliability of data transmission. Links can use different types of error-checking methods that allow recognition of corrupted data, from simple parity check, check-sum error detection, CRC error detection, and error-correction methods including repeated re-sending of corrupted seismic data that allow you to correct corrupted data. Generally, the higher (or lower) the reliability, the higher (or lower) the cost.

Local country conditions are the most important factor in the selection of an appropriate data transmission system and therefore require that the user is actively involved in the decision making process. It is essential to get information about the availability, reliability and cost of different approaches from local communication experts. The manufacturers of seismic equipment generally do not know local conditions and may be unable to correctly advise you about the best solution for your country.

• ***Recommendations:***

o Dial-up phone lines are very often proposed for seismic data transmission because they are readily available. However, they have limitations that you must be aware of. Dial-up phone lines are an appropriate choice for low seismicity regions only. Their through-put is, in spite of the high theoretical baud-rate of modern modems, frequently limited. The most modern and fast modem does not help if the phone system is of low quality. Note that a PTT system must be very reliable for successful transmission of sometimes very long event files. In developing countries, phone line system quality and reliability is often over-estimated. This easily results in inefficient data transmission and tedious repeated re-transmitting of data files. As a matter of fact, dial-up phone lines usually cannot 'digest' earthquake swarms and the numerous after-shocks after strong events. In addition, they often don't work at all for several hours after strong events due either to especially high usage of the phone system or technical difficulties. They are certainly not the right choice for networks whose predominant purpose is alarm.

o In many countries, PTT networks have specific properties and special 'tricks' which require consultations with local communication experts. Therefore, modems should be purchased locally. Pay particular attention to choosing the one which performs best under your local circumstances. Modems react differently to each phone system's particular weak point. A modem which works perfectly in one country may not be the optimal solution for another country. Consult the local experts who have practical experience in digital data transmission over local phone lines.

4. SEISMIC STATION SITE SELECTION

The matter of seismic site selection is rarely given the depth of study and attention that it requires. It is a fact that

> ... any weak motion seismic network can operate only as well as its sites allow, no matter how technologically advanced and expensive the equipment is.

If seismic noise at your sites is too high, all or a part of the benefits of modern, high-dynamic range equipment are lost. If an excessive burst- or spike-type, man-made seismic noise is present, high-trigger thresholds and therefore poor network detectability will result. If a station is situated on soft ground, VBB or even BB recording can be useless and SP signals may be unrepresentative due to local ground effects. If network layout is inappropriate, the location of events will be inaccurate or even impossible. A professional site selection procedure is, therefore, essential for success. For good sites, many factors at sites must be taken into consideration.

Generally, it is best to begin the process of site selection by choosing two to three times as many potential sites as you actually plan to use. Then you can study each one and see which sites most closely meet as many of your criteria as possible. Gradually, selecting the most promising, you will eliminate certain sites and get down to the number of sites required plus three or four. By using computer models of the few most likely network layouts and comparing the results, you will be able to make an informed decision about which layout will locate and record seismic events best.

In this paper, the site selection process is demonstrated by seeking the best placement for a local six station seismic network around a nuclear power plant.

4.1. Off-site studies

Off-site, "office" studies are the most inexpensive ones to do and are, therefore, the first to begin with. From the office, you can study maps and contact local authorities to gather information about the potential site.

The first step is to define the geographical region in which you are most interested. For this you should study known geological faults, seismo-tectonic features, and the seismicity in the area. Also compile historical and instrument-recorded events from all available earthquake catalogs and other sources. Fig. 7 shows the region for our example and the main geological faults within it. Fig. 8 shows events from catalogs, and Fig. 9 shows the final drawing of the specific region you wish to study.

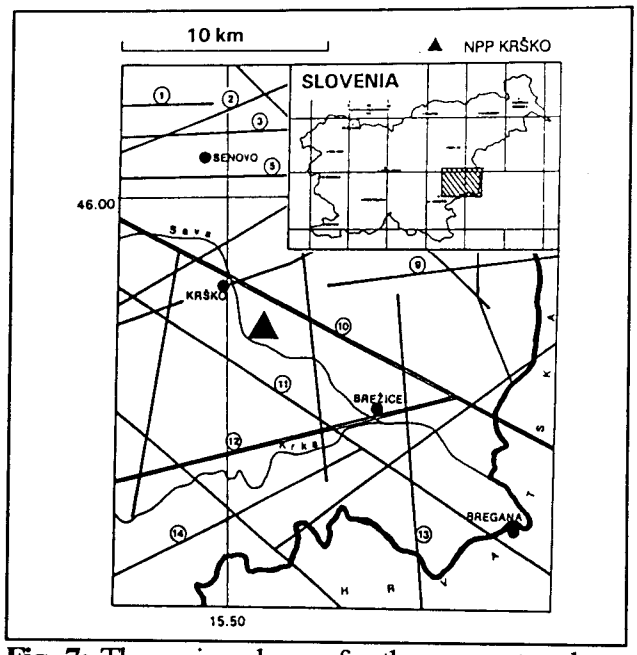

Fig. 7: The region chosen for the new network and the main geological faults within it.

Prepare a simplified map of regional seismo-geological conditions. Determine the quality of bed-rock (based on acoustic impedance of the rock shown on geological maps) for each type of bed-rock in your region and divide the region into three (or more) quality grades (Fig. 10). Usually the higher the acoustic impedance of the bed-rock, the less seismic noise and the higher the maximum possible gain of seismic station.

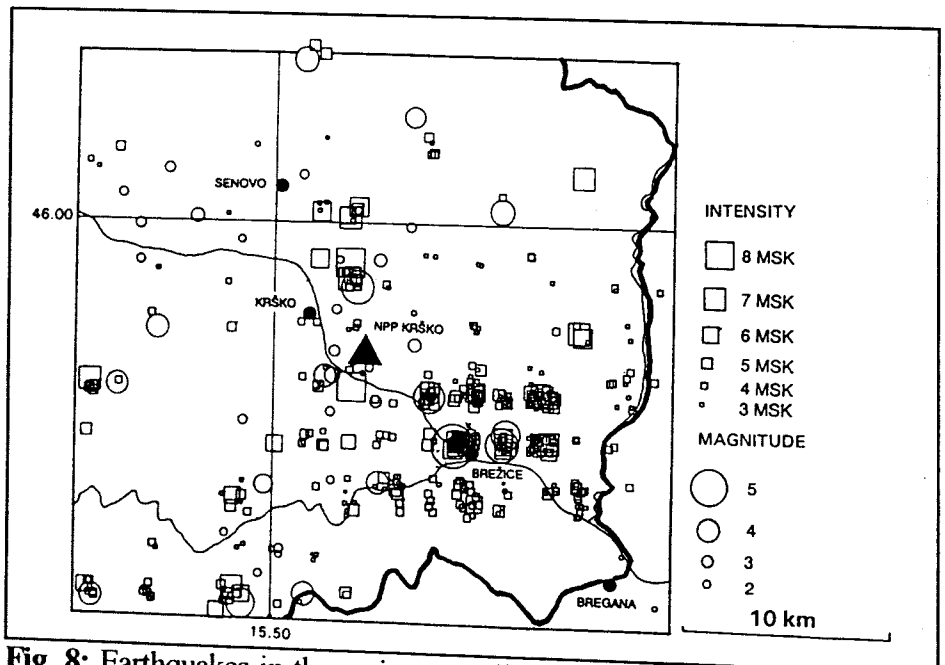

Fig. 8: Earthquakes in the region compiled from all available catalogues.

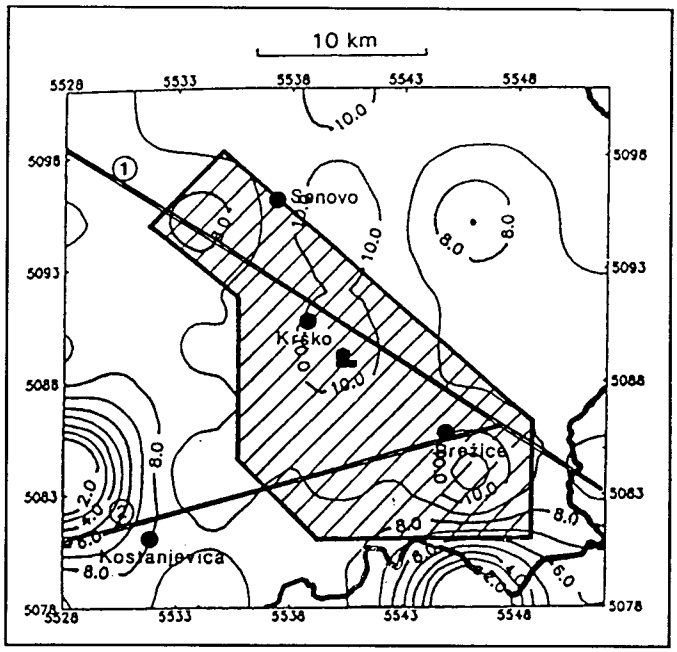

Fig. 9: Final choice of the region to be studied by the seismic network (dashed area). Isolines of released log-seismic energy in J/km^2 are also shown.

Study the topographical aspects of your possible locations. Choose sites in a "moderate" topography. Extreme mountain peaks or deep valleys are unfavorable for station operation.

Study man-made and natural seismic noise sources in your region. Road traffic, railway traffic, heavy industry, mining and quarry activities, agriculture, and any other source of seismic noise around the potential sites should all be assessed. Much of the information you will need can be found in maps and by asking questions of local authorities. Evaluate the man-made seismic noise sources, along with natural sources like oceans and lakes, rivers, waterfalls etc., according to the Manual of Seismological Observatory Practice, Willmore, Karnik, (1982). You will find a table (Fig. 11) in this manual with the minimum recommended station-site-to-noise-source distances for three levels of sensitivity of seismic stations (A very sensitive, B moderately sensitive, and C modestly sensitive), two geological conditions - hard rock and hardpan, and high and low seismic coupling between seismic noise source and station site (a,b).

Once you have gathered this information about your potential sites, draw a map similar to Fig. 12. On this map, show the possible station sites and all known seismic noise sources along with the recommended minimum distances. It will be easy to see on this map which site is influenced by which noise source and by how many of them .

Correlate RF data transmission requirements with the topography around the sites based on topographic maps. 1:50.000-scale topographic maps are most commonly used for this purpose. If you plan the use of telephone lines for data transmission, check their availability and the distances new phone lines would have to be laid. If you plan to power your stations by main

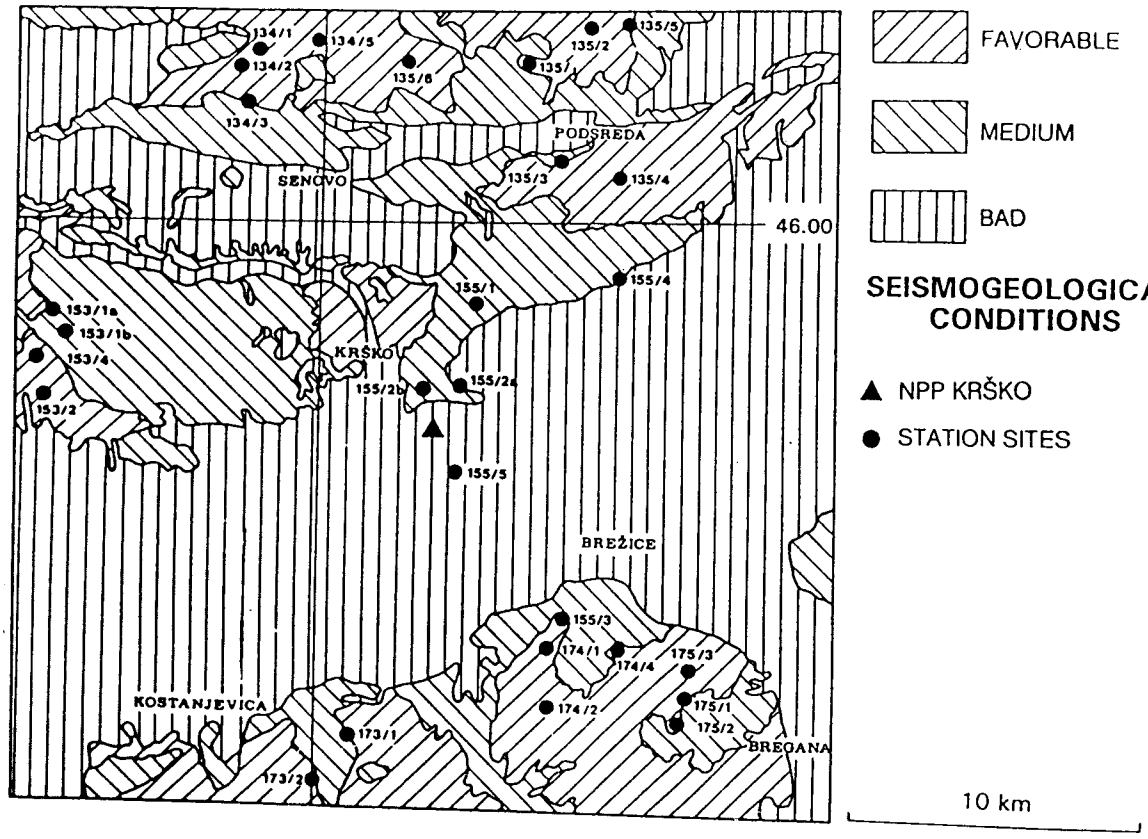

Fig. 10: The region of interest divided into three grades of bedrock and potential station sites.

power source, check the availability of main power lines and check the distances over which new power lines would have to be laid or choose solar panels as a power source.

It is also very important to study land ownership and future land use plans for the sites you are interested in. It makes no sense to undertake extensive studies if you will be unable to use certain sites because of property ownership issues or if it appears that future development will make the site unsuitable for seismic stations in near future. This information can be gathered from local and regional public officials.

Gather data about the climate at the sites from local meteorologists. Find out what the prevailing minimum and maximum temperatures are - they influence how much thermal isolation the seismic vault will require (note that seismic equipment generally needs to operate within a certain temperatur range). You will need to know about the frequency and maximum speeds of wind in the area. Wind is a primary source of seismic noise, therefore, sites with less wind are much preferable. The frequency and amount of rain will determine what kind of water-proofing measures you will need to take to keep the seismic vault dry. Annual snowfall levels determine how accessible the station will be during the winter, the waterproofing measures required, and - if solar panels are used - their installation angle and size.

SITE NAME: PULAU UBIN QUARRY		SITE #: 3			DATE: OCT.03, 1995			
SOURCE OF NOISE		HARD ROCK, GRANITE, ETC.			HARDPAN, HARD KLAY, ETC.			ACT
		A	B	C	A	B	C	km
1.Oceans,coastal mount.syst.		300	50	1	300	50	1	48
2.Large lakes		150	25	1	150	25	1	10
3.Large dams, waterfalls	a	40	10	5	50	15	5	
	b	60	15	5	100	25	10	11
4.Oil pipes	a	20	10	5	30	15	5	
	b	100	30	10	100	30	10	
5.Small lakes	a	20	10	1	20	10	1	
	b	50	15	1	50	15	1	0.25
6.Heavy machinery,reciproc.	a	15	3	1	20	5	2	
	b	25	5	2	40	15	3	1.0
7.Low waterfall, rapids	a	5	2	0	15	5	1	
	b	15	3	1	15	5	1	
8.Railway, freq.operation	a	6	3	1	10	5	1	
	b	15	5	1	20	10	1	20
9.Airports, airway traffic		6	3	1	6	3	1	5
10.Non-recipr. machinery	a	2	0.5	0.1	10	4	1	
	b	4	1	0.2	15	6	1	0.8
11.Busy highway, mech. farms		1	0.3	0.1	6	1	0.5	4.5
12.Country roads,high build.		0.3	0.2	0.05	2	1	0.5	0.15
13.Low buildings, high trees,masts		0.1	0.03	0.01	0.3	0.1	0.05	0.15
14.High fence,low trees		0.05	0.02	0.01	0.06	0.03	0.01	0.04

LEGEND:
ACT Actual distance in km.
A Seismic station with a gain of 200,000 or more at 1 Hz.
B Seismic station with a gain of 50,000 to 150,000 at 1 Hz
C Seismic station with a gain of approximately 25,000 at 1 Hz.
a Source and seismometer on widely different formations, or that mountain ranges or alluvial valleys intervene.
b Source and seismometer on the same formation and with no intervening alluvial valley or mountain range.

Fig. 11: Minimum recommended station site-to-noise-source distances according to Willmore (1982) and actual distances for a seismic station.

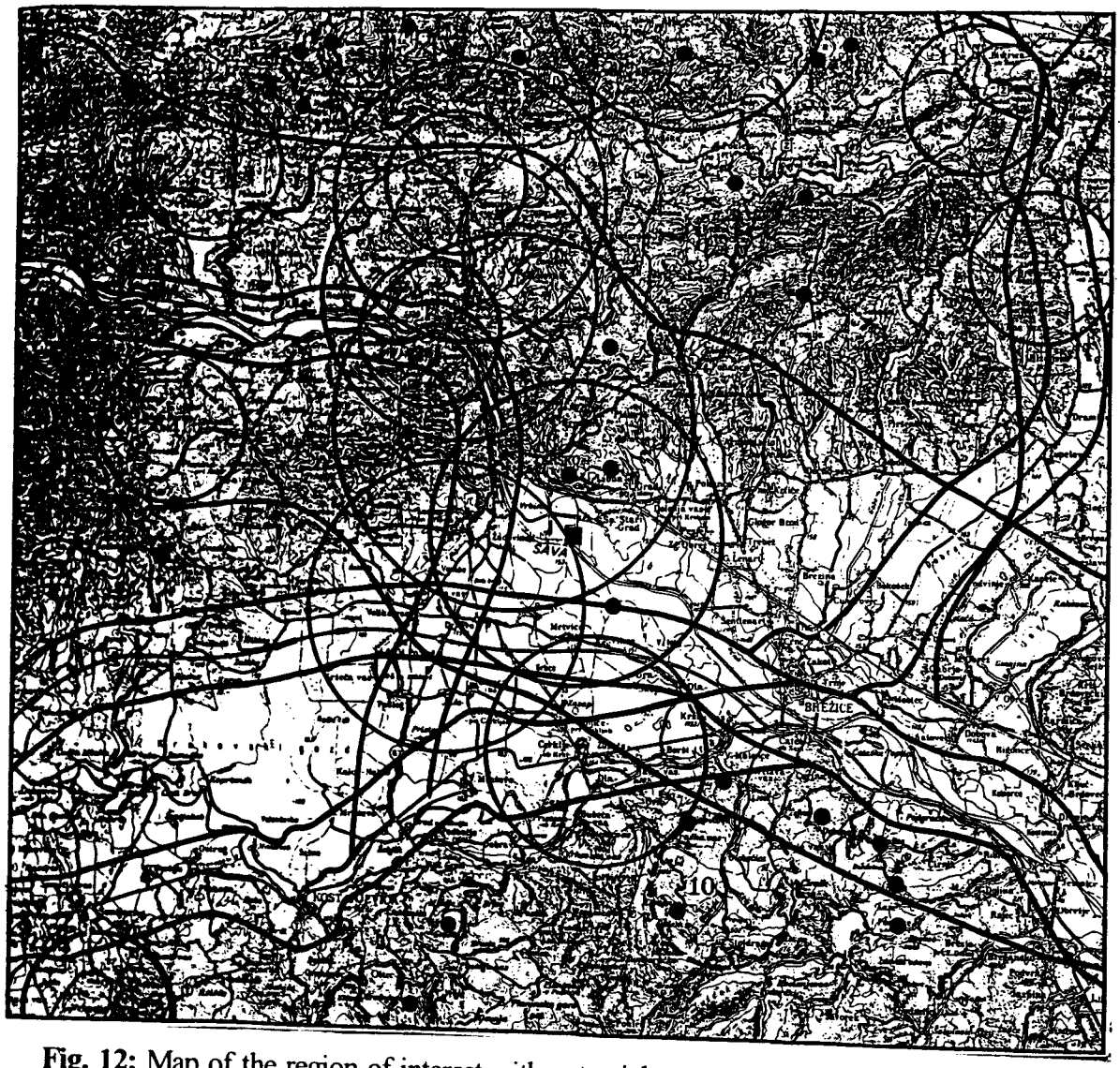

Fig. 12: Map of the region of interest with potential station sites and seismic noise sources - roads, railway, cities, industrial facilities, quarries, etc.

Insolation data will determine the proper sizes for solar panels. Gather information about the frequency of lightning to decide how great a threat it is and how many lightning mitigation measures you'll need to take.

Once you've gathered all this information, it is likely that half or more of your possible sites will be eliminated for one reason or another.

Scientific Technical Report STR 98/05
DOI: 10.2312/GFZ.b103-98055

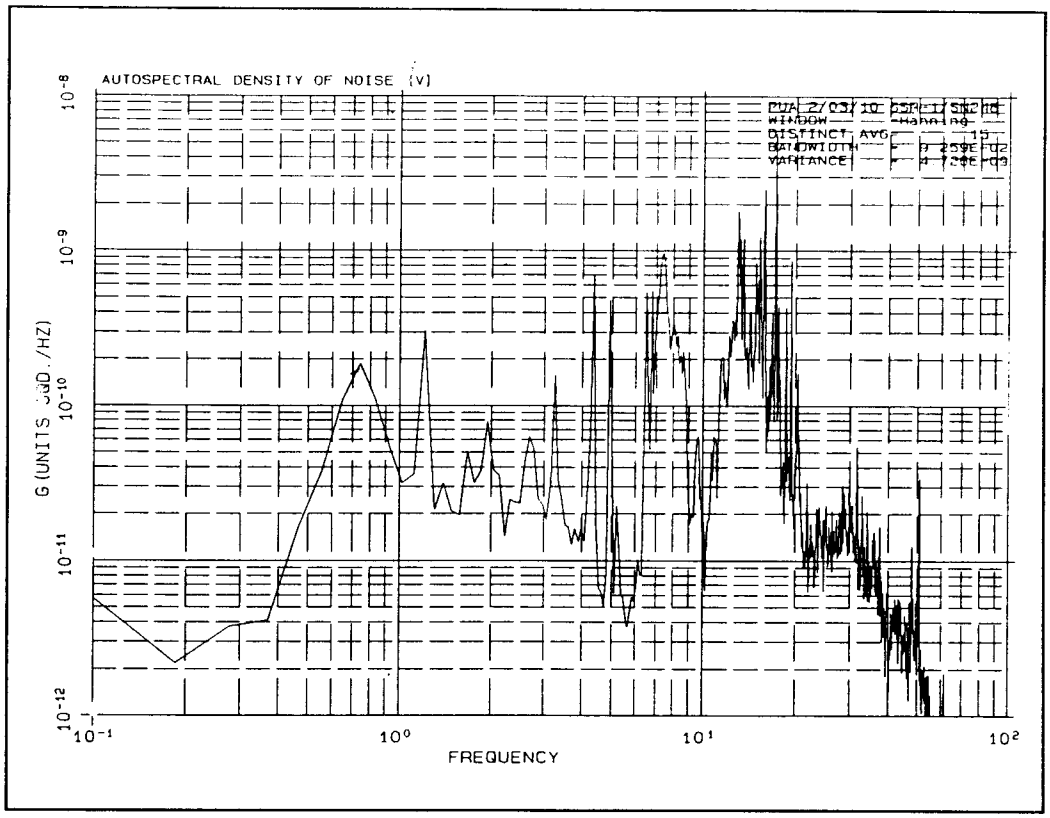

Fig. 13: A typical seismic noise spectrum (ground velocity power) at a potential seismic station site.

4.2. Field studies

The next step in the site selection process is field studies. Expect to make several visits to each site. A seismologist familiar with seismic noise measurements, a seismo-geologist, and a communication expert, if you are considering a telemetry network, should visit all sites.They should:

- *Verify* the ease (in all weather) of access to the site.
- *Search* for man-made seismic noise sources adjacent to the site.
- *Take* seismic noise measurements.
- *Study* the local seismo-geological conditions at the site.
- *Investigate* the possibilities of RF data transmission when building an RF telemetry network.
- *Verify* power and phone line availability.

Measuring seismic noise at the site is not a trivial task. Natural seismic noise varies greatly depending on the season of the year, weather conditions and innumerable (and often unforeseeable) daily occurrences. Ideally, to accurately weigh all these factors, it is best to take measurements at each site over a long period of time - long enough, in fact, to record a number of earthquake signals as well. This would allow you to compare sites based on their signal-to-noise ratio.

Unfortunately, such ideal long-term measurements are rarely taken for financial reasons. But some measurements are much better than none at all. While short-term measurements cannot provide a representative information about the noise level and its variability at the temporary potential site, they are still very useful. To assess the possible influence of long-term seismic noise variations on the actual spectrum measured at the temporary site one should gather noise data from already existing seismic stations in the region as well. By comparing noise records taken at the same time at such reference sites and the potential new sites one can, at least with respect to the more long-period natural seismic noise, weigh the representativeness of the noise data sampled at the temporary site and roughly scale it to the reference site.

Time records of seismic noise are usually re-calculated into noise spectra, which can reveal much information about the type and importance of various seismic noise sources around each site. In Fig. 13 a typical seismic noise spectrum is shown. One can easily see high contamination of the site by man-made seismic noise (frequencies around 15 Hz). Noise peaks between 3 and 5 Hz have their origin in heavy machinery working in a 4 km distant quarry. At a minimum, for future SP seismic stations, several minutes of seismic noise must be recorded in order to allow the calculation of stable seismic noise spectra in the frequency range from 0.1 to 50 Hz . At potential BB sites noise spectra must be calculated between about 0.01 and 50 Hz. This requires a minimum record duration of about twenty to thirty minutes. In order to minimize, at least to some extent, the possible biasing influence of diurnal noise variations on the site quality assessment, the measurements at the various sites should be taken at about the same time of the day. Whenever possible, use the same type of equipment and processing methods at your possible locations and at the reference station(s). This allows for simple normalization procedures to be applied to your calculations.

Study the local geology to determine its complexity and variability. As far as possible, uniform underground conditions should be preferred for seismic stations. Verify the actual quality of bed-rock as compared that given in the geological maps. Note the degree of weathering that local rocks have undergone. This gives you a rough estimate of the required depth of your seismic vault for placing your seismometers on unweathered rock. Consider seismic coupling between local noise sources and the site, and precisely determine the position of planned potential shallow profiles.

Make an RF search for potential local radio wave obstacles. Consider the immediate topography surrounding your site because it defines, to an important extent, the minimum required antenna height for reliable data transmission.

Shallow profiling is the last step in the site selection process because it is the most expensive one. It is normally done only on the most likely sites. Shallow refraction profiles reveal the quantitative rheological quality of the bed-rock and allow to determine the depth of rock weathering. The results of shallow profiling will determine the best "micro" position of the seismic vault as well as its depth. Make two profiles, about 100 meters long each and approximately perpendicular to one another. With such profiles you can determine seismic wave velocity down to a depth of about 20 to 30 meters.

If you choose not to do profiling for any reason (most likely financial), then you may expect surprises when digging your seismic vaults. Many times it is a matter of almost pure chance what you might run into. You need to dig until you reach bedrock and that can sometimes be very deep. Expect that vaults will have to be repositioned and redug if weathered bedrock

happens to be extremely deep. These possibilities often make the relatively high cost of profiling a wise investment.

4.3. Using models to determine network capabilities

Once you are very close to the final layout of your system (or better yet, to two or three possible layouts) and have decided on the final number of stations, the next step is to make a computer model of the network. Among the things you may wish to study are:

- *Network detectability* in terms of distribution minimum magnitude of events for a given number of records with a given earthquake signal-to-seismic-noise ratio (Fig.14).

- *Accuracy of event epicenter* determination in the region (Fig.15).

- *Accuracy of event hypo-center* determination in the region (Fig.16).

- *Maximum magnitude* of events that can be recorded without clipping (this requires knowledge of the gain and dynamic range of your future recording equipment).

Once you have the results from each possible layout you can choose competently the best one.

Several methods for computer modeling of a given network are described literature, but an examination of each of them is beyond the scope of this paper. In general, simple methods will suffice because the point, no matter which modeling method you use, is the comparison of results between the various layout options. Usually, estimated uncertainties of P-phase readings (± 0.1s) and P-wave velocity (± 0.3 km/s), and the sensitivity of seismic stations based on the measured RMS seismic-noise amplitudes at the sites are taken into account. A simplified and uniform seismic wave attenuation law in a homogeneous half-space or in a single layer ground model works well.

Note that the results of computer modeling based on such simplified parameters are almost never useful in an absolute sense. In general, an oversimplified seismic wave-velocity model, regional velocity variations and anisotropy, incomplete information about seismic noise at the sites, imprecise wave attenuation models, limiting conditions with respect to infrastructure, topography and accessibility etc. do not permit to put into practice, 1 : 1, the idealized optimal configuration resulting from the modelling but rather allow to assess the relative suitability of various alternative configurations. This applies both to the modelling of network detectability and location accuracy.

Several methods for direct computer calculation of optimal network layout can also be found in the literature (e.g. Kijko 1977; Rabinowitz and Steinberg 1990; Steinberg et al. 1995). However, practical considerations usually outweigh such theoretical approaches to the optimal network layout. It is a fact that in addition to theory, choosing the best layout always involves making good, educated guesses based on experience.

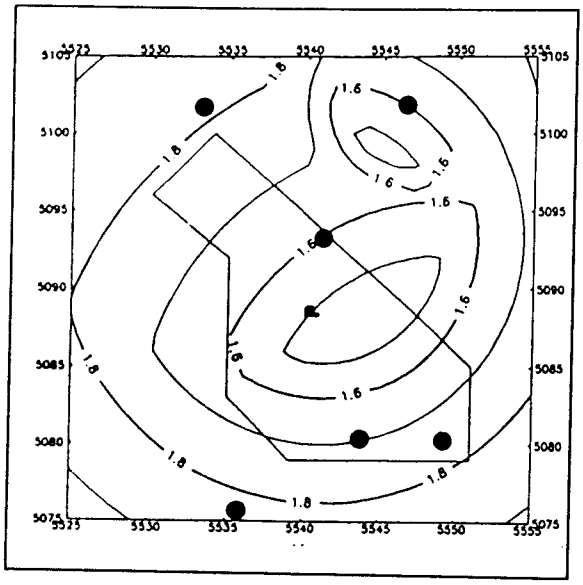

Fig. 14: Isolines of minimum magnitude of events detected on 5 stations with S/N ratio 20 dB.

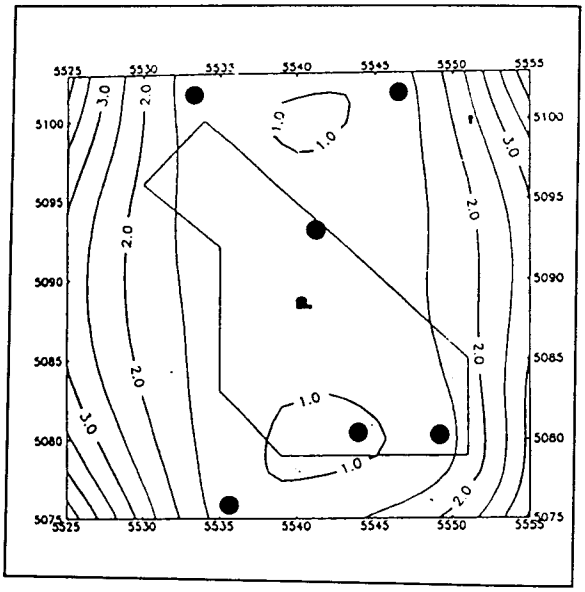

Fig. 15: Isolines of uncertainty of epicenter determination in km (SD) for final station selection.

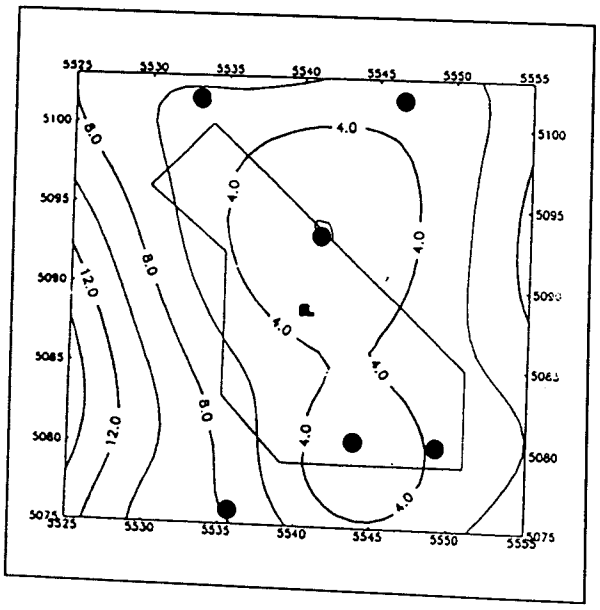

Fig. 16: Isolines of uncertainty of hypocenter determination in km (SD) for final station selection.

Scientific Technical Report STR 98/05
DOI: 10.2312/GFZ.b103-98055

5. RADIO FREQUENCY LINK SURVEY

5.1. The need for RF survey

The most common problem with seismic network equipment and the most frequent reason of unreliable operation and failures of seismic networks are inadequately designed data transmission links, particularly RF links.

> The design of RF telemetry links in a seismic network is a highly specialized and technical matter. Guess-work and the „common sense" approach usually lead to unreliable data transmission or even complete project failure.

Three main issues are often misunderstood or over-simplified:

i) The amount of data that must be transmitted in weak motion seismology is often underestimated.

ii) Seismology requires an incomparably larger information flow than many other geophysical disciplines (two orders of magnitude more than meteorology). For example, a typical single GSN seismic station with continuous data transmission produces around 30 Mbytes of data per day. These 30 Mbytes must be transmitted without errors to the network analysis center.

iii) The degree of reliability required for successful data transmission in seismology is frequently underestimated too. Interruptions, excessive noise, spikes and data errors are particularly dangerous for networks operating in triggered mode. On paper seismograms, spikes, interruptions and other interferences are "filtered out" easily by the seismologist during analysis. However, these same factors can make the results of (automatic) computer analysis totally meaningless. Frequently, a false comparison with voice RF channels is experienced. Note that voice channels allow for a much lower signal-to-noise ratio while still being fully functional because human speech is highly redundant.

An open "line of sight" between transmitters and receivers is frequently considered sufficient for a reliable RF link. This is rarely true except for very short and direct links. The real issues in link reliability are frequency of operation, Fresnell ellipsoid obstructions, the curvature of the Earth, the gradient of air reflectivity, potential wave diffraction and/or reflections, etc.

Therefore we strongly recommend a professional RF survey as a basic part of the seismic network planning procedure. The benefits of a professional RF survey are:

- Assurance that the links will meet to the desired level of reliability. (The probability of an outage in % of time in the worst month of a year is an input design parameter. Note, *there are no 100% reliable RF links*!).

- The minimum number of required links and RF repeaters in the network is guaranteed. This results in a direct customer benefit because less equipment and maintenance are required. There will also be less noise in RF FM analog networks and a smaller error rate in digital networks.

o A minimum number of licensed frequencies are required. This results in less pollution of RF space in your country and is to your direct benefit because it is much easier to obtain frequencies. Also fewer different RF spare parts are required.

o Frequencies are optimally distributed over the network which minimizes the probability of RF interference problems.

o The minimum power consumption requirement is precisely determined by calculating the minimum sufficient RF output power of the transmitters. This results in less pollution of RF space in your country and is to your direct benefit because less power consumption enables remote stations to operate longer and/or require smaller back-up batteries and solar panels.

o Robustness to technical failures and lightning of the RF network is significantly increased by proper RF layout.

o Antennae mast heights are minimized and antennae minimum-required gain and optimal polarization are accurately determined, resulting in savings on antennae and antenna mast cost.

The cost of a professional RF survey is generally one or two percent of the total investment. Its combined benefits constitute a major step towards reliable network operation and are well worth the additional spendings.

5.2. The problem of RF interferences

Radio-frequency interference caused by other users of RF space is quite a common and difficult problem in developing countries for several reasons. In some countries, the lack of discipline and confusion in RF space where army, police, security authorities, and civil authorities all operate under different (or no) rules causes unforeseeable interference. In others, poor maintenance of high power communication equipment results in strong radiation from the side-lobes of powerful transmitters that interferes with seismological links. Extensive, unauthorized use of walkie-talkies can also cause big problems. Unfortunately, in many developing countries, the use of RF spectrum analyzers, which can reveal the origin of interfering signals, is often prohibited for security reasons. In cases where foreigners are allowed to use RF spectrum analyzers, this short-term monitoring of RF space does not guarantee success because some sources may appear only very intermittently and are difficult to detect.

The best, and more or less the only, solution is to work closely with local experts who are familiar with RF conditions in the country during the design phase of your seismic network. RF interference problems are generally beyond the control of seismic equipment manufacturers. RF problems can be solved - or at least better prevented - only by involving local experts with your seismic team during the design phase.

• ***Recommendation:***

Never use existing communication towers on the tops of mountains as seismic station sites!

DOI: 10.2312/GFZ.b103-98055

Such towers appear to be an easy and inexpensive solution and are very frequently proposed by those who are unfamiliar with the requirements of good seismic stations. Such sites have several severe drawbacks. Among the most important are:

- Towers sway during windy periods causing high amplitude low-frequency seismic noise.
- There is usually a very high probability of RF interference because the RF space is being used by several 'high power' parties.
- If such sites are inhabited, it is likely there will be high man-made seismic noise due to human activities.
- The topography is rarely suitable for a seismic station,
- All such sites have diesel generators to support communication equipment during power outages; these generators are a major source of man-made, high-frequency seismic noise when in operation. And of course, these generators will surely be running after a strong earthquake because that is precisely when it is most likely that the main power will fail. Since the time during and after strong earthquakes is the most important for your network, it is clear that existing communication towers are not at all suitable for seismic sites.

5.3. What you should prepare and provide if site selection is purchased

For efficient field work the customer has to prepare the following:

- An approximate seismic network layout based on your goals,

- Regional geological maps,

- 1:50.000 (or 1:25.000) scale topographic maps covering the entire network region for RF profiling purposes, and permission to export such maps, if necessary,

- state-of-the-art road maps for easy access to potential sites during the site selection process,

- 1:5.000 scale maps (or at least 1:25.000 if 1:5.000 are not available) of the area surrounding the sites in case shallow profiles are planned,

- climatic data in the form of tables or annual reports from the country's meteorological survey (precipitation, insolation, wind, lightning threat),

- knowledgeable staff members who are well acquainted with local conditions at each proposed station site and current as well as future land use in the vicinity,

- one or two four-wheel-drive vehicles; two or three staff members (including driver),

- all required permits to enter restricted areas.

Expect one or two days of work at each potential station site, depending on the dimensions of the network and site accessibility. Be prepared to work from sunrise to sunset.

DOI: 10.2312/GFZ.b103-98055

6. PURCHASING A SEISMIC SYSTEM

6.1. The bidding process

Sending out an RFP (Request for Proposal) and asking for bids on a new seismic system is a good way to get started. When requesting bids or proposals one has to be aware of a number of important issues. Certain technical requirements and business standards must be met in order to enable later a comparison of "apples-to-apples" when analyzing the various submitted system proposals. However, many very important issues are hard to define in an RFP and then proposals can not give you the right answers regarding:

- Actual reliability of the equipment
- Availability of long-term support
- Financial stability of the manufacturer
- Actual user friendliness of the system
- Availability of spare parts in 5-10 years, etc.

In order to find a suitable and successful system, you need to invest a fair amount of additional time in research and investigation before sending out your bid specifications. You should include all relevant information in your request so that the manufacturers can put together the right technical solution for you. Do not forget to include the primary goals of the seismic network and rate their relative importance in your proposal. Too often it is not prioritized what you want to accomplish with your system. This results in unclear instructions to manufacturers and hence, disappointed customers.

While including your goals and weighing their relative importance you should not include an over-detailed technical description of the desired system. Too many details can lead to limiting your choices and may even result in disqualifying the system best suited for your goals because it cannot fulfil a relatively unimportant but specified technical requirement. Do not push manufacturers to design a new system specifically for your needs. Such systems will often be expensive, and as a "prototype," difficult to support in the long run.

While you need to be specific about your requirements, do not be unrealistic. Technology is not perfect and cannot grant each and every wish, particularly not at low prices. From a real bid specifications for a small, local network I quote: "The turn-key system must provide fully automatic, accurate, and reliable computation of location and intensity of the epicenter of regional (2,000 km) earthquakes and monitoring of distant events. These seismic measurements shall be transmitted in near real-time to the following addresses of local authorities..." In addition to these requests, the aperture of this seismic network is only about 50 km and there is not a single experienced seismologist in the country. Such unrealistic expectations, particularly with respect to 'automatic calculations', make the client-vendor relationship very difficult and virtually assure the failure of the project.

Some countries are required by law to accept the lowest bid. Qualities like services, equipment reliability, user-friendliness of the system, set-up and long-term support might be lost if you base your choice solely on who has the lowest bid and fulfills all required (but insufficient) technical requirements stated in the bid. In a legitimate desire to keep the price as low as possible, manufacturers will most probably cut support and services to a minimum. This is a dangerous situation, particularly for less experienced customers. One way to mitigate

the danger is to spell out all services required in the Request for Proposal. This is the place to be exacting; specify service and support type and duration, parts and labor warranties; pricing structure after warranties expire, timeliness requirements, etc.

6.2. Selecting a manufacturer

When you evaluate the proposals, remember to assess not only the technical qualities of the system, but the quality of the manufacturer itself. What is its reputation? How long he has been in business? Have you asked for references from users of similar systems and learned about how well the company served them?

As you near decision-making time, make a personal visit to the manufacturers you are considering; meet their people and tour their facilities. Remember that a company that serves you well before you've bought their product is more likely to continue to serve you well after you've bought and paid for their product. Often manufacturers will pay at least some of the expenses for new clients to visit their facilities and meet their staff.

Select those you wish to participate in these visits carefully. One member of the team should be the individual responsible for future operation of the seismic network. Other members should be those most knowledgeable and experienced in seismology, no matter what their position in the hierarchy or power structure of your institution or country. Of course, members must be fluent in the pertinent foreign languages.

Ask for visits with manufacturer's sales people or engineers. Data sheets themselves never give enough technical information about seismic systems. Sales persons can provide you with all the details of a particular technical solution. Such visits, however, are less appropriate during the early stage of the project when your goals are not yet clearly specified. Keep in mind that the sales person will be biased toward the equipment of the manufacturers they represent.

Generally, you should not expect the best results from companies that merely assemble systems but are not experts themselves in seismology. Such projects rarely have a happy end. Also take into consideration the size of the company. Those that are quite small may simply not have the "people-power" for long-term customer support. They may manufacture very good, technically advanced equipment, however their ability to support large projects, their longevity and system-testing capacities may cause problems for you.

6.3. Equipment selection

As already mentioned, data sheets of seismic equipment alone never give you enough information. Frequently, it is also difficult to compare the data sheets of various manufacturers because each uses its own system of specifications, measurement units and definitions of technical parameters. There are at least ten different ways of expressing intrinsic noise and dynamic range of sensors or data recorders. All of these factors must be understood in order to do an accurate comparison and this can be best accomplished through in-depth contact with the manufacturers. Be sure to ask for all possible information about the system including copies of the user manuals and the results of independent testing.

It is recommended to buy one piece of key equipment such as a sensor, a data logger, processing software with demo data or an RF link and test the product yourself. In the case of large projects with adequate financing, manufacturers will often loan you equipment for testing purposes free of charge. While it is ideal to get some first-hand experience before settling on which new system to purchase, this approach requires personnel who are knowledgeable about seismology and instrumentation. Unfortunately, in practice, however, it is usually difficult to find personnel and money for such "experiments" in most developing countries. In this case impartial advice from foreign consultants, preferably from scientific, non-commercial institutions or organizations should be solicited.

Be cautious about mixing products from different manufacturers. It is not a simple or easy task to interface between different products in terms of dynamic range, signal-to-noise ratio, full scale ranges, baud rates, processing power and power supply sources. Stay with one manufacturer if possible, or, when this is not feasible, arrange to have one manufacturer be explicitly, contractually responsible for interface problems and the functioning of the system as a whole.

Each technical seismic system, or element in that system, operates within a certain set of parameters, or "range." You should know what that range is and where your requirements will fall within that range. If the work you require means that the system, or one part in it, has to operate at the extreme end of its range on a regular basis, it is not the appropriate system or system element for you. The results are often disappointing if you plan to:

- Use the maximum possible number of channels in an FM radio-frequency link
- Acquire data with the maximum number of channels possible in a system
- Exploit the maximum number of channels in seismic data analysis software
- Operate the hardware in temperatures at the extreme range of safe operation, etc.

You would do well to find another system whose mid-range parameters can accommodate your needs. Always make sure you have a safety margin in your system for those times when it will have to operate in the extreme ranges, but don't expect it to operate accurately and reliably in the extreme ranges all the time. The data sheets provided by manufacturers usually give little information about performance ranges for their equipment. You need to get the specifics from sales reps or engineers. Note that there is always a price to pay for operating equipment under extremes. In many cases the manufacturers themselves do not have a completely clear picture what that price might be.

6.4. Seismic equipment market: It's a small, small world

The market for seismic systems and equipment is naturally quite limited, made more narrow yet by the relatively low level of investment in seismological equipment anywhere in the world. With few exceptions, instruments are produced in very small numbers. Inevitably, this limits how thoroughly new equipment is tested. This is due not to a lack of quality or commitment on the part of manufacturers in this field, but due to simple economic realities. Compared to industries with a far broader and more powerful economic base, like computers and electronics, seismic equipment moves into the field with relatively little testing, even by the most reputable manufacturer. In computers or electronics, there are millions upon millions of users field-testing the product every day! Not so in seismology. In general, this equipment arrives with a higher-than-average number of bugs and problems that will need to be solved

by the user and manufacturer working in tandem. Currently, most seismic equipment is less user-friendly than most of us would like it to be and the technical documentation frequently falls far short of the glory of the Lord. Customers are often given exhaustive amounts of information about their new system, but are rarely given complete, easy-to-follow instructions on how to set-up and use the system.

Another complicating factor is that in developing countries there is often a lack of knowledgeable experts who can set-up, operate and maintain a seismic system. For these reasons, it is generally necessary to maintain a long-term working relationship with the maker of your newly-purchased seismic system. The manufacturer's support during the initial set-up of your seismic system and a reliable, knowledgeable and friendly relationship thereafter is crucial. Make sure you feel that you can have an open, constructive and trusting relationship with the manufacturer of the system you choose. It will take both of you to establish and successfully operate your new seismic network.

7. SEISMIC STATION SITE PREPARATION

7.1. Purpose

The purpose of a seismic station site structure is:

- Protecting the equipment from temperature and humidity extremes, dust and dirt, lightning and curious animals,
- Assuring a good mechanical contact between seismic sensors and un-weathered, solid bed-rock,
- Providing a good, low-resistance electric ground for sensitive electronic equipment and lightning-protection system, and
- Providing easy and safe access to maintain and service the equipment.

The well-engineered seismic structure must also minimize distortion of seismic signals due to structure-soil interaction. This is particularly important on softer ground and at higher frequency seismic signals. It should also mitigate man-made and wind-generated seismic noise in the vicinity of the station.

Inadequate site preparation and seismometer placement can easily wipe out all the benefits of expensive, high-sensitivity, high dynamic-range equipment. For example, a station placed on unconsolidated alluvial deposits can, due to thermal and wind effects, make broad-band recording useless. It is pointless to invest in expensive equipment only to have it wasted because of improper site conditions.

7.2. Types of seismic vaults

The three main types of seismic vaults are:

- *Surface vaults.* These are the least expensive and by far the most frequently used ones, however they suffer the greatest level of seismic noise.

- *Deep vaults.* They are placed in abandoned tunnels, old mines or natural caves and are

the best locations with respect to the price/seismic-noise-performance-ratio. They frequently require, however, extensive cabling which can be expensive.

- *Bore-hole seismic stations.* Their depths ranges typically between about 50 - 2000 m. They are very good from the perspective of seismic noise, however they are also very expensive (from about US$8,000 to US$250,000 for the bore-hole itself plus the cost of bore-hole sensors which are as much as three-times higher in price than regular surface sensors). Bore-holes are used principally in regions entirely covered by alluvial deposits where no sites with good bed-rock outcroppings are available, or for the most demanding research work. Note that recording in boreholes causes frequency- and depth-dependent signal distortions which have to be corrected for when using wave-form data analysis.

Today, seismic stations are most often in vault-form. The massive, solid concrete, "seismic piers" traditionally found in seismic observatories are no longer built. No above-ground buildings or shelters are required. In fact, above-ground structures are far less desirable than in-ground vaults because of structure-soil interaction problems and the wind-generated seismic noise caused by them (Bycroft 1978, Luco et all. 1990). If such buildings already exist at the location you have chosen for your station, make sure that the seismometer vault is placed far enough away to minimize wind-generated noise and placed according to the recommendations of the Manual of Seismological Observatory Practice, Willmore, ed. (1982). The structure of the vault should be light and underground as much as possible, therefore creating little wind resistance.

7.3. A briefing on surface seismic vaults

Surface seismic vaults are usually between 1 and 2 m in diameter, depending on their depth and the amount of equipment installed and its specifications. The depth of the vault may range from about 1 to 10 m, depending on the depth, the quality, and weathering of the bedrock at the site. Round or rectangular cross-sections are equally suitable.

> Any type of above-ground shelters, or massive seismic piers at seismic station sites are undesirable. They are expensive, deteriorate dynamic range of data acquisition during windy periods and may also cause seismic signals to deteriorate during earthquakes themselves because of structure/soil interaction.

Seismic vaults with metal walls (Fig.17) made of corrugated iron, large metal tubes (like those used for reservoirs or large pipelines), or welded from metal sheets, have several advantages. When using a thin sheet of metal (with respect to the size of the vault), then pour relatively thin (20-30 cm) watertight concrete walls around the metal to add strength to the walls.

Make a flat, waterproof concrete floor, adding chemicals to make the concrete watertight. Metal walls act as a Faraday cage and thus provide ideal electromagnetic interference (EMI) shielding and the most effective lightning protection available. At the same time, the metal walls lower the impedance of the grounding system and thus make equipment grounding more effective.

To protect the sensors on the floor of the vault from water damage, build a drainage trench around the bottom of the vault. Cover the drainage pipe with wire mesh to keep small animals out.

The vault itself should be enclosed by a metal cover, which must be fixed very firmly to the ground to prevent shaking and vibration during strong winds. Such vibrations cause high seismic noise which can make stations virtually useless during high winds. The vault cover must be light enough to be handled by a single person, otherwise it takes two people for regular maintenance and service, which is unnecessarily expensive. For large-diameter vaults, it is best to make the cover in two parts. In extreme climates, metal may not be the best choice because it will get extremely hot or cold. Water resistant plywood or UV-light-resistant plastic or glas-fiber sheets are good materials to use in arid regions.

A thermal vault cover (e.g. made of a 10 to 30 cm thick styrofoam plate or disk) is also necessary to keep interior vault temperatures as stable as possible. Thermal shielding minimizes the thermal drift of sensors and electronic equipment and thus reduces the low-frequency noise of BB and VBB sensors. Thermal cover thickness depends on the climate at the site, how sensitive the equipment is (VBB sensors being the most sensitive ones!) and how much low-frequency noise one is willing to tolerate in the seismic data. Temperature changes in time are far more important than the high or low average temperatures themselves. Continental, and in particular desert, climate requires the most effective thermal insulation.

There are two thermal cover design issues that are particularly important. First, the thermal cover must be tight. Figure 17 shows a "rope" pressed into the gap between the vault's walls and the thermal cover. This "rope" is made of insulating fibers and is usually used for industrial hot water pipe insulation. Pack the insulation tightly into all the gaps between the cover and the walls or the effect of heat convection will undo the insulating effects of the cover itself. Second, do not place the thermal cover at the top of the vault, but rather at or below the level where the ground heats up during the day. In desert areas, surface ground temperatures can exceed 80^0 C, and 50^0 C at 30 cm depths are not unusual. In such conditions the thermal cover must be placed 30 - 40 cm below the ground level. A thermal cover of any thickness at the top of the vault, particularly if the vault stands significantly above the surface, has almost no effect.

VBB sensors in a seismic vault should additionally be shielded by a styrofoam box placed directly above the sensor and glued to the base plate. All other equipment should be installed outside of it so that the sensitive sensor is not touched at all during service and maintenance.

Rather than placing batteries in the same vault, create a separate, small underground container for them nearby, particularly if the batteries are the large, acid-lead type. Placing batteries in a separate area prevents equipment corrosion due to potential evaporation of battery acid vapors. The probability of this kind of problems is greater in small vaults without any ventilation.

DOI: 10.2312/GFZ.b103-98055

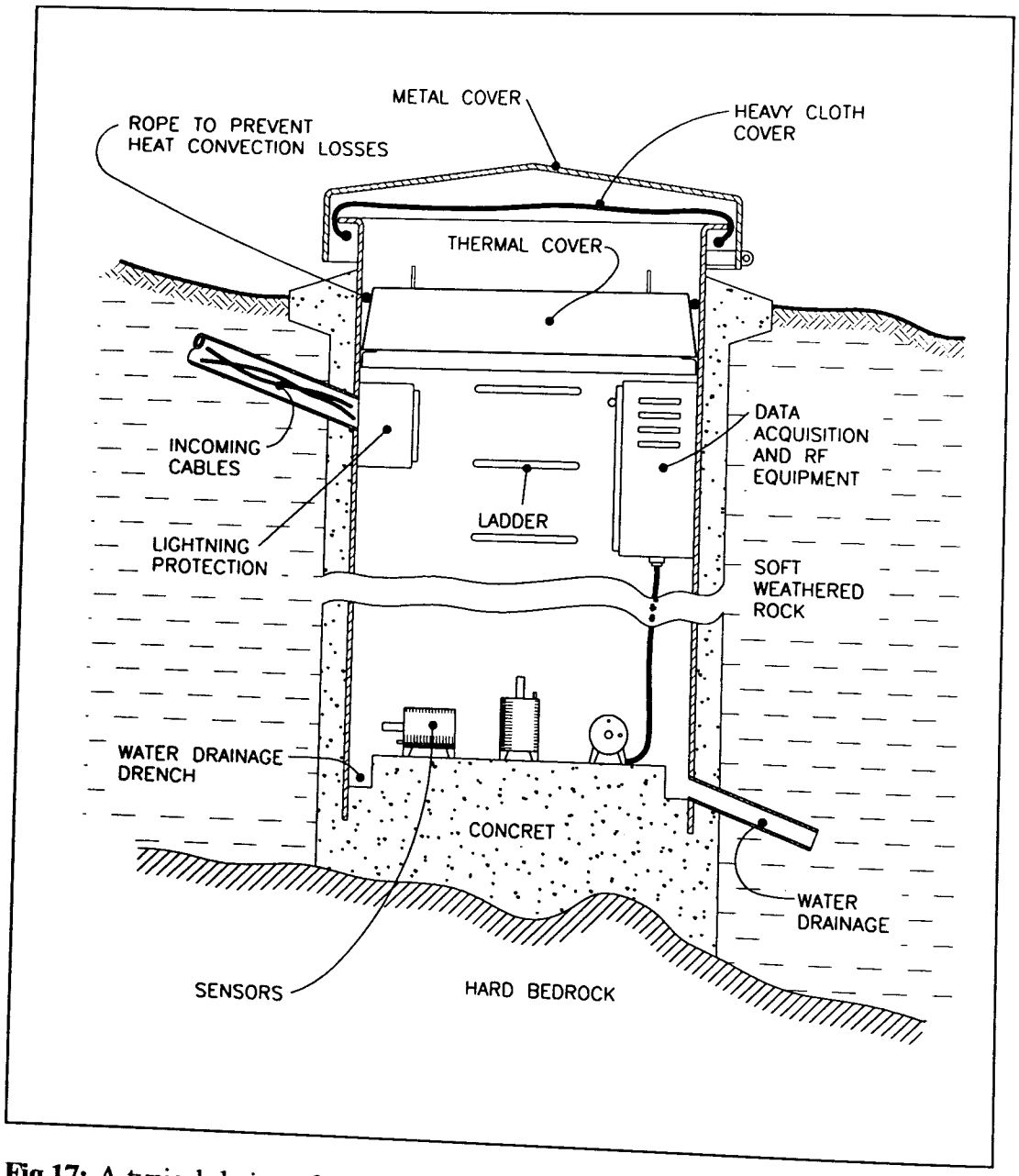

Fig.17: A typical design of a surface seismic vault.

Two vital, but often overlooked issues - with potentially fatal consequences - are lightning and grounding systems.

Proper grounding and shielding of equipment and cables keeps instrument-noise low. It also provides protection against lightning and is absolutely required for interference-free RF telemetry seismic stations. Fig. 18 shows a grounding system with a metal strip around the vault and its five legs. All metal parts at the site must be well connected, including the metal cover of the vault. For seismic vaults without metal walls, form a loose mesh around the vault by wrapping metal strips vertically and horizontally around it.

Scientific Technical Report STR 98/05
DOI: 10.2312/GFZ.b103-98055

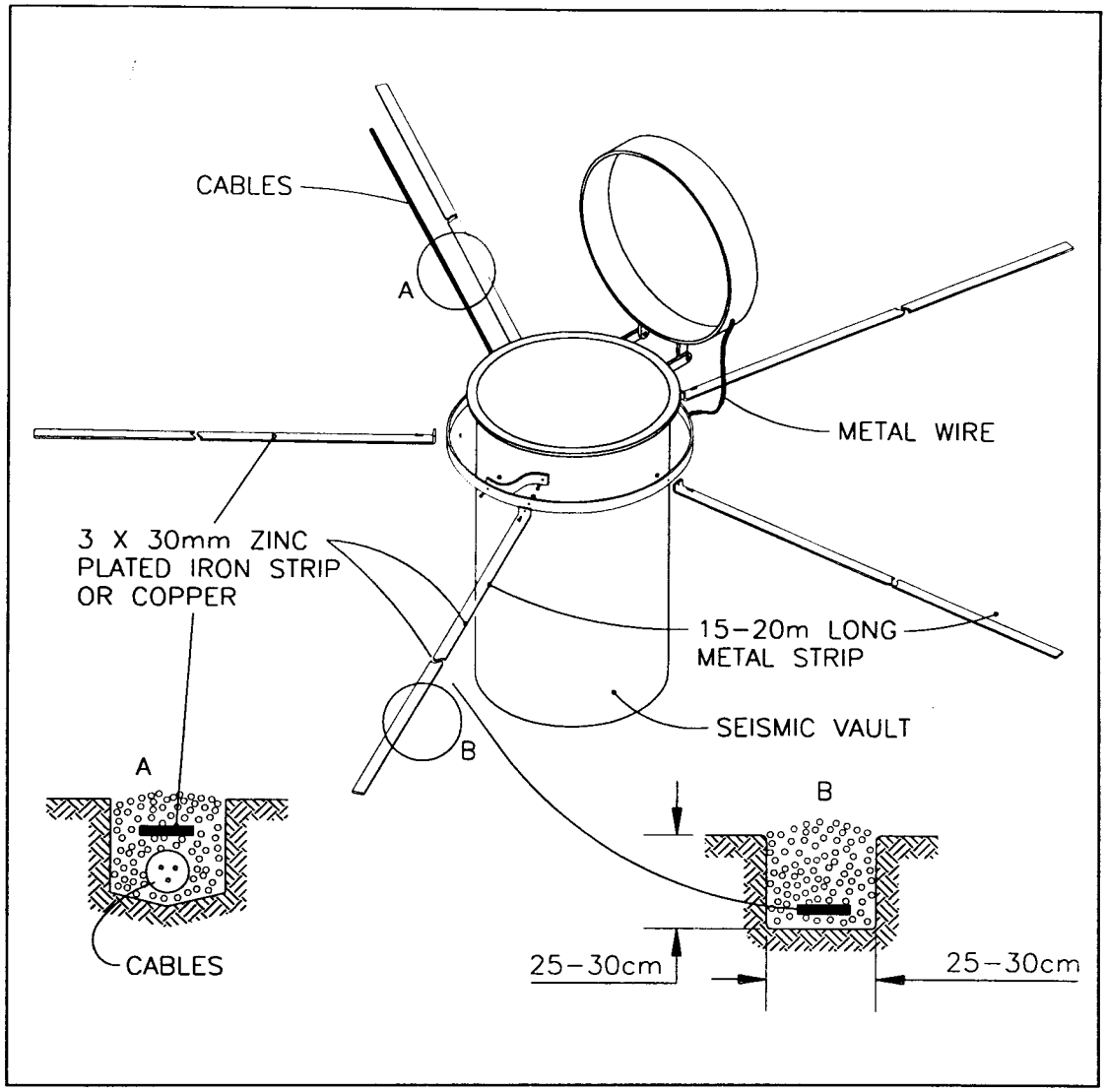

Fig. 18: A typical grounding system for a seismic vault.

The size of your grounding system depends on the climate, soil type and ground humidity. Very dry regions require special treatment. A good grounding system is usually a part of the RF link design in telemetry seismic systems. Note that any grounding system requires periodic service checks because contacts between the metal parts may eventually corrode. It is generally recommended that the grounding impedance of the system be checked once every two years. A check of lightning protection equipment and potential replacement of burned elements is one essential part of the regular maintenance visits.

The degree to which you have to protect your system against lightning will naturally depend on the lightening threat at the site. Meteorologists can give you good information about how problematic it is in your location. Of course a direct hit of lightning will cause equipment damage even with the best of protection. Fortunately, this happens very rarely. The vast majority of lightning damage is due to voltage induction surges in all the cables at the site. Lightning in the near or even far vicinity of the station can cause severe damage.

For efficient lightning protection, make all cables as short as possible with absolutely no loops of 'superficial' cables. Place lightning protection devices right on the spot where cables enter the seismic vault. They must be applied to all cables entering the vault without exception. Voltage surges usually occur in all the cables at a station (depending on their length), therefore leaving a single long cable unprotected is virtually the same as leaving all cables unprotected. Don not forget to put one leg of the grounding system exactly above the cables entering the seismic vault (main power, phone line, and/or RF cable coming from antenna mast). This metal strip keeps voltage gradients low along the length of the cables during lightning, therefore mitigating voltage surges.

Note that lightning is the most frequent cause of seismic equipment failures in the field. This requires to search for the best lightning protection avilable for the given situation and then to invest in its purchase, installation and maintenance. Several seismic networks have lost half of their equipment in less than two years after installation because they neglected to undertake adequate lightning protection measures.

In general, place data acquisition and communication equipment (modems, transmitters, receivers) on the walls of the vault in special enclosures or mounted on racks. This is the best way to prevent water damage.

If you are using an antenna mast, place it away from the vault to prevent seismic noise generated by the antenna's swinging during windy periods. The required distance is usually between 5 to 50 m, depending on a number of factors such as:

- *Maximum wind speeds* at the site (the higher the speeds, the bigger the distance)
- *Height of the antenna* (the higher the antenna mast, the bigger the distance)
- *Depth of the vault* (the deeper the vault, the smaller the acceptable distance)
- *Type of seismic coupling* between sensors and antenna base (best estimated by a seismo-geologist)
- *Measured seismic noise* at the site (very quiet sites require larger distances).

Place a fence around the vault to minimize man-made noise and to protect it against vandalism. The size of the fence, ranging from 5 x 5 m to 100 x 100 m, depends on what kind of activities go on around the site, population density in the vicinity, ground quality, natural seismic noise levels, and the depth of the vault. Be aware that proper fencing will be a significant portion of the site preparation costs!

A comment on building surface vaults: Whatever engineering and construction work is needed to prepare the site, it is usually arranged and paid for by the customer rather than the manufacturer of the seismic equipment. Very large national projects may be an exception to this rule. Site preparation will require a great deal of preparation and involvement by the customer. There are generally a number of good design alternatives from which to choose. It is recommended to hire a local civil engineering firm to design the best solution for your system. The work should be supervised by a seismologist and a civil engineer. They must make sure that the enclosure is water-tight and has good contact with solid bedrock. Your system's manufacturer can give you sketches and suggestions about how to proceed but usually he does not provide structural drawings; nor is he aware of local construction conditions. Work in tandem with a civil engineer, your local building expert. Local builders know best what materials and construction methods are available and workable in your country. Don't

"over-engineer" your project; it is usually not necessary to have an engineering firm design and oversee the whole project.

8. INSTALLATION

There are four ways to install a seismic system:

- The user installs the new system. In this option, the customer is entirely responsible for assuring that the system functions properly. In practice, especially in developing countries inexperienced with seismic equipment, this approach is rarely satisfactory.

- Installation is demonstrated by the manufacturer on a subsystem (a few stations, a sub-network). In this case, responsibility is shared by the manufacturer and user in proportions determined by who installs which portion of the system. This approach sometimes works quite well. However, at least some experience with seismic and communication equipment in the country is required for this method to work.

- The manufacturer installs the whole system with the full assistance of your technical staff. Responsibility for making sure that the system functions well lies then with the manufacturer. Since your staff will later be responsible for running, maintaining and servicing the network in the future, it is strongly recommended that they work together with the manufacturer's expert staff when installing the system. First-hand on-the-job experience of "hands-on installation" and associated problem-solving is always the best way to learn. Thus your staff, particularly in developing countries, will be best trained and served by active participation in this process.

- A turn-key installation without any assistance from the customer. Here again, the manufacturer has complete responsibility for seeing that the system functions adequately. In this case, the network will no doubt be successfully installed, but your staff members will learn nothing about how it actually works and how to solve related problems.

• ***Installation recommendations:***

- Do not accept the 'standard length' cables offered by some seismic system manufacturers. The 'standard' cables rarely work well in the field. They are usually too short or too long. As mentioned earlier, do not loop or coil extra cable length because that will increase the threat of lightning damage and unnecessarily increase system noise. Rather, ask for bulk cables with separate connectors or cables of a reasonable length and one-side mounted connectors only. You can then cut them to precisely the desired lengths in the field during installation. However, note that high quality soldering of connectors requires experience. Badly installed connectors are among the most frequent problem makers.

- Your site must be completely prepared before the manufacturer arrives to install the system. All construction work must be finished, logistics organized and access permits prepared. Time and time again, manufacturers are faced with unprepared sites or missing permits when they arrive to do the installation. This results in a significant loss of time and forces both parties to accept too many "last-minute" solutions and compromises during installation. This generally leads to less reliable and accurate work.

9. TUNING YOUR SEISMIC NETWORK

Before a seismic network can function optimally, it must be tuned to local conditions. This is especially true for networks that run in 'triggered mode'. Unfortunately, many customers are not aware that they will need to tune the system or think that the manufacturer can do this at the factory or during installation. In fact, tuning is an on-going task that cannot be done 'once and for all'. You will need to fine-tune several recording and computational parameters to local conditions in order to get the best results. This process requires time and experience. You will not be able to correctly tune the system's recording and processing parameters until you have gathered sufficient experience with natural and man-made seismic noise conditions and earthquake signals at all the sites in your network. The seismic network dimension and layout, seismicity in the region, seismic noise levels and spectra at station sites, seismic signal attenuation in the region and local earth models, etc. all play an important role in these adjustments.

Therefore, tuning a network is normally a long-term process. It takes months of systematic, well-planned and documented work. Because of the time required to accomplish this task, it simply cannot be done by your system's manufacturer. Only you can correctly tune your network while operating it. Moreover, since seismic noise conditions at the sites may change in the future, re-tuning will probably be required from time to time.

Detailed discussion of individual tuning parameters is beyond the scope of this paper. Note that not all parameters enumerated below exist in every network and that some adjustments may be missing from this list. The most common hardware and real-time processing parameters that need to be adjasted in the trigger-mode operation of networks are:

- *Seismic gain* at individual stations,
- *Signal-conditioning* filter parameters,
- *Corner frequencies* of pre-trigger band-pass filters,
- *Trigger algorithm parameters* such as: trigger and de-trigger threshold values, weights of individual stations in coincident trigger algorithms and grouping of stations in sub-regions in the coincidence trigger algorithm organization
- *Pre-event time duration*
- *Post-event time duration*
- *Minimum and/or maximum run-time duration*
- *Propagation window length* adjustment.

Off-line seismic analysis software parameters that must be prepared or adjusted for correct analysis are:

- *Sensor parameter files* containing sensor calibration data
- *Network configuration files* containing data about seismic stations
- *Automatic phase-picker parameters*

- *Earth model parameters* of event location program such as ground layer's thickness, seismic wave velocities, seismic station weights, epicenter distance weighing function, and similar parameters depending on the program used
- Magnitude-determination algorithm calibration, and
- Selection or preparation of different *macros for every-day routine analysis* of seismic signals.

Be prepared! It is quite a lot of work to acquire a complete understanding of how all these parameters can be adjusted optimally.

10. RUNNING YOUR SEISMIC NETWORK

10.1. Organizing the tasks

To keep your network error-free and in perfect working order, waiting to record earthquakes year after year, requires hard work and discipline. It is not a simple task to achieve this goal. Your staff will have to operate in a highly professional and reliable manner with:

- *Clearly defined personal responsibilities* for each task associated with the operation of the network and for other every-day record analysis and archiving activities
- *Continuous verification of all tasks* and hardware operation
- *Precision record-keeping* of all activities and in the data archives
- *Regular maintenance* of hardware and software.

Careful and continuous documentation of network operation parameters in a log-book, log-file, or in the data-base itself, is essential. This back-log information should contain all network operating parameters and their changes such as information about data acquisition parameters, station down-time, description of technical problems and solutions, description of maintenance and service work, documentation of all station calibrations and their results. The exact time when parameter or setting changes become active must be accurately recorded. This information is an integral part of archiving seismic data because only those signals recorded along with the precise conditions at the time of the recording can be properly interpreted. Defined personal responsibility with respect to altering network operation parameters and strict obedience to the established procedures is a must.

10.2. System maintenance

Maintaining a network's hardware and software is a continuous activity that inevitably requires well-trained personnel. Many vital operational parameters at the stations like back-up battery voltage, presence of charging voltage, potential software and communication problems, time keeping problems, remote station vault or equipment temperature, potential water intrusion, etc. can be remotely monitored by modem, high-end seismic systems with duplex data

transmission links. However, regular visits to the stations are still necessary, though far less frequently than in the past. Note that it is a mistake to put off in-person checks of remote stations until something goes wrong. Periodic visual checks, regular changing of batteries, checking potential corrosion problems, intrusion of small animals which may damage cables, cleaning the vaults and solar panels etc. at each station will help catch potential problems before they become big ones.

And when something does go wrong, you must be certain that you can respond immediately with the right action, personnel and spare parts. You should always maintain a good stockpile of the most common spare parts and have a well-trained technician on duty around the clock.

Batteries require constant attention. Battery failure is one of the most common, if not the number one reason for seismic equipment failures in the field. It should be noted that the output voltage alone of a battery provides almost no information about the overall health and capacity of a battery. Many types of batteries may have adequate output voltage while at the same time their charge capacity is reduced to a small fraction of its original strength. Batteries in this condition will not do the job in case of a power failure, which is almost certain to occur after damaging earthquakes.

All the batteries in your seismic system must be laboratory-tested for remaining charge capacity once a year. The batteries should be fully discharged, then fully charged, and again discharged in a controlled manner until their true charge capacity is determined. Once the charge capacity is less than 60% to 70% of the original capacity, replace the batteries with new ones. Relying solely on measurements of battery voltage will certainly lead to technical failures. Do not forget that you will need fully operational batteries after big events since it is very likely that regular power sources and power lines will be non-functional, often for quite a long time. The most important moment in the life of your seismic network, namely the event of a strong earthquake, may happen only once in a decade or even less. You should not miss it because of old batteries!

Non-chargeable batteries, particularly the lithium type, must be replaced regularly, according to the manufacturers instructions, regardless of their output voltage at the moment of testing.

10.3. Sensor calibration

You must calibrate all the sensors in your seismic system regularly - ideally, once a year!

> Strictly speaking, only those seismic signals recorded between two successive sensor calibrations that show no significant change in sensor parameters are completely reliable.

Seismic sensor calibration requires knowledge that is seldom available in developing countries. In most cases, special training is required. A good approach is to include the calibration of one or all sensors after one year of service in your purchase agreement with the manufacturer. This first-year calibration service should be done by the manufacturer with the assistance of your staff so that they can learn how to do the procedure themselves. Hands-on practice under the close supervision of a calibration specialist is highly recommended. Murphy's Laws and inadequate training and experience often ends in difficult-to-detect failures. Practice shows that mere "book learning" is often not enough when calibrating seismic sensors.

Nowadays, in the time of digital seismology, sensor and data logger transfer function representation in the 's' or 'z' plane is most commonly used. A comprehensive description of basics is given in Scherbaum (1996). A description of a popular seismometer calibration program UNICAL is given in Plesinger at all. (1995).

10.4. Archiving data

The scientific and financial value of a national archive of seismic-data will be, after several years or decades of operation of a network, very high. Therefore, extreme attention must be paid to precise data archiving and a fail-safe back-up for that data. Seismology is typically a non-experimental science in the sense that man has no control of the source and wave-propagation conditions. Lost or improperly recorded seismic data can never be re-generated by just repeating the experiment. It is, therefore, an absolute must to have a complete and reliable back-up archive. The back-up should be kept in a different physical location, no matter whether it is paper, film, tape, disk, or CD.

When you first set up a seismic network, you need to think about how to organize the data you record, being aware that you eventually will have many, many years of accumulated records.

If you have a strong-motion network or small weak-motion network in a low seismicity region which generates only a small number of records each year, you can probably get by with a DOS-directory tree organization for your data files. Nevertheless, file-name coding of events must be thoroughly thought through to prevent confusion and/or file name duplications. UNIX, Windows 95 or NT systems are more flexible than DOS in this respect because they allow longer file names.

Larger networks in moderate to high seismicity regions require true data bases for archiving purposes. Consider different options on the market carefully before you begin to log records. It is very painful to change your data coding or archiving method after several years of network operation when you have thousands upon thousands of records already in the archive.

Often, this crucial aspect of seismic system organization is overlooked or left to on-the-spot decisions by whoever is archiving records at the moment. This may work for a while, but eventually you will run into serious problems. Think through your file coding and archiving organization with the long-term future in mind!

Always keep the raw, unprocessed seismic data records (raw event files, or sequences of continuous data) in the archive along with the full documentation about the recording conditions. Processing and seismic analysis methods will change and evolve as time passes. Future generations will appreciate having your unprocessed seismic data to further their research and knowledge.

10.5. Dissemination of seismic data

International co-operation in the dissemination of seismic data is another prerequisite for high-quality operation of any new seismic network in developing countries. It is also a widely accepted international obligation. Data-sharing is the best way a less experienced institution can get feedback about the quality of its own work. By comparing your phase reading residuals, event location errors, magnitude determinations and source mechanism results, etc. with the results of others in international bulletins, you will greatly improve your own work. Any seismic analysis should include as much information as possible from neighboring regions and countries. Not only your own data, but also all available pertinent data should be used in your seismic research work. Disseminating your data will in turn facilitate easy and fast accessibility of others' data. It's important to establish a generous data-sharing relationship with other institutions. Your generosity will encourage others to be generous with you.

Normally you will regularly publish preliminary seismological bulletins (weekly, bi-weekly, or monthly), final seismological bulletins (yearly), and earthquake catalogs of the country or region (yearly, but with a few years delay so that the data can be fully analyzed). You should also immediately disseminate data from strong events. Fax, phone or the Internet are familiar forms of seismic data exchange. The Internet is used more and more to share even longer publications like seismic bulletins and waveform data.

ACKNOWLEDGEMENT

I wish to express my sincere gratitude to Prof. Dr. Peter Bormann of the GFZ Potsdam for suggesting the main topics for these two lectures in the seismology training course, for many useful hints, careful proof-reading and editorial improvements of the manuscript.

REFERENCES

Bycroft, G.N. (1978). The effect of soil-structure interaction on seismometer readings, BSSA, 68, 823

Kijko, A. (1977). An algorithm for the optimum distribution of a regional seismic network. PAGEOPH 115, 999-1009

Lee, W.H.K and Steward, S.W. (1981). Principles and Applications of Micro-earthquake Networks, Advances in Geophysics, Supplement 2, Academic Press, NY, USA

Luco, J.E., Anderson, J.G., and Georgevich, M. (1990). Soil-structure interaction effects on strong motion accelerograms recorded on instrument shelters, Earth. Eng. & Struct. Dyn. 19, 119

Plesinger, A., Zmeskal, M., and Zednik, J. (1995). PREPROC - Software for automated preprocessing of digital data, Ver.2.1, Ed.Bergman, E., NEIC Golden/FI, Prague

Rabinowitz, N. and Steinberg, D.M. (1990). Optimal configuration of a seismographic network: A statistical approach. BSSA, Vol. 80, No. 1, 187-196

Scherbaum, F. (1996). Of poles and zeros; Fundamentals of Digital Seismometry, Kluwer Academic Publisher, Boston

Steinberg, D.M., Rabinowitz, N., Shimshoni, Y. and Mizrachi, D. (1995). Configuring a seismographic network for optimal monitoring of fault lines and multiple sources. BSSA, Vol. 85, No. 6, 1847-1857

Trnkoczy, A. and Zivcic, M. (1992). Design of Local Seismic Network for Nuclear Power Plant Krsko, Cahiers du Centre Europeen de Geodynamique et de Seismologie, Luxembourg, 5, 31-41

Understanding The Earth's Dynamics and Structure (1990). The IRIS Proposal 1991-1995 to The National Science Foundation, IRIS Consortium

Willmore, P.L. and Karnik, V (Eds.) (1970/ 1982) Manual of Seismological Observatory Practice, ISC, Edinburgh, UK

PERFORMANCE ANALYSIS OF THE EASTERN AFRICAN SEISMOLOGICAL STATION NETWORK

E.Dindi

University of Nairobi, Department of Geology, P.O. Box 30197, Nairobi, Kenya,
Fax: +254-2-449-539, E-mail: uonseism@arcc.or.ke

1. INTRODUCTION

The Eastern African Seismological Network (excluding South Africa stations) consists of about 35 seismic stations spread out over the region (Fig.1). The network is thin in the east-west direction (15degrees distance) and long in the north south direction (40 degrees distance). The countries participating in this network are Eritrea, Ethiopia, Kenya, Malawi, Tanzania, Uganda, Zambia and Zimbabwe. The stations are not uniformly distributed so that large gaps exist within the area of the network. The following will give a short description of the status in each country.

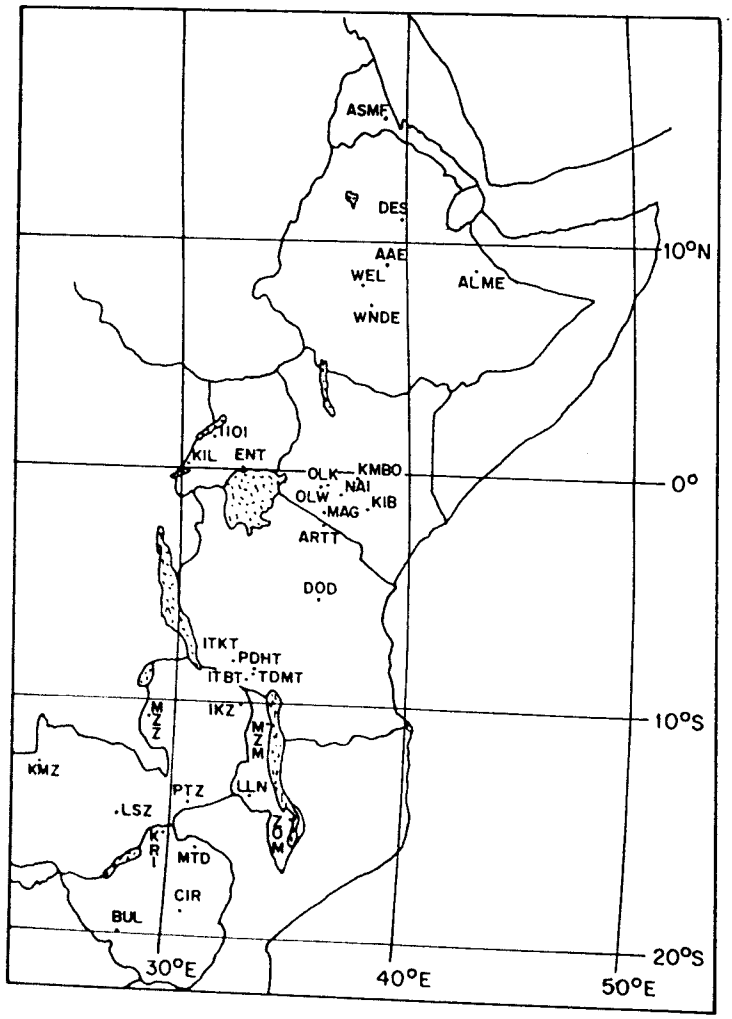

Fig. 1: Location of the existing stations of the Eastern Africa seismological network.

Scientific Technical Report STR 98/05
DOI: 10.2312/GFZ.b103-98055

Kenya has one permanent broadband IRIS station located at Kilimambogo (KMBO) and five digital Lennertz (MARS88) stations with short period seismometers. One of these stations located at Kibwezi (KIB) is permanently installed while the rest are at temporary sites.

Uganda has three permanent stations, all one component short period recording in analog form. In addition, there is one digital field station with three component accelerometer.

Tanzania has three permanent stations, all one component analog short period. In addition there is a small five station experimental digital network supported by the Royal Observatory of Belgium and the University of Uppsala.

Zambia has six permanent stations, of which the main station is Lusaka (LSZ) which is one of the IRIS stations in the network. The remaining stations are one component recording in analog form.

Zimbabwe has four permanent stations. The Buluwayo (BUL) station is the main observatory with WWSSN station and additional three component short period stations. Of the remaining three stations one is three component and the other two are one component.

Malawi operates two three component digital stations located at Zomba (ZOM) and Mzuzu (MZZ) .

Eritrea has one three component short period analog station located at Asmara and has recently acquired two new digital Nanometric stations which are planned to be installed at Massawa and Adi Keih respectively.

It can be seen from this outline that although both analog and digital stations have been in use over the years, there is a steady shift to digital stations.

2.TIMING

At the beginning of the regional cooperation initiative launched in 1993, most of the stations used timing systems other than GPS. However, in the last four years, a lot of effort has been expended in acquiring GPS clocks for the existing analog stations. This has been realized through the active support from the International Physical Sciences Program (IPPS). Thus the timing problem which was a major issue four years ago is now almost solved for most of the stations. It is now the experience in the phase identification that is still a challenge in the routine analysis of the events.

3. EFFICIENCY OF THE STATIONS IN DETECTING EVENTS

Most of the stations in use in the region have SP characteristics and are hence mainly for detection of local and regional events. However, for a number of reasons the number of stations picking up moderate events for any given period remain relatively low. Reasons

for this are various but the following stand out:

a) The high background noise level at some of the stations;

b) Frequent breakdowns of stations which are sometimes not reported;

c) Large distances between stations of the network.

In order to demonstrate the varied performance of stations in the detection of regional events, a total of 132 events, located by using 5 or more stations of the network during the period October 1993 - August 1996, were examined (Tab. 1). The idea was to find out which stations were the best in picking of these events. The calculated local magnitudes obtained for these events by using SEISAN software (Havskov and Utheim, 1992) were in the range 3.0 to 5.5

Table 1. Performance of individual stations in the detection of 132 events picked by 5 or more stations for the period October 1993 – August 1996.

STATION	NUMBER OF EVENTS PICKED
Nairobi (NAI)	102
Entebbe (ENT)	85
Dodoma (DOD)	78
Magadi (MAG)	63
Hoima (HOI)	62
Arusha(ARTT)	61
Buluwayo(BUL)	35
Pitaoke (PTZ)	31
Kilembe (KIL)	31
Kilimambogo(KMBO)	29
Langata (LAN)	23
Itumba (ITBT)	21
Mansa (MZZ)	18
Panda Hill (PDHT)	18
Kibwezi (KIB)	16
Tunduma(TDMT)	15
Olkaria(OLK)	14
Lusaka (LSZ)	10
Wendogenet(WNDE)	09
Alemaya (ALME)	08
Isoka (IKZ)	07
Weliso(WEL)	06
Itaka(ITKT)	06
Karoa(KRI)	05
Dese (DES)	03
Chiredzi(CIR)	02
Zomba(ZOM)	02
Asmara(ASME)	01

Table 1 shows that Nairobi station had the highest number of detections (102) followed by Entebbe (85) and Dodoma (78). On the other hand, 10 of the stations detected less than 10 of the 132 events. A number of factors may contribute to this disparity such as:

(a) Location of the seismic stations relative to the tectonically active areas during the period;

(b) Distance of the stations relative to other stations in the network;

(c) Non-continuous operation of stations for various reasons;

(d) Noise levels at the station sites and the sensitivity settings and capabilities of the stations.

Stations closest to the most active parts of the rift system such as Nairobi, Entebbe, Dodoma, Magadi, Hoima and Arusha had the best detectability partly by virtue of being closest to the epicentres of the events. It should be noted that the central and northern parts of Tanzania and of the western rift were quite active during the period (Fig. 2).

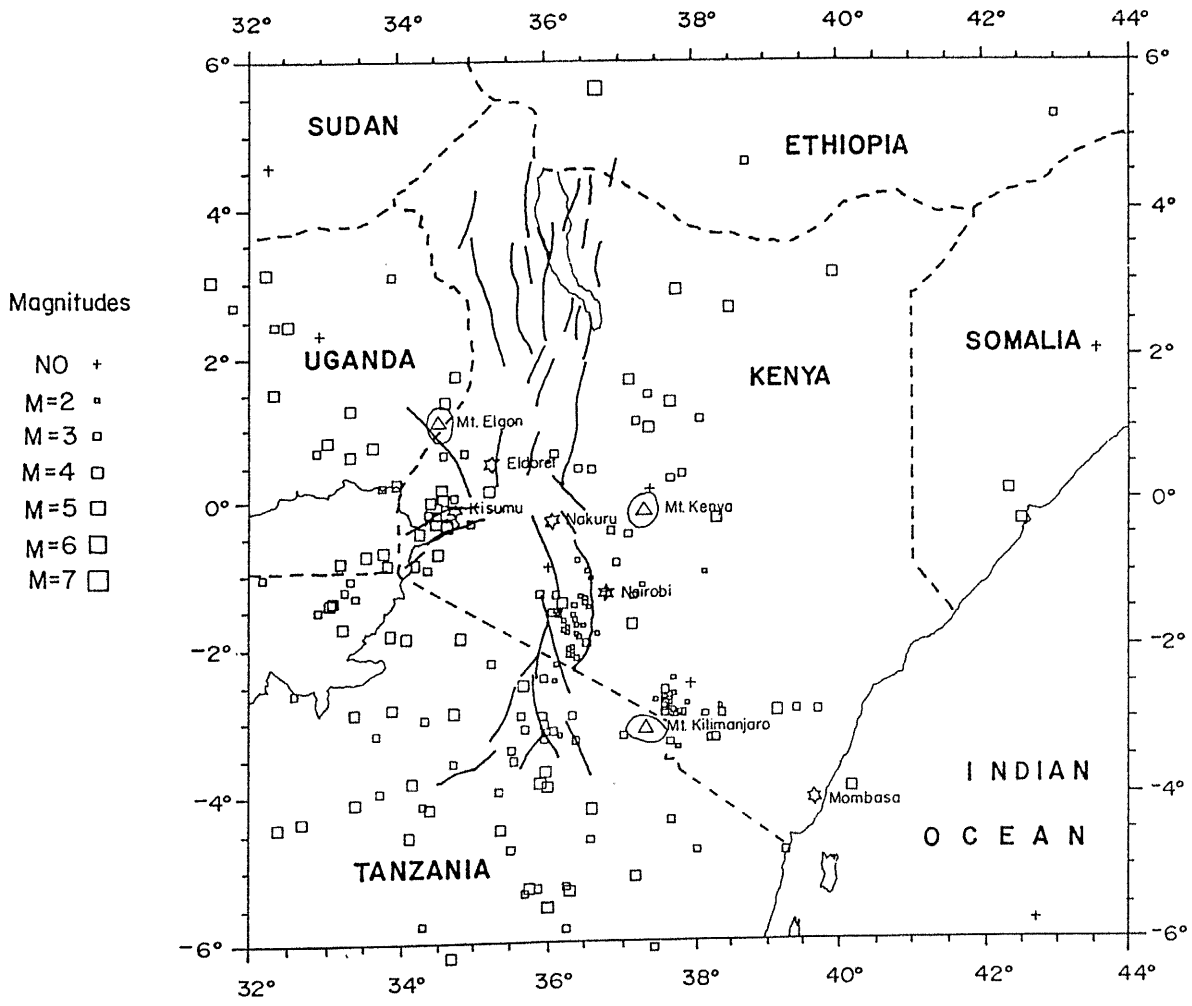

Fig. 2: Seismicity map of the most active sections of the Rift System (data 1993-1996)

Isolated stations on the extreme ends of the station network such as ASME and ZOM hardly recorded aany event because of their large distances away. Some of the stations such as KMBO, LAN, KIB, although located close to the active zones were operational only for a short duration during the period. This partly explains the few events detected by the station.

Finally, the problem of noise level also contributed to the non-detectability of events. For example, the Olkaria (OLK)station which was initially located within the Central Kenyan Rift Valley had to be relocated elsewhere as the noise from the local geothermal system was quite high. The performance of the station was extremely poor so that the few regional events were of very poor quality.

On the other hand, it was of interest to note that the Nairobi (NAI) station despite being located at a noisy site detected so many events. This is due to the fact that apart from the station being operational continuously during the period, it was possible by applying software to redeem most of the poor quality events. Many of the analysis centres in the region do not have the facilities for this type of event analysis and of course for analog records there is not much one can do.

It should also be pointed out here that some of the digital stations are not capable of capturing the whole event window for events coming from beyond a certain distance due to the limited flexibility in the trigger settings. Thus, for some events, only the S phases were detected.

The 132 events considered above are only those located by 5 stations or more. The actual number of events located during the period October 1993-August 1996, including events located locally by fewer stations, comes to about 1200. The difference between this total and the events considered above is due to the inclusion of events with magnitudes generally less than 3.0 which can be located only by nearby stations.

4. DETECTION THRESHOLD

The detection capabilities of a network depend upon station distribution, instrument sensitivity and background noise levels. It is, therefore, not possible to workout accurate figures for a region such as Eastern Africa where various instruments are in use and where the noise levels and absorption characteristics of the rocks are unknown.

However, in order to obtain a rough estimate of the network capability, a b-value plot with 0.1 resolution was made using 1206 earthquakes with local magnitudes obtained by use of the SEISAN analysis software (Havskov and Utheim, 1992). For these 1206 events the threshold magnitude was approximately 3.0 and the data seemed complete up to magnitude 5.5. An a value of 5.7 was obtained with a b-value of 1.34. Considering the limitations mentioned above, these figures can only be treated as very rough estimates.

Scientific Technical Report STR 98/05
DOI: 10.2312/GFZ.b103-98055

5. DISTANT EVENTS

So far, the only stations in the region that have been active in detecting distant events are the WWSSN stations which were located in Ethiopia(EAA), Kenya(NAI), Zambia(LSZ) and Zimbabwe(BUL). Some of these stations have now been upgraded to broadband digital thus enhancing their capabilities even further. However, the working group in the region has not been keen to work on distant events as the priority has been on local and regional events. For distant events, normally only the first arrivals are picked and the data send to international data centres for analysis.

6. CONCLUSIONS

The potential of the Eastern Africa seismic station network is high. The performance of the stations has not attained, however, their optimal level. There is still a lot of room for improvement in the performance of the existing stations. In order to increase the quality and quantity of the events detected by the network the following steps are necessary:

(a) There should be a slight improvement in the geographical distribution of stations to fill in the large gaps between stations;

(b) Efforts should be made to replace the remaining analog stations with digital ones;

(c) There should be increased usage of modern analysis software in order to redeem most of the poor quality events which are otherwise left without analysing;

(d) Efforts should be made to ensure that the stations operate continuously without prolonged breakdowns.

REFERENCES

Dindi, E, Havskov, J, Iranga M., Jonathan E., Lombe D.K., Mamo A., and Turyomu-rugyendo G. (1995). Potential Capability of the East African Seismic Stations. Bulletin of the Seismological Society of America. Vol. 85 No. 1 pp 354-360.

East ern and Southern Africa Seismology Working Group (1993). Workshop in East Africa on Seismology, Dar-es-Salaam.

Eastern and Southern Africa Seismology Working Group (1994). Regional Seismological Bulletin (October, 1993- December, 1993), Nairobi

Eastern and Southern Africa Seismology Working Group (1994). Regional Seismological Bulletin (January, 1994 - April 1994), Entebbe

Eastern and Southern Africa Seismology Working Group, (1995). Regional Seismological Bulletin (May, 1994 - August 1994), Ethiopia

Eastern and Southern Africa Seismology Working Group (1996). Regional Seismological Bulletin (September 1994 - February 1995), Malawi

Eastern and Southern Africa Seismology Working Group (1996). Regional Seismological Bulletin (March 1995- August 1995), Zimbabwe.

Eastern and Southern Africa Seismology Working Group (1996). Regional Seismological Bulletin (September 1995 - February 1996). Zambia

Eastern and Southern Africa Seismology Working Group (1997). Regional Seismological Bulletin (March 1996 - August 1996). Eritrea.

Havskov, J and Utheim T (1992). SEISLOG and SEISAN: A complete System for Seismic Data Acquisition and Analysis, Vol. 5, Cahiers du Centre Europeen de Geodynamique et de Seismologie, Luxembourg

Stangl R.L and Dindi E.W. (1997). Seismicity of Kenya and adjacent areas. (in press)

INSTRUMENTATION AND DATA ANALYSIS PRACTICE IN KENYA

Dirk Hollnack

University of Nairobi, Department of Geology, P.O. Box 30197, Nairobi, Kenya,
Fax: +254-2-449-539, E-mail: uonseism@arcc.or.ke

1. INTRODUCTION

A continuous observation of the seismic activity in Kenya started in 1963 when one of the WWSSN-stations (World Wide Standarized Seismograph Network) was installed in Nairobi. This seismograph, which was first operated by the Mines and Geology Department of the Ministry of Environment and Natural Resources and was handed over to the Geology Department of the University of Nairobi in 1964. This Nairobi WWSSN station was the only permanent earthquake-station in Kenya for about 30 years. It recorded thousands of local and regional earthquakes which could not be located properly since for most of these events no recordings from other stations were available. Therefore, no complete picture of the seismicity could be drawn and the amount of earthquakes in Kenya was underestimated for decades. Nevertheless, these data were the basis for several investigations as for example Rodrigues (1970), Loupekine (1971), Shah (1986), Ochieng (1993), and Kataka (1995).

Between 1964 and 1994 several microearthquake networks were established on temporary basis, designed for special research targets. Above all, the **K**enya **R**ift **I**nternational **S**eismic **P**roject (KRISP) has to be mentioned, a co-operation of various international working groups. The field campaigns of KRISP took place in 1985, 1989-90 and 1993-95 and were divided into refraction seismic experiments and temporarily established earthquake networks. The main results of these investigations have been published in KRISP Working Party (1991), Achauer *et al.* (1994), Keller *et al.* (1994), and Prodehl *et al.* (1997).

The seismological networks of KRISP were mainly designed for the observation of teleseismic events and, therefore, the analysis of the field data was carried out only for the far-distant earthquakes. But from the fact, that many local events were recorded by the different temporary networks and not by the WWSSN station it became obvious that the seismicity in Kenya is higher than known before. This led to the conclusion that the local earthquake activity in Kenya has to be studied in more detail by a permanent seismological survey. Therefore, a project, sponsored by the GTZ (German Society for Technical Co-operation), was started in 1990 at the Geology Department of the University of Nairobi, which still continues. Up to now a data centre and five digital portable seismograph systems of type MARS-88 (Lennartz Electronics) were purchased. Besides this new project, the old WWSSN station has been exchanged by a modern IRIS/GEOFON system (USGS and GFZ Potsdam) in 1995 which is also operated by the Seismology Section of the University of Nairobi.

DOI: 10.2312/GFZ.b103-98055

This paper will give some details about the development and actual state of the seismic network of the University of Nairobi, called University Network in brief. Additionally, first results of this network, concentrating on the local seismic activity during the period between October 1993 and August 1996, are presented. As far as available, data of the Eastern and Southern African Regional Seismological Working Group (ESARSWG) were used to improve the localisation results of this network. ESARSWG is a data exchange and analysis co-operation between several East and South African countries,

2. THE KENYAN SEISMIC NETWORK

The activities to establish a local seismological network in Kenya started in 1990. During the first two years five MARS-88 stations were purchased and tested and a preliminary test network installed. The MARS-88 are digital performance instruments, manufactured by Lennartz Electronics in Germany. They can record three channels with a sampling rate of up to 500 samples/s. The Kenyan instruments are equipped with 1 Mbyte RAM, a magneto-optical disc (OD) with a capacity 2 x 310 Mbytes for data storage and Lennartz LE-3D active short-period (1 Hz) three component seismometers. For the time base Lennartz GPS-clocks are used, keeping the time error in the MARS-88 systems within 1 ms. The power-supply for these instruments can either be main power (240 V AC) or from 12 V batteries, rechargeable by solar panels.

During the test phase of the instruments some hard- and software-problems came up which had to be solved first. After this a final large scale test was carried out until May 1993, followed by a participation in the KRISP 1993-95 experiment (Ritter *et al.*, 1995). The installation of the present University Network started in early 1994 and is still under progress. The current station distribution is shown on the map in Fig.1. Station co-ordinates and operation times are listed in Table 1.

The first station was installed at Lake Magadi (MAG), close to the Kenya-Tanzania border. This station is operating smoothly until today, only interrupted by some short failures caused by minor technical problems.

Also in February 1994 the second station, named Langata (LAN), was installed in the Nairobi National Park. Although the performance of this station was very good, it was dismantled in January 1995 because it was too close to the Nairobi University where the IRIS/GEOFON broadband system was set up for a test-phase. Meanwhile the IRIS/GEOFON station was moved to Kilima Mbogo (KMBO) some 40 km NE of Nairobi. Therefore, it is planned to rebuild LAN soon.

The KMBO station is equipped with two broadband seismometers for three components (Vertical, N-S and E-W). One seismometer is of type STS-1 covering the ULP, VLP and LP frequencies and the other is of type STS-2 for the VSP frequency range. In addition, there is a 3-component force-balance accelerometer of very low gain and of 1g full scale deflection.

Another station, which was running from April to August 1994 about 200 km SE of Nairobi at Kibwezi (KIB), was also temporarily dismantled when the solar-panel was stolen. This station was reinstalled in June 1996 after building a strong brick hut.

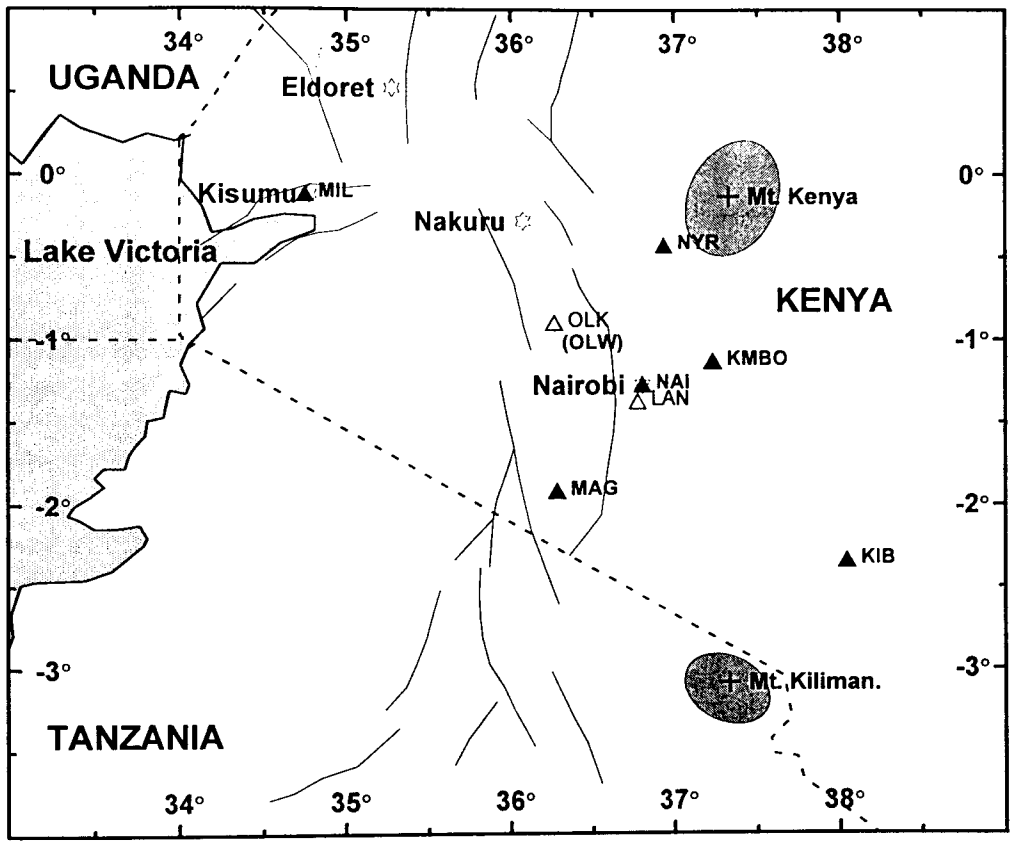

Fig. 1: Location map of the University of Nairobi seismological network. Actual stations are indicated by filled triangles and former station locations by open triangles.

Table 1: Co-ordinates and operating periods of the University Network stations.

Name	Code	Working Period	Latitude	Longitude	Elevation (m)
Nairobi	NAI	since 1963	1.274 S	36.804 E	1692
Magadi	MAG	since Feb.'94	1.918 S	36.287 E	660
Kibwezi	KIB	Apr.'94 - Aug.'94 since Jun.'96	2.340 S	38.046 E	775
Langata	LAN	Feb.'94 – Jan.'95	1.377S	36.773E	1707
Olkaria	OLK	Mar.'95 - Nov.'96	0.888 S	36.324 E	1751
Olkaria West	OLW	Nov.'96 – Apr.'97	0.886 S	36.264 E	1780
Kilima Mbogo	KMO	since Sep.'95	1.135 S	37.234 E	1950
Kisumu	MIL	since Feb.'97	0.114S	34.751E	1140
Nyeri	NYR	since Apr.'97	0.429S	36.937E	1900

Scientific Technical Report STR 98/05
DOI: 10.2312/GFZ.b103-98055

The Station OLK, which is located close to the Olkaria geothermal power plant (near Naivasha), was installed in March 1995. The performance of this station was highly disturbed by noise from the geothermal field. Therefore, as well as for improving the station distribution of the network, the instrument was moved to the Mount Kenya region. There it is now operating as a temporary installation in Nyeri (NYR). The final and permanent location for this station is planned in Meru, north-east of Mount Kenya.

Up to now one MARS-88 system is operating at the campus of the University of Nairobi (NAI), at the old WWSSN-site. There, also the IRIS/GEOFON system was running for a 9 month test phase. During the last 30 years the artificial noise of the growing city increased so much that the running of a seismological station at this site nearly became useless. Therefore, this instrument will soon be moved to LAN. The fifth and last available MARS-88 will be installed at Kisumu/Lake Victoria in the near future.

The configuration of the University Network is restricted to the Rift Valley around Nairobi in order to keep the cost and the time required for the maintenance of the stations low. Only within the currently covered area it is possible to service the stations within one day of travel. An extension of the network would be possible only by the use of modem stations.

3. DATA ACQUISITION AND PROCESSING

The acquisition and analysis of seismic data at the Nairobi data centre is a heterogeneous process since the recordings of the IRIS/GEOFON instrument and the MARS-88 instruments are in different binary formats. The IRIS/GEOFON station at Kilima Mbogo is connected by radio telemetry to the data processing unit at the Geology Department where the data are stored continuously on a hard-disk as well as on streamer-tape. For a fast overview of the daily data, two 24-hours continuous analogue recordings of the vertical ground motion are plotted, one for the short period and one of the long period data stream. Based on these recordings time windows are determined which include seismic events. By using the KERMIT program the data of these windows are transferred in ASCII format to a PC of the data centre where they are controlled and prepared for a conversion into binary format. Via Ethernet the data are copied to the SUN workstation and converted into ISAM files and stored in monthly directories for analysis.

Except NAI, which is running in continuous mode and viewed on a daily base, all other MARS-88 stations are working on event-trigger mode. Their maintenance as well as changing of the optical discs is done monthly. All data stored on the optical discs are downloaded at the Department of Geology into a database on the SUN computer and viewed. The earthquake recordings are converted into ISAM-format and also copied in the monthly directories as for the IRIS/GEOFON data.

For the basic analysis of the seismograms the program XPITSA (Scherbaum and Johnson, 1994) is used. The arrival times of each event, the azimuth and the first motion at the vertical component are converted into Nordic format (Havskov and Lindholm, 1994) and transferred into a SEISAN database which is used by all members of the ESARSWG.

For earthquake localisation the pick-files in Nordic format are copied into a SEISAN data base. The SEISAN package contains a modified version of HYPOCENTER (Lienert et al.,

1986) which can accept more phases, locate teleseismic events and use input in Nordic format directly from the data base. This program can also locate with one station if P-arrival, S-arrival and azimuth are given. This possibility is only utilised for events with epicentral distances of less than 100 km to the recording station and if the determination of the first ground motion at all three components is doubtless and corresponds with the direction of a particle-motion diagram.

Since the crustal structure in the study area varies considerably several velocity models have been tested by Kataka (1995), mainly based on the results of the KRISP experiments (KRISP Working Party, 1991). As a good approximation for the study area he found a simple two layer model with an upper layer of 14 km thickness and a P-wave velocity of $V_p = 6.2$ km/s. The second layer has a P-wave velocity of $V_p = 6.6$ km/s and reaches down to the Moho at 37 km depth. For the upper mantle a velocity of $V_p = 8.1$ km/s is given. The S-wave velocities are calculated by using a V_p/V_s ratio of 1.73.

For control purposes the local magnitudes are determined in two ways. First they are computed from integrated horizontal traces within XPITSA which includes the formula of Bakun and Joyner (1984). The second magnitude value is determined during the localisation of the events. Therefore, the displacement amplitudes of the horizontal traces in nm are entered into the database. The formula used to calculate the local magnitude is:

$$M_L = a * \log(amp) + b * \log(dist) + c * dist + d$$

where a (0.925), b (0.91), c (0.00087), d (-1.31) are constants, amp is the maximum ground amplitude (zero-peak) in nm and dist is the epicentral distance in km. The numbers given in brackets with the constants are the values used by the ESARSWG members. In average the local magnitudes calculated with XPITSA and with SEISAN do not differ more than 0.1. However, further works to improve the magnitude determination as well as the localisation model for Kenya are in progress.

Many of these results are preliminary. For the final solutions additional information from the other members of the ESARSWG, which are meeting twice a year, are included. Thus it is possible also to locate earthquakes outside the Nairobi Network with reliable results.

4. SEISMIC ACTIVITY IN KENYA AND ADJACENT AREAS

In order to give an idea about the seismic activity in the area of the University Network all earthquakes, localised between October 1993 and August 1996 and grouped in magnitude classes ranging from $M_L \leq 2$ to $M_L \leq 5$, have been depicted in Fig.2. During this time interval 435 earthquakes out of more than 2000 could be located in the study area, which covers the region from 1°N to 4°S and from 33°E to 39°E. Since the arrival times of the ESARSWG network were available for the whole period also a number of events outside the Nairobi Network could be located with reliable results.

Fig. 2 clearly shows three regions of prominent seismicity. First, the Rift Valley between Nakuru and its extension into northern Tanzania, second the region north, north-east and east of Mt. Kilimanjaro and third, Western Kenya and Lake Victoria region around Kisumu. The occurrence of a large number of small earthquakes ($M_L \leq 3$) in the Rift Valley and near the

station Kibwezi can be explained by the distribution of the seismic stations used for the localisation of the earthquakes.

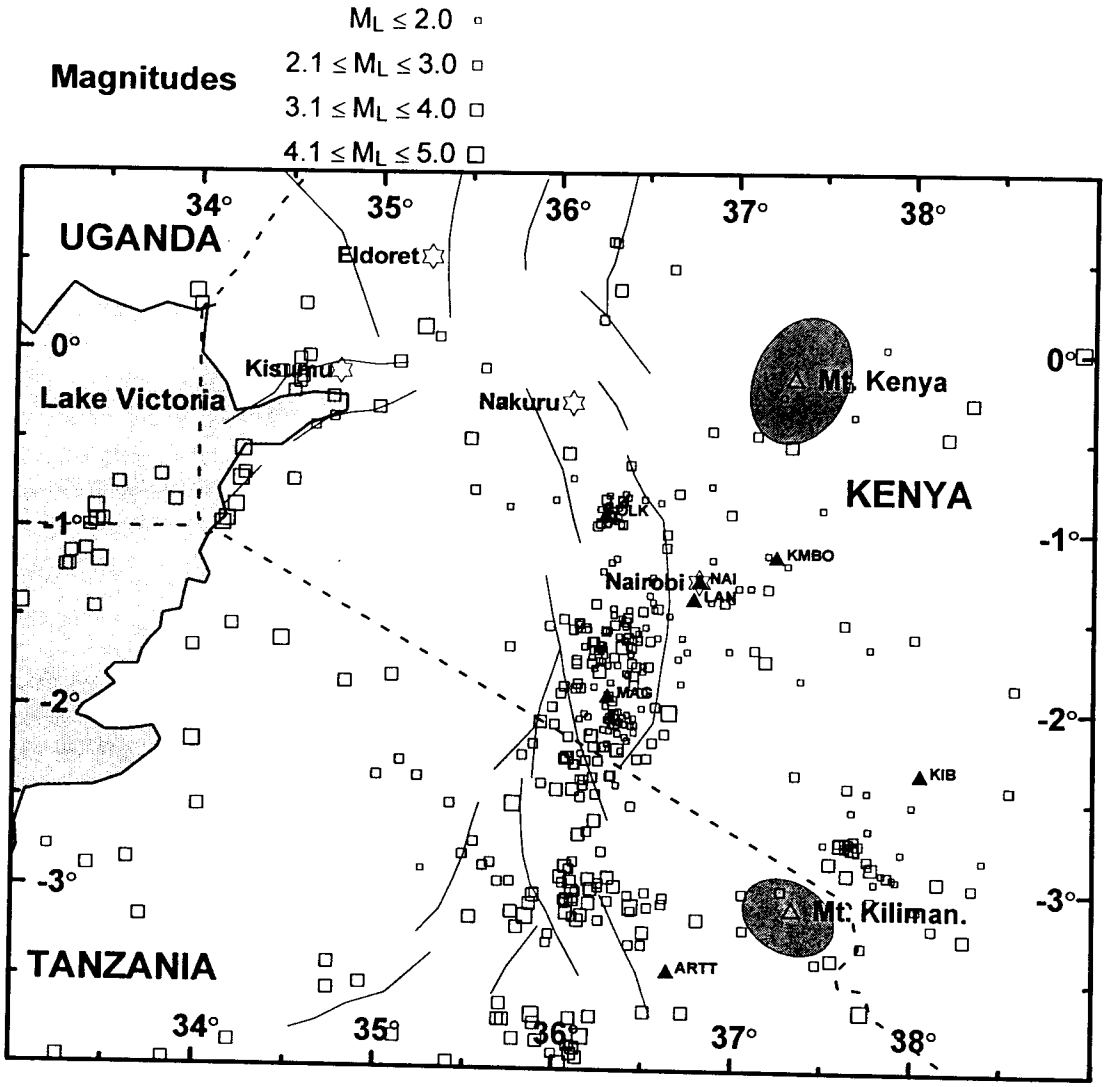

Fig. 2: The seismicity in Kenya between October 1993 and August 1996. The 435 earthquakes shown in the study area are grouped in different magnitude classes.

On the whole, the seismicity in Kenya can be characterised as moderate. Nevertheless, the earthquake activity has to be monitored continuously because on the one hand, stronger earthquakes have occured from time to time and on the other hand, its detailed investigation is of high interest from a scientific point of view.

REFERENCES

Achauer, U., the KRISP Teleseismic Working Group (1994). New ideas on the Kenya rift based on the inversion of the combined dataset of the 1985 and 1989/90 seismic tomography experiments. Tectonophysics **236**, 305-329.

Bakun, M.M. and Joyner, W.B. (1984). The Ml scale in central California. Bull. Seismol. Soc. Am. **74**, 1827-1843.

Havskov, J. and Lindholm, C. (1994). The SEISAN earthquake analysis software for the IBM PC and Sun, version 4.0. Manual, Institute of Solid Earth Physics, University of Bergen, Norway, 139 pp.

Kataka, M.O. (1995). Regionalisation of seismic velocities for precise earthquake localisations in Kenya. M.Sc. thesis, University of Nairobi, Nairobi.

Keller, G.R., Prodehl, C., Mechie, J., Fuchs, K., Khan, M.A., Maguire, P.K.H., Mooney, W.D., Achauer, U., Davies, P.M. Meyer, R.P., Braile, L.W. Nyambok, I.O. and Thompson, G.A. (1994). The East African rift system in the light of KRISP 90. In: Prodehl, C., Keller, G.R. and Khan, M.A. (Editors), Crustal and upper mantle structure of the Kenya rift, Tectonophysics **238**, 453-464.

KRISP Working Party (1991). Large-scale variation in lithospheric structure along and across the Kenya Rift. Nature **354**, 217-249.

Lienert, B.R., Berg, E. and Frazer, L.N. (1986). Hypocenter: An earthquake location method using centered, scaled, and adaptively damped least squares. Bull. Seism. Soc. Am. **76**, 771-783.

Loupekine, I.S. (1971). A catalogue of felt earthquakes in Kenya, 1892-1969. Publ. Seism. Unit, University of Nairobi.

Ochieng, A.O. (1993). Seismic energy mapping and strain release pattern of Kenya. M.Sc. thesis, University of Nairobi.

Prodehl, C., Mechie, J., Ritter, J.R.R., Fuchs, K., Keller, G.R., Khan, M.A., Jacob, B., Nyambok, I.O. and Obel, J.D. (1997). The KRISP 94 lithospheric investigation of southern Kenya - the experiments and their main results. In: Fuchs, K., Altherr, R. Müller, B., and Prodehl, C., Stress and stress release in the lithosphere. Tectonophysics (in press).

Ritter, J.R.R., Fuchs, K., Kaspar, T., Lange, F.E.I., Nyambok, I.O. and Stangl,R.L. (1995). Seismic images illustrate the deep roots of the Chyulu Hills volcanic area, Kenya. EOS **76**, 273 and 278.

Rodrigues, E.B. (1970). Seismological studies of the East Africa Rift System. Ph.D thesis, University College, Nairobi.

Shah, E.R. (1986). The seismicity of Kenya. Ph.D thesis, University of Nairobi, Nairobi.

Scherbaum, F. and Johnson, J. (1994). Programmable interactive toolbox for seismological analysis (PITSA). IASPEI Software Library Volume 5, Seism. Soc. Am., El Cerrito, CA.

SEISMIC DATA ACQUISITION AND ANALYSIS

Michael Baumbach

GeoForschungsZentrum Potsdam, Division 2: Solid Earth Physics and Disaster Research,

Lecture presented at the Advanced Study Course on Seismic Risk („SERINA")
September 21-27, 1997, Thessaloniki, Greece

1. THE RECORDING SYSTEM

Time series recorded by seismic stations depend on the source mechanism of the earthquake considered, on the velocity and attenuation structure of the propagation medium and on the recording system used. Additionally, they might be superimposed by ambient seismic noise. The recording system includes the seismometer and the data recorder. When we try to derive information about the earthquake source, the Earth structure, or local site effects we have to be aware, that the results may be affected by the recording system. One has to know, therefore, the basic properties of the recording system in order to correct the recorded time series or the derived source or medium parameters accordingly.
The first part of the lecture deals with the seismometer and the different techniques used for digitising the analogue output signal of the seismometer. Further, methods for estimating the quality of recording systems are described.

1.1 The Seismometer

In order to understand how the recorded signal can be related to the ground motion we analyse the equation of motion of a vertical pendulum seismometer (figure. 1).

Its equation of motion is:

$$k\,x + D\,\dot{x} + m\,(\ddot{x} + \ddot{y}) = 0 \qquad (1)$$

x - displacement of the suspended mass relative to the ground
y - displacement of the ground (true ground motion)
k - spring constant
D - friction coefficient
m - suspended mass

When applying the Fourier transform to equation (1) we get

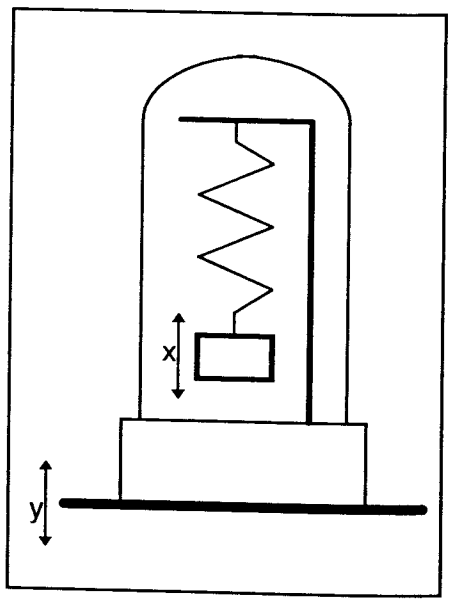

Fig. 1: Pendulum seismometer without transducer

Scientific Technical Report STR 98/05
DOI: 10.2312/GFZ.b103-98055

$$X(\omega) = Y(\omega)\ \omega^2 / (\omega_0^2 + 2\,i\,h\,\omega\,\omega_0 - \omega^2) = Y(\omega)\ T(\omega) \qquad (2)$$

with $\omega_0^2 = k/m$ $\omega_0 = 2\ \pi\ f_0$ - angular eigenfrequency of the seismometer
and $h = D/(2\,m\,\omega_0)$ - damping constant

The expression

$$T(\omega) = \omega^2 / (\omega_0^2 + 2\,i\,h\,\omega\,\omega_0 - \omega^2) \qquad (3)$$

is denoted as frequency response function and its inverse Fourier transform as impulse response function of the system. Indeed, a Delta impulse $\delta(0)$ has a flat spectrum $\delta(\omega) = 1$. Therefore, the inverse Fourier transform of (2) gives the response of the seismometer to an impulse input. According to (2) the seismometer output can be calculated either by multiplying the ground motion spectrum with the frequency response function and subsequent Fourier transformation of $X(\omega)$ into the time domain or by convolving the ground displacement y(t) with the impulse response function T(t), i.e. $x(t) = y(t) * T(t)$.

The general shape of the frequency response of a seismometer can be derived from (3): at small frequencies ($\omega << \omega_0$) the response is proportional to ω^2, at high frequencies ($\omega >> \omega_0$) the response is -1. The behaviour in the vicinity of the eigen- or corner frequency ω_0 depends strongly on the seismometer damping constant h.

The motion of the pendulum can be measured by a capacitive or inductive transducer. In case of a capacitive transducer the measured voltage is proportional to the displacement of the suspended mass. In case of an inductive transducer a coil, connected to the seismometer mass, is moving through a permanent magnetic field. The induced voltage is proportional to the velocity of the seismometer mass. This introduces an additional $i\omega$ in the numerator of the seismometer frequency response function. Further, the generator constant G of the seismometer coil has to be taken into account. The transducer resists to the motion of the seismometer mass and therefore changes the damping constant h. For an electromagnetic sensor, we finally get the frequency response function

$$T(\omega) = G\ i\,\omega^3 / (\omega_0^2 + 2\,i\,h\,\omega\,\omega_0 - \omega^2). \qquad (4)$$

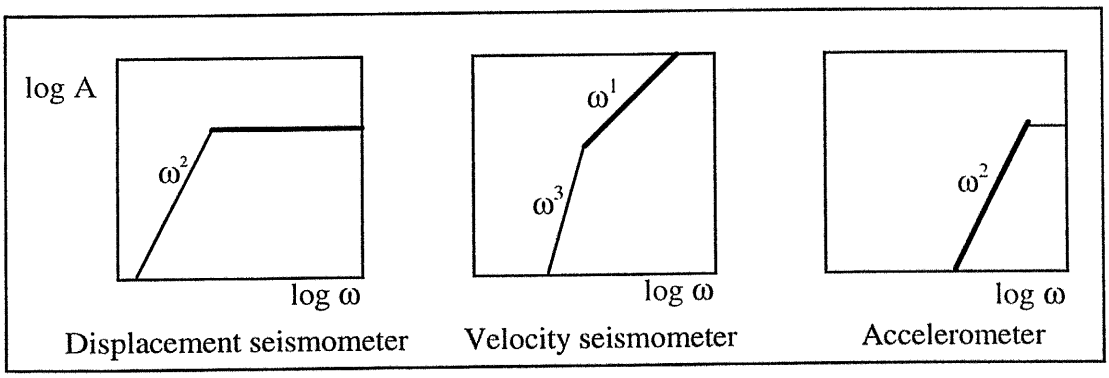

Fig.2: Response curves for different seismometer types, A: displacement amplitude
ω: angular frequency

Usually, the damping constant h is set to 0.7. For $h \geq 1$ the pendulum returns to the resting state (zero position) after initial elongation (release test, zero initial velocity) without oscillations (h = 1: critical damping).

Figure 2 shows the frequency response curves of displacement and velocity seismometers and an accelerometer. Below the corner frequency a displacement seismometer records acceleration. Therefore, accelerometers usually consist of sensors with high eigenfrequencies (e.g. 60-100 Hz).

Equation 3 is a specific example for the calculation of the system response of general linear time invariant systems, which will be described by linear differential equations (Scherbaum, 1994). The general expression for the frequency response function of such a systems is:

$$T(\omega) = C \frac{(i\omega - z_1)(i\omega - z_2)(i\omega - z_3)\ldots(i\omega - z_m)}{(i\omega - p_1)(i\omega - p_2)(i\omega - p_3)\ldots(i\omega - p_n)} \qquad (5)$$

where C is a constant and p_j and z_j are the so called poles and zeros of the system. They are complex numbers and describe the system completely.

The poles and zeros of equation (3) are

$$p_{1,2} = (-h\omega_0, \pm \omega_0 \sqrt{(1 - h^2)}) \qquad z_{1,2,3} = (0, 0). \qquad (6)$$

1.2 Digital data recorder

Before sampling the analogue data they have to pass through an ant-alias lowpass filter which should remove all signal energy above the so-called Nyquist frequency f_n, that is half the sampling frequency f_s . Otherwise, the sampling process would map this energy into the frequency band from 0 to f_n and distort the digitised time series. Therefore, anti-alias filtering has to be done using analogue filters. Analogue filters of course influence the recorded trace what has to be taken into account when analysing the data. They change both the amplitude and the phase spectrum. The corner frequency of the analogue filters is usually about 30% f_n, what means, that a significant portion of the frequency range is lost or its spectral amplitudes being distorted.

Over the last years the dynamic range of the analogue to digital converters has been permanently improved. Nowadays, 24 bit converters are becoming a standard, although there are still 16 bit systems on the market and a lot of 12 bit systems are still in use in many countries. The theoretical dynamic range DR of digital systems is being calculated in Decibels [db] as

$$DR = 20 \log (A_{max} / A_{min}) = 20 (n - 1) \log 2 \approx 6 (n - 1). \qquad (7)$$

n is the number of bits of the AD-converter and -1 takes into account, that one bit is used for storing the sign of the sample.

Methods for increasing the dynamic range of AD-converters

1. Gain ranging

Gain ranging AD-converters sample the same analogue signal from different channels with amplifications differing by $i = 2^k V$ (k - integer constant, V is the voltage corresponding to 1 count at the lowest amplification). The sample to be stored will be selected by a logic unit from the AD-board that has the highest amplification and is not yet off-scale. The data are usually stored in gain ranging format which consists of the mantissa m (output of the converter) and an exponent n of i which shows the gain amplification. The amplitude in counts can then be derived as

$$A = m\ i^n . \qquad (8)$$

Other more recent gain ranging systems use instead of AD-boards with different preamplifiers one single programmable preamplifier which checks the input voltage of the AD-converter and reduces, if required, the preamplification. It should be underlined, that the use of gain ranging AD-converters increases the dynamic range but decreases the internal resolution (larger amplitude steps for greater amplitudes compared with smaller ones).

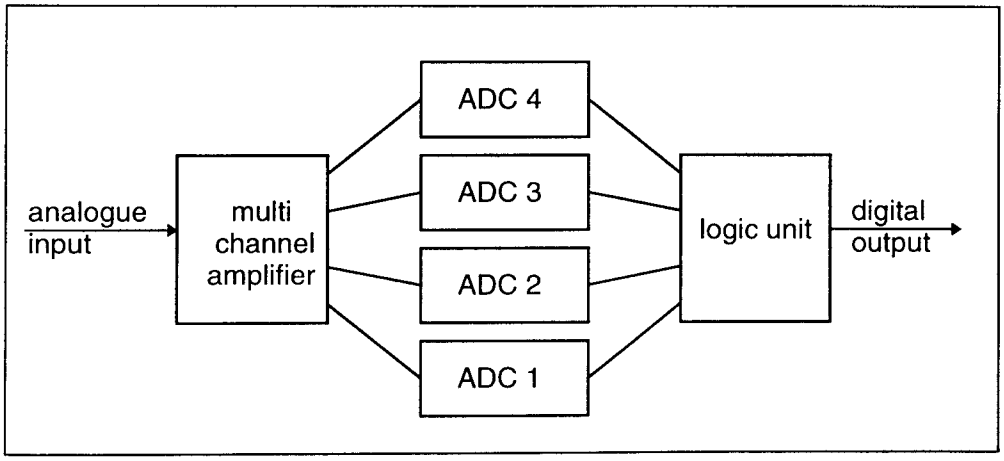

Fig. 3: Schema of a gain ranging ADC

2. Oversampling

Oversampling means, that the primary sampling rate is larger than the final sampling rate desired. The method (Oppenheim and Schafer, 1989) is based on the assumption, that the quantization noise has a variance that is independent of the sampling rate. This is true if the quantization noise has a probability density function which is flat between $\pm Q / 2$, where Q is the quantization step. The variance of the quantization noise equals $Q^2 / 12$. When applying the Parseval theorem, which states that the energy in the time domain equals the energy in the frequency domain, we get for two different Nyquist frequencies f_1 and f_2 and a given time series of quantization noise

Scientific Technical Report STR 98/05
DOI: 10.2312/GFZ.b103-98055

$$\int_{t_1}^{t_2} n(t)^2\,dt = \int_{-\omega_1}^{\omega_1} N_1(\omega) N_1^*(\omega)\,d\omega = \int_{-\omega_2}^{\omega_2} N_2(\omega) N_2^*(\omega)\,d\omega . \qquad (9)$$

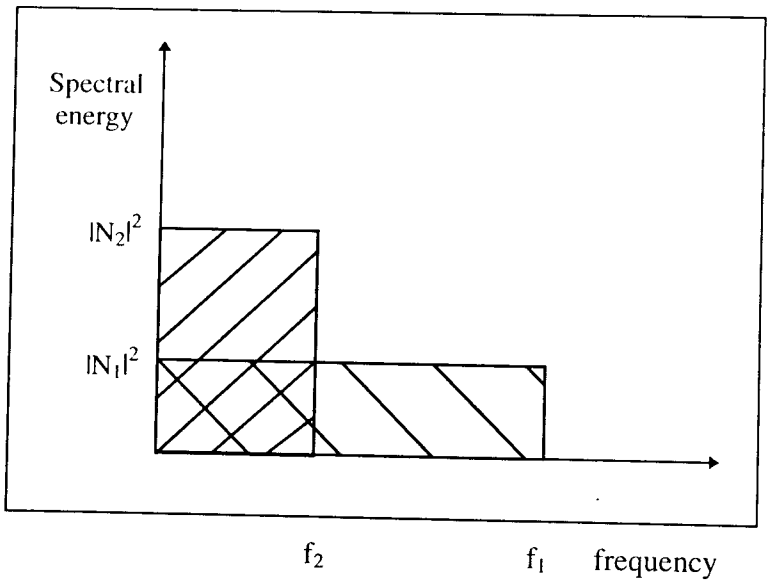

Fig. 4: Principle of oversampling

N_1 and N_2 are the spectral noise amplitudes for Nyquist frequencies $\omega_1=2\pi f_1$ and $\omega_2=2\pi f_2$, N_1^* and N_2^* are the complex conjugates of N1 and N2. The time integral does not depend on the sampling rate and therefore on the Nyquist frequency. This results in a different spectral noise amplitude $N(\omega)$ for different Nyquist frequencies ω_1 and ω_2.

$$|N_1| / |N_2| = \sqrt{(f_2/f_1)} \qquad (10)$$

Digital lowpass filtering of an oversampled time series with full floating point accuracy (decimation filter) and subsequent resampling with a lower sampling rate decreases the noise level by $\sqrt{(f_2 / f_1)}$ and therefore increases the dynamic range of the recording system. For example, a recording system with an oversampling ratio f_1 / f_2 of 16 (PDAS-100, TELEDYNE Geotech) increases the dynamic range by a factor of 4 what corresponds to an enhancement of the number of bits by 2.

1.3 Properties of modern recording systems

There are several seismic recorders with different parameters on the market. When selecting a recorder for a specific purpose one has to check what system has the optimum parameters for the data to be recorded. This chapter describes the most important parameters and shows, how to derive them.

1. Dynamic range

According to equation 7 we have to find the the maximum and minimum signal amplitude for computing the dynamic range of a data recorder. The maximum amplitude for the given recorder can be simply derived from its clipping level in counts. The minimum amplitude of a seismic signal that can be identified in a record depends on the eigennoise of the recorder in counts. A comparison of sinus oscillations with different amplitudes (model of a seismic trace) superimposed by normally distributed noise with standard deviation σ (eigennoise of the recording system) shows, that a seismic signal can be detected starting from an amplitude of $\sqrt{2}\,\sigma \approx 1.4\,\sigma$ (figure 5), which is assumed as minimum amplitude for the computation of the dynamic range of the recorder (DR=20 log (A_{max}/A_{min}) in db).

For checking the dynamic range in the frequency domain we have to compare the spectra of the sinus signal and the noise. For the transformation into the frequency domain we use the discrete Fourier series. The length of the time series was selected as a multiple of the period of the test signal. In this case the sinus test function is orthogonal to all basis functions so that only one Fourier coefficient describes the test signal in the frequency domain. In order to compare the noise and signal parameters we apply the Parseval theorem to the given time series f_i. In order to get power instead of energy we divide the equation by the length of the time series T.

$$N^{-1} \sum_{i=1}^{N} f_i^{\,2} = \tfrac{1}{2} \sum_{k=1}^{N/2} |F_k|^2 \qquad (11)$$

N is the number of samples f_i and F_k are the complex Fourier coefficients.

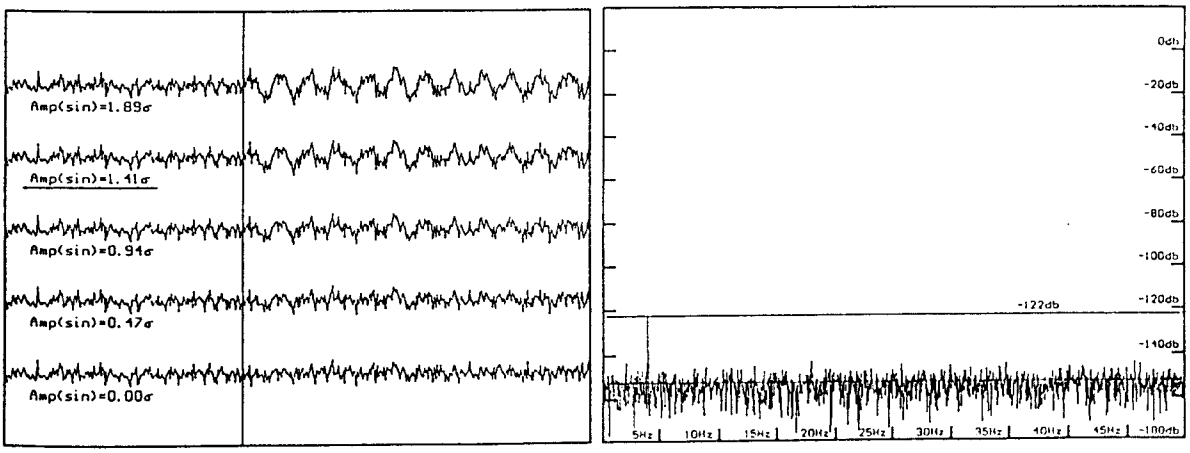

Fig. 5: Synthetically generated noise (σ = 3.6, typical for a REFTEK 72A07 Recorder) with superimposed sinus oscillations of different amplitudes (left) and corresponding spectrum for noise and sinus oscillations with amplitude of 1.4 σ. The spectrum is displayed in db relative to the clipping amplitude of the recorder (0 db). The single peak in the spectrum is due to the sinus test signal.

Scientific Technical Report STR 98/05
DOI: 10.2312/GFZ.b103-98055

The ratio of the power of the noise n_i to the power of the sinus signal $s_i = A_0 \sin(\omega t_i)$ can be derived in the time and frequency domain as

$$\sum_{i=1}^{N} n_i^2 \Big/ \sum_{i=1}^{N} s_i^2 = 2\sigma^2 / A_0^2 \quad \text{and} \quad \sum_{i=1}^{N/2} |R_i|^2 / A_0^2 \qquad (12)$$

respectively. R_i are the Fourier coefficients of noise. For the assumed minimum signal amplitude of $A_0 = 1.4\,\sigma \approx \sqrt{2}\,\sigma$ we get, that the signal power equals the noise power. From (12) we conclude, that the amplitude of the minimum detectable seismic signal can be computed simply from the noise spectrum:

$$A_0 = \sqrt{(\sum |R_i|^2)} \qquad (13)$$

Expression (13) shows, that there is a simple way to compute the dynamic range of a recording system from the spectrum of the eigennoise and the clipping amplitude in counts.

$$DR = 20 \log (A_{clip} / \sqrt{(\sum |R_i|^2)} \qquad (14)$$

Figure 5 displays the minimum spectral amplitude calculated according to (13) as a solid line at -122db. It well agrees with the spectrum peak, caused by the minimum detectable sinus signal. When using the spectral noise level as the minimum spectral amplitude one would significantly overestimate the dynamic range (e.g. by 30 db for the given example according to figure 5). All tests were done with a sampling frequency of 100 Hz. One has to keep in mind that the dynamic range changes with sampling frequency for recorders with oversampling.

2. Recorder noise

The eigennoise of the recorder has to be measured with shorted input. For a given AD-converter the usable dynamic range depends on the standard deviation of the eigennoise measured in units of counts. Three high gain recorders were tested:

- REFTEK 72A07, Refraction Technology, 24 bit AD-Converter
- PDAS100, TELEDYNE Geotech, 16 bit ADC, gain ranging, oversampling
- MARS88 Lennartz Electronic, 16 bit ADC, oversampling.

The standard deviation of the noise ranges between 1.2 and 22.1 counts, what corresponds to a difference of about 4 bits. Figure 6 shows the noise spectrum and the distribution of noise amplitudes. The least significant bit was best selected for the MARS88, in order to get the highest dynamic range for the given system.

Some recorders for temporary field installations are optimised for low power consumption (REFTEK 72A07). This may result in a step-like baseline shift if external devices (hard disk, GPS) are temporarily switched on. Further, temperature changes may cause a low frequency base line drift. These effects introduce additional noise.

Scientific Technical Report STR 98/05
DOI: 10.2312/GFZ.b103-98055

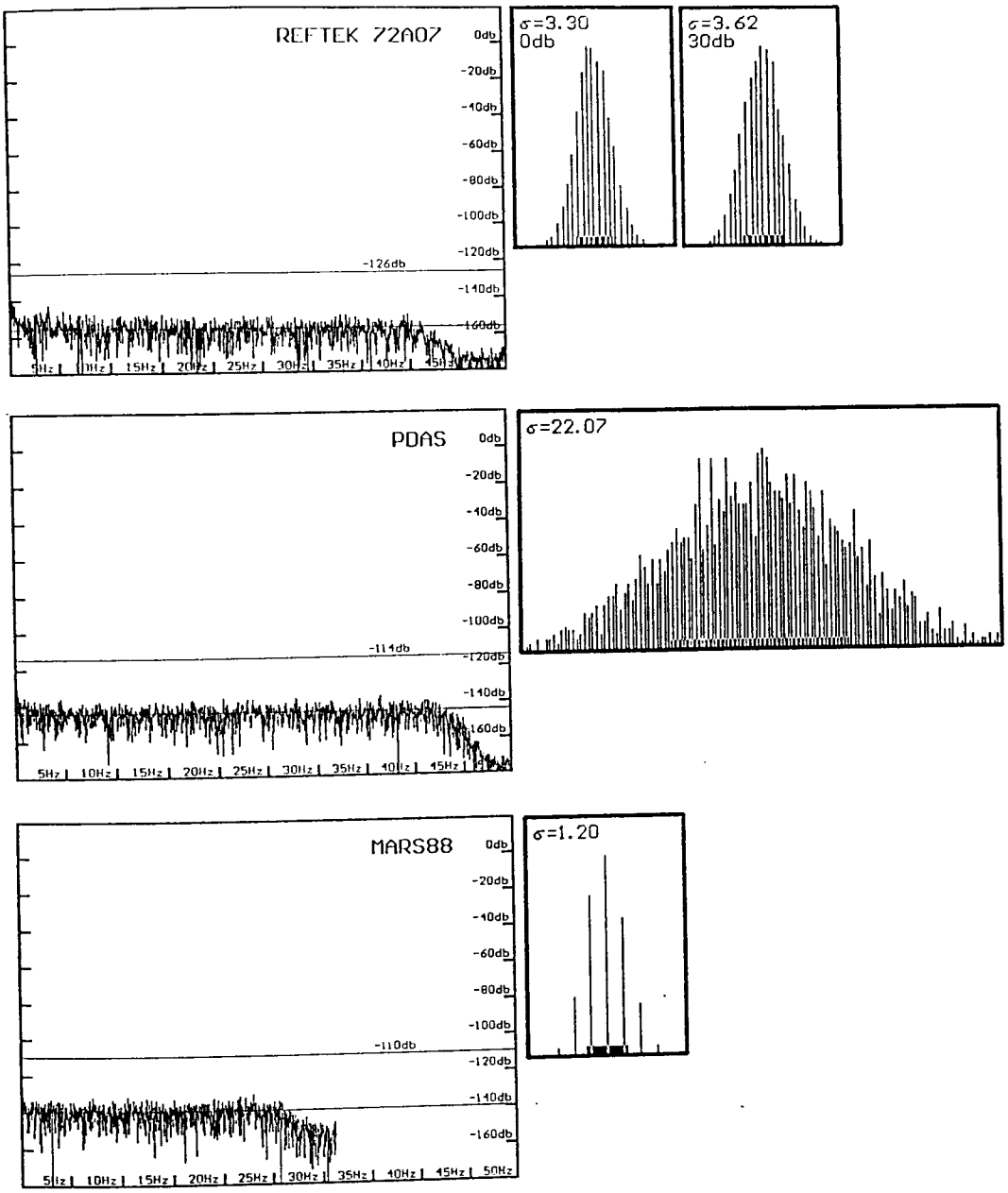

Fig. 6: Spectra of recorder noise for shorted input, usable dynamic range and amplitude distribution of noise samples, σ – standard deviation of noise in counts.

3. Resolution

Recorders without gain ranging do not show resolution changes for different amplitudes (no change of quantization step). Figure 7 shows the spectra of two records with a 4 Hz- sinus signal and amplitudes close to the clipping level and 60 db below the clipping level, respectively. The overtones are due to the limited stability of the sinus generator. Remarkable is the different noise level. Although the MARS88 uses oversampling (no gain ranging ADC), the resolution decreases as a result of storing the data in a gain ranging format. The data quantization step therefore increases with amplitude and decreases the system resolution, what results in a higher noise level for signals with large amplitudes (30 db for the given example).

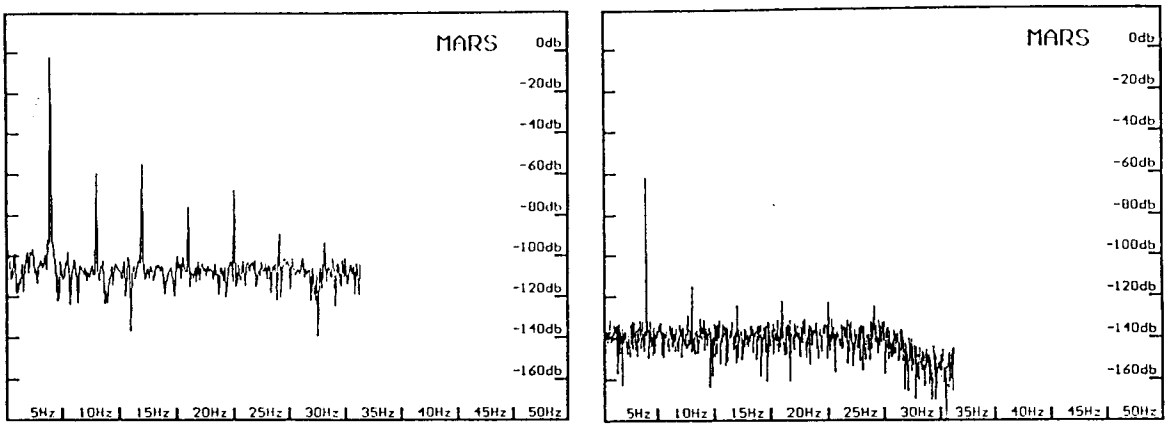

Fig. 7: Spectra of noise records superimposed by sinus oscillations of different amplitudes. The data were stored in gain ranging format.

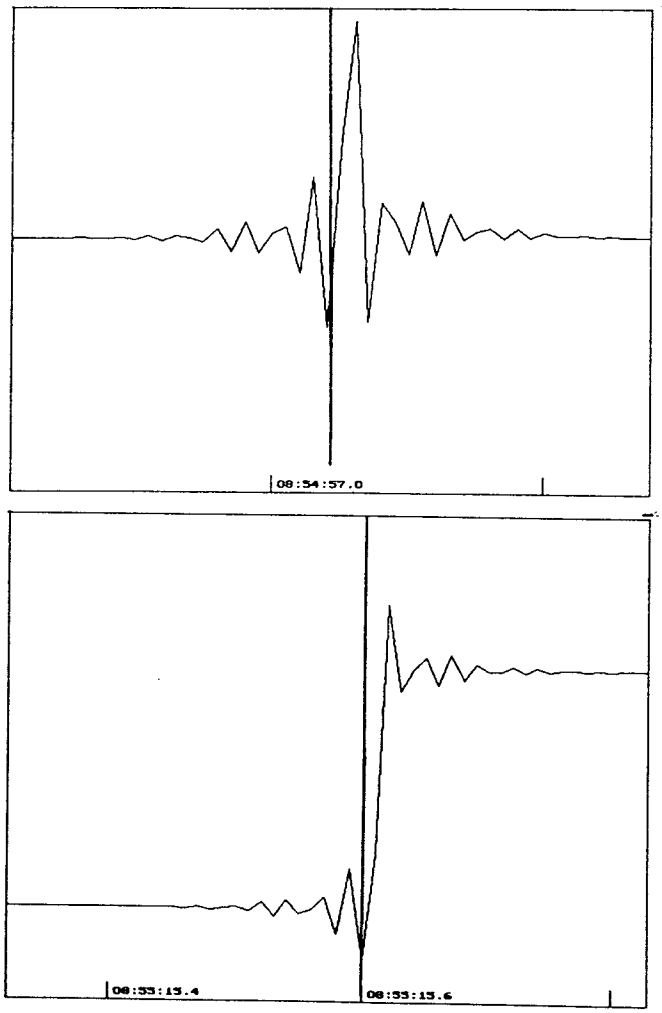

Fig. 8: Records, showing acausal effects for impuls (above) and step test functions (below). The exact time of the beginning of the impuls and step, respectively, is marked by the vertical bar.

4. Anti-alias filter

In modern high gain seismic recorders are usually linear phase finite impulse response (FIR) filters implemented (Scherbaum and Bouin, 1997a). They are used as digital anti-alias filters and sampling noise decimation filters for recorders using the oversampling technique. They are very steep stable filters and expand the usable frequency range up to 80% of the Nyquist frequency f_n in contrast to analogue filters which have a passband approximately up to 30% of f_n. Analogue filters are always causal filters and cause a phase distorsion of the input signal within the passband of the filter. Linear phase filters pass signals within the passband undistorted, except for a constant time shift. A filter which additionally corrects this time shift is called zero phase filter. These filters are acausal and produce oscillations before the onset approximately with the Nyquist frequency. This is a result of the two-sided impulse response of the linear or zero phase filters. Figure 8 shows records of step and impulse functions with remarkable precursory signals. In case of seismic records they might be misinterpreted as earlier arrivals. In general, onset times picked from linear or zero phase filtered traces will be always too early.

Zero phase filters are implemented in most high gain recorders (QUANTERRA, REFTEK, MARS, PDAS, ORION). There is one strong motion recorder on the market (ALTUS K2 from Kinemetrics) with a linear phase filter which produces a time shift, depending on the sampling rate: shift of 0.38 sec for 100 Hz, 0.156 sec for 250 Hz. This shift has to be taken into account when data of different recorder types are processed and analysed together. The acausal effects can be removed by post filtration (Scherbaum,1997a). For some recorders the corresponding programs can be requested (Scherbaum, 1997b).

2. SEISMOMETER SIMULATION

For the estimation of some seismological parameters (e.g. arrival times, amplitudes, periods) records with a specific seismometer response are more suitable or even required to make them comparable with related readings from standardized seismic networks (e.g. WWSSN stations). Further, the estimation of source parameters of earthquakes in the time domain requires the simulation of a broadband displacement record.

Figure 9 shows the displacement spectrum of a vertical component P-wave of an M_s=5.8 rockburst (Teutschenthal, Germany) as derived from a velocity broadband record at station TNS of the German Regional Seismograph Network (GRSN). The source spectrum, corrected for wave propagation effects, shows the typical shape: at low frequencies a constant amplitude and at high frequencies an ω^{-3} decay. The high frequency decay usually ranges between ω^{-2} and ω^{-3}. The seismic moment $M_0 = \mu A \bar{D}$ (μ - shear modulus, A - area of the rupture plane, $\bar{D}$ average static dislocation) can be derived in the frequency domain from the low-frequency amplitude level ($\omega \rightarrow 0$) of the P- or S-wave or in the time domain from the P- or S-displacement integral. Additionally, the corner frequency of the P- or S-wave spectrum (figure 9: 1.5 Hz for P) or the duration of the P- or S-pulse in the time domain allow to estimate the size of the rupture plane. Figure 9 displays a noise spectrum in addition to the P-wave ground motion spectrum. At a frequency of 0.1 Hz the noise spectrum exceeds the P-spectrum. In the given case, for $f < 0.15$Hz no signal can be recovered from the record because of the high noise level. The usable frequency range increases with increasing magnitude and decreasing epicentral distance.

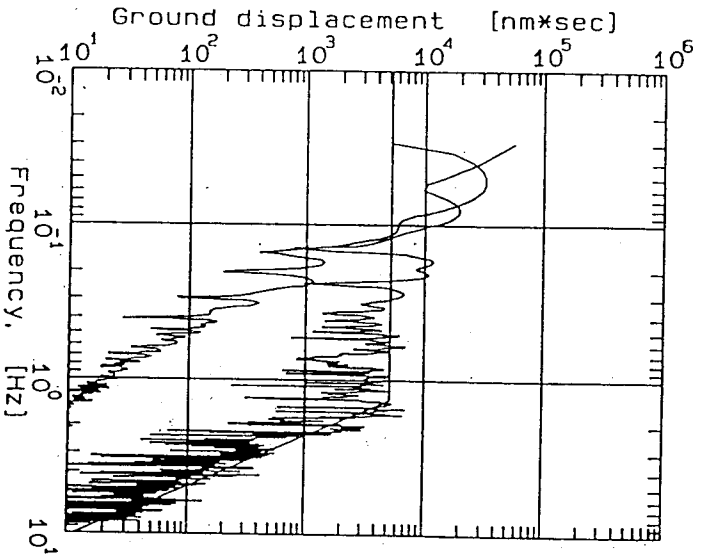

Fig. 9: Source spectrum of a P-wave record (rockburst) and related noise spectrum

Simulation theory starts with the Laplace transform L which transforms the time function f (t) into a function of the complex variable $s = \sigma + i\,\omega$ (for complete theory see Plesinger et al., 1996)

$$L(f(t)) = F(s) = \int_{-\infty}^{+\infty} f(t)\, e^{-st}\, dt \qquad (15)$$

As physical model linear time invariant systems (LTI) are adopted. They can be described by a differential equation of the general form (14) with x as input- and y as output (see equation 1 as example)

$$\sum_{m=0}^{M} b_m\, y^{(m)} = \sum_{n=0}^{N} a_n\, x^{(n)} \qquad (16)$$

(m) and (n) denote the m-th or n-th derivative. The ratio of the Laplace transform of the output signal to the Laplace transform of the input signal gives the system transfer function H(s).

$$H(s) = \frac{\sum_{n=0}^{N} a_n\, s^n}{\sum_{m=0}^{M} b_m\, s^m} = C\, \frac{\prod_{n=0}^{N} (s - z_n)}{\prod_{m=0}^{M} (s - p_m)} \qquad (17)$$

z_n and p_m , the roots of the numerator and denominator are called zeros and poles of the transfer function, respectively. When replacing s by $i\,\omega$ we get the Fourier spectrum of the transfer function (compare with equation 5).

A practical example is the transfer function of a seismometer (3) as derived above. For deriving a simulation filter H(s) one has to divide the transfer function V(s) of the desired seismometer by that of the seismometer, which was used for recording, U(s)

$$H(s) = V(s) / U(s) \qquad (18)$$

and check the result for stability. According to Plesinger et al. (1996) a transfer function is stable, if

- the number of zeros is less than or equal to the number of poles
- there are no pure imaginary poles or poles at the origin of the co-ordinate system
- the real part of all poles is negative
- both complex poles and zeros occur in conjugate pairs.

There are different methods of transition from a continuous to a sampled record. One of them is the bilinear Z-transform

$$s = \frac{2}{\Delta t} \frac{z-1}{z+1}, \qquad \Delta t \text{ is the sampling interval, z is a complex variable.} \qquad (19)$$

When replacing s according to (19) in the transfer function H(s), derived for seismometer simulation according to (18), we get an expression like

$$H^*(z) = \frac{V^*(z)}{U^*(z)} = \frac{c_0 + c_1 z^{-1} + c_2 z^{-2} + \ldots + c_n z^{-n}}{1 + d_1 z^{-1} + d_2 z^{-2} + \ldots + d_m z^{-m}} \qquad (20)$$

c_i and d_i are real numbers, V*(z), U*(z), and H*(z) are the bilinear Z-transforms of the transfer functions of the seismometer to be simulated, as well as of the seismometer which was used for recordings and of the simulation filter. The shifting theorem of the Z-transform

$$W^*(z)\, z^{-k} \equiv w_{l-k} \qquad (21)$$

states, that the multiplication of a Z-transform with z^{-k} results in a time shift of the corresponding discrete time series w_l by k samples. The application of this shifting theorem (21) converts equation (20) into a difference equation

$$v_l = c_0 u_l + c_1 u_{l-1} + c_2 u_{l-2} + \ldots + c_n u_{l-n} - d_1 v_{l-1} + d_2 v_{l-2} + \ldots + d_m v_{l-m}. \qquad (22)$$

(22) is the equation of an ARMA-filter (auto regressive moving average filter): The new filtered sample is computed from the weighted average of the current and the last n samples of the original time series u_l and the last m samples of the filtered time series v_l. Such type of filter is rather easy to program.

The bilinear Z-transform produces non-linear distortions of the frequency scale. By prewarping (inverse predistortion) the corner frequencies ω_i of the seismometers or filters using the formula (23) this effect can be corrected.

$$\omega_i = \frac{2}{\Delta t} \tan(\Delta t\ \omega_i / 2) \qquad \Delta t \text{ is the sampling interval} \qquad (23)$$

Scientific Technical Report STR 98/05
DOI: 10.2312/GFZ.b103-98055

The simulation can be stabilised by limiting the frequency range to the one within which the simulation is exact. This bandwidth depends on the noise level and on the steepness of the simulation filter. There is a complete software package for simulation filtering available (PREPROC, Plesinger et al., 1996)

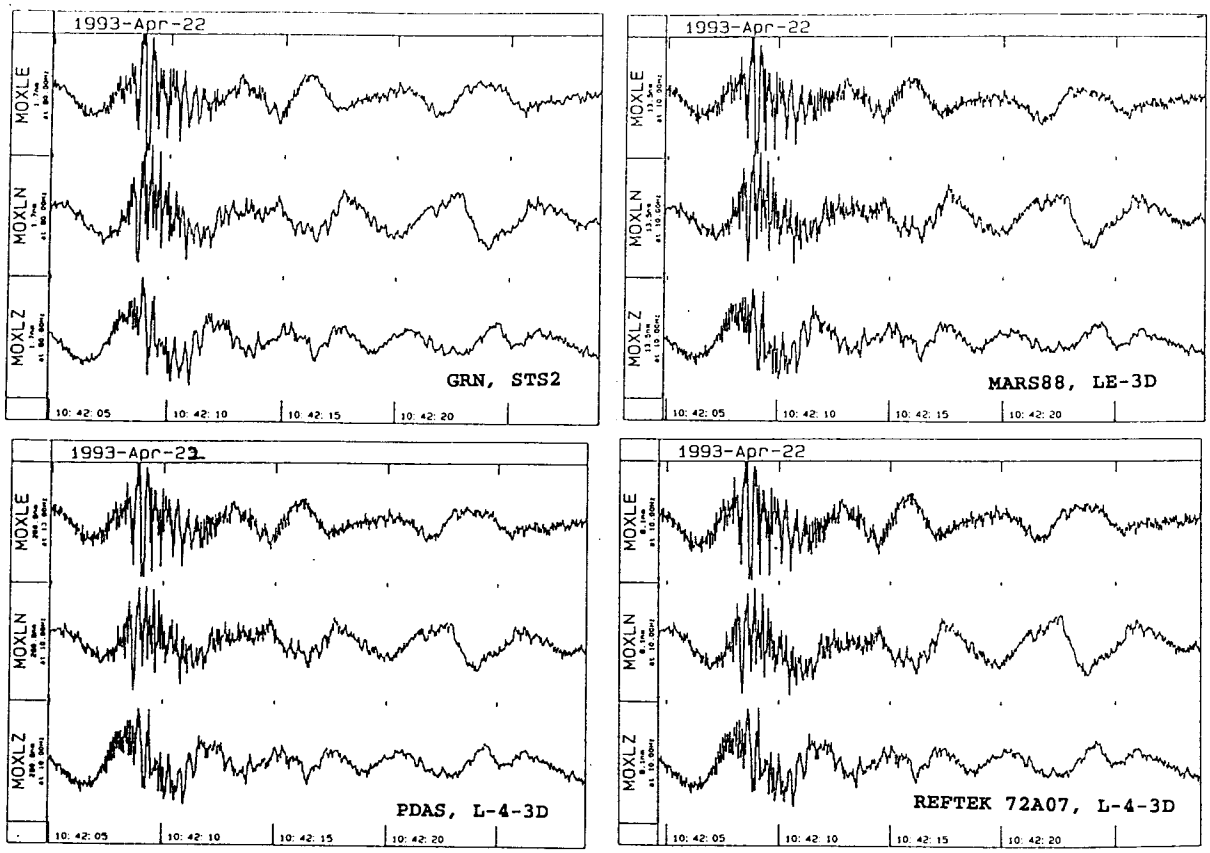

Fig. 10: Simulated records of a seismometer with an eigenperiod of 5 sec derived from records of a GRSN broadband station (200 sec)(upper left) and 2 short period (1 sec) stations left and right below. A primary record of the same event from a station with an intermediate period seismometer (5sec) is shown for comparison (upper right).

Figure 10 shows a quarry blast , recorded by 4 different systems at the same location:

1. permanent station MOX, German Regional Seismograph Network, seismometer STS2 (T=100 sec), recorder: Quanterra
2. field stations: MARS88, seismometer LE-3D (T=5sec)
   PDAS100, L4-3-D (T=1sec)
   REFTEK 72A07 L4-3-D (T=1sec).

For comparison the STS2 and L4-3-D-records were transformed into a record of a LE-3D seismometer (T=5sec). The simulated records do not show any remarkable difference.

Figure 11 shows records of an Mb=6.4 Alaska earthquake (13.5.1993) from a virtual velocity seismometer with an eigenperiod of 20 sec (damping: 0.7 of critical), derived from a broadband record (left: German Regional Seismograph Network, station BRG, seismometer

Scientific Technical Report STR 98/05
DOI: 10.2312/GFZ.b103-98055

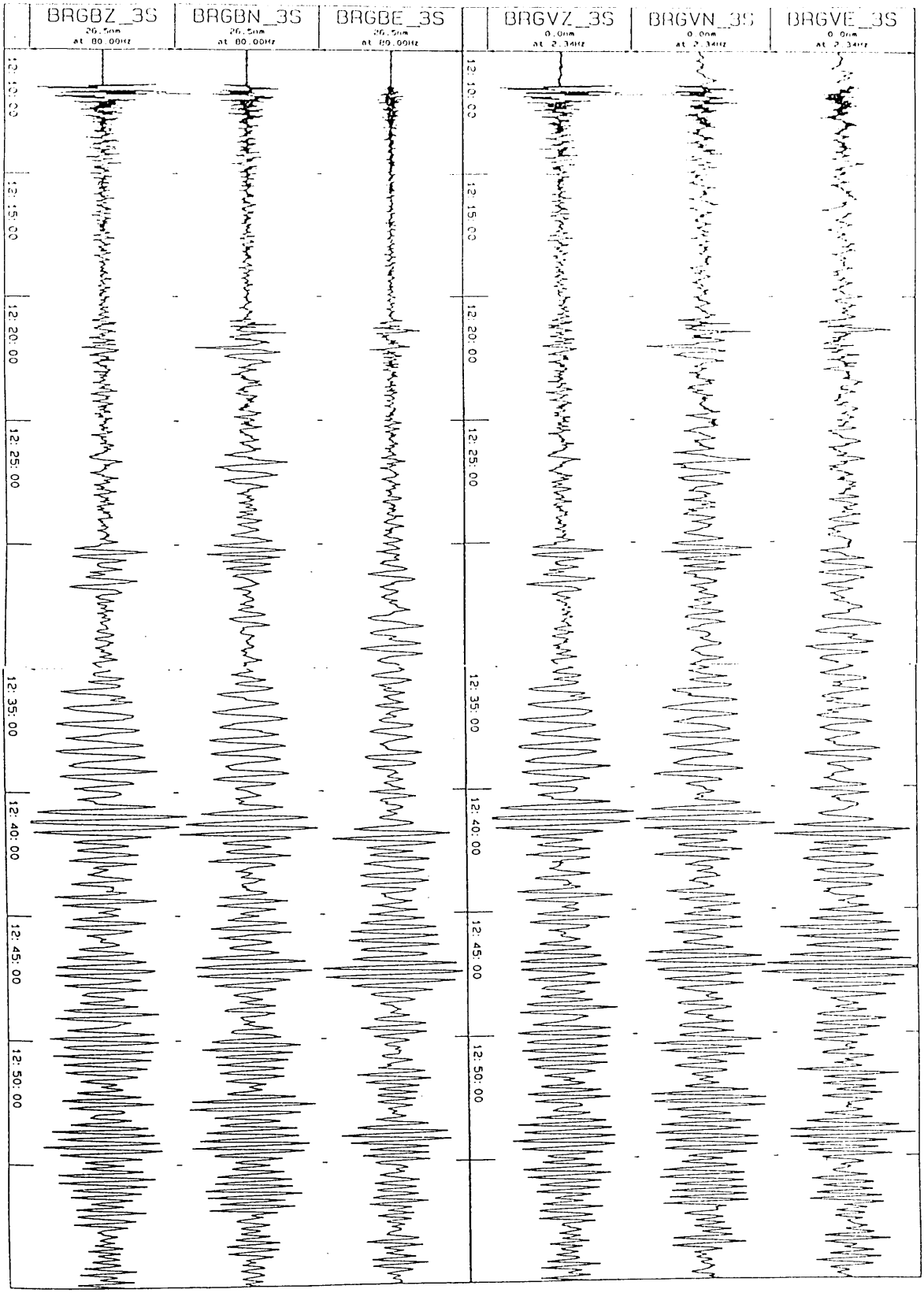

Fig. 11: Comparison of two simulations of intermediate period seismometer records (eigen-period 20 sec) derived from records of a broadband (200 sec),(left) and a short period (1 sec) seismometer (right), respectively. (Alaska earthquake, 13.5.1993, Mb=6.4)

STS2, T = 200 sec) and from a PDAS-recorder, equipped with a short period seismometer (right: Mark L4-3-D, T = 1sec). This example shows, that at least for the vertical component a good short-period seismometer can be used for simulating intermediate period records. The horizontal components of a MARK L4-3-D seismometer are mechanically less stable than the vertical component. This results in a higher noise level compared with the vertical component. The simulation of seismometers becomes important, when in the course of large projects different seismometers and data loggers are used together and the scientific objectives require a uniform station response. Further, parameter estimations in routine seismological analysis have to be derived from seismometers with internationally agreed dedicated response curves which remain unchanged over long time spans.

3. COMPARISON OF RECORDED AND SYNTHETIC SEISMOGRAMS

The normal way of deriving models of the earth structure is to extract arrival time, period and amplitude information from seismograms in order to use these data in inversion procedures (e.g. derivation of velocity models from travel time data). Waveform methods, which fit theoretical seismograms to records are usually limited to low frequencies and small velocity perturbations because of the problem to find analytical solutions for heterogeneous media with large velocity contrasts. Further, one should have rather dense station networks. The standard nowadays for calculating theoretical seismograms for local earthquakes is a horizontally layered velocity model. Programs based on the original Thompson-Haskell matrix method show instabilities at high frequencies. Wang (1997) derived a new stabilisation method which allows fast and correct computation of high frequency seismograms for point sources with a given source mechanism. This method was applied to aftershock records of the Mb=6.3 Killari intraplate earthquake of September 29, 1993.

The factors contributing to the strong damage and the high death toll (12000 people) caused by the Killari earthquake were:
1. high population density
2. occurrence at night time
3. the area was assumed to have the lowest seismic risk in India
4. traditional building style (basalt stones without cement or concrete)
5. strong ground motion amplification.

Figure 12 shows the epicentre distribution of the Killari aftershocks (Baumbach et al. 1994). They were recorded with 3 digital PDAS-stations, 4 strong motion stations and 9 analogue stations (magnetic tape records). The velocity recordings have a rather monofrequent character (Fig. 13). This is a first hint for ground motion amplification caused by a thin low-velocity surface layer. The resonance frequencies for a vertically incident S-wave are $f_n=(2n+1)V_s/4H$. H is the thickness of the surface layer and V_s is the S-velocity, n=0,1,2,... . The coda of the records is very long. This could be caused by high crustal scattering and low attenuation. The geological underground consists of granite, covered by a 300 m basalt layer and few meters of black soil. The depth of the basalt could be estimated at some places from wells. Figure 14 displays spectra at PDAS station sites with epicentre distances of 5 to 10 km. They show typical spectral peaks with an amplification of 5-8 due to the surface layer. Some of the spectra display overtones. The amplification peaks are within the frequency range of the corner frequencies of the P- and S-waves from low magnitude aftershocks. Therefore, it is impossible to estimate reliably their source parameters from the P- or S-spectrum.

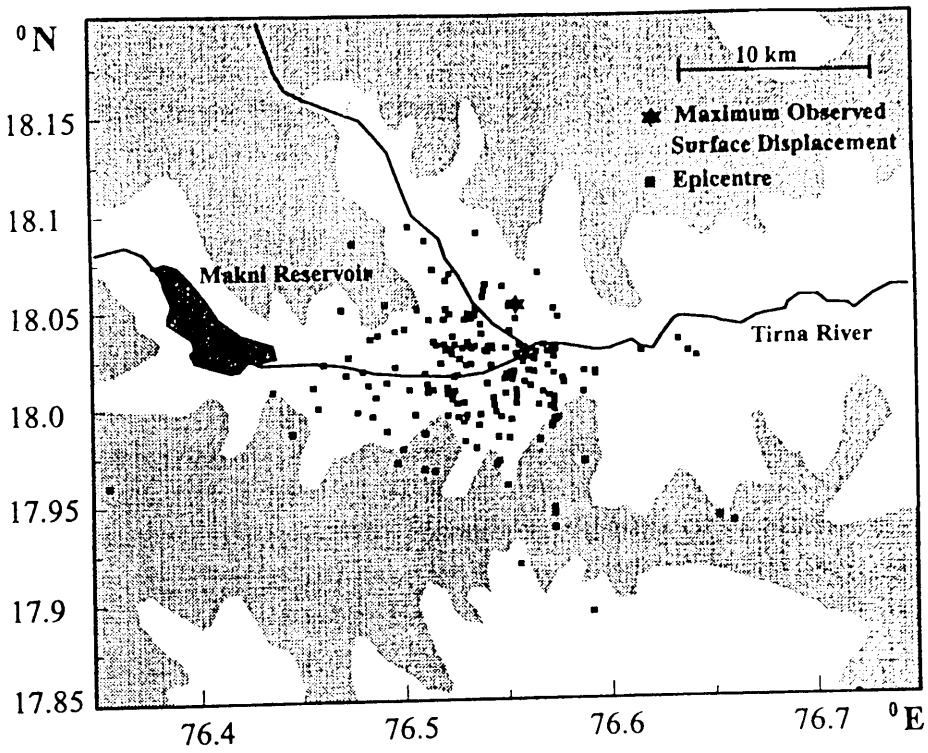

Fig. 12: Epicentres of Killari aftershocks

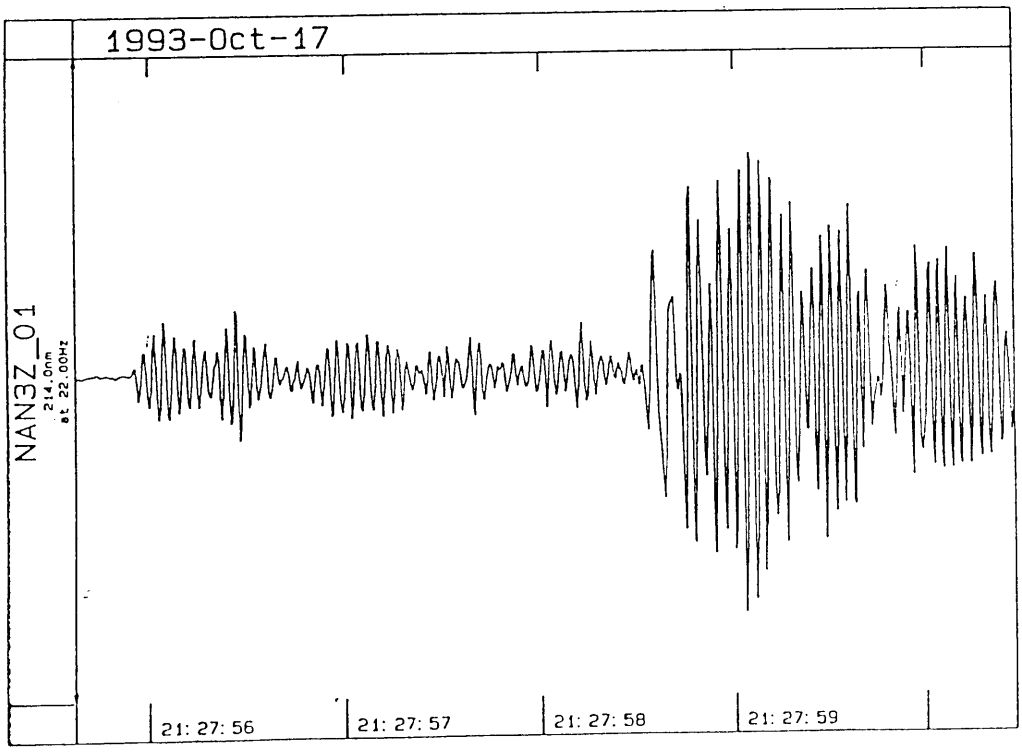

Figure 13: Velocity record of a Killari aftershock

Scientific Technical Report STR 98/05
DOI: 10.2312/GFZ.b103-98055

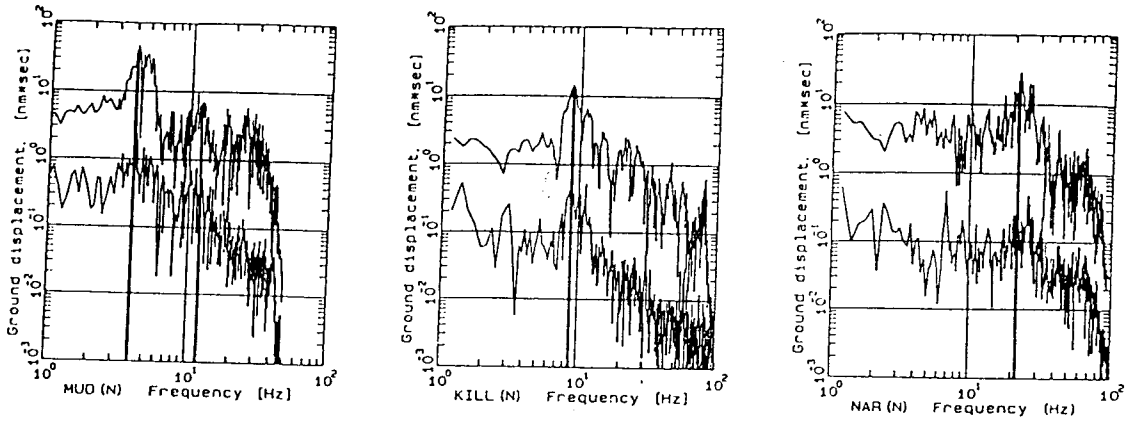

Fig. 14: Spectra of aftershocks (upper trace, horizomtal components) showing soil amplification effects. Noise spectra are indicated for comparison (lower trace).

To analyse the ground motion amplification in detail theoretical seismograms were calculated for the following velocity model:

Layer	thickness [km]	ρ [g / cm ^{3}]	V_p (km / sec)	V_s (km / sec)	Q_p	Q_s
1	0.005	1.3	1.2	0.2	80	20
2	0.300	2.5	4.5	2.6	500	220
3	∞	2.7	6.0	3.5	800	270

The assumed layer thicknesses coincide well with the results from drillings in the epicentre area of the Killari earthquake, carried out in 1996 (Gupta, 1996, personal communication).

Figure 15 shows the synthetic displacement seismograms for an epicentral distance of 20 km and a thrust mechanism. The upper three traces (radial, transversal and vertical) show the displacement at the surface, the lower ones at a depth of 5 m (soil-basalt boundary). Remarkable are the high frequency oscillations after the P- and S-onsets caused by the surface soil layer. The second onset after the P-wave at 00:00:04 could be misinterpreted as reflection from a deep crustal boundary. Both, travel time and amplitude studies showed that this is an inhomogeneous P-wave, guided at the 300 m deep basalt/granite boundary.

Finally, theoretical seismograms were computed for an aftershock and a small 3-station network with an aperture of 8 km. The 3-component seismograms were recorded by PDAS-stations. For analysis they were converted into Wood-Anderson records. The typical spectra of the stations MUD, KIL and NAR (figure 14) show different resonance frequencies: 4 Hz, 10 Hz and 20 Hz, respectively. These differences are caused by different thickness of the surface layer and result in different periods of the S-wave onset (fig. 16). The above shown velocity model gives a resonance frequency of 10 Hz and is therefore typical for station KIL. The fault plane solution was calculated from polarity readings only, because the amplitudes are strongly influensed by the surface layer. The S-wave periods and amplitudes of the Killari (KIL) radial component record are in good agreement with the corresponding synthetic seismogram. The amplitudes of the recorded and calculated transversal and vertical component records differ remarkably. The other stations show differences in periods because of the wrong model

thickness of the uppermost layer. Because of the dominant influence of the uppermost layer, a better fit could be expected when using models with different soil thickness for different stations.

The P-polarities of records and synthetics coincide for all stations. Differences in the amplitudes show that the fault plane solution calculated with only 12 P-polarities is less accurate. Further modelling with different source mechanisms, different source duration and different surface and intermediate layers could probably improve the fit.

The calculations show, that the analysis of dense network recordings of aftershocks of strong earthquakes could contribute to the estimation of ground motion amplification caused by low velocity surface layers. The results could be used for microzonation studies.

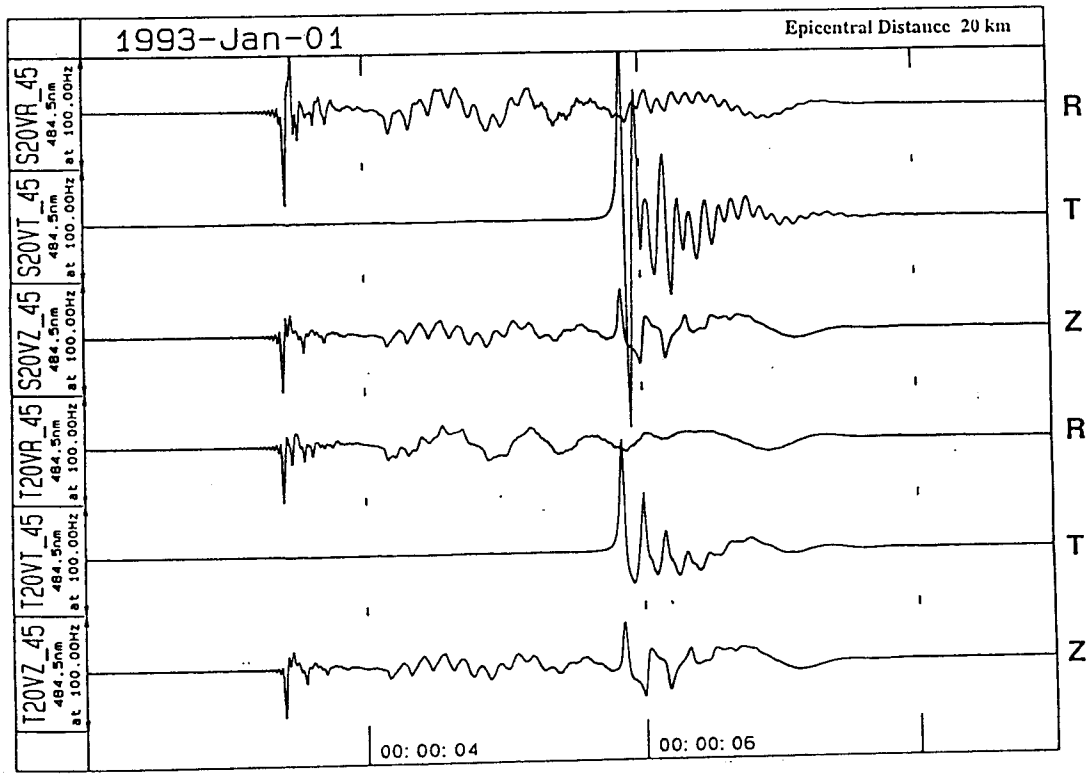

Fig. 15: Synthetic seismograms for a Killari aftershock with thrust mechanism. Upper traces: surface displacement, lower traces: displacement at 5 m depth

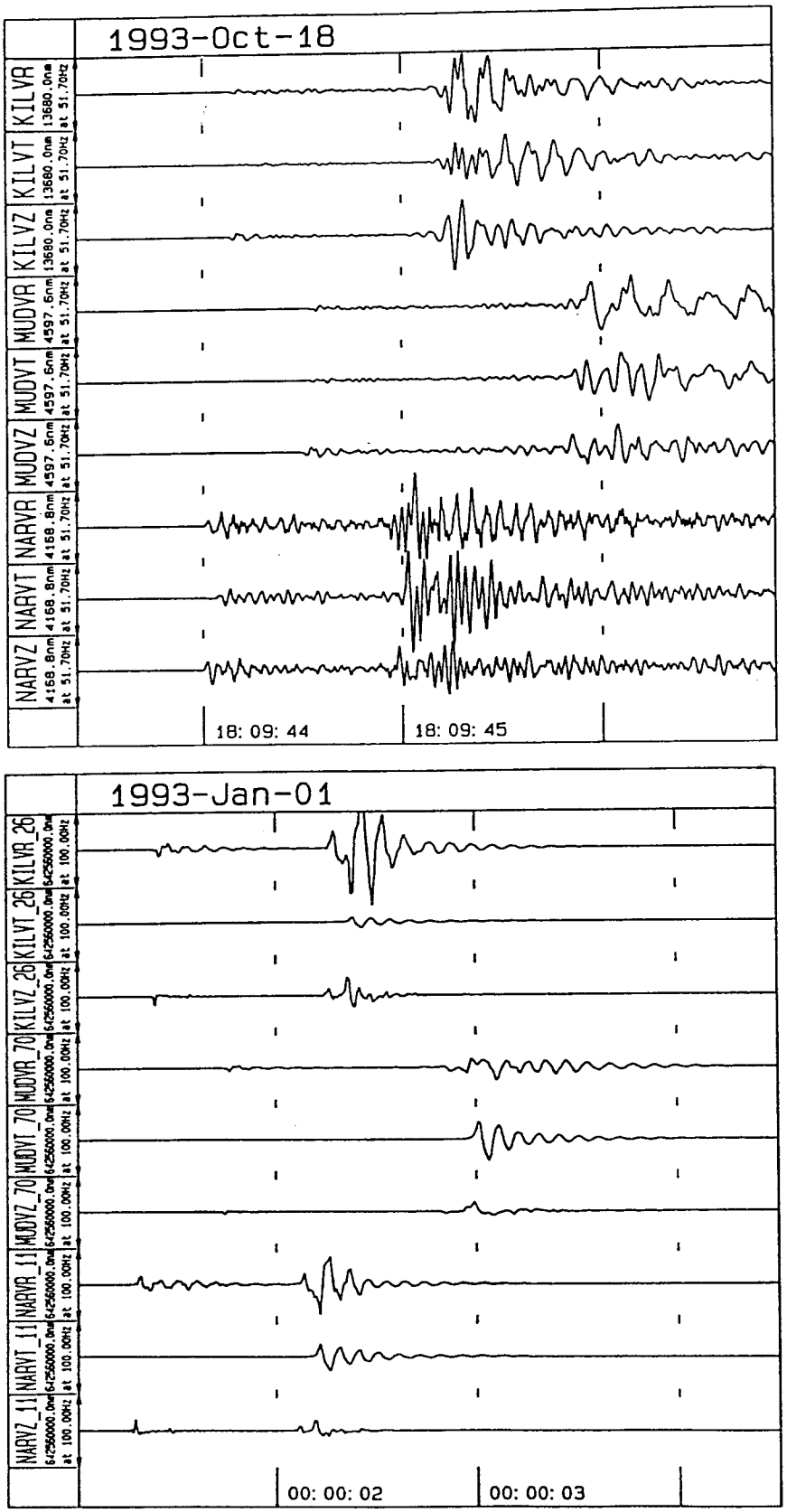

Fig. 16: Comparison of records (top) and synthetics(bottom) for a 3 station network

References

Baumbach, M., H. Grosser, H.G. Schmidt, A. Paulat, A. Rietbrock, C.V.Ramakrishna Rao, P. Solomon Raju, D. Sarkar and Indra Mohan. Latur earthquake, Memoir 35, 1994, Geological Society of India, pp. 33-63.

Baumbach, M., H. Grosser: Erprobung von Registrierapparaturen für die Task Force Erdbeben. GFZ Potsdam, 1994.

Oppenheim, A.V., R.W. Schafer, Discrete time signal processing. Prentice Hall, 1989

Plesinger, A., Zmeskal, M. and J. Zednik: Automated preprocessing of digital seismograms: Principles and software, Version 2.2, E. Bergman, ed, Prague & Golden, 1996.

Scherbaum, F.: Basic concepts in digital signal processing for seismologists. Lecture notes in Earth sciences, Vol. 53. Springer Verlag, Berlin Heidelberg, 1994.

Scherbaum, F. and M.-P. Bouin: FIR filter effects and nucleation phases. Submitted to Geophys. J. Int.: 1997a February 18.

Scherbaum, F.: Zero phase filters in digital seismic acquisition systems: blessing or cure ? Submitted to EOS: 1997b February 25.

Wang, R.: A new algorithm of wavenumber integration method for synthesising high frequency seismograms. 57. Annual meeting of the German Geophysical Society, Potsdam, March 3-7, 1997, Programme and abstract volume.

"SEISAN" INTRODUCTORY TRAINING COURSE

Jens Havskov

University of Bergen, Norway
July 1997

1. INTRODUCTION

This SEISAN training course is intended as a short introduction to SEISAN and how to use it. It assumes some knowledge of basic seismological processing and basic computer knowledge. During the course, the SEISAN manual, version 6.0, Havskov, (1997), will be used, in addition to these notes. The goal of the exercises is to be able to handle the SEISAN data base, pick phases, locate the events and display the results. There is also a short exercise in doing fault plane solutions and determining spectral parameters.
SEISAN is a large system with many options and this course will only deal with the most basic operations. However, it should hopefully be sufficient to get started with SEISAN.

2. OVERVIEW OF SEISAN

The main goal of SEISAN is to have a simple system for routine processing of all kinds of seismic observatory data, whether digital, analog, broad band, teleseismic or local data. Another important goal is to be able to store and retrieve all data in a single system so that when one analysis like spectral analysis require a hypocenter and an attenuation function, these parameters should automatically be available if obtained at some earlier time or already given in a parameter file. In SEISAN, this is achieved by having a simple event oriented data base storing all data in chronological order. Once the user has found the relevant event to work with, no other steps are needed to access all data related to this event. This requires that station coordinates, crustal models etc are stored in a standard way.

Batch processing: Since SEISAN is used for routine observations, there is also a need for processing large data sets in one go. In SEISAN, any part of or all of the database can be reprocessed with new parameters. If e.g. a new crustal model becomes available, a single command will relocate all events in the data base and give the changes in location relative to the old model. If trace plots are required for any number of events, this can also be done with one command.

Computer independent: The system operates on UNIX (mainly Sun) and PC (DOS and Windows95/NT) and all types of files can be moved between the two systems without any kind of reformatting. It is thus e.g. possible to preprocess data on a PC and move the data to Sun for further processing and storage.

Scientific Technical Report STR 98/05
DOI: 10.2312/GFZ.b103-98055

Advanced analysis: By having all parameters collected in a single data base, and by adjusting well known analysis programs like PITSA to SEISAN, further data analysis becomes much easier compared to having to reformat data for each new analysis tool. Thus SEISAN has a series of well known analysis programs integrated and has as a goal to integrate more to take advantage of the unified data base and associated formats in SEISAN.

Learning SEISAN then involves as a first major step to become familiar with the data base and how to manipulate data in the data base as well of how to input and output data from the data base. Once this is mastered, different kinds of analysis can be done following similar steps.

3. INSTALLATION

If SEISAN already has been installed, skip this section.

SEISAN for PC and Sun is normally distributed on a CD, the alternative is floppies, ZIP drive or tape. Here it is assumed that a CD is available. Normally SEISAN comes in one file, ZIP file for PC and a compressed tar file for Sun.

- Copy the file from the CD to the directory under which SEISAN is going to be installed.
- Follow the instructions in the SEISAN manual section 3. In order to get SEISAN operating with the test data included, the only parameters to set are the paths to the data base and software. The remaining parameters can be dealt with later.
Once the software has been installed and paths set, reboot the computer (on Sun, source the .SEISAN file).
- Give a command (e.g. "wo" to move to working directory) to check that it is installed. If that works, try command dirf, if no protests, the software is successfully installed.

4. BASICS OF THE "SEISAN" DATA BASE

The data is organized in a database like structure using the file system. The smallest basic unit is a file containing original phase readings (arrival times, amplitude, period, azimuth, apparent velocity) for one event. The name of that file is also the event ID, which is the key to all information about the event in the database. Although the database in reality only consists of a large number of sub-directories and files (all of which the user has access to), the intention is that by using the surrounding software, the user should rarely need to access the files directly, but rather do all work from the user's own directory using the SEISAN software.

The whole SEISAN system is located in sub directories residing under the main directory SEISMO (can have a different name). The data base and associated parameter files consist of the following:

```
REA:  Earthquake readings and full epicenter solutions in a database
DAT:  Parameter and fixed data files, e.g. station coordinates
WAV:  Digital waveform data files
CAL:  System calibration files
```

The directory structure is used as a tree like structure for quick access to individual files in the REA directory, which therefore will appear as a simple database to the user. Figure 1 shows the tree structure of the SEISAN data base.

Figure 1: Directory tree structure of SEISAN data base part.

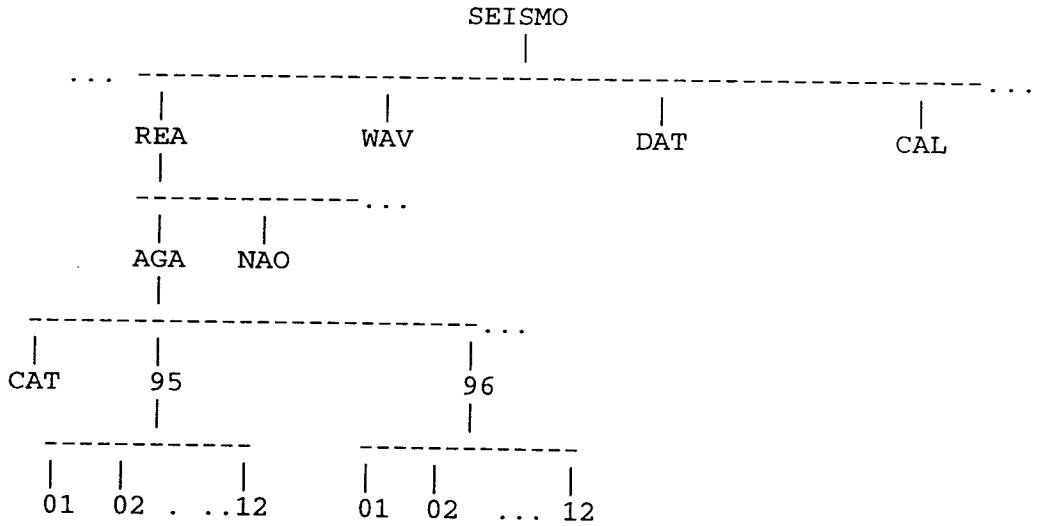

4.1 REA directory and data base

The REA directory contains phase readings and derived source information like hypocenters, fault plane solutions etc. The REA directory has one or several subdirectories corresponding to separate data bases, for simplicity it is here assumed that only the data base AGA is present (see Figure 1). For quick reference and interactive work the events are stored in single files (S-files) in yearly directories and monthly subdirectories. When new data is entered into the data base, it is stored as individual event files. However, once the interactive work has finished, the single event files are overwritten with the final location and additionally stored in monthly files, which are only changed when updating the data base.

The monthly files, called CAT-files for catalog, are stored separately in the CAT directory and primarily used for quick searching and backup for the single files.

The key files in the data base are the S-files. Each S-file contains original phase readings in the Nordic format (see example below) which includes file names of all corresponding waveform files. One event is one file. Each event has an ID line. The ID line contains a unique ID which

will follow the event through all following operations. The ID line also contains status information about the event like last action as e.g. when it was updated.

Table 1: A typical S-file

The first line is the header with origin time, location and magnitudes, in this case 2 magnitudes. The line type (last column) is 1.
The second lines gives the event ID, line type I.
The third line gives the name of the associated waveform file, in this case from Sun, line type 6.
The fourth line is a comment line, line type 3.
The fifth line is a header line for the phase lines, line type 7, followed by the phases lines, one per line. The abbreviations are:

```
Input parameters:
STAT SP     : Station and component
IPHAS       : Phase with onset
W           : Phase weight, HYPO71 style
HRMM SECON  : Hour, minute and seconds
CODA        : Coda length (secs)
AMPLIT PERI: Amplitude (nm) and period (sec)
AZIM VELO   : Azimuth (deg) and apparent velocity of arrival at station
SNR         : Signal to noise ratio for phase

Output parameters:
AR          : Azimuth residual
TRES        : Arrival time residual
W           : Weigh used in location
DIS         : Epicentral distance in km
CAZ         : Azimuth from event to station
```

```
 1993 1014 1638 24.1 L  58.285   6.356 16.0  BER  8  .8 2.6CBER 2.3LNAO        1
 ACTION:UPD 97-03-25 21:28 OP:jh   STATUS:               ID:19931014163824     I
 9310-14-1638-01S.NSN_23                                                       6
     535  SOUTHERN NORWAY, this line is comment                                3
 STAT SP IPHASW D HRMM SECON CODA AMPLIT PERI AZIMU VELO SNR AR TRES W  DIS CAZ7
 KMY  SZ EP       1638 43.75   99                                  .010  122 328
 KMY  SZ ES       1638 59.09                                       .810  122 328
 BLS5 SZ EP       1638 44.83  101                                  .210  127   3
 BLS5 SZ ES       1638 59.60                                      -.210  127   3
 ODD1 SZ EP       1638 53.18  122                                  .910  182   5
 EGD  SZ EP       1638 57.89  122                                 -.3 9  230 343
 EGD  SZ ES       1639 23.23                                      -.2 9  230 343
 BER  SZ EP       1638 59.23  105                                 -.3 9  241 346
 ASK  SZ EP       1639  0.91  113                                 -.2 9  254 344
 ASK  SZ ESG      1639 33.37                                     -1.9 9  254 344
 SUE  SN EP       1639  9.70  156                                  .2 9  322 343
 NRA0 S  EPn      1639 19.25       20.0  1.7  20.4  9.452.0 -8  -.1 9  401  49
 NRA0 S  EPg      1639 26.92            228.7  6.7 6.0  0 -1.9 9  401  49
 NRA0 S  ESn      1640 01.69            232.3  4.7 3.6  3  1.4 9  401  49
 NRA0 S  ELg      1640 15.09            222.4  3.4 6.2 -6  -.4 9  401  49
```

For more details on the S-file, see p. 195 of the SEISAN manual.

The S-files are used as input for location and, when making a permanent update, also for output. Events are classified as either L, R or D for local, regional or distant event respectively. This information is given in the header line of the S-file as well as in the S-file name.

Interactive work with the S-files in the data base is done with the program EEV. This program will enable the user to point to any event in the data base and do interactive work with that event.

The catalog in the CAT directory is accessed ONLY with the SELECT command. This command searched the data base for events of particular interest.

4.2 Waveform data, the WAV directory

This directory contains files with digital waveform data. The directory normally has no subdirectories or any other organization since there is only room for a small part of the waveform data corresponding to the entries in the REA data base. However, in case of using very large disks, WAV can also, be subdivided (see SEISAN manual).

The S-file will, in addition to seismic parameters, also have a list of waveform file names associated with the event (see example above, line type 6 lines). This means that the S-file contains ALL information about available data for a particular event.

The analysis system (like EEV) will always look in the users own directory and then in WAV for a waveform file.

4.3 Calibration data, the CAL directory

The CAL directory contains calibration files, one for each channel of digital data. For details see SEISAN manual. For this exercise, it is assumed that the calibration files are already there.

4.4 Parameter files, the DAT directory

The DAT directory contains station files, program parameter files like channels to be plotted on default. Parameters used for spectral analysis are also stored here as well as map contours. Changes to the files in this directory will only have to be done occasionally, and most often when a new crustal model is to be used or new stations added. It is assumed for this exercise, that no changes are needed.

ACKNOWLEDGEMENT

This manuscript was revised by K. Atakan and B. Storheim. B. Storheim also tested all the exercises.

REFERENCES

Havskov, J (1997), editor. The SEISAN earthquake analysis software for the IBM PC and SUN. Version 6.0. Manual, Institute of Solid Earth Physics, University of Bergen, Norway.

EXERCISES ON THE USE OF "SEISAN"

Jens Havskov
University of Bergen, Norway

In all the following exercises, a reference to a page number, means reference to the SEISAN manual.

Exercise 1: Interactive work with the data base using EEV

COMMANDS CAN BE ENTERED IN UPPER OR LOWER CASE EXCEPT ON SUN WHERE PROGRAM NAMES MUST BE GIVEN IN LOWER CASE.

SEISAN has test data in the default data base AGA from October and November, 1993. Due to limitations of space on the distribution, there is only digital data for a few of the events. For details of EEV, see p 24.

Always work in the work directory \seismo\wor, use command "wo" to get there.

Type "eev 9310", that points you to the first event for October, 1993. You will see the essential information about the event (p 28) like origin time, location and magnitude. The letter L, R or D indicate whether it is a local, regional or distant event. To move around the data for that month, try the following commands (terminated with a CR)

Return: go to next event
"b" : move back one event
"11": move to event # 11
"d12": move to the first event on the 12'th or later

The event shown, can be operated on with several commands (upper or lower case), try these:

t: type the event (S-file) to see the parameters
tt: ---------- only header line
e: edit event file
l: locate event
d: delete event (do not confirm !!)

Note: The editor is NE on PC and vi on Sun. To change to another editor, see p 12.

To see all commands, type "?"

Question 1.1
How many events does the month have ?

Question 1.2
How many local, regional and distant events are there ?

Question 1.3
What happens when you type return when positioned at the last event of the month ?

Question 1.4
Locate an event: The last output line gives the location in decimal degrees. How does that location compare to the data base location ?
Edit the event (command "e") and change one of the P-readings by 5 seconds. Locate again, what is the difference in the location ? Examine the details of the location in file print.out. This can be done from EEV with command "one print.out" (PC) or "ovi print.out" (SUN). "o" in front of "ne" means giving the command ne to the operating system.
How many iterations was used to locate the event ?

Question 1.5
Position at event October 4 at 2021. Edit the event and add the following reading to the event:
Station BER, component SP, Phase P, time 20 22 29.0
Exit from the editor and relocate event. Does the new station appear on the output ? How much did the location change ?

Question 1.5
Try command "c" (p 26). Explain what it does and check that it works.

Question 1.6
Try command "r" (p 26), explain what it does.

If you have SEISAN installed on a Windows95 system, try the same commands, see p 30.

Question 1.7
As mentioned above, not all events have digital waveform files available. Make a crosscheck between the file names of waveform file names in the WAV directory (type WA to go there) and the events in the data base (check for line type 6 in the S-file) to find which events have digital data available.

Exercise 2: Selecting data from the data base and making an epicenter map

An important task is to extract data out of the data base for further analysis like epicenter plotting or exchange with other agencies. If the data base has been updated meaning that data is available in the CAT directory, this is most easily done with the SELECT command, otherwise use the COLLECT command (p 93). These commands will extract data out of the data base data in any given time interval, and the SELECT program can in addition use many selections criteria (magnitude, location etc) to further limit the data extraction. The data is extracted to one file in the same format with events separated with blanks. For this exercise, only the SELECT program will be used.

Go back to WOR directory with command "wo". Start select program with command

SELECT, use time limits 9310 to 9311 and default data base. When menu comes up, select magnitude limits (6), give limits, make another return (see also p 89). You will now get an output file select.out with selected events. Edit the file to see what it looks like.

Question 2.1
How many events were selected out of the total available ? How many waveform files were available for these events ? How was the distribution of local, regional and distant events ?

Plot the selected events using command EPIMAP. Follow instructions, p 82,
use defaults for most parameters and select.out as input epicenter file name. The latitude - longitude range should be 59-63 and 0-20 respectively.
EPIMAP generates a file epimap.cmd with the plot commands every time it runs. This file can be edited to run the same map with e.g. a new input file. Try the command "epimap epimap.cmd" to plot the same map again without answering questions.

Question 2.2
When the plot is on the screen, try commands "p" and "z", explain what they do.

Exercise 3: Putting new dat into the data base

Data can come into the data base in two forms, parameter data and/or waveform data (see exercise 4). For this exercise, it is assumed that parameter data (readings) are available either from a different agency or entered manually through SEISAN program NEWEVE. For the exercise, a test file with readings from August 1995 is available (file name august.95 in DAT directory). The format is the same as used in all other S-files and CAT files. In order to put he data into the data base, the necessary directory structure must be in place. If not already there, create it with command MAKEREA (p 15). Make a directory structure for all of 1995 and use data base name AGA.

Question 3.1
How many directories were made with MAKEREA ?

Now that the directory structure is in place, the data is put into the data base with program SPLIT (p 94), which splits up the input file with many events to single S-files in the data base.

Question 3.2
Use EEV on the month of August 95, and find how many events there are.

Exercise 4: Plotting digital data

Digital data is plotted and analyzed with program MULPLT. The program is capable of doing general phase picking, correct for instrument response, produce ground corrected seismograms for determining Ml, Mb or Ms, determine azimuth of arrival for 3 component stations and do

spectral analysis. The program can also read in theoretical arrival times for global phases for help in identifying phases.
MULPLT operates either as a database independent program (started with command MULPLT) or in connection with the data base (started from EEV with command "p"). If the program works independently of EEV, it will create an output file mulplt.out in Nordic format - with the readings and results of spectral analysis.
Running MULPLT using command MULPLT, the program asks for a file name or file number of a waveform file. To use the number, it is assumed that a list of interesting files has first been created and numbered in a file FILENR.LIS using command DIRF, see p 96. By giving the number, the file corresponding to the number is used. By giving a "?", the list with numbers is displayed and a new number can be given. In the first exercise, MULPLT will be used from EEV.

- Start EEV on October 93
- Move to an event with digital data
- Type "p" to plot. When first question comes up, answer "0" and make 2 returns (p 52-53)
- When plot comes up try the following:
  Get options: Click on the "MENU" bar. MENU or single letter commands can be used (p 61)
  zoom: Put cursor to the right, push mouse left button or space bar, move mouse to the left, repeat
  Back to original: Do in reverse order (right - left)
  Filter: Click filter limits (e.g. ".1-1.0") 0.1 to 1.0 Hz, click on "Plot" or push "x" followed by "r"
  Push "b" , then "r" (filtered from 5 to 10 hz)
- Select channels: Click on "Other" and select channels or click on channel name on left hand side and type "r" or click on "Plot"
- Plot one channel at a time: Click "Togle", back to multi trace, click "Togle"
- All commands are one key press or click on menu, to see all type "?" or click on "Help"
- Quit by typing "q" or click on "Quit", you are now back to EEV

Plotting events directly with MULPLT without using the data base:

Move to \seismo\wav directory: "wa"
Make a list of waveform files: "dirf 9*.*", use all files starting with 9
Check list of files : "type filenr.lis", on Sun "cat filenr.lis"
Plot event : "mulplt", give event number e.g. "2", then option "0"
Plot next event in list : Press "f" or click on "Next"

In this way, many events can sequentially be plotted for quick inspection.

Question 4.1: Are all available channels plotted ?

Putting a new digital recorded event into the data base:
- Start MULPLT, when asked about filename, answer "?" to get the event list, select the event from August 95, use option "0" to plot the event.
- When event is on the screen, click on "Regis" and answer questions (event is local) (p 62), then quit.

The event is now put into the data base as a new event. Check that it is there by using EEV on August 95.

Question 4.2
What information is now available for the August event in the data base ?

Exercise 5: Phase picking

Phases picked will enter the data base and, when plotting from EEV, phases already present in the S-file will be shown on the plot (p 62). In this exercise, phases will be picked and put into the data base.

- Start EEV for August 95
- Move to event on August 22 at time 1:40 using the "d22" command
- Plot event with "p"

Question 5.1: Are there phases picked already for this event ?

- Go back to EEV and type the event with command "t"

Question 5.2: Are there readings available in the data base (S-file) ?

- If readings are already present, edit the event and delete all phase lines (lines below the phase header line), DO NOT DELETE OUTER LINES.

- Plot event in multi trace mode. When the traces are on the screen, move cursor to the P-phase for the first trace, press "1", move to the S-phase press "8" and to the end of the coda and press "c" (phase keys are defined on the top of the screen in single trace mode). As the phases are picked, they will be displayed. Do the same with the remaining traces and quit.

- Check readings available : "t" for type to see readings

Question 5.3: How many phase lines are present in S-file ?

- Locate event : "l"

Question 5.4: Does the location and magnitude look "reasonable", how big is the RMS and how large is the largest residual ?

The above phase picking was done in multi trace mode. For more detailed picking, use single trace mode (p 61):

- Plot event, when menu comes up, make a return, next comes station selection, just click on "ok". The first trace is then shown and you zoom in on that to make picks. The phases are now picked on the lower trace. Zoom in on some the previous picks. Pick phases with polarity (p 63). Try zoom on top trace before selecting window for lower trace (p 54).

Question 5.5: What is the advantage of using single trace mode compared to multiple trace mode when picking phases ?

- In EEV, use command "update" (p 28), explain what happens, what changes do you see in the S-file ?

Exercise 6: Magnitude determination

All currently used magnitudes can be determined with SEISAN. In exercise 5, coda magnitude was calculated, here we shall calculate local magnitude Ml, body wave magnitude Mb and surface wave magnitude Ms. In order to determine magnitudes based on amplitudes, response information must be available in the system. The response files have already been installed in the CAL directory for this exercise. The definition of the magnitude scales are given on p 40-41.

Local magnitude Ml

In order to determine Ml, amplitudes must be read on a Wood Anderson seismograph. In SEISAN, the original trace is corrected for instrument response and converted to a synthetic Wood Anderson trace (p 65). Then the maximum amplitude is read.

- Select the August event from exercise 5, plot the event in single trace mode. Select Wood Anderson trace by clicking on "WA", select a window around the maximum amplitude. The lower trace will now show the Wood Anderson simulated trace with amplitude scale of nanometers. Pick the amplitude (p 63) and store with an E-phase. Do the same for all stations and exit plot.

Question 6.1
Inspect the amplitude readings in the data base (S-file), how do the amplitudes vary with distance ?

- Locate the event. At the end of the listing, the magnitudes calculated for each station is shown.

Question 6.2
How well do the Ml values for the different stations agree ?

Body wave magnitude Mb

Mb is defined using SP seismographs with a peak gain around 1 sec. Modern SP instrument have a flat velocity response from 1 to e.g 20 Hz so, like for Ml, SEISAN simulates the old SP response (p 65).

- Select event October 2,1993 at 9:45, plot the signal in single trace mode. Click on "Mb" button and select a window around the P-phase. On the lower trace, the corrected seismogram will appear. Pick amplitudes for several stations and exit the plot.

- Locate event, the magnitudes will appear for each station as for Ml.

Question 6.3
How well do Mb for different stations agree, how do they agree with PDE magnitude (found in S-file) ?

Surface wave magnitude

Ms is supposed to be read near the 20 sec period. In SEISAN, this is simulated by making the ground correction and filtering between 16 and 24 secs (p 66).

- Select event November 11, 1993 at 00:29, plot the signal in single trace mode. Since this data is from a broad band station, it must be filtered to "see" the signals. Try with filter 0.01 0.1 Hz on the LZ channel. Click on "Ms" and select a window around the surface waves. On the lower trace, read the maximum amplitude, go to next trace with "F" and quit.

Question 6.4
What is the period and amplitude read (remeber units) ?

- Locate the event.

Question 6.5
How does your determined Ms compare to the PDE magnitude (found in S-file) ?

Exercise 7: Fault plane solution

In SEISAN, the fault plane solution can be determined with first motions (p 122).

- Select the August 1995 event and determine polarities for all stations. The polarities are best seen when using zoom in zoom in single trace mode. Fix the depth to 20 km (p 44). Then chose option "f" and proceed with the fault plane solution (p 122).

Question 7.1
How well is the solution restrained ?

Exercise 8: Spectral analysis

The standard displacement spectral analysis determining seismic moment, stress drop and source radius can be done with SEISAN (p 71). As with other parameters, the results of the analysis is stored in the data base. In addition to the spectral parameters, the moment magnitude Mw will also be determined using the seismic moment and the hypocentral distance (p 72). It is therefore important, that before doing any spectral analysis, that the data base has been updated, meaning that epicentral distances are store in the data base.

- Select the August 1995 event, plot in single trace mode
- Click on "Spec" on the menu and select a window around the S-waves (about 10 - 20 secs long), select displacement spectrum when question comes up. The displacement spectrum is now displayed. With cursor, select the 3 points defining the spectral level and slope (p 76), enter "f" and the spectral values are displayed. Enter "f" again and the values are stored in the S-file. Quit the plotting program.

Question 8.1
Are the spectral parameters stored in the S-file ?

Question 8.2
How does the Mw magnitude compare to Ml ?

Question 8.3
How big is the stress drop and source radius ?

Exercise 9: Reading global phases using IASPEI91 tables

The IASPEI91 travel time tables can be used to help reading phases (p 64). In order to calculate the theoretical times, the hypocenter and origin time must be known. In SEISAN, this means that the data is available in the S-file in the header line or another hypocenter line (type 1). Chose event on November 11 at 00:29.
- Calculate theoretical times: Command "iasp". This will calculate theoretical arrival times for all stations given in the S-file.

- Plot event: Command "p", select LPZ channel and plot with filter 0.01-0.1 Hz. The theoretical phase swill now be displayed with a prefix "y" and displayed below the trace. There will be very many phases, try to zoom to identify a few.

Question 9.1
Which phases could be identified ?

Question 9.2
Try to identify phases pP for event October 2, 1993 at 9:45. Relocate after identifying the phase(s), what can you say about the depth ?

HOW TO RETRIEVE DATA FROM IRIS/USGS STATIONS

Sue McLafferty

Albuquerque Seimic Lab, Kirtland AFB East, Bldg. 10002, Albuquerque,
New Mexico 87115, U.S.A., Fax: +1-505-846-6973, Email: sue@asl.cr.usgs.gov

1. OVERVIEW

Data can be retrieved from the IRIS/USGS stations in either decompressed ASCII format or in compressed binary (SEED) format.

Choices of ACSII format data include "Expanded variable record length ascii", "Expanded fixed record length ascii" and "SAC ascii digital counts". There is a limit of 10.000 samples per request (8.3 minutes of 20 sample/second data). SEED data is a much more efficient way to transfer and store data than ascii data but requires a program that will decode the data (such as DIMAS or rdseed). The limit per request varies from hours to days of data depending on the sample rate of the data. The method of data retrieval depends both on the desired data format and the type of connection available between the analysis computer and the IRIS/USGS station computer.

To access the IRIS/USGS computer at the user's station, the user can set up either a direct serial connection or a LAN (Local Area Network) connection. The direct serial connection requires that a cable be connected from a serial port on the analysis computer to a serial port which is configured as a spare terminal on the IRIS/USGS computer. The LAN connection requires that network software (including TCP/IP programs telnet and ftp) be running on the analysis computer and that the appropriate ethernet cable and transceiver are available.

Remote IRIS/USGS stations can be accessed either by dial-up (telephone) connection or by an Internet connection depending on the station. The dial-up connection requires that the analysis computer be connected via a modem to a phone line. The Internet connection requires that you have access to the Internet and that the analysis computer has the programs telnet and ftp. For a current list of station phone numbers and network addresses, contact the Albuquerque Seismic Labs (a list current to 10/97 is attached to this handout). The list is also available on the web site http://aslwww.cr.usgs.gov/stations/dialup.html.

2. HOW TO RETRIEVE DECOMPRESSED ASCII DATA

The basic method for retrieving ASCII format data is to capture/log a retrieve session to a file on the analysis computer. A retrieve session entails connecting to the IRIS/USGS station and logging in as user=seed and password=data. This starts a program called retrieve which allows the user to select and transmit the requested data.

Scientific Technical Report STR 98/05
DOI: 10.2312/GFZ.b103-98055

The method that is used to log the retrieve session and connect to the station computer will depend on the type of analysis computer and the software running on the computer. For a PC running Windows95, the program Hyperterminal will allow the user to connect to the station computer through a direct serial connection or by dial-up connection. The Transfer menu option "Capture Text" will allow to user to log the retrieve session. The Windows95 program Telnet will allow the user to make a network connection to the station (either a LAN or Ineternet connection). The Terminal menu option "Start Logging" will allow the user to log the retrieve session.

Once the user is connected to the station computer, the retrieve session will be the same no matter what method was used to connect to the computer. The following is an example of a retrieve session to request SAC ascii data. The session is annotated with comments delimited by asterisks (*comment*):

OS-9/68K V2.4 Motorola VME147 - 68030 97/10/03 19:52:49

User name?: seed *Enter seed for the User name*
Password: *Enter data - the Password will not be displayed*
Process #29 logged on 97/10/03 19:52:53
Welcome!

WELCOME to the Global Telemetered Seismograph Network (GTSN) - DP

...please wait

Data Retrieval System / GTSN - DP / GT1X

Please type your name and organization - up to 50 characters:
****
sue mclafferty - asl *Enter your name and organization*

Data Retrieval System / GTSN - DP / GT1X
Copyright 1986-1994 by Joseph M. Steim & Quanterra, Inc.
Retrieve (C) 1986-1994 - Release 35/06-1213- 68020- FPU

type ? for help

Command? ? *Enter ? to display the help menu shown below*

Data Retrieval System / GTSN - DP / GT1X
Retrieve (C) 1986-1994 Quanterra, Inc. - Release 35/06-1213- 68020- FPU
"C <C/E>" = Change buffer from/to continuous/event data
"T <V/F/C/CS/S/P>" = select Transmission file format
"F <W/S/L/V...>" = select optional Filters

"E [ALL]/<DATE> <DATE> [<SEEDNAMES>]" = Examine available data or logs
"S <SEEDNAME> <DATE>" = Setup single data channel to retrieve
"G" = start or resume sending selected segment
"G P[LOT]" = Plot selected segment on 4014 terminal
"G <S/B>" = Store selected segment to local/backup file
the following 4 methods are available for SEED binary transfer:
"K <SEEDNAMES> <DATE> <DATE> [MAXREC] [TIMETOL]" = via Kermit
"X <SEEDNAMES> <DATE> <DATE> [MAXREC] [TIMETOL]" = via STP
"V <SEEDNAMES> <DATE> <DATE> [MAXREC] [TIMETOL]" = archiVe local file
"I <SEEDNAMES> <DATE> <DATE> [MAXREC] [TIMETOL]" = via uuencode
"R" = send station description
"L[|B|C] [ALL]" = view entries in event, caliB, or Clock Log
"P" = display active Processes
"U <N>" = view User log <N> entries backward
"Y[T] <N> [<M>]" = view [<M>] activitY log <N> entries backward
"M <message text>" = send Message to station operator
"Q" = Quit on-line session. CTL-"C" is ABORT key.
<SEEDNAMES> supports wildcards (i.e. BH?,?LZ,???) and DET|CAL|TIM|MSG

Command? t *Enter t to select the transmission format*

Possible transmission formats are:

"C" - Compressed hexadecimal ascii
"CS" - Compressed hexadecimal ascii SEED
"V" - Expanded variable record length ascii
"F" - Expanded fixed record length ascii
"S" - SAC ascii digital counts
"X" - Exit to main command menu

Transfer mode? s *Enter s to select SAC ascii digital counts*

Current transmission mode is SAC ascii

Transmit card numbers with each line of data? (y/n): n *Enter n for no*
card numbers
Command? s bhz 97/10/2 1:00:00 *Select the channel and start time for*
data retrieval
...scanning available channels

Search requested starting at 1997/10/02 01:00:00

Time window begins in segment 4 at buffer record 14419

Maximum number of samples to transfer? 25 *Select number of samples*
limit=10000 samples

Buffer server is processing your request

skipping first 1759 samples...
transmission will begin at requested starting time within -0.009113 sec

...event detector on in record starting at 1997/10/02 00:58:32

Use the "G" command to begin transmission
or to re-transmit data received incorrectly.

Command? g *Enter g to transmit the data*

Start (31) and end (35) cards to transmit?<CR> *Enter <CR> for all cards*

```
   0.0500000 -12345.0000000 -12345.0000000 -12345.0000000 -12345.0000000
  -0.0091130    1.1908870    0.0000000    0.0000000    2.0000000
-12345.0000000 -12345.0000000 -12345.0000000 -12345.0000000 -12345.0000000
-12345.0000000 -12345.0000000 -12345.0000000 -12345.0000000 -12345.0000000
-12345.0000000 -12345.0000000 -12345.0000000 -12345.0000000 -12345.0000000
-12345.0000000 -12345.0000000 -12345.0000000 -12345.0000000 -12345.0000000
-12345.0000000   40.5800018  -122.5400009  300.0000000 -12345.0000000
-12345.0000000 -12345.0000000 -12345.0000000 -12345.0000000 -12345.0000000
-12345.0000000 -12345.0000000 -12345.0000000 -12345.0000000 -12345.0000000
-12345.0000000 -12345.0000000 -12345.0000000 -12345.0000000 -12345.0000000
-12345.0000000 -12345.0000000 -12345.0000000 -12345.0000000 -12345.0000000
-12345.0000000 -12345.0000000    0.0000000    0.0000000 -12345.0000000
-12345.0000000 -12345.0000000 -12345.0000000 -12345.0000000 -12345.0000000
-12345.0000000 -12345.0000000 -12345.0000000 -12345.0000000 -12345.0000000
   1997    275      1      0      0
     0      6      0      0     25
 -12345  -12345  -12345  -12345  -12345
     1      1     11  -12345  -12345
 -12345  -12345     40  -12345  -12345
 -12345  -12345  -12345  -12345  -12345
 -12345  -12345  -12345  -12345  -12345
     1      1      1      1      0
GT1X  H972750100ZVBB
-12345 -12345 -12345
-12345 -12345 -12345
-12345 -12345 -12345
-12345 -12345 -12345
-12345 -12345 -12345
-12345 -12345 -12345
-12345 -12345 -12345
    2649.0     2649.0     2649.0     2649.0     2649.0
    2650.0     2649.0     2649.0     2650.0     2649.0
    2649.0     2649.0     2650.0     2649.0     2649.0
    2649.0     2649.0     2649.0     2649.0     2649.0
    2650.0     2649.0     2650.0     2649.0     2649.0
```

Command? q *Enter q to quit the retrieve session*

...normal termination

...vbb data retrieval system logged out

IMPORTANT NOTE: Do not close the Hyperterminal or Telnet window before entering "q" to quit the retrieve session.

Once disconnected from the computer, the user should close the log session file. Depending on the analysis application, the file will probably need to be edited to remove all extraneous command lines (non-data).

The following is an example of expanded variable length ascii format data:

GT1X 1997/10/02 01:00:00 -0.009113 SEC Z VBB 20.00 SPS UNFILTERED 25

2649 2649 2649 2649 2649 2650 2649 2649 21193
2650 2649 2649 2649 2650 2649 2649 2649 21194
2649 2649 2649 2649 2650 2649 2650 2649 21194
2649 0 0 0 0 0 0 0 2649

The following is an example of the expanded fixed length ascii format data:

GT1X 1997/10/02 01:00:00 -0.009113 SEC Z VBB 20.00 SPS UNFILTERED 25

2649	2649	2649	2649	2649	13245
2650	2649	2649	2650	2649	13247
2649	2649	2650	2649	2649	13246
2649	2649	2649	2649	2649	13245
2650	2649	2650	2649	2649	13247

3. HOW TO RETRIEVE SEED DATA

Since SEED data is in binary rather than ascii format, the procedure to log a retrieve session will not work. Two of the available procedures entail making a file on the IRIS/USGS computer and then transferring the file

For data requests using a direct serial connection or dial-up connection, the Windows95 program Hyperterminal will allow the user toconnect to the station computer. The retrieve program option "K" is used to generate a file which is then transferred to the analysis computer using Kermit protocol. See the "Procedure to retrieve data using Kermit" in the DIMAS (Display, Interactive Manipulation and Analysis of Seismograms) operations manual for the details.

For data requests using a network connection, the telnet program will allow the user to connect to the station computer. The retrieve program option "V" is used to create an archive local file. The program ftp (on the analysis computer) is used to transfer the file to the analysis computer and delete the file from the IRIS/USGS computer. See the "Procedure to create and copy a SEED data file via the network" in the DIMAS manual for details.

If the user is running the DIMAS software on the analysis computer, the DIMAS program NETRD will also allow the user to retrieve SEED data using a network connection. This is the preferred method as it does not create files on the IRIS/USGS computer disk.

Scientific Technical Report STR 98/05
DOI: 10.2312/GFZ.b103-98055

Scientific Technical Report STR 98/05
DOI: 10.2312/GFZ.b103-98055

GeoForschungsZentrum Potsdam

Global Seismograph Network

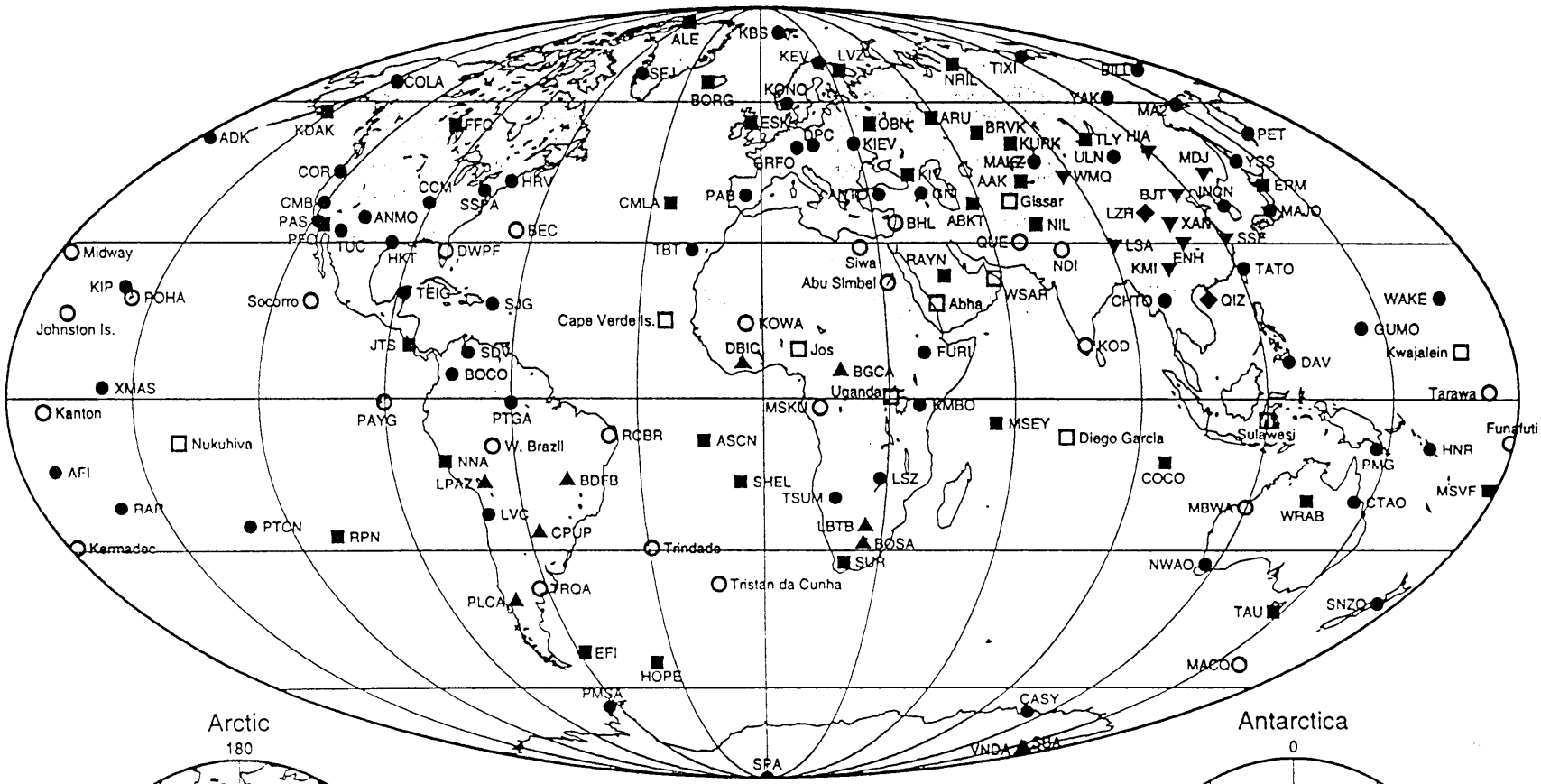

USGS Albuquerque Seismological Laboratory

September 1997 (RLW/CRH)

Station Phone numbers and Internet Addresses

A phone line or internet connection enables many IRIS/USGS Global Seismic Network stations to provide users data recorded within minutes of a data request. The table below contains the current phone number and/or internet addresses available for digital data retreival from IRIS/USGS GSN stations. The Data Collection Center updates the table whenever changes or additions occur.

Contact the Data Collection Center, webmasters@asl.cr.usgs.gov or (505) 846-5646, for information regarding accounts and passwords for data retrieval from stations.

The most recent change to the table occurred on 2 Sep 1997, 11:27:13 MDT.

Station	Location	Phone Number	Internet Address	Notes
ADK	Adak, Alaska	907-592-3724	-	-
AFI	Afiamalu, Western Samoa	685-27-028	-	-
ANMO	Albuquerque, New Mexico	505-846-0384	anmo.cr.usgs.gov	-
ANTO	Ankara, Turkey	90-312-210-1273	-	-
BILL	Bilibino, Russia	4217-62-25742	-	NOTE: limited success with the dialup at present time.
BOCO	Bogota, Colombia	5-71-338-4537	200.3.149.8	-
CASY	Casey, Antarctica	672-12-846	-	-
CCM	Cathedral Caves, Missouri	314-245-6555	-	-
CHTO	Chaing Mai, Thailand	66-53-220-506	-	-
COLA	College, Alaska	907-474-5913	cola.giseis.alaska.edu	-
COR	Corvalis, Oregon	541-737-0853	-	-
CTAO	Charters Towers, Australia	61-7-3365-2374	ctao.seis.uq.edu.au	-
DAV	Davao, Philippines	63-82-97-1290	-	-
GNI	Garni, Armenia	-	194.67.210.253	-
GUMO	Guam, Marianas Islands	671-637-4647	202.128.5.75	-
HNR	Honiara, Solomon Islands	677-25-165	-	-
HRV	Harvard, Massachusetts	508-456-3099	hrv.harvard.edu	NOTE: The telnet connection is not working at this time.
HKT	Hockley, Texas	512-346-3292	129.116.194.225	-
INCN	Inchon, Republic of Korea	82-273-46988	incn.kma.go.kr	-
KBS	Ny-Alesund, Spitzbergen	47-79-027129	193.156.10.249	-

KEV	Kevo, Finland	358-16-678550	-	-
KIEV	Kiev, Ukraine	380-41-222-7206	-	-
KIP	Kipapa, Hawaii	808-689-7413	140.90.183.151	-
KMBO	Kilima Mbogo, Kenya	254-2-445896	-	-
KMI	Kunming, Yunnan Province, China	86-871-5212583	-	NOTE: limited success with the dialup at this time
KONO	Kongsberg, Norway	47-55-32-6101	kono.ifjf.uib.no	-
LSA	Lhasa, Tibet, China	86-89163-39567	-	-
LSZ	Lusaka, Zambia	260-1-250-774	-	-
LVC	Limon Verde, Calama, Chile	56-55-322-407	165.182.34.175	-
MAJO	Matsushiro, Japan	81-262-78-9393	-	-
MA2	Magadan, Russia	7-413222-0154	194.87.56.194	-
MDJ	Mudanjiang, China	86-453-652-8858	-	-
NWAO	Narrogin, Australia	61-9-295-2880	-	-
PAB	San Pablo, Spain	34-2-541-6132	-	-
PET	Petropavlovsk, Russia	7-415-22-59136	195.9.105.45	-
PMG	Port Moresby, New Guinea	675-326-0864	-	-
PTGA	Pitinga, Brazil	55-92-723-1194	-	-
RAR	Rarotonga, Cook Islands	6-82-27-446	-	-
SDV	Santo Domingo, Venezuela	57-61-840	-	NOTE: The dialup does not work presently, this may be problem with local telephone company VSAT.
SFJ	Sondrestrom Fjord, Greenland	299-113-69	-	-
SJG	San Juan, Puerto Rico	787-263-5934	-	-
SNZO	South Karori, New Zealand	64-4-472-3833	131.203.44.28	-
SPA	South Pole, Antarctica	-	199.4.250.15	NOTE: The satellite is only visible for about 6 hours a day - expect a large failure rate.
SSE	Sheshan, Shanghai, China	86-21-57654170	-	-
SSPA	Standing Stone, Pennslyvania	814-667-4486	-	-
TSUM	Tsumeb, Namibia	264-672-20717	-	-
TATO	Taipei, Taiwan	886-2-783-9920	140.109.80.44	-

Scientific Technical Report STR 98/05
DOI: 10.2312/GFZ.b103-98055

TBT	Taburiente, Canary Island, Spain	34-22-24-4679	-	-
TIXI	Tiksi, Yakutia, Russia	7-41167-53434	-	NOTE: Dialup is currently inoperative
TUC	Tucson, Arizona	520-621-1733	-	-
ULN	Ulanbatar, Mongolia	-	202.131.1.100	-
WAKE	Wake Island	808-424-2148	-	-
WMQ	Urumqi, Xinjiang Province, China	86-991-2625262	-	-
XAN	Xian, China	86-29-5954447	-	-
YAK	Yakutsk, Russia	7-41122-6-28-21	194.87.244.5	-
YSS	Yuzhno Sakhalinsk, Russia	75-0441-62518	193.124.51.66	-

ISOP AND GARNET
(Notes on Two Projects for International Data Exchange and Cooperation in Seismology)

Eric Bergman

Global Seismological Services, 601 16th St., #C390
Golden, Colorado 80401 USA
Phone/fax: +1 (303) 278-4089 ,Email: bergman@seismo.com

1. INTRODUCTION

The concept of an International Seismological Observing Period (ISOP) was first discussed among seismologists over 10 years ago. Over the years, the project has at times moved forward rapidly, with healthy levels of funding and dedicated personnel. For the past few years, the project has been somewhat dormant, but continues to be a frequent topic of discussion and planning among seismologists interested in the long-term health of seismology as a global observational science. Regardless of any specific observations which may be carried out under ISOP, it has proven to be a very useful concept in providing seismologists with a point of reference concerning the kinds of activities which are needed to ensure continued productive work in this field throughout the world.

In this lecture I will discuss the reasons why a project like ISOP is important for global seismology, and to convince you that ISOP is more of an organizing principle than a specific set of observational or scientific exercises which need to be accomplished. In other words, the goals of ISOP are best met by a variety of activities arising from the legitimate needs and interests of seismologists who are involved in operating seismic observatories worldwide.

The GARNET (Global Alliance of Regional Networks) project is a relatively recent off-shoot of ISOP which at the moment represents perhaps the most active part of the ISOP community. It is an excellent example of adaptation of the ISOP concept to specific national and regional initiatives in seismology. I will discuss the scientific basis of GARNET briefly, and focus on the organizational aspects in order to emphasize the fact that the best way for seismologists to make progress in a field which is chronically underfunded (or funded inappropriately) is to exploit opportunities for COMMUNICATION, COOPERATION, AND COORDINATION.

2. ORIGIN OF ISOP

The idea for ISOP was originated by Prof. Thomas Jordan of MIT in the mid-1980s when he made a tour of many seismic observatories worldwide. He was struck by the great variations he encountered. In some places observatories were fully staffed by enthusiastic and well-trained seismologists who routinely analyzed all records thoroughly and reported readings to international data centers. In others he found facilities barely fulfilling the basic requirements of observatory operation and contributing little or nothing to global data collection and exchange.

Scientific Technical Report STR 98/05
DOI: 10.2312/GFZ.b103-98055

The easy answer for how to improve such sad circumstances is: more money, more equipment, and more people with more training. But we all know this rarely is possible, and then usually only for a few years after a major earthquake. The rest of the time, seismology is mostly ignored. Yet the value of seismological data lies to a large extent in maintaining long-term high quality observational programs. So how can we bring about any significant improvement without large investments of money? How can seismologists maintain observatory operations at a professional level during the lean years? The answer is that through enhanced levels of communication, cooperation, and coordination, seismologists can make optimal use of the instrumentation, resources, facilities and personnel available, build stronger arguments for increased local support of seismology (especially in the "out-years" between major earthquake disasters), and build morale and professionalism of observatory staff, and continue to contribute vital data toward solution of first-order scientific problems.

Therefore, ISOP is not so much a specific scientific exercise or research project, but rather a strategy for making the best use of limited resources, and which can be expected to yield a variety of benefits, including direct contributions to the science of seismology. It is necessary to have examples of how such a strategy can be implemented, and the ISOP project is closely identified with a particular application related to secondary body wave phases. However it must be remembered that the real point of ISOP is to stimulate additional ideas along these lines which meet the real needs of seismological researchers and observatory personnel.

3. EXAMPLES:

3.1 Enhanced reporting of secondary bodywave phases

This effort is based on several simple observations:

1) Secondary bodywave observations are of great importance to a variety of major seismological research efforts.
2) Such phases are not reported as often as they could be.
3) The geographical pattern of reporting is currently very uneven and yields biased estimates of Earth structure
4) The geographical distribution of readings and their quantity and quality could be greatly improved with a simple observational program based on special "ISOP Events" for which participating stations would make a special effort to do a full analysis, and also forward the data to international data centers.

Efforts are underway to start such an observing program, and all interested persons are encouraged to participate at whatever level is comfortable for them.

3.2 Station-based analysis of digital seismic data

This effort grew out of the project discussed above when it became clear that the spread of digital seismic stations is actually inhibiting the traditional task of seismogram analysis at many observatories. There seem to be three main reasons:

1) The dangerous attitude that digital stations are "special" and do not need to be routinely analyzed as analog records once were.
2) Difficulty in gaining access to the digital data stream at the stations, particularly the very high quality "global" broadband observatory stations for which the standard procedure is to send data tapes away to a distant data center.
3) Inadequacy of software to support routine analysis. Research-grade software is often very inappropriate for routine processing.

The ISOP project has been a consistent champion of the view that the health of global observational seismology requires that seismologists be able to carry out efficient and effective routine analysis of data from their local stations. This has several desirable effects:

1) It greatly improves the maintenance given to stations, reduces down-time, improves data quality, and lowers maintenance costs.
2) It is essential for the training of new generations of seismologists, and maintenance (or even growth!) of seismological expertise in developing countries.
3) It reduces the amount of data which is never analyzed at all - the dirty secret of seismology.

Later in this course we will demonstrate some software which has been developed recently to help address this problem at IRIS/GSN stations. It is not a complete answer_no one software package ever could be_but it is necessary to constantly maintain a focus on this need, and to encourage development of appropriate software at every opportunity. A corollary to this effort is the need to organize and distribute effective training in certain aspects of digital signal processing which have a great influence on the analysis of digitally-recorded data.
Seismologists need to help each other in this effort, because no funding agency is likely to support a global campaign to deal with these problems in their infinite variations from observatory to observatory. A solution will require the commitment of seismologists at all levels of the global infrastructure.

4. GARNET: SECOND GENERATION ISOP

The idea for Global Alliance of Regional Networks came to Hiroshi Inoue a few years ago as a natural merging of two other projects, ISOP and the Japanese J-Array project. Fortunately, this idea also coincided with the announcement of a major new scientific initiative in Japan, called Superplume. Superplume is an umbrella project which includes a variety of geophysical observing programs aimed at the broad understanding of the structure and dynamics of the Pacific upwelling of the same name. Thus, it needed to have an international (hemispheric) scale, which is rather new for Japanese earth scientists.

4.1 J-array

The J-Array experiment was conceived by Prof. Ando, starting in the early 1990s, as a way to circumvent the notorious difficulty in Japan of exchanging data from the many regional seismic networks. The networks were mostly operating short-period instruments with various forms of telemetry and digital recording at a network data center. Partly the problem was political, and

Scientific Technical Report STR 98/05
DOI: 10.2312/GFZ.b103-98055

partly technical and logistical. Ando was inspired in part by the success of Vidale and Benz in using huge stacks of California network data, which were all available from one source (the USGS) to study weak secondary phases and deep-Earth structure.
Ando succeeded in establishing a program in which all participating networks were supplied with a standard mass-store device (MO-drive) which made a continuous record of selected channels in a standard format. The cartridges were mailed periodically to a central office, where they were combined with the data from all other networks, and then waveform sections from the entire country-scale J-Array network were extracted for events of interest, usually large (especially deep) events near Japan. But excellent records of teleseisms were obtained as well, and a whole generation of young Japanese researchers found ample material for PhD theses and published papers in this data.

4.2 The extension to GARNET

Inoue recognized that J-Array-style networks could be created from regional and national networks throughout the Pacific region and make a strong contribution to the Superplume project. In addition he understood the philosophy of the ISOP project and saw the potential benefits to participating networks and to the practice of global observational seismology.
The basic concept for GARNET, then, is that hardware, software, and training will be supplied to participating networks at no cost. The nature of hardware required will vary from network to network, but the standard situation is assumed to be a network of short-period instruments with analog telemetry to a network center. GARNET hardware is a complete digital acquisition and analysis system based on PC technology, with GPS timing, mass-store capability, networking, and peripherals. There will be a capability to run Windows-based software and also Unix-based software, through a freely-distributable Unix clone OS. Software will include advanced programs for normal network analysis, advanced research analysis, and array analysis.
Representatives of participating networks will be brought to special training courses in Japan, and possibly at regional training centers, for training in hardware installation and maintenance, and software use. This is paid by the Superplume project also. The only obligation of participating networks is agreement to exchange data for selected (ISOP) events. Each network will receive back all the waveform data submitted by all participating networks, on CD-ROM. The first training course is being held this December in Tsukuba, Japan, with representatives of about 10 pilot networks.

4.3 GARNET down the road

Because of the scientific focus of Superplume, funding for GARNET networks is limited to the Pacific region and Asia. Clearly it is desirable to see the GARNET concept expanded globally, however, and discussions are beginning on ways to do this in other regions. Some existing networks could participate in the data exchange program of GARNET with no additional hardware upgrades, and this will be encouraged.

Another step for GARNET would be to move data exchange to the Internet as that becomes more widely available. Then the process could become almost completely automated, and form the basis for a variety of regional data exchange programs aimed at improving the ability to carry out national monitoring programs.

5. SUMMARY

I hope these ideas have at least given you a sense of how important it is for seismologists to keep in mind the global perspective as you make decisions about your organization's activities, and your own career. Seismology is an inherently global science that cannot afford to lose sight of the fact that we make progress only through an extremely complex system of voluntary cooperation. There is no shortage of data around_in fact we are drowning in it! The challenge is to see if we can find ways to work more effectively with each other to do something useful with it.

If you interested in learning more about either the ISOP or GARNET projects, please contact me.

Scientific Technical Report STR 98/05
DOI: 10.2312/GFZ.b103-98055

BANDWIDTH-DEPENDENT TRANSFORMATION OF NOISE DATA FROM SPECTRAL INTO TIME DOMAIN AND VICE VERSA. PART I: INTRODUCTION AND METHODOLOGY

Peter Bormann

GeoForschungsZentrum Potsdam, Division 2: Solid Earth Physics and Disaster Research
Telegrafenberg, D-14473 Potsdam, Germany

1. INTRODUCTION

Noise data for site quality assessment are collected with a wide range of instruments, both analog and digital, of different bandwidth, resolution and transfer functions. Accordingly, noise appearence in seismic records, amplitude- and frequency-wise, differs as do the various kinds of noise spectra derived therefrom. They are not easily comparable amongst each other and with older presentations of noise "spectra" derived from analog records. This is illustrated by the following figures. Fig. 1 represents a kind of classical noise spectrum as derived by visual amplitude and period readings in analog seismic records. Depicted are the envelops of the maximum and minimum peak amplitudes of seismic noise that might be expected on land in rural environment over a rather long interval of time (about one year).

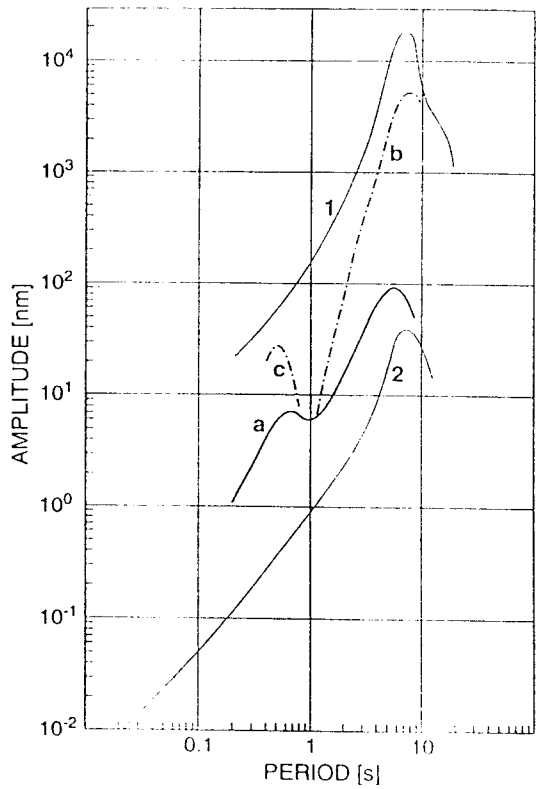

Fig. 1. Envelopes of maximum and minimum peak amplitudes for rural environments as determined from analog records of different type over a long time-span according to Brune and Oliver (1959) (curve 1 for high-noise sites and curve 2 for very low-noise sites) together with envelope curves of peak noise amplitudes at station MOX in Germany at times of minimum (curve a) and maximum noise (curves b and c).

Scientific Technical Report STR 98/05
DOI: 10.2312/GFZ.b103-98055

The new global high noise and low noise models (NHNM and NLNM) published by Peterson (1993) in units of dB referred to 1 $(m/s^2)^2/Hz$ are depicted in Fig. 2. They represent the upper und lower bound envelopes of a cumulative complilation of representative ground acceleration power spectral densities $\mathbf{P_a}$ determined for noisy and quiet periods at 75 world-wide distributed digital stations. Peterson's original curves have been complemented by us with the respective curves $\mathbf{P_v}$ and $\mathbf{P_d}$ calculated according to equation (8) below.

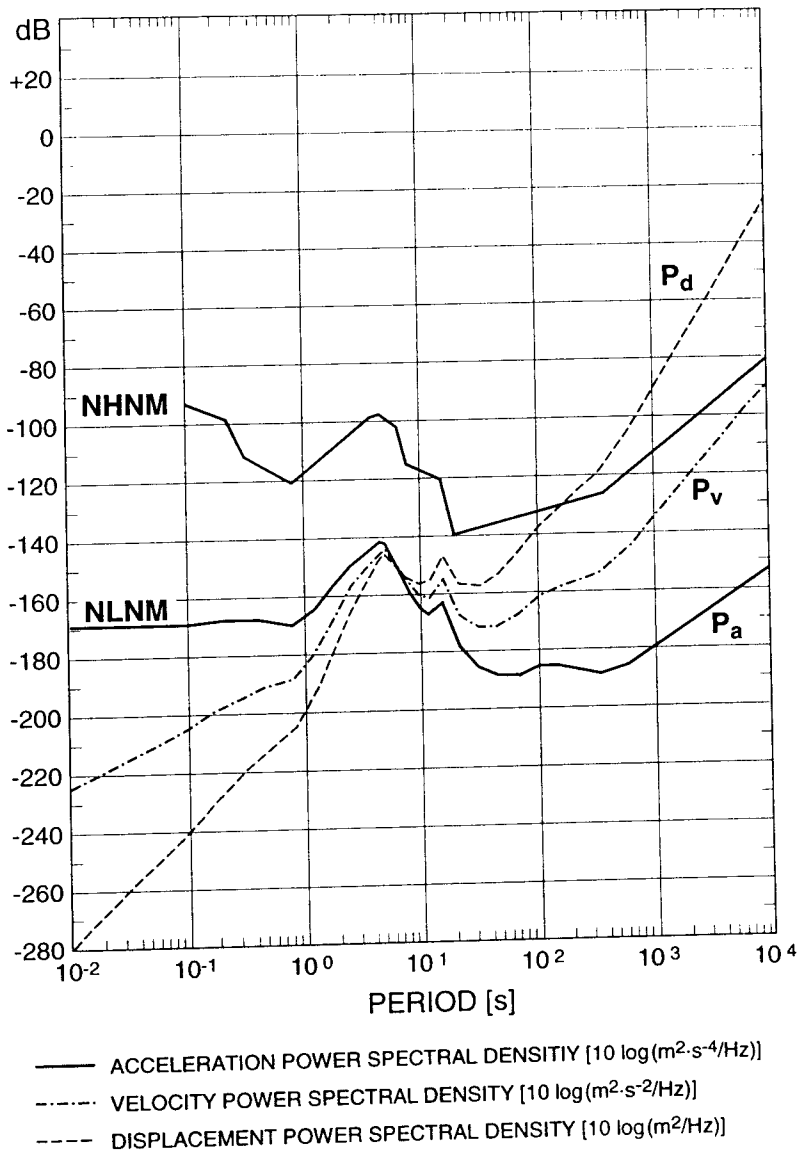

Fig. 2. Envelope curves of the new global high (NHNM) and low noise model (NLNM) according to Peterson (1993) in units of dB related to 1 $(m/s^2)^2/Hz$ and the respective curves calculated by the author for the displacement and velocity power spectral density $\mathbf{P_d}$ and $\mathbf{P_v}$ in dB related to 1 $(m/s)^2/Hz$ and 1 m^2/Hz, respectively.

Other presentations of global ambient seismic noise and signal conditions were presented by Aki and Richards (1980) in form of ambient noise velocity power density spectra (Fig. 3) and of amplitude spectral density for seismic waves and noise (lower bound) (Fig.4).

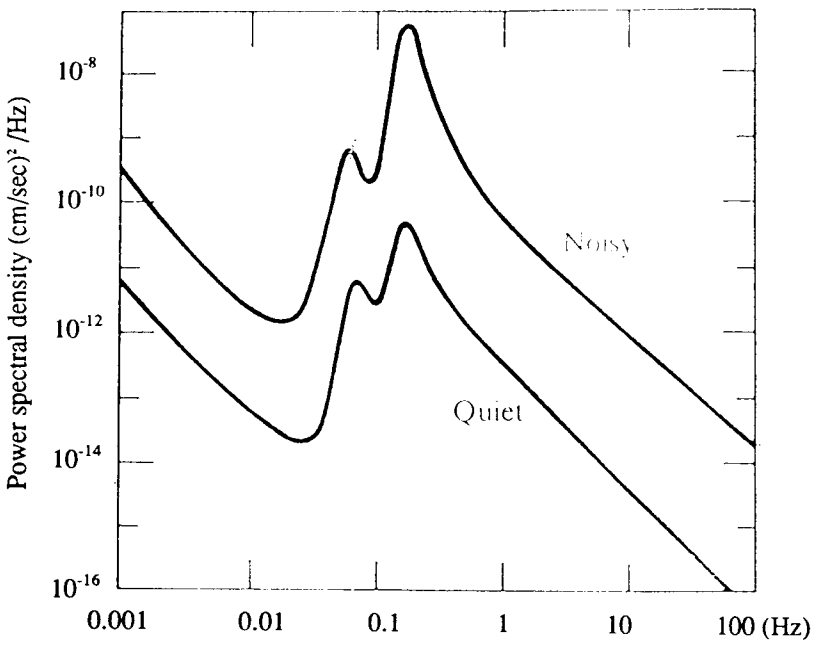

Figs. 3: Velocity power spectra of ambient seismic noise at noisy and quiet conditions for a typical station on hard basement rock (from: QANTITATIVE SEISMOLOGY: THEORY AND METHODS, Volume 1 by Aki and Richards © 1980 by W.H. Freeman and Company. Used with permission).

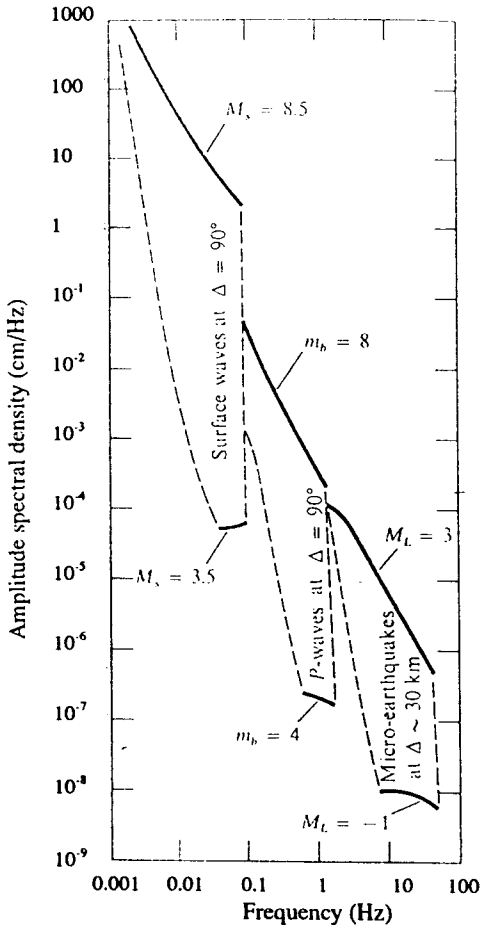

Fig. 4 Ranges of amplitude spectral densities for seismic waves. The lower bound is limited due to ambient seismic noise (from: QANTITATIVE SEISMOLOGY: THEORY AND METHODS, Volume 1 by Aki and Richards © 1980 by W.H. Freeman and Company. Used with permission).

Finally, we present in Fig. 5 a 15 s record segment of ambient seismic noise from a local seismic station site investigation carried out in NW Iran (left) together with the related displacement power density spectrum (right).

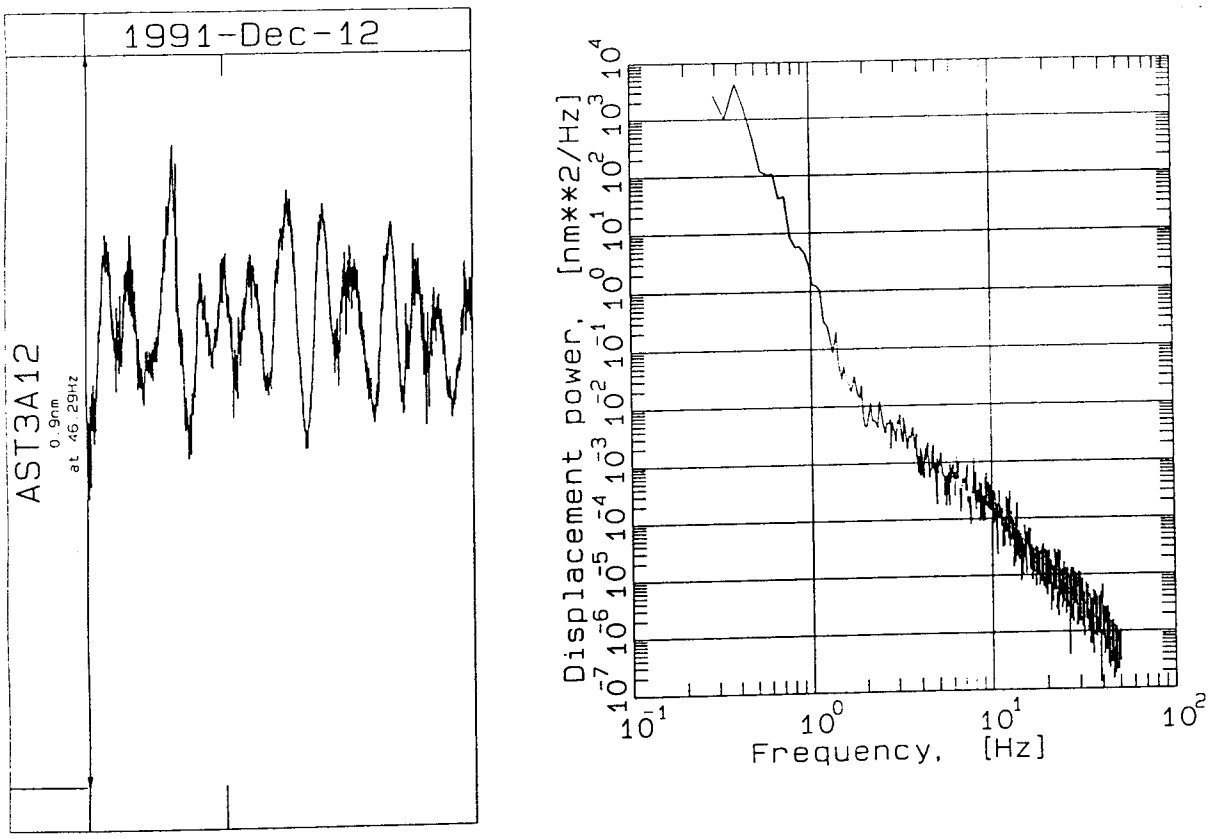

Fig. 5: Record section of seismic background noise at a quiet site in NW Iran (left) together with the related displacement power spectral density spectrum (right). The latter was calculated from 6 moving and 50% overlapping intervals, 4096 samples long each, i.e. from a total record length of about 80 s.

With the following exercise we want to demonstrate that characteristic values from all these different spectral presentations can be transformed into one another and that both old „classical" noise presentations and modern ones derived from digital data correspond to each other rather well within the limits of accuracy and representativeness.

But having determined noise power density spectra from digital records it is not so obvious what this means in terms of ground motion amplitudes and appearance of noise in records of different bandwidth and vice versa. Therefore, we present below not only the relationships to be used for the convertion of power and amplitude spectra into different kinematic units but also for calculating from spectral representations of seismic noise for different bandwidth the related frequency-dependent root-mean-square (RMS) or average peak amplitudes (APA). These relationships will then be practiced in the following exercises.

Scientific Technical Report STR 98/05
DOI: 10.2312/GFZ.b103-98055

2. CONVERSION OF SIGNAL AND NOISE SPECTRA INTO DIFFERENT UNITS

Nowadays digital recordings allow proper computational spectral analysis. For a transient signal f(t) the Fourier transform F(ω) exists with

$$F\omega) = \int_{-\infty}^{\infty} f(t) \exp(i\omega t)\, dt = |f(\omega)| \exp^{i\phi(\omega)} \quad \text{and} \tag{1}$$

$$f(t) = (2\pi)^{-1} \int_{-\infty}^{\infty} F(\omega) \exp(-i\omega t)\, d\omega. \tag{2}$$

$|F(\omega)|$ is the *amplitude spectral density* with the unit m/Hz and $\phi(\omega)$ the *phase-delay spectrum* with the units deg, rad or 2πrad. But contrary to *coherent transient seismic signals* f(t) of finite length, as in seismograms from explosions or earthquakes, irradiated by defined localized sources, *ambient seismic noise* is a more or less *stationary stochastic process* without a defined phase-delay spectrum. Therefore, a more suitable spectral presentation of seismic noise is the *power spectral density* P(ω). It is the Fourier transform of the autocorrelation function $P(\tau) = < f(t)\, f(t+\tau) >$, i.e.

$$P(\omega) = \int_{-\infty}^{\infty} P(\tau) \exp(i\omega\tau)\, d\tau. \tag{3}$$

The symbol < > indicates averaging over the time t. Depending on whether f(t) is a displacement (d), velocity (v) or acceleration (a) record, P(ω) is given in units m^2/Hz, $(m/s)^2/Hz$ or $(m/s^2)^2/Hz$.

When converting displacements $x = a_d \sin\omega t$ into the related velocities dx/dt or accelerations d^2x/dt^2 then one has to consider that the respective velocity and acceleration amplitudes are $a_v = a_d\, \omega$ and $a_a = a_d\, \omega^2$, respectively, with $\omega = 2\pi f$ (f - frequency in Hz). Consequently, knowing the displacement power spectral density value $P_d(\omega)$ one can calculate the respective values of the velocity (P_v) or acceleration power spectral density (P_a), i.e.

$$P_v(\omega) = P_d\, \omega^2 = 4\pi^2 f^2\, P_d \tag{4}$$

and

$$P_a(\omega) = P_d\, \omega^4 = 16\pi^4 f^4 P_d = 4\pi^2 f^2 P_v \tag{5}$$

or vice versa.

If the power spectral density is expressed in units of dB referred to 1 $(m/s^2)^2/Hz$ it can be written as:

$$P_a[dB] = 10 \log (P_a / 1\ (m/s^2)^2/Hz). \tag{6}$$

When substituting in (4) and (5) the frequency f by the period T = 1/f in s we get:

$$\mathbf{P}_v[\mathrm{dB}] = \mathbf{P}_a[\mathrm{dB}] + 20 \log (T/2\pi) \quad (7)$$

and

$$\mathbf{P}_d[\mathrm{dB}] = \mathbf{P}_a[\mathrm{dB}] + 40 \log (T/2\pi) = \mathbf{P}_v[\mathrm{dB}] + 20 \log (T/2\pi). \quad (8)$$

Accordingly, $\mathbf{P}_a = \mathbf{P}_v = \mathbf{P}_d$ applies for period $T = 2\pi = 6.28$ s and $(\mathbf{P}_d - \mathbf{P}_a) = 2 \times (\mathbf{P}_v - \mathbf{P}_a) =$ const. for any given period and negative for $T < 2\pi$ and positive for $T > 2\pi$ (cf. Fig. 2).

3. CONVERSION OF SPECTRAL AMPLITUDES OR POWER DENSITIES INTO RECORDING AMPLITUDES

According to Aki and Richards (1980) the amplitude of a wavelet f(t) at t = 0 can be *roughly approximated* by the product of the amplitude spectral density and bandwidth of the wavelet, i.e.

$$f(t)_{t=0} = |F(\omega)| \, 2 (f_u - f_l) \quad (9)$$

with f_u and f_l as the upper and lower corner frequencies of the band-passed signal. Likewise, if the power spectral density defined for noise is $P(\omega) = P$ within the frequency band $f_l < f < f_u$ and $P(\omega) = 0$ otherwise, then the *mean square amplitude* is

$$< f^2(t) > = 2P (f_u - f_l). \quad (10)$$

Thus, for a given bandwidth, we can approximately relate the noise *power spectral density* to its *root mean square* (RMS) amplitude:

$$a_{RMS} = \{2P (f_u - f_l)\}^{1/2}. \quad (11)$$

Proper determination and comparability of PSD at different frequencies require octave filtering. Increasing the frequency of a signal by one octave means doubling its frequency. Accordingly, a band-passed signal (or filter) with n octaves of bandwidth has corner frequencies

$$f_u = 2^n f_l \quad (12)$$

and *a geometric center frequency* f_o of

$$f_o = (f_u \times f_l)^{1/2} = f_l \times 2^{n/2}. \quad (13)$$

From this follows for the *relative bandwidth* **RBW**

$$(f_u - f_l)/ f_o = (2^n - 1)/ 2^{n/2}. \quad (14)$$

and (11) becomes

$$a_{RMS} = (P \times f_o)^{1/2} \times \{ 2 (2^n - 1)/ 2^{n/2} \}^{1/2} = (P \times f_o)^{1/2} \times (2 \, \mathbf{RBW})^{1/2} \quad (15)$$

Accordingly, the relative bandwith for a 2-octave filter is 1.5 and for a 2/3-octave filter 0.466.

Aki and Richards (1980, vol.1, p. 498) converted PSD into ground motions by putting the bandwidth of the noise signal half the considered (center) frequency, i.e. by assuming $f_u - f_l = 0.5\ f_o$. This is equivalent to the assumption of a bandwidth of approximately 2/3-octaves. For this special case one gets:

$$(< f^2(t) >)^{1/2} = a_{RMS} = (P \times f_o)^{1/2}. \qquad (16)$$

Other authors (e.g. Fix, 1972; Melton, 1978) have used an integration bandwith of 1/3-octave only for computing RMS amplitudes from PSD. Melton reasoned that this is nearly ±10% about the center period in width and thus close to the tolerance with which an analyst can measure the period on an analog seismogram. Therefore, using a 1/3-octave bandwidth seemed to him a reasonable convention for calculating RMS noise amplitudes from PSD. The differences as compared to RMS values based on 1/4- or 1/2-octave bandwidths are less than 20%. But 1/3-octave RMS amplitudes will be only about 70% or 50% of the respective RMS amplitudes calculated for 2/3- or 1-octave bandwidth, respectively. Typical response curves of narrowband seismographs well suited for recording of transient body-wave onsets have bandwiths between about 1 and 3 octoves. Choosing a constant one octave filter bandwidth for comparing amplitudes of noise and transient seismic signals seems to be rather appropriate , therefore.

For RMS amplitudes determined according to (11) or (15) there is a 95% probability that the *instantaneous peak* amplitudes of a random wavelet with Gaussian amplitude distribution will lie within a range of $2a_{RMS}$. Peterson (1993) could show, that both broadband and long-period noise amplitudes follow indeed very closely a Gaussian probability distribution. In that case the absolute peak amplitudes of the narrowband filtered signal envelopes should follow closely a Rayleigh distribution. In case of an ideal Rayleigh distribution the theoretical *average peak amplitudes* (APA) are 1.253 a_{RMS}. Peterson (1993) measured from test samples of narrowband filtered VBB and LP noise records APA values between 1.194 and 1.275.

The exercises below aim at transforming data values from these different spectral presentations into the related other forms, to compare their mutual comparability and representativeness and to calculate for different signal bandwidth the RMS ground amplitudes corresponding to selected spectral density values.

REFERENCES

Aki, K. and Richards, P.G. (1980). Quantitative seismology - theory and methods. W.H. Freeman and Company, San Francisco, Vol.1, chapter 10: principles of seismometry, 477-524

Bormann, P. (1997). Conversion and comparability of dat presentations on seismic background noise. Journal of Seismology (submitted).

Brune, J.N. and Oliver, J. (1959). The seismic noise of the Earth´s surface. BSSA 49, 349-353

Fix, J.E. (1972). Ambient Earth motion in the period range from 0.1 to 2560 sec. BSSA, 62, 1753-1760

Peterson, J. (1993). Observations and modeling of seismic background noise. U.S. Geol. Survey Open-File Report 93-322, 95p

BANDWIDTH-DEPENDENT TRANSFORMATION OF NOISE DATA FROM SPECTRAL INTO TIME DOMAIN AND VICE VERSA. PART II: EXERCISES

Peter Bormann

GeoForschungsZentrum Potsdam, Division 2: Solid Earth Physics and Disaster Research
Telegrafenberg, D-14473 Potsdam, Germany

Note:

- The equation and figure numbers given below refer to Part I: Introduction and methodology !

*- The solutions to the exercises below will be handed out to you for comparison **after** you have finished the exercise on your own!*

Exercise 1: Determine the relative bandwidth (RBW) of an

a) 1-octave filter

b) 1/2-octave filter

c) 1/3 octave filter

d) 1/4-0ctave filter

using equation (14).

Exercise 2: Calculate for the noise maximum in Fig. 3 the corresponding RMS particle velocity and displacement.

a) Estimate the velocity power maximum from Fig. 3 (Note logarithmic scale!)

b) Give this value also in units of $(m/s)^2/Hz$

c) Estimate the frequency f_o related to this maximum

d) Calculate the RMS particle velocity amplitude by considering eq. (15) and a a relative bandwidth of 2/3 octaves

e) Transform this RMS particle velocity determined under d) into the corresponding RMS particle displacement considering eq. (4)

f) Give the *amplitude spectral density* for the displacement amplitude determined under e) considering eq. (9)

g) Compare the value calculated under f) with Fig. 4 and discuss the reason for the „notch"-shaped lower boundary of the range of seismic signal-amplitude spectral

density shown in this figure.

Exercise 3: Transform the displacement power values of Fig. 5 at f = 1 Hz and f = 10 Hz in

a) units of m^2/Hz

b) acceleration power values with units $(m/s^2)^2/Hz$

c) the values determined under b) in units of dB refered to 1 $(m/s^2)^2/Hz$ according to eq. (6) and compare the result with the respective values in Fig. 2 for the New Low Noise Model (NLNM).

Exercise 4: Determine from Fig. 2 the NHNM-values in units of $(nm/s^2)^2/Hz$ for

a) f = 1 Hz

b) f = 0.1 Hz

Exercise 5: Transform the values determined under 4. into the corresponding RMS displacement amplitudes considering a signal of 1/3 octave bandwidth and compare the result with the respective amplitudes in Fig. 1. Discuss possible discrepancies.

Exercise 6: Transform the *peak noise* amplitude in Fig.1 for curve 1 at T ≈ 6 s into the respective acceleration power spectral density in units of $(nm/s^2)^2/Hz$ assuming a bandwidth of the signal of 1/3 octave.

Exercise 7: Express the result of 6. in dB referred to 1 $(m/s^2)^2/Hz$.

Exercise 8: Compare the result of 7. with the respective value for the NHNM in Fig. 2 and discuss possible discrepancies.

SOLUTIONS

Note: Reading errors may result in slight deviations. But they should not be > 10%!.

1. a) 0,7071

b) 0.3483

c) 0.23156

d) 0.1735

2. a) 5×10^{-8} $(cm/s)^2/Hz$;

b) 5×10^{-12} $(cm/s)^2/Hz$;

c) 0.16 Hz;

d) $a_{oRMS}\approx 9\times10^{-7}$ m/s;

e) $a_{oRMS}\approx 9\times10^{-7}$ m;

f) $|f(\omega)| \approx 5.6\times10^{-6}$ mm/Hz

3. a) 2×10^{-18} m^2/Hz at 1 Hz and 1.5×10^{-22} m^2/Hz at 10 Hz;

b) 3.12×10^{-15} $(m/s^2)^2/Hz$ at 1 HZ and 2.3×10^{-15} $(m/s^2)^2/Hz$ at 10 Hz;

c) - 145 dB for 1 Hz and -146 dB for 10 Hz, i.e. the noise power at this station is about 20 dB higher than for the NLNM.

4. a) and b) ≈ -117 dB, i.e. $\approx 2\times10^{6}$ $(m/s^2)^2/Hz$;

5. a_{oRMS} = 24 nm at 1 Hz and 770 nm at 0.1 Hz. These amplitudes are about 4 to 6 times smaller than those in Fig. 1. The reason is that the latter are RMS and not peak amplitudes. Besides this, the amplitudes in Fig. 1 were most probably measured with seismographs of typically 1 to 2 octaves bandwith. According to eq. (11) their amplitudes would then be 1.8 to 2.5 times larger than those recorded with 1/3 octave bandwidth only.

6. $P_{acc} = 1.65\times10^{9}$ $(nm/s^2)^2/Hz$;

7. - 87.8 dB referred to 1 $(m/s^2)^2/Hz$;

8. The value under **7.** is about 9 dB larger than for the NHNM (≈ -97dB). This corresponds to a factor of almost 3 in amplitude. The reason is that the NHNM represents RMS and not maximum peak amplitudes! With 95% probabilty the latter are within the range of about 2xRMS! Additionally, the assumed bandwith of the noise signals in Fig. 1 of 1/3 octaves only was not correct (cf.. answer to **5.**).

IDENTIFICATION AND ANALYSIS OF SHORT-PERIOD CORE PHASES. PART I: REQUIREMENTS AND GUIDELINES

Peter Bormann[1] and Siegfried Wendt[2]

[1] GeoForschungsZentrum Potsdam, Division 2: Solid Earth Physics and Disaster Research, Telegrafenberg, D-14473 Potsdam, Germany

[2] Universität Leipzig, Institut für Geophysik und Geologie, Geophysikalisches Observatorium Collm, D-04758 Collm, Germany

1. WHY SHOULD WE LOOK FOR CORE PHASES?

Oldham (1899) was the first to identify in records of the M = 8.7 Assam earthquake of 1897 the three main types of waves predicted by Poisson and Rayleigh. He surmised from the substantial delay of P-waves beyond epicentral distances of 120° and the then missing S-waves the probable existence of a molten core, which Wiechert had hypothesized the year before to consist of iron. Gutenberg (1913) then determined the depth of the core-mantle boundary (CMB) with rather high accuracy (2900 km below the earth surface) and to inferred a drop in the velocity of longitudinal waves by almost 40% beneath the CMB. Such a two-shell earth causes refraction phenomena analogous to the optical caustic formed by a spherical lense. Such a caustic was found to exist indeed at D ≈ 145°. Later, Inge Lehman (1936) identified a phase named by her P′. It arrived before the caustic within the shadow zone for primary mantle P-waves. Its existence and observed travel times let her conclude „... that inside the core there is an inner core in which the velocity is larger than in the outer core".

Since that time detailed investigations of refracted, reflected and converted core phases have revealed more details of the CMB, the discontinuity between the outer and inner core (ICB) and of the transition layers above them. Indications for the existence of negative velocity gradients above and scattering irregularities at the CMB, for attenuation anomalies and anisotropy etc. have been found. The identification, verification and quantification of such phenomena provides crucial clues for a more realistic parameterization of these boundary layers and for deeper insights into their nature. This will result in improved modellings which are crucial for understanding the interaction and coupling between the inner and outer core as well as between core and mantle. They govern the thermal, compositional, kinematic and dynamic history of the earth, the driving forces for the episodic cycles of increased orogenitic and magmatic activities throughout the earth history, the origin and drift of the geomagnetic field and of many other fundamental geophysical processes.

Improving existing earth models requires to identify more comprehensively related seismic phases and to determine more precisely their travel times. Currently, more than 10% of all first onsets published by the World Data Center A (NEIS) in Earthquake Data Reports (EDR) are core phases. To look for first arrivals only is, regrettably, still the prevailing practice at seismological observatories. But model improvements require urgently to identify and report secondary arrivals as well which sometimes follow very closely. Only by this way we will be able to verify with real data the precise position of focal points, cusps and receding branches in travel-time curves as they can be calculated from earth models. These characteristic

Scientific Technical Report STR 98/05
DOI: 10.2312/GFZ.b103-98055

features respond very sensitive to changes in the model parameters.Additionally, one has to study the amplitudes and waveforms too. They depend not only on the geometry and velocity distribution but also on the attenuation structure of the earth. Its anelastic part is closely related to the rheology and thus to the thermal and compositional properties of the earth.

Besides this, one should look not only for the various direct core phases but also for reflected and converted ones as well. They often sample parts of the earth which are not passed by recorded direct refracted waves. This may be due to the inhomogeneous distribution of seismic sources and receivers or because of the specifics of the velocity distribution. The uppermost outer core, e.g., is not sampled by any of the direct core phases. The reason is, that their rays are refracted towards the deeper parts of the core because of the strong velocity decrease below the CMB (cf. Fig. 2). Consequently, only core phases which are reflected back into the core at the CMB will sample those parts of the uppermost outer core. Comparing the spectral amplitudes from multiple reflections of this type is well suited for better constraining the attenuation properties in those parts and the acoustic impedance contrast at the CMB.

Thus, a detailed identification and analysis of the various types of core phases on a global scale by seismic observatories may yield unique data for verifying or improving existing earth models. Besides this, a more careful analysis and reporting of such phases to international data centers may also help to improve their routine determination of basic source parameters of seismic events such as magnitudes and hypocentral co-ordinates. This applies, in particular, when the events occur in regions which are not well covered by local or regional stations while in other parts of the world, at „core phase distances", good seismic networks with low detection thresholds may exist. This is true, e.g., for seismic stations in central and northern Europe with respect to events in the SW Pacific (Fig. 1a). Many seismic stations in Africa have, besides the SW Pacific, also the seismically very active regions of the Aleutian Islands, Alaska and California within the PKP distance range (Fig. 1b and c).

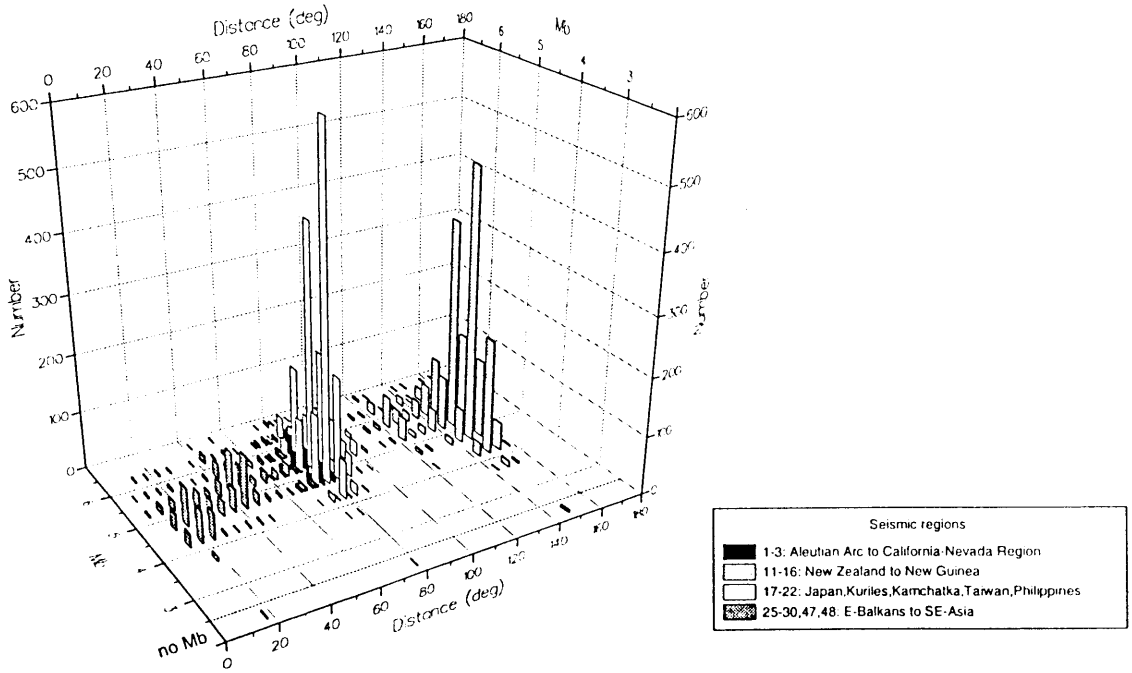

Fig. 1a

Fig. 1: Number of period (T) and amplitude (A) readings of selected seismic stations as contained in EDR of NEIS, 1990-95, as a function of magnitude and distance. a) Collm (CLL), Germany; b) Silverton (SLR),South Africa; c) Bulawayo (BUL), Zimbabwe.

Station Silverton (SLR)

EDR 1990 - 1995; SLR with T/A-values

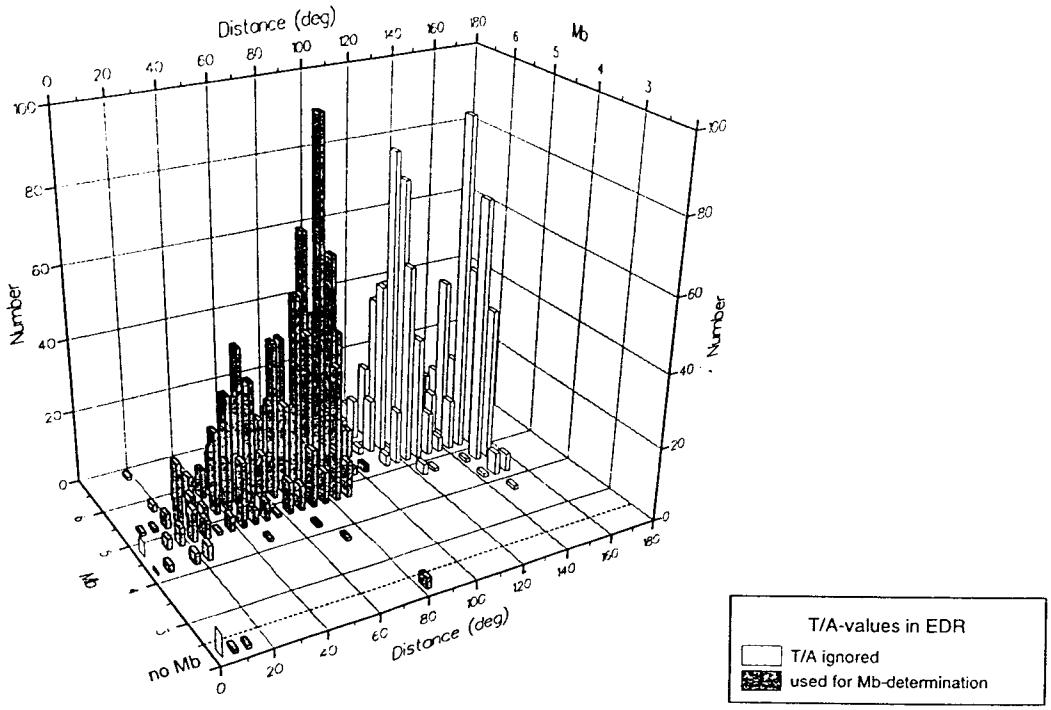

Fig. 1b

Station Bulawayo (BUL)

EDR 1990 - 1995; BUL with T/A-values

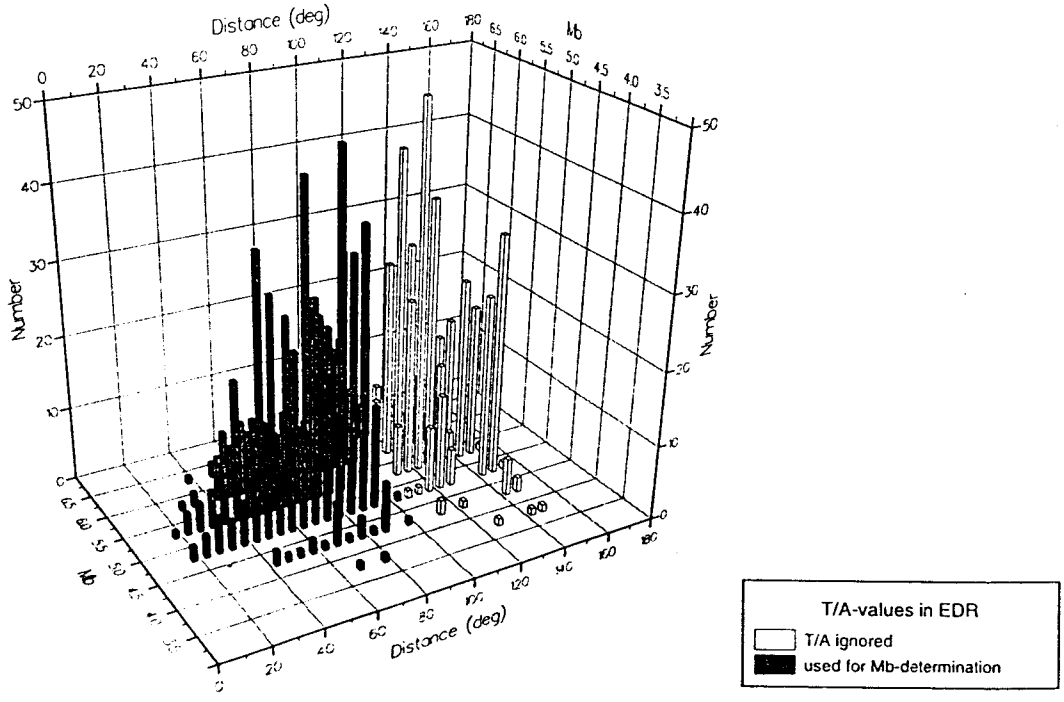

Fig. 1c

Until now it is standard practice at the international seismological data centers to use P-wave onsets up to epicentral distances of about 100° only for the determination of body-wave magnitudes m_b. But, as obvious from Fig. 1, the seismic station Collm in Germany, has reported to the EDR of NEIS almost as many period (T) and amplitude (A) readings for PKP core phases between $110° < D < 160°$ as for teleseismic P-waves. Thus, not using PKP for magnitude determinations, is a waste of potentially useful information. Often NEIS is unable to give m_b values because of lacking suitable P-wave data although reliable A and T values reported for PKP were readily available.Therefore, we will present in the following exercise newly derived calibration functions for magnitude determination from PKP phases.

In case of strong earthquakes or underground nuclear explosions, reflected core phases such as PKPPKP, PKKP or their multiples (up to P7KP has already been observed!) may appear in seismic records as small but rather distinct short-period onsets. They are well separated in time (about 10 to 80 min.) from P, PKP, PP, PcP or other short-period phases related to the main event. Therefore, station operators frequently interprete them as P-wave onsets from another event (cf. Fig. 9 below). Although this misinterpretation is mostly recognized by the automatic data association procedures at the international data centers, often enough this has not been the case. Ambraseys and Adams (1986) reported, that misinterpreted PKKP arrivals at the LASA array in Montana, USA, resulted in the location and reporting to the International Seismological Center (ISC) of spurious events in western and central Africa with magnitudes between 4 to 6. They had nothing to do with real seismicity there and thus could have biased significantly hazard assessments based on uncorrected catalogue data.

This highlights the importance of a priori correct phase identification at seismic observatories. With this introduction and the following guidelines and exercises on the identification of core phases in short-period seismic records we intend to develop the needed problem awareness and skills of station operators on this important issue. Although we are aware that modern interactive data analysis programms allow to call for all travel-time curves theoretically expected at a given distance and to overlay them on the records, thus aiding a correct phase identification, we prefer to demonstrate the sequence of logic steps to be followed when interpreting a seismic record. Only this will allow a correct phase interpretation even without knowing beforehand details about the source location, distance, depth etc. from data centers.

Our emphasis is on short-period core phases because only high-gain short-period (or accordingly filtered broadband) records provide sufficient world-wide data of these mostly weak phases with good time-resolution. This is documented by Fig. 2 which also reveals, that different kind of direct and/or reflected/converted core phases are observable in practically all teleseismic distance ranges. The stronger direct core phases may be recorded in all instruments but the different PKP onsets appearing beyond the caustic within a few seconds to each other are integrated in broadband recordings to a more or less complex long-period wavelet which does not allow precise onset time determinations of these individual phases without special processing.

Fig. 2 (next two pages): Relative frequency of occurrence of secondary phases with respect to first arrival P or number n of analysed events (hatched column = 100%) in records of different types of seismographs at station MOX of earthquakes from different regions and distance ranges: A -short-period; B - KIRNOS broadband, C - long-period (in brackets if less clear or frequent). Signatures for source depth h are: white column - $h <$ 70 km, Δ - 70 km $\leq h \leq$ 300 km, ◊ - $h <$ 300 km. For more details cf. Bormann (1972)

Scientific Technical Report STR 98/05
DOI: 10.2312/GFZ.b103-98055

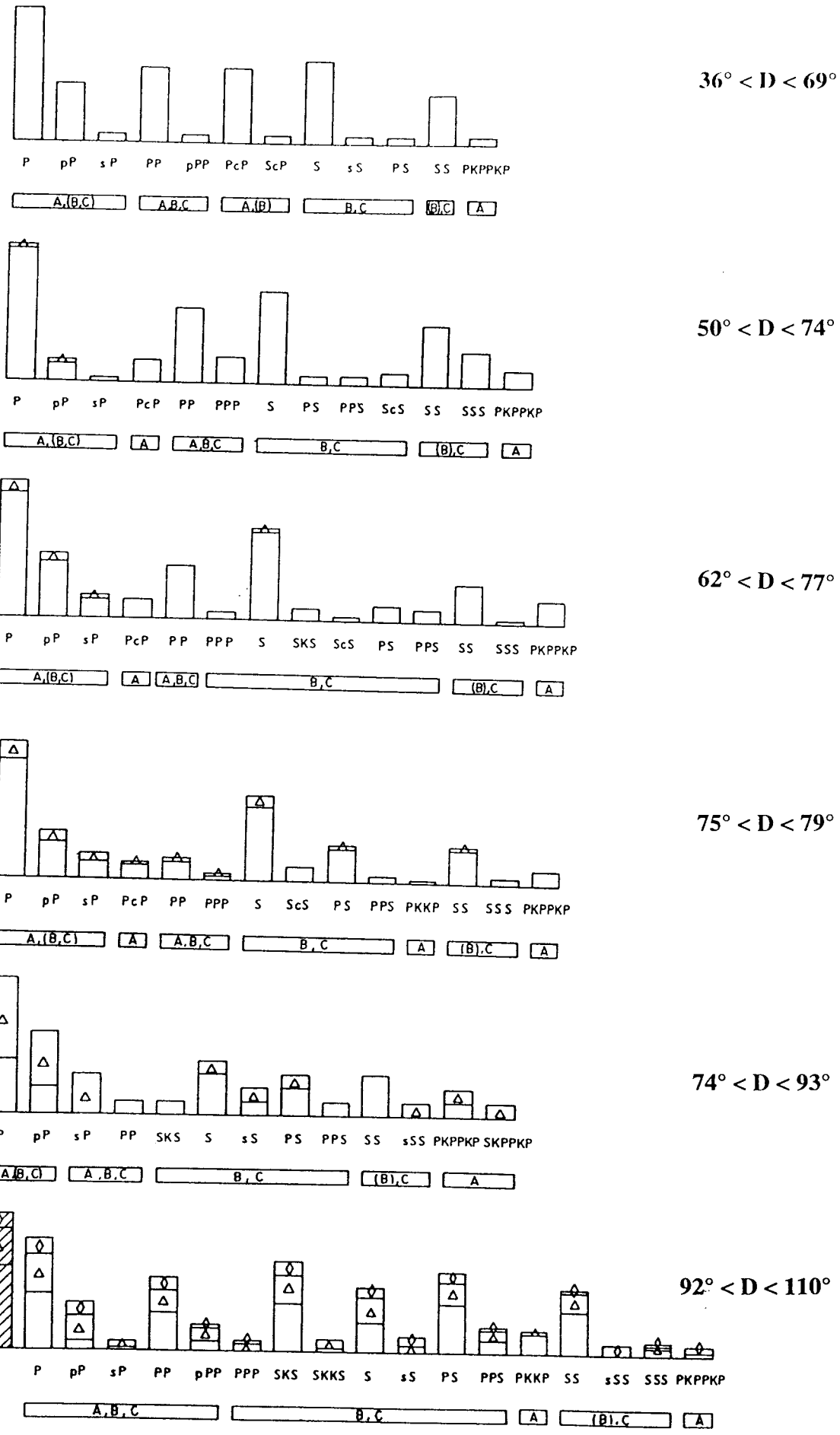

Fig. 2a: Figure caption see page before.

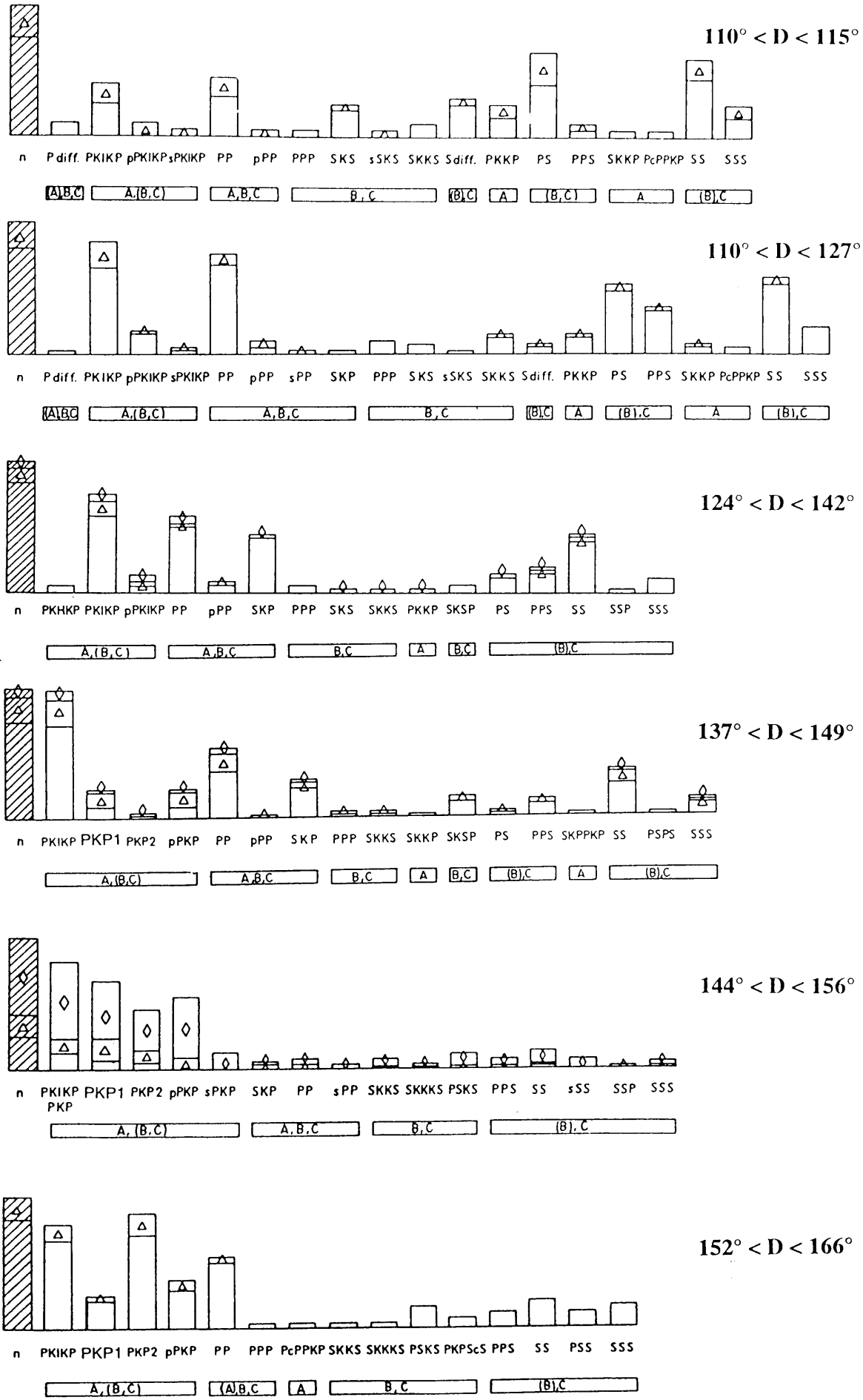

Fig. 2b: Figure caption see page before but one

DOI: 10.2312/GFZ.b103-98055

2. RAY PATHS AND TRAVEL TIMES OF PKP PHASES

Fig. 3 shows the ray paths and travel-time curves for PKP phases according to the IASPEI 1991 velocity model (IASP91 for short; Kennett 1991). Recommended by the International Association of Seismology and Physics of the Earth Interior (IASPEI) the latter is the currently most often used one-dimensional earth model. The caustic effect due to this velocity structure is clearly to be seen. The three different core phases PKP1, PKP2 and PKIKP reach the point B at a distance of about 145° at the same time while being more or less clearly separated for larger distances. The symbol P stands for ray segments travelled as a longitudinal wave through the earth mantle while the symbols K and I stand for travelling as a longitudinal wave through the outer or inner core, respectively. PKP2 forms the receding travel-time branch between the points A and B (focus). From thereon PKP1 exists up to the point C, forming a prograde branch. According to IASP91, the ray which was totally reflected due to the velocity increase at the inner core boundary arrives at nearly 155°. This gives rise to the formation of a cusp at point C with the receding branch of the inner core reflection PKiKP going back to point D at about 114°. Since the branch CD follows within ≤ 2 s only after PKP1, PKP2 or PKIKP, respectively, and since, according to Fig. 4, the theoretically expected related wave amplitudes are for D > 135° smaller than for the other three phases, this branch has not been depicted in Fig. 3. PKIKP forms, from the cusp at point D up to 180°, the prograde travel-time branch DF. Accordingly, these three considered PKP-phases are nowadays often discerned by adding the branch symbols (mostly as lower case letters) instead of using the classical notation given above.

3. AMPLITUDE-DISTANCE RELATIONSHIPS FOR PKP PHASES

Besides the systematic, distance-dependent travel-time differences the amplitude ratio of the different direct longitudinal core phases is another important identification criterion. According to the normalized theoretical amplitude-distance curves shown in Fig. 4 below PKIKP is the weakest phase for D < 155°. Exeptions may be sometimes observed week amplitude forrunners. These phases, annotated PK(P) by Hales, 1995 and PKHKP in the initial publication by Bolt (1964), are due to energy scattered from the CMB. These rather incoherent phases may arrive between about 130° and 144° up to 17 s before PKIKP(cf. Fig. 6).

For D < 135° PKiKP, following PKIKP within a second, may have several times larger amplitudes. Between 143° < D < 155° the intermediate phase PKP1(PKPbc) is theoretically expected to have amplitudes about 2 to 10 times larger than that of PKIKP, followed by PKP2(PKPab) with about 1.5 to 4 times larger amplitudes (cf. Figs. 4-6).

According to ray theory PKP1 is supposed not to exist any more for D > 155° for the models IASP91 (Fig. 3) and 1066B (Fig. 4), but due to diffraction around the inner core this phase is often observed up about 160° but then generally as the weakest of the direct core phases.

According to Fig. 4 PKP2 is expected to become somewhat smaller than PKIKP beyond about 155°. This does not agree with our observations up to about 164°. They show PKP2 generally with 2-4 times, sometimes even more larger amplitudes than PKIKP (Figs. 5 and 6). This is also reflected in the magnitude calibration functions Q of these 3 phases as depicted in Fig. 5 of the exercise, with Q being smaller when the relative amplitude is larger.

Scientific Technical Report STR 98/05
DOI: 10.2312/GFZ.b103-98055

Raypaths and travel time curves of core phases PKIKP, PKP1, PKP2

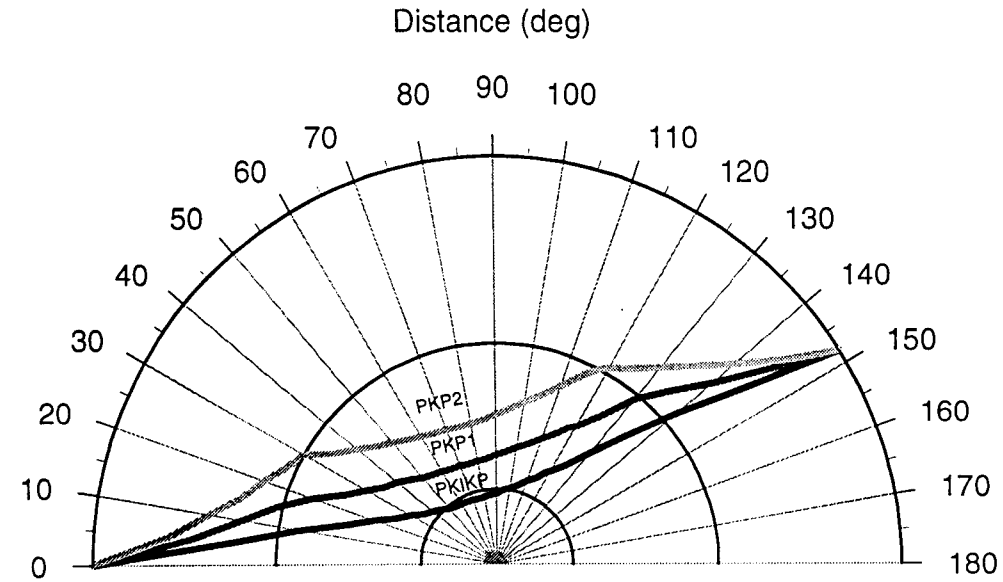

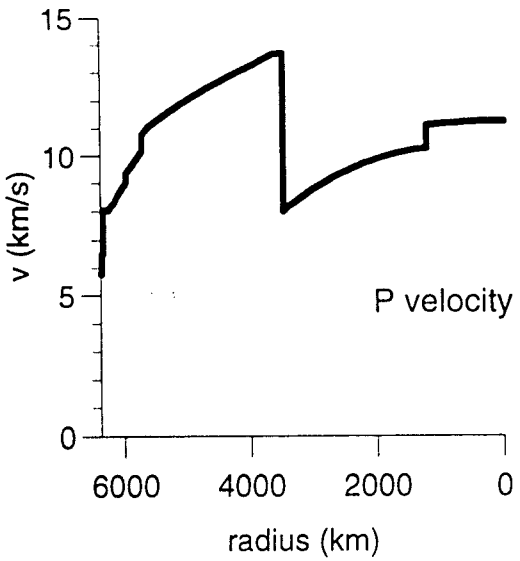

P velocity values for model iasp91

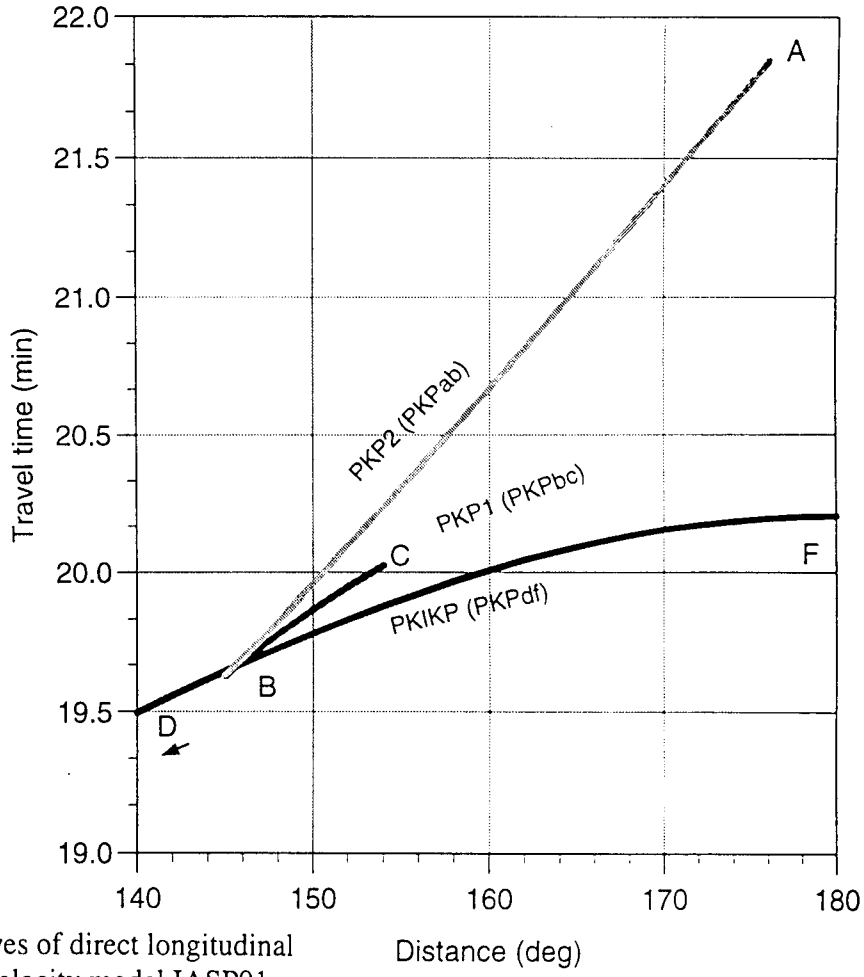

Fig.3: Ray paths and travel-time curves of direct longitudinal core phases according to the velocity model IASP91

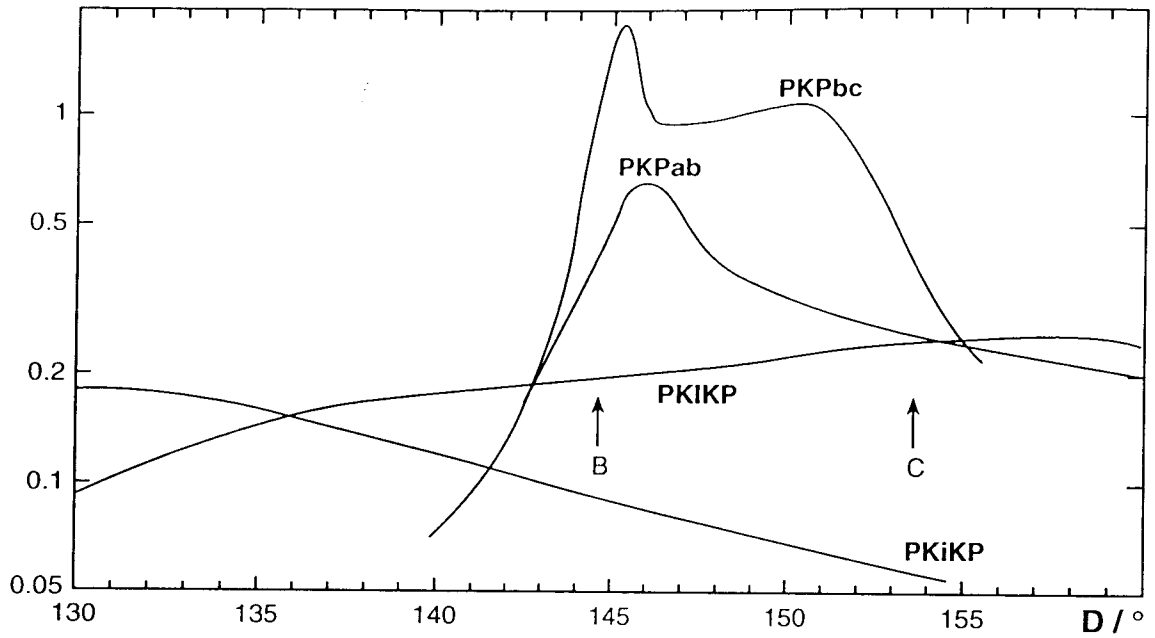

Fig. 4: Smoothed amplitude-distance relationships for the core phases PKIKP, PKiKP, PKP1 and PKP2 as calculated for the model 1066B (modified according to Houard et al. 1993).

Fig. 5 below summarizes the average relative experimental A-D relationships for two ranges of source depth h as determined from data of station CLL. It provided the basis from which the new PKP magnitude calibration functions depicted in Fig 5 of the exercise were derived. Fig. 6 depicts a typical record section for PKP observations at the seismological station Collm (CLL), Germany. It illustrates the essential amplitude features discussed above which differ significantly in many respect from the theoretical relationship in Fig. 4.

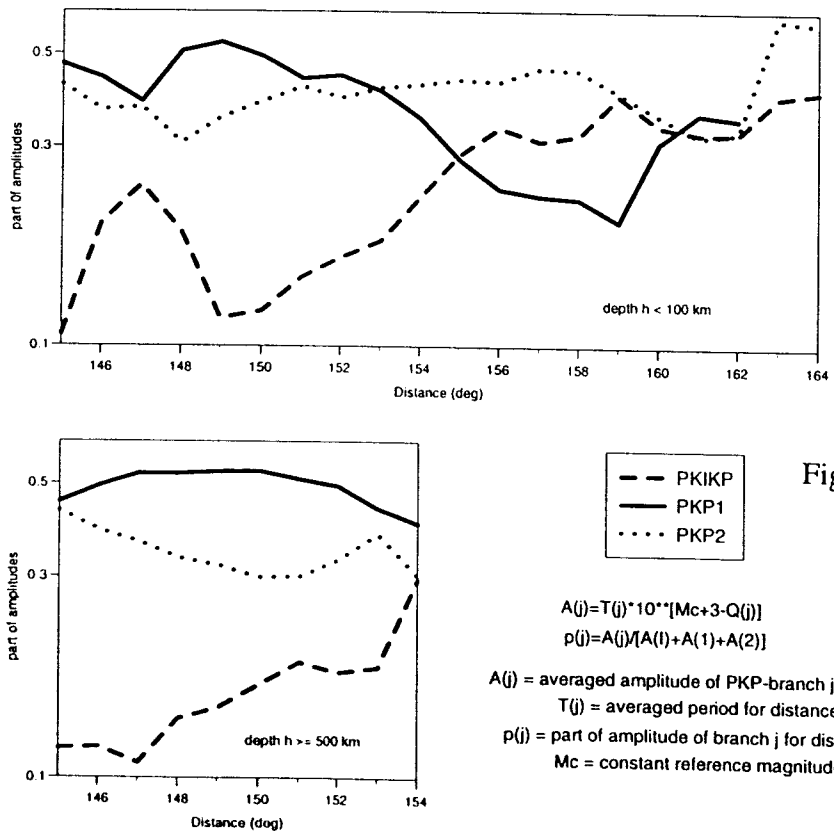

Fig. 5:

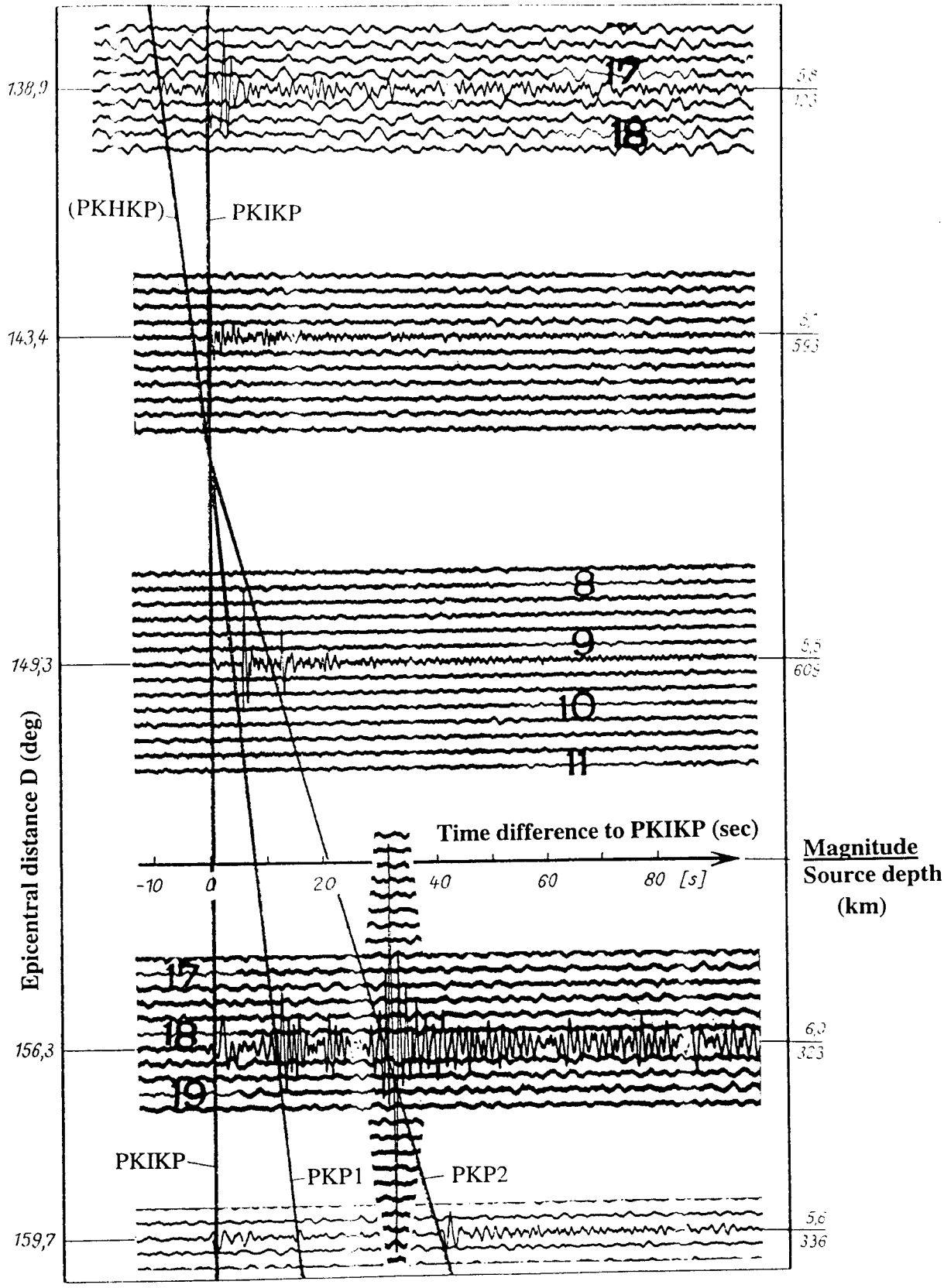

Fig. 6: Typical short-period recordings of core phases (PKHKP), PKIKP, PKP1 and PKP2 in the epicentral distance range 138° < D < 160° as recorded at station CLL, Germany. They are shown together with the differential travel-time curves for these phases according to Bolt (1964). The German version of this figure was made available by courtesy of Dr. B. Tittel.

Scientific Technical Report STR 98/05
DOI: 10.2312/GFZ.b103-98055

4. ADDITIONAL CHARACTERISTICS OF PKP-ONSETS

As can be infered from Fig. 3 above, PKP-onsets have much larger amplitudes in vertical components than in horizontal ones. This is equivalent to a rather small slowness ranging between 0 s/° (in case of PKIKP at D = 180°) and 4.44 s/° for PKP2 at the same epicentral distance. The latter value corresponds to that of mantle P-waves at D > 98°. The slowness values near the caustic vary between 1.7 s/° for PKIKP and < 4 s/° for PKP2. Availing of data from a station network or array one can determine the slowness from the onset-time differences and use the slowness values both for event location as well as an additional identfication criterion (e.g. Schlittenhardt, 1996).

The differential time pPKP - PKP (i.e. depth phase - direct core phase) is, in a first approximation, nearly independent of the epicentral distance (cf. Fig. 4 in part II: Exercise). This allows to determine D with rather good accuracy (better than about 1.5°) just from the travel-time differences of the 2 or 3 pronounced direct core phases just from records of a single station even without knowing the source depth. In case of clearly developed depth phases one may sometimes be able to recognize the same sequence of onsets with different amplitudes as for the direct core phases. If this is not the case, then one should determine the focal depth always from the time difference between pPKP and the strongest PKP-onset.

5. REFLECTED CORE PHASES

In case of stronger events, reflected core phases may be observed besides direct ones, sometimes with up to 4 (or even more) repeated reflections. These phases may be observed at practically all teleseismic distances with delays behind the first arriving P or PKP onsets ranging from about 10 minutes up to about 80 minutes depending on the number of multiple reflections. These phases are clearly discernible only in high-magnifying short-period records. Most frequently observable are the single reflection PKKP and PKPPKP, the latter sometimes called P´P´. The respective n-fold reflections are sometimes annotated for short as PnKP or nPKP, respectively. Fig. 7 shows ray pathes for PKKP, PKPPKP and P4KP while Fig. 8 presents a record cutout with the latter phase, weak but still distinct and superimposed on more long-period „signal noise". Fig. 8 in the exercise (part II) shows several record examples for both PKPPKP and PKKP. They illustrate that these phases may indeed erroneously be interpreted by station operators as being P or PKP first arrivals from independent events.

PKKP is observable mainly in the distance range 80° < D < 127° with about 13 to 19 min behind P or 9.5 to 12 min behind PKIKP (cf. Fig. 2 above and Fig. 6 of the exercise).. PKPPKP is observable between 10° < D ≤ 105° (cf. Fig. 2 and Fig. 7 of the exercise). In this range it follows the P-onset after about 40 to 24 min.

A particular advantage of these phases is again the small depth dependence of their travel-time differences to P and PKP, respectively. Consequently, their identification allows very good distance estimates from single station records even without knowing the source depth. Because of the inverse differential travel-time curves of PKKP and PKPPKP with respect to P and PKP their identification can be facilitated by comparing the onset times at neighbouring stations. An additional interpretation aid is the determination and comparison of the polarization for both the first arrival and the PKKP or PKPPKP onset, respectively, from 3-component records. According to Fig. 7 above their azimuths should be opposite to that of P.

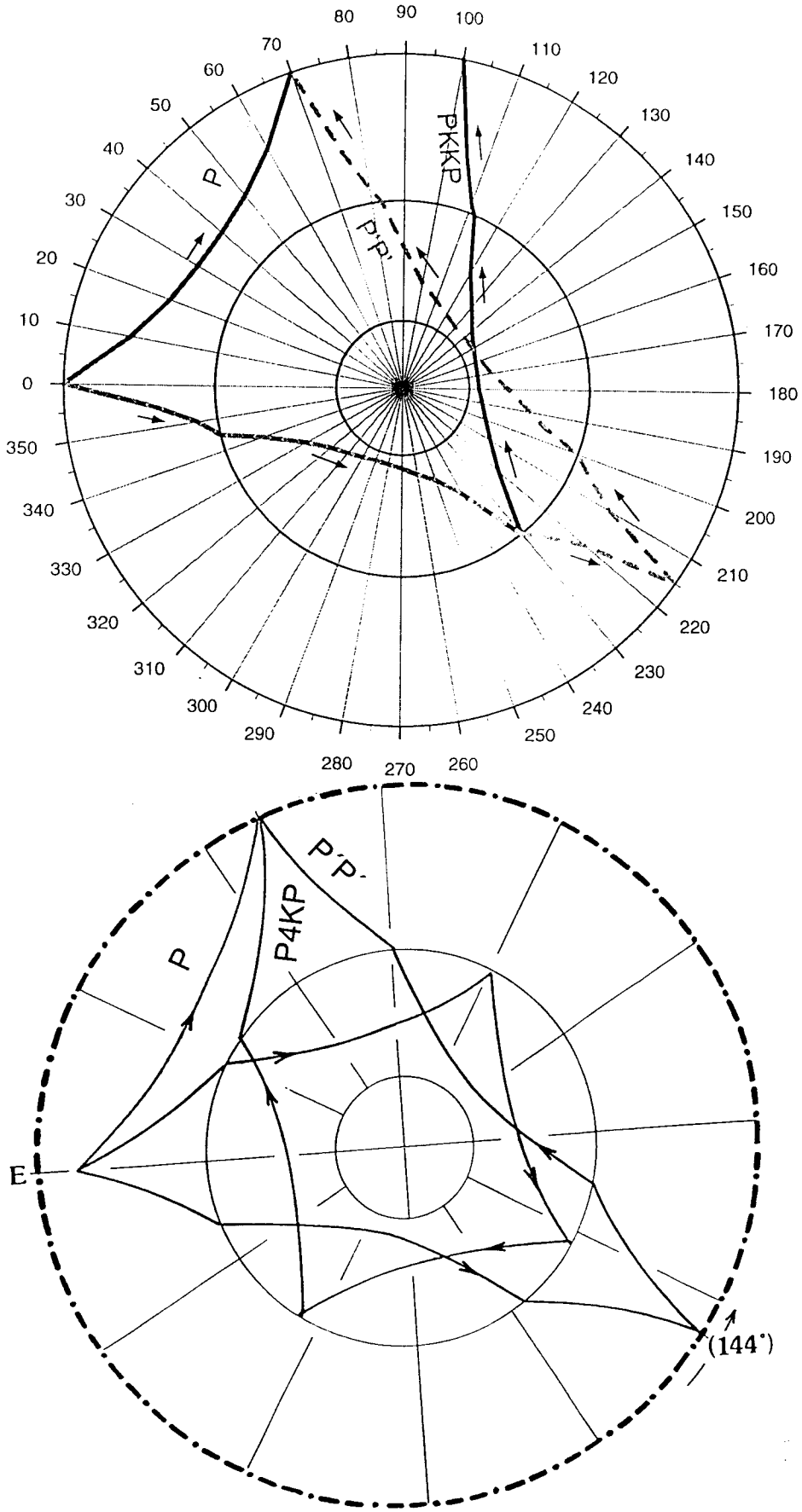

Fig. 7: Ray pathes for P, PKKP and PKPPKP (P´P´) (above) and for P4KP (below).

Scientific Technical Report STR 98/05
DOI: 10.2312/GFZ.b103-98055

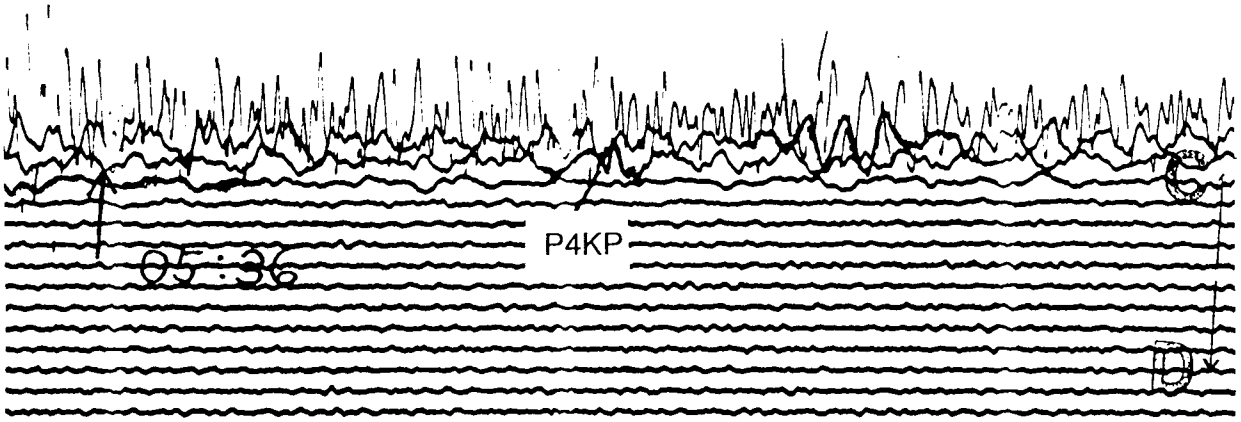

Fig. 8: Week onset of the multiple reflection P4KP in short-period records of station CLL at the epicentral distance D = 71° from a deep earthquake underneath Sachalin Island (date: 12.05.1990, h = 605 km, m_b 6.5). The related ray path is depicted in the lower part of Fig. 7.

Multiple reflections from the inner side of the CMB such as P3KP, P4KP and P5KP are observed, if at all, at about 37 ± 1 min after the first arriving wave. The latter is in case of P3KP the P-wave at around 10° epicentral distance, in case of P4KP the P-wave between 45° < D < 75° and for P5KP the PKIKP between about 130° < D < 150°.

Sometimes, also converted core reflections such as SKPPKP or SKKP can be observed in short-period recordings. Contrary to this, converted or reflected core phases which have travelled along both ray segments through the mantel as S-waves are mostly observed in broadband or long-period records (cf. Fig. 2).

5. SUMMARY DISCUSSION

From the discussions above, comparing theoretical with experimental travel-time- and amplitude-distance relationships and cf.also to Figs. 1 - 7 of the exercises we can conclude:

1.) Between about 145° and 160° the longitudinal core phases PKIKP, PKP1 and PKP2 follow a rather typical distance-dependent travel-time difference and amplitude pattern. This allows to identify these phases and to determine the epicentral distance of the related event with rather high accuracy (better than 1.5°) from short-period records of just a single seismic station. The same applies for using the travel-time differences between P or PKIKP to reflected core phases such as PKKP, PKPPKP or their multiples.

2.) This pattern is well developed, especially in case of deep earthquakes with no close-up crustal depth phases interfering with this typical wave group.

3.) Experimental data about core phases may still deviate significantly from those predicted on the basis of current best earth models. This highlights not only the urgent need to provide the international data centers with much more carefully identified and measured data about core phases. It also alarms us not to base our interpretations and measurements exclusively on theoretically expected travel-time branches and onset times or amplitude-distance relationships. Distinct and well correlated phases may still exist clearly beyond to limits to

which currently available theoretical travel-time curves have been defined, and also their amplitudes may differ significantly from the predicted ones.

4.) The depth-dependent magnitude calibration curves as derived from PKP amplitude readings at the station CLL (cf. Fig. 5 in part II: Exercise) allow m_b determinations from core phases with an accuracy of better than ± 0.2 magnitude units. Their applicability should be tested at other stations of the world -wide network.

ACKNOWLEDGEMENT

The authors wish to thank Dr. Bernd Tittel from the Geophysical Observatory Collm (CLL) for valuable discussions and suggestions, for making the German Figs. 6 - 8 available to us and for his many years of dedicated and inspiring work on seismic core phases in routine observatory practice.

REFERENCES

Bolt, B.A. (1964). The velocity of seismic waves near the earths center. Bull. Seism. Soc. Am., **54**, 1, 191-208.

Bormann, P. (1967). Aufzeichnungen longitudinaler Kernphasen an der Station Moxa und ihre Interpretation. In: Stelzner, J. und Bormann, P.. Seismologisches Bulletin 1965 - Station Moxa. Akademie-Verlag Berlin 1967, 10-15.

Bormann, P. (1972). A study of relative frequencies of body-wave onsets in seismic registrations of station Moxa. In: Bormann, P. and Stelzner J. (1972). Seismological Bulletin 1967 - station Moxa (MOX), Akademie-Verlag Berlin, 379-396.

Gutenberg, B. (1913). Über die Konstitution des Erdinnern, erschlossen aus Erdbebenbeobachtungen. Physik. Zeitschrift **14**, 1217-1218.

Haddon, R.A.W. and Cleary, J.R. (1973). Precursors to PKIKP and seismic wave scattering near the mantle-core boundary. Phys. Earth Planet. Interiors 7,495-497

Hales, A.L. (1995). Comment on „Amplitudes of core waves near the PKP caustic, from nuclear explosions in the South Pacific recorded at the „Laboratoire de Detection et Geophysique" network in France" by S. Houard et al., Bull. Seism. Soc. Am., **85**, 3, 957-958.

Houard, S., Plantet, J.L., Massot, J.P. and Nataf, H.C. (1993). Amplitudes of core waves near the PKP caustic, from nuclear explosions in the South Pacific recorded at the „Laboratoire de Detection et Geophysique" network in France. Bull. Seism. Soc. Am. **83**, 6, 1835-1854.

Kennett, B.L.N. (Editor)(1991). IASPEI 1991 Seismological Tables. Research School of Earth Sciences, Australian National University, 167 pp.

Scientific Technical Report STR 98/05
DOI: 10.2312/GFZ.b103-98055

Lehmann, I. (1936). P′. Bur. Centr. Seismol. Int. A., **14**, 87-115.

Oldham, R.D. (1899). Report on the great earthquake of 12th June 1897. Mem. Geol. Survey, India, **29**, 1-379.

Schlittenhardt, J. (1996). Array analysis of core-phase caustic signals from underground nuclear explosions: Discrimination of closely spaced explosions. Bull. Seism. Soc. Am., **86**, 1A, 159-171.

IDENTIFICATION AND ANALYSIS OF SHORT-PERIOD CORE PHASES. PART II: EXERCISES

Siegfried Wendt[1] and Peter Bormann[2]

[1] Universität Leipzig, Institut für Geophysik und Geologie, Geophysikalisches Observatorium Collm, D-04758 Collm, Germany

[2] GeoForschungsZentrum Potsdam, Division 2: Solid Earth Physics and Disaster Research, Telegrafenberg, D-14473 Potsdam, Germany

1. IDENTIFICATION AND ANALYSIS OF DIRECT PKP PHASES

Clear short-period vertical component PKP seismograms of a single station contain all information needed to determine *source depth* h, *epicentral distance* D and *magnitude* m_b with an accuracy of ± 30 km, better ± 1.5° and ± 0.3 magnitude units, respectively. In case of strong events and the availability of identically calibrated horizontal components with good signal-to-noise ratio, additionally the source azimuth can be determined with an accuracy of about ± 5°- 10° and thus the approximate location. As a guideline a compilation of typical core phase recordings at the station MOX from events between 140° < D < 160° is shown in Fig. 1. From this it becomes clear that the typical three-phase pattern PKIKP, PKP1 and PKP2 is only well developed for D > 147°. Around 145° all three phases come together forming a rather sharp impulsive onset. At D < 145° small amplitude precursors of waves scattered from the core-mantle boundery (CMB) may occur (phase notation PKHKP or PK(P), cf. also part I).

The first record example also illustrates that in case of crustal earthquakes closely following depth phases may complicate the wave pattern and mimic a core phase triplication typical for D > 146°. But in case of deeper events with sharp onsets and no or small signal coda the triplication is rather distinct. Note in the last two examples of Fig. 1 well developed depth phases which are obviously related to the strongest direct phase PKP2. The depth phases pPKP may follow up to about 2.5 min later in case of a maximum possible source depth of 700 km. When the primary core phases are rather strong, two or three related depth phases may be discernable.

All steps of determining h, D, Az and m_b will be practiced in the following based on not annotated copies of records given in Figs. 2. In these records 1 mm corresponds to about 1 s. Full minutes start at the left side of the 2 s long gap or „fainting" of the record traces.

1.1 Depth determination

Fig. 3 gives the IASPEI 91 differential travel times Δt of the depth phases pPKPab (or pPKP2), pPKPbc (or pPKP1) and pPKPdf (or pPKIKP) to their respective direct phases as a function of source depth h.

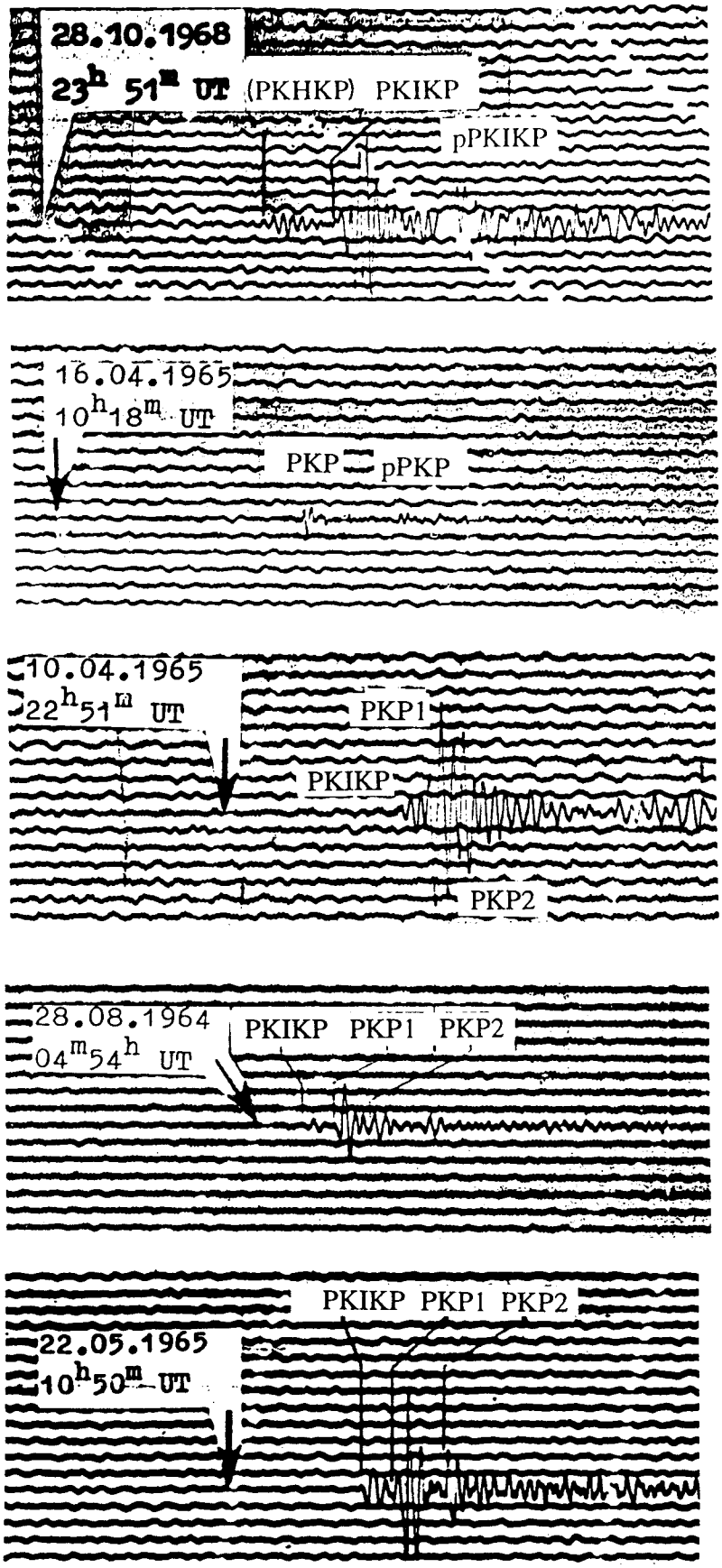

D = 135.5°
h = 60 km
m_b = 5.9
Santa Cruz Islands

D = 144.7°
h = 62 km
m_b = 5.0
New Hebrides

D = 146.2°
h = 543 km
m_b = 5.9
Fiji Islands

D = 148.3°
h = 580 km
m_b = 5.4
Fiji Islands

D = 149.6°
h = 578 km
m_b = 5.8
Fiji Islands

Fig. 1a: Figure caption see next page

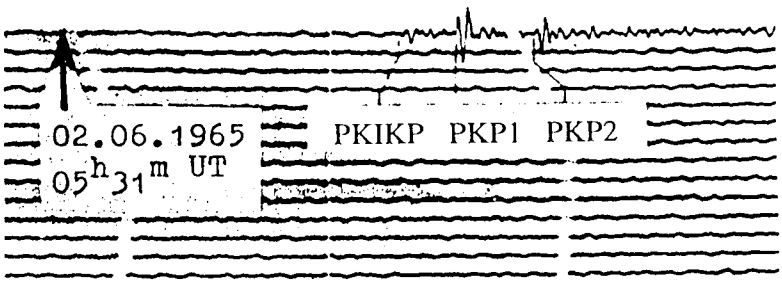

D = 151.3°
h = 539 km
m_b = 5.6
Fiji Islands

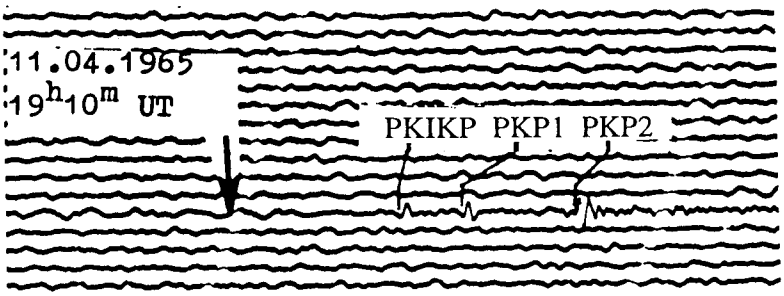

D = 153.6°
h = 581 km
m_b = 5.6
South of Fiji Islands

D = 159.1°
h = 231 km
m_b = 5.5
Kermadec Islands

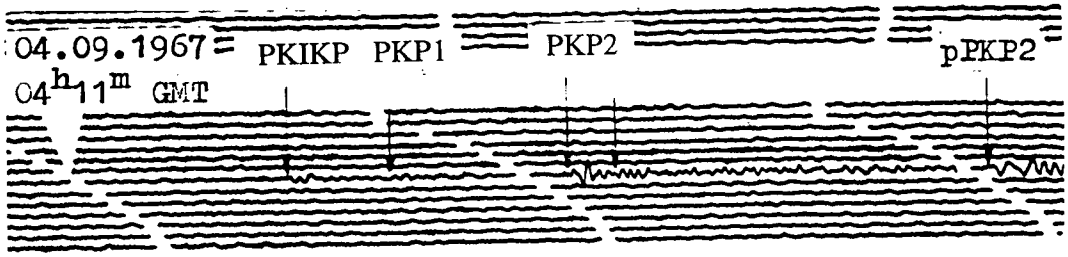

D = 159.5°
h = 235 km
m_b = 5.5
South of Kermadec Islands

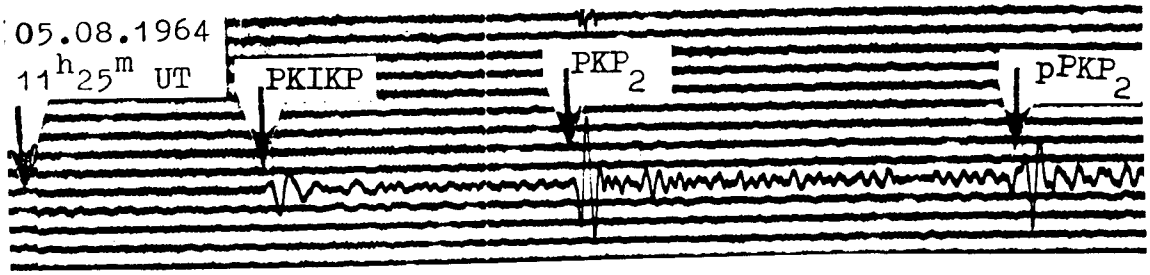

Fig. 1a (page before) and 1b (above): Examples of short-period records of direct longitudinal core phases in the distance range 135° < D < 161° at station MOX, Germany. 1 mm in the records corresponds to about 1 s. All source data according to NEIS - National Earthquake Information Service, USA.

Scientific Technical Report STR 98/05
DOI: 10.2312/GFZ.b103-98055

Scientific Technical Report STR 98/05
DOI: 10.2312/GFZ.b103-98055

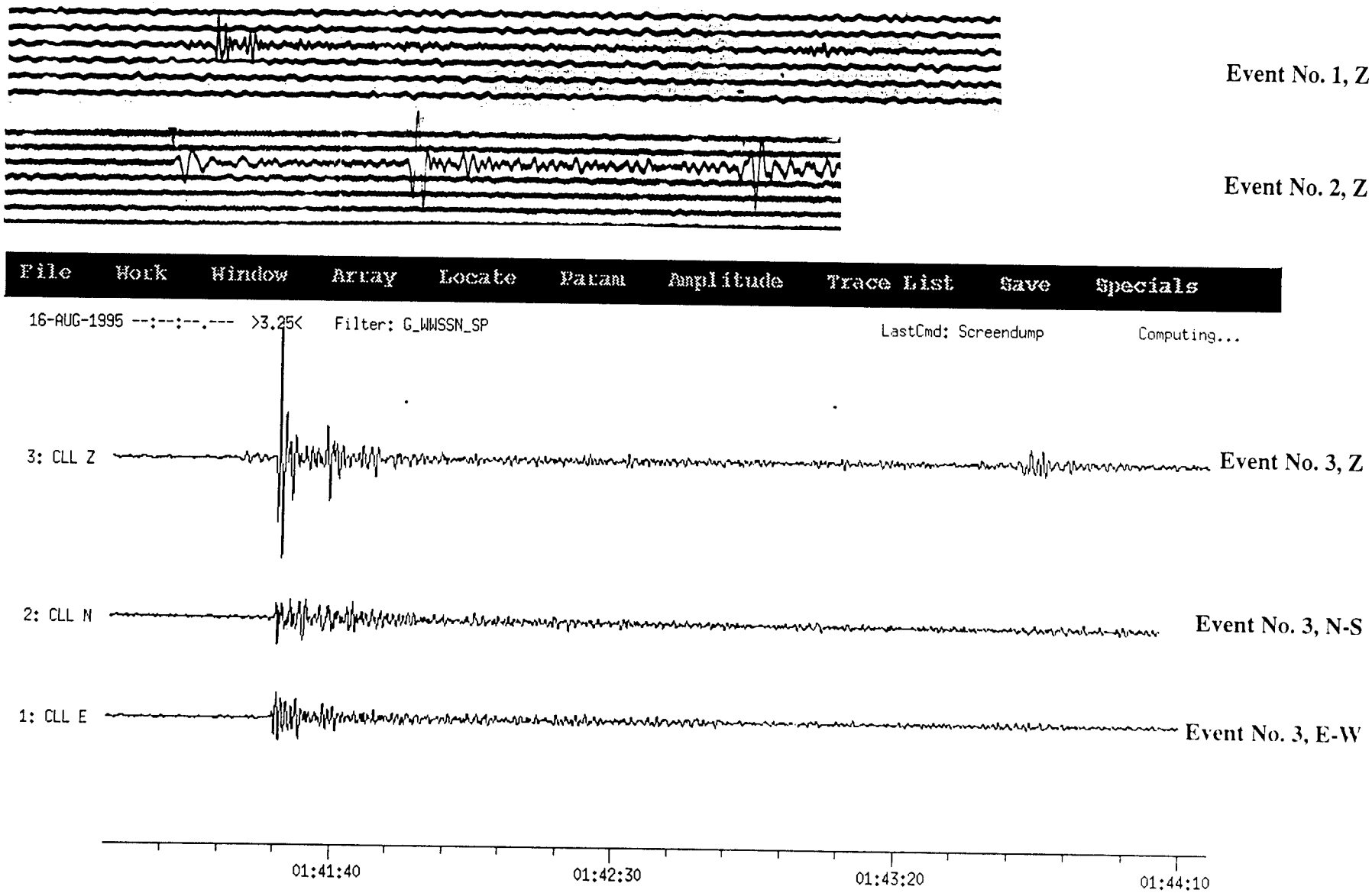

Fig. 2: Recordings of direct longitudinal core phases and related depth phases from records of station CLL (Nos. 1 and 3) and MOX (No. 2)

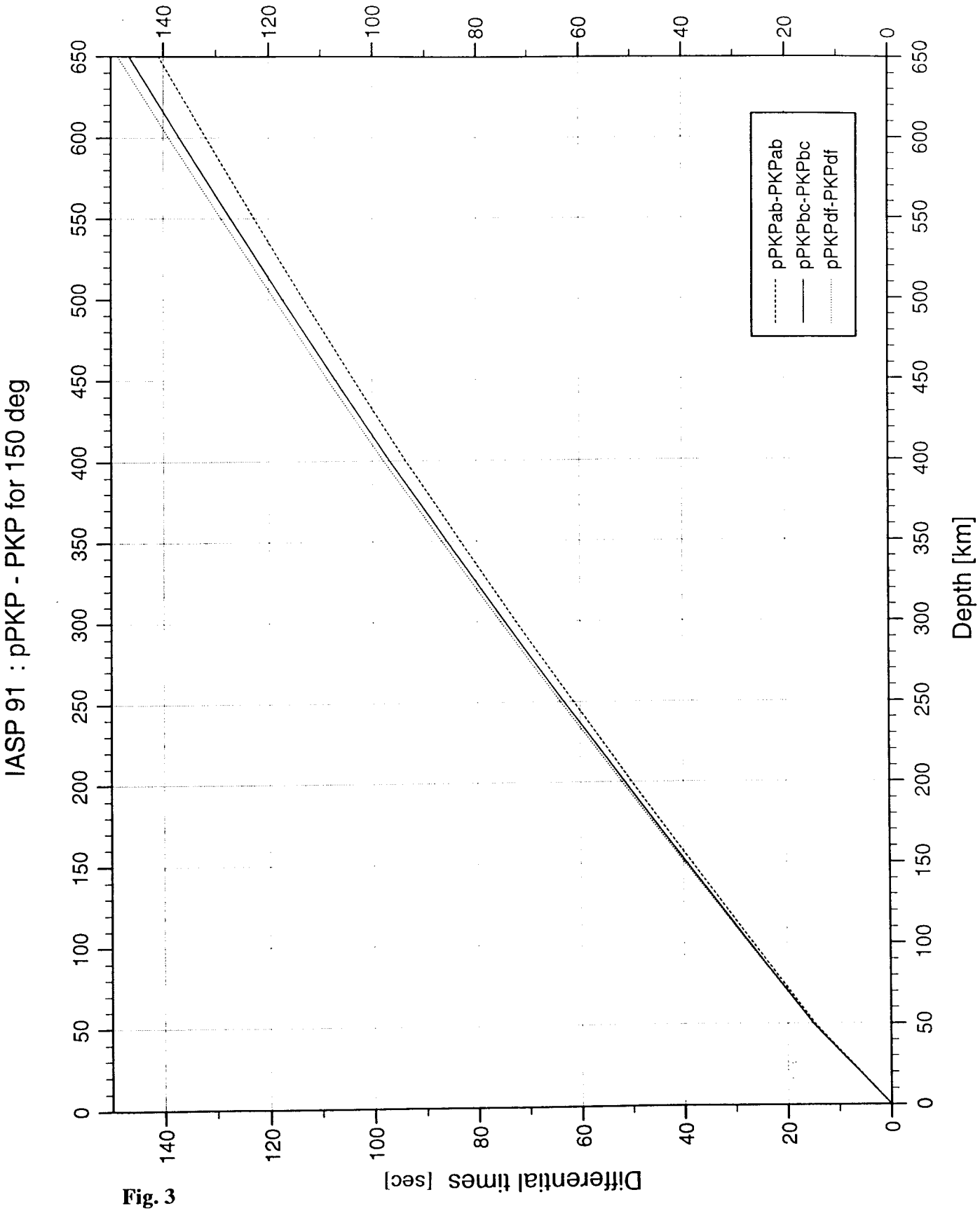

Fig. 3

Scientific Technical Report STR 98/05
DOI: 10.2312/GFZ.b103-98055

Exercise 1:

- Make a table with event No., phase pair, Δt, h(Δt), h(average), h(NEIS), δh which is h(Δt) or h(average) - h(NEIS).

- Try, to identify in at least one of the 3 Z-component records all three depth phases related to PKIKP, PKP1 and PKP2.

- Determine h(Δt) and h(average), where possible, from all Z-component records shown in Fig. 2 and write your results into the table ! You will then be given the values h(NEIS).

- Determine δh and assess the accuracy of your h-determinations as compared to NEIS.

Note: If the pPKP group is less distinct relate its onset to the strongest direct core phase !

1.2 Distance determination

Fig. 4 gives the IASPEI 91 depth-dependent differential travel-time curves for PKPbc-PKPdf and PKPab-PKPdf, respectively. Thus, having identified two or three of these phases, D can be determined.

Exercise 2:

- Make a table with event No., time-differences Δt(PKP1-PKIKP) and Δt(PKP2-PKIKP), h, D(Δt), D(fit), D(NEIS) and δD which is D(Δt or fit) - D(NEIS).

- Measure and write down for each event in Fig. 2 the Δt(PKP1-PKIKP) and/or Δt(PKP2-PKIKP), if possible with an accuracy of better than 0.5 s.

- Determine D(Δt) for all time differences and D(average) for each event in Fig. 2 by taking into account the source depth determined under 1.1.

- Use the transparent overlay of Fig. 4 and try a best fit with all phases, taking h into account ! Write down your D(fit) ! You will then be given the values for D(NEIS).

- Determine $\delta D(\Delta t)$ and δD(fit) and assess the accuracy of your own distance determinations as compared to NEIS.

The origin time of the event could additionally be determined knowing the absolute onset times measured, h and D as determined above and consulting a published absolute travel-time curve or table (e.g. Kennett 1991).

1.3 Azimuth determination

The back-azimuth in degrees against North can be determined from the relationship $\mathbf{Az = \arctan (A_E/A_N)}$ with A_E and A_N as the trace amplitudes measured in mm from the equally calibrated records of the E-W and N-S components.

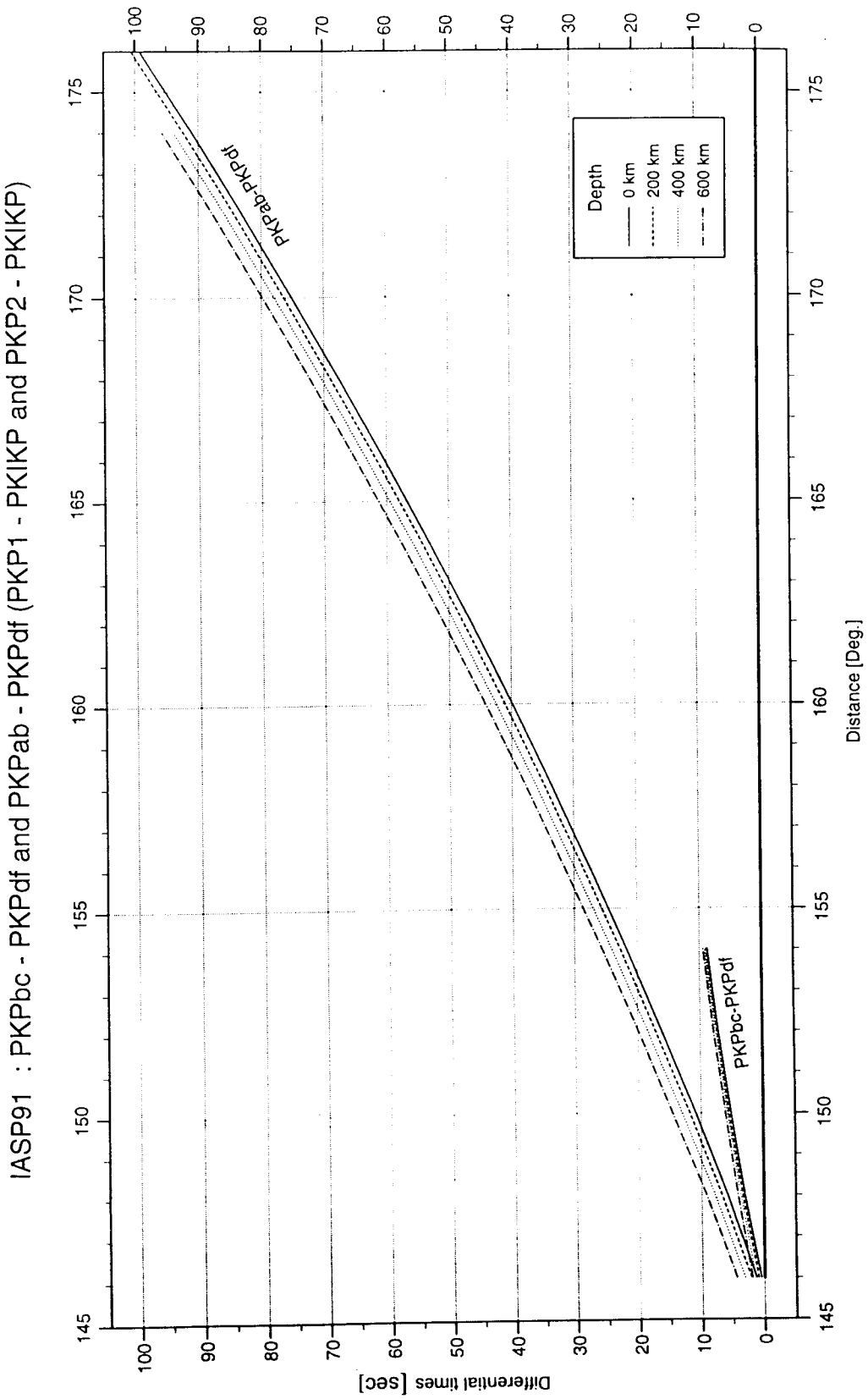

Fig. 4

Scientific Technical Report STR 98/05
DOI: 10.2312/GFZ.b103-98055

Note: Be carefull in deciding about the proper quadrant in which the determined angle is situated by comparing the polarities in all three records !

Exercise 3:

- Determine Az from the 3-component records of event No. 3 in Fig. 2 for which you have already determined D !

- Find the source area by using the global map with D and Az isolines centered around station CLL ! Write down the name of the source area. You will then be given the name of the source area as determined by NEIS.

- Assess the achievable accuracy of a single station location as compared to NEIS.

1.4 Magnitude determination from direct longitudinal core phases

Although several versions of magnitude calibration functions Q for PKP waves have already been proposed earlier, no generally accepted calibration functions for core phases do exist until now. Miyamura (1974) considered only shallow earthquakes. Janský et al. (1977) were the first to publish preliminary depth-dependent calibration functions. They allowed magnitude determinations based on measurements of the maximum A/T ratio (A - amplitude in nm, T - period in s) from the whole PKP-wave group regardless of what branch of the travel-time curve it is related to. Kowalle et al. published Q functions for the first PKP onset measured at station MOX, Germany, and for CLL single phase measurements for source depth $h < 100$ km and $h > 500$ km. Wendt and Tittel (1991) used 26 Tuamotu underground nuclear explosions and the Homogeneous Magnitude System (HMS), developed by Christoskov et al. (1978 and 1985) to determine station corrections, magnitudes and a calibrating function for PKP (maximum amplitudes of the group only) for the rather limited distance interval 143° to 148°.

In the exercise we will use detailed depth- and distance-dependent functions Q(D, h) which were determined by one of us (S. Wendt) for all three direct core phases appearing in the range D= 145° - 164°. The isoline-plots of Q(D, h) shown in Fig. 5 were derived from a total of about 4000 A/T-readings between 1970 and 1994 at station CLL, Germany. We determine m_b(PKP) by using the relationship:

$$m_b(PKP) = \log_{10} (A/T) + Q(D, h)$$

with amplitude A in μm (10^{-6} m), period T in s, epicentral distance D in degree and source depth h in km. To determine the „true ground motion" amplitude A in nm from the measured trace amplitudes we need to correct the latter for the period-dependent magnification of the seismograph. In case of Fig. 2 the records No. 1 and 3 were made with a frequency response according to the magnification values given in the table below while for event No. 2 the magnification was half of these values.

Period (sec)	0.8	1.0	1.2	1.4	1.6	1.8	2.0	2.4
Magnification	54 250	52 440	49 210	44 090	37 550	30 660	24 420	14 000

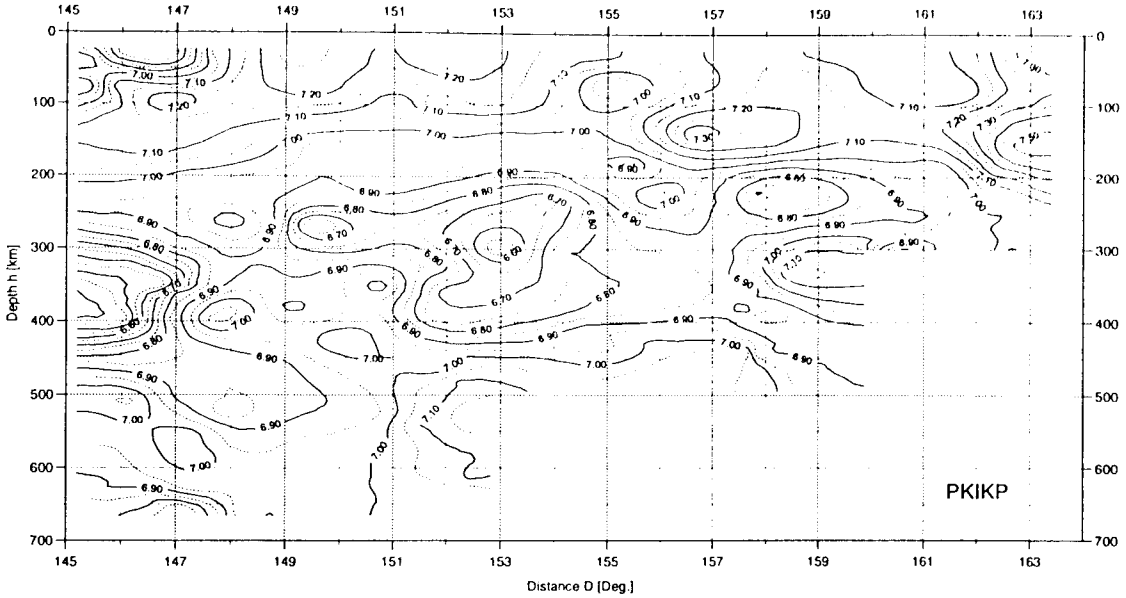
PKIKP
Depth h [km]
Distance D [Deg.]

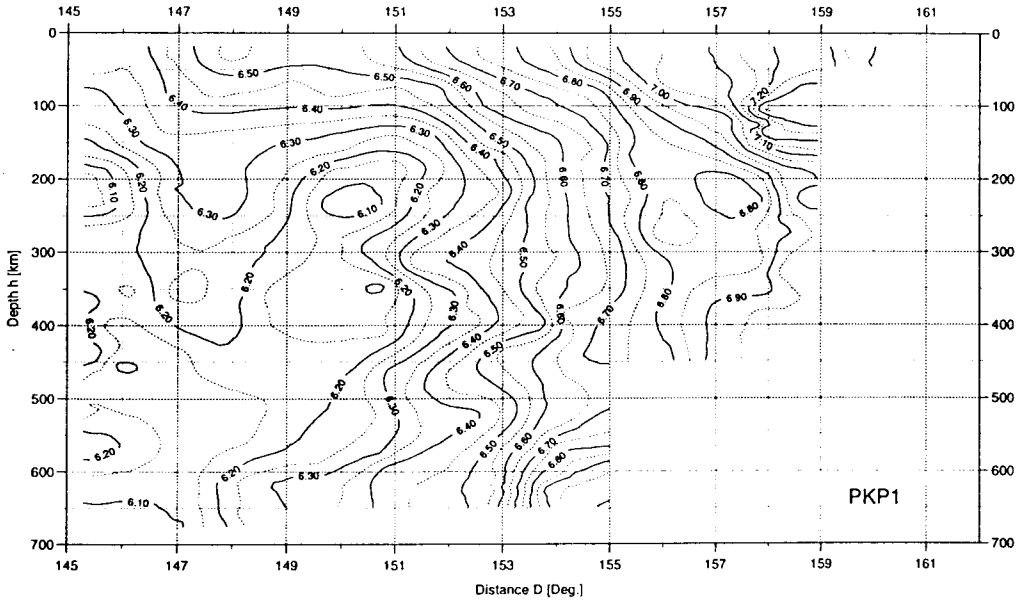
PKP1
Depth h [km]
Distance D [Deg.]

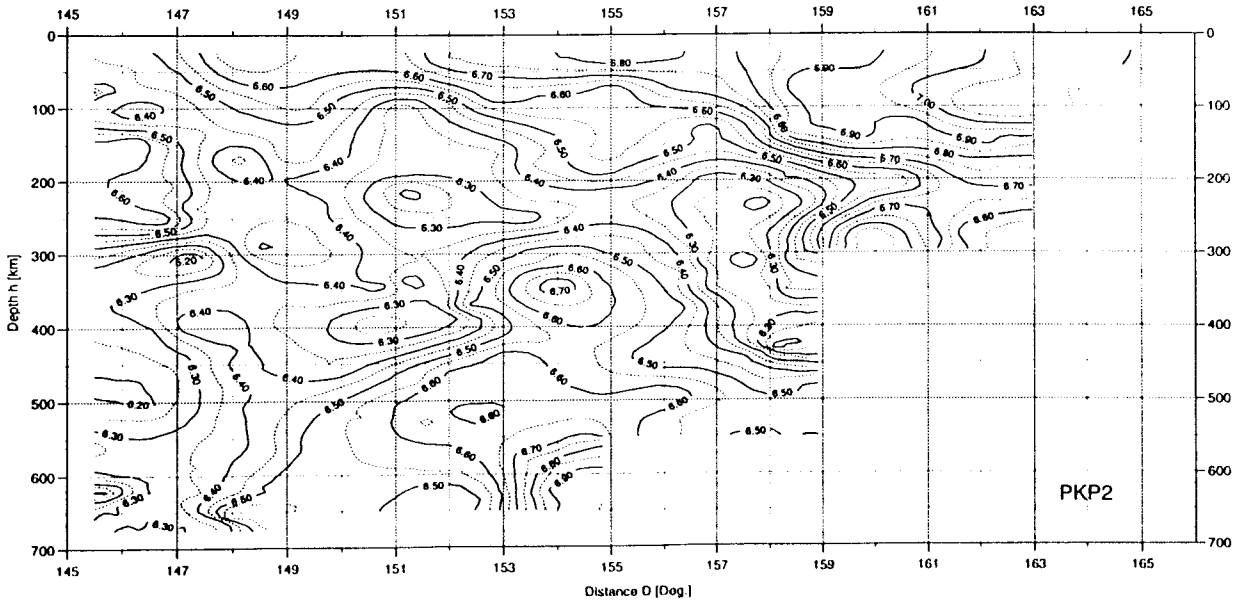
PKP2
Depth h [km]
Distance D [Deg.]

Fig. 5

Exercise 4:

- Make a table with colums for event No., D, h, phase name, T in s, corresponding magnification value M, A (trace in mm), A („true" in nm), log A/T , Q (D, h), m_b (phase), m_b (average), m_b(NEIS) and δm_b which is m_b(average) - m_b(NEIS). The m_b(NEIS)-values will be given to you after you have completed your own determinations.

- Determine log A/T, Q (D,h), m_b(phase) for all identified phases of direct core phases for the three events in Fig. 2 using the the Q(D, h) plots in Fig. 5 and determine m_b(average). You will then be given the values of m_b(NEIS).

- Determine δm_b for your own m_b(phase) and m_b(average) determinations. Assess the accuracy of your magnitude determinations from PKP measurements as compared to the global average m_b(NEIS) values determined from teleseismic P-wave readings.

2. DISTANCE DETERMINATIONS BY USING REFLECTED CORE PHASES

Reflected longitudinal core phases such as PKKP and PKPPKP (cf. section 5 in part I) are very suitable for distance determinations at single stations since they are nearly independent of source depth. Fig. 6 show both theoretical and observed travel-time differences of PKKP - P and PKKP - PKP depending on epicentral distance D, while Fig. 7 gives the respective relationship for PKPPKP - P.

Exercise 5:

- Make a table with event No., phase difference, respective time difference Δt, related epicentral distance D(observed), D(NEIS) and δD which is D(observed) - D(NEIS).

- Determine Δt(PKKP-P or PKP) and Δt(PKPPKP-P), respectively, for the 4 events shown in Fig. 8. You will then be given the values D(NEIS).

- Calculate δD and assess the accuracy of single station D-determinations using reflected longitudinal core phases.

ACKNOWLEDGEMENT

The authors wish to thank Dr. Bernd Tittel from the Geophysical Observatory Collm (CLL) for valuable discussions, suggestions, and careful prove-reading, for making the German version of Fig. 6 available to us and for his many years of dedicated and inspiring work on seismic core phases in routine observatory practice.

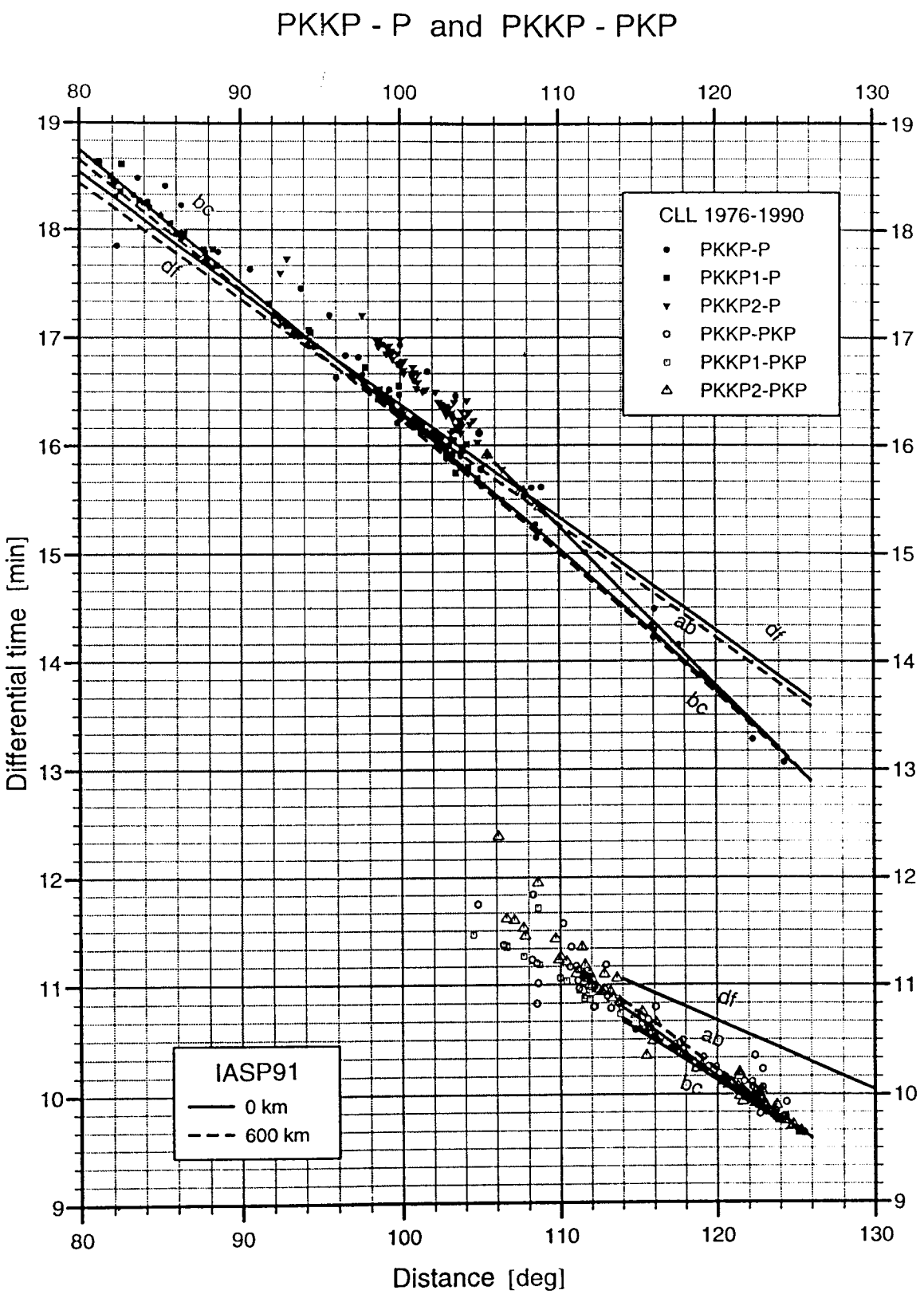

Fig. 6: Comprison between theoretical (IASP 91) and observed travel-time differences for PKKP-P and PKKP-PKP at station CLL as a function of epicentral distance and source depth.

Scientific Technical Report STR 98/05
DOI: 10.2312/GFZ.b103-98055

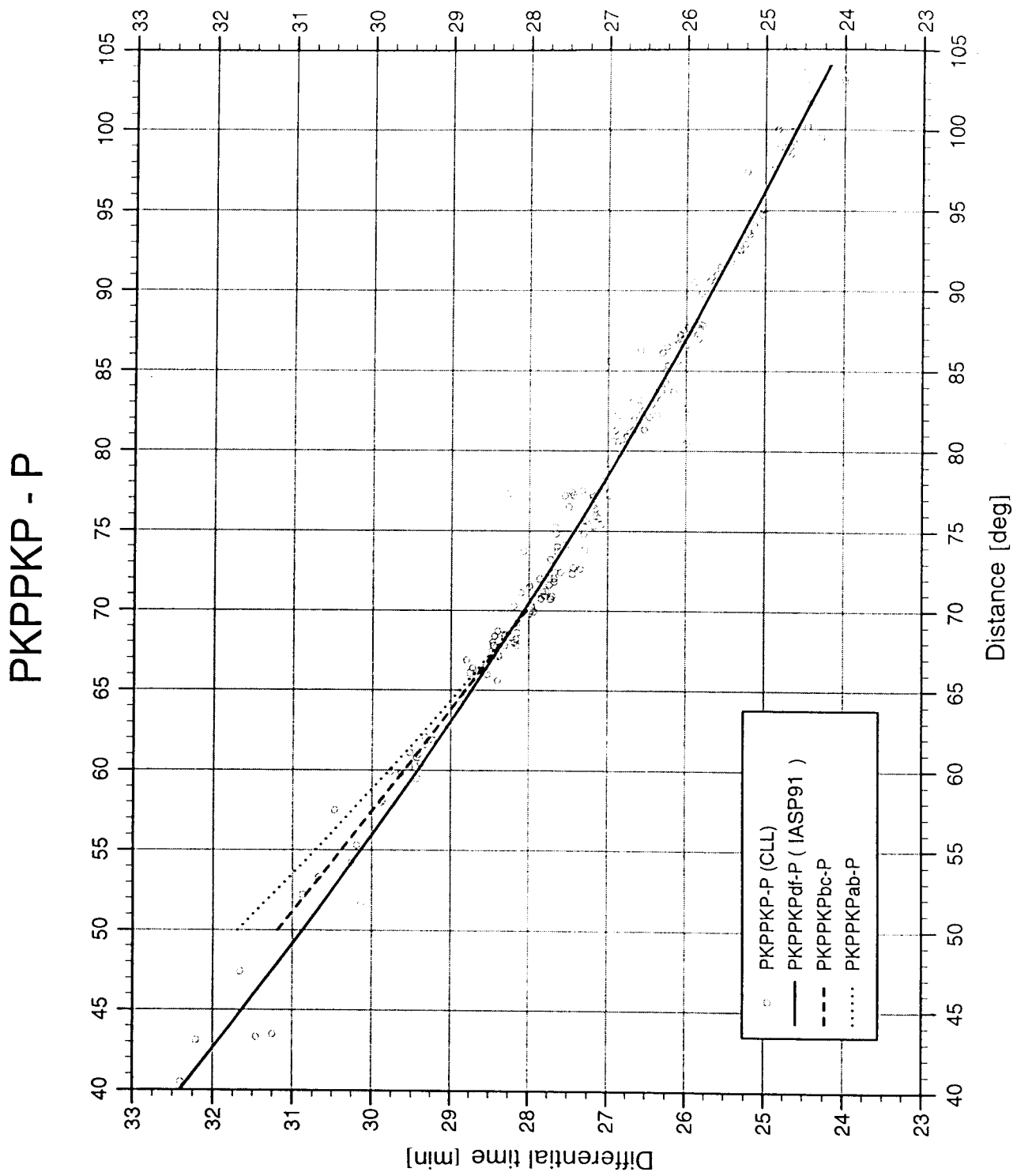

Fig. 7: Comparison between theoretical (IASP91) and observed travel-time differences PKPPKP - P at station CLL depending on epicentral distance.

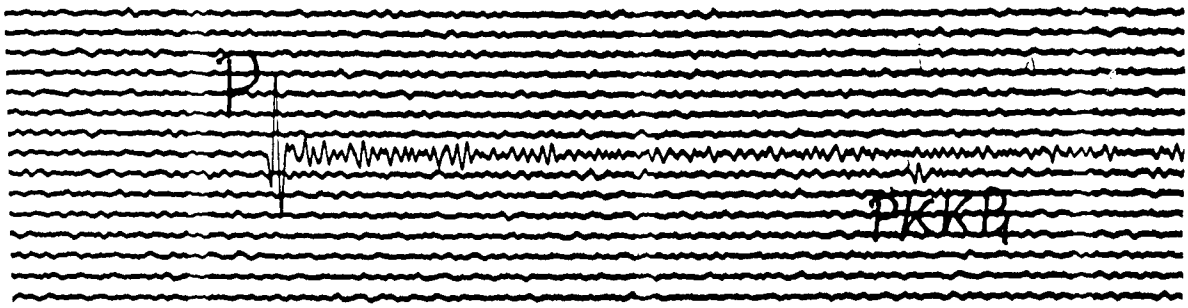

24.08.1995 Mariana Islands: H = 01:55:34.4, D(CLL) = ° ?, h = 588 km, m_b = 6.0

13.07.1994 Banda Sea: H = 11:45:23.4, D(CLL) = ° ?, h = 159 km, m_b = 6.5

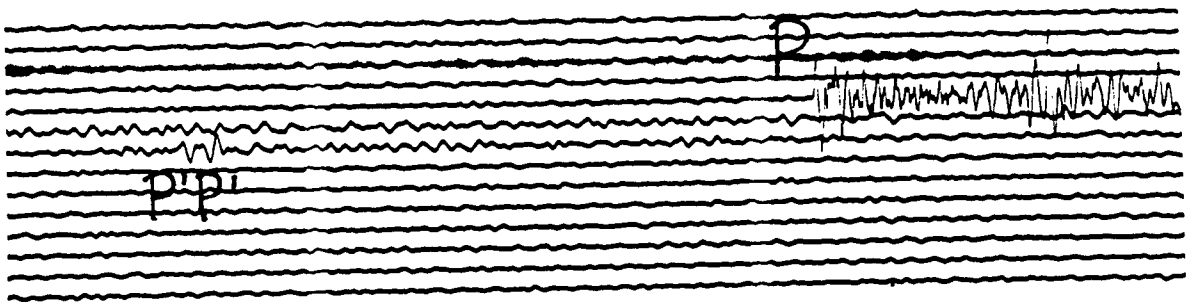

08.08.1994 Myanmar: H = 21:08:31.7, D(CLL) = ° ?, h = 122 km, m_b = 6.1

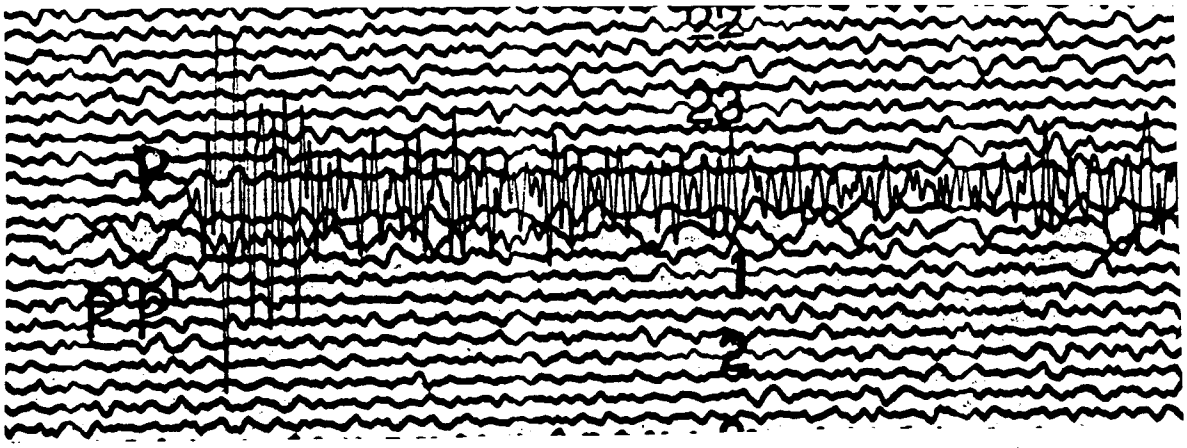

18.02.1996 North of Ascension Island: H = 23:49:27.8, D(CLL) = ° ?, h = 10 km, m_b = 6.3

Fig. 8: Short-period recordings of reflected longitudinal core phases PKKP and PKPPKP (P´P´) at station CLL, Germany. Neighbouring traces are 15 min apart from each other!

Scientific Technical Report STR 98/05
DOI: 10.2312/GFZ.b103-98055

REFERENCES

Bath, M. (1984). Earthquake magnitudes based on PKP and SKP waves. In: The O.G.S. Silver Anniversary Volume, O.G.S. Trieste, p.93-108

Christoskov, L., Kondorskaya, N.V. and Vanek, J. (1978). Homogeneous magnitude system of the Eurasian continent. Tectonophysics, **49**, 131-138.

Christoskov, L., Kondorskaya ,N.V. and Vanek, J. (1985). Magnitude calibrating functions for a multidimensional homogeneous system of reference stations. Tectonophysics, **118**, 213-226.

Janský, J., Ruprechtová, L. and Tittel, B. (1977). Magnitude determination based on short-period core waves. Studia geoph. et geod. **21,** 267-273.

Kennett, B.L.N. (Editor)(1991). IASPEI 1991 Seismological Tables. Research School of Earth Sciences, Australian National University, 167 pp.

Kowalle, G., Tittel, B. and Bormann, P. (1983). Determination of a magnitude calibration function using short-period readings of PKP. Tectonophysics, **93**, 289-294.

Miamura, S. (1974). Determination of body-wave magnitudes for shallow earthquakes in the New Zealand and Macquarie Loop regions using PKP data. Phys. Earth Planet. Int., **8**, 167-176.

Tittel, B. (1977). Zur Bestimmung von Erdbebenmagnituden aus longitudinalen Kernwellen. Gerlands Beitr. Geophysik, **86**, 79-85.

Wendt, S. and Tittel, B. (1991). Calibration function and station corrections for PKP waves in the vicinity of a caustic.Studia geoph. et geod., **35**, 213-220.

SOLUTIONS

Exercise 1: NEIS calculated for the three events the following hypocentral depths:

No.1	h = 435 km
No. 2	h = 235 km
No. 3	h = 540 km

Your own determinations should be within about ± 20 km to these values.

Exercise 2: NEIS calculated for the stations which recorded these three events the following epicentral distances:

No. 1	$D = 148.5^{\circ}$
No. 2	$D = 159.5^{\circ}$
No. 3	$D = 150.0^{\circ}$

Your own determinations should be within $< \pm 2^{\circ}$ to these values.

Exercise 3: Event No. 3 was in the Fiji Islands. Its azimuth as seen from the station CLL was

$Az = 26^{\circ}$.

Your own determinations should be within $< \pm 10^{\circ}$ to this value.

Exercise 4: NEIS determined for the three events from global P-wave data the following body-wave magnitudes:

No. 1	$m_b = 5.0$
No. 2	$m_b = 5.5$
No. 3	$m_b = 5.3$

Your own determinations should be within ± 0.5 magnitude units to these values.

Exercise 5: NEIS determined for the four events the following epicentral distances to CLL:

No. 1	$D = 98.3^{\circ}$
No. 2	$D = 111.2^{\circ}$
No. 3	$D = 66.3^{\circ}$
No. 4	$D = 57.3^{\circ}$

Your own determinations should be within $< \pm 2^{\circ}$ to these values.

Scientific Technical Report STR 98/05
DOI: 10.2312/GFZ.b103-98055

DETERMINATION OF FAULT PLANE SOLUTIONS

Michael Baumbach, Peter Bormann and Helmut Grosser

GeoForschungsZentrum Potsdam, Division 2: Solid Earth Physis and Disaster Research
Telegrafenberg, D-14473 Potsdam, Germany

1. INTRODUCTION

For pure shear mechanisms the P-wave amplitude distribution is described by

$$A_P(\Theta, \phi) = \sin\Theta \ \sin 2\phi \qquad (1)$$

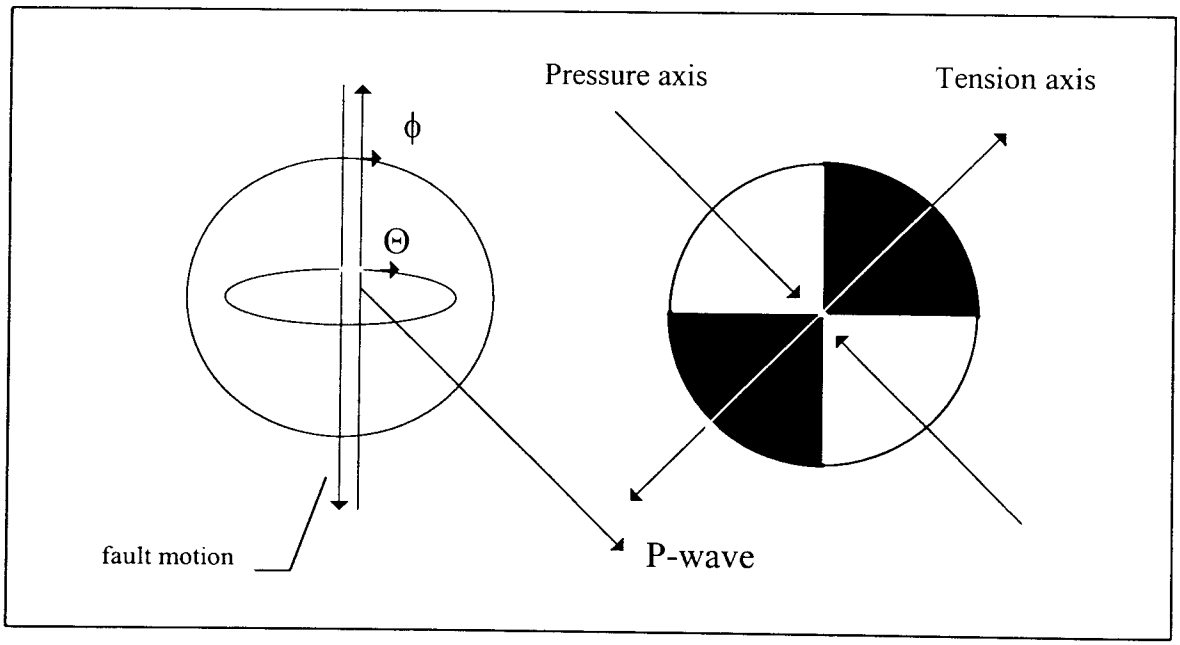

Figure 1: P-wave radiation pattern for a shear fault. Black areas: polarity +, white areas -

This expression divides the focal sphere into 4 quandrants. In each quadrant the sign of the P-wave first motion (polarity) does not change. Opposite quadrants have the same polarity, neighbouring quadrants different polarities. The focal sphere is an imaginary sphere with the hypocentre in it's centre. The position of the quadrants on the focal sphere depends on the orientation of the active fault and the slip direction. Therefore, the estimation of the P-wave first motion polarities and their backprojection onto the focal sphere allows to find the focal mechanism of a shear event (fault plane solution). The only problem is, that the hypocentre and the wave propagation from the source to the individual stations must be known. This may be difficult for a heterogeneous model with 2D or 3D-velocity structure.

In most applications 1D-layered velocity models are accepted (layers with constant velocities and velocity discontinuities at the boundaries). The majority of location programs (e.g. Hypo71, Hypoellipse, Hypoinvers) require this type of velocity model. During location procedure the wave propagation is calculated. The azimuth AZM and the take-off angle AIN at which the P-wave, arriving at a given station, leaves the focal sphere are listed in the output files. The remaining problem to be solved is to find the distribution of P-polarities on the focal

Scientific Technical Report STR 98/05
DOI: 10.2312/GFZ.b103-98055

sphere and to estimate the angles, describing the focal mechanism. For manual fault plane solutions the lower half of the focal sphere is being projected onto a plane. For estimation of angles an equal angle (Wulff net) or equal area projection (Schmidt net) is required. Since only the lower half of the focal sphere is used, one has to project the upper half onto the lower one. This is easily possible because of spherical symmetry of the radiation pattern (Fig.2 & 3).

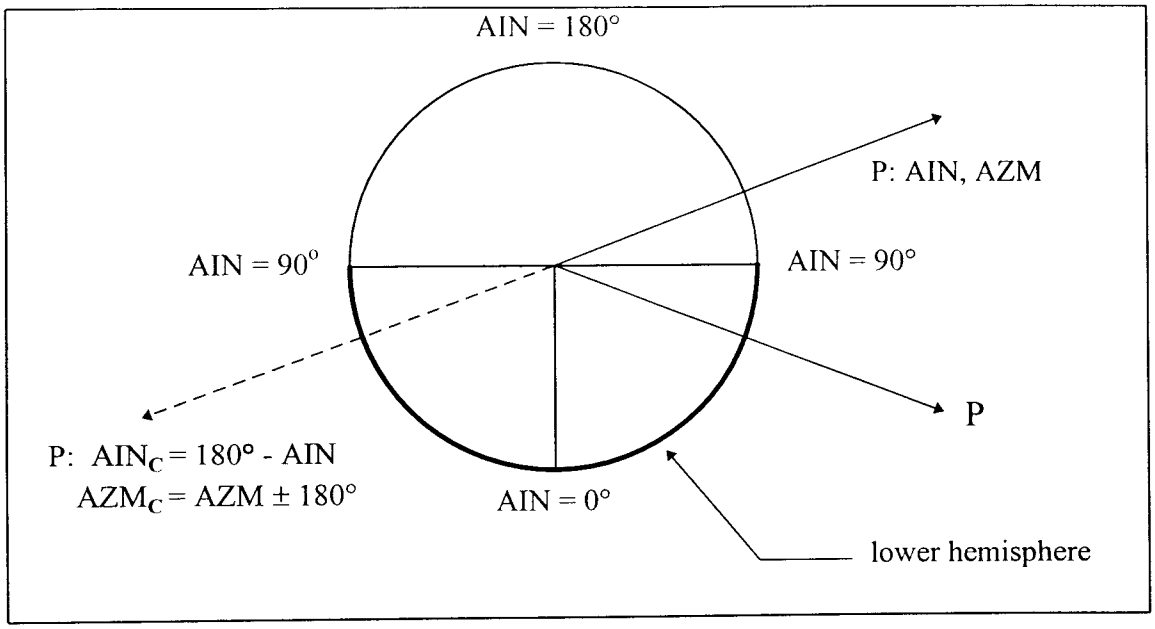

Fig. 2: Transformation of a ray leaving the focal sphere upwards into a downward ray with same polarity and changed incidence angle and azimuth.

Fig. 3 (below): Two rays, leaving the focal sphere in opposite directions, reach - because of the symmetry of radiation pattern - the stations 1 and 2 with the same polarity. The crossing point of the upgoing ray with the focal sphere can, therefore, be remapped according to the formulae given in Fig. 2 into a crossing point with the lower hemisphere which conincides with the ray crossing-point for station 2.

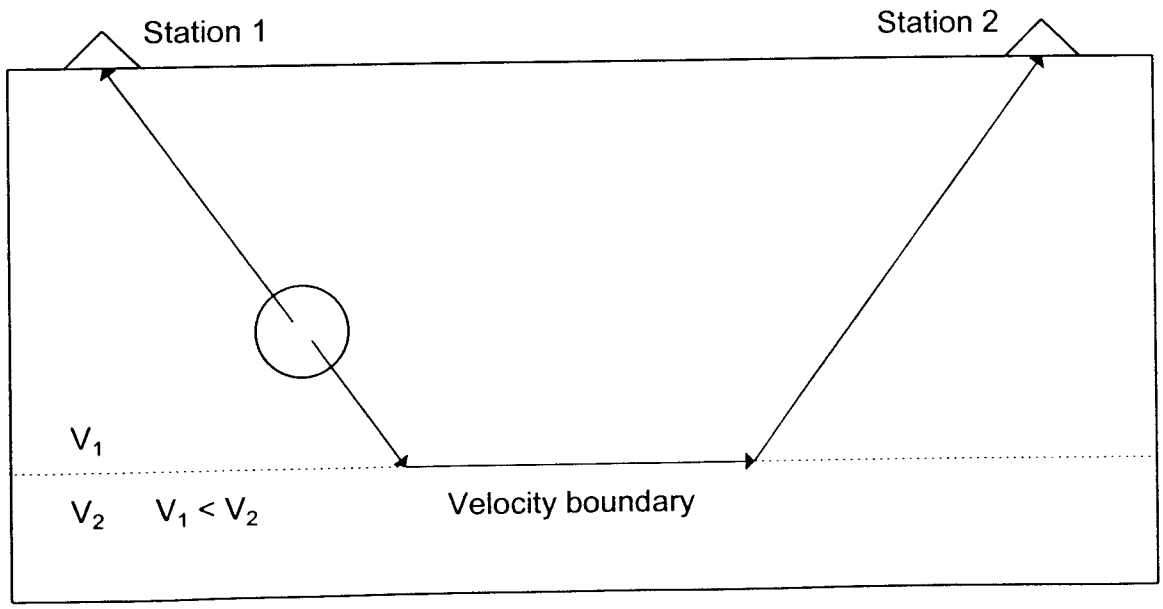

Fig. 4 shows the angles which describe the orientation and motion of a fault plane and Fig. 5 shows their determination in the Wulff net projection. The **strike angle** ϕ is measured clockwise against North ($\mathbf{0° \le \phi \le 360°}$). To resolve the 180° ambiguity, it is assumed that when looking into the strike direction the fault dips to the right hand side (i.e. its fault-trace projection is towards the right of the Wulff net center). The **dip angle** δ describes the inclination of the hanging wall against the horizontal ($\mathbf{0° \le \delta \le 90°}$). The **rake angle** λ describes the displacement of the hanging wall relative to the foot wall ($\mathbf{-180° \le \lambda \le 180°}$). $\lambda = 0$ corresponds to slip in strike direction, $\lambda > 0$ means upward motion of the hanging wall (i.e. *reverse or thrust faulting component*) and $\lambda < 0$ downward motion (i.e. *normal faulting component*).

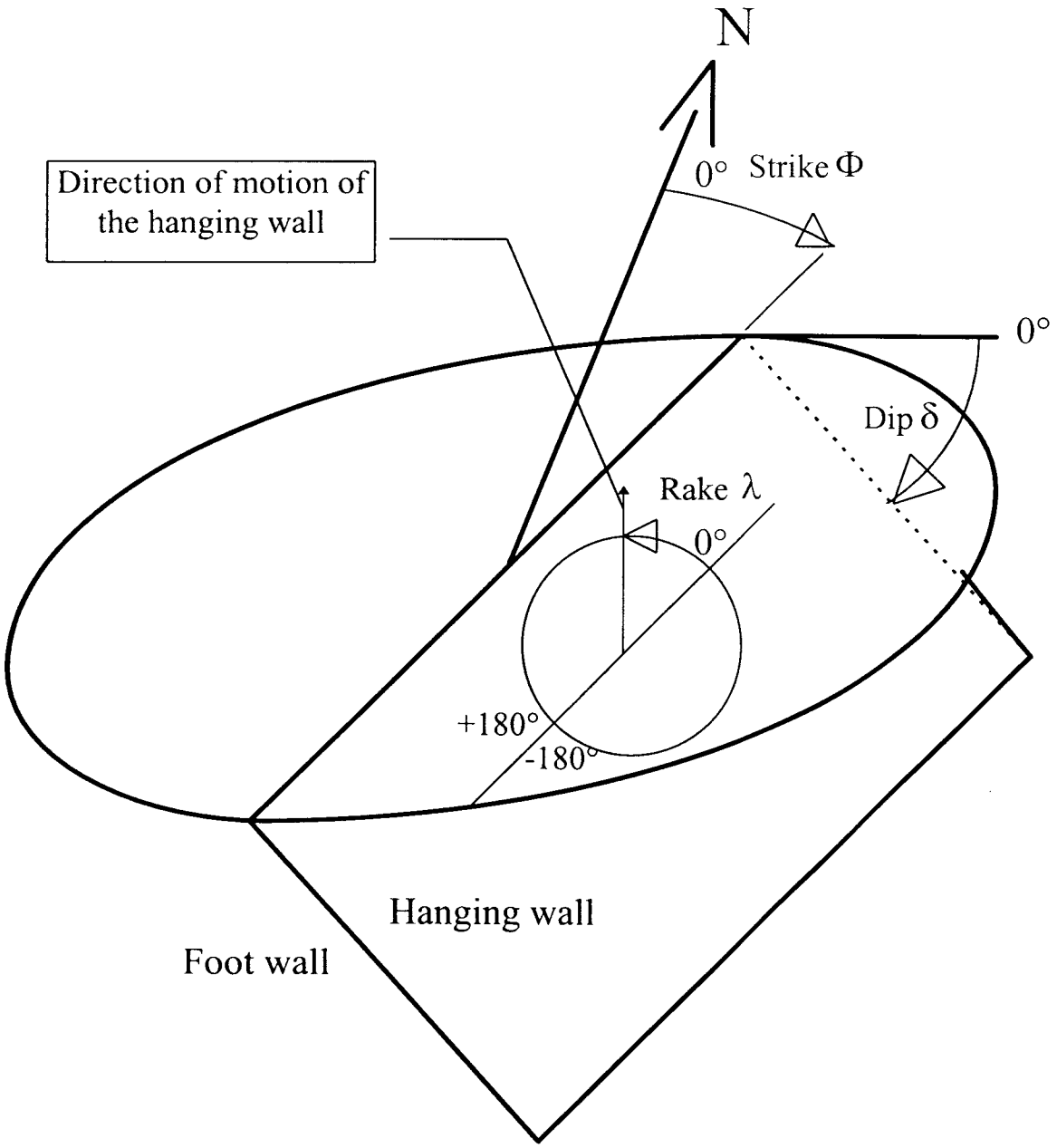

Fig. 4: Angles describing the orientation and motion of faults

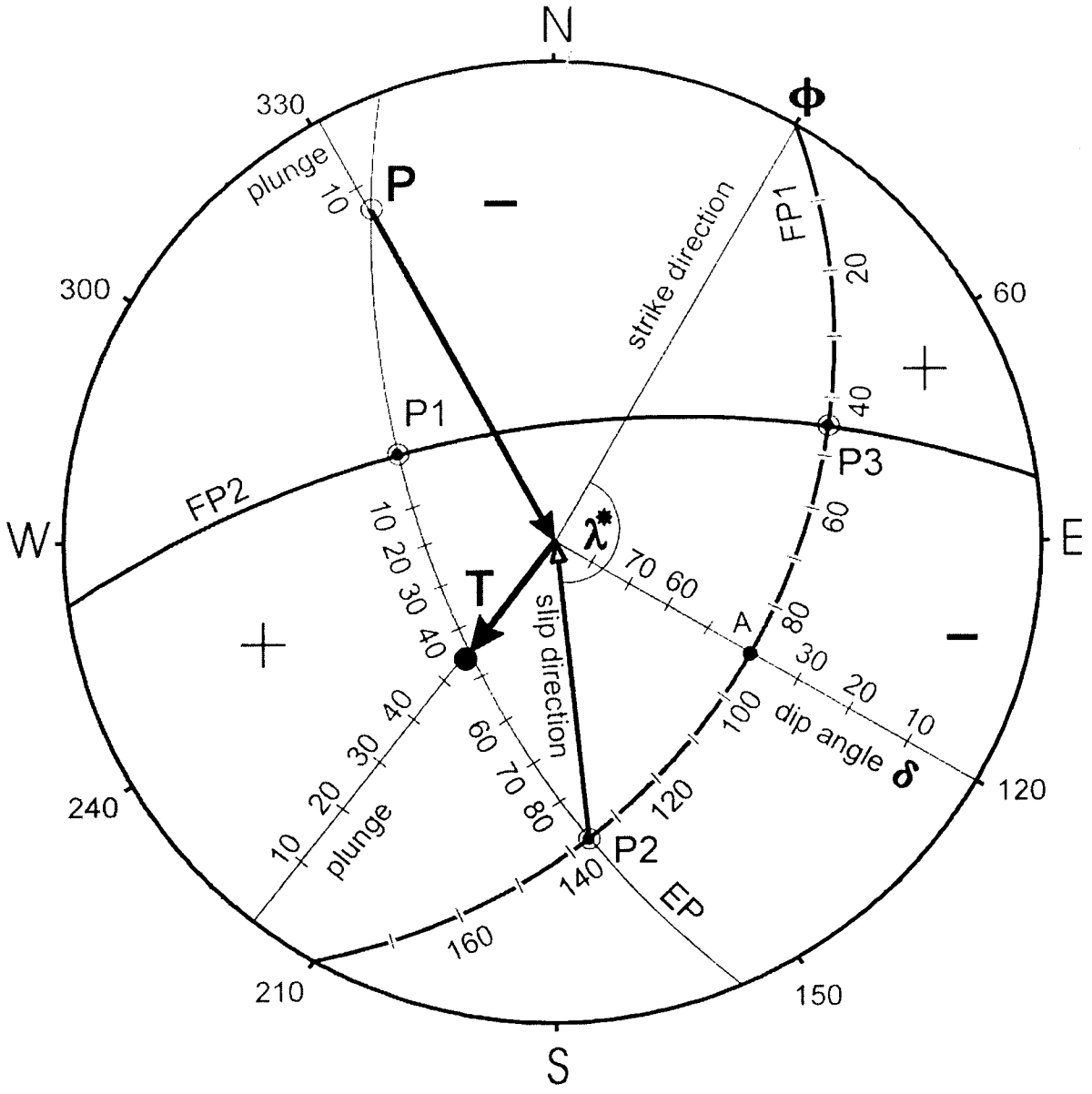

Fig. 5: Determination of the fault plane parameters Φ, δ and λ in the Wulff-net diagram. The polarity distribution, slip direction and projection of FP1 shown do qualitatively correspond to the faulting case depicted in Fig. 4. For abbreviations used see text.

In Fig. 5 P1, P2 and P3 mark the positions of the poles of the planes FP1 (fault plane), FP2 (auxilary plane) and EP(equatorial plane) in their Wulff-net projections. From Fig. 5 it is obvious that all three planes are perpendicular to each other (i.e. 90° apart) and intersect in the poles of the respective third plane, i.e. FP1 and FP2 in P3, FP1 and EP in P2 etc. Note that on the basis of polarity readings alone it can not be decided whether FP1 or FP2 was the really acting fault. A discrimination from seismological data alone requires additionally a study of the azimuth dependence of frequency (*Doppler* effect!) and amplitudes or waveforms. On the other hand, seismotectonic considerations or field evidence from surface rupture in case of strong earthquakes may allow to resolve this ambiguity. Figs. 6 and 7 depict several basic types of earthquake faulting and their appearance in Wulff-net projections, respectively.

Scientific Technical Report STR 98/05
DOI: 10.2312/GFZ.b103-98055

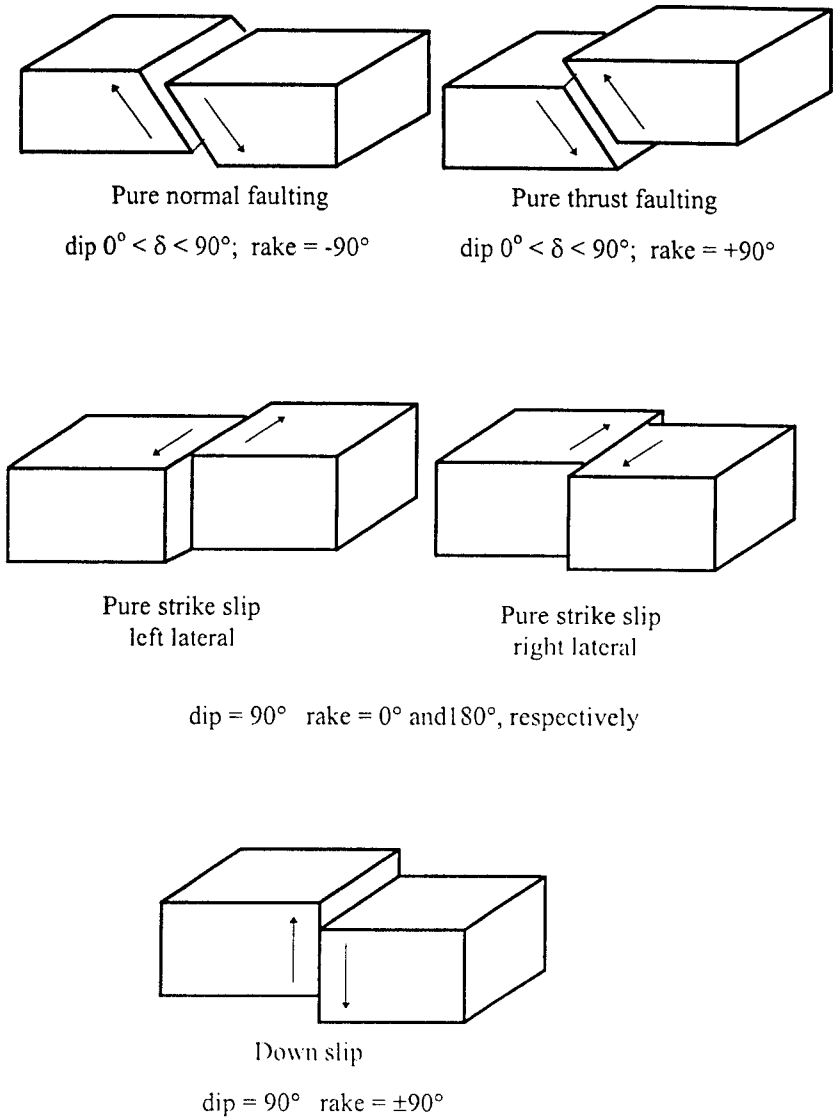

Fig. 6: Basic types of earthquake faulting for some selected dip and rake angles. Note that mixed types of faulting do occur when $\lambda \neq 0$, 180° or ± 90°., e.g. normal faulting with strike-slip component or strike-slip with thrust component. Also, dip angles may vary between $0° < \delta \leq 90°$. For fault plane traces and polarity distributions of these faulting types in the Wulff diagram see Fig. 6.

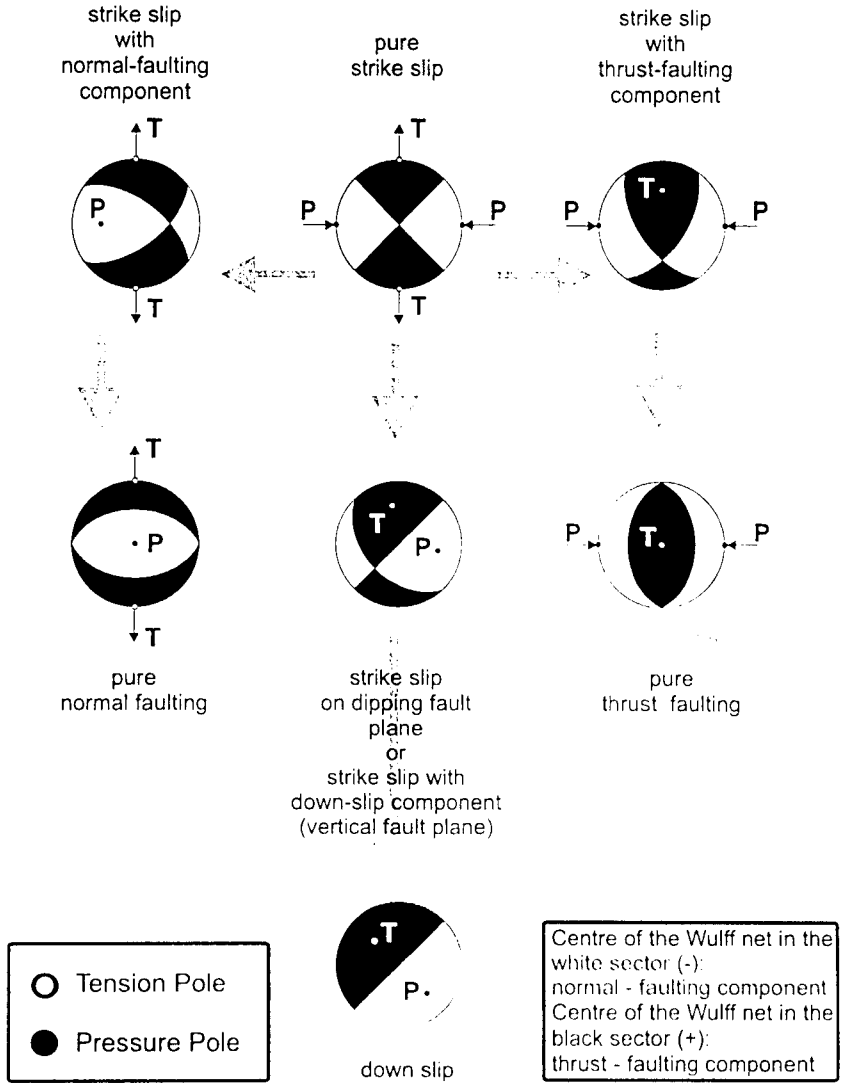

Fig. 7. Wulff-net projections of the cut-traces of the fault planes and of the penetration points of the T- and P-axes through the lower half of the focal sphere for different faulting mechanisms. White sectors correspond to negative and black sectors to positive first-motion polarities.

GeoForschungsZentrum Potsdam

2. DATA AND RELATIONSHIPS

When localizing near events with HYPO71 the values for both the azimuth AZM and for the take-off angles AIN of the rays leaving the source for each station are given in the localization output file together with the polarity readings made under column PRMK (U = up = +; D = down = -). Tab. 3 gives an example for an aftershock of the Erzincan earthquake of 1992. When one wishes to determine the focal plane solution for teleseismic events one can find in the bulletins of the International Seismological Center (ISC) data for polarity readings at reporting stations (↑ for up and ↓ for down) and calculated AZM values. A cut-out example is shown in Fig. 7 which also gives results of seismic moment tensor and fault plane solutions as calculated by various international data centers or agencies. But these bulletins do not give values for AIN. They can be calculated by using the relationship

$$\sin AIN = v_P(h) \times (r_o/r_h) \times S_o(\Delta, h)/111.11 \qquad (2)$$

with $S_o(\Delta, h)$ being the slowness observed on the Earth's surface (in units s/deg) at the epicentral distance Δ (in degree) as a function of the hypocentral depth h (in km), $v_P(h)$ being the P-wave velocity at the depth h and $r_o = 6371$ km the Earth's radius; $r_h = r_o - h$.

Tab. 1 gives the respective values v_P for P-waves and Tab. 2 for $S_o(\Delta, h)$ according to the IASPEI91 velocity model (Kennett, 1991).

Tab. 1: P-wave velocities as a function of depth h according to the IASPEI 1991 Seismological Tables (Kennett, 1991) in the depth range 0 km ≤h ≤ 760 km

h (km)	v_P (km/s)	h (km)	v_P (km/s)	h (km)	v_P (km/s)
0	5.8000	171	8.1917	660	10.2000
20	5.8000	210	8.3000	660	10.7900
20	6.5000	271	8.5227	671	10.8192
35	6.5000	371	8.8877	760	11.0558
35	8.0400	410	9.0300		
71	8.0442	410	9.3600		
120	8.0500	471	9.5650		
120	8.0500	571	9.9010		

Scientific Technical Report STR 98/05
DOI: 10.2312/GFZ.b103-98055

Tab. 2: Slowness values $S_o = dT/d\Delta$ of Pn, P or PKP_{df} first arrivals at the Earth´s surface as a function of hypocentral depth h according to IASPEI 1991 Seismological Tables (Kennett, 1991)

		S_o (in s/deg)			
Phase	**Δ (in deg)**	h = 0 km	h = 100 km	h = 300 km	h = 600 km
Pn (P)	2	13.75	12.90	7.91	4.01
	4	13.75	13.49	10.96	6.91
	6	13.74	13.58	11.95	8.60
	8	13.72	13.60	12.25	9.48
	10	13.70	13.59	12.26	9.90
	12	13.67	13.29	12.12	10.05
	14	13.64	12.91	11.03	10.06
	16	12.92	12.43	10.91	9.17
	18	12.33	10.97	10.73	9.10
P	20	10.90	10.81	10.50	9.02
	22	10.70	10.58	9.12	8.90
	24	9.14	9.11	9.03	8.83
	26	9.06	9.02	8.91	8.76
	28	8.93	8.90	8.83	8.66
	30	8.85	8.82	8.75	8.56
	32	8.77	8.74	8.65	8.45
	34	8.67	8.64	8.54	8.33
	36	8.56	8.52	8.42	8.21
	38	8.44	8.40	8.29	8.08
	40	8.30	8.26	8.16	7.95
	42	8.17	8.13	8.03	7.82
	44	8.03	7.99	7.89	7.69
	46	7.89	7.85	7.75	7.56
	48	7.55	7.71	7.61	7.42
	50	7.60	7.56	7.47	7.29
	52	7.46	7.42	7.33	7.15
	54	7.31	7.28	7.19	7.02
	56	7.17	7.13	7.05	6.88
	58	7.02	6.99	6.90	6.74
	60	6.88	6.84	6.76	6.61
	62	6.73	6.70	6.62	6.47
	64	6.59	6.55	6.48	6.33
	66	6.44	6.41	6.33	6.19
	68	6.30	6.27	6.19	6.05
	70	6.15	6.12	6.05	5.91
	72	6.00	5.97	5.90	5.77
	74	5.86	5.83	5.76	5.63
	76	5.71	5.68	5.61	5.49
	78	5.56	5.53	5.46	5.34
	80	5.40	5.38	5.31	5.20

Tab. 2: cont.

		S_0 (in s/deg)			
Phase	**Δ (in deg)**	h = 0 km	h = 100 km	h = 300 km	h = 600 km
P	82	5.25	5.22	5.16	5.04
	84	5.09	5.07	5.01	4.90
	86	4.94	4.92	4.85	4.72
	88	4.74	4.72	4.69	4.65
	90	4.66	4.65	4.64	4.61
	92	4.61	4.61	4.60	4.57
	94	4.58	4.57	4.55	4.51
	96	4.52	4.51	4.49	4.44
	98	4,45	4.44	4.44	4.44
P_{diff}	100-144	4.44	4.44	4.44	4.44
PKP_{df}	114	1.92	1.92	1.92	1.92
	116-122	1.91	1.91	1.91	1.91
	124-126	1.90	1.90	1.90	1.90
	130	1.88	1.88	1.88	1.88
	136	1.84	1.84	1.84	1.83
	140	1.80	1.79	1.79	1.78
	142	1.76	1.76	1.76	1.75
	144	1.73	(1.72)	(1.72)	(1.71)
	146	1.68	1.68	1.67	1.66
	148	1.63	1.62	1.62	1.60
	150	1.57	1.56	1.55	1.54
	152	1.49	1.49	1.48	1.47
	154	1.42	1.41	1.40	1.39
	156	1.33	1.33	1.32	1.30
	158	1.24	1.23	1.23	1.21
	160	1.14	1.14	1.13	1.11
	162	1.04	1.03	1.03	1.01
	164	0.93	0.93	0.92	0.91
	166	0.82	0.82	0.81	0.80
	168	0.71	0.70	0.70	0.69
	170	0.59	0.59	0.58	0.58
	172	0.47	0.47	0.47	0.47
	174	0.36	0.36	0.35	0.35
	176	0.24	0.24	0.24	0.23
	178	0.12	0.12	0.12	0.12
	180	0.00	0.00	0.00	0.00

Scientific Technical Report STR 98/05
DOI: 10.2312/GFZ.b103-98055

Tab. 3: HYPO71 output file from an Erzincan aftershock

DATE	ORIGIN	LAT N	LONG E	DEPTH	MAG	NO	DM	GAP	M	RMS	ERH	ERZ
920412	319 12.99	39-31.11	39-52.46	3.13		28	4	87	1	0.08	0.3	0.2

STN	DIST	AZM	AIN	PRMK	HRMN	P-SEC	TPOBS	TPCAL	DLY/HL	P-RES	P-WT	AMX	PRX	CALX
ALI	3.7	40	130	IPD0	319	9.10	0.95	0.92	0.07	-0.03	1.10	0	0	0.00
ME2	7.1	134	114	IPD0	319	13.84	1.75	1.47	0.29	-0.01	1.10	0	0	0.00
KAN	7.7	197	112	IPD0	319	12.20	1.51	1.57	0.02	-0.08	1.09	0	0	0.00
YAR	8.2	48	111	IPD0	319	13.83	1.74	1.66	0.06	0.02	1.10	0	0	0.00
PIT	9.2	337	109	IPD0	319	14.75	1.82	1.83	0.03	-0.04	1.10	0	0	0.00
ERD	13.6	313	103	IPD0	319	15.58	2.65	2.64	-0.07	0.09	1.09	0	0	0.00
DEM	14.3	330	102	IPD0	319	14.84	2.75	2.76	-0.03	0.02	1.10	0	0	0.00
GIR	14.4	301	102	IPU0	319	12.55	2.73	2.78	-0.10	0.06	1.10	0	0	0.00
UNK	16.2	336	101	IPD0	319	12.05	3.04	3.10	-0.05	-0.01	1.10	0	0	0.00
SAN	17.2	76	62	IPU0	319	15.35	3.26	3.29	-0.03	0.00	1.10	0	0	0.00
PEL	18.6	327	62	IPD0	319	16.69	3.76	3.54	0.18	0.05	1.10	0	0	0.00
GUN	22.6	290	62	IPU0	319	16.20	4.11	4.20	-0.16	0.07	1.09	0	0	0.00
ESK	22.7	312	62	IPU1	319	16.59	4.50	4.22	0.30	-0.01	0.82	0	0	0.00
SOT	23.8	318	62	IPD1	319	16.52	4.43	4.40	0.20	-0.17	0.75	0	0	0.00
BA2	27.3	79	62	IPU0	319	16.92	4.83	4.99	-0.16	0.01	1.10	0	0	0.00
MOL	28.8	297	62	IPU0	319	18.06	5.13	5.24	-0.04	-0.06	1.09	0	0	0.00
YUL	29.3	67	62	IPU0	319	11.80	5.06	5.32	-0.22	-0.04	1.10	0	0	0.00
ALT	31.5	59	62	IPD0	319	17.67	5.58	5.68	-0.17	0.07	1.10	0	0	0.00
GUM	32.0	320	62	IPU0	319	13.95	5.47	5.77	-0.02	-0.28	0.54	0	0	0.00
GU2	32.0	320	62	IPD0	319	17.79	5.70	5.77	-0.03	-0.04	1.10	0	0	0.00
BAS	35.6	308	62	IPD0	319	19.89	6.96	6.36	0.51	0.09	1.09	0	0	0.00
BIN	36.4	295	62	IPU0	319	19.14	6.21	6.49	-0.28	0.00	1.10	0	0	0.00
HAR	38.7	24	62	IPD0	319	18.73	6.64	6.88	-0.13	-0.11	1.06	0	0	0.00
KIZ	42.2	311	62	IPU0	319	21.08	8.15	7.47	0.26	0.43**	0.03	0	0	0.00
ACR	47.5	311	62	IP 0	319	16.40	8.69	8.34	0.23	0.12	1.07	0	0	0.00
AKS	48.7	284	62	IPD0	319	20.34	8.25	8.55	-0.38	0.09	1.09	0	0	0.00
SUT	49.6	295	62	IPU0	319	21.30	8.37	8.69	-0.25	-0.07	1.09	0	0	0.00
HEY	59.8	307	62	EPN1	319	22.69	10.60	10.39	0.14	0.07	0.74	0	0	0.00

NEIC Moment tensor solution: s23, scale 10^{17}Nm; M_{rr}–3.05; $M_{\theta\theta}$–0.97; $M_{\phi\phi}$4.03; $M_{r\theta}$–2.51; $M_{r\phi}$–1.95; $M_{\theta\phi}$2.71. Depth 272km; Principal axes: T 6.09,Plg17°,Azm117°; N –1.36, Plg27°,Azm216°; P –4.73,Plg57°,Azm358°; Best double couple: M_o5.4×10^{17}Nm; NP1:ϕ_s172°,δ36°,λ–140°. NP2: ϕ_s48°,δ68°,λ–60°.

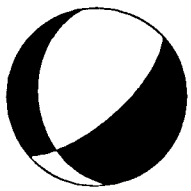

*HRVD 05d 13h 24m 15s7±0s2, 39°10N±°02×15°39E±°02, h295km±.8km, Centroid moment tensor solution. Data used: GDSN; LP body waves: s50,c**; Half duration: 1s9. Moment tensor: Scale 10^{17}Nm; M_{rr}–2.17±.06; $M_{\theta\theta}$–1.97±.10; $M_{\phi\phi}$4.14±.09; $M_{r\theta}$–3.51±.09; $M_{r\phi}$–3.29±.09; $M_{\theta\phi}$0.01±.09. Principal Axes: T 5.83,Plg27°,Azm103°; N 0.32,Plg30°,Azm210°; P –6.15,Plg48°,Azm339°. Best double couple: M_o6.0×10^{17}Nm, NP1:ϕ_s146°,δ33°,λ–157°. NP2:ϕ_s37°,δ78°,λ–60°.*

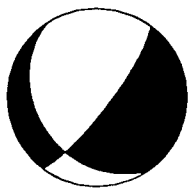

ISC 05d 13h 24m 11s4±0s13, 39°16N±°016×15°18E±°014, h290km±1.3km, (h286km±2.7km:pP–P), n757, σ1s04/729, Mb5.7/107, 119C-155D, Southern Italy

OVO	**Vesuviano**	**1.77**	**340**	**↑*i*P**	**13 24 57.2**	**+1.5**
MCT	**Mte Cammarata**	**1.95**	**219**	**P**	**13 24 57.7**	**+0.6**
FG4	**Candela**	**1.99**	**8**	**P**	**13 24 58.2**	**+0.9**
MEU	**Monte Lauro**	**2.07**	**186**	**dP**	**13 24 56.8**	**–1.3**
PZI	**Palazzolo**	**2.14**	**186**	***e*P**	**13 24 57**	**–1.7**
FAI	**Favara**	**2.21**	**213**	**dP**	**13 24 59.5**	**+0.1**
MSC	**Monte Massico**	**2.23**	**336**	**↑*i*P**	**13 25 01.1**	**+1.6**
SGG	**Gregorio Matese**	**2.30**	**345**	**↑*i*P**	**13 25 01.9**	**+1.8**

Fig. 8: Cut-out of the ISC bulletin (left) with NEIC and Harward (HRVD) moment tensor fault plane solutions (right) for the Italy deep earthquake of Jan. 05, 1994. In the columns 3 to 5 of the bulletin the following data are given: 3 - epicentral distance in degree, 4 - backazimuth AZM in degree, 5 - phase code and polarity.

Tab. 4: Original and corrected values of ray azimuth (AZM and AZMc) and take-off angles (AIN and AINc) towards stations of a temporay network which recorded the Erzincan aftershock of April 12, 1994. The original values were taken from Tab.3. Calculate the corrected ones. Other abbreviations used: STA - station code, POL - P-wave first motions (U = up = +; D = down = -). 8×tan(AINc/2) is the distance of the given polarity mark on the Wulff net from its center in cm.

STA	AZM (degree)	AIN (degree)	POL	AZMc (degree)	AINc (degree)	8×tan(AINc/2) (cm)
ALI	40	130	-			
ME2	134	114	-			
KAN	197	112	-			
YAR	48	111	-			
ERD	313	103	-			
DEM	330	102	-			
GIR	301	102	+			
UNK	336	101	-			
SAN	76	62	+			
PEL	327	62	-			
GUN	290	62	+			
ESK	312	62	+			
SOT	318	62	-			
BA2	79	62	+			
MOL	297	62	+			
YUL	67	62	+			
ALT	59	62	-			
GUM	320	62	+			
GU2	320	62	-			
BAS	308	62	-			
BIN	295	62	+			
HAR	24	62	-			
KIZ	311	62	+			
AKS	284	62	-			
SUT	295	62	+			

Tab. 5: Selected data for five seismic stations at different epicentral distances Δ and back-azimuth AZM which reported for the deep earthquake in Southern Italy on Jan 05, 1994 (h = 286 km) polarity readings for the first P or PKP onset in the ISC bulletin.

STA	Δ (deg)	AZM (deg)	POL	r_0/r_h	$v_h/111.1$ (deg/s)	$S_0(\Delta,h)$ (s/deg)	AIN (deg)	AZMc (deg)	AINc (deg)
SGG	2.30	345	+						
KHC	10.03	354	-						
BTH	12.25	294	+						
ZAK	60.02	48	-						
PAE	154.8	324	-						

3. EXERCISES

3.1 Exercise on fault plane determination for the Erzincan aftershock

Task 1:
The original data given in Tab. 4 may need to be corrected in order to assure uniform lower hemisphere projection!. If AIN > 90° add in the table the corrected take-off angles and the corrected azimuths with: AINc = 180° - AIN, AZMc = AZM ± 180°.
In case of AIN < 90° :the original values remain unchanged.

Task 2:
Compute the distance d of the sign entries from the center of the Wulff net according to
d = 8 × tan(AINc / 2).

Task 3:
Mark the P-wave first motion signs in the Wulff net (Fig. 9) according to the calculated values for d and the ray azimuth AZMc. The azimuth is measured clockwise from North, i.e. 0° = North, 90° = East etc. Use the sign + for + polarities (trace up = compressional first motion) and o for - polarities (trace down = dilatational first motion).

Task 4:.
Try to find - by by rotating the Wulff net over the plotted data - a great circle which separates as good as possible the expected quadrants with different first motion signs. This great circle represents the intersection trace of one of the possible fault planes with the lower half of the focal sphere (FP1). Note that switching polarities close to each other may be due to uncertain readings in case of small amplitudes which are indicative for the week P-wave radiation in the strike direction of nodal planes!

Task 5:
Mark point A at the middle of FP1 and find, perpendicular to it, the pole P1 of FP1, 90° apart (cf. Fig. 5). All great circles, passing this pole are perpendicular to the great circle of FP1. Since the second possible (auxiliary) fault plane (FP2) must be perpendicular to the FP1, it has to pass P1. Find, accordingly, FP2 which again has to separate areas of different polarity.

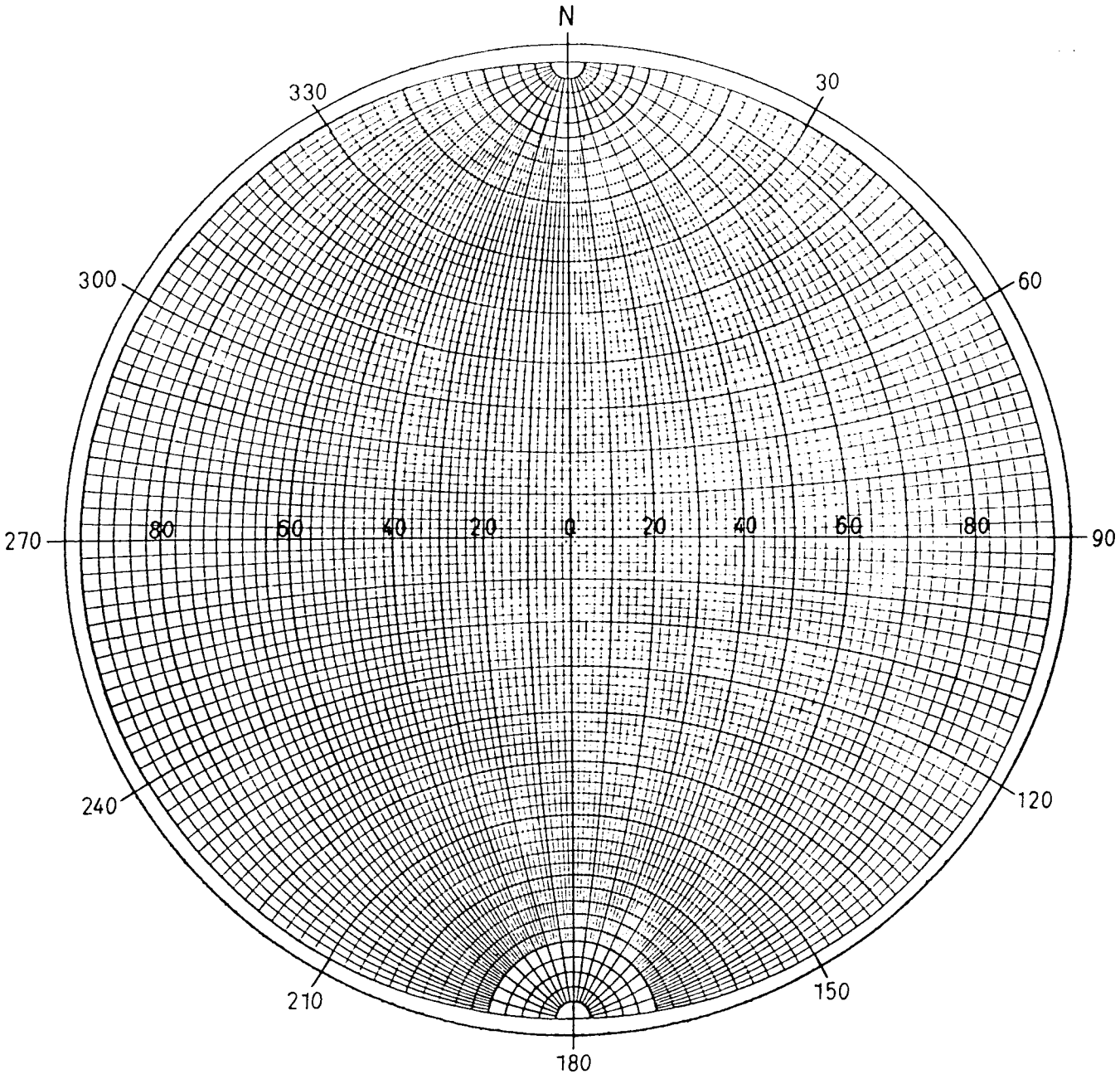

Fig. 9: The equal angle Wulff net

Scientific Technical Report STR 98/05
DOI: 10.2312/GFZ.b103-98055

Task 6:
Find the pole P2 for FP2 and delineate the equatorial plane EP. The latter is perpendicular to both FP1 and FP2 , i.e. a great circle through the poles P1 and P2. The intersection point between FP1 and FP2 is the pole of the equatorial plane (P3).

Task 7:
Mark the position of the pressure and tension axes on the equatorial plane and indicate their direction towards (P) and from the center (T) of the Wulff net, respectively (cf. Fig. 5). Their positions on the equatorial plane lie in the centre of the respective dilatational (-) or compressional (+) quadrant, i.e. 45° away from the intersection points of the two fault planes with the equatorial plane. Note:

All angles on the Wulff net have to be measured along great circles!

Task 8:
Mark the slip vectors, connecting the intersection points of the great circles, representing the fault planes and the equatorial plane, with the centre of the Wulff net. If the centre of theWulff net lies in a tension quadrant, then the slip vectors point to the Wulff net centre. If it lies in a pressure quadrant, then the slip vector points in the opposite direction. The slip vector shows the direction of displacement of the hanging wall.

Task 9:
Determine the azimuth (strike direction ϕ) of both FP1 and FP2. It is the angle measured clockwise against North between the directional vector connecting the center of the Wulff net with the end point of the respective projected fault trace lying towards the right of the net center.

Task 10:
Determine the dip angles δ (against the horizontal) for both FP1 and FP2 by putting their projected traces on a great circle of the Wulff net. Measure δ as the difference angle from the outermost great circle towards the considered fault plane trace.

Task 11:
The rake angle λ is positive in case the center of the Wulff net lies in the tension (+) quadrant (i. e. an event with a thrust component) and negative in case it lies in the pressure (-) quadrant (event with a normal faulting component). In the first case λ is $180° - \lambda^*$. λ^* has to be measured on the great circle of the respective fault plane between its crossing point with the equatorial plain and the respective azimuth direction of the considered fault plane (cf. Fig. 5). In the second case $\lambda = -\lambda^*$. For a pure strike slip motion ($\delta = 90°$) $\lambda = 0$ defines a left lateral strike-slip and $\lambda = 180°$ defines a right-lateral strike-slip.

Task 12:
The azimuth of the pressure and the tension axes, respectively, is equal to the azimuth of the line connecting the center of the net through the P and T point with the azimuth circle of the

Wulff net. Their plunge is the respective dip angle of these vectors against the horizontal (to be measured as for δ).

Task 13:
Estimate the parameters of the fault planes and of the stress axes for the Erzincan aftershock and insert your results into the following table:

	strike	dip	rake
Fault plane 1			
Fault plane 2			

	azimuth	plunge
Pressure axis		
Tension axis		

Note that the angles may range between:

$0° <$ strike $< 360°$ $\quad 0° <$ incidence angle $< 180°$
$0° <$ azimuth $< 360°$
$0° <$ dip $< 90°$
$0° <$ plunge $< 90°$
$-180° <$ rake $< 180°$

3.2 Exercise on the determination and check of take-off angles for the Italian earthquake

Task 1:
Calculate for the data given in Tab. 5 the still blank values for r_o/r_h, $v_h/111.11$, $S_o(\Delta, h)$ and AIN using the relationship (2) and the values tabulated in Tabs. 1 and 2. When required, interpolate linearly as a first approximation.

Task 2:
Decide whether your ray has left the upper or lower half of the focal sphere and whether or not you need to calculate AINc and/or AZMc. Complete Tab. 5 accordingly.

Task 3:
Use the values in Fig. 7 for the fault-plane solution of NEIC and reconstruct in the Wulff net both related great circle nodal (fault) planes by applying the inverse procedure as in 3.1 above. Compare your nodal planes with that of NEIC based on long-period wave form data (Fig. 7).

Task 4:
Also draw the P and T axis, determine the + and - quadrants and check whether the short-period polarity readings of the stations given in Tab. 5, taking into account the AZMc and AINc determined above, are consistent with the fault plane solution of NEIC .

Scientific Technical Report STR 98/05
DOI: 10.2312/GFZ.b103-98055

4. SOLUTIONS

Note : Angles determined in the exercise 3.1 by eye-fit to the data may be uncertain by about ± 10°. This accuracy is acceptable. Even PC assisted fits to the data, as demonstrated by a complement to the exercise, will produce different acceptable solutions within about the same error range with only slightly different standard deviations. Additionally, one has to be aware, that even different fitting algorithm/error-minimization procedures may produce for the same data results within this range of uncertainty. Uncertainties due to not ideal distribution of polarity data in the Wulff diagram, erroneous polarity readings, differences in model assumptions (e.g. in the velocity models used) and with respect to the assumed constant angular (45°) relationship between the fault plane on the one hand and the stress and tension axis on the other hand, may even result in still larger deviations between the model solution and the reality in nature. Below the authors give the data for their own eye-fitting solutions as a reference together with the calculated values (in brackets) for FP2, the P and T axis when assuming that the eye-fit values for FP1 are correct. If your results differ by more than about 20° or even show different type of faulting mechanism then you should critically check your data entries and fits in the Wulff net again.

Exercise 3.1

	strike	dip	rake
Fault plane 1 (FP1)	276°	39°	70°
Fault plane 2 (FP2)	132° (121.1°)	54°(53.8°)	111° (105.5°)

	azimuth	plunge
Pressure axis	205° (200.1°)	7° (7.5°)
Tension axis	90° (79.6°)	73° (75.4°)

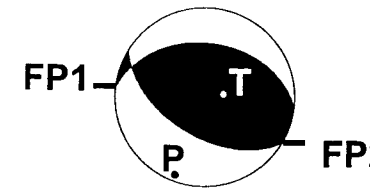

Exercise 3.2

STA	Δ (deg)	AZM (deg)	POL	r_o/r_h	$v_h/111.1$ (deg/s)	$S_o(\Delta,h)$ (s/deg)	AIN (deg)	AZMc (deg)	AINc (deg)
SGG	2.30	345	+	1.047	0.07722	8.68	(44.6)	44.6	165
KHC	10.03	354	-			12.35	87.1	87.1	354
BTH	12.25	294	+			12.18	71.2	71.2	294
ZAK	60.02	48	-			6.77	33.2	33.2	48
PAE	154.8	324	-			1.37	6.4	6.4	324

EXERCISE ON THE DETERMINATION OF SPECTRAL SOURCE PARAMETERS

Michael Baumbach and Peter Bormann

GeoForschungsZentrum Potsdam, Division 2: Solid Earth Physics and Disaster Research
Telegrafenberg, 14473 Potsdam

1. Methodology and data

The parameters to be estimated are:

- Seismic moment $M_o = \mu \bar{D} A$ with μ - shear modulus
  $\bar{D}$ - average source dislocation
  A - size of the rupture plane
- Source dimension R
- Stress drop $\Delta\sigma$

These parameters can be estimated both in the time and frequency domain. For estimation in the time domain the records have to be converted into true ground motion displacement records. This may cause problems, if the bandwidth of the recording system is limited (e.g. short-period records) or if the phase response of the system is not well known. For estimation in the frequency domain only the amplitude response curve is needed.

In this exercise source parameters are estimated in the frequency domain only. Figure 1 shows a velocity record (vertical component) of an aftershock of the 1992 Erzincan earthquake (Turkey). Figure 2 shows the related *displacement spectrum* of the P-wave. The calculated spectrum was corrected for the amplitude response of the recording system (both response of the velocity seismometer and antialias filter of the recorder). Further, the P-wave spectrum was corrected for attenuation $\exp(i\omega t/2Q_p)$. Q_p had been estimated beforehand from coda Qc-observations in the area under study assuming that $Q_p = 2.25\ Q_c$ (only if $Q_c = Q_s$, i.e. no attenuation of compressional energy, and $V_p/V_s = 1.73$). In addition, a noise spectrum, treated in the same way as the P-wave spectrum, was computed and plotted in order to select the suitable frequency range for analysis (with signal-to-noise ratio SNR > 1).

Typical P- and S-wave spectra show at low frequencies a constant amplitude level and at high frequencies a decay of f^{-2} to f^{-3}. In double logarithmic scales the spectrum can be approximated by two straight lines. The intersection point is the corner frequency which allows to estimate the size of the rupture plane.

2. Reading of parameters from figure 2

2.1 Select in figure 2 the frequency range (f_1 - f_2) that can be used for analysis.

f_1 = ... Hz $\qquad$ f_2 = ... Hz

Scientific Technical Report STR 98/05
DOI: 10.2312/GFZ.b103-98055

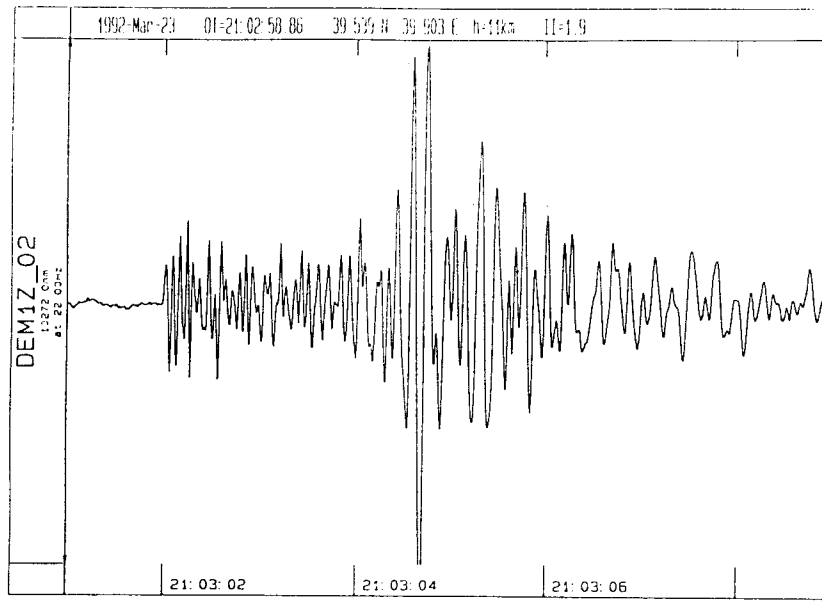

Fig.: 1: Record of an Erzincan aftershock (vertical component)

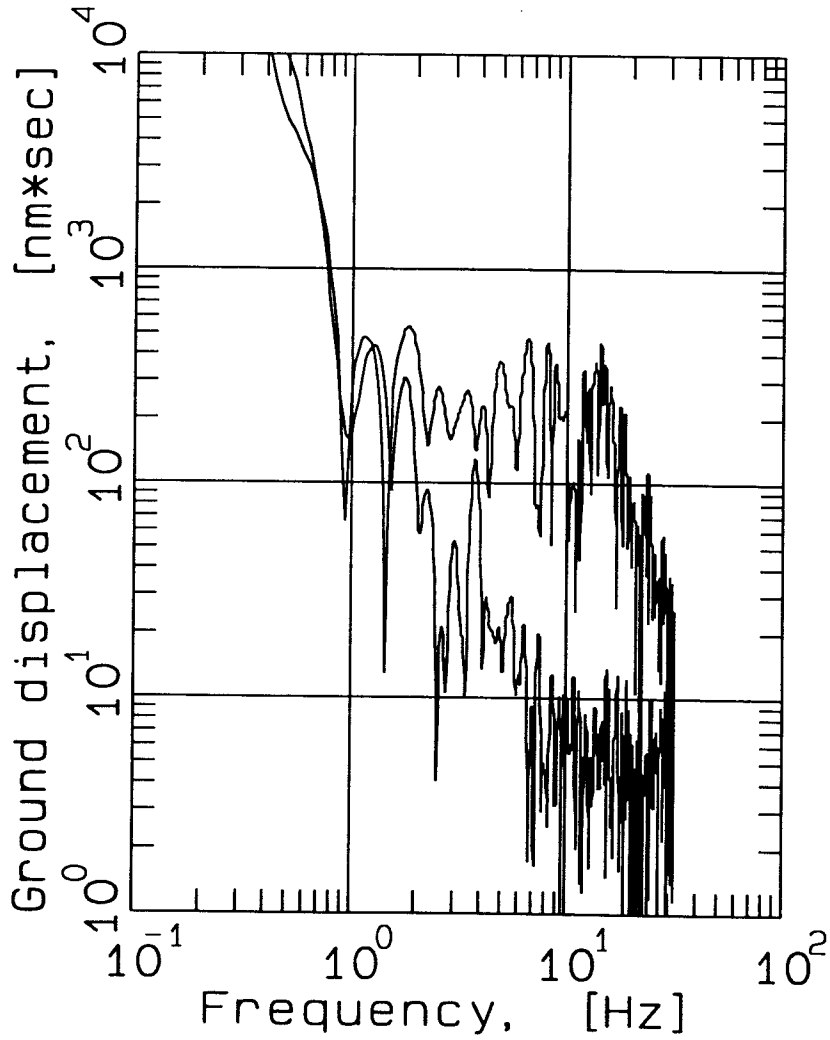

Fig.: 2: P-wave and noise spectrum of the record shown in figure 1.

2.2 Estimate the low-frequency level u_0 of the spectrum by approximating it with a horizontal line. Note the logarithmic scales and ordinate dimension in nm s = 10^{-9} m s.

u_0 = ... m s

2.3 Estimate the exponent n of the high frequency decay f^{-n}, mark it by an inclined straight line.

n = ...

2.4 Estimate the corner frequency fc_p (intersection between the two drawn straight lines).

fc_p = ... Hz

3. Parameter calculations

3.1 Seismic moment

Under the assumption of a homogeneous Earth model and constant P-wave velocity V_p, M_o can be determined from the relationship:

$M_o = 4\ \pi\ \rho\ V_p^3\ \rho\ u_o\ /\ (A\ S_a)$ with:

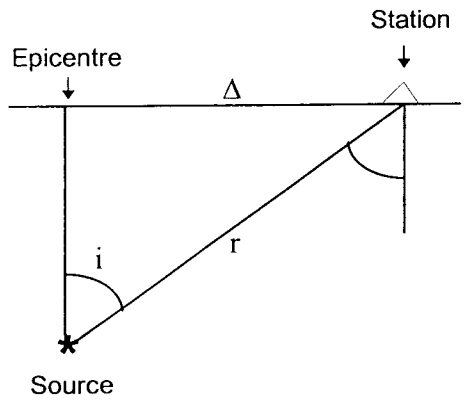

density	$\rho = 2{,}7$ g/cm^3
P-wave velocity	$V_p = 6$ km/sec
source depth	$h = 11.3$ km
epicentral distance	$\Delta = 18.0$ km
travel path	$r = \sqrt{(h^2 + \Delta^2)}$
incidence angle	$i = \arccos(h / r)$
surface amplification	S_a
averaged radiation pattern	$A = 0.64$

Note the differences in dimentions used! M_o has to be expressed in the unit Nm = kg m^2 s^{-2}. S_a can be determined by linear interpolation between the values given in table 1. It was computed for the above given constant values of V_p and ρ (homogeneous model) and assuming a V_p / V_s - ratio of 1.73. i is the angle of incidence, measured from the vertical.

Calculate for the above given case the values for r, i, S_a and M_o

r = ... km i = ... ° S_a = ... M_o = ... Nm

Scientific Technical Report STR 98/05
DOI: 10.2312/GFZ.b103-98055

Table 1: Surface amplification S_a for P-waves; i is the incidence angle

i	S_a	i	S_a	i	S_a
0	2.00	30	1.70	60	1.02
5	1.99	35	1.60	65	0.90
10	1.96	40	1.49	70	0.79
15	1.92	45	1.38	75	0.67
20	1.86	50	1.26	80	0.54
25	1.79	55	1 .14	85	0.35

3.2. Size of the rupture plane

For estimating the size of the rupture plane and the source dislocation one has to adopt a kinematic (geometrical) model, describing the rupture propagation and the geometrical shape of the rupture area. For the exercise computations have to be made for three different circular models, which differ in the source time function and the crack velocity V_{cr}. V_S is the S-wave velocity, here, as common, assumed to be $V_S = V_P / \sqrt{3}$.

Table 2: Parameters of some commonly used kinematic rupture models

1. Brune . . . . . (1970)	$V_{cr} = 0.9\ V_s$	$K_p = 3.36$	$K_s = 2.34$
2. Madariaga I . . . (1976)	$V_{cr} = 0.6\ V_s$	$K_p = 1.88$	$K_s = 1.32$
3. Madariaga II . . . (1976)	$V_{cr} = 0.9\ V_s$	$K_p = 2.07$	$K_s = 1.38$

The source radius R has to be computed by using the formula

$$R = V_s\ K_{p/s} / 2\pi\ fc_{p/s}$$

with $fc_{p/s}$ - the corner frequency of the P- or S-waves, respectively, and K_p and K_s being the related model constants. Only K_p has to be used in the exercise (P-wave record!).

The size of the circular rupture plane is $A = \pi R^2$. $\Rightarrow A_1 =$ .....m^2, $A_2 =$ m^2, $A_3 =$ m^2.

.

3.3. Source dislocation D

The average source dislocation $\bar{D}$ can be computed from the expression $M_o = \mu\ \bar{D}\ A$

with the shear modulus $\mu = V_s^2\ \rho$ and $V_s = V_p / 1.73$.

The average dislocation is $\bar{D} = M_0 / (\mu A)$. Determine $\bar{D}_1$ = ...m, D_2 = ... m, D_3 = ... m.

3.4 Stress drop

The static stress drop $\Delta\sigma$ describes the difference in shear stress on the fault plane before and after the slip. According to Keilis Borok (1959) the following relationship holds for a circular crack with a homogeneous stress drop:

$\Delta\sigma = 7 M_0 / (16 R^3)$.

The stress drop is expressed in the unit of Pascal $Pa = N m^{-2} = kg m^{-1} s^{-2} = 10^{-5}$ bar.

Summarize your results for R, A, $\bar{D}$ and $\Delta\sigma$ according to the circular models given above in the table below.

Model	R [m]	A [m^2]	$\bar{D}$ [m]	$\Delta\sigma$ [MPa]
1. Brune				
2. Madariaga I				
3. Madariaga II				

Note: Since $\Delta\sigma \sim R^{-3}$ the estimate of stress drop very much depends on f_c, a parameter which can not be estimated very precisely from real spectral data. In case of non-circular, e.g. rectangular fault ruptures, even two corner frequencies may exist which are controlled by the width W and the length L of the rupture plane. Additionally, differences in the assumed mode of crack propagation (e.g. unilateral, bilateral, radial) and crack propagation velocity V_{cr} influence the parameters calculated from spectral data. Accordingly, stress drop values may be uncertain by about two orders of magnitude. Therefore, in studying possible systematic differences in source parameters derived from spectral data for events in a given area for which similar modes of faulting and crack propagation can be assumed with good reason one should alway stick to using one type of model.

REFERENCES

Brune, J. N. (1970). Tectonic stress and the spectra of shear vaves from earthquakes. J. Geophy. Res. 75, 4997-5009.

Keilis Borok, V. I. (1959). On the estimation of the displacement in an earthquake source and of source dimensions. Ann. Geofis. 19, 205-214.

Madariaga, R. (1976). Dynamics of an expanding circular fault. BSSA 66, 639-666.

DOI: 10.2312/GFZ.b103-98055

SOLUTIONS

Note that individual visual parameter readings from Fig. 2 might be somewhat biased but they should not differ by more than about ± 10% from the mean. Acceptable average values for the read and calculated parameters are for:

2.1 $f_1 = 2$ Hz, $f_2 = 30$ Hz

2.2 $u_o = 3 \times 10^{-7}$ m s

2.3 $n = 3$

2.4 $f_{cp} = 14.4$ Hz

3.1 $i = 58^o$, $S_a = 1.07$, $M_o = 6.8 \times 10^{13}$ N m

3.2 $R_1 = 129$ m, $A_1 = 5.23 \times 10^4$ m^2

$R_2 = 72$ m, $A_2 = 1.63 \times 10^4$ m^2

$R_3 = 79$ m, $A_3 = 1.96 \times 10^4$ m^2

3.3 $\mu = 3.24 \times 10^{10}$ kg m^{-1} s^{-2}

$\bar{D}_1 = 4.0 \times 10^{-2}$ m

$\bar{D}_2 = 1.3 \times 10^{-1}$ m

$\bar{D}_3 = 1.1 \times 10^{-1}$ m

3.4 $\Delta\sigma_1 = 13.8$ MPa

$\Delta\sigma_2 = 79.7$ MPa

$\Delta\sigma_3 = 60.3$ MPa

NEOTECTONICS AND STRESS PATTERN IN AFRICA

Isaac O. Nyambok

University of Nairobi, Department of Geology, P.O. Box 30197, Nairobi, Kenya,
Fax: +254-2-449-539, E-mail: uonseism@arcc.or.ke

1. INTRODUCTION

Neotectonics and stress patterns are very important elements in the zonation and evaluation of seismic hazard. These two elements are closely associated with active faults and seismotectonics, while active faults are, in turn, often associated with other geohazards such as volcanism, fluid and gas activity, hydrogeological changes, landslides etc. A combined approach of geological techniques, remote sensing, and correlation of existing seismic geophysical, geodetic, and hydrogeological data not only allows us to identify active faults and determine their structural and kinematic parameters, but also to characterize regimes of recent crustal movement (neotectonics), estimate some parameters of potential earthquakes, and better understand the relations between mechanical properties of rocks and recent crustal movement. The most reliable manifestations of neotectonic events are offsets of young topographic, geological and/or cultural features, recent and prehistoric seismic ruptures, chains of hypocenters of recent earthquakes, and recent displacement recorded by repeated geodetic measurements.

It is noteworthy that strain rates in intraplate regions are 2 or 3 orders of magnitude lower than those in the plate boundaries. More commonly, intraplate seismicity is characterized by a diffuse pattern of few moderate to large events per century, and a few concentrated clusters of modern day seismicity (Nyambok and Ochieng, 1997). Thus while macro- and instrumental seismicity records may be sufficient in plate boundary zones, seismic hazard assessment in the intraplate regions may be somewhat problematic and to rationally evaluate seismic hazard, in such regions, consideration should be given to additional tectonic and geophysical information that can explain the source of intraplate seismicity and possible focal mechanisms for localisation of such deformations or ruptures. Data on neotectonics and contemporary stress field are critical in this regard.

2. NEOTECTONICS

The areas of major neotectonic events are the East Africa Rift System, the mobile belts of southern Africa, the faulted volcanic field of Cameroon, the shear zone of Ghana, Togo and Benin, Rokelides and Mauritanides fault zone of Liberia - Senogambia region and the Cape Range of South Africa.

Scientific Technical Report STR 98/05
DOI: 10.2312/GFZ.b103-98055

The East African Rift System is undoubtedly an area of major neotectonics. It stretches from the Red Sea to Mozambique with two branches so named western branch and eastern branch (Ethiopian Rift and Kenya Rift) (Fig. 1).

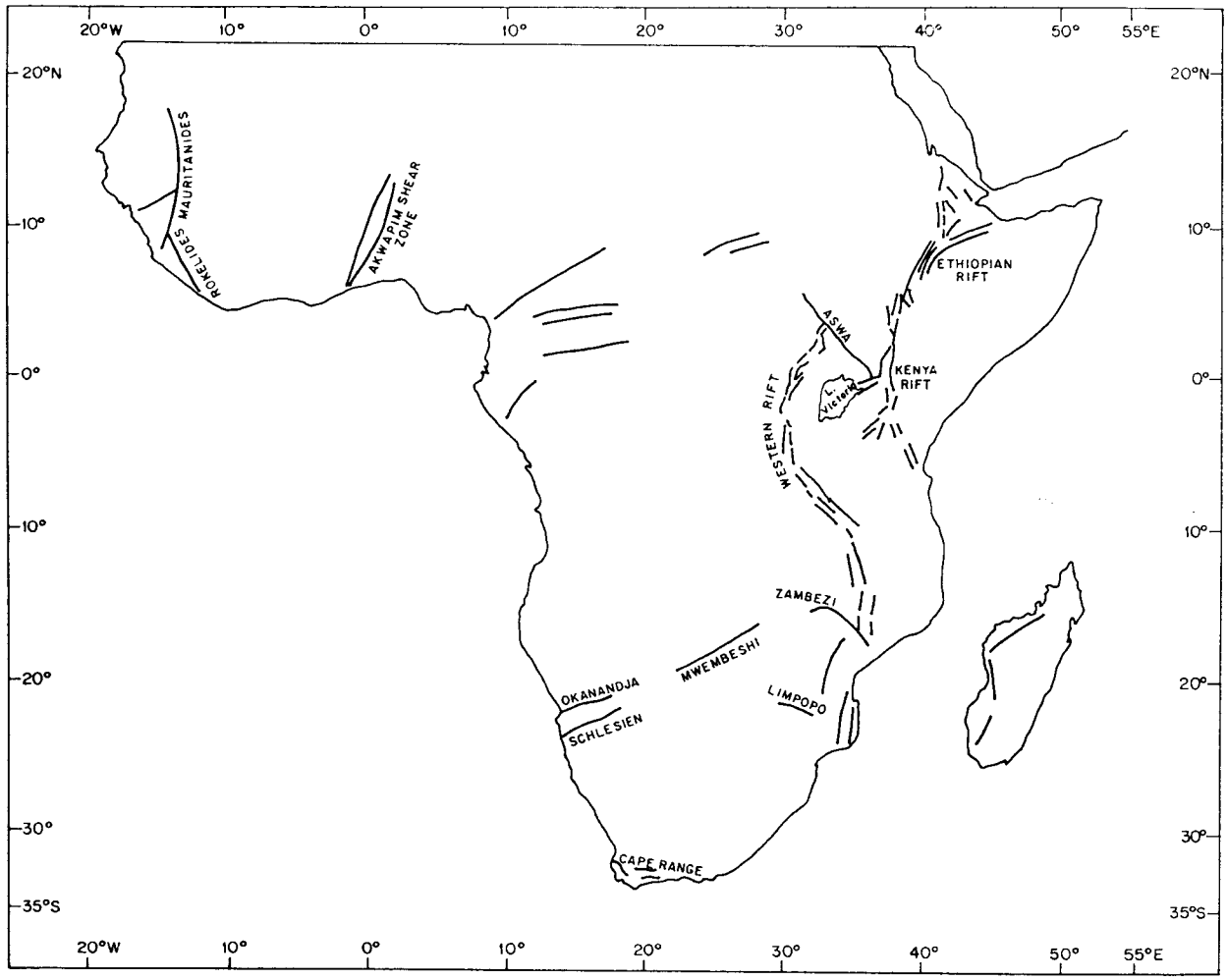

Fig. 1: Faults associated with earthquakes in sub-saharean Africa

The western branch is a well defined rift valley extending in an area from 4°N to 9°S with its floor occupied by several lakes. At the northern part the rift faulting dies out in a series of en echelon faults which terminate against the Aswa Shear Zone. The general faulting mechanism of the Rift is an extensional axis trending E-W to ESE-WNW with normal fault movement, giving a relative upward movement to the Ruwenzori host block compared to the surrounding country. However, the tectonics of Tanganyika-Rukwa-Malawi zone display a transcurrent fault movement (Tiercelin, et. al., 1988). Volcanism is restricted to small sections of the rift, with Nyiragongo and Nyamuragira volcanoes of the Virunga volcanic field currently being the most active (Hamaguchi, et. al., 1992; Zana, et al., 1992; and Kasahara, et al., 1992).

The eastern branch of the East African Rift System can be divided into the Ethiopian Rift and Kenya Rift. In the Ethiopian Rift recent deformation is essentially restricted to an eight kilometer wide zone of intense faulting (Wonji fault belt) which follows the axis of the Rift in an en echelon pattern. On the other hand the Kenya Rift is 60-80 km wide and about 1 km deep traversing the Kenya dome. The Kenya Rift floor has undergone extensive fracturing with recent volcanism and geothermal activity. Faulting patterns in the Kenya Rift indicate E-W and oblique (NW-SE) tensional stress. However, south of 3°S, the faulting is not confined to narrow rift floor but spreads out in a fan arrangement of block faulting. The area of the Manyara and Eyasi faults have been very seismically active compared with the rest of the Kenya Rift in the past few decades.

Other neotectonic events in southern Africa, not associated with the East African Rift System, occur in the mobile belts like the Zambezi and Limpopo Mobile belts. There are also neotectonic events associated compressional Cape Range. In West Africa, neotectonic events occur in the Mt. Cameroon faulted volcanic line, Akwapim and "Rodelides-Mauritanides" shear zones. These are mostly subjected strike-slip movements incorporating limited dip-slip movements (normal faulting).

3. STRESS PATTERNS

It is generally observed that areas of intraplate active extension such as the East African Rift System are often associated with regions of high topography. In such a case, horizontal extensional stress derived from buoyancy forces related to crustal thickening and/or lithospheric thinning in these regions dominate the horizontal intraplate compressional stress field due to plate driving forces.

As Nyambok and Ochieng (1997) pointed out that most seismicity and deformation in the Sub-Saharan Africa are concentrated in the East African Rift System. However, low level seismicity persists throughout the continent. Zoback, et. al. (1989) noted that the plate tectonic setting of Africa, surrounded by mid-ocean ridges and a continental collision in the north, would suggest that the interior of the African plate should be subjected to compressional stress field. A zone of NNW compression has been identified from earthquake focal mechanisms and geological evidence along the northernmost boundary of the African continent which is consistent with the convergence of the African and Eurasian plates. Recent stress data suggest the existence of a midplate compressive stress regime in Central and West Africa with a maximum horizontal stress orientation of approximately E-W orientation outside the East African Rift. As shown in Fig. 2 all these stress data show a relatively consistent pattern of strike-slip deformation or rupture. A similar approximately E-W maximum horizontal stress orientation is also observed in borehole breakout data from 11 wells covering an area of over 1000 km wide in the Sudan (Bosworth et al. 1992). The approximate boundary between this western midplate compressional regime and the eastern rift extensional zone is indicated by the dashed line in Fig. 2.

The general uniformity of the approximate E-W maximum horizontal stress orientation from both focal mechanism well data throughout Central and West Africa can be used to define a seismotectonic province for seismic hazard assessment. A local rotation of maximum

Scientific Technical Report STR 98/05
DOI: 10.2312/GFZ.b103-98055

horizontal stress is evident, namely 50-60° clockwise rotation within the East African rift relative to Central and West Africa (Fig. 2) due to extensional buoyancy forces caused by lithospheric thinning. Thus the stress data permit zoning of a broad region within a continent with very little additional geological or geophysical information. Identification of the broad scale regional stress patterns allows definition of local stress perturbations due to local geologic or tectonic structure. Using available geologic and geophysical data, the local stress effect of the structures can be modelled and used to obtain valuable stress magnitude constraints at hypocentral depths and help to explain causes of localised seismicity.

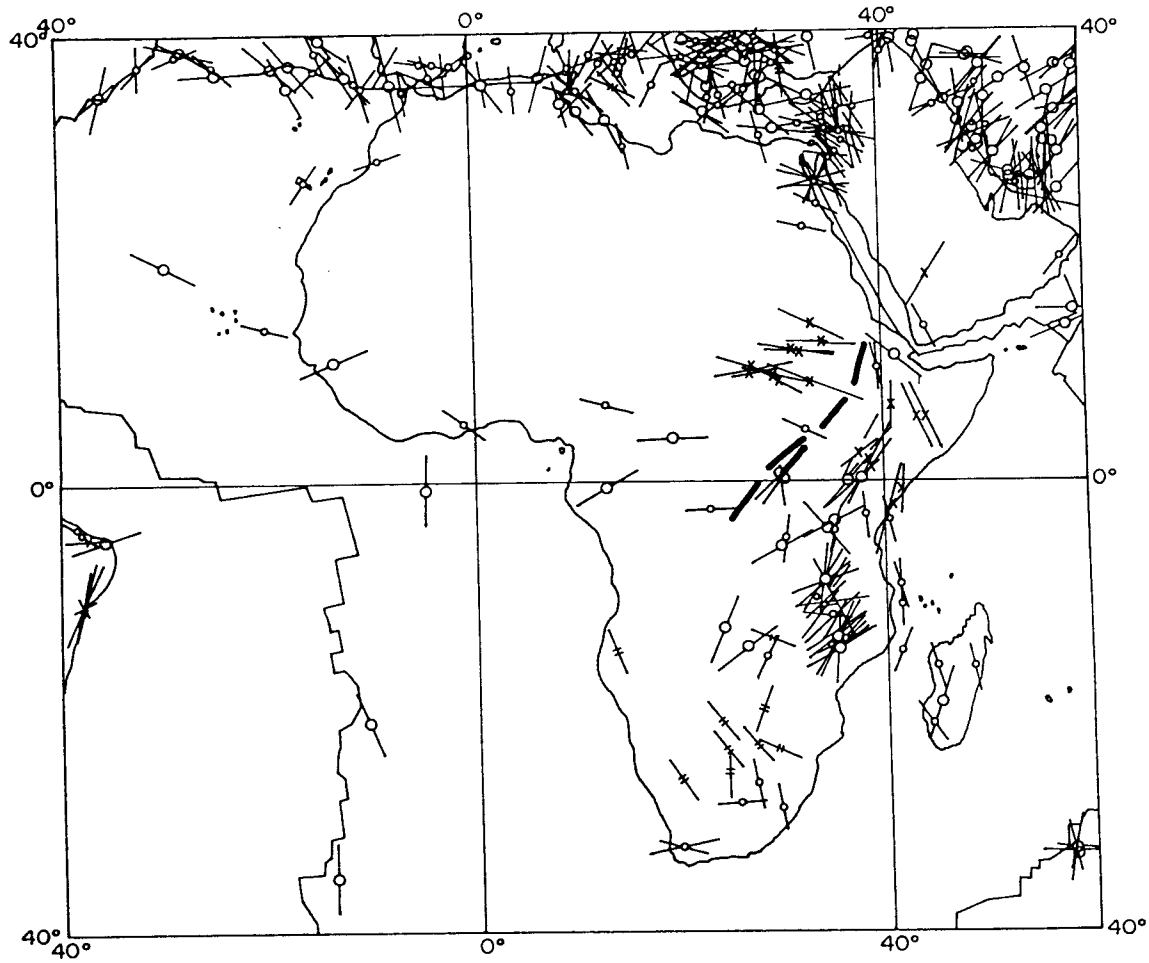

Fig. 2: Maximum horizontal stress orientation in Africa. Stress data according to Zoback et al. (1989). Heavy dashed line indicates the eastern limit of the midplate compressional province.

Scientific Technical Report STR 98/05
DOI: 10.2312/GFZ.b103-98055

REFERENCES

Bosworth, W., Strecker, M.R. and Blisnuik, P.M. (1992). Integration of East African palaeostress and present - day stress data: implications for continental stress field dynamics. J. Geophys. Res.97 : 11851-11865.

Hamaguchi, H., Nishimura, T. and Zana, N. (1992). Process of the 1977 N yiragongo eruption inferred from the analysis of long-period earthquakes and volcanic tremors. In: C.J. Ebinger, H.K. Gupta and I.O. Nyambok (Editors), Seismology and Related Sciences in Africa. Tectonophysics, 209 : 241-254.

Kasahara, M., Hamaguchi, H., Tanaka, K., Zana, N. and Kabwik, M. (1992). Recent horizontal crustal movements in and around volcano Nyamuragira, Zaire. In: C.J. Ebinger, H.K. Gupta and I.O. Nyambok (Editors). Seismology and Related Sciences in Africa. Tectonophysics, 209 : 263-268.

Nyambok, I.O. and Ochieng, A.O. (1997). Seismic hazard assessment of sub-saharan Africa. A GSHAP contribution. In: I.O. Nyambok and D.W. Ichang'i (Editors). Proceedings of the GSA 95 International Conference - 10th Conference of the Geological Society of Africa. 275-286.

Tiercelin, J.J., Chorowicz, J., Bellon, H., Richert, J.P., Mwambene, J.T. and Walgenwitz, F. (1988). East African Rift System: Offset, age and tectonic significance of the Tanganyika-Rukwa-Malawi intracontinental transcurrent fault zone. Tectonophysics, 148 : 241-252.

Zana, N., Tanaka, K., and Kasahara, M. (1992). Main geophysical features related to the Virunga Zone, western rift, and their volcanological implications (Extended Abstract). In: C.J. Ebinger, H.K. Gupta and I.O. Nyambok (Editors). Seismology and Related Sciences in Africa. Tectonophysics, 209 : 255-257.

Zoback, M.L., Zoback, M.D., Adams, J., Assumpcao, M., Bell, S. Bergman, E.A. Blumling, P., Brereton, N.R.,. Denham, D.,Ding, J., Fuchs, K., Gay, N. Gregersen, S., Gupta, H.K., Gvishiani, A., Jacob, K., Kelin, R., Knoll, P., Magee, M., Mercier, J.L., Muller, B., Paquin, C., Rajendorn, K., Stephansson, O., Suarez,G., Suter, M. Udias, A., Xu, Z.H., and Zhizhin, M. (1989). Global patterns of tectonic stress. Nature, 341 : 291-298.

Scientific Technical Report STR 98/05
DOI: 10.2312/GFZ.b103-98055

QUARTERNARY VOLCANIC EVENTS IN AFRICA

Isaac O. Nyambok

University of Nairobi, Department of Geology, P.O. Box 30197, Nairobi, Kenya,
Fax: +254-2-449-539, E-mail: uonseism@arcc.or.ke

1. INTRODUCTION

Studies of the seismicity of sub-saharan Africa show that there are well defined zones of earthquake occurrence. Nyambok and Ochieng (1977) have shown that the East Africa Rift System, extending from Eritrea-Ethiopia into southern African shear zones of Ghana - Togo and Liberia-Guinea-Senegambia, the Cape Range of South Africa and the Cameroon Volcanic Line, are areas within which earthquakes occur. Apart from the Cameroon Volcanic Line, there are several volcanic centres some of which are associated with the East African Rift System such as Virunga volcanic field and others that are mantle-plume derived such as Mt. Kenya, Mt. Kilimanjaro etc. which also show associated earthquake activities.

It is generally apparent that earthquakes originating from volcanic activities are of low to medium magnitudes. However, this does not suggest that these volcanic centres are aseismic rather that large magnitudes are either infrequent and/or crustal stresses caused by the upwelling magmas are being released through small magnitude tremors. In order to look at the current geophysical changes, we shall herewith focus on Quaternary volcanic centres, namely volcanoes that can be regarded as active. Another important interrelationship between active volcanoes and seismicity, is the use of seismic activities as precursors to identify possible imminent volcanic eruptions.

2. QUARTERNARY VOLCANOES AND SEISMIC ACTIVITIES

2.1 Cameroon

In Cameroon, the main active volcano is Mt. Cameroon which is a part of the 1400 km chain of volcanic centres knows as the Cameroon Volcanic Line (Fig. 1). Mt. Cameroon which is located on the continental margin approximately midway along the Line, has erupted four times this century in 1922, 1954, 1959 and 1982. Prior to this, the earliest authenticated eruption occurred in April, 1909 (de Swadt, 1956). These eruption records coupled with the recent gas disasters of lakes Monoun and Nyos of 1984 and 1986 respectively may suggest that the volcanic field is entering into a significant activity stage. This volcanic Line may represent hot spots which are manifestations of mantle-plumes a way from an extensional rift, in this case the Benue Trough having a similar geological setting as in the eastern branch of the East African Rift System. The mantle-plume would thus be generated by the sink of the convective mass movement.

DOI: 10.2312/GFZ.b103-98055

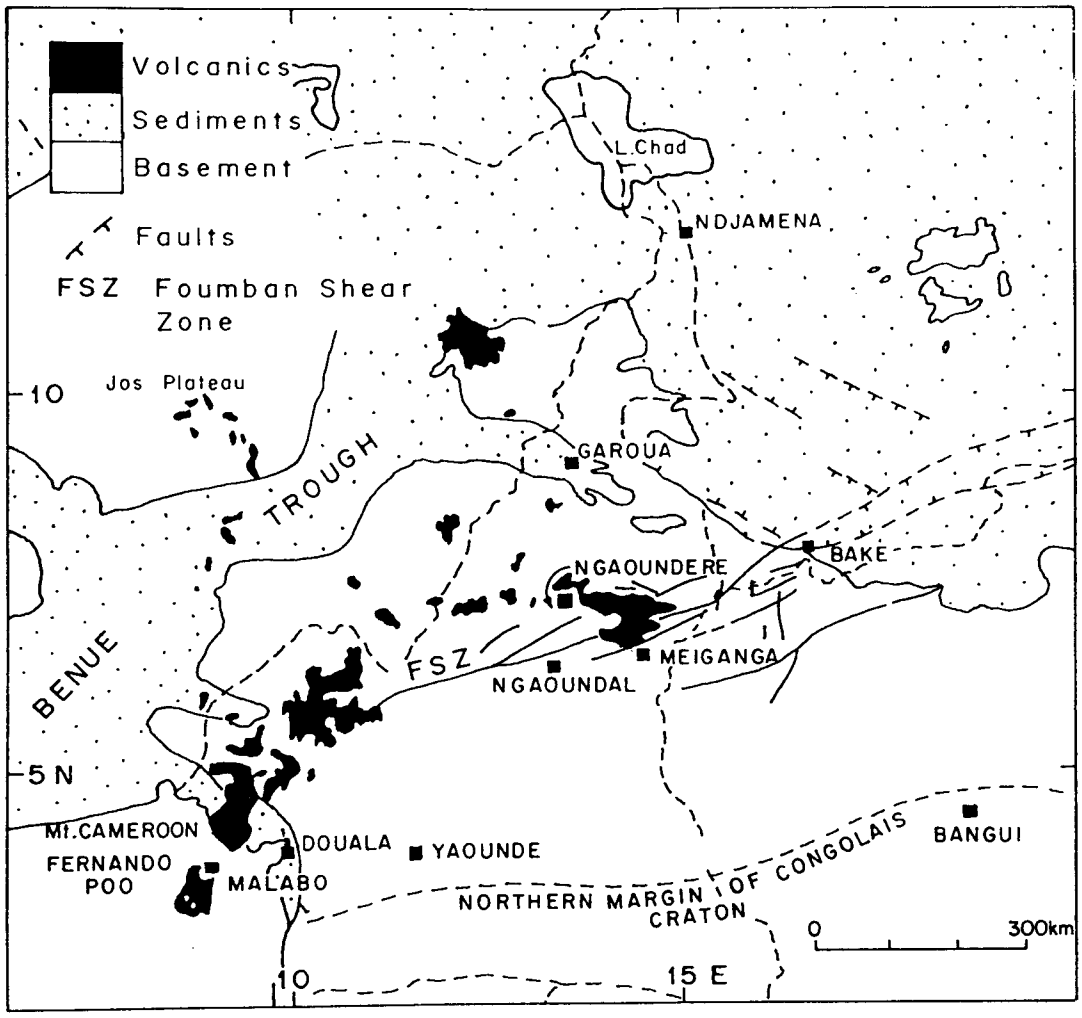

Fig. 1: Tectonic setting showing the Cameroon volcanic line

Approximately 20 felt earthquakes are reported to have occurred in the period 1615 to 1984 (Ambraseys and Adams, 1986), most of which are epicentred in the province of the Cameroon Volcanic Line. Ambraseys and Adams (1986) reported that the earliest documented felt earthquake in Cameroon occurred in 1852 in the Mt. Cameroon region. Between 1852 and 1907, at least 6 felt earthquakes occurred in Cameroon, most of them associated with Mt. Cameroon. For example the February 1922 eruption of Mt. Cameroon was characterized by the occurrence of an earthquake swarm.

2.2 Cape Verde

Fogo has remained an active volcano in the Cape Verde. The most recent eruption occurred in April, 1995 which generated lava flows throughout the month. The eruption was accompanied by explosive activity and emission of pyroclastic material. While the eruption stopped by the end of April, fumarolic activity remained intense in May, 1995, especially along the main NE-SW fault.The eruption constructed a cinder cone and an edifice that reached 160 m high. Although there is no seismic information on the eruption, it is reasonable to assume that minor and microearthquakes occurred prior and during the eruption.

Scientific Technical Report STR 98/05
DOI: 10.2312/GFZ.b103-98055

2.3 East African Rift System

In the East African Rift System, there is an areal relationship between the rift faulting and volcanic eruptions. However, there are also off-rift volcanoes such as Mt. Kenya and Chyulu Hills.

Table 1: Centres of Quarternary Volcanic activities in the East African Rift System

Country	Ethiopia	Kenya	Tanzania	Uganda	Congo	Rwanda
Volcanic Centers	Amoissa Butajira Edd Mega Fantale Sabober Wonchi Alid Ayelu Erta Ale Dendi Garabaldi Shala Zukwala	Telekis Barrier Emuruan-gogolak Silali Paka Kilombe Menengai Eburru Longonot Suswa North Isl. Central Island	Mt.Kiliman-jaro Mt. Meru Ngorongoro Ol Donyo Lengai Gelai Kitumbieni Rungwe Kiejo	Katwe-Kikorong Mikeno Virunga-Bufumbira	Nyamuragira Nyiragongo	Kavisimbi Visoke Sabinyo

NB: Sources of Information: Smithsonian Institutions Global Volcanism Network; MacDonald, 1987; Tesha, et. al., 1992; Dawson, 1992; Nyambok, 1985; Nyambok, 1992; Nyambok and Chorowicz, 1997; Hayashi et. al., 1992; Hamagachi et. al., 1992 and Zana, et. al., 1992.

Among the listed Quarternary volcanoes in the East African Rift System, four are known to be currently active, namely Ol Donyo Lengai, Nyiragongo, Nyamuragira and Erta Ale. The faulting pattern of the East African Rift System is given in Fig. 2 while the Quarternary centres of Kenya, Tanzania, Uganda, Rwanda and Zaire are given in Figs. 3-5.

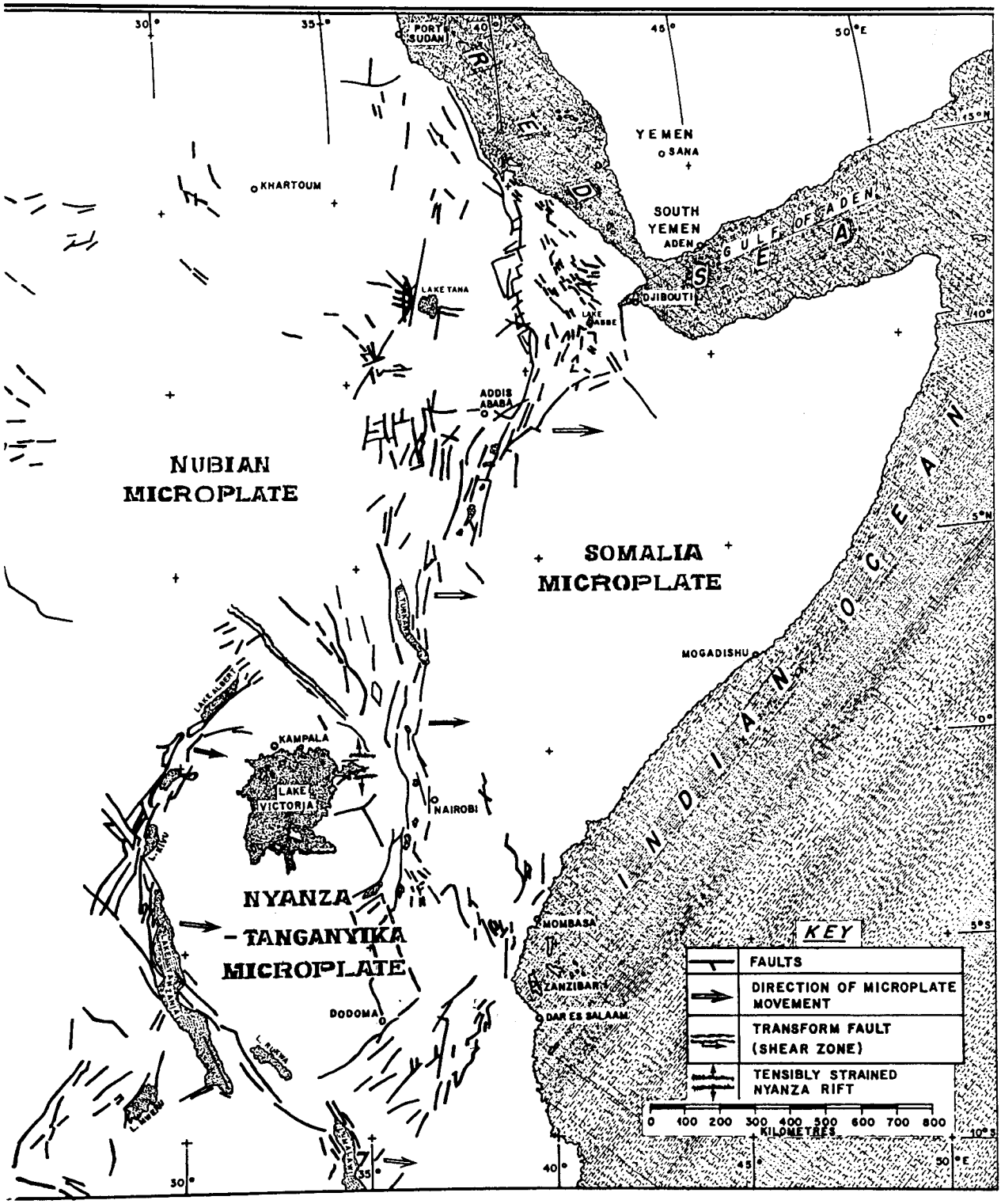

Fig. 2: Structural evolution of rift system in eastern Africa

Scientific Technical Report STR 98/05
DOI: 10.2312/GFZ.b103-98055

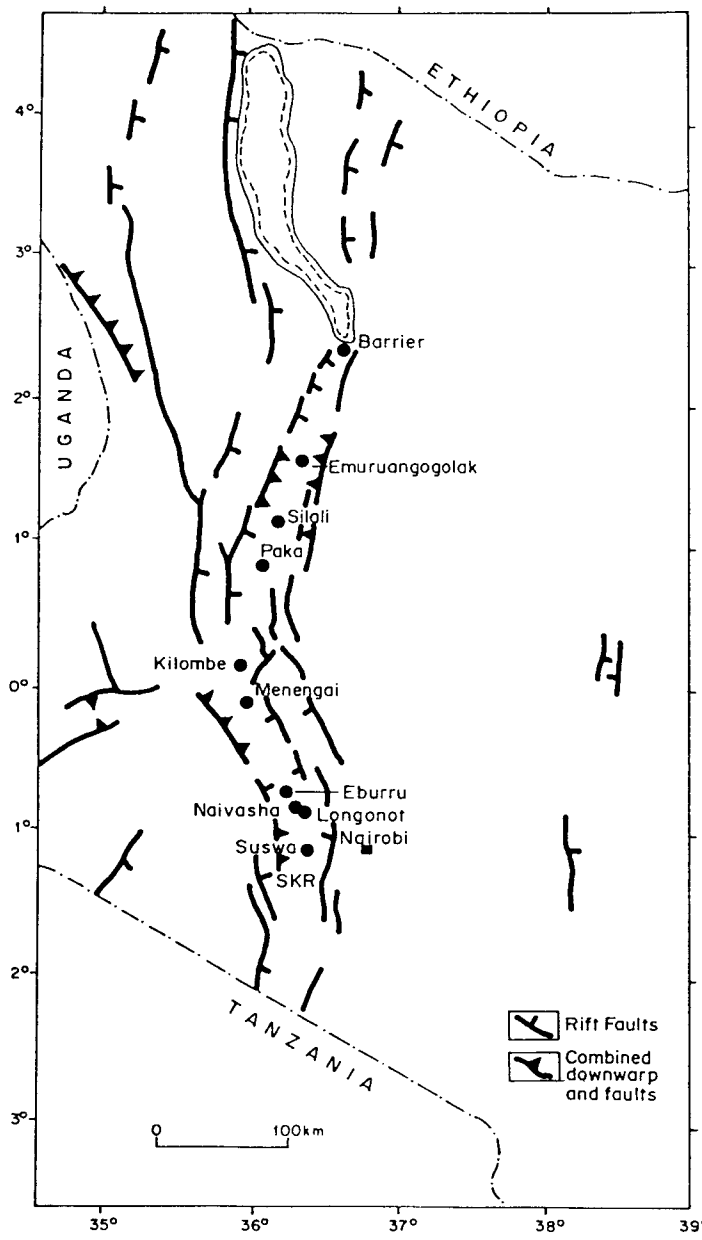

Fig. 3: Locality map of the late Quarternary central volcanoes

The four known active volcanoes referred to above are hereunder briefly described. The Eastern rift branch contains two active centres namely Erta Ale in Ethiopia and Ol Doinyo Lengai in Tanzania. In the case of Arte Ale, recent observations made in December, 1965 revealed fumarolic activity in the northern part of the caldera while a secondary pit crater was seen in the south-eastern part of the main pit. Within the central part of the caldera a lava lake is located at the top of a small lava shield. The diameter of the pit-crater was 140 m and the lava lake was 90 m below the rim whose activity was characterized by intermittent fountaining from as many as four locations at a time. Ol Donyo Lengai continues with magmatic eruptions of carbonatite lapilli. Normally the eruptions extends to an average of 10 m above the crater and the pyroclastics cover an area of about 0.1 km^2. The eruption is usually accompanied by very small lava flows.

Scientific Technical Report STR 98/05
DOI: 10.2312/GFZ.b103-98055

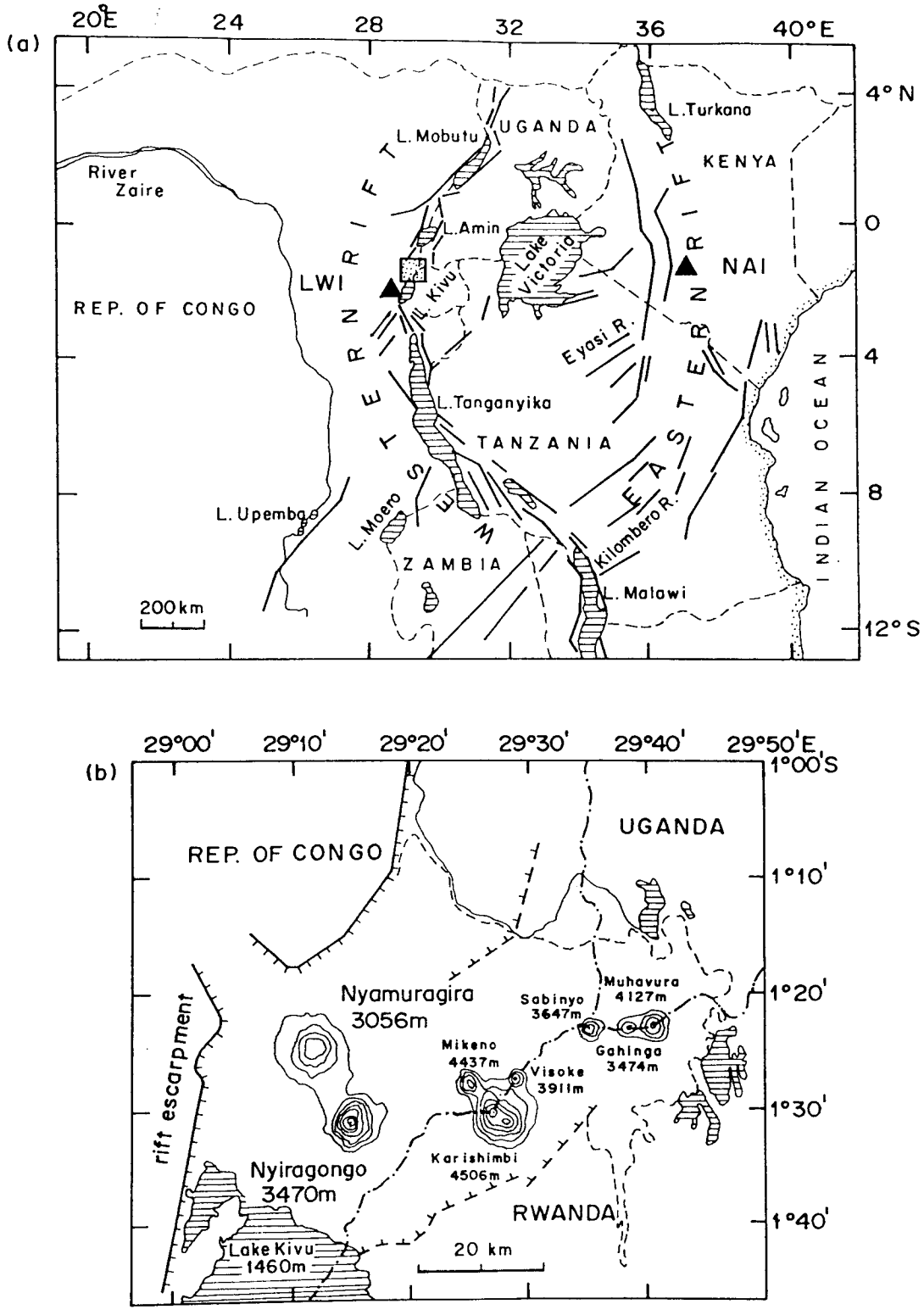

Fig. 4: (a) The western and the eastern rift branches of the East African Rift System. At the position of the hatched rectangle is the Virunga volcanic field.
(b) Virunga volcanic field comprising eight volcanoes.

Scientific Technical Report STR 98/05
DOI: 10.2312/GFZ.b103-98055

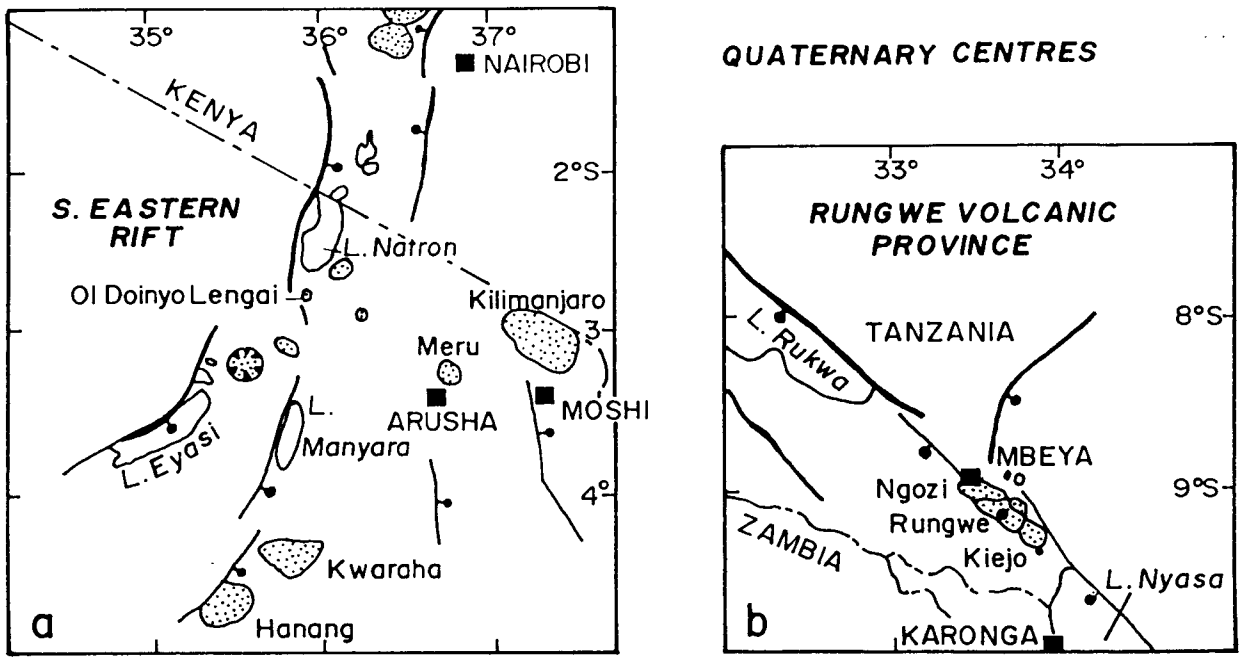

Fig. 5: Quarternary eruptive volcanic centers (shaded) in (a) the eastern rift branch and (b) the Rungwe area of the western rift branch.

The other active volcanoes, namely Nyiragongo and Nyamuragira occur in the western rift branch. Vigorous lava production has continued at Nyamuragira building 23 cinder cones along 2.5 km zone that trends generally NE. The eruptions main phases produce substantial lava flows terminally accompanied by ejections of bombs, lava fragments and ash. Microearthquakes are usually triggered by the lava extrusions and ash emissions. The lava extrusions usually produce phonolitic tephrite scoria. Nyiragongo, on the other hand, had a major eruption in 1977. It had a long-lived lava lake in the summit crater for about 50 years in the period of 1928-1977 (Hamaguchi et. al., 1992). During the 1977, Nyragongo completely lost its long-lived lava lake, and a big crater with a depth of 800 m was formed at the top. Seven earthquakes triggered by the Nyiragongo eruption were recorded at Lwiro seismograph station.

The other areas of active volcanoes are found in the Indian Ocean islands of Comoro and Reunion. In the Comoro Island, there is a Karthala active volcano which is basaltic shield volcano. In the last century, at least eight eruptions have occurred. In this case, the volcanic activity is generally characterized by effusive activity but at least one eruption was of phreatic character. These eruptions are often accompanied by seismic events, some of which are precursors.

In the Reunion Island, Piton de la Fournaise erupted in 1991 after a quiescent period of 14 months from the last eruption in 1990. An eruptive fissure opened at an altitude of 2,510 m along the southern edge of Dolomieu crater and extended toward the eastern flank of the volcano. This fissure with a general orientation of N55°E was composed of several *en echelon* segments, some of which did not produce lava flows or spatters. Small quantities of lava poured out into the southeastern part of the Dolomieu Crater or around Maillard crater, but the main part of the lava was emitted by the lower end of the fissure and flowed for about 2 km. Interestingly fountaining at the vents remained very weak.

Prior to the eruption, deformation monitoring network, indicated increasing values showing a general inflation pattern in the summit zone of the volcano. At the same time, the seismic swarm ended with the appearance of the volcanic tremors and the starting of the lava outflow.

REFERENCES

Dawson, J.B. (1992). Neogene tectonics and volcanicity in the North Tanzania sector of the Gregory Rift Valley: contrasts with the Kenya Sector. In: R. Alther (Editor), The Afro-Arabian Rift System. Tectonophysics, 204 (spec. sect.): 81-92.

de Swardt, A.M.J. (1956).The 1954 eruption of Cameroon Mountain. Rec. geol. surv. Nigeria, Kaduna, 35-40.

Hamaguchi, H., Nishimura, T. and Zana, N. (1992). Process of the 1977 Nyiragongo eruption inferred from the analysis of long-period earthquakes and volcanic tremors. In: C.J. Ebinger, H.K. Gupta and I.O.Nyambok (Editors), Seismology and Related Sciences in Africa. Tectonophysics, 209 : 241-254.

Hayashi, S., Kasahara, M., Tanaka, K., Hamaguchi, H., and Zana, N. (1992). Major element chemistry of recent eruptive products from Nyamuragira volcano, Africa (1976-1989). Extended Abstract. In: C.J. Ebinger, H.K. Gupta and I.O. Nyambok (Editors), Seismology and Related Sciences in Africa. Tectonophysics, 209: 273-276.

Macdonald, R. (1987). Quarternary peralkaline silicic rocks and caldera volcanoes of Kenya. In: F.G. Fitton and B.G.J. Upton (Editors), Alkaline Igneous Rocks. Geological Society Special Publications, 30 : 313-33.

Nyambok, I.O. (1985). Evolution of the East African rift system with special emphasis on the central rift of Kenya: a new model. Kenya Journal of Science and Technology Series A, 6(2), 83-90.

Nyambok, I.O. (1992). Chyulu Range and Yatta Plateau: geology. In: Kenya from Space: An aerial atlas. East African Educational Publishers, Nairobi, 116-1127.

Scientific Technical Report STR 98/05
DOI: 10.2312/GFZ.b103-98055

Nyambok, I.O. and Chorowicz, J.(1997). Satellite imagery study of the tectonic setting of a volcano: Menengai caldera in the Kenya Rift. In: I.O. Nyambok and D.W. Ichang'i (Editors), Proceedings of the GSA 95 International Conference - 10th Conference of the Geological Society of Africa. 671-286.

Nyambok, I.O. and Ochieng, A.O. (1997). Seismic hazard assessment of sub-saharan Africa: A GSHAP contribution. In I.O. Nyambok and D.W. Ichang'i (Editors). Proceedings of GSA 95 International Conference - 10th Conference of the Geological Society of Africa. 275-286.

Tesha, A.L., Ebinger, C.J. and Nyamweru, C. (1992). Rift-related volcanic hazards in Tanzania and their mitigation (Extended Abstract). In: C.J. Ebinger, H.K. Gupta and I.O. Nyambok (Editors). Seismology and Related Sciences in Africa. Tectonophysics, 209: 277-279.

Zana, N., Tanaka, K. and Kasahara, M. (1992). Main geophysical features related to the Virunga zone, western rift and their volcanological implications (Extended Abstract). In: C.J. Ebinger, H.K. Gupta and I.O. Nyambok (Editors), Seismology and Related Sciences in Africa. Tectonophysics, 209: 255-257.

KRISP - A JOINT KENYAN-GERMAN PROGRAMME FOR THE COMPLEX INVESTIGATION OF THE EARTH'S CRUST IN THE KENYAN RIFT SYSTEM

C. Prodehl[1], J. Mechie[2] and O. Novak[1]

[1] Geophysical Institute, University, Hertzstr. 16, D-76187 KARLSRUHE, Germany
[2] GeoForschungsZentrum Potsdam, Telegrafenberg, D-14473 POTSDAM, Germany

1. INTRODUCTION

From 1985 to 1995 a major investigation of the lithosphere underneath the Kenyan part of the East African rift system has been carried out by the Kenya Rift International Seismic Project (KRISP) during several geoscientific campaigns using geological, petrological, and geophysical methodologies. The geophysical investigations comprised in particular seismic studies during three major campaigns in 1985 (KRISP85), 1989-90 (KRISP90) and 1993-1995 (KRISP94). The KRISP group is an international team with scientists from Kenya, Germany, U.K., U.S.A. and Ireland as the leading parties and furthermore from Denmark, France, and Italy. The projects were funded from the European Community, Germany, U.S.A., and U.K. KRISP concentrated mainly on refraction-seismic and teleseismic field experiments, but also included various phases of geological and petrological field studies as well as a magnetotelluric field campaign in 1995 and the installation of a seismological network by the University of Karlsruhe which is now being operated under the supervision of the University of Nairobi (Department of Geology).

The first international seismic campaign, KRISP-85, was primarily a test experiment for the later seismic refraction surveys of 1990 and 1994 and consisted of the observation of an axial profile between Lake Baringo and Lake Naivasha using underwater shots and a short cross-rift line north of Mount Susua using borehole shots (KRISP Working Group, 1987). In addition a major teleseismic survey was carried out consisting both of a 500 km long linear array of 22 stations from Lake Magadi to Garissa and of a 100 x 110 km two-dimensional array covering the rift and its flanks from Lake Magadi to Lake Bogoria by 15 three-component stations with an average spacing of 35 km. Both arrays recorded teleseismic events for a time period of three months from September to December 1985 (Dahlheim et al., 1989; Green and Meyer, 1992).

The seismic refraction/wide-angle reflection survey of KRISP-90 was carried out in a 4-weeks period in January and February 1990. It consisted of three profiles: one extending along the rift valley from Lake Turkana to Lake Magadi (lines A, B, C in Fig. 1), one crossing the rift at Lake Baringo (line D in Fig. 1), and one being located on the eastern flank of the rift proper (line E in Fig.1). A total of 206 mobile vertical-component seismographs, with an average station interval of about 2 km, recorded the energy of underwater and borehole explosions to distances of up to about 550 km. During the teleseismic survey an array of 65 seismographs was deployed to record teleseismic, regional and local events for a period of about 7 months from October 1989 to April 1990. The elliptical array spanned the central portion of the rift

(*on the following page*)

Fig.1: Location map of the KRISP '90 and KRISP '94 seismic refraction wide-angle reflectionsurveys. The 1985 refraction - wide-angle reflection lines extended from Lake Baringo to Lake Magadi and across the rift just north of the Susua volcano.

Scientific Technical Report STR 98/05
DOI: 10.2312/GFZ.b103-98055

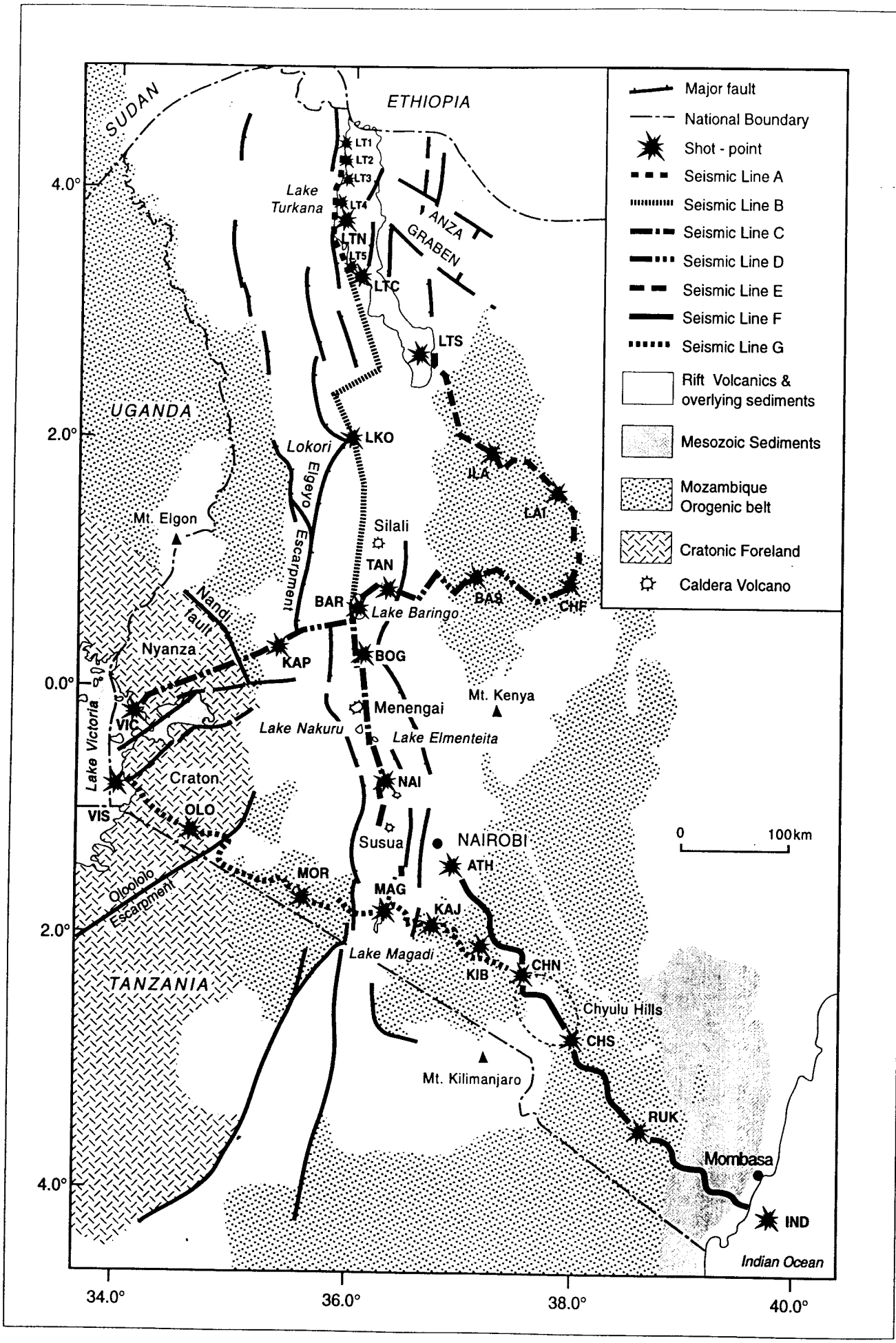

Fig. 1

Scientific Technical Report STR 98/05
DOI: 10.2312/GFZ.b103-98055

GeoForschungsZentrum Potsdam

and the adjacent flanks, with Nakuru at its center, and covered an area about 300 x 200 km, with an average station spacing of 10-30 km (Prodehl et al., 1994).

KRISP 94 involved a teleseismic tomography experiment of the Chyulu Hills area in July and August 1993, a seismic refraction - wide-angle reflection survey across southern Kenya from Lake Victoria to the Indian Ocean in 1994, seismicity studies of southern Kenya from 1993 to 1995, a seismicity study of the Lake Magadi area in February 1994, a gravity study along the seismic-refraction lines performed before and after the seismic-refraction study, and a magnetotelluric study of southern Kenya in February 1995 (Fuchs et al.,1997). During the tele-seismic survey an array of 31 seismographs was deployed to record teleseismic, regional and local events for a period of about 3 months from June to August 1993. The elliptical array covered an area about 150 km (N-S) x 100 km (E-W) and spanned the central portion of the Chyulu Hills and its surroundings, with an average station spacing of 10-30 km. The seismic refraction - wide-angle reflection survey was carried out in a 2-weeks period in February 1994. It consisted of two profiles: one extending from Lake Victoria across the western flank and the southernmost Kenya rift at Lake Magadi (line G in Fig. 1), the other extending from Athi River near Nairobi across the eastern flank of the rift, traversing the Chyulu Hills and terminating at the Indian Ocean near Mombasa (line F in Fig. 1). A total of 204 mobile seismographs, with an average station interval of about 2 km, recorded the energy of underwater and borehole explosions to distances of up to 730 km (Prodehl et al., in Fuchs et al., 1997).

This contribution will concentrate on the refraction seismic studies, but will also briefly discuss the results of the teleseismic tomography. We will discuss the main results of crustal and upper-mantle structure of the Kenya rift and its flanks by presenting a fence diagram and we will discuss in more detail the seismic-refraction data by describing in some detail the correlation of phases and their attribution to the corresponding depth ranges.

2. CRUSTAL STRUCTURE OF THE KENYA RIFT SYSTEM DERIVED FROM THE SEISMIC-REFRACTION DATA

The seismic refraction - wide-angle reflection experiments carried out between 1985 and 1994 in the Kenya rift (KRISP '85, KRISP '90 and KRISP '94; Fig. 1) show that, below sedimentary layers in the basins, the crystalline crust consists of three layers: an upper crust (basement) with velocities from 6.0 to 6.3 km/s, a middle crust with velocities of 6.4 to 6.7 km/s and a lower crust with velocities of 6.8-7.0 km/s. The crust is underlain by upper-mantle material with velocities above 8.0 km/s outside the rift, with the only exception underneath the Chyulu Hills in southeastern Kenya (7.9 km/s), but upper-mantle velocities immediately under the Moho of the Kenya rift proper are below 8.0 km/s (Fig.2).

The model (fence diagram in Fig. 2) shows major crustal thickness variations both along and across the rift. Along the rift axis crustal thickness varies from 35 km in the south beneath the Kenya dome to 20 km in the north beneath the Turkana region (KRISP Working Group 1987; KRISP Working Party 1991; Prodehl et al. 1994; Prodehl et al., in Fuchs et al., 1997). To a large extent this variation is accomplished by the thinning of the 6.8-km/s basal crustal layer. Due to the distribution of crustal thickness beneath the rift flanks, it can be stated that the major amount of variation in crustal thickness along the rift axis is due to the Tertiary rifting episode. The decrease in crustal thickness northwards from the Kenya dome can be correlated with changes in surface topography (northwards decrease), rift width (northwards increase), surface estimates of extension (5-10 km in the south and 35-40 km in the north) and Bouguer gravity, the regional northwards increase of which can be explained entirely by the change in crustal thickness (Mechie et al. (b), in Prodehl et al., 1994).

Scientific Technical Report STR 98/05
DOI: 10.2312/GFZ.b103-98055

Scientific Technical Report STR 98/05
DOI: 10.2312/GFZ.b103-98055

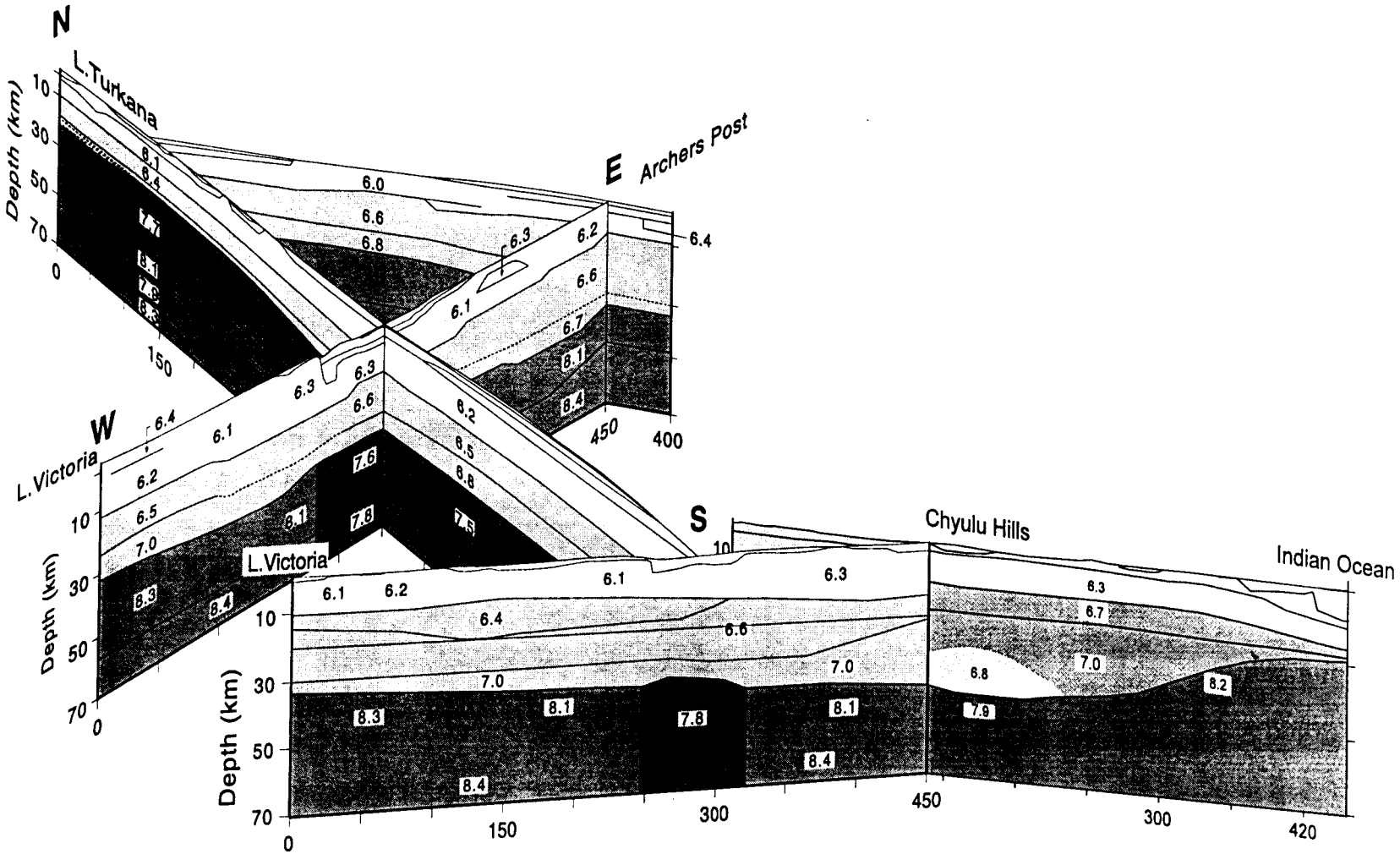

Fig.2: Fence diagram showing crustal and uppermost mantle structure of the Kenya rift from Lake Turkana to Lake Magadi and beneath the neighbouring flanks from Lake Victoria to Archers Post north of the Kenya dome and from Lake Victoria to the Indian Ocean south of the Kenya dome. P-wave velocities are shown in km/s. The cross-hatched pattern represents anomalous mantle beneath the rift axis. (after Birt, 1996, and Novak, 1997).

The profile completed in 1990 across the rift north of the Kenya dome at the latitude of Lake Baringo shows that the low uppermost mantle P-wave velocity (P_n) of 7.5-7.7 km/s and crustal thinning of 5-10 km is confined to below the surface expression of the rift (Mechie et al. (b), in Prodehl et al., 1994). An abrupt change in Moho depths and P_n velocities occurs as the rift boundaries are crossed. Beneath the rift flanks normal P_n velocities of 8.0-8.2 km/s occur (Maguire et al., Braile et al., Prodehl et al., all in Prodehl et al., 1994).

The profile completed in 1994 across the rift south of the Kenya dome at the latitude of Lake Magadi also shows a low uppermost mantle P_n velocity of 7.8 km/s confined to beneath the surface expression of the rift (KRISP Working Group 1995; Birt et al., in Fuchs et al., 1997). However, the crustal thinning beneath the rift along this profile is much subdued and to the west towards Lake Victoria the crust remains thin with a total thickness of around 34 km. In contrast, east of the rift, in the vicinity of the Chyulu Hills Quaternary volcanic field some of the thickest crust (38-44 km) encountered so far beneath Kenya is revealed over a distance of about 250 km. Further southeast the crust thins to 20-25 km towards the Indian Ocean. The seismograms from the region of the Chyulu Hills Quaternary volcanic field are of a reverberatory nature from immediately behind the first arrivals to beyond the Moho reflection P_MP. This reverberatory nature could possibly be caused by the intrusive equivalents of the volcanic outpourings in the Chyulu Hills. Beneath the Chyulu Hills the uppermost mantle P_n velocity is around 7.9 km/s and a zone of reduced velocity is also present at the base of the crust (Novak et al. (a, b), in Fuchs et al., 1997).

Below the 750 km long axial rift profile, P_n velocities are low being 7.5-7.8 km/s. However, under the northern part of the rift two layers with velocities of 8.1 km/s and 8.3 km/s are embedded in the low velocity material at 40-45 km and 60-65 km depth respectively. In contrast, the wide-angle data show that beneath the Kenya dome in the southern part of the rift low mantle velocities occur down to at least 65 km depth. This mantle velocity structure indicates that the depth to the onset of melting is at least 65-70 km beneath the northern part of the rift and is thus not shallower than the depth (50-70 km) to the onset of melting under the Kenya dome to the south (Keller et al. (a), in Prodehl et al., 1994; Mechie et al., in Fuchs et al., 1997). Reflecting interfaces within the uppermost mantle also occur beneath the eastern flank and cross-rift profiles. Below the northeastern flank profile E, a reflector at about 45 km depth has been detected while beneath the cross-rift profiles reflectors at 45-65 km depth have been identified, below both the eastern and western flanks (Mechie et al., in Fuchs et al., 1997) and, in the case of the cross-rift profile south of the Kenya dome at the latitude of Lake Magadi, crossing the rift itself (Byrne et al., in Fuchs et al., 1997).

3. UPPER-MANTLE STRUCTURE FROM TELESEISMIC TOMOGRAPHY

The two seismic tomography studies of KRISP-85 and KRISP-90 (Achauer et al.,1992; Achauer and the KRISP Working Group, in Prodehl et al., 1994) have imaged the three-dimensional velocity structure of the Kenya rift and its flanks down to 150 km depth between Lake Magadi in the south and Lake Baringo in the north (Fig. 3). Using an inversion algorithm of Aki et al. (1977), relative velocity changes are obtained from the traveltime residuals observed by the seismic-array stations.

The inversion algorithm requires a pre-set block model in which the thickness of layers is fixed by definition of the interpreter. While the depths remain constant during the entire inversion procedure, horizontal velocity variations are calculated for each layer by iteratively comparing the observed and the model-derived traveltime residuals, until the deviation between observed and model-derived data reaches a minimum. The tomography model chosen for the Kenya rift consists of two crustal and three upper-mantle layers (Achauer et al., 1992).
- The upper crustal layer (layer 1, surface to 10 km depth) exhibits the velocity structure immediately below the recording sites. Its strong lateral variations are mainly due to sediments and volcanics close to the surface under the neigbourhood of the stations.

Scientific Technical Report STR 98/05
DOI: 10.2312/GFZ.b103-98055

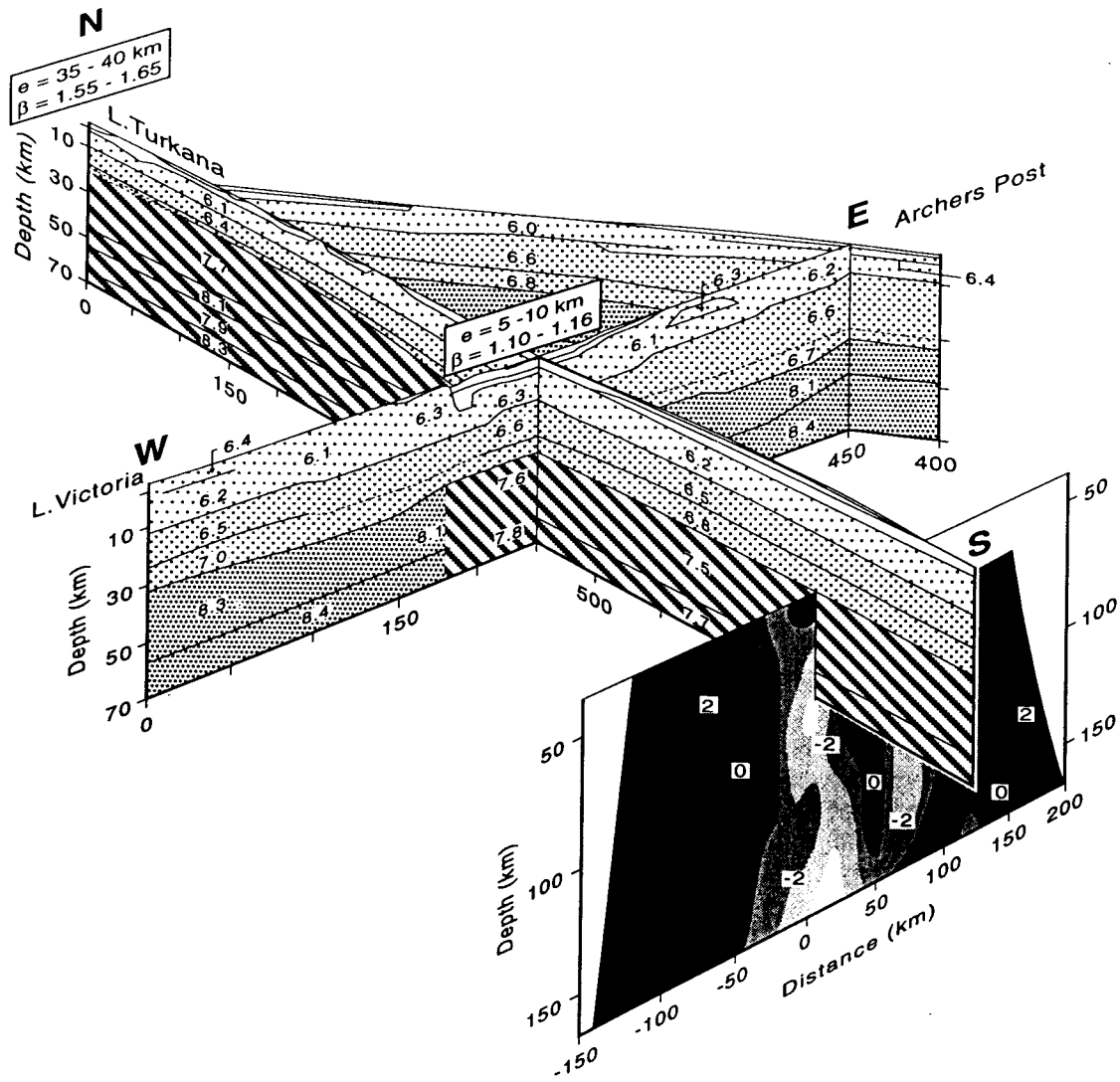

Fig.3: Fence diagram showing crustal and uppermost-mantle structure of the Kenya rift from Lake Turkana to Lake Naivasha and beneath the neighbouring flanks from Lake Victoria to Archers Post. P-wave velocities are shown in km/s. Also shown are relative velocity variations from teleseismic delay time studies across the rift at 1°S (Achauer and the KRISP Working Group, in Prodehl et al., 1994, this volume). Teleseismic velocity perturbations are contoured at 1% intervals and shaded at 2% intervals. Slow perturbations are light coloured, fast perturbations are dark coloured. For more detailed velocity information for the crustal sections, see corresponding cross sections in enlarged form in individual papers of KRISP-90 (N-S-profile: Mechie et al. (b), W-E-profile: Maguire et al., Braile et al., NW-SE-profile: Prodehl et al., all in Prodehl et al., 1994).

- The lower crustal layer (layer 2, 10 - 35 km depth) shows up to 12% velocity variations (about 0.8 km/s) with high velocities under the rift axis and low velocities beneath the flanks. The rift presents significant variations in velocity along strike with lowest velocities in the center of the rift between Lakes Bogoria and Naivasha.
- The uppermost mantle layer (layer 3, 35-65 km depth) shows a variation of 10% and, contrary to the lower crustal layer, low velocities beneath the rift. This low-velocity zone seems to terminate northwards towards Lake Bogoria. Of interest is its continuation in the direction of the young Nyanza trough to the west towards Lake Victoria.
- The intermediate upper-mantle layer (layer 4, 65-105 km depth) shows a pronounced relative low velocity beneath the rift axis through the entire rift up to Lake Baringo as far as observations are available. The velocities vary by 12.5% (about 1.0 km/s) in the south and by 8% in the north. Only small variations can be recognized when moving from south to north. The low-velocity zone remarkably correlates with the rift bounding faults. There is a slight deflection to the east under the eastern flank north of Lake Bogoria.
- The deepest mantle layer (layer 5, 105-145 km depth) is similar to layer 4, but the anomalous low-velocity zone is broader and the velocity changes are around 9%. The deflection of the low-velocity zone under the eastern flank is more pronounced.

To demonstrate the relationship and difference between seimic-refraction and tomography modelling, the fence diagram of KRISP-90 is shown here in Figure 3 which does not include the southernmost east-west line (profiles F and G in Fig. 2), but does include instead a tomographic cross section across the southern Kenya rift (Fig. 3; from Keller et al. (b), in Prodehl et al., 1994). Based on laboratory measurements on dry peridotite at pressures up to 1 GP and temperatures of 1300°C, where 6-8% partial melt were observed causing a 12% velocity decrease, it is suggested that there are regions of up to 5-6% partial melt in the upper mantle under the Kenya rift proper where extensive low velocities are observed (Green et al., 1991; Achauer et al., 1992; Achauer and the KRISP Working Group, Mechie et al.(a), both in Prodehl et al., 1994).

The tomographic investigations of KRISP-94, performed in 1993, covered only the crust and upper mantle of the Chyulu Hills in southeastern Kenya (dashed oval between CHN and CHS in Fig. 1; Ritter and Kaspar, in Fuchs et al., 1997). Though they reached only to a maximum of 140 km depth, the results indicated velocity contrasts of 4-5% at the most in the lower crust and the uppermost mantle between 20 and 90 km depth, which are considerably less than those obtained for the Kenya rift at the same depth range (Fig. 4). The cross section of Figure 4 shows crust and upper-mantle structure underneath the Chyulu Hills.

It combines the seismic-refraction model for the crust (Novak et al. (a, b), in Fuchs et al., 1997) and the tomography model for the upper mantle (Ritter and Kaspar, in Fuchs et al., 1997). Haug and Strecker (1995) suggest that this youngest volcanic field on the eastern rift shoulder is placed on much thicker and therefore thermally less weakened lithosphere.While for the Kenya rift it is concluded that the mantle contains partial melt caused by major heating of the uppermost mantle and upwelling of hot material, the smaller-scale anomaly under the Chyulu Hills is more likely due to the existence of small magma chambers within the crust and uppermost mantle feeding the Holocene volcanic field and disturbing the crust-mantle boundary (Ritter and Kaspar, Novak et al. (b), both in Fuchs et al., 1997). A zone of partial melt corresponding to the zone of slightly decreased seismic velocity below the Chyulu South shotpoint (CHS) is also inferred by the geoelectric structure (Simpson et al., in Fuchs et al., 1997).

Scientific Technical Report STR 98/05
DOI: 10.2312/GFZ.b103-98055

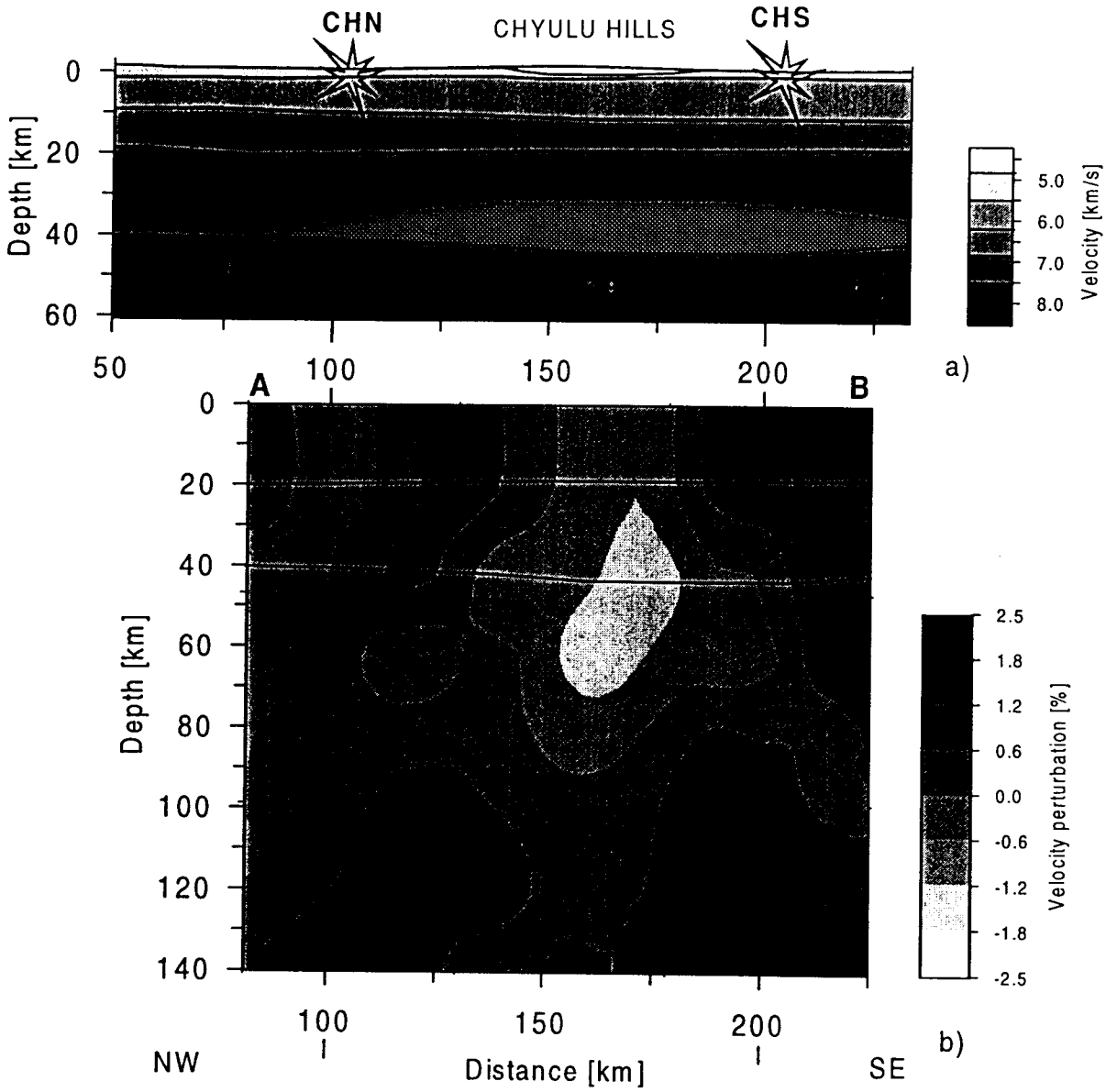

Fig.4: (a)Part of the seismic-refraction model along line F (see Figs. 1 and 2) compared at the same scale to
(b) the cross section through the teleseismic-tomography model along line F. Displayed are perturbations of the compressional wave velocity in percent relative to the starting model (from Novak et al. (b), in Fuchs et al., 1997).

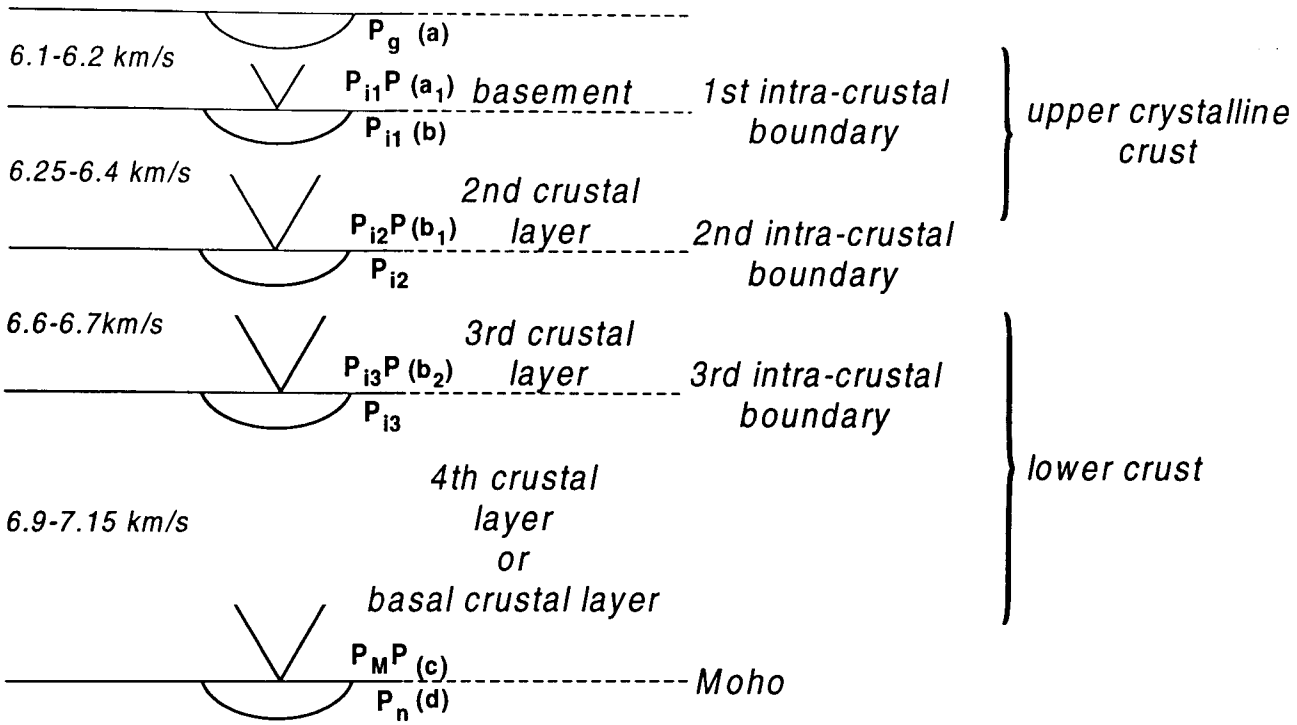

Fig.5: Presentation of the phases correlated and their notation in the record sections of Figs. 6-10.

4. INTERPRETATION OF THE SEISMIC-REFRACTION DATA

4.1 General observations

This contribution is particularly devoted to the description of the seismic-refraction data. The phases which can be identified in the individual record sections are shown in Figure 5. The data will be described in some detail and are presented as assemblages of record sections in Figures 6 to 10.

Details of the individual profiles will be discussed below separately for each line, but some general observations can be made beforehand. The general notation of the phases is shown in Figure 5. All correlations are shown as traveltime curves: P_g (*a*), P_{i1}, (*b*), P_n (*d*) are phases refracted beneath a boundary resp. diving into the underlying layer. $P_{i1}P$ (a_1) is a reflection from the top of the crystalline basement, $P_{i2}P$ (b_1), $P_{i3}P$ (b_2), etc. are phases reflected from intracrustal boundaries. P_MP (*c*) is the reflection from the Moho, and d_1, d_2, etc. are reflections from subcrustal boundaries. It should be noted, however,that *"b"* is not used uniquely by different authors. In some record sections (e.g., Fig.6), *"b"* denotes simply the reflection from the top of the lower crust. The individual phases marked in the record sections of Figures 6-10

Scientific Technical Report STR 98/05
DOI: 10.2312/GFZ.b103-98055

correspond to theoretical traveltimes which have been recalculated from the final models for the individual lines A to G (Fig.1) which are combined in the fence diagram (Fig.2).

With the exception of basin areas along the rift proper as, e.g. Lake Turkana, where a several km thick succession of low-velocity sediments has been assumed (see, e.g., Gajewski et al., in Prodehl et al., 1994), sedimentary cover is thin to negligible as can be recognized from the P_g-phase (*a*) where it is observed close to the 0-axis in many record sections at the distance range from 0 to about 100 km indicating seismic basement with velocities of 5.5 km/s near the surface and between 5.95 and 6.25 km/s at greater depths.

On most record sections two major phases can be correlated in secondary arrivals (Figs. 6 - 10) with more or less clarity. Phases b_1, b_2 are reflected from intracrustal boundaries at about 10 and 20 km depth (Fig.2). The P_MP-phase (*c*) is, in most cases, well observed with strong amplitudes and is always interpreted as the reflection from the crust-mantle boundary. At large distances, from 150 km onwards, a first-arrival P_n-phase (*d*) can be detected which originates from a wave refracted along or diving into the uppermost mantle. Though not always identified, phase *d* as predicted from the models in Figure 2 has been plotted on most record sections, also on those of intermediate shotpoints where the observation range was too short to trace mantle refractions in first arrivals. Finally, also at large distance ranges on the profiles recorded from the Lake Turkana shots, a phase d_1 can be correlated, which follows phase *d* by some tenths of a second and is reflected from a boundary within the subcrustal lithosphere. On the profiles within the rift a second phase d_2 is interpreted as reflection from an additional subcrustal boundary.

Differential signatures typical for graben areas as well as such for the flanks can be detected already when viewing the data sets as a whole without going into details. Note the appearance of either P_MP*(c)* or $P_{i1}P$, $P_{i2}P$ *(b_1, b_2)* alone or together, reflectivity patterns, existence of a P_n-phase *(d)* etc. at the individual assemblages and models.

4.2 KRISP-90 - axial line (lines B and C)

In order to accomplish the above mentioned aims a 600 km long axial line was completed between Lakes Turkana and Magadi in two deployments, B and C (Fig. 1). The northern end of deployment B starts in the Lake Turkana basin (Plio-Pleistocene and Holocene sediments). Subsequently, the line crosses the Kerio basin (km 190 - km 253, Holocene sediments), exposed Precambrian crystalline basement, the Lokichar basin (km 256 - km 280, Neogene and Quaternary sediments), Upper Miocene volcanics (to km 330), Pliocene volcanics (to km 388), Pleistocene volcanics, the Baringo basin (km 453 - km 482, Holocene sediments), Pleistocene volcanics (to km 510), Holocene volcanics, Holocene sediments of the Naivasha basin (km 600 to km 617) and finally, between km 674 and the southern end of deployment C, Pleistocene volcanics. The data of this line have been interpreted by Mechie et al. (b) (in Prodehl et al., 1994) and the traveltime curves shown in the record sections have been re-calculated from the model for lines B and C shown in Figures 2 and 3.

(on the two following pages)

Fig.6: Record sections of the Kenya rift from Lake Turkana to Lake Naivasha (KRISP 90, axial line; lines B and C in Fig. 1). The phase-correlating curves correspond to the travel times calculated from the model shown in Figs. 2 and 3. Shotpoint is at km 0.

(a) Observations from north to south. (b) Observations from south to north.

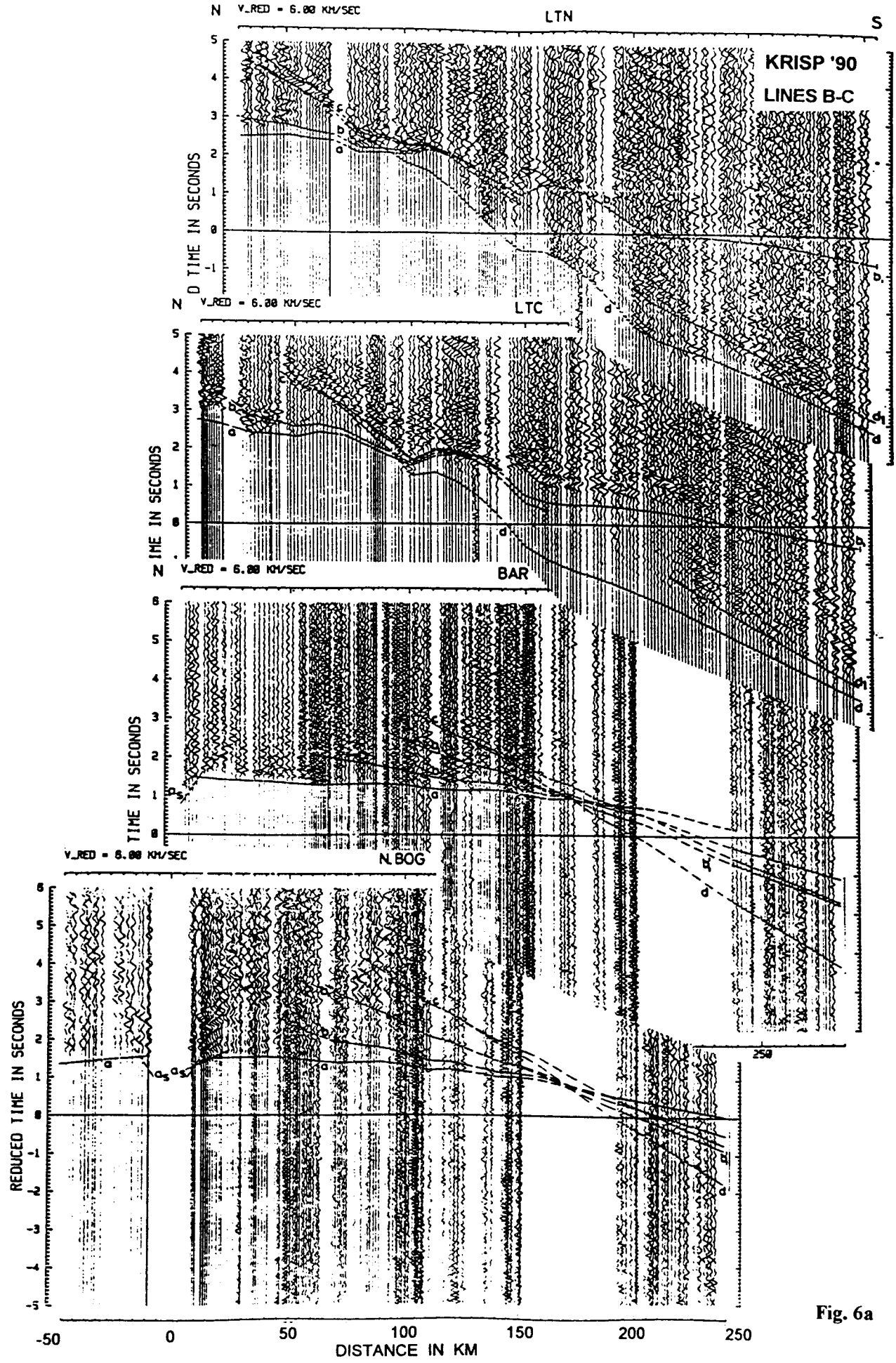

Fig. 6a

Scientific Technical Report STR 98/05
DOI: 10.2312/GFZ.b103-98055

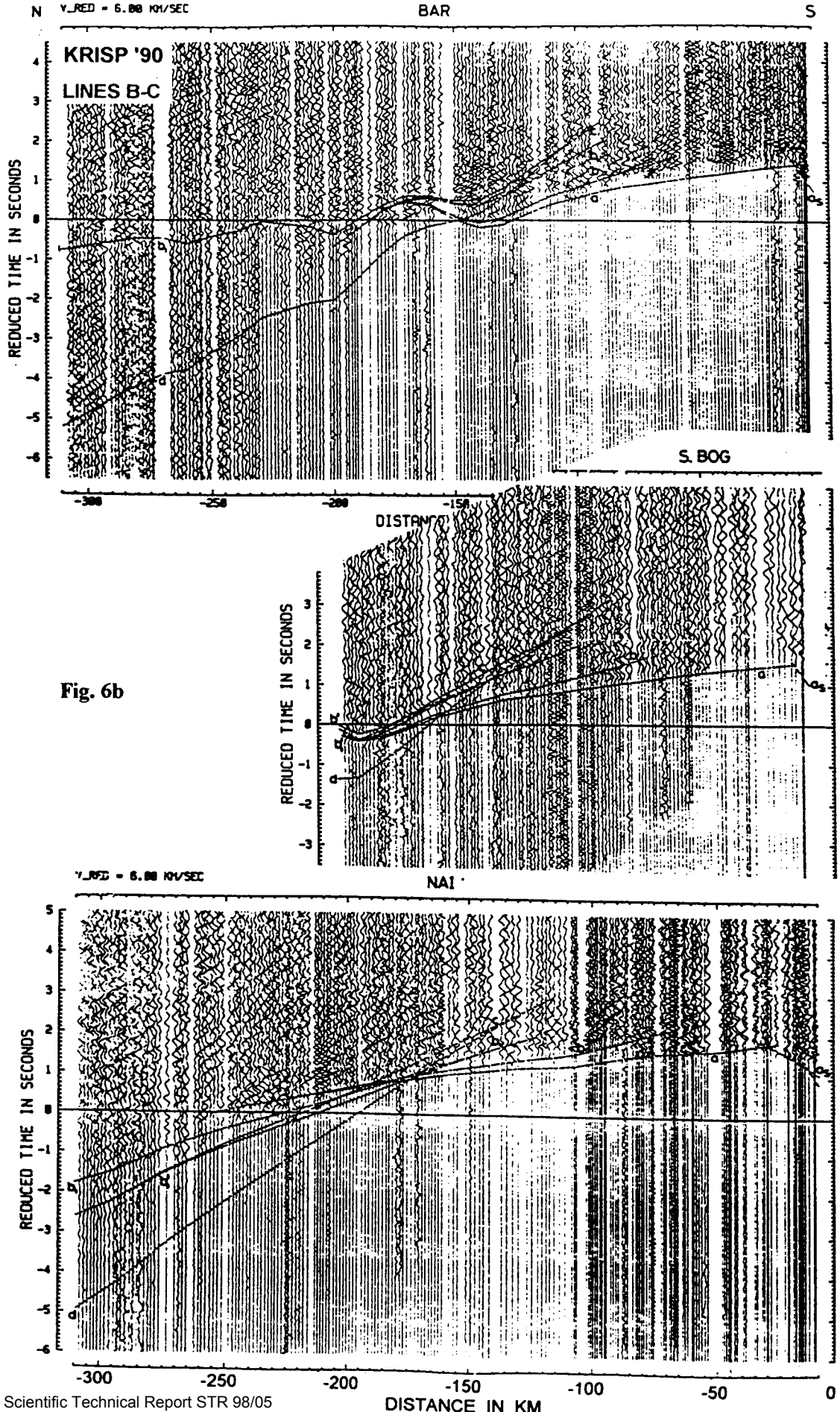

Fig. 6b

Scientific Technical Report STR 98/05
DOI: 10.2312/GFZ.b103-98055

The record sections for LTN and LTC (Fig.6a) show clearly the P_g (*a*) and P_n (*d*) phases, the first arrival refractions through the upper crystalline crust and the uppermost mantle respectively. The topography of the base of the rift basins can be well recognized in the travel-time advances and delays of the P_g and P_n phases. Of all the record sections, those from LTN and LTC show the P_MP phase (*c*), the reflection from the crust-mantle boundary (Moho), most clearly. Although the intracrustal phase *b* ($P_{i3}P$), the reflection from the top of the lower crust, cannot be identified with any certainty on either the LTN or LTC record sections, it can be recognized on the record section for LT4, which is nearby LTN, recorded to the south along line A (Gajewski et al., in Prodehl et al., 1994).

On the BAR-S (Fig. 6a) and BAR-N (Fig.6b) record sections, the first-arrival refracted phases a_s through the rift infill can be recognized out to about 15 km distance, after which the P_g phase (*a*) becomes the first arrival out to about 150 km distance. Beyond about 150 km distance, P_n (*d*) can sometimes be seen as the first arrival. The phase *b* ($P_{i2}P$) can be recognized on both the BAR-N and BAR-S record sections while the intracrustal phase b_l ($P_{i3}P$), the reflection from the top of the basal crustal layer, can be recognized on the BAR-S record section. Whereas it is possible to identify the P_MP (*c*) phase on the BAR-S record section it is not possible to do so on much of the BAR-N record section.

On the two BOG record sections (Figs.6a, b), in addition to the first arrival phases through the rift infill and the P_g (*a*) phase, the P_n (*d*) phase can be seen from BOG recorded to the north beyond about 150 km distance (Fig. 6a). From BOG recorded to the south (Fig. 6b) both the *b* ($P_{i2}P$) and b_l ($P_{i3}P$) phases can be seen while the *c* (P_MP) phase can be identified in recordings both north and south from BOG.

On the NAI-N record section (Figs.6b), beyond the first-arrival phases a_s through the rift infill, P_g (*a*) can be recognized out to about 150 km. Beyond about 160 km, P_n (*d*) occurs as a very weak first arrival in comparison to the crustal phases. Phases *b* ($P_{i2}P$) and b_l ($P_{i3}P$) can be identified. The combined energy of *c* (P_MP) and b'_l (P_{i3}), the refracted phase through the basal crustal layer, can be recognized on the NAI-N record section at distances greater than 200 km. The combined energy which is the dominant energy in the record section at distances greater than 200 km is the energy which was taken to be the first arrival in the data recorded northwards from the shot in Lake Bogoria in the 1968 experiment.

4.3 KRISP-90 - northern cross-rift line (line D)

The 450km long cross-rift line was completed as KRISP 90 deployment D between Lake Victoria in the west and Chanlers Falls in the east. The location of the recording sites was along the crooked line shown on Figure 1. The topographic and geological variation along the profile is extremely large. The geology is roughly from west to east:
Km 0: Lake Victoria is on meta-sediments, km 0 - 55 km: volcanics and intrusives of the Nyanza craton - Archaean greenstone belt, km 55 - 110: granitoid belt, at km 110: Nandi Fault, km110 - 130: Precambrian Mozambique orogenic rocks, east of km 130: relatively flat-lying Middle Miocene volcanics of the Uasin Gishu plateau - the Elgeyo escarpment (the major western bounding fault of the Kenya Rift) - 500m down the escarpment: outcrop of hornblende-biotite gneiss of the Mozambique belt in the footwall of the Elgeyo fault, in its hanging wall: an unknown thickness of Tertiary sediments and volcanics which are covered in the Kerio Valley by recent alluvial sediments, basement with block rotation in the uplifted Kamasia Hills, which on the seismic line are covered with Pliocene and Miocene volcanics, from km 215 (in the central part of the Rift): Quaternary sediments and volcanics thin along the profile to the east beneath Lake Baringo, km 255 - 265: further cover of recent sediments, continuation of Miocene and Pliocene volcanics on the eastern side of the Rift to about km 320, continuing to the eastern end of the line: Precambrian basement gneisses of the Mozambique orogenic belt, covered occasionally by recent fluvial deposits.

Scientific Technical Report STR 98/05
DOI: 10.2312/GFZ.b103-98055

The cross-rift line was interpreted by two research teams (Braile et al., Maguire et al., both in Prodehl et al., 1994), each using a different interpretation technique, but both resulting in quite similar models. Here we follow Maguire et al. who describe their phase identification of the principal seismic phases on the record sections shown in Fig. 7a and b as follows:

- Pg (phase *'a'*) the first arrival, a diving wave through the upper crust. It is clearly seen on all the sections but in most cases increased gain is required, indicating small velocity gradients in the upper crust;
- Pi (phase *'b'*) a diving wave from below a mid-crustal boundary is observed on the record sections from BAR and TAN;
- $P_{i1}P$, $P_{i2}P$ (phases *'b_1 '*, *'b_2 '*) at least one and sometimes two intracrustal reflections are seen on most record sections;
- P_MP (phase *'c'*), the Moho reflection can be seen more or less clearly from all shots;
- P_n (phase *'d'*), the first arrival refracted wave from the uppermost mantle can be observed from all shot points but is weak on some sections;
- An upper mantle reflection (phase *'d_1'*), from below the Moho is seen on the section from VIC. A phase labelled *'x'*, seen on some other sections may be a pre-critical phase of the same origin, but could alternatively be a converted phase or multiple.

Discussion of the individual arrivals from each shot is best accomplished in relation to the modelled phases produced after complete interpretation of the whole data set. The traveltime curves shown in the record sections of Figure 7a and 7b are re-calculated from the model for line D shown in Figures 2 and 3.

Shotpoint VIC (Fig.7a)
The first arrival phase *'a'* is delayed by about 0.4 seconds between 0 and 30km (for a reduction velocity of 6km/s) and has an apparent velocity of near 6.1km/s out to 150km. The modelled critical point of phase *'b_1'* is at about 75km. This is a high amplitude reflection from the top of a layer of velocity 6.5km/s at a depth of about 12km. Pre-critical energy is seen as close as 40km. A second, weaker reflection *'b_2'* with a critical point at about 135km is from a lower crustal boundary at a depth of about 25km. The strongest later arrival seen across the section is phase *'c'* a low frequency reverberative phase with a critical point at 95km. It can be ray-traced to about 210km, at which distance the observed phase emerges slowly from precursory energy. Beyond the cross-over distance with phase *'d'* at about 150km, the crustal phases result in an almost monotonic reverberation across the section from a reduced time of about 0.5 seconds. Phase *'d'*, the diving wave into the mantle, is rather weak but recorded out to the maximum distance and well-modelled except for an advance between about 240 and 280km. A mantle reflection phase *'d_1'* is identified immediately after phase 'd' with a modelled critical point at about 270km.

Shotpoint KAP to the east (Fig.7a)
The KAP shotpoint was sited on the Uasin Gishu phonolites which cause a small near-source delay for phase *'a'*. The 0.4 seconds delay on the first arrival phase *'a'* decreases towards the Rift margin before a large delay is introduced at about 30 km where the energy enters the Rift

(on the two following pages)
Fig.7: Record sections across the central Kenya rift from Lake Victoria eastward through Lake Baringo (KRISP 90, cross line; line D in Fig. 1). The phase-correlating curves correspond to the travel times calculated from the model shown in Figs. 2 and 3. Shotpoint is at km 0.

(a) Observations from west to east. (b) Observations from east to west.

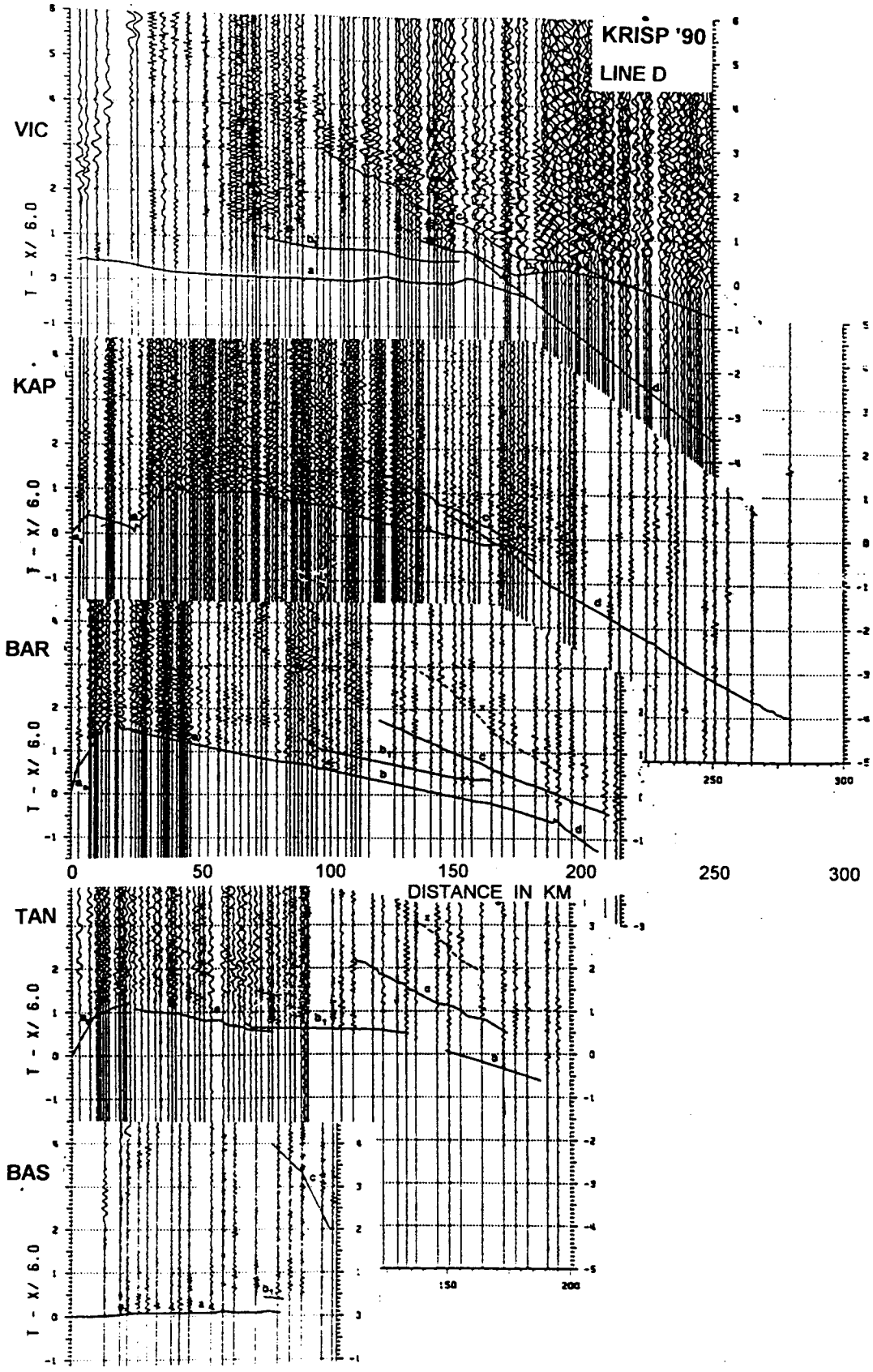

W 0 50 100 150 200 E

DISTANCE IN KM

Fig. 7a

Scientific Technical Report STR 98/05
DOI: 10.2312/GFZ.b103-98055

Fig. 7b

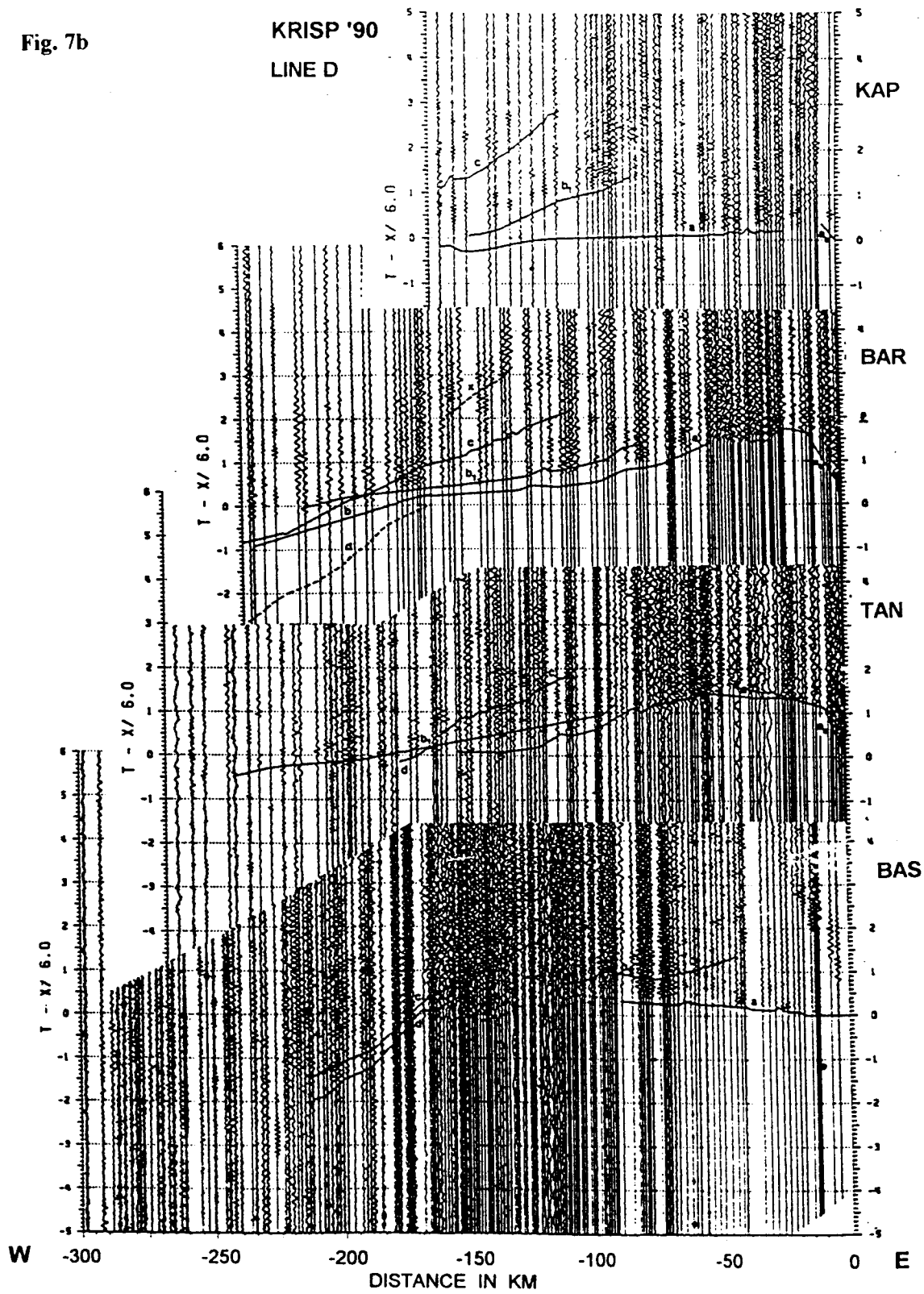
KRISP '90
LINE D
KAP
BAR
TAN
BAS
T - X/ 6.0
W
-300
-250
-200
-150
-100
-50
0
E
DISTANCE IN KM

proper. Within the Rift the energy is reverberative and of low signal-to-noise ratio, making identification of arrivals difficult. Phase *'c'* is almost impossible to identify near the modelled critical point at about 100km, but is consistent with the diffuse energy observed beyond about 140km from the shotpoint. Phase *'d'*, although weak, can be clearly identified to a distance of about 220km.

Shotpoint KAP to the west (Fig.7b)
The large-amplitude phase *'b_1'* is modelled with a critical point at about 80km advancing to a reduced time of about 0.1 seconds at 140km from KAP. Phase *'c'* can be identified on the most distant few seismograms, but the separation of the traces and its relatively low amplitude make positive identification of its onset tenuous. It is modelled with a critical point at about 105km.

Shotpoint BAR to the east (Fig.7a)
The large delay at the source is indicative of the thick, low velocity Rift infill, the first arrival out to about 65km emerging from the surface sediments and two underlying layers above the basement. Phase *'a'* can be modelled to 110km at which point it intersects a high-velocity block in the upper crust, and beyond which the observed arrival decreases in amplitude. The diving wave *'b'* from the lower crust produces the weak first arrival occurring between about 100 and 200km. Phase *'b_1'* itself is a clear, but weak reflection from the base of the upper crust with a critical point at about 100km from BAR. It has a complex ray path when passing through the high velocity block. Phase *'c'* with a critical point at about 120km, extends back to within about 95km of BAR, at which point it must be pre-critical. It originates from the Moho at a depth of about 34km beneath the eastern margin of the Rift, and becomes diffuse beyond about 150km from the shotpoint. Phase *'d'* is seen as a clear first arrival and occurs beyond about 190km from BAR. A further high amplitude phase *'x'* can be seen on the combined plot apparently following phase *'c'*. It can be modelled quite successfully as a reflection from a deep interface at about 55km, but it has to be pre-critical energy. Alternatively, it can be modelled as multiple energy from the upper crustal layer and the further possibility of it being a converted phase should not be ruled out.

Shotpoint BAR to the west (Fig.7b)
Once again there is a delay of some 1.5 seconds at the shotpoint, indicative of a substantial thickness of low-velocity sediments and volcanics above the crystalline basement. The first arrival out to about 40km originates in sequence from the surface layer (2.2km/s), and the two underlying layers (3.8 and 5.8km/s) before being overtaken by phase *'a'*. A delay in phase *'a'* at approximately 55km occurs over the Kerio basin and is followed by an advance over the basement outcrop at the base of the Elgeyo escarpment. There is a cross-over to a higher velocity phase *'b'* at about 160km. It is difficult to identify exact onsets of later phases on the reverberative traces. However, phase *'b_1'* correlates with energy concentrated at about 100km from the shotpoint, and asymptotically tends towards phase *'a'* at long offsets. The combined plot of the four Lake Baringo shots successfully enhances the second arrival energy identified as phase *'c'*. The critical point is modelled at about 105km. Phase *'d'* is poorly defined but can be positively identified on at least two traces. Ray-tracing does not produce any diving rays, therefore the observed times are indicated in Figure 7b by a dashed line. Once again there is a later phase *'x'* following *'c'*, similar to that identified on the section from BAR to the east. The same statements apply concerning its origin.

Shotpoint TAN to the east (Fig.7a)
To the east of the Tangulbei shotpoint, the first arrival comprises phases from the Rift infill and the crystalline basement to a distance of about 80km. The model does not enable this phase to continue beyond the high-velocity upper-crustal block, and it can be seen that the amplitude of the first arrival is apparently attenuated at about this distance. The reflection from the base of the upper crust *'b_1'* has a critical point at about 75km. A diving phase *'b'* from the top of the mid-crustal layer is identified from about 150 to 190km. Phase *'c'* is diffuse, but identifiable with a critical point at about 110km. A later high-amplitude, diffuse phase *'x'* can be identified, modelled as a pre-critical reflection from the intra-mantle boundary at a depth of

Scientific Technical Report STR 98/05
DOI: 10.2312/GFZ.b103-98055

about 55km, but the same statements apply as were made for the equivalent phase observed on the BAR section.

Shotpoint TAN to the west (Fig.7b)
The first arrival to 150km represents diving waves from layers within the Rift and the crystalline basement, phase *'a'*. Thereafter it can be seen continuing towards 200km from the shotpoint. There is good correlation between the modelled and observed arrivals across the complex structure of the Kerio Valley and Elgeyo escarpment. Phase *'b_1'* can be observed with a critical point at about 90km. No other intra-crustal phases can be confidently identified in the reverberative coda. Similarly, phase *'c'* is poorly defined but is modelled with a critical point at about 105km. There is no well defined mantle diving wave, phase *'d'*. Given the reciprocal time from VIC to TAN, this should occur at about -4.8 seconds reduced time at the farthest offset recording on the section. Calculated times for phase *'d'* can only be obtained by ray-tracing for rays emerging at about 160km.

Shotpoint BAS to the east (Fig.7a)
Phase *'a'* is clearly observed to the east of BAS. Its amplitude on the normalized section decreases when the large-amplitude phase *'b_1'* appears. Phase *'b_1'* arises as the reflection from the top of the mid-crustal layer and is consistent with this interface rising towards CHF and the modelled depth on the flank line E (Fig.2). It is probable that the high-amplitude phase occurring at about 2.5 seconds reduced time on the two traces at the end of the section is phase *'c'* modelled as the pre-critical reflection from the Moho.

Shotpoint BAS to the west (Fig.7b)
Phase *'a'* is modelled to 42km from BAS. Beyond this distance it is overtaken by a diving wave entering the high-velocity block beneath the shotpoint, required to accommodate the advance in first arrivals from about this distance. It can only be modelled to a distance of about 90km. Phase *'b_1'* is a strong reflection with a critical point at about 65km, a pre-critical phase being identified back to about 45km. Later phases are masked by the strongly reverberative signal and low signal-to-noise ratio, but phase *'c'* may be identified and is modelled with a critical distance of 130km. An important phase *'d'* can be identified at a distance of 200km, and is reasonably modelled by waves passing through the sub-Rift anomalous upper mantle zone having a velocity of about 7.6km/s. There is no evidence for a mantle reflection originating from below the Moho.

4.4 KRISP-90 - northern flank line (line E)

Line E is a diagonal line with one end in the rift, rather than a purely flank line. An added complication is the proximity of the Jurassic Anza rift. Particularly towards its northwest end, it lies on structures which form the flanks of not one, but two rifts, one Jurassic to Tertiary (Anza Rift) and the other Tertiary to recent (Kenya Rift). The topography along the line varies from approximately 300 m (Lake Turkana) to a maximum of less than 1000 m. The line runs along the northeastern margin of a basement rock complex (MOE, 1987). Basement rocks outcrop at many sites near the line, and the sedimentary cover is thin to neglegible.

Contrary to lines B to D, the record sections of this line are plotted for the complete deployment, the corresponding shotpoint being marked by 0 in Figure 8. The flank line E was interpreted by Prodehl et al. (in Prodehl et al., 1994). Their phase identification of the principal seismic phases on the record sections shown in Fig. 8 is as follows:

Shotpoint CHF to the northwest (Fig.8)
The first-arrival phase *a* (P_g) is relatively weak and is followed by a strong reflection a_1 which is interpreted as a reflection from a shallow high-velocity reflector within the basement. This phase is also seen on the short section of CHF-SE. Phase *b* is very well modelled. Because of the geometry of this section of the crust, a corresponding refracted phase *b'* is also present, but does not appear until beyond 100 km. A further intracrustal phase, b_1, is only

seen at larger distances, beyond about 130 km. The strongest event in secondary arrivals is phase *c* (P_MP), a quite strong and low-frequency phase which emerges from relatively strong precursory energy. Phase *d* (P_n), while rather weak, is fairly clear and well modelled beyond 150 km distance from CHF.

Shotpoint LAI to the southeast (Fig.8)
As in the CHF-NW section, an outstanding feature is the strong reflection a_1 which closely follows phase *a* (P_g). Any phase *b* and b_1 is not apparent. Phase *c* (P_MP) is well recorded from about 90 km outwards and appears to have a slightly lower dominant frequency content than the precursory lower crustal energy, but it is to a certain extent masked by a 'noisy' lower crust which is probably highly reflective.

Shotpoint LAI to the northwest (Fig.8)
From LAI to the northwest, the high-velocity reflector is not evident and a reflected phase a_1 has to be interpreted differently. Here, between 40 and 80 km, the two phases a_1 and *b* can be modelled as both being reflected from two interfaces at around 10 km depth. A phase *b'* is observed but not very strongly. In addition, a weak wide-angle reflection b_1 from the lower-crustal layer can be followed at 50 - 150 km distance from the shotpoint. In the reverse direction from ILA it is seen at a similar time and distance range. The phase becomes more distinct near 130 km. Phase *c* is rather complex, sometimes with the maximum energy significantly delayed with respect to the first onset of the phase. Patches of low amplitude and apparent delays may indicate a disturbed crust-mantle boundary.

Shotpoint ILA to the southeast (Fig.8)
The first arrivals recorded east of ILA (8 - 15 km) and travelling near the surface may pass through a lava flow or some other high-velocity body, to produce the observed early arrivals, otherwise phase *a* (P_g) is well matched by the model. East of ILA the top of the mid-crustal layer (reflected phase *b*) drops quite steeply near km 210 (Fig.2), with a depth increase from about 7 km to about 10 km. It then rises gradually eastwards without reaching the shallow depth attained northwest of ILA. Southeast of km 210, a weak reflector (phase a_1) persists at about 7 km depth. Similar to LAI-NW, a "refracted" phase *b'* is seen at larger distances which is well fitted by arrival times predicted by the model. Phase *c* is well matched at its inner end near 100 km. The observed phase continues beyond 140 km, but here it is obscured by the earlier phase b_1. Phase *d* cannot be correlated in this short record section.

Shotpoint ILA to the northwest (Fig.8)
Though observed from the same shot, the profile ILA-NW differs considerably from the observations in SE direction. The energy recorded in later arrivals is much more diffuse. Nevertheless, though with difficulty, the main phases can also be identified here. Phase *b* is a reasonably good phase from about 40 km outwards, with some evidence for subcritical arrivals. An analogue to phase a_1 cannot be seen here. Phase b_1 would be subcritical on this short section and there is not much evidence for it, though the predicted model travel times have been plotted into the record section. Phase *c*, finally, is a relatively strong and predominantly low-frequency arrival beyond about 80 km distance from ILA.

(on the following page)
Fig.8: Record sections of the northern eastern rift zone flank of the Kenya rift from Lake Turkana towards southeast (KRISP 90, flank line; line E in Fig. 1). The phase-correlating curves correspond to the travel times calculated from the model shown in Figs. 2 and 3. Position of shotpoint is marked by 0, observations are both to NW and SE, except for shotpoint LTS which is to the left (NW) of the recording line.

Scientific Technical Report STR 98/05
DOI: 10.2312/GFZ.b103-98055

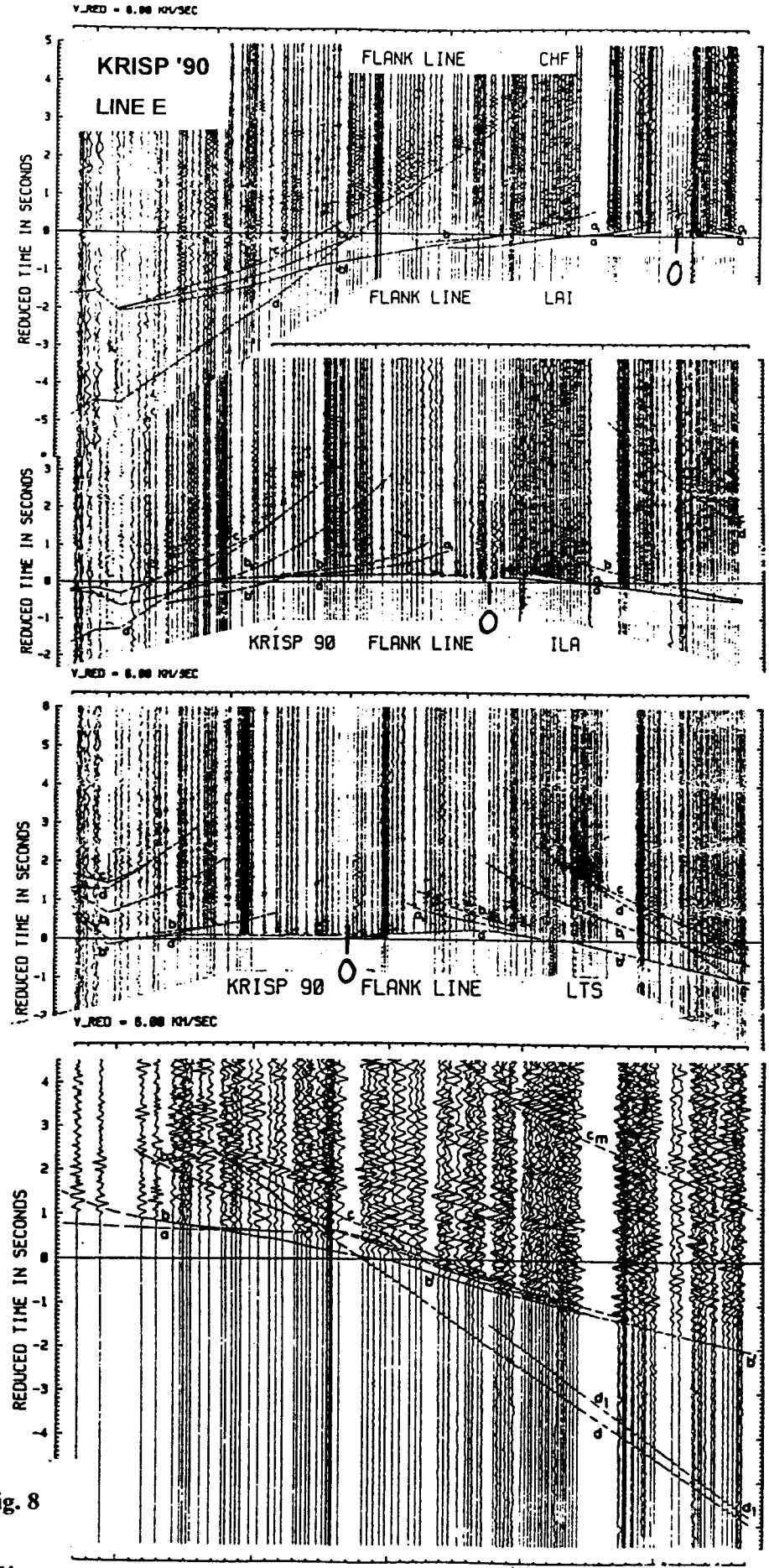
KRISP '90
LINE E
FLANK LINE
CHF
FLANK LINE
LAI
KRISP 90
FLANK LINE
ILA
KRISP 90
FLANK LINE
LTS
REDUCED TIME IN SECONDS
NW
50
100
150
200
250
SE
DISTANCE IN KM

Fig. 8

Shotpoint LTS to the southeast (Fig.8)
As the shotpoint was about 35 km off the eastern shore of Lake Turkana, only the outer end of phase *a* has been recorded. Phase *b*, reflected from 10 km depth, is visible only over a short distance range, from the beginning of the observed data (35 km from the shotpoint) to about 110 km (Fig.8). A corresponding "refracted" phase *b'*, correlated from 100 to near 160 km, is interpreted as a diving wave generated by a positive gradient in the middle crust beneath 10 km depth. Phase b_1 is a strong reflection with its critical point around 150 km, continuing for more than 100 km with evidence for subcritical energy to distances as small as 60 km, whereas further to the southeast around Illaut (ILA) the intermediate boundary between middle and lower crust near 20 km depth appears partly as a second-order discontinuity which, on the borehole shot data, produces a quite weak to almost absent reflection b_1 preceding phase *c*. Phase *c* is correlated from 90 to 240 km. It is a reasonably strong phase, but is also rather complex. Beyond 100 km from LTS there is a short stretch where the phase appears to be delayed. This may indicate a considerably more complex crust-mantle boundary than the model in Figure 2 can illustrate as it is based on pure ray tracing. Beyond 150 km distance, at about 3.5 seconds after the main bulk of P-phases, a strong phase $c_m$can be correlated which can be traced to the end of the line. This phase is interpreted as a multiple reflection being twice reflected between surface and Moho. The LTS-SE record section includes at least two other strong and persistent multiple phases, some of which may be dog-leg multiples which are hard to model. The two phases between 170 and 220 km, approximately parallel to the first-arrival pattern and delayed approximately 1.5 and 3.0 sec, are probably multiples in the sedimentary layers near the shotpoint. There are clear arrivals of the phase *d* (P_n) on only 10-12 stations. Nevertheless, the phase *d* (P_n) is clearly visible and can uniquely be correlated to the end of line E. P_n arrivals from the reversing shotpoint CHF are weak and their onsets not always certain. From around 200 km distance outwards there is good evidence for a subcrustal reflection d_1 which can also be correlated on the data of LTC-SE not shown here.

4.5 KRISP-94 - flank line through the Chyulu Hills (line F)

Line F extended over the eastern flank of the Kenya rift from Athi River (30 km southeast of Nairobi) across the Chyulu Hills volcanic field to the Indian Ocean near Mombasa (Fig.1). The key area of interest on line F is the Chyulu Hills range, a Quaternary volcanic field, situated about 150 km east of the Kenya rift, and close to the border with Tanzania, just 40 km north of Mt. Kilimanjaro. The Chyulu Hills consist of hundreds of cones predominantly aligned in a northwest-southeast direction embedded in the flat surrounding basement of the Mozambique belt. Most of the eruptions took place during the late Pleistocene and Holocene and the youngest flows are of historical age. The record sections in Figure 9 were compiled and interpreted by Novak et al. (a)(in Fuchs et al., 1997).

Except for record section IND all inline record sections (Fig.9) reveal a similar seismic picture. The sedimentary cover is thin to negligible as the P_g-phase observed on ATH, CHN, CHS and RUK in the distance range 0 to 50 km has basement velocities of 6.1-6.2 km/s. The record section IND features a time offset of nearly 2 s for the P_g-phase. A thick local sedimentary cover of about 8 km is used to explain this time offset. A very prominent arrival on the borehole-shot record sections is the P_{i3}-phase which travels through the lower crust. On

(on the following page)
Fig.9: Record sections of the southern eastern rift zone flank of the Kenya rift from Nairobi through the Chyulu Hills to the Indian Ocean (KRISP 94, line F in Fig. 1). The phase-correlating curves correspond to the travel times calculated from the model shown in Figs. 2 and 4. Position of shotpoint is marked by 0.

Scientific Technical Report STR 98/05
DOI: 10.2312/GFZ.b103-98055

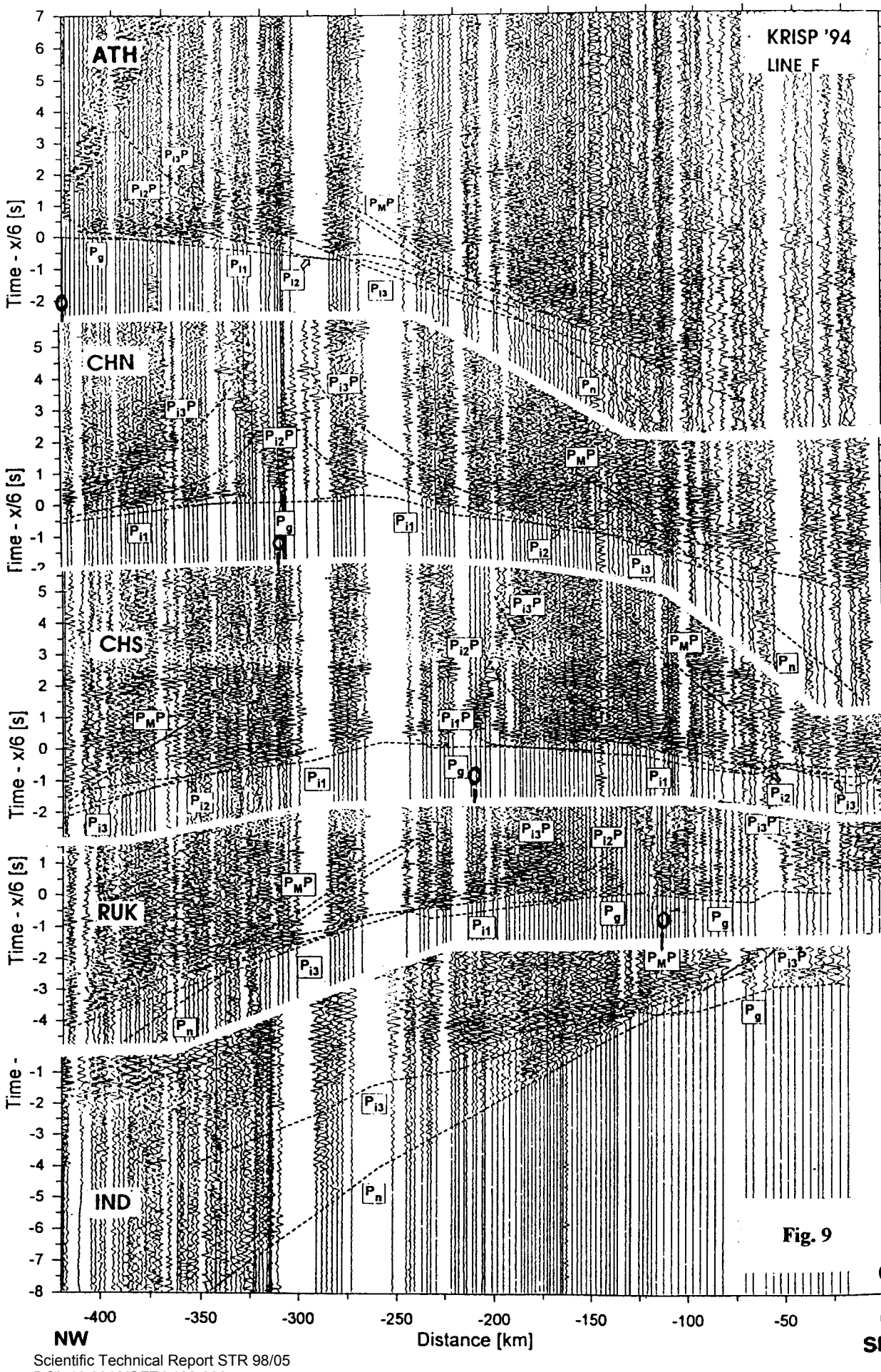

Fig. 9

Scientific Technical Report STR 98/05
DOI: 10.2312/GFZ.b103-98055

all borehole record sections the P_MP-phase (reflection from the crust-mantle boundary), is hard to identify, especially on the record sections CHN (to the south) and RUK (to the north). The region sampled by P_MP for these particular sections corresponds to the region immediately beneath the Chyulu Hills (Fig. 4). This indicates a transitional nature for the Moho in this area, possibly the result of thermal disturbances related to the recent volcanism in the Chyulus. Strong reverberations which start directly behind the first arrivals and mask secondary arrivals complicates phase identification. This long coda could be generated by heterogeneous upper and lower crust. At distances beyond about 230 km a first arrival phase P_n can be detected on the record sections ATH, CHN, RUK and IND. Though not always easy to identify, the P_n-phase as predicted from the final crustal model (Figs. 2 and 4), has been plotted on all record sections.

The record section of the underwater shot IND (Fig. 9) shows features which are not observed on the borehole-shot record sections. There is an absence of high frequencies, in contrast to the borehole shots which seem to be broader band sources. The P_n-phase and strong undercritical reflections, which occur in small distances, are the dominant phases on the record section IND which is in contrast to the four borehole record sections. The P_MP-phase has a critical distance of about 50 km which is much less than critical distances of P_MP on the other record sections, where it is generally about 140 km. This fact indicates that the crust-mantle boundary rises significantly towards the Indian Ocean (Fig. 2).

Shotpoint ATH to the southeast (Fig.9)
The first arrival phase P_g is very well seen. Directly behind the P_g-phase a reflection is generated. This reflection from the first intra-crustal boundary can be observed nearly along the entire profile. The corresponding refracted phase (P_{i1}) is also present and can be identified as a first arrival to a distance of 120 km. The arrivals of this phase are rather weak and are followed by $P_{i2}P$, the second intra-crustal reflection. The refracted waves (P_{i2}) travelling through the third layer can be identified as first arrivals only over a very small distance range between 135-150 km. We observe good reflected energy from the lower boundary of this layer ($P_{i3}P$). The P_{i3}-phase refracted in the lower crust can be observed from 150-270 km. On this record section the arrivals of the P_{i3}-phase are not very pronounced as P_MP has its strongest amplitudes in the same distance range. Phase P_n is very weak and clear arrivals can be identified only on some traces, nevertheless it has been correlated up to 300 km.

Shotpoint CHN to the northwest (Fig.9)
Only phases travelling in the upper part of the crust can be observed here. The P_g-phase has a lower velocity (6.0 km/s) than the P_g of ATH. It is followed by a clear reflection from the first intra-crustal boundary. The refracted phase in the second crustal layer (P_{i1}) can be correlated from about 35 km to the end of the record section. The reflected phase from the top of the third crustal layer ($P_{i2}P$) is not seen very clearly but the reflection from the top of the lower crust ($P_{i3}P$) can be correlated.

Shotpoint CHN to the southeast (Fig.9)
On this record section the first arrival phase P_g is observed up to 30 km where it is delayed due to the low-velocity material located at the surface in the area of the Chyulu Hills (Fig. 4). P_{i1} suffers a delay over the first few kilometres and is overtaken at km 135 by P_{i2}, travelling through the third crustal layer. The corresponding reflection ($P_{i2}P$) is seen at subcritical distances. The fourth first-arrival phase P_{i3} can be identified beyond 160 km, where it is clearly observed, but then becomes less well defined due to noisy traces and the delay from the sedimentary cover at distances greater than 230 km. The reflection from the top of the lower crust ($P_{i3}P$) is seen but is masked by a seismic reverberation signal which starts immediately after the first-arrival phases. The interpretation of the most dominant reflection phase on this record section is difficult: the part beyond 165 km is modelled as P_MP, the part before 165 km might be sub-critical but shows an offset of half a second. It is not obvious whether we are dealing with one or two phases. An indication of the correct position of the modelled P_MP-phase are some observed P_n arrivals which if correlated correctly run directly into the modelled critical point for P_MP.

Scientific Technical Report STR 98/05
DOI: 10.2312/GFZ.b103-98055

Shotpoint CHS to the northwest (Fig.9)
The recorded seismograms show features similar to those generated by ATH. Secondary arrivals are even more difficult to identify due to the long coda of the first arrivals. P_g is rather weak and travels through the low-velocity feature at the surface of the Chyulu Hills area (15-30 km) (see also Fig. 4). Also the refracted phase P_{i1} travelling through the second crustal layer is influenced at short distances by this low velocity zone. This phase can be modelled to a distance of 125 km where it is then overtaken by the diving wave (P_{i2}) generated in the third crustal layer. As in the ATH record section, this phase is only observed as the first arrival over a short distance range (125-155 km). The refracted phase in the lower crust (P_{i3}) shows first arrivals to the end of the record section. The reflection from the crust-mantle boundary (P_MP) is difficult to identify.

Shotpoint CHS to the southeast (Fig.9)
This part of the record section is quite similar to CHS-northwest. The arrivals still have a relatively long coda but it is attenuated faster than on the seismograms recorded in the northwestern part of the record section. Secondary arrivals are thus visible which give better seismic control of the crust in this area and towards the Indian Ocean. The P_g-phase can be observed to a distance of about 30 km. Similar as on the ATH record section, this phase is followed immediately by the reflection from the bottom of the basement. The refracted phase of the second crustal layer (P_{i1}) can be identified into a distance of almost 150 km. The critical and sub-critical reflections corresponding to the top and the bottom of the third crustal layer can be identified as later arrivals in the distance range 30-150 km. All phases appearing at more than 150 km from the shotpoint are strongly influenced by the sedimentary cover near the Indian Ocean. Sediments here have a thickness of about 1 km which increases up to 8 km at the end of the profile. The most prominent phase on this record section is the P_MP-phase which shows a strong convex curvature, indicating an uprising of the Moho towards the Indian Ocean.

Shotpoint RUK to the northwest (Fig.9)
This record section shows features which are characteristic and similar on both record sections CHS-northwest and CHS-southeast. Secondary arrivals are visible up to a distance of 150 km. Beyond that distance long signal codas mask secondary arrivals, especially the normally dominant phase P_MP which we were not able to identify at all. The P_g-phase is observed out to 50 km, and stronger reflections from the basement directly behind that phase are missing. The first arrivals of the P_{i1}-phase are rather weak in the distance range 60-110 km where phase $P_{i2}P$ reflected from the bottom of this layer appears as a second arrival. Between 120 and 175 km the P_{i1}-phase is delayed by the low-velocity feature at the surface in the Chyulu Hills area. The P_{i2}-phase could be identified, as on the previous record sections, only over a very small distance range which also corresponds to the Chyulu Hills area (Fig. 4). The refracted phase in the lower crust (P_{i3}) can be observed unambiguously from 175 km to the end of the profile. Due to the fact that we could not identify a P_MP-phase on this record section it is an interesting feature that very weak but visible P_n arrivals can be observed in the distance range of 225-300 km so that the P_n-phase of ATH-southeast is reversed.

Shotpoint RUK to the southeast (Fig.9)
Modelling of phases correlated on this record section revealed the sedimentary cover of the coastal area, near Mombasa (Fig. 2). The P_g-phase indicates still a high basement velocity of about 6.2-6.3 km/s and can be observed to 50 km. The P_{i1} phase is delayed by 0.3 s. Two major secondary arrivals can be observed beyond a distance of 60 km. The first one we identified as the reflection from the top of the lower crustal layer ($P_{i3}P$). The interpretation of the second reflection is still open.

Shotpoint IND to the northwest (Fig.9)
Seismograms recorded from the deep underwater shot IND show very different seismic characteristics when compared with the borehole shot record sections described above. The frequency content is much lower and phases, like the P_n-phase, travelling through the uppermost mantle, are dominant on this record section. The first arrival phase P_g is strongly delayed by 1.8 s. This is due to sedimentary cover which is about 8 km thick near the coast. All other phases refracted in the crust appear as secondary arrivals. The only one which could be identified was the P_{i3}-phase diving through the lower crust. A strong seismic signal appears between 270 and 420 km about 2 s behind the P_{i3}-phase, but is not yet identified. The most interesting feature in this record section is a phase we observe from 110 km to the end of the profile as a first arrival. We assume it is the P_n-phase. Its nature is rather complex. From 110 to 170 km amplitudes are extremely strong which may be due to the trace normalisation. At greater distances P_n loses much of its clarity because several mantle reflection phases appear directly behind it. In the distance range of 20-60 km several undercritical phases are present.

4.6 KRISP-94 - southern cross-rift line (line G)

Line G was 430 km long and cuts across the southern part of the Kenya Rift, the precise location being constrained by the need to follow driveable roads (Fig. 1). It crosses the rift at the alkaline soda lake at Magadi, just north of the border with Tanzania, and terminates at the Chyulu Hills in the east. At the western end of the line, Archean intrusives and meta-sediments (older than 2.5 Ga) form the surface geology. Near the OLO shotpoint, the craton is disturbed by a series of intrusions running parallel to the profile. Just the west of the Oloololo Escarpment, the Archean basement is obscured by a cover of Miocene phonolite lava. The Oloololo Escarpment is a striking linear fault-scarp, with an exposed throw of 400m. It may mark the boundary between the Archean rocks to the west and the Proterozoic rocks to the east The profile is forced to take a northerly detour in order to descend the steep escarpment, before dropping down onto the flat plains of the Masai Mara. The basement rocks are partially obscured by a blanket of Miocene phonolite lavas and recent alluvial soils. East of the Mara plains, Proterozoic rocks of the Mozambique Belt are exposed in the folds and thrusts of the Loita Hills. The Loita Hills are terminated to the east by the 2000m high Nguruman Escarpment, marking the western boundary of the Tertiary Kenya Rift. The elevation of the rift floor (650m above sea level at this point) is the lowest along the whole line. The floor of the rift valley is covered by a sequence of extensively faulted trachyte and basalt lavas. Lake Magadi occupies an elongated depression at the eastern side of the rift basin. The eastern margin of the rift is made up of a series of small 'step-faults', rising in elevation to reach outcropping Proterozoic basement near the Kajiado shotpoint (KAJ). There are no tracks that follow the optimum course of the E-W profile between the MAG and KAJ shotpoints, and a deviation some 20 km to the north was required (Fig. 1). The profile then crosses an area of patchy sediments before reaching the basaltic cones at the edge of the Quaternary Chyulu Hills range, where the CHN shotpoint is located on a small area of exposed basement. The record sections in Figure 10a, b were compiled and interpreted by Birt et al. (in Fuchs et al., 1997).

(on the following two pages)
Fig.10: Record sections of the southern Kenya rift from Lake Victoria through Lake Magadi to the Chyulu Hills (KRISP 94, line G in Fig. 1). The phase-correlating curves correspond to the travel times calculated from the model shown in Fig. 2. Position of shotpoint is marked by 0.

(a) Observations with shotpoints west of rift valley. (b) Observations with shotpoints within and east of rift valley.

Scientific Technical Report STR 98/05
DOI: 10.2312/GFZ.b103-98055

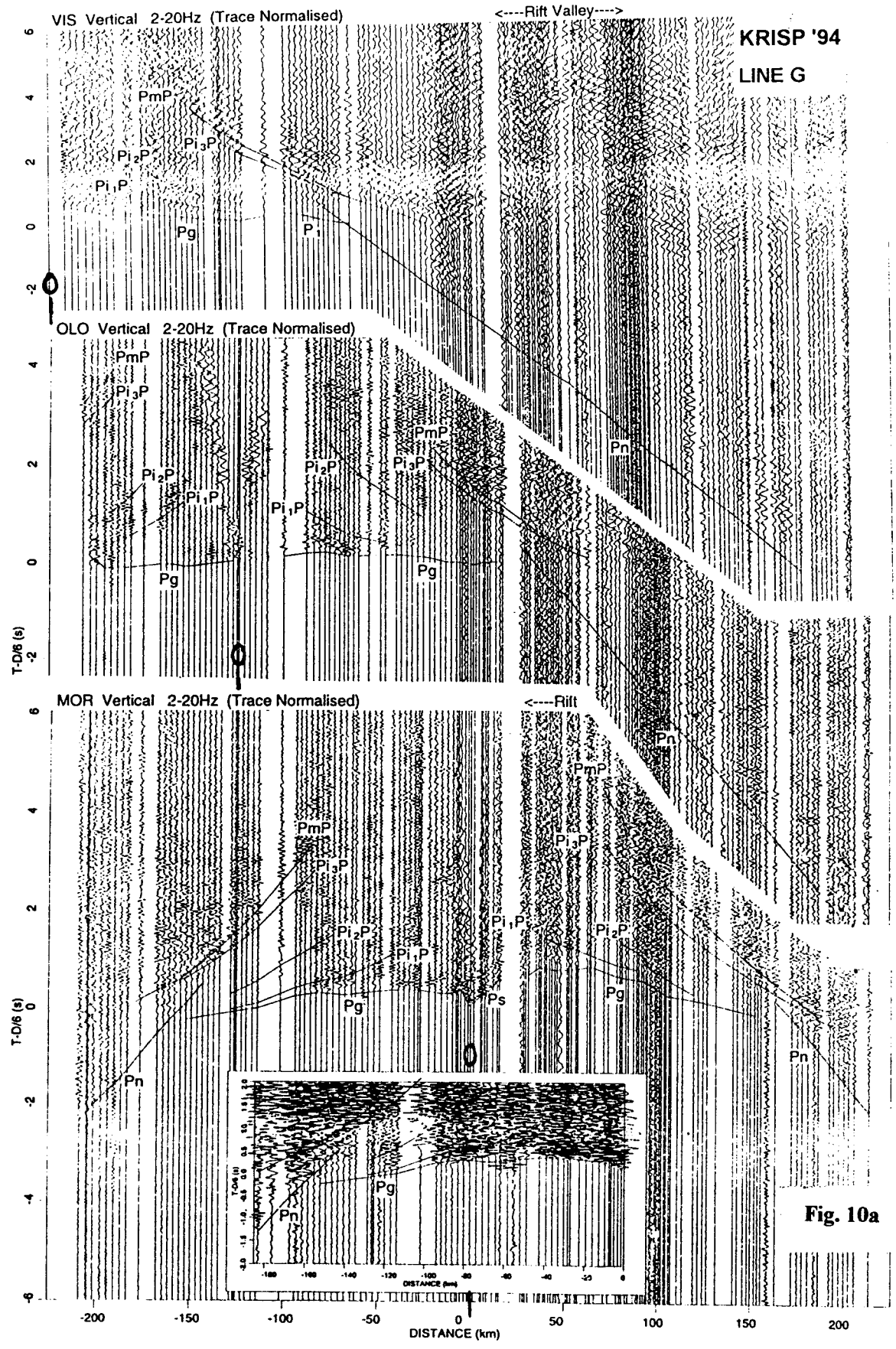
VIS Vertical 2-20Hz (Trace Normalised)
<----Rift Valley---->
KRISP '94
LINE G
PmP
Pi3P
Pi2P
Pi1P
Pg
P1
Pn
OLO Vertical 2-20Hz (Trace Normalised)
MOR Vertical 2-20Hz (Trace Normalised)
<----Rift
Ps
T-D/6 (s)
DISTANCE (km)
W
E

Fig. 10a

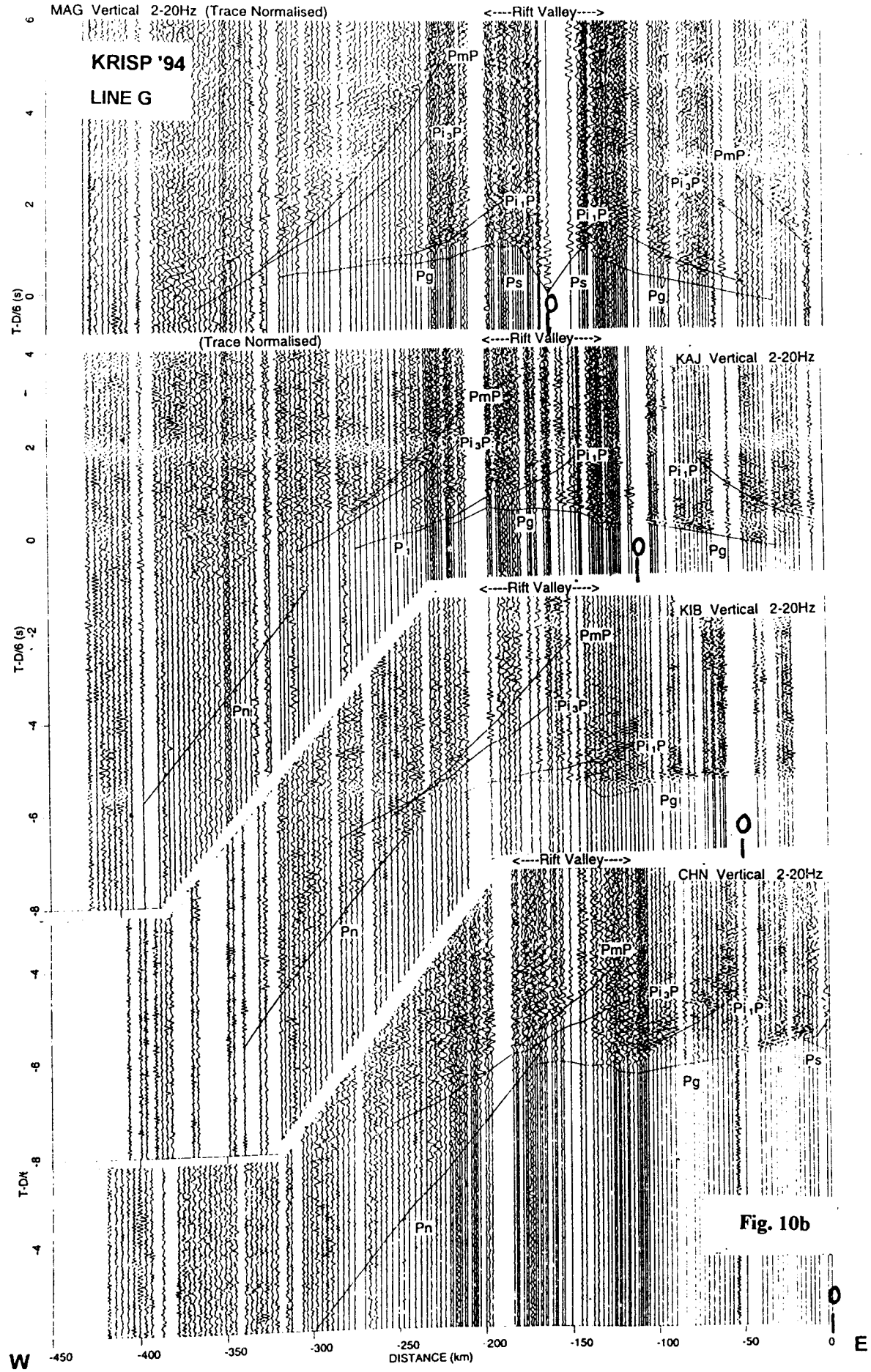

Fig. 10b

Scientific Technical Report STR 98/05
DOI: 10.2312/GFZ.b103-98055

Shotpoint VIS (Fig.10a)
The underwater shot from VIS generated strong but low-frequency energy that resonates at about 4 Hz. The basement arrival P_g has an apparent velocity of slightly higher than 6.0 km/s, but is delayed by 0.4s with respect to the shot instant, indicating a sedimentary sequence with slow P-wave velocities immediately beneath the shotpoint in the lake. The P_g phase can be identified out to 120 km, and two crustal reflections are picked behind this. The second reflection ($P_{i_2}P$) is weak and is only identified from shots at the western end of the profile, VIS, OLO and MOR. Beyond 120 km a diving wave in the mid-crust with an apparent velocity of 6.45 km/s becomes the first arrival, with P_n (the diving wave below the Moho) emerging at about 180 km and continuing until the end of the profile. Immediately in front of the strong Moho reflection (P_MP) is a reflection from the lowest crust ($P_{i_3}P$) which crosses over at 160 km to become the dominant phase. P_MP dies away quickly, indicating a high velocity gradient in the lower crust. The energy from the $P_{i_3}P$ reflection probably extends across much of the section, but it is not clear to pick.

Shotpoint OLO (Fig.10a)
The P_g arrival has an apparent velocity of slightly above 6.0 km/s but is delayed by about 0.2s 25-100 km east of the shotpoint. The upper crustal reflections can be seen, although $P_{i_1}P$ is very weak to the east. $P_{i_3}P$ can be clearly picked in advance of P_MP, but neither phase can be correlated at offsets less than 100 km. P_n becomes the first arrival at about 160 km, but is initially obscured by noisy data within the rift, becoming clearer beyond 250 km.

Shotpoint MOR (Fig.10a)
Close to the shotpoint, the first arrival is a direct wave (P_S) in a surface layer, with slightly higher velocities (4.8 km/s) to the east. The basement diving wave P_g is delayed by the low-velocity layer at the surface, with a much bigger delay (0.75s) towards the rift basin in the east. The reverberative nature of the seismograms within the rift is a feature common to many of the sections, and also the previous KRISP experiments (line D, Maguire et al., in Prodehl et al., 1994). P_MP is a strong phase in both directions, although it is partially obscured towards the east at offsets less than 100 km by reverberations after the lowest crustal reflection. P_n (with an apparent velocity of 8.1-8.2 km/s) can be clearly identified in both directions.

Shotpoint MAG (Fig.10b)
This shotpoint is within the rift itself, and the shot hole was drilled into volcanics at the surface. The direct wave has an apparent velocity of 4.5 km/s and delays the P_g arrival by 1s to the west, but slightly less towards the east, indicating an asymmetric rift basin. Crustal reflections are obscured by the reverberative signal within the rift, and P_MP is the strong, dominant phase. The observed critical points (75 km to the west, but 110 km to the east) indicate that the Moho is deeper towards the eastern end of the profile (Fig. 2). P_n cannot be seen in either direction. It is interesting to note that the frequency content of the $P_{i_3}P$ and P_MP reflections is different. At low frequencies (below 15 Hz), P_MP is the obvious and dominant phase, with $P_{i_3}P$ hardly visible, but at higher frequencies (above 15 Hz), $P_{i_3}P$ becomes much clearer, with the mantle reflection almost vanishing. The increased separation between $P_{i_3}P$ and P_MP compared with VIS, OLO and MOR suggests that the lowest crustal layer is thickening towards the rift.

Shotpoint KAJ (Fig.10b)
West of the shotpoint, P_g has an apparent velocity of about 6.0 km/s, but is soon delayed by about 0.5s due to the low velocity volcanics in the rift valley basin. To the east, the apparent velocity is higher (6.1-6.15 km/s), increasing to 6.2-6.3 km/s at 40 km. From 115 to 165 km west of the shotpoint, the P_1 diving wave below the mid-crustal layer is the first arrival, with an apparent velocity of 6.45 km/s, beyond which P_n can be picked until 280 km. In contrast to the MAG section, the lowest crustal reflection $P_{i_3}P$ is the dominant phase at low frequencies, and only in the higher frequencies does the P_MP reflection become clearer. This change in character may be caused by the KAJ shot sampling the lowest crust beneath the active rift zone, whilst MAG samples to the west of this.

Shotpoint KIB (Fig.10b)
This shot was an additional quarry blast which provided useful signals out to 300 km, but care must be taken in interpretation, especially at near offsets, since the shotpoint was some 10 km north of the recording profile, and was situated in limestone rather than crystalline basement. The P_g arrival has an apparent velocity of 6.2 km/s, and is delayed at 90 km by the rift basin. Upper crustal reflections behind this first arrival are difficult to pick because it is followed by a 1s wide zone of scattered or reverberative energy. P_n crosses over to become the first arrival at 175 km, and mantle refractions can be followed for almost 300 km from the shot. The long cross-over distance (compared with about 150 km for VIS and OLO) is another indication that the Moho is deeper on the eastern side of the rift. The lower crustal and P_MP reflections are not as strong as on some of the other sections.

Shotpoint CHN to the west (Fig.10b)
This shotpoint, situated on the northern flank of the Quaternary Chyulu Hills, shows a small delay in the first arrivals due to a near-surface low-velocity layer, with an apparent velocity of 5.4 km/s that could represent volcanic material. Beyond the delay, the P_g arrival has an apparent velocity of 6.2-6.3 km/s until it is delayed by the rift basin, showing that the basement velocity has significantly increased from west to east across the profile. The strong $P_{i_1}P$ reflection, with the critical point at 55 km, marks the onset of a 1s band of reverberation that appears similar to that seen from KIB. P_n crosses over P_g at 175 km to become the first arrival, and mantle refractions can be traced until 300 km. The start of the $P_{i_3}P$ and P_MP reflections are obscured by the reverberations behind the mid-crustal reflection, but become clearer beyond 175 km. P_MP is followed by a wide package of reverberating energy, especially in the central rift zone.

CONCLUSIONS

The crust under the Kenya rift is thickest (about 35 km) near the apex of the Kenya topographic dome where updoming is apparently the controlling feature and where the rift valley floor is at its maximum elevation and the amount of extension across the rift is small. To the north, the crust thins dramatically to about 20 km near Lake Turkana at the northern end of the domal uplift, where the amount of extension is higher and the elevation of the rift floor is at its lowest. Although there is evidence of underplating in the form of a relatively high velocity lower crustal layer, there are no major seismic velocity anomalies in the middle and upper crust which would suggest pervasive magmatism. Under southern Kenya, relatively thin crust (less than 35 km) was found under the rift valley and the areas extending westward to Lake Victoria. The most interesting feature, however, is an unusually thick crust (up to 44 km) extending eastwards from the rift for over 300 km towards the continental margin near the Indian Ocean where a more normal thickness of 25-30 km is reached. Weak supercritical reflections from the Moho suggest a transitional boundary in the region of the Chyulu Hills volcanic field, a major Quaternary feature.

Detailed teleseismic tomography studies were only carried out in central and southern Kenya. The south-central Kenya rift is clearly associated with sharply defined lithospheric thinning and very low upper mantle velocities down to depths of over 150 km (Achauer and the KRISP Working Group, in Prodehl et al., 1994). There the lithospheric mantle has been thinned much more than the crust. To the north, under the Turkana region, high velocity layers detected in the upper mantle appear to require the presence of anisotropy with preferred orientation of olivine crystals (Keller et al. (a), in Prodehl et al., 1994).

Summarizing the characteristics of crust and upper-mantle structure shown in Figures 2 - 4 for the entire Kenya rift system and its flanks, the following physical parameters may be regarded as typical:

Scientific Technical Report STR 98/05
DOI: 10.2312/GFZ.b103-98055

- Internal crustal structure variations in the rift zone are significant in all parts of the Kenya rift.
- Strong crustal thickness variations occur along the entire rift system, reaching from less near 20 km to more than 35km.
- Rift and flank crusts may differ substantially both in structure and velocities.
- The crust-mantle boundary in rift areas is usually not a sharp boundary, but a transitional zone.
- The uppermost-mantle (P_n) velocity in the rift zone is always less than 8 km/s.
- The uppermost-mantle (P_n) velocity under the flanks is always equal to or greater than 8 km/s, an exception being the Chyulu Hills in southern Kenya.

When viewed within the context of other observations, the physical characteristics and differences illustrated in Figures 2 - 4 lead to important conclusions concerning rift evolution in general:

- Internal crustal variations are often reflected in near-surface faulting, volumes and compositions of igneous activity, amount of extension, and timing of magmatic and tectonic events.
- All crustal sections represent more or less stretched and thinned continental crust.
- Crustal thickness variation may be viewed as a function of rift development. The further the rifting process has progressed, the thinner is the crust.
- The flanks may be highly influenced by rifting in those parts which are close to the rift. Broad upwarping and/or a transitional crust-mantle boundary may be signs of approaching rifting.
- Recent volcanic activity may disturb crustal interfaces; as well it may disrupt the Moho as evidenced particularly in the Chyulu Hills.
- The entire Kenya rift appears to be underlain by a heated upper mantle as evidenced by low P_n-velocities and the observed heat flow anomalies (Wheildon et al., in Prodehl et al., 1994). Under parts of the rift zone which are narrow in their surface expession, the width of the heated upper mantle zone is also relatively narrow (Achauer and the KRISP Working Group, in Prodehl et al., 1994; Braile et al., 1995).
- The presence of hot mantle material beneath the Kenya dome since the onset of volcanism 15-20 Ma ago is compatible with the abrupt change of P_n-velocities at the rift boundaries (Mechie et al., in Fuchs et al., 1997).
- Petrological interpretations of the seismic velocities beneath the Kenya rift indicate that the lower crust beneath the rift probably consists of a mix of high-grade metamorphic rocks, mafic intrusives, and an igneous mafic residuum accreted to the base of the crust during differentiation of a melt derived from the upper mantle (Mooney and Christensen, in Prodehl et al., 1994; Hay et al., 1995). The upper mantle may contain up to 5% basaltic melt, except within the high-velocity layers under the northern Kenya rift which can only be explained by some crystal orientation (anisotropy) (Mechie et al. (a), in Prodehl et al., 1994; Mechie et al., in Fuchs et al., 1997).

ACKNOWLEDGEMENTS

We want to express our special thanks to the membrs of the KRISP Local Organizing Committee, in particular to its chairman J.D. Obel, vice-chairman I.O. Nyambok, and secretary D. Riaroh as well as to its members S. Gaciri, , H.T. Macharia, J. Mukinya, D.K. Nzioka, W.S. Okoth, and J.P. Patel. Thanks are due to the Kenyan Government and the understanding officials who made the experimental work possible. The University of Nairobi, Egerton University, JKUCAT, the Ministry of Energy, the Department of Mines and Geology, the Survey of Kenya, the Department of Fisheries, the Kenya Navy, the Ministry of Water Development, the National Environment Secretariat, the National Council for Science and Technology, Kenya Power and Lighting, the Kenya Marine and Fisheries Research Institute, the Kenya Posts and Telecommunications Corporation, the Kenya Police, Contratours, Inside Africa Safaris, Hertz Corporation, Payless Car Hire, Rasul's Car Hire and Tours, Aquadrill,

Silanga, TWIGA Chemical Industries, all made vital contributions to the programmes. Mrs. D. Zola took care of all KRISP business at Nairobi, was available at any time on radio and telephone and offered her house to be used as KRISP office, laboratory and communication center by the installation of a radio station.

The work was financed by the German Research Society (DFG) and the state of Baden-Württemberg via the collaborative research center SFB 108 "Stress and Stress Release in the Lithosphere" at the University of Karlsruhe, the European Community under SCI contract 00064 (involving U.K., Denmark, France, Germany, Ireland, and Italy) and under the Human Capital and Mobility Programme under contract no. CHX-CT930308 (DG12COMA) (involving U.K., Denmark, Ireland, and Germany), the Continental Dynamics Program of the National Science Foundation (N.S.F.) in U.S.A. (University of Texas at El Paso, Purdue University, Stanford University, University of California at Los Angeles, University of Wisconsin), the U.S. Geological Survey, and the Natural Environmental Research Council (N.E.R.C.) in the U.K. The help of the diplomatic representatives of the E.C., U.K., U.S.A., and UNESCO and, in particular, the continuous support of the German Embassy are greatly acknowledged. The German Academic Exchange Service (DAAD) and the National Science Foundation (N.S.F., U.S.A.) helped with special funds to support travel and subsistence for long-term visits of scientists in Kenya and of Ph.D.students in Germany and U.S.A., respectively. The German Company for Technical Cooperation (GTZ) supported the technical realization of a local seismological network, based at the University of Nairobi, Kenya.

REFERENCES

Achauer, U., Maguire, P.K.H., Mechie, J., Green, W.V., and the KRISP Working Group, 1992. Some remarks on the structure and geodynamics of the Kenya rift. In: P.A. Ziegler (Editor), 1992. Geodynamics of Rifting, Volume II. Case history studies on rifts: North and South America, Africa. Tectonophysics, 213: 257-268.

Aki, K., Christoffersson, A. and Husebye, E.S., 1977. Determination of the three-dimensional seismic structure of the lithosphere, J. Geophys. Res., 82 : 277-296.

Birt, C.S., 1996. Geophysical investigation of active continental rifting in southern Kenya. Ph.D. Thesis, Leicester University, Leicester, 214 pp.

Braile, L.W., Keller, G.R., Wendlandt, R.F., Morgan, P., and Khan, M.A., 1995. The East African Rift System. In: Olsen, K.H. (Editor), Continental rifts: Structure, evolution, tectonics (CREST). Elsevier, Amsterdam, pp. 213-232.

Dahlheim, H.A., P.M. Davis, and U. Achauer, 1989. Teleseismic investigation of the East African rift, Kenya. J. Afr. Earth Sci., 8, 461-470.

Fuchs, K., Altherr, R., Müller, B. and Prodehl, C. (Editors), 1997. Structure and dynamic processes in the lithosphere of the Afro-Arabian rift system. Tectonophysics, 278, in press

Green, W.V., Achauer, U., and Meyer, R.P., 1991. A three-dimensional seismic image of the crust and upper mantle beneath the Kenya rift. Nature, 354: 199-203.

Green, W.V., and Meyer, R.P., 1992. Array observations of PKP phases across the Kenya rift: implications for structure and tectonics. In: Altherr, R. (Editor), The Afro-Arabian rift system. Tectonophysics, 204 (spec. sect.): 41-58.

Haug, G.H., and Strecker, M.R., 1995. Volcano-tectonic evolution of the Chyulu Hills and implications for the regional stress field in Kenya. Geology, 23: 165-168.

Scientific Technical Report STR 98/05
DOI: 10.2312/GFZ.b103-98055

Hay, D.E., Wendlandt, R.F. & Keller, G.R., 1995. The origin of Kenya rift plateau-type flood phonolites: Integrated petrologic and geophysical constraints on the evolution of the crust and upper mantle beneath the Kenya Rift. J. Geophys. Res., 100: 10,549-10,557.

KRISP Working Group, 1987. Structure of the Kenya rift from seismic refraction. Nature, 325: 239-242.

KRISP Working Party, 1991. Large-scale variation in lithospheric structure along and across the Kenya rift. Nature, 354: 223-227.

KRISP Working Group, 1995. A new look at the lithosphere underneath southern Kenya. EOS Trans. Am. Geophys. Union, 76: 73, 81-82.

Novak, O., 1997. Ph.D. Thesis, University College Dublin, Dublin, pp.

MOE, 1987. Geological map of Kenya with structural contours. Ministry of Energy of Kenya, scale 1:1,000,000.

Prodehl, C., Keller, G.R. and Khan, M.A. (Editors), 1994. Crustal and Upper Mantle Structure of the Kenya Rift. Tectonophysics, 236, 483 pp.

Titles of referenced publications in Prodehl et al. (1994):

Achauer, U., and the KRISP Working Group, 1994. A three-dimensional image of the upper-mantle structure beneath the central Kenya rift from teleseismic investigations.

Braile, L.W., Keller, G.R., Mooney, W.D., and Patel, J.P., 1994. Modelling the 2-D seismic velocity structure across the Kenya rift.

Gajewski, D., Schulte, A., and Riaroh , D., 1994. High-resolution investigation of the Lake Turkana crust - ray trace modelling.

Keller, G.R., Mechie, J., Braile, L.W., Mooney, W.D., and Prodehl, C., 1994a. Seismic structure of the uppermost mantle beneath the Kenya rift.

Keller, G.R., Prodehl, C., Mechie, J., Khan, M.A., Mooney, W.D., Achauer, U., Davis, P.M., Meyer, R.P., and Nyambok, I.O., 1994b. KRISP 90 in the framework of continental rifting.

Maguire, P.K.H., Swain, C.J., Masotti, R., and Khan, M.A., 1994. A crustal and uppermost mantle cross-sectional model of the Kenya rift derived from seismic and gravity data.

Mechie, J., Fuchs, K., and Altherr, R., 1994a. The relationship between seismic velocity, mineral composition and temperature and pressure in the upper mantle - with an application to the Kenya rift and its eastern flank.

Mechie, J., Keller, G.R., Prodehl, C., Gaciri, S., Braile, L.W., Mooney, W.D., Gajewski, D., and Sandmeier, K.-J., 1994b. Crustal structure beneath the Kenya rift from axial profile data.

Mooney, W.D., and Christensen, N.I., 1994. Composition of the crust beneath the Kenya rift.

Prodehl, C., Jacob, A.W.B., Thybo H., Dindi, E., and Stangl, R., 1994. Crustal structure on the northeastern flank of the Kenya rift.

Wheildon, J., Morgan,P., Williamson, K.H., Evans, T.R., and Swanberg, C.A., 1994. Heat flow in the Kenya rift zone.

Titles of referenced publications in Fuchs et al. (1997):

Birt, C.S., Maguire, P.K.H., Khan, M.A., Thybo, H. and Mechie, J., 1997. The influence of Pre-Existing Structures on the Evolution of the Kenya Rift Valley - Evidence from Seismic and Gravity Studies.

Byrne, G.F., Jacob, A.W.B., Mechie, J. and Dindi, E., 1997. Seismic structure of the upper mantle beneath the southern Kenya rift from wide-angle data.

Mechie, J., Prodehl, C., Keller, G.R., Khan, M.A., and Gaciri, S.J., 1997. A model for structure, composition and evolution of the Kenya rift.

Novak, O., Prodehl, C., Jacob, B., and Okoth, W., 1997a. Crustal structure of the Chyulu Hills, southeastern Kenya.

Novak, O., Ritter, J.R.R., Altherr, R., Byrne, G.F., Sobolev, S.V., Garasic, V., Volker, F., Kluge, C., Kaspar, T., and Fuchs, K., 1997b. An integrated model for the deep structure of the Chyulu Hills volcanic field, Kenya.

Prodehl, C., Ritter, J.R.R., Mechie, J., Keller, G.R., Khan, M.A., Jacob, B. Fuchs, K., Nyambok, I.O., Obel, J.D., and Riaroh, D., 1997. The KRISP 94 lithospheric investigation of southern Kenya - the experiments and their main results.

Ritter, J.R.R. and Kaspar, T., 1997. A tomography study of the Chyulu Hills, Kenya.

Simpson, F., Haak, V., Khan, M.A., and Sakkas, V., and Meju, M, 1997. The KRISP-94 magnetotelluric survey of early 1995: first results.

Scientific Technical Report STR 98/05
DOI: 10.2312/GFZ.b103-98055

CRITICAL REVIEW OF METHODOLOGIES OF SEISMIC HAZARD ASSESSMENT APPLIED IN MEDITERRANEAN COUNTRIES OF AFRICA AND THE NEAR EAST

D. Benouar

USTHB, Civil Engineering Institute, BP 32 EL-ALIA, Bab Ezzouar, Alger, Algeria
CRAAG, BP 63, Bouzareah, Alger, Algeria

1. INTRODUCTION

The main purpose of this work is to establish a uniform catalogue of all earthquakes reported in the Maghreb region, which satisfies the conditions of homogeneity, and to derive from this basic data set the general laws governing the space and time distribution of earthquake occurrences in the seismic source zones, and to evaluate the seismic hazard.

For the Maghreb region, earthquake hazard constitutes a constant threat to human life and property, sometimes causing major economic losses and disruption. The rapid urbanisation, development of critical engineering works such as dams, nuclear power plants, industrialisation of cities with modern types of buildings and the concentration of populations living or settling in hazardous areas are matters of growing concern, as they contribute to heavier loss of life and increase considerably the cost of disaster damage. The environment concerns and an increased official and public awareness of earthquake hazards have, in the last decade, led to a rapid rise of interest in seismicity and, seismic hazard and risk evaluations in the Maghreb countries. In order to assess the seismic hazard with a certain degree of reliability, an earthquake data of the region under survey which are as complete, homogeneous and accurate as possible are needed. For this purpose, and from the point of view of long term prediction and seismic hazard assessment, it is imperative that input data in the catalogues of the Maghreb countries be revised and homogenised.

2. DEFINITION OF THE REGION UNDER SURVEY

By « the region under survey » it will be meant hereafter the main country to investigate and adjacent regions. Actually, for the evaluation of seismic hazard in any country it is necessary to take into consideration also the seismic sources which lie outside its borders, but which can affect its territory. Thus, the investigation will cover also earthquakes the epicentral zones of which do not fall within the country of interest but which may affect its seismic hazard assessment.

The region under consideration, which is defined as the Maghreb, includes Algeria, Morocco, Tunisia and the south Iberian Peninsula, it is limited by the 20°N and 38°N and 10°W and 12 °E, and shown in Map 1. The term Maghreb is used here to illustrate the extent of the interest of the project, although Algeria constitutes the main concern. For the Maghreb region, as well as for other regions of the World, it is imperative to look beyond the boundaries of each country when evaluating seismic hazard. In fact, there are various reasons for investigating beyond the boundaries of each country and looking rather into the north African-south Iberian Peninsula region, designated as the Maghreb in this study, as a unit and for evaluating the

Scientific Technical Report STR 98/05
DOI: 10.2312/GFZ.b103-98055

final seismic hazard of the entire zone under similar criteria: (1) Similar geological process: the countries limiting the western part of the Mediterranean Sea and its adjacent continuation in the Atlantic Ocean have had, since hundred million years ago, the same tectonic process marked by a relative motion alternating between left and right lateral along the border of the African and Eurasian plates; (2) Similar present compressional state of stress: the actual state of stress in the whole zone is dominated by a compression with a principal axis along the NNW-SSE direction. (3) Similar historical development: the historical development of the countries in the region shows many common factors, such as cultural background, which lasted for several centuries and are still apparent today. Similarities in population settlements, building stock characteristics and socio-economic and demographic conditions, etc., are very important parameters in the whole process of seismicity studies in the zone under consideration. The selection of this area allows investigation of any earthquake, affecting although not occurring in a specific zone of the Maghreb, which may influence the seismic hazard assessment in any particular site of the region. The term Atlas is used here to define the block containing the Atlas mountains along the whole north Africa (Map 1.).

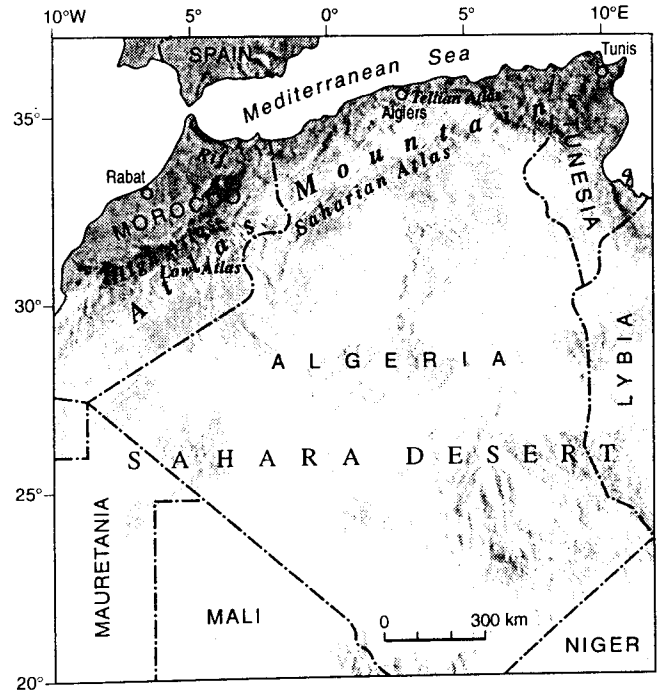

Map 1: Limits of the region under study

3. PERIOD OF CONSIDERATION

The period before 1900 is to be extended as back in time as far as the data allow. The problem of timing in this period, which is carried out by historical records, is usually expressed according to various calendars or time systems. The use of different calendars which are not directly convertible into those in use today is a constant hazard.

The period between 1900 and 1990 deals with the twentieth century which is characterised by a rapid development on instrumental seismology and by adequate seismological services

Scientific Technical Report STR 98/05
DOI: 10.2312/GFZ.b103-98055

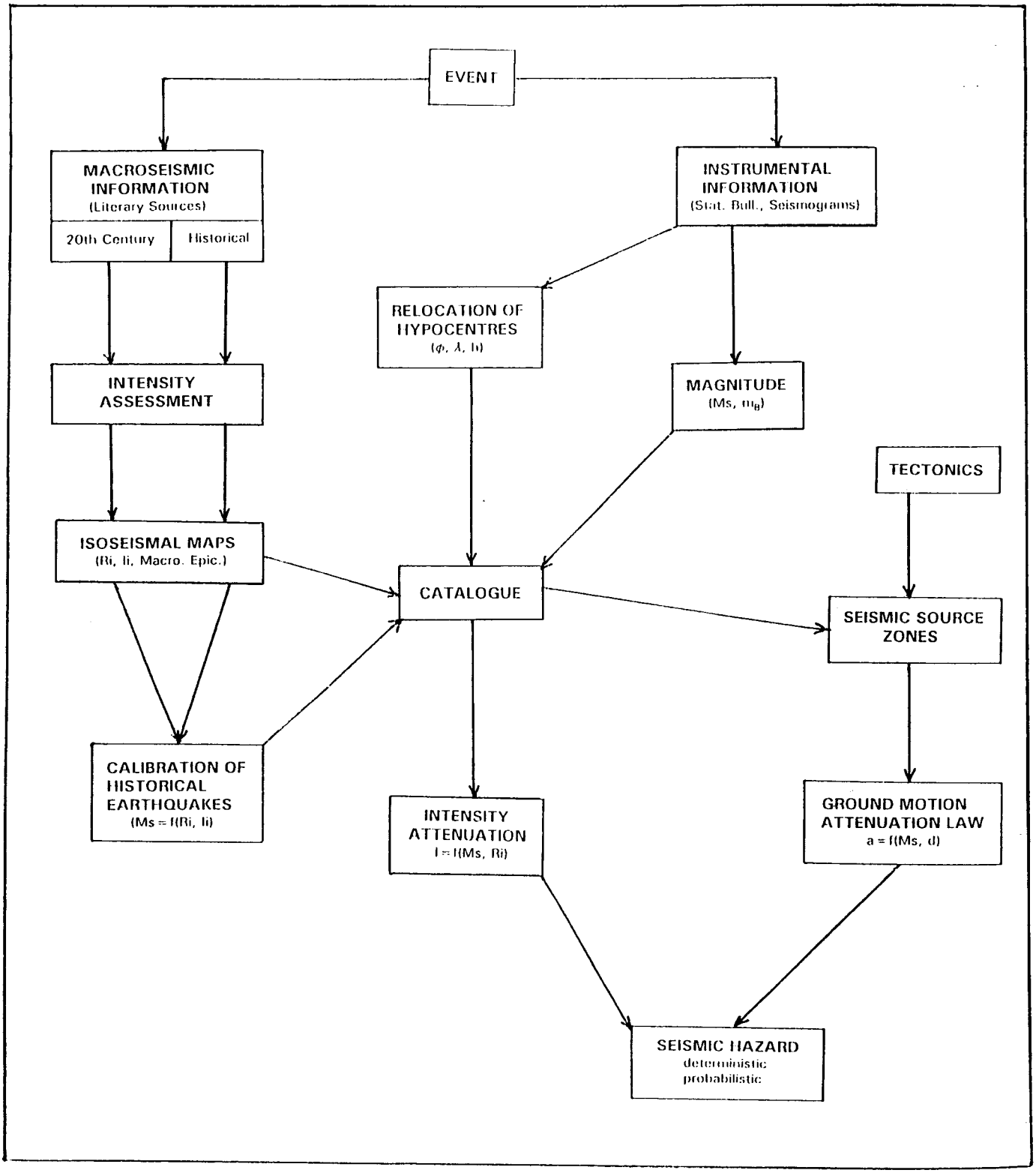

Fig. 1: Flow-chart of the general methodology of the re-evaluation of seismicity and assessment of seismic hazard

operating in and around countries of the Maghreb. It has been found that during this period of time, homogeneous data for earthquakes above a certain magnitude can be obtained for the entire region under survey. However, the overall detection capability was significantly reduced for long periods of time during the unstable years between 1914 and 1922 and again between 1940 and 1947 as a result of permanent or temporary suspension of some stations and services. This period had also been marked by the development of national seismographic stations in the Maghreb countries, where the number of operating stations increased from one station in 1917, to two in 1948, to four in 1957 and to nine in 1990 in Algeria. For Morocco, it increased from one station in 1937, to two in 1964, to four in 1968 and to fourteen in 1990. For Tunisia, from one station in 1937 to six in 1990.

4. GENERAL METHODOLOGY

This paragraph presents the methodology used to re-evaluate the seismicity of Algeria and adjacent regions, during the twentieth century. This required (1) the retrieval and revision of both macroseismic and instrumental information, (2) the development of a methodology for the assessment of seismicity, (3) the application of techniques of completing the homogenised available data, (4) the establishment of a homogeneous and complete earthquake catalogue for the region under survey, (5) the geographic distribution of the earthquakes in order to define the seismic source zones in the region, (6) the calibration of the Atlas block and Algerian earthquakes and (7) the derivation of intensity-attenuation relationships in the Atlas zone and Algeria. This work has allowed the assessment of seismic hazard in the Maghreb region, the Atlas block, Algeria and at eight major urban cities in Algeria.

The procedure which is used to re-evaluate the seismicity of Algeria and surrounding regions is given by the flow-chart in Figure 1. It is clear that for historical earthquakes (pre-instrumental events) and even for twentieth century earthquakes for which there are no instrumental data, but for which intensities and radii are available, their magnitudes are calculated from macroseismic data (using calibration relationships).

4.1. Instrumental Information

Earthquake instrumental recordings in and around the Maghreb region started late in the last century which were by today's standards very limited. The first instrument in north Africa was installed by 1917. Most of the seismographic stations covering the Maghreb countries were operating in southern Europe, thus all to the north, resulting in a narrow range of azimuthal distribution of stations around the epicentre and contributing to east-west positioning uncertainty. Stations such as those at Cairo (Egypt) and Ksara (Lebanon) give some additional east-west control. For a better understanding of the instrumental data in the

Scientific Technical Report STR 98/05
DOI: 10.2312/GFZ.b103-98055

Maghreb countries, it is important to know about the historical development of seismographic station network in and around the region under investigation. For this purpose a detailed study of the historical development of the seismographic station network in and around the Maghreb countries is presented in Benouar (1993).

4.1.1. Seismological bulletins

Monthly bulletins of various seismological stations and international organisations have been used along this study for checking the event itself, completing and/or determining missing characteristics of the event. The main seismological bulletins consulted in this study are those of the International Seismological Summary (ISS, 1913-1963), the International Seismological Centre (ISC, 1964-1982) and the National Earthquake Information System (NEIS, 1983-1990) ; they are summarised in Table 1. They may be used to re-evaluate hypocentral locations, origin time and exceptionally to determine source mechanism.

Table1: Main sources used in the compilation of the Maghreb countries earthquake catalogue

SOURCES	TIME COVERAGE 1900	1950	1990	(*)
+Ilee (1925)	11 — 24			I/M
+Sieberg (1932)	— 26			I/M
Ilee (1932)	11 — 31			I/M
+Rodriguez (1932-40)	— 33			I/M
+Roux (1934)	— 33			I/M
+Ilee (1950)	— 11			I/M
+Rothe (1950)	— 49			I/M
Debrach (1952)	32 — 51			I/M
Grandjean (1954)	40 — 50			I/M
Gutenberg et al.(1954)	04 — 52			I/M
+Ben Osman (1960)	— 55			I/M
+Ambraseys (1962)	— 58			I/M
+Munuera (1963)	— 60			I/M
+Rothe (1980)	— 77			I/M
Duverge (1969)	10 — 67			I/M
Karnik (1969)	01 — 55			I/M
Rothe (1969)	53 — 69			I
Benhallou et al.(1971)	51 — 70			I
+Roussel (1973)	— 70			I/M
Ben Sari (1978)	01 — 80			I/M
Hatzfeld (1978)	72 — 75			I
Frogneux (1980)	71 — 78			I
+Mezcua et al.(1983)	— 80			I/M
+Woodward-Clyde (1984)	— 81			I/M
+Benhallou (1985)	— 80			I/M
Cherkaoui (1988)	01 — 84			I/M
ISS (1913-63)	13 — 63			I
BCIS (1950-63)	50 — 63			I
ISC (1964-82)	64 — 82			I
NEIS(1983-90)	83 —			I

+: catalogue including earthquake data from pre-1900 period.
I: Instrumental catalogue
M: Macroseismic catalogue
I/M: Instrumental and Macroseismic catalogue

4.1.2. Seismograms

Seismograms are the fundamental observational records to study the various parameters of earthquakes and earth's interior. They are recorded at seismographic stations all over the world and are usually stored locally. The relocation of hypocentral location will be mostly accomplished using original seismograms as well as bulletin data if wave forms are missing.

4.2. Relocation of Hypocentres

The relocation of Hypocentres is a fundamental problem in seismological observations and research. In regions well covered with seismographic stations, it is believed that instrumental locations are more precise than macroseismic epicentres. However, this is not the case of the Maghreb countries where neither the quality of the data nor the azimuthal distribution and number of stations is suitable for an accurate epicentral location, particularly before 1960. Whenever, the instrumental data permits, it is imperative that earthquakes before 1960 be relocated, using the present location ISC procedure, to obtain a reliable geographical distribution of epicentres which may lead to a better seismotectonic interpretation so that hidden features be revealed. In this project, some Algerian earthquakes have been relocated to show the degree of accuracy of the British Association for the Advancement of Science (BAAS:1899-1917) and the International Seismological Summary (ISS: 1918-1963), presented in Table 2. It is found that the location error reaches values about an average of 16 km, still remains important since it represents about 2 to 3 times the radius of the meizoseismal area, in comparing relocated positions and macroseismic ones, where it is an average about 65 km between relocated and ISS epicentres which is a significant improvement.

Table 2: Comparison of original (ISS), relocated (ISC) and macroseismic epicentres for some Algerian earthquakes

Date	ISS (1)	relocated (2)	Macroseismic (3)	(1-2) (km)	(2-3) (km)
1910 Jun. 24	36.0°N 4.0°E	36.3°N 3.7°E	36.23°N 3.43°E	47	30
1922 Aug. 25	36.5°N 1.5°E	36.4°N 1.3°E	36.42°N 1.20°E	25	11
1924 Mar. 16	35.0°N 6.0°E	35.4°N 5.8°E	35.42°N 5.90°E	50	11
1924 Nov. 5	35.3°N 3.5°E	36.6°N 3.0°E	36.64°N 2.91°E	154	11
1928 Aug. 24	34.3°N 1.3°E	35.9°N 0.9°E	35.94°N 0.88°E	183	5
1934 Sep. 7	36.0°N 1.1°E	36.2°N 1.6°E	36.30°N 1.70°E	60	16
1937 Feb. 10	36.6°N 7.5°E	36.4°N 7.2°E	36.38°N 7.52°E	40	35
1943 Apr. 16	36.1°N 4.6°E	35.9°N 4.0°E	36.09°N 4.48°E	70	57
1946 Feb. 12	35.7°N 4.8°E	35.7°N 4.8°E	35.70°N 5.00°E	2	20
1959 Nov. 7	36.4°N 2.5°E	36.4°N 2.5°E	36.41°N 2.48°E	6	8

(1-2) Location error between ISS and relocated epicentres

(2-3) Location error between relocated and Macroseismic epicentres

Scientific Technical Report STR 98/05
DOI: 10.2312/GFZ.b103-98055

4.3. Determination of Magnitudes

The magnitude scale allows to classify earthquakes objectively and independently of local ground conditions and environment. The aim in this study is to determine anew or to revise and to unify existing magnitudes; it is to produce a file of reliable data which could reflect, as homogeneously and completely as possible, the seismicity of the region under study.
Body-wave magnitude m_b is calculated using Gutenberg and Richter formula:

$$m_b = \log(A/T)_{max} + Q(D,h) + S \qquad (1)$$

where $(A/T)_{max}$ is the maximum amplitude-period ratio in the wave classes (PV, PH, PPH and SH) and Q(D,h) is a calibrating function which depends on epicentral distance D, focal depth h and wave type.

Surface-wave magnitude M_S is calculated using the Prague formula given by:

$$M_S = \log(A/T)_{max} + 1.66\log(D) + 3.3 \qquad (2)$$

where $(A/T)_{max}$ is the maximum value of the ration of the ground displacement amplitude in microns, T is the corresponding period in seconds and D is the focal distance in degrees.

For the early years of this century, when Milne seismographs were operating, M_S is calculated using the calibrating Ambraseys and Melville formula given by:

$$M_S = \log(2A_t) + 1.25\log(D) + 4.06 \qquad (3)$$

where $(2A_t)$ is the double trace ground displacement amplitude (peak-to-peak) in millimetres and D is the focal distance in degrees.
For a variety of reasons, many earthquakes in the Maghreb region remain without surface-wave magnitudes or simply without any type of magnitude. To solve this problem, M_S are estimated when possible from semi-empirical relationships, derived in this work, between M_S and m_b or M_S and M_L or by using the number of stations that reported the event to the ISS or ISC. M_S for historical earthquakes, may also be estimated from the radius of perceptibility (r_3) which is defined as the mean epicentral distance of an area within which the shaking was felt with an intensity equal to or greater than III (MSK) by using a relationship between M_S and r_3, or by using the relationship between M_S and I_o. Table 3 shows all these relationships derived for the Maghreb region to estimate the equivalent surface-wave magnitude to complete and homogenise the earthquake catalogue.

Table 3: Relationships used to estimate equivalent surface-wave magnitude

$M_S = 0.47 + 0.86(m_b)$		
$M_S = 1.40 + 0.76(M_L)$		
$M_S = a + b(\log(NS))$		
$a = 3.69$	$b = 0.86$	for the period 1919 - 1930
$a = 2.77$	$b = 1.50$	for the period 1931 - 1949
$a = 2.59$	$b = 1.41$	for the period 1950 - 1963
$a = 1.35$	$b = 1.44$	for the period 1964 - 1990
$M_S = -0.04 + 2.56 \log(r_3)$		
$M_S = 1.36 + 0.47 (I_o)$		

4.4. Macroseismic information (literary sources)

Documentary source materials are essential for a retrospective reconstruction of the macroseismic field data of past earthquakes. However, it is clear that the results of any study based mainly on an inventory of data available from various sources is subject to the quality and completeness of the information. Thus, the earthquake data available today will determine the accuracy of this work and the significance of the conclusions drawn. Sources of information are found in local and European documentary materials, newspapers, administrative records, special studies, scientific reports, private diaries and various books. Such materials are found to be available in libraries and archive centres across the Maghreb countries and the Mediterranean European countries such as Spain, Italy and, particularly France.

4.4.1. Catalogues

Although catalogues or listings of earthquakes in the Maghreb region are available, they cover different time periods, incomplete at a given region, and are grossly deficient in several respects, particularly in magnitude, depth and location. Some of these catalogues are new, some incomplete for any given region or time period, some out-of-date or at second hand, some others are oversimplified and misleading. The most important and accessible catalogues and other publications containing information about earthquakes in the Maghreb region are listed in references in Benouar (1993, 1994). For the early times in Algeria, only one reliable earthquake catalogue for the province of Algiers has been found dating back to the fourteenth century (Ambraseys and Vogt, 1988). In Tunisia, the earthquake catalogue compiled by Rothé (1980) dates from 410 but does not contain enough information about the sources used. For Morocco, Ramdani et al. (1988) published a listing on historical earthquakes. Mezcua and Martinez (1983) compiled an earthquake catalogue for the Ibero-Maghreb region for the period 500 BC - 1980. For some events, especially those prior to 1960, epicentral locations, magnitudes and other pertinent earthquake characteristics are inaccurate or simply not available.

The first task was to make an inventory of all existing catalogues, covering the whole region or parts of it and period under investigation, shown in Table 1, and to compare and combine their entries. The number of estimates inventoried for the Maghreb reached 12,447 for 7,724 earthquakes reported of which 2,061 have surface-wave magnitude equal to or greater than 3.0. This methodology has allowed the estimation of the accuracy of the various catalogues and, in particular, the identification of the sources consulted in their compilations as well as the procedures used in the determination of the earthquake parameters. These catalogues, despite their incompleteness and inhomogeneity, constitute important references, in terms of both felt and recorded seismic activity, and should be considered as the starting point for the revision of the seismicity of the region under consideration. Additional macroseismic information, collected during this project, are used to answer ambiguities among previous catalogues.

4.4.2. Contemporary accounts

These documentary sources could be classified under two general headings which are: the official reports and the general public information (local and foreign newspapers). The first

type includes published and unpublished scientific works, official reports, administrative correspondence, private letters and military records. The second type of document, although written for public consumption, generally presents the effects of the event according to the geographical and political circumstances. Some of these reports contain detailed information, mentioning names of damaged cities, villages, douars and even buildings, houses and streets, behaviour of the population and animals, effects on nature, relief operations, photographs and interviews with people. This type of archives has played a major role in the revision of the knowledge of the seismicity of the Maghreb. From his accounts, generally, one is able to retrieve the historical context during which the earthquake occurred.

4.4.3. Other documentary sources

Another new source of information appearing during the twentieth century is unpublished technical reports related to the construction of large engineering structures. Most of these reports contain invaluable information accumulated in situ by engineers or geologists after an earthquake or in specific studies made to evaluate local seismic hazard.

4.5. Intensity assessment

Intensity assignment presents also one of the main reasons for inhomogeneity. Intensity value is usually attributed in terms of different scales, sometimes even unspecified. Newly retrieved data should be re-assessed according to one suitable scale and correlate the old data with it.

Intensities in this study are re-assessed with reference to the Medvedev-Sponheuer-Karnik - MSK- (1981) intensity scale, using standard criteria and macroseismic information retrieved from various sources mentioned earlier.

For a wise analytical study of past earthquakes, and better understanding of the information contained in the contemporary sources, one should take into account the political, socio-economic and demographic conditions, times of peace or war, cultural and religious backgrounds as well as the building stock characteristics of the period concerned. From these factors that may influence the macroseismic information, the buildings play a major role in the frame of intensity estimations. Because the building stock in the Maghreb countries, as that in the Middle East, has numerous variable characteristics such age, building materials and structural systems, an extensive investigation was carried out in order to reveal what type of constructions were exposed and what state they were in during the period of the concerned earthquake.

In this research, Intensities IX (MSK) and higher are assigned to the sites where destruction was complete (intensity depending of the nature of buildings) and there was great loss of life. Broadly, this means that within the area containing the fault-breaks associated with the earthquake, masonry and adobe structures were totally destroyed, many of which collapsed completely, causing casualties. Intensities VI to VIII (MSK) are consistent with a rigid interpretation of the MSK intensity scale. Lower intensities IV to V (MSK) were attributed solely on felt effects and on evidence of lack of damage to low-quality types of constructions. For the very low intensities II to III (MSK), negative reports were also taken into account; generally in the absence of very low intensity observations, intensity III^{+} (MSK) is assumed to be the boundary of the felt area.

4.6. Isoseismal maps

An intensity map, that is the distribution of observed intensity data points of an earthquake, is the best compromise between the qualitative nature of historical records and the quantitative needs of the users. An intensity map illustrates at a glance how good is the knowledge of the earthquake itself; the total number of intensity data points, their density and azimuthal coverage can be used for assessing quality factors.

From intensity data when enough, an isoseismal map is constructed and a macroseismic epicentre located for each studied earthquake. Radii (R_i) and intensity (I_i) are reported in the catalogue. The location of macroseismic epicentres is of great value, in terms of tectonic feature determinations, particularly during the first half of this century when instrumental data were still unreliable. As an output of the processing of isoseismal maps, attenuation relationships are derived.

4.7. Calibration of historical earthquakes

The calibration of historical earthquakes represents the magnitude-intensity relationship model for the region under survey. One of the results of the revision of the data set presented in Table 4 is the derivation of a relationship from which the surface-wave magnitude Ms can be estimated from macroseismic information. This can be achieved by fitting the pairs Ii and Ri with their corresponding surface-wave magnitude Ms.

From the isoseismal map using the pairs I_i and R_i with their corresponding surface-wave magnitude M_S, a relationship $M_S = f(R_i, I_i)$ can be easily derived. The result of the regression analysis of the data of the Atlas block which consist of 32 events and 124 (I_i, R_i) pairs is :

$$Msc = -2.36 + 0.596j^{-1}\Sigma(Ii) + 0.0016j^{-1}\Sigma(Ri) + 2.71j^{-1}\Sigma(\log(Ri)) \qquad (4)$$

where $j \geq 1$ is the number of isoseismals available for the determination of the mean value of the equivalent Msc of a particular earthquake, Ri is the focal distance that corresponds to the average epicentral radii (in km) of isoseismal Ii.

The derived relationship, which represents the equivalent surface-wave magnitude, M_{SC}, in terms of felt effects, could be used to assign magnitudes to historical and even to 20th century earthquakes which have no instrumental data but for which isoseismal radii and intensities are available.

4.8. Catalogue

All the previous section of this paragraph contribute to a homogeneous, complete and as accurate as possible catalogue. For most of the seismic hazard assessment methods, the earthquake catalogues represent the main, if not the only, seismological data sample and it is considered as the « maximum possible today » earthquake information in the region.

The structure of this catalogue should include: Serial number, Date: Year, Month and Day, Time of origin of the event: Hours, Minutes and Seconds in Universal Time (UT),

Scientific Technical Report STR 98/05
DOI: 10.2312/GFZ.b103-98055

GeoForschungsZentrum Potsdam

Table 4: Selected data of the seismic events used in the regression analysis for the determination of magnitude-intensity and intensity-attenuation relationships in the Atlas and Algeria.

Event no.	Date	Epicentre		Ms	mean radius (km) of isoseismals (MSK)								Site
					D_3	D_4	D_5	D_6	D_7	D_8	D_9	D_{10}	
1	1903 SEP. 23	36.00N	2.83E	5.60	-	-	-	34	-	-	-	-	Moudjebeur. AL
2	1908 AUG. 4	36.41N	6.61E	5.23	-	-	-	-	21	13	-	-	Constantine. AL
3	1922 AUG. 25	36.40N	1.30E	5.10	98	56	-	-	18	7	-	-	Tenes. AL
4	1924 MAR. 16	35.40N	5.80E	5.35	-	-	-	-	21	8	-	-	Mac-Mahon. AL
5	1924 NOV. 5	36.60N	3.00E	4.80	86	53	32	20	14	6	-	-	Ben Chabane. AL
6	1928 AUG. 24	35.90N	0.90E	5.40	113	-	42	-	-	9	-	-	Inkermann. AL
7	1934 SEP. 7	36.30N	1.70E	5.10	100	60	42	28	9	-	-	-	Carnot. AL
8	1936 OCT. 14	32.00N	6.20W	4.90	-	52	43	30	-	-	-	-	Tilougit. MO
9	1937 FEB. 10	36.40N	7.50E	5.20	103	48	52	35	22	10	-	-	Guelma. AL
10	1943 APR. 16	35.90N	4.00E	5.30	-	-	-	-	20	9	-	-	Mansoura. AL
11	1946 FEB. 12	35.70N	4.82E	5.55	125	-	51	-	28	13	-	-	Berhoum. AL
12	1947 AUG. 6	36.31N	6.68E	5.00	67	45	32	24	17	8	-	-	Constantine. AL
13	1949 FEB. 17	36.52N	5.24E	4.74	77	48	34	20	9	-	-	-	Kherrata. AL
14	1950 MAY. 10	32.70N	5.50W	5.30	165	119	71	26	-	-	-	-	Kerrouchen. MO
15	1954 SEP. 9	36.31N	1.47E	6.70	280	-	138	-	48	34	24	15	Orleansville. AL
16	1955 MAY. 8	36.53N	1.46E	4.75	95	57	-	22	11	-	-	-	Boucheral. AL
17	1955 JUN. 5	36.31N	1.50E	5.11	104	-	45	27	-	-	-	-	Beni Rached. AL
18	1959 NOV. 7	36.38N	2.55E	4.90	110	68	40	24	16	9	-	-	Bou Medfaa. AL
19	1959 DEC. 12	35.72N	0.56W	4.55	84	53	28	18	11	-	-	-	Oran. AL
20	1960 FEB. 21	36.04N	4.17E	5.12	80	-	40	-	22	13	-	-	Beni Ilman. AL
21	1960 FEB. 29	30.45N	9.62W	5.70	242	178	97	22	14	10	-	-	Agadir. MO
22	1960 DEC. 5	35.58N	6.54W	4.70	-	-	30	-	-	-	-	-	Atlantic Coast. MO
23	1964 NOV. 15	34.85N	5.47W	4.50	75	54	18	-	-	-	-	-	Ouezzane. MO
24	1965 JAN. 1	35.61N	4.40E	5.45	121	79	56	36	-	13	-	-	M'Sila. AL
25	1968 APR. 17	35.24N	3.73W	4.80	75	48	30	-	-	-	-	-	Boudinar. MO
26	1970 APR. 7	34.87N	3.90W	4.50	-	36	22	-	-	-	-	-	Adjir. MO
27	1977 JAN. 19	36.56N	8.43E	4.60	55	41	23	15	6	-	-	-	Ain Soltane. TU
28	1980 OCT. 10	36.16N	1.40E	7.45	425	257	203	130	70	44	21	-	El-Asnam. AL
29	1985 OCT. 27	36.34N	6.92E	5.70	125	95	60	38	20	9	-	-	Constantine. AL
30	1986 JAN. 28	31.98N	5.39W	4.90	127	66	21	-	-	-	-	-	Khenifra. MO
31	1988 APR. 9	31.44N	9.75W	4.20	46	31	22	-	-	-	-	-	Atlantic Coast. MO
32	1989 OCT. 29	36.78N	2.44E	5.68	153	112	56	43	19	9	-	-	Chenoua Mount. AL

AL: Algeria MO: Morocco TU: Tunisia

Instrumental epicentre: latitude and longitude with estimation of accuracy, Macroseismic epicentre: latitude and longitude, Focal depth, Magnitudes: M_S, mb, M_L with eventually estimation of accuracy, Seismic moment $\log(M_O)$, Epicentral intensity, intensities with corresponding radii (I_i, R_i), Number of reporting stations: NS, Site of maximum felt intensity, References, Remarks. Table 5 shows the global structure of the Maghreb earthquake catalogue.The catalogue should go back in time as far as possible in order to extend the seismic history of the region under consideration.

The distribution of the epicentral locations of all earthquakes reported in the Maghreb region during the period 1900-1990 is shown in Map 2.

4.9. Intensity Attenuation

Despite the increase in numbers of strong-motion accelerographs, intensity continues to be a necessary measure of the size of ground shaking in earthquakes. When evaluated consistently for a large (enough) number of seismic events to represent the seismic activity of a region, macroseismic intensity, as other semi-empirical measures may disclose regular isoseismal models which can be taken to represent a simple radiation pattern associated with a point source. This approach remains very practical for an efficient evaluation of the interaction between earthquakes and environment and, thus for for seismic hazard and risk.

One of the results of the revision of the data set presented in Table 4 is the derivation of a relationship from which the intensity at any site can be estimated. The Atlas data which consist of 123 (I_i, R_i) pairs corresponding to 32 events is used to derive an intensity-attenuation relationship $I = f(M_S, R_i)$ for the Atlas Block.

$$I = 5.16 + 1.48(Ms) - 0.000745(R) - 4.73\log R \qquad (5)$$

with $R = (D^2 + h^2)^{1/2}$.

This model is found to predict quite accurately the fall-off of intensity with distance. The rate at which intensity die-out with distance is of great importance for the assessment of the seismic intensities to be expected at a given site as a result of an earthquake. Intensity distribution may be used to estimate focal depth and together with other parameters, to estimate the size of an event.

4.10. Tectonics

It is generally agreed that earthquakes have occurred along faults. Thus, the first step is to identify and classify the tectonic and geological faults. The identification of the tectonic process plays an important role in modelling earthquake occurrences.

4.11. Seismic source zones

The definition of seismic source zones is based upon the interpretation of geological, geophysical and seismological information. The configurations of individual sources could be point source, line source, area source or volume source, depending upon the type of source chosen and the ability to define its geologic space.

Scientific Technical Report STR 98/05
DOI: 10.2312/GFZ.b103-98055

GeoForschungsZentrum Potsdam

Table 5: Shows the global structure of the Maghreb earthquake catalogue.

No	YR	MNH	DY	HR	MN	SC	LAT(N)	LON	DEP	Ms	OBS	Mb	M	ML	ISC	NS	RMK	SITE	REFERENCES
124	1954	SEP	9	1	4	37	36.31	1.47	-	6.7	-	7	6.8	-	10MK	211	*.M	BENI.RACHED..AL	BEN,NNA,ISS,CGS,MEZ
125	1954	SEP	9	1	49	48	36.00	1.50	-	5	-	-	6.7	-	10MK	-	A	LAMARTINE..AL	KAR,HHB,ROT
126	1954	SEP	9	2	49	48	36.00	1.50	-	6.2	-2	6.7	-	-	11MK	-	A	LAMARTINE..AL	MEZ
127	1954	SEP	9	2	52	24	36.28	1.47	-	4.7	-	-	-	-	6MK	-	A	WARNIER..AL	BCS,MEZ,CGS,KAR
128	1954	SEP	9	4	14	42	36.00	1.50	-	4.5	-	-	-	-	-	-	A	LAMARTINE..AL	KAR
129	1954	SEP	9	5	5	12	36.00	1.50	-	4.5	-	-	-	-	-	-	A	LAMARTINE..AL	KAR
130	1954	SEP	9	9	28	42	36.28	1.47	-	5.1	-	6	5.5	6	10MK	64	A	WARNIER..AL	BCS,ISS,CGS,KAR,HHB
131	1954	SEP	10	5	44	5	36.60	1.30	-	6.3	-	6	6	6.2	8MK	146	A	TENES..AL	BEN,ISS,MEZ,CGS,KAR
132	1954	SEP	16	6	7	3	36.00	1.50	-	4.5	-	-	-	-	-	-	A	LAMARTINE..AL	KAR
133	1954	SEP	16	22	18	17	36.28	1.47	-	4.8	-	4	-	-	7MK	-	A	WARNIER..AL	BCS,MEZ,KAR
134	1954	OCT	10	5	44	31	36.48	1.30	-	6	-3	-	-	6.2	9MK	-	A.M	MONTENOTTE..AL	BCS
135	1954	OCT	12	19	23	29	36.25	1.70	-	4.5	-	6	-	-	7MK	-	A	OUED.FODDA..AL	MEZ,BCS,KAR
136	1955	FEB	4	5	12	17	36.50	1.66	5	4.8	-	4.6	4.8	-	8MK	-	A	F.GARNIER..AL	MEZ,ALI,KAR,BCS,HHB
137	1955	MAY	8	21	38	59	36.53	1.46	5	4.8	-	4.6	4.9	-	7MK	48	*.M	BOUCHERAL..AL	BEN,ISS,MEZ,CGS,KAR
138	1955	JUN	5	14	56	13	36.31	1.50	5	5.1	-	4.7	5.8	-	8MK	98	*.M	BENI.RACHED..AL	BEN,ISS,KAR,MEZ,CGS
139	1955	DEC	24	13	7	9	36.40	1.70	5	4.8	-	-	4.8	-	6MK	11	A	CARNOT..AL	BCS,ROS,MEZ,KAR
140	1956	FEB	14	9	53	43	36.50	1.50	5	4.7	-	4.6	5.9	-	7MK	103	-	CAVAIGNAC..AL	ISS,MEZ,CGS,BCS,HHB
141	1956	AUG	16	2	9	40	36.91	-8.61	5	5	-1	5	-	-	6MK	50	-	SE..C.S.VICENTE	MEZ,ISS,ALI,CGS,BCS
142	1957	FEB	20	4	41	1	36.24	8.93	-	5.1	-	5.6	5.6	-	9MK	102	-	LA.MERJA..TU	ISS,MEZ,CGS,BCS
143	1957	JUN	28	21	23	49	36.10	1.38	15	4.8	-	4.4	5	-	7MK	53	-	SENDJAS..AL	NNA,ISS,MEZ,CGS,BCS
144	1957	JUL	15	9	36	30	36.00	-7.50	100	4.6	-2	4.8	-	-	4MK	-	-	W.GIBRALTAR	BCS,MEZ,CGS
145	1958	JAN	26	8	34	54	36.50	1.30	-	4.8	-	-	-	-	6MK	3	A	TENES..AL	MEZ,BCS
146	1958	MAY	17	5	25	33	31.81	11.28	-	5.1	-1	-	-	-	-	58	-	LYBIA	ISS,CGS,BCS
147	1959	MAY	24	13	19	32	36.12	4.51	5	4.8	-	-	-	4.5	8MK	-	-	MANSOURA..AL	ISS,MEZ,CGS,BCS,IMP
148	1959	AUG	23	22	21	29	35.73	-3.23	20	4.6	-2	4.8	5.5	-	6MK	-	-	ALBORAN	ISS,MEZ,MOS,CGS,BCS
149	1959	AUG	30	3	24	53	35.68	-3.14	-	4.6	-2	4.8	5.1	-	6MK	-	-	ALBORAN	ISS,MEZ,CGS,BCS
150	1959	SEP	30	16	57	30	35.00	-3.00	5	4.6	-2	4.8	4.8	-	2MK	-	-	ALBORAN	CGS,MEZ,BCS
151	1959	NOV	7	2	32	7	36.38	2.55	-	4.9	-	5.1	5.5	-	8MK	-	*	BOU.MEDFAA..AL	BEN,ISS,MOS,CGS,MEZ
152	1959	DEC	12	20	0	5	35.72	-0.56	-	4.5	-	4.3	-	-	7MK	-	-	ORAN..AL	BEN,ISS,MEZ,BCS
153	1960	FEB	21	8	13	33	36.04	4.17	5	5.1	-	5.5	5.8	5.9	8MK	131	*	BENI.ILMAN..AL	BEN,ISS,MOS,MEZ,CGS
154	1960	FEB	29	23	40	16	30.45	-9.62	-	5.7	-	6	6.2	-	10MK	-	*	AGADIR..MO	BEN,ISS,CGS,MOS,MEZ
155	1960	OCT	9	2	3	0	32.00	-5.20	-	4.6	-1	-	4.7	-	6MK	24	-	ASSOUL..MO	MEZ,BCS
156	1960	DEC	5	21	21	47	35.58	-6.54	34	4.7	-2	4.9	-	-	7MK	-	-	ATLANTIC	ISS,MEZ,CGS,BCS
157	1961	OCT	6	3	21	9	36.50	1.25	-	4.5	-1	3.9	-	-	6MK	20	-	N.ORLEANSVILLE..AL	ALI,MEZ,BCS
158	1961	DEC	2	12	40	14	36.35	8.39	35	5.2	-2	5.5	4.5	-	-	-	-	GHARDIMAOU..TU	ISS,MOS,MEZ,CGS
159	1962	FEB	11	13	32	46	37.30	-7.10	33	4.6	-2	4.8	-	-	-	-	F	B.VERA.ALMERIA.SP	MDD
160	1962	SEP	4	15	11	45	36.60	-8.75	5	4.5	-2	4.7	-	-	4MK	-	-	SE.CABO.SAN.VINCENT	MEZ,PAY
161	1962	NOV	5	8	29	50	37.50	-2.80	-	4.5	-2	4.7	-	-	-	-	-	GRANADA..SP	PAY
162	1963	MAR	31	14	58	4	35.26	-9.10	13	5.1	-2	5.4	5.2	-	3MK	-	-	ATLANTIC	MEZ,AVE,MDD,BCS
163	1963	JUN	20	19	47	34	35.55	-3.74	40	4.9	-2	5.1	4.3	-	4MK	-	-	ALBORAN	ISS,MDD,MEZ,BCS
164	1963	SEP	4	5	6	46	36.02	5.27	39	5.6	-	6.3	5.7	-	-	-	-	AIN.TAGROUT..AL	ISS,MOS,MEZ,BCS,HHB

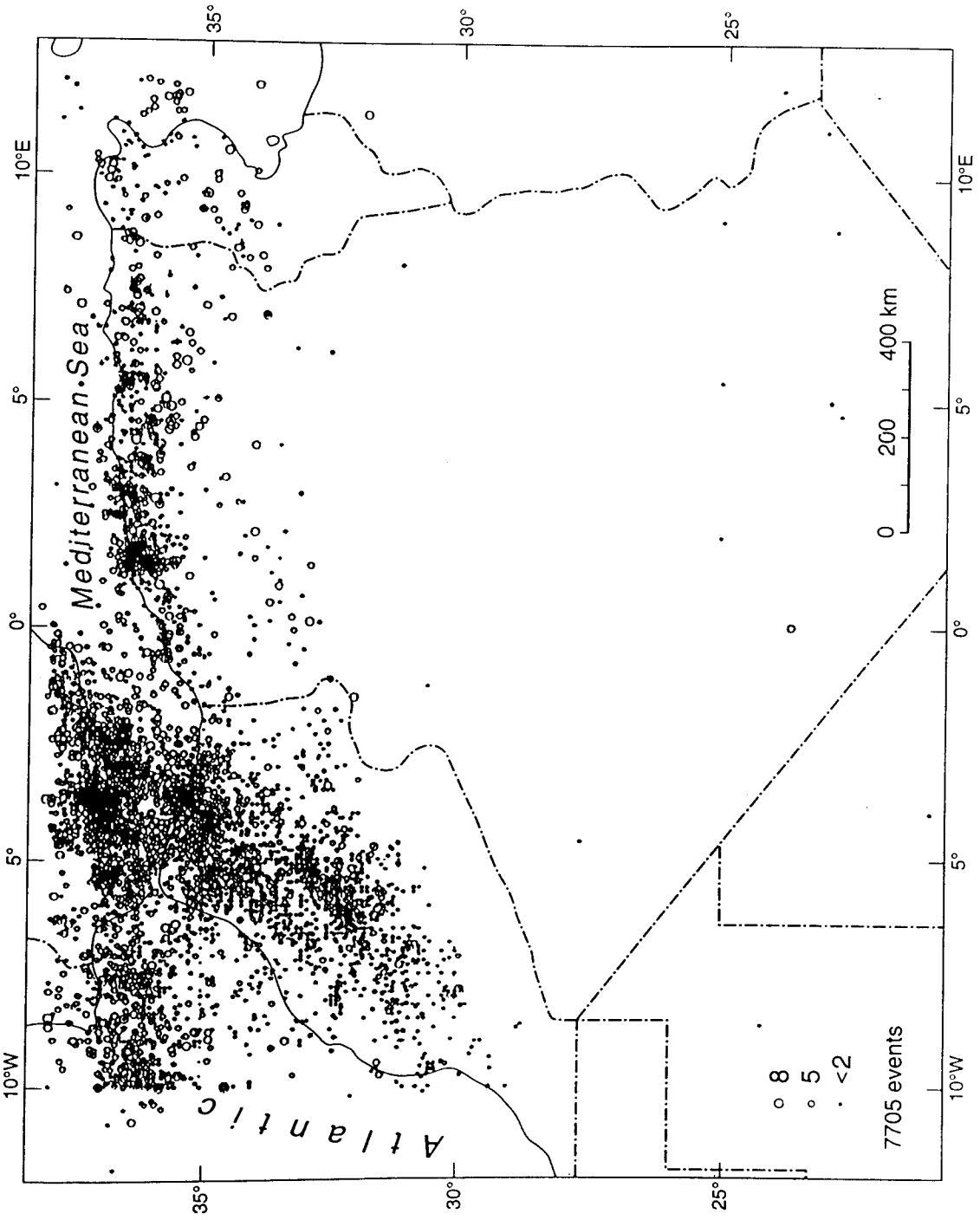

Map. 2: Illustrates the distribution of the epicentral locations of all earthquakes reported in the Maghreb region during the period 1900-1990

4.12. Strong ground motion attenuation law

The maximum ground motion to be expected in the site within a given time period constitutes a crucial problem in earthquake engineering. A large number of strong ground motion attenuation laws in terms of magnitude, distance, site geology, and in some cases other factors, using various models and data sets have been derived for various parts of the world.

Ground motion attenuation laws depend on the concerned region. Very often, due to the absence of strong motion data for the region under study, an attenuation law is selected from a region of similar tectonic process. The ground motion attenuation law is given in the form of $a = f(M_S, d_i)$. In this work, Ambraseys and Bommer (1991) PGA attenuation law derived for Europe, of which the data contain mainly Mediterranean data, including the Algerian on, is used. To show this, the available Algerian data has been fitted to the attenuation law of Ambraseys and Bommer (1991) which is presented in Fig. 2.

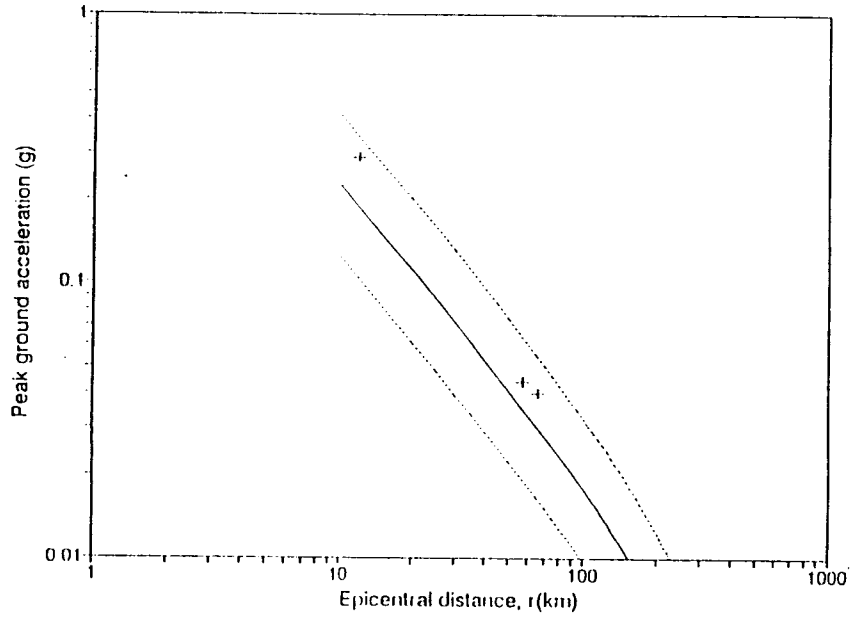

Fig. 2: Shows the relationships of the Algerian strong motion data (Chenoua earthquake, Ms = 5.70). The solid line shows the values predicted by the Ambraseys and Bommer attenuation law (1991), and the dashed lines are the 84-precentile values of the predicted.

4.13. Seismic hazard evaluation

In deterministic seismic hazard analyses, seismic sources are assigned maximum earthquakes which are assumed to occur at the location, within the source, closest to the site of interest. This approach uses the ground motion attenuation to estimate the ground motion parameter at a given site.

$$a = f(M_S, d_i) \qquad (6)$$

The probabilistic seismic hazard analysis allows the use continuous events and models. This consists of the evaluation of the probability of occurrence of an earthquake strong enough to cause damage within a given region or site and in a given time interval:

$$P(a< A/M_S, d_j) \qquad (7)$$

To illustrate this approach in this research work: (1) The seismic hazard is evaluated using Gumbel type I asymptotic distribution in the Maghreb region, Atlas zone and Algeria, shown in Fig. 3,4, 5 respectively.

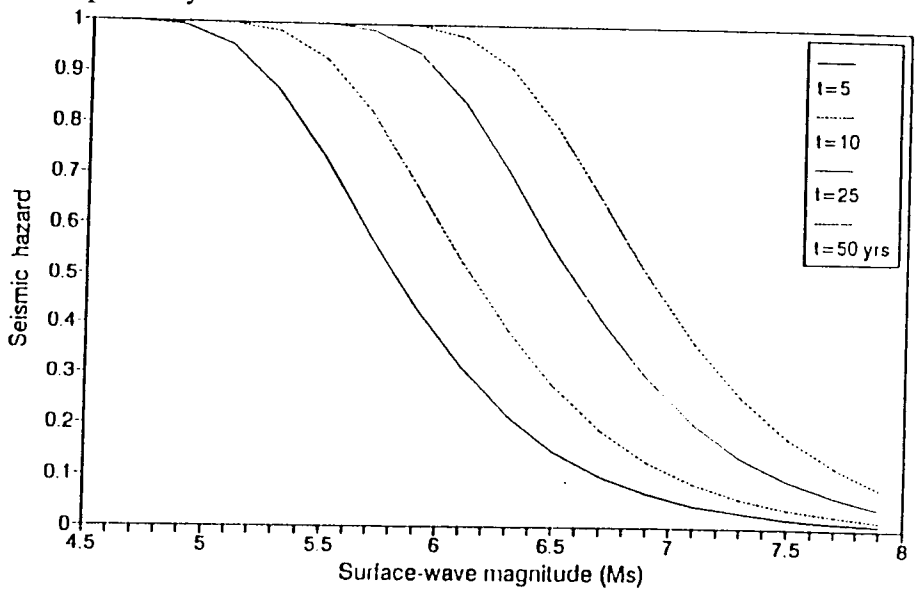

Fig. 3: Seismic hazard for a sample of earthquake magnitudes and return periods in the Maghreb region

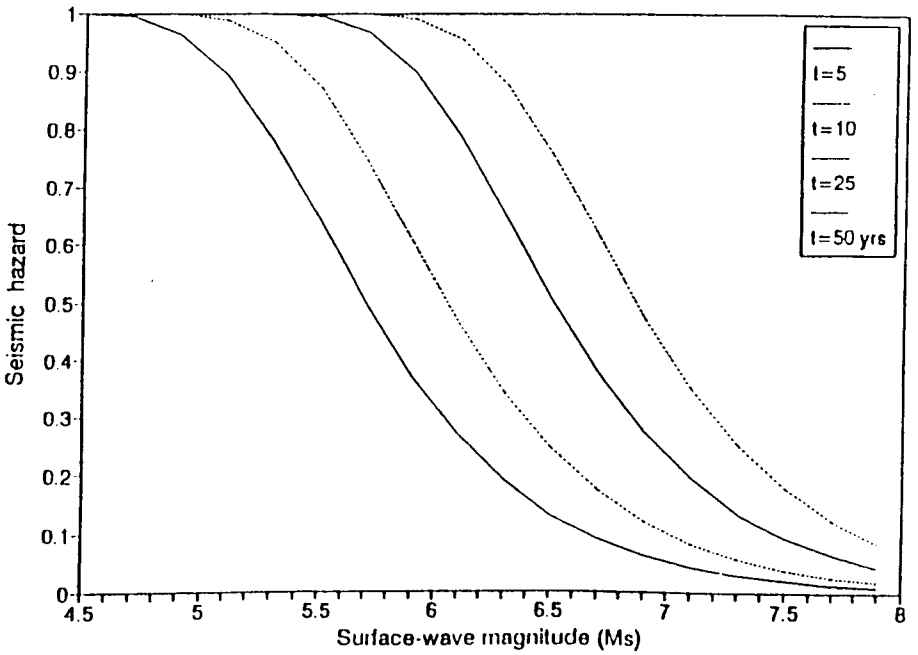

Fig. 4: Seismic hazard for a sample of earthquake magnitudes and return periods in the Atlas block

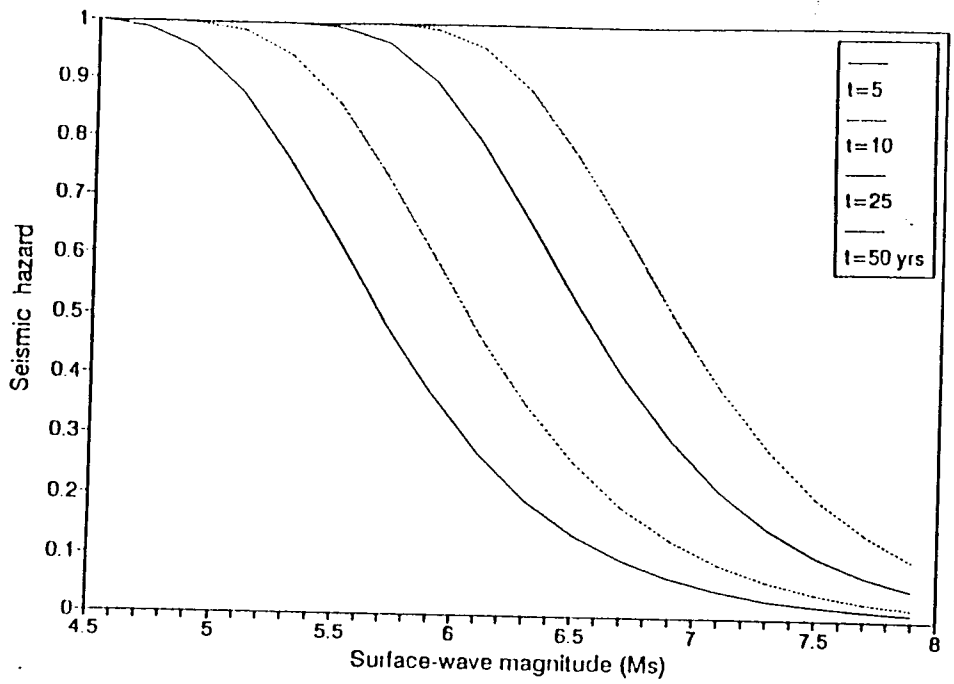

Fig. 5: Seismic hazard for a sample of earthquake magnitudes and return periods in Algeria

(2) The estimation of modal magnitude return periods using Gumbel type I distribution at major urban cities in Algeria is presented in Table 6.

Table 6: Results of seismic hazard analysis for most important cities in Algeria

City	Parameters		Magnitudes for		Mean return Period for Magnitudes (Years)			
	U	B	50-	100-yr RP	4.5	5.0	5.5	6.0
Alger	4.37	0.64	6.8	7.3	1.2	2.5	5.8	12.7
Oran	3.98	0.58	6.2	6.6	2.4	5.8	13.7	32.5
Annaba	4.24	0.51	6.2	6.6	1.6	4.4	11.8	31.5
Constantine	4.25	0.48	6.1	6.4	1.7	4.8	13.5	38.0
Chlef	4.18	0.64	6.7	7.2	1.6	3.6	7.8	17.1
Setif	4.27	0.53	6.3	6.7	1.5	4.0	10.2	26.2
Mascara	4.09	0.50	6.0	6.3	2.3	6.2	16.8	45.6
Msila	4.32	0.57	6.5	6.9	1.4	3.3	8.0	19.1

(3) The evaluation of seismic hazard at the site of Algiers based on peak ground motion acceleration using Cornell's method is terms of return period (Fig. 6) and in terms of probability of exceedance (Fig. 7).

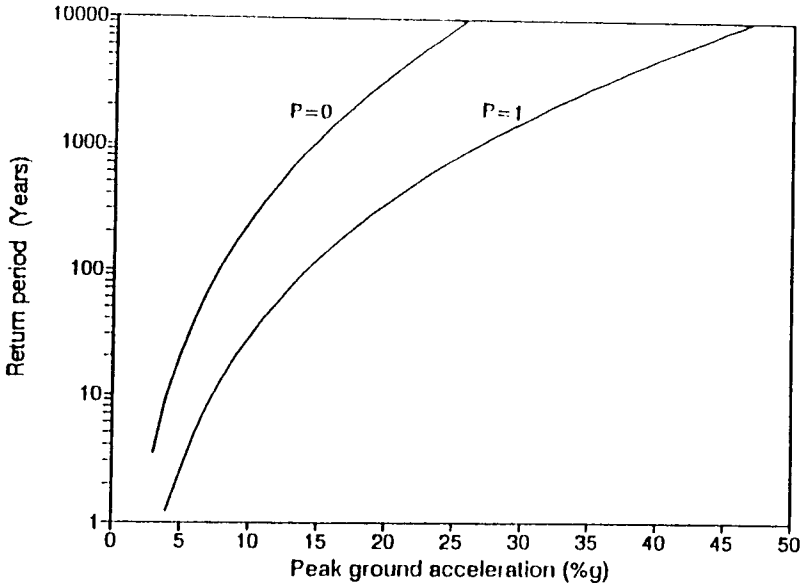

Fig. 6: Return period of different PGA at Algiers for P=0 and P=1

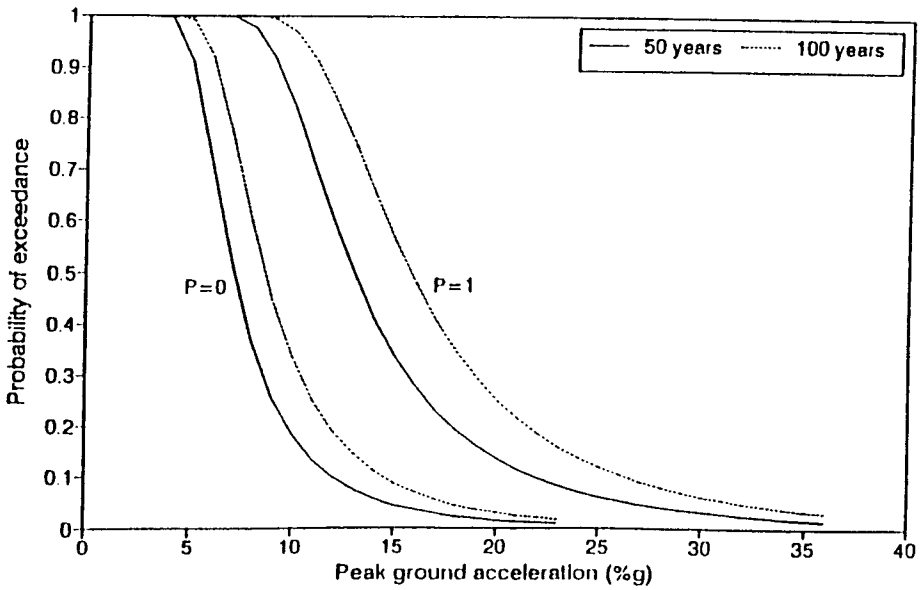

Fig. 7. Probability of exceedance of different PGA at Algiers for an economic life of 50 and100 years

Scientific Technical Report STR 98/05
DOI: 10.2312/GFZ.b103-98055

5. CONCLUSION

This methodology and the consistency process of the available data, particularly magnitude determinations and intensity estimations, ensure a high degree of homogeneity for the whole period under investigation. This has led to a homogeneous and complete earthquake catalogue for the Maghreb region which can be used in seismic hazard and risk evaluations in this region. The catalogue compiled in this work is stored as a computer file for ease of use. The last years have seen an important development of methods and computer routines for the assessment of seismic hazard. For most of these methods the catalogue presents the main, if not the only, seismological data set and it is assumed as the « maximum possible » information, upon which the evaluation of seismic hazard and risk relies to a large extent. However, this research clearly demonstrates that in order to investigate the pattern of current tectonic activity or to evaluate long term seismic hazard in a certain region, seismic information should go back in time as far as possible.

ACKNOWLEDGEMENT

I would like to thank Professor N.N. Ambraseys for the supervision and guidance of my research. This research has been achieved as part of the study of the seismicity of Algeria and adjacent regions, during the 20th Century, supported by an Arab-British Chamber Foundation grant.

REFERENCES

Ambraseys, N.N., (1962). The seismicity of Tunis. Ann. Di Geofisica. Vol. XV. No. 2-3, 233-244.

Ambraseys, N.N., (1971). Values of historical records of earthquakes. Nature, 232, 374-379.

Ambraseys, N.N. and Vogt, J., (1988° Material for the investigation of the seismicity of the region of Algiers. Europ. Earthq. Eng., 3, 16-29.

Ambraseys, N.N., and Bommer, J., (1991). The attenuation of ground accelerations in Europe. Earthq. Eng. & Struct. Dynamics, Vol. 20, 1179-1202.

Annuaires et Annales de l'Institut de Physique du Globe de Strasbourg (France) publiés entre 1920 et 1972 sous la direction de E. Rothé puis J.P. Rothé.

Archives du Gouvernement Général d'Algérie, 1900-onwards (unpublished).

Benhallou, H., (1985). Les catastrophes sismiques de la région d'Echéliff dans le contexte de la sismicité historique de l'Algérie. Thèse de Doctorat es-science, USTHB/IST, Alger.

Benouar, D., 1993. The seismicity of Algeria and adjacent regions, during the twentieth century. Ph.D. thesis, Imperial College of Science, Technology and Medicine, Civil Engineering Dpt., London.

Benouar, D., (1994). Materials for the investigation of the seismicity of Algeria and adjacent regions during the twentieth century. Special issue of Annali di Geofisica, No. 37, Vol. 4, July.

British Association for the Advancement of Science (BAAS). Seismological Investigation Reports 1899-1917, London, UK.

Cherkaoui Maknassi, M.T., (1991). Contribution à l'étude de l'aléa sismique au Maroc. Thèse de Doctorat, Université Joseph Fourier de Grenoble, France.

International Seismological Centre (ISC), Newbury, Berkshire, 164-onwards.

International Seismological Summary (ISS), Kew Observatory, Richmond, 1918-1963.

Meghraoui, M., (1988). Géologie des zones sismiques du Nord de l'Algérie (paléosismologie, tectonique active et synthèse sismotectonique). Thèse de Doctorat d'Etat, Université de Paris Sud, Centre d'Orsay, France.

Mezcua, J. And Martinez, J.M., (1983). Sismicidad del area Ibero Mogrebi. Seccion de Sismologia, Inst. Geogr. Nacional. Madrid.

Munuera, J.M., (1963). Datos basicos para un estudio de sismicidad en la area de la peninsula Iberic (seismic data). Memorias del Instituto Geographico y Catastral, tome XXXII, Madrid, pp.93.

Ramdani, M., Tadili, B., and El Mrabet, T., (1988). The present state of knowledge on historical seismicity of Morocco. Proc. Symp. on calibration of historical earthquakes in Europe and recent developments in intensity interpretation, European Seismological Commission, Sofia, 23-28 August 1988, pp. 258 - 279.

Rothé, J., (1980). Catalogue des séismes tunisiens. Manuscript (unpublished).

EARTHQUAKE HAZARD MAPS OF THE MAGHREB COUNTRIES (ALGERIA, MOROCCO, TUNISIA) AND THEIR SUITABILITY FOR PRACTICAL MEASURES OF RISK MITIGATION: A CASE STUDY

Djillali BENOUAR

USTHB, Civil Engineering Inst. BP 32, El-Alia, Bab Ezzouar, Alger, Algeria
CRAAG, BP 63, Bouzareah, Alger, Algeria

1. INTRODUCTION

All the Maghreb countries, as many other earthquake-prone regions in the world, are becoming more and more concerned with social and economic consequences of earthquake Hazard. The earthquake hazard constitutes a constant threat to human life and property, sometimes causing major economic losses and disruption. The rapid urbanisation, development of critical engineering facilities such nuclear power plants and dams, industrialisation of cities with modern types of buildings, the growing density of populations living in hazardous areas, new settlements in previously unoccupied zones and new vulnerable installations are of growing concern, as they contribute to heavier loss of human lives and increase greatly the costs of disaster damage. All these aspects force the governments and the population alike to consider better counter disaster strategies.

The first phase in reducing the risk of the society from earthquake hazard is an assessment of the hazard itself. Earthquake risk prevention, whether it includes seismic resistant design, land use management, city planning, earthquake insurance, public education or legislation, should be based on a sound knowledge of earthquake hazards, i.e. on the estimation of future seismic effects in a given region or at a given time interval, 50, 100 and 250 years. Although it is recognised that the occurrence of earthquakes is not inherently random, deterministic prediction of time, intensity and location of future event has not been possible until today. Therefore the best way to assess the seismic hazard at present is to treat the past earthquake data available by the probabilistic approach which is justified by the lack of the region seismotectonic map. The analysis of the seismic hazard presented in this work considers the contribution of all possible earthquakes and computes the probabilities that selected earthquake parameters will be exceeded within a particular exposure time.

One of the causes for concern in this part of the world was the absence of reliable data for the estimation of the appropriate earthquake design parameters. Until recently, although earthquake catalogues and or listings in the Maghreb countries were available, they cover different time periods, use different types of magnitudes, are incomplete at a given region and are grossly deficient in several respects, particularly in magnitude, depth and location. For some events, especially those prior to 1960, epicentral locations, magnitudes and other pertinent earthquake characteristics are inaccurate or simply not available (Benouar, 1993). Therefore, both seismic hazard analysis and construction of earthquake hazard maps were made difficult in the Maghreb countries by the lack of homogeneous, accurate and complete data. Due to these deficiencies, Benouar (1993) has compiled a newly revised earthquake catalogue for the Maghreb and the southern of Iberian peninsula. Today, after the re-evaluation of the seismicity of the Maghreb countries (Benouar, 1993), it becomes possible to produce earthquake hazard maps in this region of the world. An earthquake hazard map for engineering purposes is a map that specifies the levels of the maximum ground motions

Scientific Technical Report STR 98/05
DOI: 10.2312/GFZ.b103-98055

(forces) for earthquake-resistant design. Seismic hazard maps are practical tools, which serve engineering as well as land use and urban planning purposes, because they provide important guidance when it is not feasible to do the earthquake hazard assessment at particular sites. These maps give a good indication on the scope of expected strong shaking for moderate to large earthquakes.

For this purpose, this research work is intended to evaluate the seismic hazard and to establish earthquake hazard maps in the Maghreb countries -Algeria, Morocco, Tunisia-. The findings of this work should be an integral part of the whole process of economic and social development in the region considered. They constitute a fundamental means which guide officials at the national and regional levels in the formulation of development strategies in seismically active zones, land use management, revision and enforcement of appropriate building codes and policies of decision-making for protection measures against earthquake risk affecting the region under survey. It is of interest to mention that earthquake hazard maps produced for engineering purposes may be different in various ways depending both upon the expected use and the interests of the scientists constructing the maps. For instance, a seismic hazard map for a tall building should be different from one adequate for a low-height structure ; an earthquake hazard map for a nuclear power plant might well be very different from a typical housing unit.

2. DELIMITATION OF THE REGION UNDER STUDY

The region under study, which is called hereafter « Maghreb », includes Algeria, Morocco, Tunisia and south Iberian Peninsula, is limited by the latitudes 20°N and 38°N and the longitudes 10°W and 12°E, and is presented in Figure 1. As a matter of fact, there are various reasons for investigating beyond the geographical borders of each country and looking rather into the north African-south Iberian Peninsula region as a unit for a homogeneous final seismic hazard assessment in the whole zone under similar criteria : (1) Similar geological process: the countries limiting the western part of the Mediterranean Sea and its adjacent continuation in the Atlantic Ocean have had, since hundred million years ago, the same tectonic process marked by a relative motion alternating between left and right lateral along the border of the African and Eurasian tectonic plates. (2) Similar present compressional state of stress : the present state of stress in the entire region is dominated by a compression with a principal axis along the NNW-SSE direction. (3) Similar historical development: the historical development of the countries of the region shows numerous common factors, such as cultural background, which lasted for several centuries and are still apparent today. Similarities in population settlements, building stock characteristics and socio-economic and demographic conditions, etc., are very important parameters in the general process of seismic hazard analysis in the region under consideration. The choice of delimitation of this zone allows investigation of any earthquake, affecting although not necessarily occurring in a particular country, which may influence the seismic hazard assessment in any specific country of the region under survey. The term « Atlas » is used to define the block comprising the Atlas mountains along the whole north African coast (Fig. 1).

3. REGIONAL SETTING AND SEISMICITY

The Maghreb region has a relatively moderate seismicity despite the apparent tectonic activity of that thrust zone of 2,300 km long and 400 km wide. This region, which comprises the Atlas ranges bordering the western Mediterranean Sea and the southern Iberian peninsula, has

experienced, since hundred million years ago, a common tectonic evolution characterised by a relative motion between the left and right lateral along the African and Eurasian plates (Patriat et. al., 1982). Because the region under consideration is not in subduction zone, it my be considered that the corresponding deformations due to plate convergence are concentrated to a great extent in the North African mountains, which exhibit many characteristics of plate collision tectonics. Recent tectonics studies of McKenzie (1972), Dewey et al. (1973), Alvarez et al. (1974), Taponnier (1977), Groupe de Recherche Neotectonic de l'Arc de Gibraltar (1977), Hatzfeld (1978), Patriat et al. (1982) and Philip and Meghraoui (1983) have shown that the recent collision between the African and Eurasian plates mainly produced compressive tectonics where thrust and strike-slip deformations are associated. These deformations show a main NNW-SSE shortening direction.

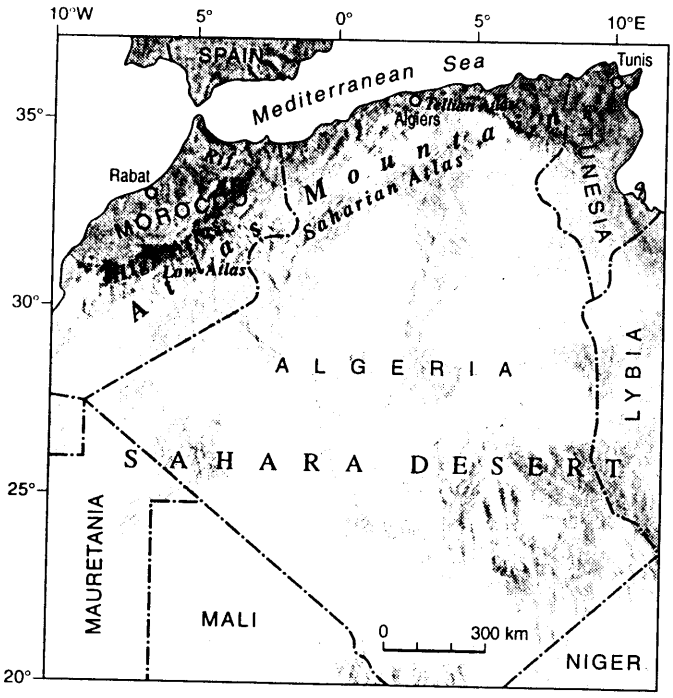

Fig. 1: Map showing the limits of the region under consideration

In examining the epicentral map (Fig. 2) of the Maghreb region and south Iberian Peninsula, it can clearly be seen that most of the seismic activity in North Africa is concentrated along the Atlas mountains. These mountains form a geological section distinct from the rest of the continent. The Atlas portion, which spreads out from Agadir in Southwest Morocco, crossing northern Algeria, to the gulf of Gabes in Tunisia, is delimited by the Mediterranean sea in the north and the east, the Sahara desert in the south and by the Atlantic Ocean in the west. The Atlas block is constituted by two main chains of mountains separated by High plateaux : the Tell Atlas and the Sahara Atlas. The Tell Atlas consists of a succession of mountain ranges, plateaux and valleys, with the principal direction of the relief roughly parallel to the north African coastline. The High Plateaux lie between the Tell Atlas and the Sahara Atlas with their basins of internal drainage (Chotts). These two main chains are relatively distinct in Algeria and Morocco, but they join each other progressively and merge into one another in Tunisia where, near Zaghouan, they are separated by a closely vertical fracture. In east central Algeria, in the Hodna region, these mountains are linked by branches. From the tectonic point of view, the Atlas block constitutes a section of the Alpine folding axis which extends from

the Pyrenées to the eastern and western Alps, to the Carpathians, to the Apennines, to the Beatic cordillera and spreads out westward to the Acores. This entire block was uplifted during the Alpine crustal movement which started by the end of the Jurassic period, recommenced in the Upper Cretaceous and continued into the middle and probably the Upper Miocene. There are no indications of folding during earlier periods with a predominant direction of movement from north to south (Ambraseys, 1962). As a matter of fact, this region is still subjected to a relatively slow rate of tectonic readjustments which cause light earthquake shocks along the Atlas ranges, except for the Orléansville 1954 and El-Asnam 1980 (Algeria) earthquakes which had been generated by a sudden release of potential energy. The existence of active faults in the zone is very much consistent with the orogenics of the region.

The analysis of the seismicity in the Maghreb as a whole suggests that the long return period of relatively strong earthquake shocks in Tunisia and in Southwest Morocco (Agadir, 1960) seems to be typical to the orogenics of the two ends of the Atlas mountain ranges. It appears that the crustal readjustments of the two extremes of the Atlas release their potential energy by numerous slight earthquake shocks which draw little attention. In Algeria, the central part of the Atlas, these readjustments are more sudden and sometimes destructive. Except the Orléansville 1954 and El-Asnam 1980 earthquakes, the seismicity of the Maghreb countries is light to moderate (Benouar, 1993).

For a better understanding of the seismicity of the Maghreb countries, additional seismic information and more field evidence of recent tectonics are needed (Benouar, 1993). A particular need is expressed for further extensive significant sample of seismicity, especially of the larger earthquakes, covering much more than the period of the twentieth century, which is minutely brief on the time-scale involved in tectonic processes. Thus, despite the significant amount of data for earthquakes in the twentieth century, it is imperative to retrieve macroseismic seismic information covering the period before 1900 and as far back in time as possible. The most reliable and accessible catalogues and other publications containing information about earthquakes in the Maghreb region are listed in references in Benouar (1993, 1994a). For the early times in Algeria, only one reliable earthquake catalogue for the province of Algiers has been found dating back to the fourteenth century (Ambraseys and Vogt, 1988; Benhallou et al., 1994). In Tunisia, the earthquake catalogue compiled by Rothé (1980) dates from 410, but does not contain enough information about the sources used. For Morocco, Ramdani et al. (1988) published a listing of historical seismicity. Cherkaoui (1988) published a catalogue of the seismicity of Morocco and surrounding areas for the period 1901-1984. Mezcua and Martinez (1983) compiled an earthquake catalogue for the Iberian-Maghreb region included between 30°N and 38°N and between 20°W and 12°E for period 500 BC-1980. However, much of the macroseismic data required for an investigation of the region under study has to be retrieved from many other documents, a process which requires co-ordinated research and extensive field work. By there history, the Maghreb countries and the Iberian Peninsula have always been an important zone for different civilisations and should therefore have a long and well-recorded history. Research into the cultural background would certainly reveal many other earthquakes. Work on this subject, a slow and painstaking process, is being carried out and is giving valuable information about the seismicity and tectonics of areas in the region.

Scientific Technical Report STR 98/05
DOI: 10.2312/GFZ.b103-98055

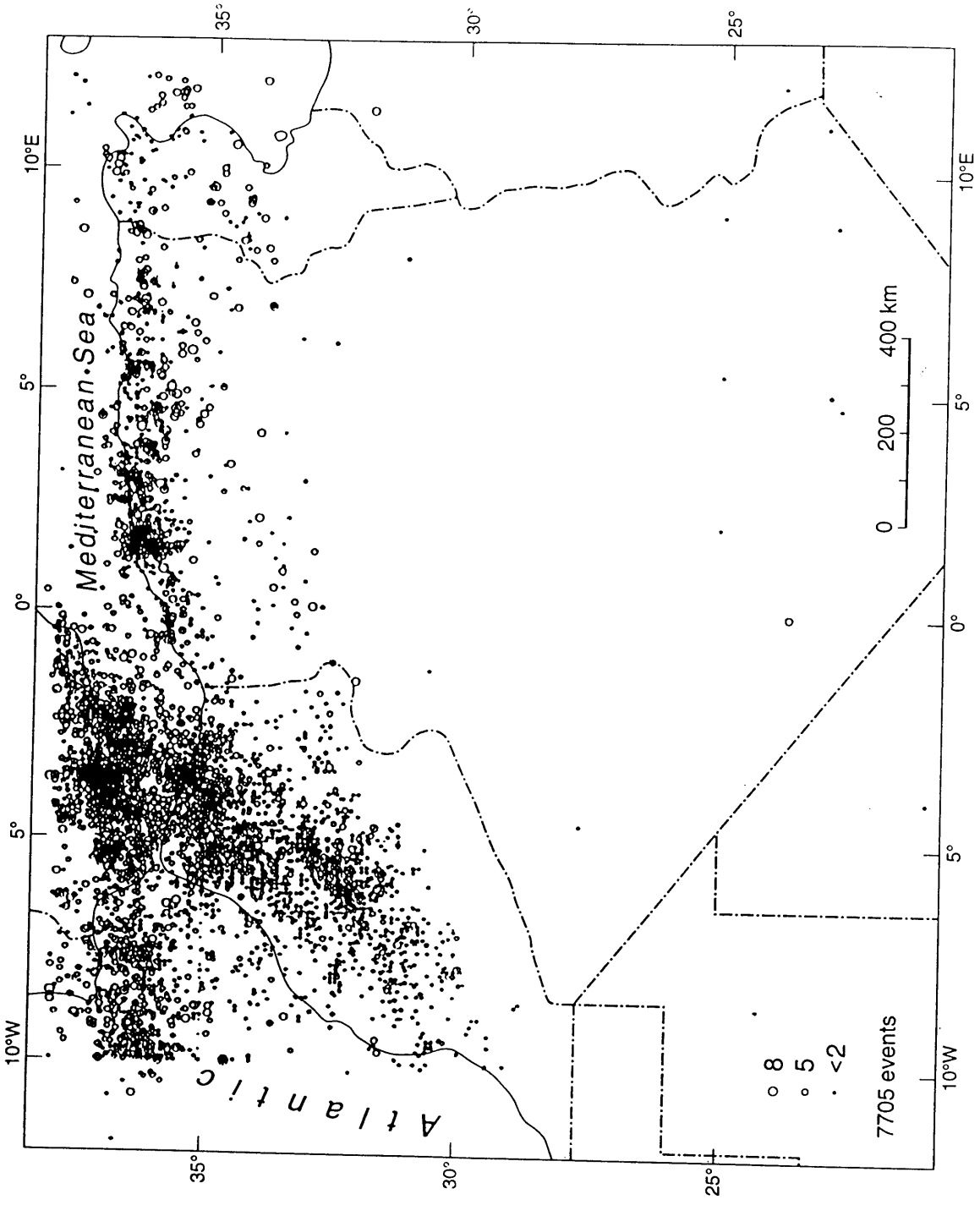

Fig. 2: Illustrates the distribution of the epicentral locations of all earthquakes reported in the Maghreb region during the period 1900-1990

4. SEISMIC HAZARD EVALUATION METHODLOGY

A great development of methods and computer routines for the assessment of seismic hazard has been achieved during the last years (a complete list of references would be out of the scope of this paper, but some of them can be found in Mayer-Rosa and Shenk, 1989; Mayer-Rosa et al., 1993). However, it is of interest to mention some of them as Lomnitz and Epstein (1966), Cornell (1968), Esteva (1968), Milne and Davenport (1969) who used the Poisson process and derived the general basis for the most complete analysis of the whole seismic hazard problem with the inclusion of the propagation mechanism of the ground motion. Shah and Vagliente (1972) employed the Markov model of earthquake prediction in seismic hazard analysis. For most of these methods the catalogue represents the principal, if not the only, earthquake data sample and it is assumed as the maximum possible information available today, upon which the assessment of seismic hazard relies to a great extent.

Earthquake hazard analysis in a given site is assessed in this research work using the well known Cornell's method as is achieved for the site of Algiers by Benouar (1996). A brief summary of the methodology is presented in the following section.

4.1. Summary of analysis method

The seismic hazard estimation in a given site depends upon the definition of the following four conditions :

1) *An earthquake source model.* This is based on geological evidence, geotectonic zone, historical seismicity, earthquake sources are identified and modelled as a line, area or dipping plane. In this study, annular source model is used.

(2) *A seismicity model.* The seismicity of each of the modelled sources is first settled from the earthquake catalogue of the region under investigation. The recurrence relationship correlating the size of the past seismic events with the frequency is derived. The seismicity model is usually taken as :

$$\log_{10}(N) = a - b(M) \qquad (1)$$

and must be normalised per unit area and per unit time. Where a and b are regression constants and N is the cumulative number of seismic events exceeding or being equal to a given magnitude M in a given region and within a certain period of time and M is the surface-wave magnitude. This model may also be written as :

$$\nu = N = f_m(M) \qquad (2)$$

where ν is the occurrence rate.

(3) *An attenuation model of ground motion information.* The attenuation model for ground motions is a very important parameter in the seismic hazard assessment. It defines the transfer of ground motions from the source to a particular site as a function of magnitude, distance and soil conditions. Here the peak ground acceleration is used to characterise the ground motion; the attenuation law is in the following form :

$$\log_{10}(y) = b_1 + b_2(M) - b_3\log_{10}(r) - b_4(r) \quad (3)$$

where $r^2 = d^2 + h^2$, r is the hypocentral distance (in km), d is the epicentral distance (in km), h is the focal depth (in km), M is the surface-wave magnitude and y is the peak ground acceleration (in g). In earthquake hazard analysis this expression is inverted and written as follows

$$M = f(y, r) \quad (4)$$

(4) A recurrence forecasting model. Numerous statistical models have been tested in various research papers; however, for practical reasons, earthquakes are considered to be random events, and the homogeneous Poisson process is employed, which implies assumptions of stability and independence over time. Since hazard analysis is defined as the occurrence of ground motions equal to or greater than a specified value, the probability of exceedance is used. For the Poisson distribution this may be expressed as

$$p = 1 - \exp(-\nu t) \quad (5)$$

where ν is the rate of occurrence of seismic events of particular peak magnitude over a given time t. By combining equations (2), (4) and (5) for each point source :

$$\nu = f_m(M), \qquad M = f_M(y,r), \qquad p_t = 1 - \exp(-f_M(m(y, r))t) \quad (6)$$

Cornell then introduced the assumption that the occurrence of earthquakes at different sources is independent and, since the sum of Poisson processes is itself also a Poisson process with a mean rate equal to the sum of each mean recurrence rate of each source, equation(6) for a point source can be integrated to obtain the probability of exceedance of a specified peak ground acceleration in any type of source (line, area, volume). For an annular source, and taking R equals r/h, Papastamatiou and Sarma (1988) show that the probability of exceedance may be expressed as

$$p_t = 1 - \exp(-CGy^{-\beta/b2}t), \quad (7)$$

where

$C = 10^{a}(b_1)^{\beta/b2}$,

$G = 2\Pi h(1-\delta)\int R^{-\delta}\exp(-\varnothing R)dR$,

$\beta = b\log(10)$,

$\delta = \beta b_3/b_2 - 1$,

$\varnothing = h\beta b_4/b_2$.

Where R_{max} is the maximum value of R determined by the minimum significant acceleration at the site and the upper bound magnitude M_{max}. Equation (7) gives the probability of

Scientific Technical Report STR 98/05
DOI: 10.2312/GFZ.b103-98055

exceedance of peak ground acceleration y over time t. The return period, the waiting time interval between two consecutive seismic events of same characteristics, is given by

$$T = 1/p_1(-CGy)^{fi/b2} \quad (8)$$

4.2. Earthquake source data sample

As in any quantitative analysis, the data sample for a seismic hazard assessment are critical. It is clear that the findings of any study based mainly on an inventory of data available from different sources is subject to the quality and completeness of the information. Thus, the earthquake data available today will determine the accuracy of this research work and the significance of the conclusions drawn. All newly compiled earthquake catalogues for the Maghreb region and the Southern Iberian-Peninsula are used which are Rothé (1980), Mezcua and Martinez (1983), Cherkaoui (1988), Ambraseys and Vogt (1988), Ramdani et al. (1988), Benouar (1994a), Benhallou (1985) and Benhallou et al. (1994). The detail of these catalogues is presented in Benouar (1994a). It is of interest to mention that the newly earthquake data catalogue compiled for the Maghreb countries and the southern Iberian Peninsula by Benouar (1993) during the period 1900-1990 has been revised. This catalogue is as homogeneous, complete and accurate as the available macroseismic and instrumental data allow. Although, most of the historical seismic events known (pre-1900) of the region under study have been included in this work but they are still not re-evaluated.

Because the Atlas region is in a collision, earthquakes occur generally at small depths. The focal depth remains the most uncertain of hypocentral co-ordinates; its estimation from teleseismic data alone is not accurate enough to determine small differences in focal depths of less than 10 km. In North Africa, more than 70 per cent of the earthquakes with focal depths available are found to have occurred at less that 15 km. Favier et al. (1981), Ouyed and Hatzfeld (1981) and Ouyed et al. (1982) have shown, in studying more than 500 aftershocks of the El-Asnam 1980 earthquake, that most of the shocks occurred at less than 15 km, among which more than 50 per cent were found at around 4 km. In Benouar (1993), in Algeria, 62 percent of the earthquakes with focal depths available are found to have occurred at less than 10 km and 95 per cent at less than 33 km. 16 events were reported at depths between 33 and 60 km; in Tunisia, among 186 earthquakes identified, only 56 have had depth values reported among which 26 events occurred at depths of less than 12 km, 44 at less than 33 km and 11 at depths between 35 and 79 km. This shows that the Maghreb region is characterised by shallow earthquakes with 70 per cent occurring at a depth less than 15 km. In this research work, a focal depth of 10 km is assumed for all earthquakes with unknown focal depths. Earthquakes with focal depths greater than or equal to 100 km are excluded from analysis.

Due to the lack of a seismotectonic map in the region under investigation, there is a significant uncertainty on long term rates of earthquakes and on individual faults based on trenching studies, etc.; the twentieth century seismicity in general provides the best available earthquake data for assessing seismic hazard in the Maghreb countries. This means that in evaluating seismic hazard at any site we can do no better today than to assume that future earthquakes will tend to take place very close to past seismic events, i.e. to estimate seismic hazard based on history of seismic occurrence around the site. The findings of Benouar (1996) suggests that small events be removed from seismic hazard analysis in the Maghreb countries (i.e. disregarding data with occurrence rates greater than 1.0 per year). Then, the evaluation of earthquake hazard at a site is carried only if the number of earthquakes in the area considered

Scientific Technical Report STR 98/05
DOI: 10.2312/GFZ.b103-98055

(200 km radius around a given site) is larger than 10 and the surface-wave magnitude is equal to or greater than 4.0.

4.3. Attenuation model for peak ground acceleration

The quantitative evaluation of seismic hazard at any particular site within a region requires an attenuation law for the Peak Ground Acceleration (PGA). The maximum ground motion to be expected in the site within given time period constitutes a crucial problem in earthquake engineering. For the Maghreb zone , as in many other parts of the world, no PGA attenuation law has been derived, due principally to the shortage of strong motion data. However, to evaluate the seismic hazard in this region, an attenuation law has to be adopted from the literature. A large number of attenuation relationships, predicting strong ground motions in terms of magnitudes, distance, site geology, and in some cases other parameters, using various models and data sets have been derived for different parts of the world. Reviews of these laws are made in Idriss (1978), Boore and Joyner (1982), campbell (1985) and Joyner and Boore (1988). Examples include the attenuation law derived by Ambraseys (1995) for Europe and Middle East including North Africa, which includes strong ground motion data from Algeria, for which the horizontal and the vertical component are shown respectively in equations (9) and (10) which are used in this work:

Mean Ambraseys (1995) PGA attenuation laws for Europe

(a) Horizontal acceleration

$$\log_{10}(y_h) = -1.43 + 0.245(M) - 0.0010(r) - 0.786\log_{10}(r) \qquad (9)$$

with $r^2 = d^2 + h^2$

(b) Vertical acceleration

$$\log_{10}(y_v) = -1.72 + 0.243(M) - 0.00174(r) - 0.750\log_{10}(r) \qquad (10)$$

with $r^2 = d^2 + h^2$

where y_h and y_v are respectively the horizontal and vertical PGA (in g), r, d, h and M are the same as defined above.

4.4. Attenuation of acceleration response spectrum

The response spectrum is the best representation of ground motion because it gives the possibility to take into account the natural period of the structure. It constitutes the basis of most seismic resistant design and defines the relation between the period of the structure considered and the lateral forces. The response spectrum is of great importance for engineering purposes since it represents the maximum response, to the given ground motion, of a sample of single-degree-of-freedom models of structures. Also, the spectral attenuation of ground motion allows to assess a structure's natural period-dependent seismic hazard at any site and thus period-dependent seismic zoning.

Several authors have derived spectral attenuation laws which are reviewed in Joyner and Boore (1988). Molas and Yamazaki (1995) developed two different models to predict the acceleration of response spectra based on magnitude, distance and site conditions. Examples used in this work are Molas and Yamazaki (1995) spectral attenuation law, which are given in respect to the structure natural undamped period and a 5 per cent damping ratio, are used to produce an earthquake hazard maps based on the structure's period in the Maghreb countries.

4.5. Attenuation of intensity law

In spite of the increase in numbers of strong motion accelerographs, intensity continues to be a necessary measure of the size of ground shaking in earthquakes. When evaluated with a consistent process for a large enough number of earthquakes, to assess the seismicity of a given region, the intensity may reveal regular isoseismal models which can be taken as a simple radiation pattern associated with a point source. This approach is very practical for an efficient evaluation of the interaction between environment and earthquakes, and therefore seismic hazard and risk. For most of developing countries, the intensity may constitute a better correlation with damage than peak ground acceleration alone. Earthquake hazard studies based on intensity have been made by various scientists (e.g. Cornell, 1968). Benouar (1994a) derived an intensity-attenuation model for the Atlas block. This attenuation relationship in terms of MSK intensity and distance in the Atlas block is developed by using an earthquake data sample which consists of 123 (Ii, Di) pairs corresponding to 32 seismic events, where Ii is the intensity (MSK) corresponding to the mean radius Di. The Benouar (1994a) mean intensity attenuation expression for the Atlas block is :

$$I = 5.16 + 1.48(M) - 0.00074(r) - 4.73\log_{10}(r) \qquad (11)$$

where $r^2 = d^2 + (4.82)^2$, I is the intensity (MSK), M is the surface-wave magnitude, r is the focal distance (km) and D is the epicentral distance (km).

This expression is used to construct earthquake zoning maps based on intensity in the Maghreb countries.

5. RESULTS OF SEISMIC HAZARD MAPPING

The first step in reducing the risk in the community from earthquake hazard is an evaluation of the hazard itself. Seismic hazard mapping constitutes a fundamental mean towards mitigating the seismic risk. A seismic hazard map for engineering use is a map that specifies the level of expected loads for earthquake-resistant design. It is the basis for introducing low-cost earthquake-resistant building design and construction as well as for land use planning and siting new critical engineering facilities such as nuclear power plants and dams. They are a permanent working document, provisional judgements on future seismic activity.

5.1. Methodology

The evaluation of seismic hazard within a given zone consists of subdividing it into a large enough number of grids of which the intersections represent the sites where the selected seismic hazard parameters (e.g. PGA, Intensity, Return Period, etc.) are evaluated. Then contour lines or areas are drawn, linking all different sites with equal seismic hazard. The contour lines map is known as an earthquake hazard map for the zone under investigation.

Scientific Technical Report STR 98/05
DOI: 10.2312/GFZ.b103-98055

The Maghreb region, as defined in Figure 1, has been first divided into ninety-nine grids having sides of two degrees. These grids have been subdivided in their turn into 441 grids with sides of 0.1 degree which constitute 46,659 grid points and for which earthquake hazard has been evaluated using Cornell's method (1968). This shows that seismic hazard has been estimated in about every 10 km distance which could illustrate the trend of seismic hazard with an appreciable degree of reliability.

5.2. Seismic hazard maps

Seismic hazard Analysis in the Maghreb is assessed in terms of (1) absolute peak ground acceleration, (2) expected peak ground horizontal and vertical acceleration for a 10 per cent probability of exceedance (i.e. 90 per cent probability that the specific parameter will not be exceeded, (3) intensity (MSK) all these for an economic lifetime of 50, 100 and 250 years, (4) return period in years for PGA $\geq$ 100 cm/s^2 (0.10g) which is considered as an important acceleration in engineering practice, and (5) expected structure's period-dependent spectral absolute amplitudes (in gals) for a 10 per cent probability of exceedance . To illustrate the seismic hazard in the Maghreb region only the following maps are presented.

Fig. 3 shows the geographical distribution of the absolute peak ground acceleration using Ambraseys horizontal-PGA attenuation law for T = 100 year return- period.

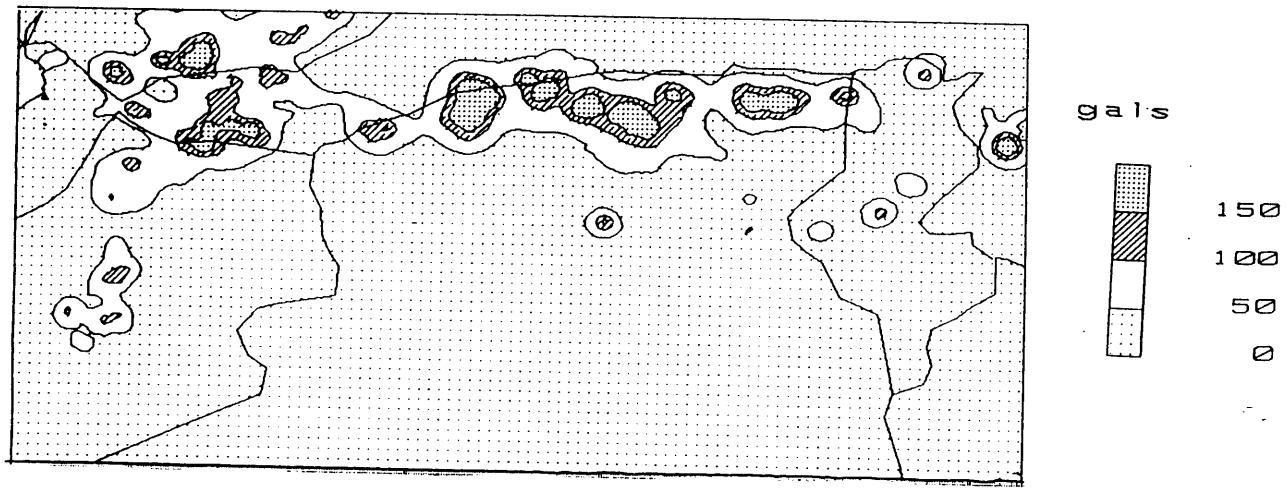

Fig. 3: 100-year absolute peak ground acceleration (in gals) using Ambraseys (1995) horizontal PGA attenuation law

The next Figures. 4 and 5 show the geographical distribution of expected peak ground acceleration for a 10 per cent probability of exceedance in an economic lifetime of T = 100 years using Ambraseys (1995) horizontal and vertical PGA attenuation laws, respectively while Figure 6 depicts the geographical distribution of absolute intensity, according to the MSK scale, for an economic lifetime of T = 100 years using Benouar's (1994b) intensity-attenuation law. Fig. 7 presents then the related geographical distribution of seismic hazard in terms of return period in years for PGA $\geq$ 100 cm/s^2 using Ambraseys (1995) horizontal-PGA attenuation law.

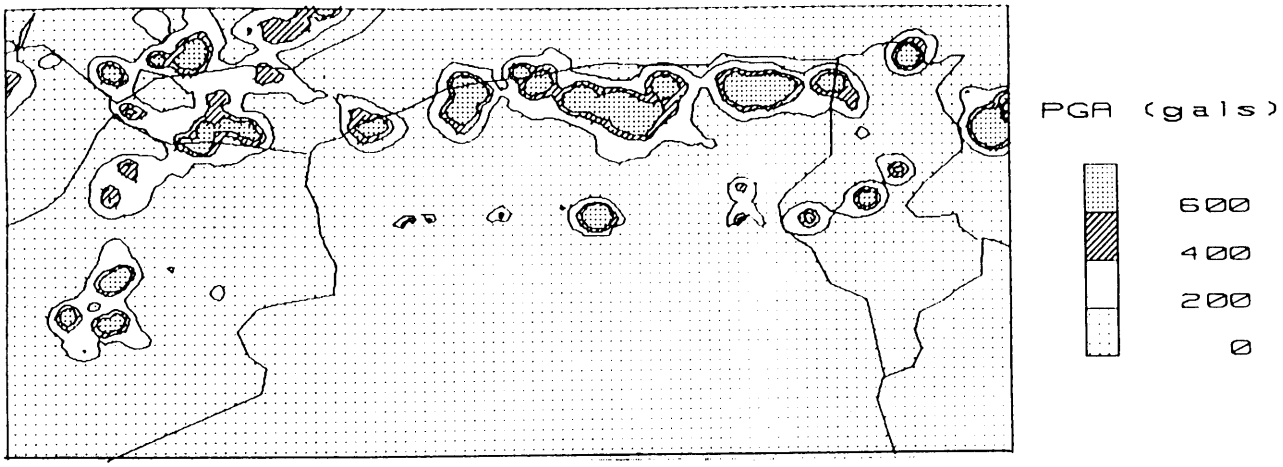

Fig. 4: Expected peak ground acceleration (in gals) for a 10 per cent probability of exceedance in an economic lifetime of T = 100 years using Ambraseys (1995) horizontal-PGA attenuation law.

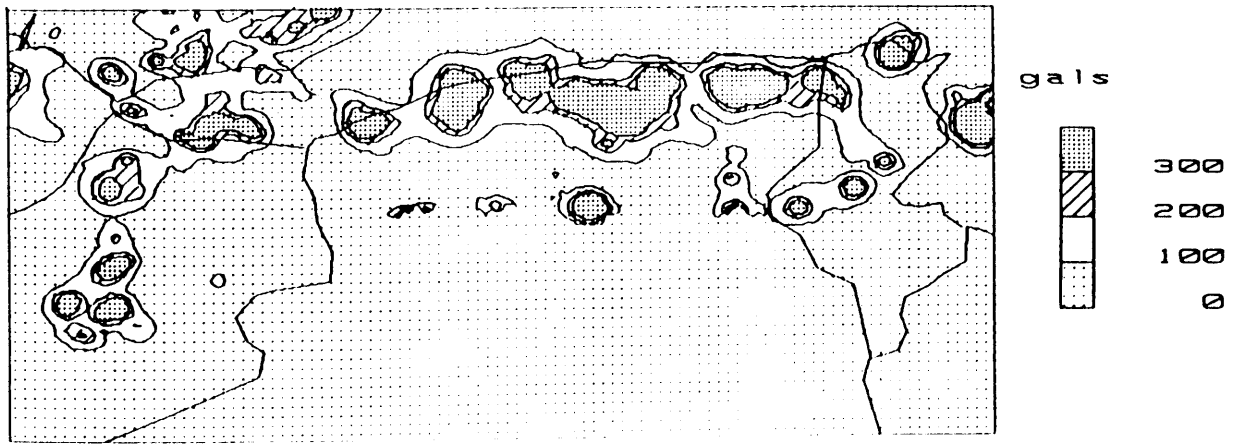

Fig. 5: Expected peak ground acceleration (in gals) for a 10 per cent probability of exceedance in an economic lifetime of T = 100 years using Ambraseys (1995) vertical-PGA attenuation law

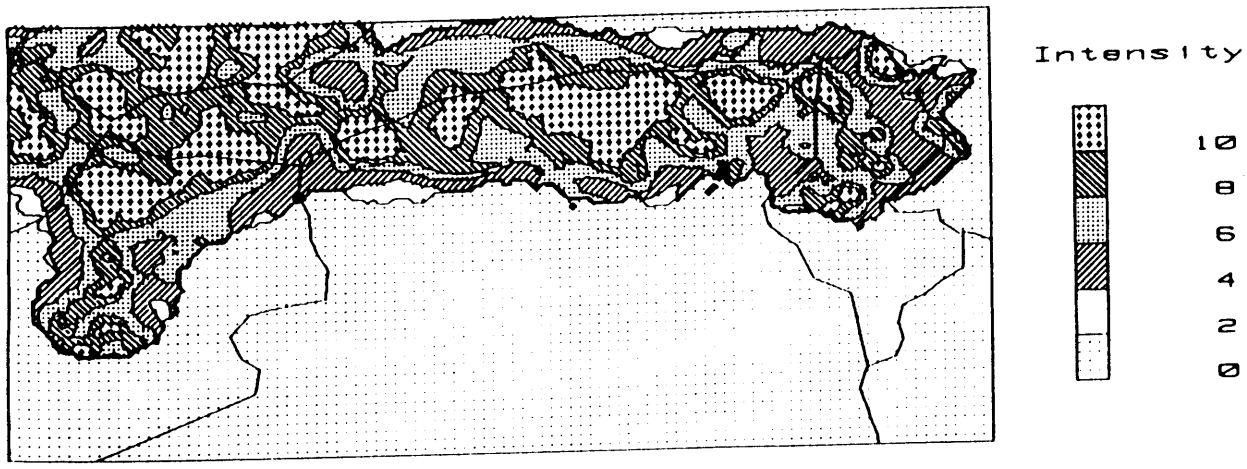

Fig. 6: Geographical distribution of absolute intensity (MSK) for an economic lifetime of T = 100 years using Benouar´s (1994b) intensity-attenuation law.

Scientific Technical Report STR 98/05
DOI: 10.2312/GFZ.b103-98055

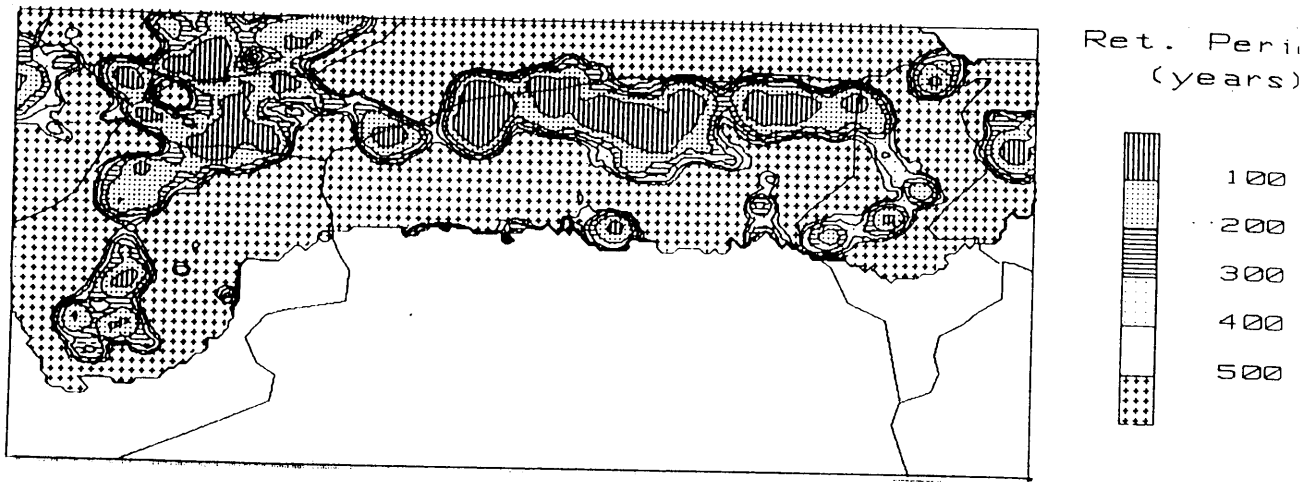

Fig. 7: Geographical distribution of seismic hazard in terms of return period in years for PGA ≥ 100 cm/s^2 using Ambraseys (1995) horizontal-PGA attenuation law.

The following three Figures. 8 a - c show the expected absolute PGA spectral amplitudes (in gals) for the typical eigenperiods of structures in this region, i.e. for periods of (a) T = 0.1 s, (b) T = 0.3 s and (c) T = 1 s using Molas and Yamazaki (1995) spectral attenuation law. These maps reveal a high seismic hazard for such types of structures in central eastern Algeria.

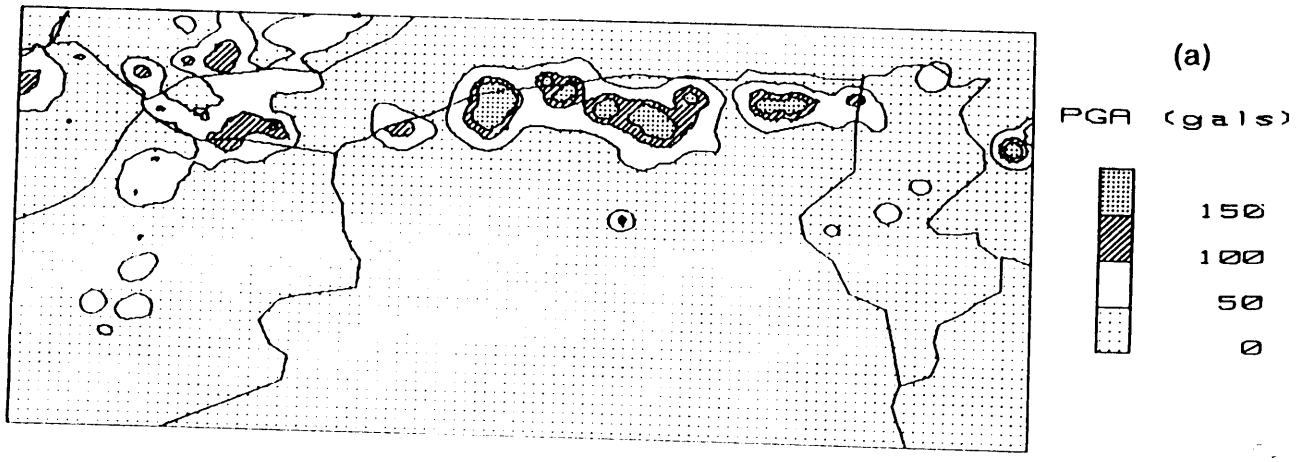

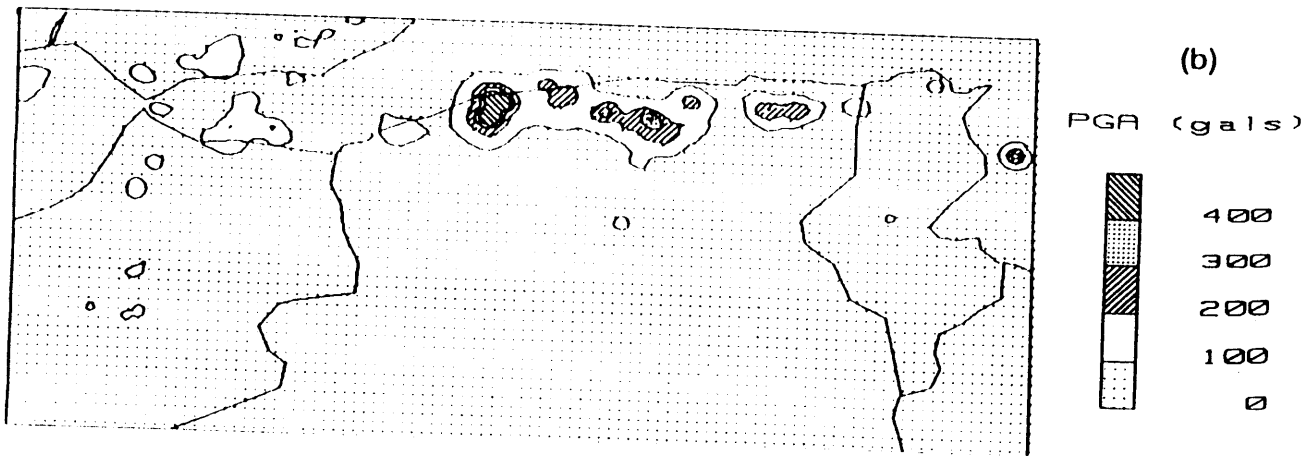

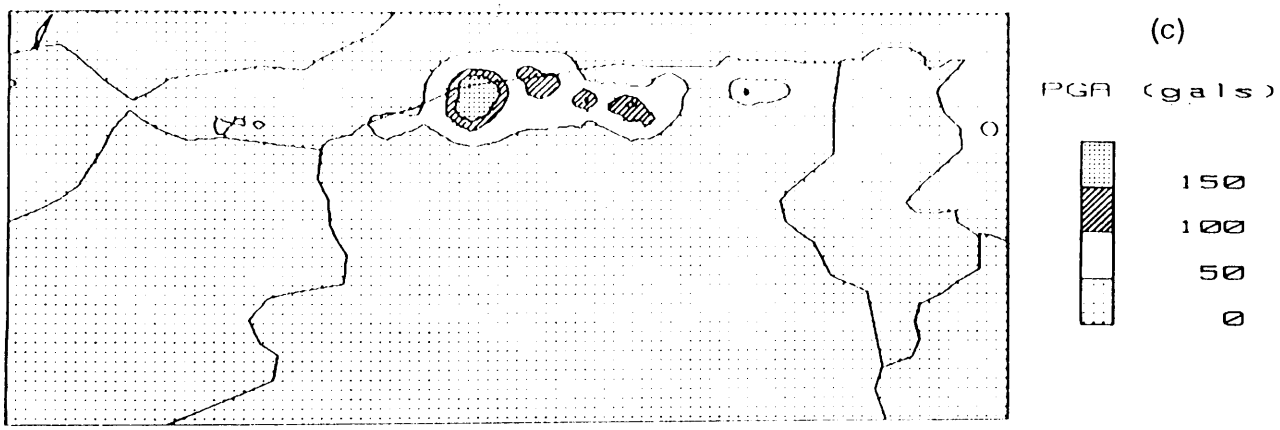

Fig. 8 a - c: Geographical distribution of expected absolute PGA spectral amplitudes (in gals) for typical eigenperiods of structures with a) T = 0.1 s, b) T = 0.3 s and c) T = 1 s, using Molas and Yamazaki (1995) spectral attenuation law.

6. CONCLUSIONS AND RECOMMENDATIONS

These newly earthquake hazard maps in the Maghreb region are drawn in terms of absolute peak ground acceleration, expected peak ground accelerations for a 10 per cent probability of exceedance for 50, 100 and 250 years, MSK intensities and in terms of return period in years for PGA $\geq$ 100 cm/s^2. They should be of great use in the formulation of social and economic development strategies in the whole region under study.

All these maps suggest that high seismic zones in the Maghreb region are found in regions where past destructive earthquake occurred as in El-Asnam, Algiers, Constantine and Setif in Algeria which is in good agreement the seismicity map of the area under study. In western part of the Maghreb region which includes Morocco and the southern Iberian Peninsula, it may be concluded from the seismic hazard maps that high seismic hazard is found in the Rif and High Atlas which constitutes the western branch of the Algerian Atlas mountains. In Tunisia, there is clear division as in Algeria, a seismic north and an aseismic south. The zone north of 34°N presents a higher seismic hazard. The highest earthquake hazard in the part of the world is concentrated in the coastal band of about 200 km wide and along the border of the African and Eurasian tectonic plates which are in collision. This clearly follows the Atlas mountains block from Agadir in south-western Morocco to Tunis (Tunisia) which experiences alternatively low and moderate earthquakes.

I conclude that, given a lack of a seismotectonic map of the Maghreb region, it is reasonable to assume that future earthquakes will tend to occur in areas in which they have occurred in the past, and with rates similaire to historic rates. It is important to recall that whenever enough earthquake data historical or instrumental are accumulated, the seismic hazard maps should be revised consequently. However, the occurrence of a large earthquake in the zone considered may modify these maps. But, it should be kept in mind that a good earthquake zoning map is a permanent map and should not be dependent on individual events. This may be reached when the earthquake data in the catalogue is complete and the time span of the historical seismicity is large enough to include seismic events with long return periods.

This research work is addressed to a broad range of users including high-level government officials, administrators, planners, insurance and reinsurance companies, civil engineers, architects, earth scientists, seismologists and technical experts. It should constitute an integral part of the whole process of economic and social sustainable development in the Maghreb countries. It provides a fundamental means which should guide officials at the national and regional levels in the formulation of development strategies in seismically active zones, land use management, city planning, development or revision of building earthquake-resistant building and construction codes, reinforcement of vulnerable existing buildings, siting new critical engineering projects as well as decision-making of policies for preventive measures against earthquake risk affecting the region considered. The results of this work, coupled with vulnerability analysis, must guide, stimulate and facilitate the efforts of the respective governments, the earthquake engineering and the disaster mitigation planning communities to take specific practical preventive measures to reduce earthquake risk.

Until the seventies, the rate of investments in large urban and industrial development in North African countries was very small and several places non-existing, as a result, there have been no significant economic losses. This may explain that during this century, earthquakes, although they have caused the loss of at least 17,000 human lives, injured about 27,000 and made homeless approximately 550,000 others, the damage in economic terms has been relatively small which mainly due to the types of building prevailing in this part of the world (Benouar, 1993). For instance, the Melouza earthquake (M5.0) of 21 February 1960 killed 47 people, injured 129 and rendered homeless 4900 others ; it destroyed 600 housing units, based on 1960 replacement values the cost of damage amounted FFr 500 Millions; but in contrast, the El-Asnam 1980 (M7.4) caused the loss of more than 3,000 human lives, injured about 9,000 and made homeless at least 400,000 people, it destroyed more than 600,000 housing units, official buildings and public works, and caused damage estimated by official reports at U.S. $5 billions. But today, obviously, with the spread of urban civilisation and important investments in large engineering works in seismic active areas, as the Maghreb region, the toll to be taken by future large earthquakes, and particularly the economic losses, are very likely to increase considerably. The population of the Maghreb countries approaches 70 millions distributed unequally with most living in a mere 6 per cent of the total area which is considered as cultivable and also in cities.

Disaster mitigation constitutes a necessity for urban inhabitants, an obligation for governments and a strategic resource for investment promoters.

Insurance must play a more advanced role, in the mitigation of earthquake disasters in the Maghreb countries, which until now is however neglected. Any insurer who deals with earthquake risk in a modern professional way must have enough knowledge about earthquake size and probability of occurrence, (i.e. with earthquake hazard), in the region under interest. The results of this work may also be used to evaluate the seismic risk by converting probabilistic estimates of selected earthquake parameters into losses or damage potential, through a loss function, for which the insurer is most interested to answer specific insurance questions like rating of risks, determining acceptable levels of risks and to what extent.

In recognition of the constant threat to the major investments at risk in this part of the world from strong earthquakes, governments of the respective countries, with the help of international specialised organisations, should multiply and join their efforts to continue the study and analysis of the seismicity of the concerned region with a view to mitigating the earthquake risk; this is a field of research where interaction and co-operation of teams may give the best results in the short time.

REFERENCES

Alvarez, W., Cocozza, T. and Wezel, C., 1974. Fragmentation of the Alpine orogenic belt by microplate dispersal. Nature, 248, 309-314.

Ambraseys, N.N., 1962. The seismicity of Tunis, Ann. Di Geofisica, Vol. XV, No.23, 233-244.

Ambraseys, N.N. and Vogt, J., 1988. Material for the investigation of the seismicity of the region of Algiers. European Earthquake Engineering, 3, 16-29.

Ambraseys, N.N., 1995. The prediction of earthquake peak ground acceleration in Europe. Earthq. Eng. & Struct. Dynamics, Vol. 24, 467-490.

Benhallou, H., 1985. Les Catastrophes Séismiques de la Région d'Echéliff dans le Contexte de la Séismicité Historique de l'Algérie. Thèse de Doctorat Es-Science, IST-USTHB, Alger.

Benhallou, H., and et al., 1994. Les seismes en Algérie de 1365 à 1992. Publication du Centre de Recherche en Astronomie, Astrophysique et Géophysique, Dpt. Etudes et Surveillance Sismiques, CRAAG, Alger-Bouzaréah.

Benouar, D., 1993. The seismicity of Algeria and adjacent regions during the twentieth century, Ph.D Thesis, Civil Engineering Department, Imperial College, University of London, pp. 712.

Benouar, D., 1994a. Materials for the investigation of the seismicity of Algeria and adjacent regions during the twentieth century, Special Issue of Annali di Geofisica, XXXVII, No.4, 459-860.

Benouar, D., 1994b. Magnitude-intensity and intensity-attenuation relationships in the Atlas zone and Algerian earthquakes, Earthq. Eng. & Struct. Dyn. Vol. 23, 717-727.

Benouar, D., Molas, G.L., and Yamazaki, F., 1996. Earthquake hazard mapping in the Maghreb countries, Earthq. Eng. & Struct. Dyn. Vol. 25, 1151-1164.

Boore, D.W. and Joyner, W.B., 1982. The empirical prediction of ground motion. Bull. Seism. Soc. Am. 72, S43-S60.

Campbell, K.W., 1985. Strong motion attenuation relations: a ten-year perspective. Earthquake spectra 1, 759-804.

Cherkaoui Maknassi, M.T., 1988. Fichier des séismes du Maroc et des régions limitrophes 1901-1984. Trav. Inst. Scie. Rabat, Série géol. Géog. Phys. No 17, pp.158.

Cherkaoui Maknassi, M.T., 1991. Contribution à l'étude de l'aléa sismique au Maroc. Thèse de Doctorat, Université Joseph Fourier de Grenoble. France.

Cornell, C.A., 1968. Engineering seismic risk analysis, Bull. seism. Soc. Am. 58, 1583-1606.

Dewey, J.F., Pitman, W.C, Ryan, W.B ;F. and Bonnin, J., 1973. Plate tectonics and the evolution of the Alpine system. Bull. Geol. Soc. Am., 84, 3137-3180.

Epstein, B. and Lomnitz, C., 1966. A model for the occurrence of large earthquakes. Nature, Vol. 211, No. 5052. 954-956.

Esteva, L., 1968. Bases para la formulacion de decisiones de diseno sismico. Instituto de Inginiera, No.182, Universidad Nacional Autonoma de Mexico.

Favier, E., Ferrieux, H., Goula, X., Hellal, E., Messen, N., Mohammadioun, B., Mohammadioun, G. and Oudahmane, S., 1981. Etudes des répliques du séisme du 10 Octobre 1980. In Actes des Journées Scientifiques sur le Séisme d'El-Asnam. Alger, 15-16 Juin.

Groupe de recherche Néotectonique de l'Arc de Gibraltar, 1977. Histoire tectonique récente (Tortonien à Quarternaire de l'Arc de Gibraltar et des bordures de la mer d'Alboran), Bull. Soc. Geol. Fr., 19 (3), 575-614.

Hatzfeld, D., 1978. Etude séismotectonique de la zone de collision Ibéro-Maghrébine. Thèse, Institut de Recherches Interdisciplinaires de Géologie et de Mécanique, Grenoble (France).

Idriss, I.M., 1978. Characteristics of earthquake ground motions. Proc. ASCE conf. earthquake eng. & soil dyn. Pasadena, California I, 1151-1265.

Joyner, W.B. and Boore, D.W., 1988. Measurement, characterization and prediction of strong ground motion. Proc. ASCE conf. earthquake eng. & soil dyn., Park City, Utah, 43-102.

Mayer-Rosa, D. and Schenk, V., (Editors). 1989. Special issue on TERESA, Test Regions for Evaluations of Algorithms for Seismic Hazard Assessment in Europe, Natural Hazards, 2, 3-4.

Mayer-Rosa, D. and Sleijko, D., 1993. Assessment of seismic hazard for the Sanio-Matese area, Southern Italy (project « TERESA ». In Special issue on the meeting « Irpinia Dieci Anni Dopo », XXXVI, No.1.

McKenzie, D., 1972. Active tectonics of the Mediterranean region. Geophys. J. R. Astr. Soc. London, 30, 109-185.

Mezcua, J. and Martinez, J.M., 1983. Sismicidad Del Area Ibero Mogrebi. Seccion de Sismologia, Inst. Geogr. Nacional. Madrid.

Milne, W.G. and Davenport, A.G., 1969. Distribution of earthquake risk in Canada. Bull. Seism. Soc. Am., 59, 729-754.

G.L. Molas and F. Yamazaki. The effect of source depth and local site to the attenuation charcteristics of response spectra. Proc. 23rd JSCE earthq. eng. Symp., pp. 69-72, 1995.

Munuera, J.M., 1963. Datos basicos para un estudio de sismicidad en la area de la peninsula Iberica (seismic data). Memorias del Instituto Geographico y Catastral, tome XXXII, Madrid, pp.93.

Ouyed, M. and Hatzfeld, D., 1981. Le séisme du 10 Octobre 1980: Etude Séismotectonique. in In Actes des Journées Scientifiques sur le Séisme d'El-Asnam. Alger, 15-16 Juin.

Ouyed, M., Yielding, G., Hatzfeld, D. and King, G.C.P., 1982. An aftershock study of the El-Asnam (Algeria) earthquake of 1980. Geophys. J. R. Astr. Soc., 73, 605-639.

Papastamatiou, D. and Sarma, S.K., 1988. Physical constraints in engineering seismic hazard analysis. Earthq. Eng. & Struct. Dyn., 16, 967-984.

Patriat, P., Segoufrin, J., Schlich, R., Goslin, J., Auzende, J.M, Benzart, P., Bonnin, J. and Olivet, J.L., 1982. Les mouvements relatifs de l'Inde, de l'Afrique et de l'Eurasie. Bull. Soc. Geol. France, 24, (2), 363-373.

Philip, H. and Meghraoui, M., 1983. Structural analysis and interpretation of the surface deformations of the El-Asnam earthquake of October 10, 1980. Tectonics, 2, 17-49.

Philip, H. and Cisternas, A., 1985. El terremoto de El Asnam del 10 Octubre de 1980. In: Udias, A., Munoz, D. And Buforn, E. (Editors) Mecanismo de los terremotos y tectonica. Editorial de la Universidad Complutense de Madrid.

Ramdani, M., Tadili, B., and El-Mrabet, T., 1988. The present state of knowledge on historical seismicity of Morocco. Proc. symposium on calibration of historical earthquakes in Europe and recent developments in intensity interpretation, European Seismological society, Sofia, 23-28 August, 258-279.

Rothé, J.P. 1980. Catalogue des séismes tunisiens. Manuscrit (Unpublished).

Shah, H.C. and Vagliente, V.N., 1972. Forecasting the risk inherent in earthquake resistant design, in Proc. int. conf. on microzonation, Vol.2.

Tapponnier, P., 1977. Evolution tectonique du system Alpin en Méditerranée: Poinçonnement et écrasement rigide plastique. Bull. Soc. Géol. France, 19(3), 437-460

Scientific Technical Report STR 98/05
DOI: 10.2312/GFZ.b103-98055

CURRENT STATE OF THE ART, PROBLEMS AND PRELIMINARY RESULTS OF SEISMIC HAZARD ASSESSMENT IN SUB-SAHARAN AFRICA

Isaac O. Nyambok

University of Nairobi, Department of Geology, P.O. Box 30197, Nairobi, Kenia,
Fax: +254-2-449-539. E-mail: uonseism@arcc.or.ke

1. INTRODUCTION

Disastrous earthquakes in sub-Saharan Africa have been limited and have drawn equally limited investigations. Even these limited investigations have tended to be restricted to the discrete individual earthquake events, rather than integrated seismic hazard assessment. In this respect, areas of high seismic risk are not fully understood.

Nonetheless, sub-Saharan Africa is known to have many earthquakes associated with tectonic and volcanism within the continent, especially the active rift in East and Central Africa (Fairhead and Stuart, 1982; and Iranga, 1992). Most of these earthquakes have caused relatively less loss of life and damage to property. However, with increased population concentration in urban centres, structural development projects and lifeline systems, the impact of earthquakes are bound to be felt more in sub-Saharan Africa and most likely with devastating consequences. The lowest cost but most cursory level of zonation is based on past earthquake magnitudes or seismic intensities (Task Committee TC4 of ISSMFE, 1993). The distribution of seismograph stations in sub-Saharan Africa is still so sparse in many countries that even in the period for better determined instrumental positions, many earthquakes are mainly identified by their felt effects and therefore to have better correlations of seismic data a regional or international approach in necessary. It is with this in mind that the author and other collaborators embarked on seismic hazard study of the sub-Saharan Africa as a contribution to the Global Seismic Hazard Assessment Program (GSHAP) (Nyambok & Ochieng, 1997).

2. BASIC DATA

Earthquake effects have been noted and documented in historical records, but it is only with the emergence of seismic instruments that a detailed and precise study of their occurrence and location in the last a hundred or so years has been possible. An extensive collection of earthquake data is available for sub-Saharan Africa most of which go back beyond instrumental seismicity (Fig. 1). The earliest known earthquake in sub-Saharan Africa occurred in 1071. However, the earlier data are scanty and may not be representative of all the earlier seismic events. This may be ascribed to the lack of instrumentation in those years which must have resulted in many unrecorded earthquakes, especially those of low magnitudes. The main obstacles in seismic data are the brief time span of instrumental catalog (Paivi and Kijko, 1992), distribution of seismograph stations (Ambraseys and Adams, 1991) and inadequate standardisation of instrumentation and non standard types of buildings. The detection of earthquakes, however, increased with instrumentation (see Figures 2-5).

Scientific Technical Report STR 98/05
DOI: 10.2312/GFZ.b103-98055

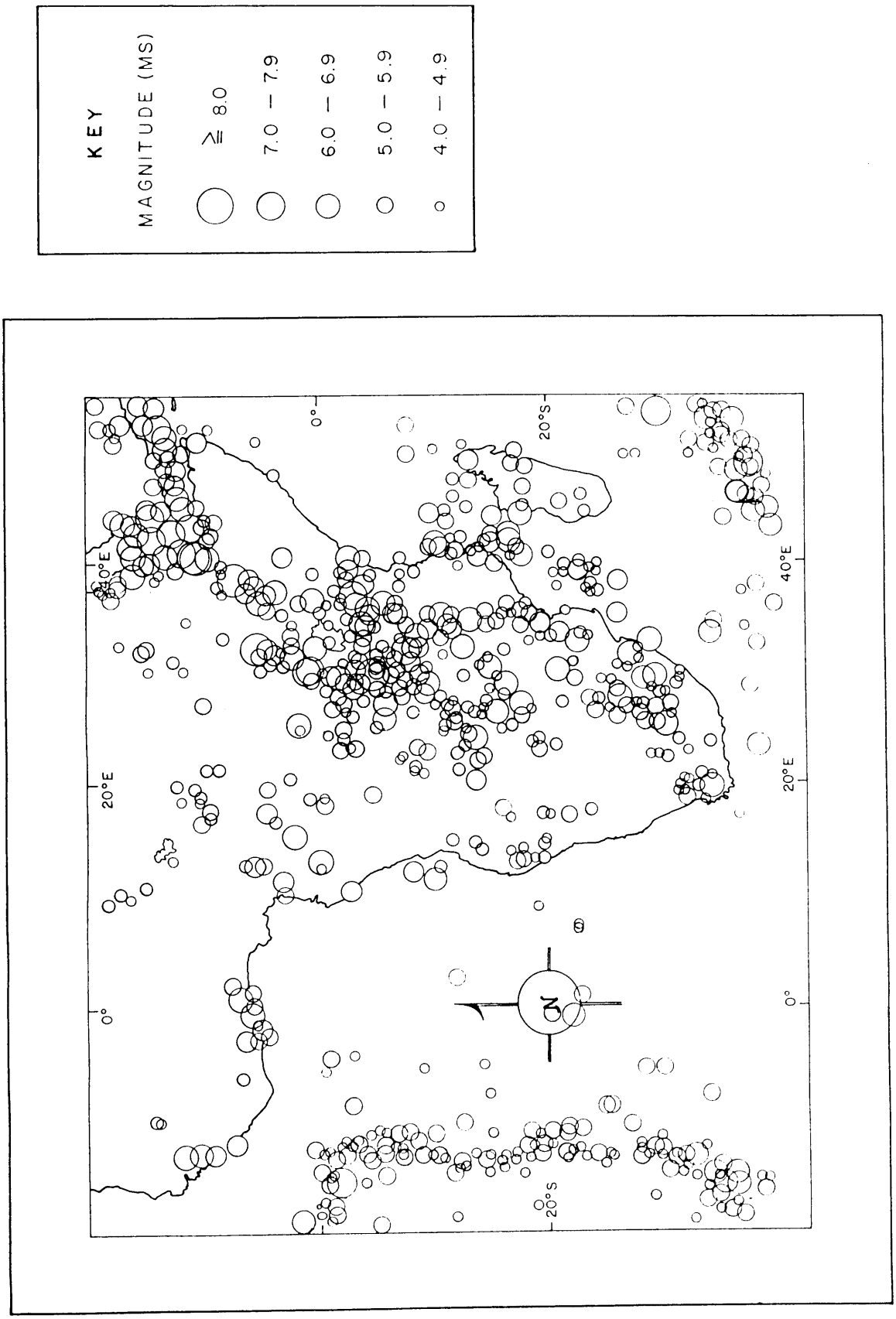

Fig. 1: Sub-Saharan African earthquake distribution

Scientific Technical Report STR 98/05
DOI: 10.2312/GFZ.b103-98055

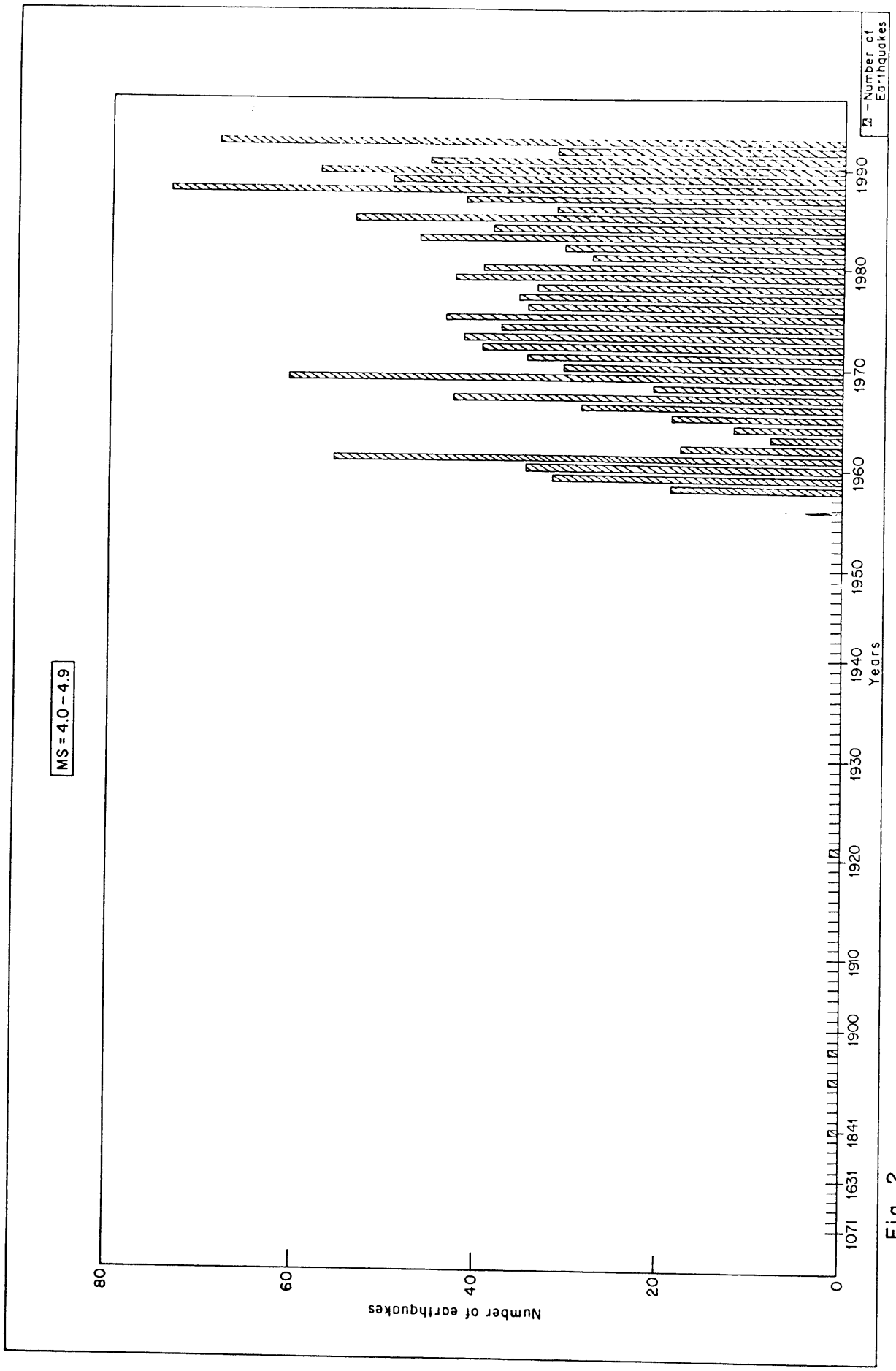
MS = 4.0 – 4.9
Number of earthquakes
0
20
40
60
80
1071
1631
1841
1900
1910
1920
1930
1940
1950
1960
1970
1980
1990
Years
Number of Earthquakes

Fig. 2

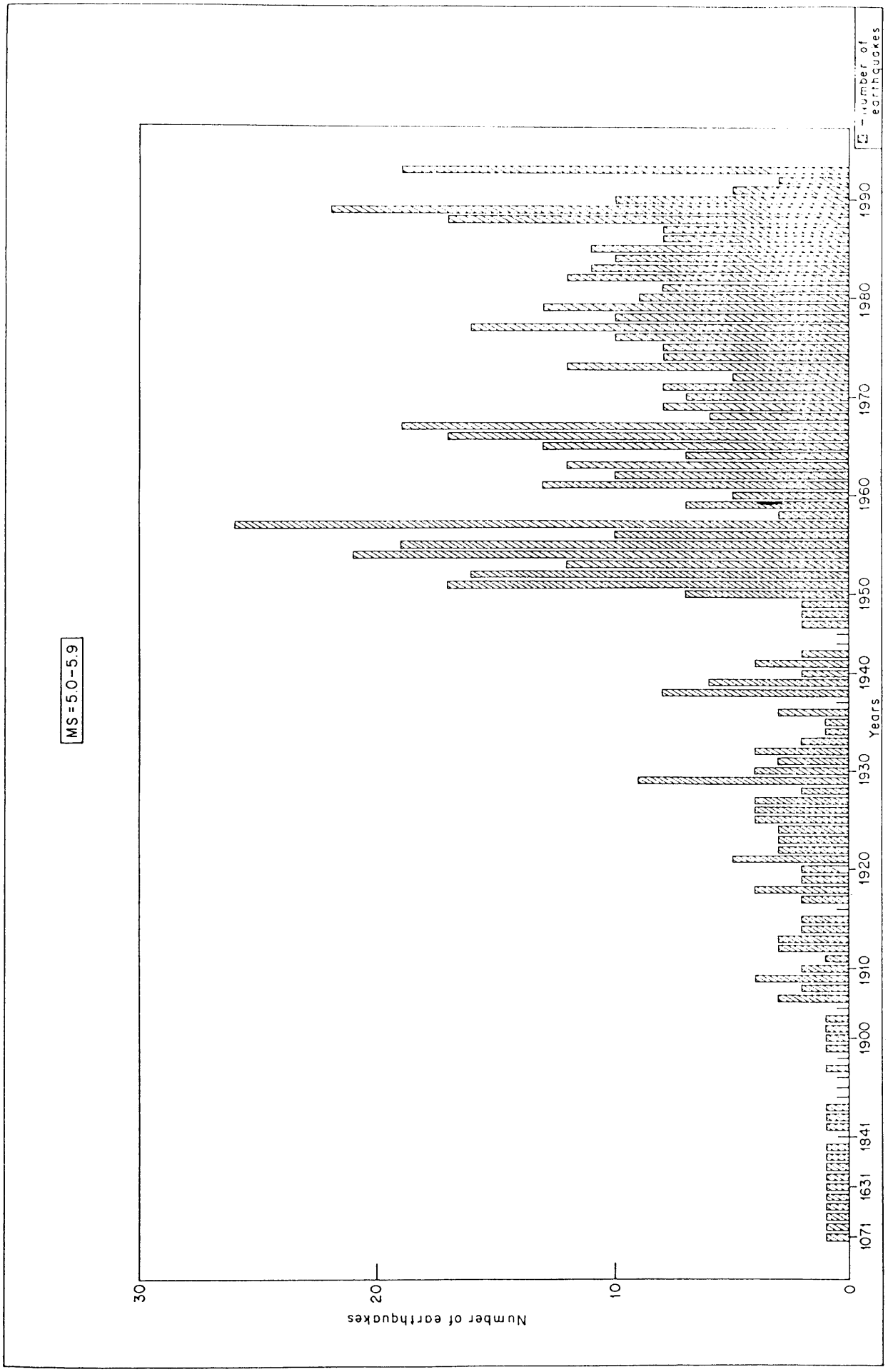
MS=5.0-5.9
Number of earthquakes
0
10
20
30
1071
1631
1841
1900
1910
1920
1930
1940
1950
1960
1970
1980
1990
Years
Σ - number of earthquakes

Fig. 3

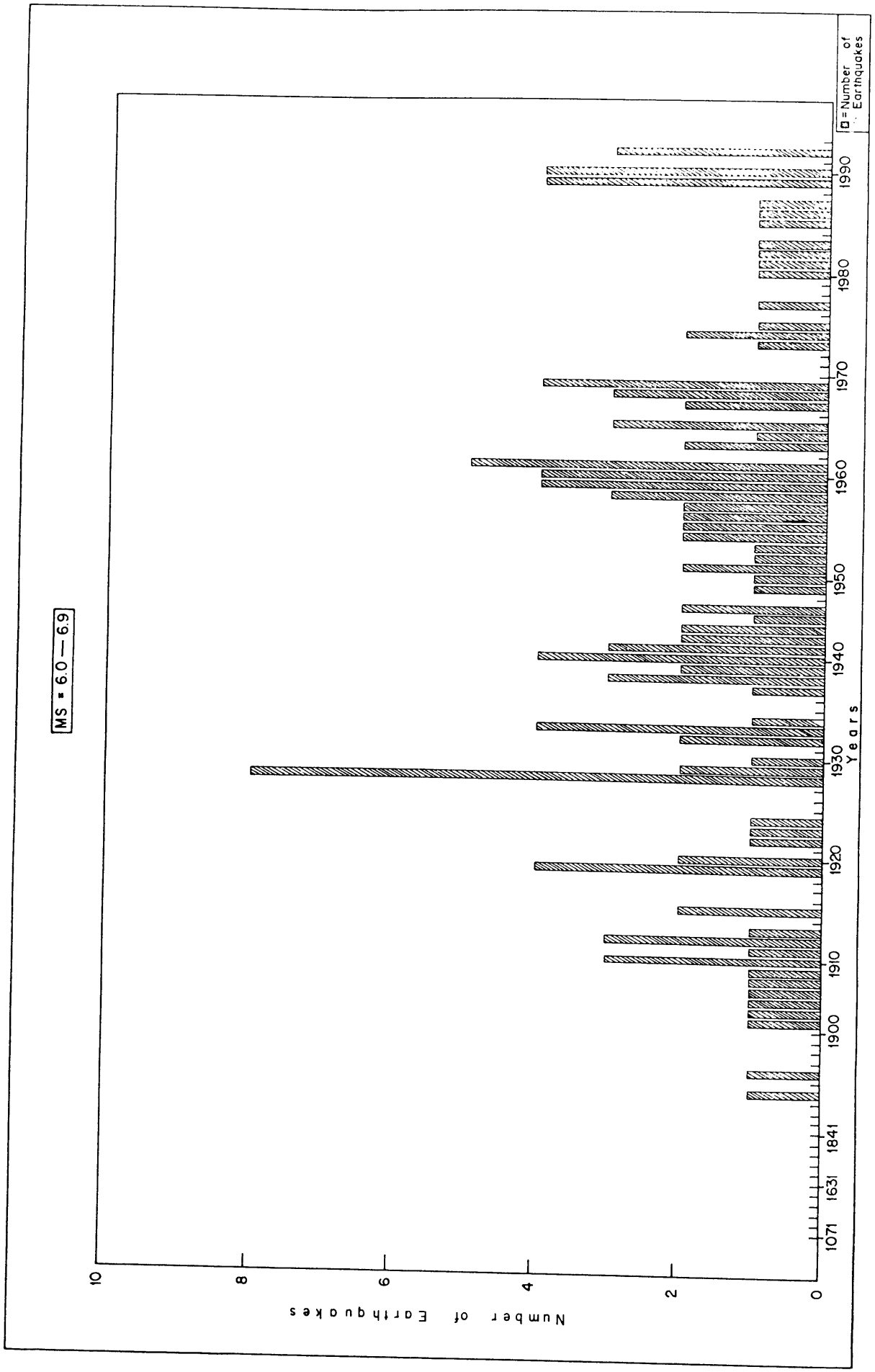
MS = 6.0 — 6.9
Number of Earthquakes
Years
Number of Earthquakes
0
2
4
6
8
10
1071
1631
1841
1900
1910
1920
1930
1940
1950
1960
1970
1980
1990

Fig. 4

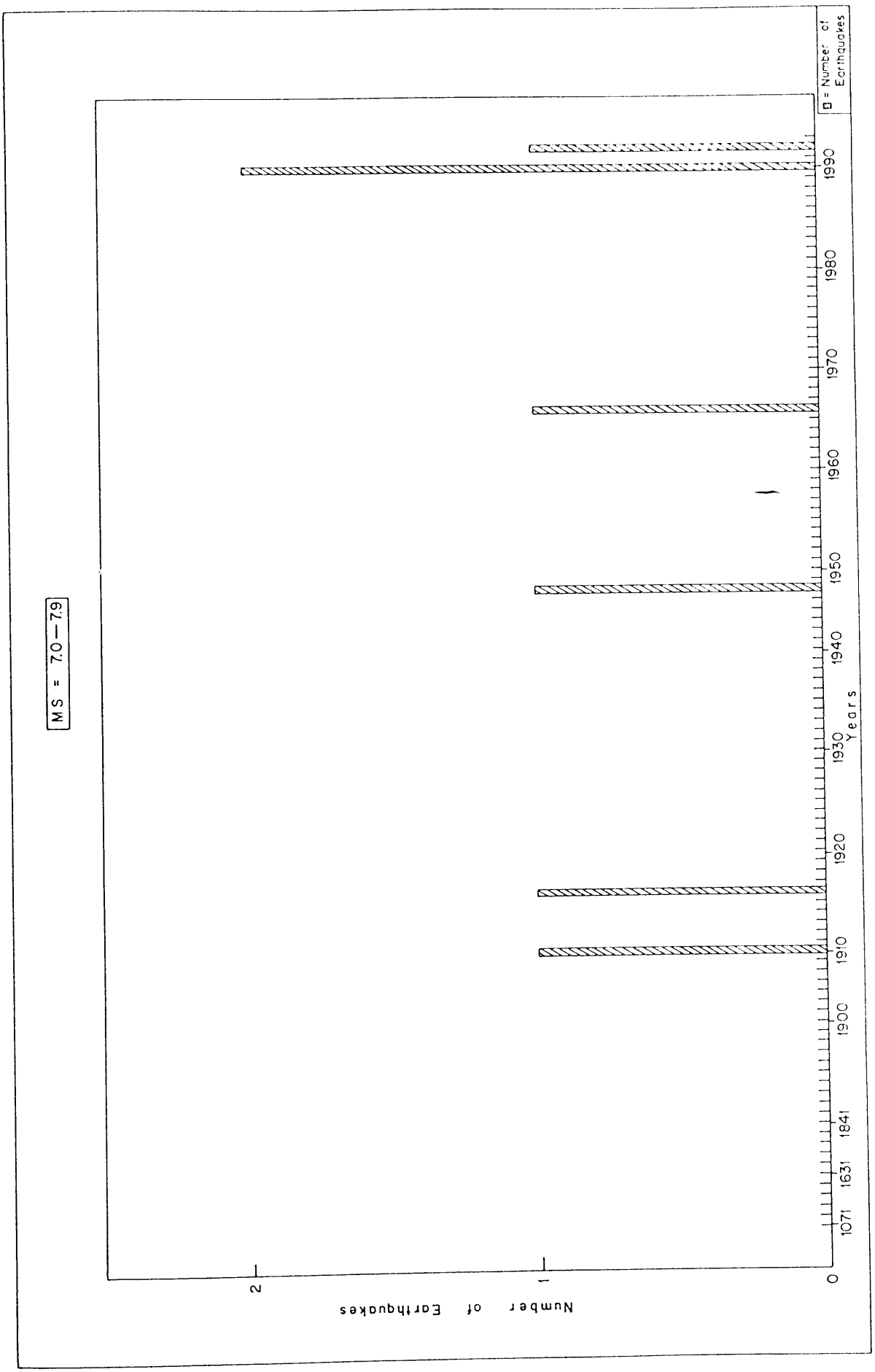
D = Number of Earthquakes
MS = 7.0—7.9
Number of Earthquakes
0
1
2
Years
1071
1631
1841
1900
1910
1920
1930
1940
1950
1960
1970
1980
1990

Fig. 5

In this study, a catalogue of 2780 earthquakes of surface magnitude ≥ 4 from various sources has been prepared. The seismic data are used to assess the energy release distribution of the earthquakes in sub-Saharan Africa. To start with, the distribution of epicentres as shown in Fig. 1 shows that the majority of earthquakes occur along active faults and mobile belts. There are seismically active centres spread over the whole sub-continent, but the most active region is the East African Rift System.

The catalogue contains seismic data of earthquakes of surface magnitudes Ms ≥ 4.0 and the sub-continent is bounded by latitudes 35°S and 20°N and longitudes 20°W and 55°E. The seismic data parameters such as time (month, year, date and origin time), location (altitude and longitude), depth, locating agency, magnitude and reporting agency. Intensities are not yet included because of varied local conditions, and nonstandard types of buildings and infrastructure. The data presented are both historical and instrumental.

Because instrumentation is a recent development in the study of earthquakes and the early macroseismic information depended very much on the population awareness and distribution, these seismic data are therefore not homogeneous or standardised in time and space. This is discernible in Figure 2 which is a histogram of low magnitudes (Ms = 4.0 - 4.9) earthquakes. There were hardly any earthquake of this range of magnitude before mid-20th century. It is doubtful and perhaps not true that only four earthquakes of this magnitude range occurred before 1958. The palicity of the earthquakes is most likely due to lack of seismic instruments and also the sparse population which could provide macroseismic information. This makes a strong case for palaeo-seismic studies. On the other hand, the number of earthquakes recorded increased tremendously in the late 1950s up to the present.

Figure 3 shows an increase in the number of earthquakes even in the early years before instrumental seismicity in Africa, which can be attributed to the stronger earthquakes that affected larger areas, hence many people felt them. This appears also to be the case in Figure 4. However, in Figure 5, the number of earthquakes decreased because there are generally fewer earthquakes of very high magnitudes. This does not imply that the sub-Saharan Africa is a seismic or devoid strong earthquakes it may just mean that the many small earthquakes which occur give rise to the reduction of seismic strain and thus likewise reduce the chances of strong large earthquakes, especially in extensional stress areas.

The data on the magnitudes were collected from several sources and were not vigorously correlated in order to detect any analytical errors. These errors commonly arise from the measurements of amplitudes, non-standardised instruments used and even the manipulation of the conversion formulae. However, the preinstrumental earthquakes whose magnitudes were uncertain, were assigned a uniform magnitude of Ms =5. Although these early earthquakes have their magnitudes thus fixed, there were some strength indications based on the reported intensities (I_0). The epicentral intensities (approximate) were used to estimate the local magnitude (M_L) applying the formula

$$M_L = 2/3\ (I_0) + 1.$$

3. DATA ANALYSIS

The data were analysed on the basis of seismic energy releases as suggested by Båth (1982a, b). All earthquakes bounded by latitudes 20°N and 35°S, and longitudes 20°W and 55°E were analysed using squares of sizes 3° x 3°. The use of squares in this study was found to give the best fit as compared to circular sampling technique. The method used is maximum likelihood with the earthquake with maximum magnitude within the square representing that area. They were analysed such that all the earthquakes that fall within or at the boundary of the square and had the highest magnitude had its magnitude value put at the centre of the square. The squares were then shifted latitudinally and longitudinally with overlaps of 1° in both directions. This resulted in the analysis of 999 squares for the whole of sub-Saharan region. The overlapping was undertaken to harmonise the energy release boundaries in the squares since the seismic activities are not strictly bounded by the squares. In effect, the magnitude centre points are only 2° apart latitudinally and longitudinally.The application of this approach resulted in seismic energy mapping of sub-Saharan Africa. Isomagnitude lines were then drown of similar magnitude range joined together. This was done at a magnitude value thus resulting in the range Ms = 4.0 - 4.9, Ms = 5.0 - 5.9, Ms = 6.0 - 6.9 and Ms ≥ 7.0 being delineated (Fig. 6). The approach makes the data more reliable because of the uncertainty in magnitude determination. The magnitude ranges reduce or absorb the errors.

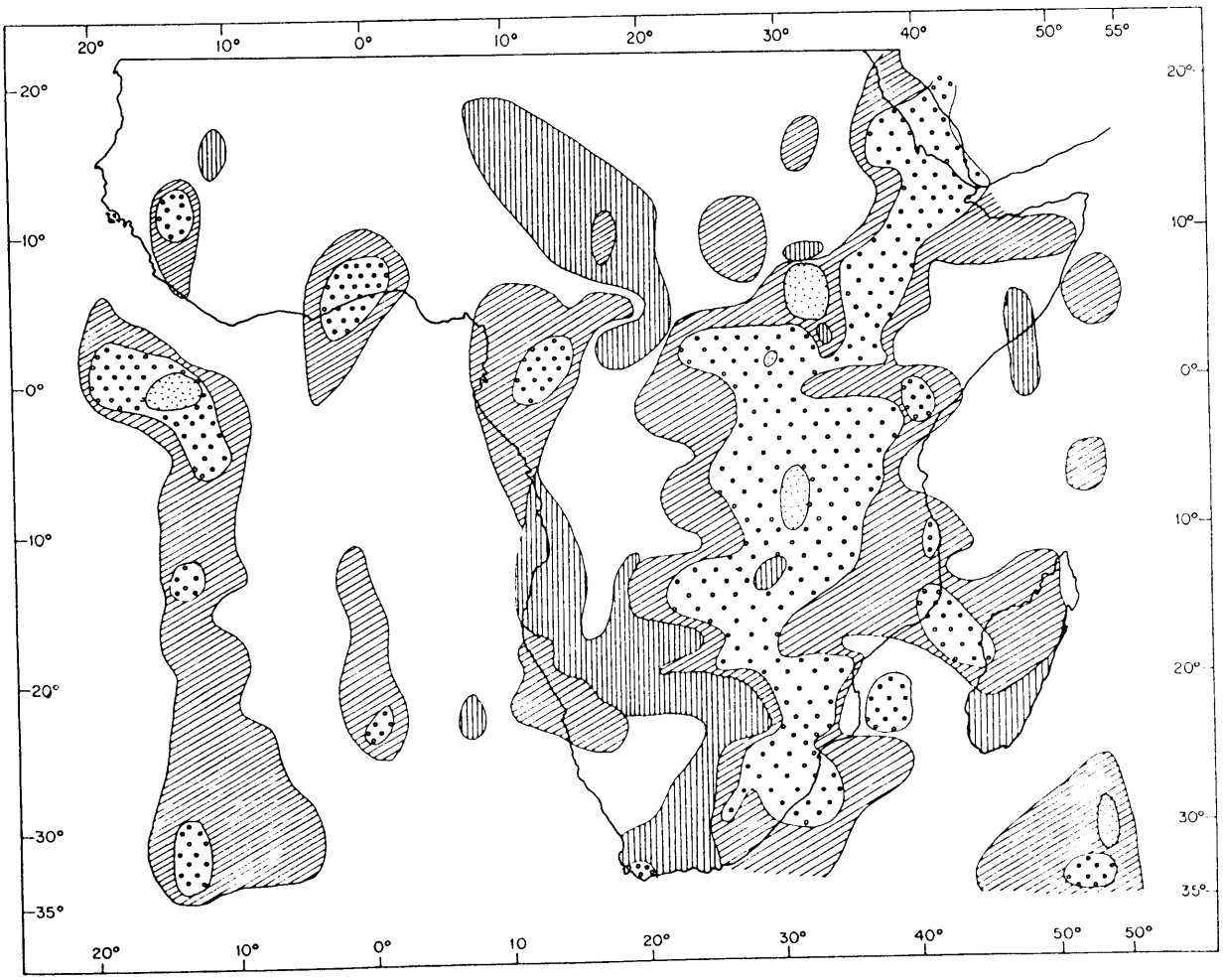

FIG. 6 : SEISMIC ENERGY MAP OF SUB-SAHARAN AFRICA USING MAXIMUM MAGNITUDES (Ms)

4. INTERPRETATION

Seismicity of sub-Saharan Africa has mainly been influenced by the tectonic episodes which affected the region. However, volcanic activities especially mantle-plume events have also generated seismicity in sub-Saharan Africa. Areas of highest magnitudes (Ms $\geq$ 7.0) are found around Lake Tanganyika and Lake Kivu and in the southern Sudan. In the case of Lake Tanganyika, the most seismic parts are southeastern and central areas while the southwest of Lake Kivu is the most active seismically in the Lake Kivu area. These areas which are within the western branch of the East African Rift System are more seismically active than the eastern branch of the Rift System. The difference between the two branches could be attributed to the fact that the western branch is characterised by brittle Precambrian rocks which preferentially fracture under strain. Earthquake generating stress in this area is predominantly of normal faulting type with significant strike-slip contributions (Tanaka et al., 1980; Zana and Tanaka, 1981). The eastern branch on the other hand is mainly characterised by volcanic rocks which under strain deform plastically and thus do not fracture readily which may lead to the generation of frequent minor earthquakes. another area of the highest magnitudes is found in southern Sudan which is associated with the Aswa Shear Zone.

The second highest seismic area encompasses the whole of the eastern branch of the East African Rift System from the Red Sea in Ethiopia and Eritrea to northern Tanzania, traversing Kenya as well. The magnitude range of the earthquakes is Ms = 6.0-6.9. This is also an area of intense tectonic and volcanic activities. It is apparent that these two earth processes are the cause of strong seismicity in this area. The magnitude range of seismic events is the same in Malawi, Mozambique, northeastern south Africa, the extreme western part of Madagascar, the cape Rangwe in south Africa, the faulted volcanic province of Cameroun, the Akwapim Shear Zone in Ghana and Togo, and "Rokelides and Mauritanides" faulted province of West Africa. Major earthquakes can also occur in Africa in areas with little or no surface expression of tectonic events (Ambraseys and Adams, 1992). Some of the intraplate earthquakes are events caused by the strains which are constantly present in the earth;s crust even in places far removed from the plate boundaries. The build up of strain to the point of rupture is somewhat slower within the plates than at boundaries and as a result there are infrequent, large earthquakes within the plates which come as surprises to the population. The areas of low seismicity are large parts of West Africa, central Africa and south-west Africa. These are areas associated with basins such as Niger, Tchad, Congo and Namibia basins. These basins are mainly filled with sedimentary sequences which tend to flow and deform under strain rather than rupture, thereby releasing low seismic energies, microseismicity and minor seismicity.

REFERENCES

Ambraseys, N.N. and Adams, R.D. (1991). Reappraisal of major African earthquakes, south of 20°N, 1900-1930. Natural Hazards 4, 389-419.

Ambraseys, N.N. and Adams, R.D. (1992). Reappraisal of major African earthquakes, 1900-1930. (Extended Abstract). In: C.J. Ebinger, H.K. Gupta and I.O. Nyambok (Editors), Seismology and Related Sciences in Africa. Tectonophysics, 209, 313-320.

Bath, M., 1982a. Seismic energy mapping applied to Turkey. Tectonophysics, 82, 69-87.

Fairhead, J.D. and Stuart, G.W. (1982). The seismicity of the East African rift system and comparison with other continental rifts. In: G. Palmason (Editors), Continental and Oceanic Rifts. Geodym. Ser. Am. Geophys. Union, 8, 41-61.

Iranga, M.D. (1992). Seismicity of Tanzania: distribution in time, space, magnitude and strain release. In: C.J., Ebinger, H.K., Gupta and I.O. Nyambok (Editors), Seismology and Related Sciences in Africa. Tectonophysics, 209, 313-320.

Nyambok, I.O. and Ochieng, A.O. (1997). Seismic hazard assessment of sub-Saharan Africa. A GSHAP contribution. In: I.O. Nyambok and D.W. Ichang'i (Editors), Proceedings of the GSA 95 International Conference - 10th Conference of the Geological Society of Africa, 275-286.

Paivi, M and Kijiko, A. (1992). Seismic hazard in East Africa: an example on the application of incomplete and uncertain data (Extended Abstract). In C.J. Ebinger, G.K., Gupta and I.O. Nyambok (Editors), Seismology and Related Sciences in Africa. Tectonophysics, 209, 311-312.

Tanaka, K., Horiuchi, S., Sato, T. and Zana, N.(1980). The earthquake generating stress in the western Rift Valley of Africa. J. Phy. Earth, 29, 45-47.

Task Committee, TC 4 of ISSMFE (1993). Manual for zonation of seismic geotechnical hazards. Published by the Japanese Society of Soil Mechanics and Foundation Engineering.

Zana, N. and Tanaka, N. (1981). Focal mechanism of major earthquakes in the western Rift Valley of East Africa. Tohoku Geophy. J., 28, 119-121.

Zana, N., Kamba, M., Katsongo, S. and Janssen, T.H. (1989). Recent seismic activity of the Kivu Province, western Rift Valley of Africa. Phy. of the Earth and Planetary Interiors, 58, 52-60.

Scientific Technical Report STR 98/05
DOI: 10.2312/GFZ.b103-98055

SEISMIC HAZARD ASSESSMENT IN EASTERN AND SOUTHERN AFRICA: Test area in the East African rift system

Fekadu Kebede

Geophysical Observatory, Science Faculty, Addis Ababa University, P. O. Box 1176, Addis Ababa, Ethiopia; Fax: +251-1-117 253; E-mail: observatory.aan@telecom.net.et

Contributors to the results presented here: K. Atakan, L. S. Chapola, D.J. Hlatywayo, F. Kebede, D. K. Lombe, V. Midzi and G. Turyomurugyendo.

1. INTRODUCTION

The East African Rift system mainly extends in the NNE-SSW direction and is the best example of continental rifting on land. Several attempts devoted to studying the current status of rifting in Eastern and Southern Africa have been performed by many researchers (e.g. Shudofsky, 1985). This rift system joins the world wide oceanic rift system via the Afar depression and the Gulf of Aden (Fig. 1).

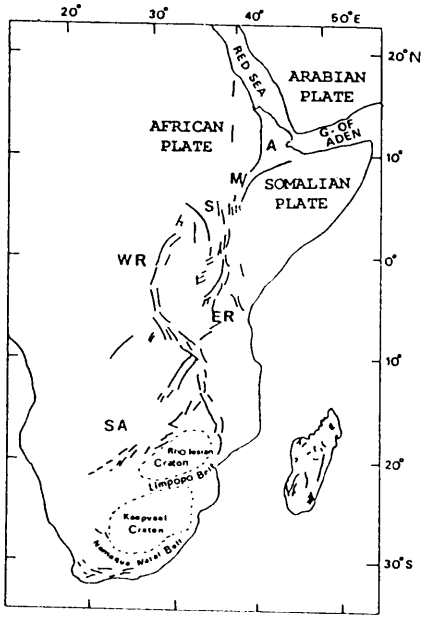

Fig.1. Major structural elements and regions along the East African rift system and the southern Red Sea (after McConnell, 1972). A, M, S, WR, ER and SA denote the Afar Depression, the Main Ethiopian rift system, the southernmost rifts of Ethiopia, the Western rift, the Eastern rift and the southern part of Eastern Africa, respectively. Lines show fault belt orientations.

In the northern part of the region under study three major plates, namely the African (Nubian), Somalian and Arabian plates meet. From tectonic point of view the northern part of the rift, specifically the Afar triple junction, is more complex than the southern part. The seismic

Scientific Technical Report STR 98/05
DOI: 10.2312/GFZ.b103-98055

activity is higher in the central and northern part than in the southern part of the East African rift system. In general the region is seismically active and characterized by extensional tectonics.

In subsequent sections we will briefly present the past and present experience we have, inputs and methods used, recently obtained results and discussion for the seismic hazard assessment in the region.

2. EARLIER WORK DONE ON SEISMIC HAZARD ASSESSMENT IN THE REGION

Regarding seismic hazard assessment, attempts have been made by several researchers to produce seismic hazard maps for different segments of the East African rift system. Employing the extreme value approach Gouin (1976) produced the first seismic hazard map for the Horn of Africa for a return period of 100 years. Since then several new developments have taken place. Thus, attempts are also recently made to revise the hazard map for the Horn of Africa by Kebede and Asfaw (1996) and Kebede and Van Eck (1997). They employed the probabilistic approach as developed by Cornell (1968) and McGuire (1976, 1993) and produced hazard maps of peak horizontal ground acceleration for various annual probabilities of exceedence. Also, Hlatywayo (1995), Twesigomwe (1996), Chapola (1997) and Lombe (1997) produced hazard maps for Zimbabwe, Uganda, Malawi and Zambia, respectively, using the same probabilistic approach employed for the Horn of Africa. In producing the hazard maps each researcher prepared input parameters independently. Moreover, the time periods of the catalogue used in the hazard assessment by each researcher are also different.

Therefore, the main objective of the Eastern and Southern Africa Regional Seismology Working Group (ESARSWG) is to produce a seismic hazard map of the region by using:

1. A revised and updated catalogue for the whole region;
2. The same approach for defining seismic source zones and other input parameters;
3. A better (regional) ground motion attenuation relation;
4. A common technique that agrees with the one recently recommended by the Global Seismic Hazard Assessment Program (GSHAP).

3. INPUT PARAMETERS

3.1. Removal of aftershocks from the catalogue

The occurrence of the main shock (largest earthquake of the sequence) observed during a seismic activity is due to the permanent tectonic process going on in the region under consideration while the occurrence of aftershocks is due to the readjustment required to the new stress state in the same region. Thus, the catalogue has to be cleaned from aftershocks. For the results presented here removal of aftershocks is performed using the guidelines formulated by Lazarov and Christskov (1981). In identifying aftershocks the model uses size of the earthquake, time difference between the occurrence of the main shock and aftershock and location of the aftershock (distance) with respect to that of the main shock.

3.2. Characterizing seismicity

To characterize the seismicity of the region, which is a fundamental input in the analysis of seismic hazard, the Gutenberg and Richter relation (Gutenberg and Richter, 1954) is used:

$$\log N(m) = a - b\,m \qquad (1)$$

where N (m) is the cumulative number of earthquakes with magnitude greater than or equal to m. The slope b in equation (1) characterizes the seismicity and gives the relative abundance of small and large earthquakes for a given region under study. Regarding the b-value, Kebede and Kulhánek (1994) and others have shown that different parts of the region have different characteristic seismicity, each with its own b-value. Thus, to determine the b-value and other input parameters a sub- catalogue for each source zone is extracted from the main catalogue compiled for the whole region. Then, earthquake magnitudes in each sub-catalogue are grouped into magnitude classes with center magnitudes of 4.5, 5.0, 5.5, 6.0, 6.5, 7.0 and 7.5. Estimation of the b-value for each source zone is performed using the maximum likelihood method (Weichert, 1980). From all the source zones b-values ranging from 0.58 to 1.28 are obtained.

3.3. Activity rate

Knowing the completeness of the catalogue in time with respect to magnitude the activity rate, i.e. the number of earthquakes having magnitudes greater than or equal to the lowest threshold magnitude that occur per year in each zone, can be obtained by taking the cumulative number of earthquakes in each magnitude class and dividing it by the corresponding time period of completeness. For all the source zones, activity rates ranging from 0.05 to 3.17 are obtained.

3.4. Seismic source zones

Various major zones of seismicity and crustal deformation contributing to seismic hazard exist in Eastern and southern Africa. Although studies devoted to mapping of active faults and other geomorphic studies have not been performed to the level desired, recent seismicity studies and developments in the understanding of the tectonics of the region suggest the identification of twenty one seismic source zones as the main contributors of damaging earthquakes for the seismic hazard assessment in the region (see Fig. 2).

Each seismic zone is defined by some homogeneity in its observed seismicity (earthquake epicenters) and tectonic characteristics (major faults). The main tectonic features that exist in the region according to Fig. 1 are: the axial trough of southern Red Sea, Afar depression and its western margin including the Djibouti area, the western Gulf of Aden, the Main Ethiopian rift system and the southernmost rifts of Ethiopia, the Western rift including the Aswa shear zone in southern Sudan, the Eastern rift, and the NE-SW trending seismicity zones that are not associated with major rift structures in southern Africa. Knowledge of the tectonics of these regions forms the basis for characterizing the areal extent and configuration of source zones. The input parameters are given in Table 1.

Here we would like to emphasize the preliminary nature of the identification of source zones in the region. A thorough investigation based on a multi-disciplinary approach should be carried out to have well-defined seismic source zones for future seismic hazard assessment.

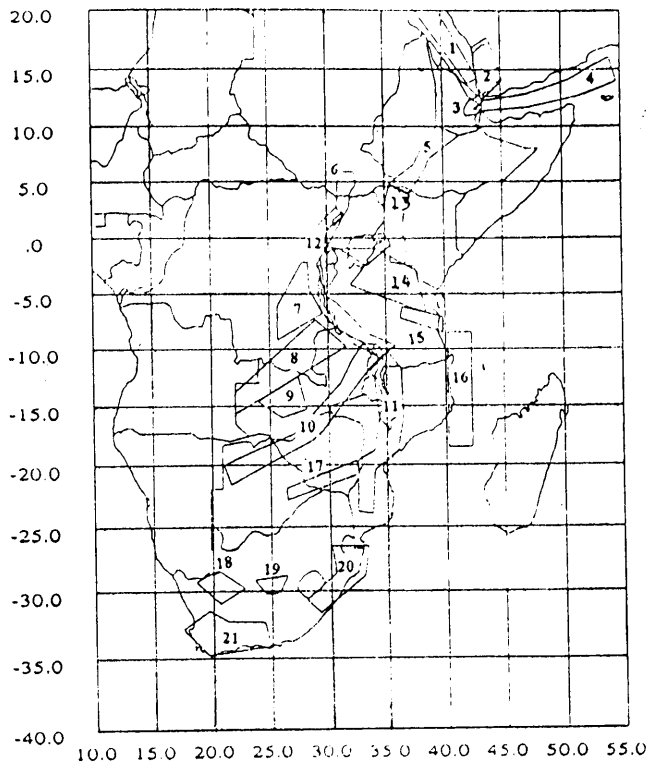

Fig. 2. Seismotectonic source zones contributing to hazard evaluation in The Eastern and Southern Africa. Numbers 1-21 in the figure show seismic source zones. (After ESARSWG Committee, 1996).

Table 1. Parameters used for seismic source zones. In the table M_0, M_1, λ and h denote lower threshold magnitude, upper threshold magnitude, activity rate and depth, respectively.

Zone	M_0	M_1	b-value	λ	h
1	**4.5**	**6.7**	**0.90**	**0.64**	**10.0**
2	**4.5**	**7.1**	**0.98**	**0.16**	**10.0**
3	**4.5**	**6.8**	**0.68**	**1.24**	**10.0**
4	**4.5**	**6.5**	**1.06**	**2.54**	**10.0**
5	**4.5**	**6.8**	**0.58**	**0.39**	**10.0**
6	**4.5**	**7.8**	**0.90**	**3.17**	**10.0**
7	**4.5**	**7.8**	**1.21**	**0.43**	**10.0**
8	**4.5**	**7.1**	**0.97**	**0.46**	**10.0**
9	**4.5**	**7.1**	**1.03**	**0.06**	**10.0**
10	**4.5**	**7.1**	**0.71**	**0.42**	**10.0**
11	**4.5**	**7.3**	**0.93**	**0.70**	**10.0**
12	**4.5**	**6.7**	**1.26**	**0.55**	**10.0**
13	**4.5**	**7.4**	**0.59**	**0.14**	**10.0**
14	**4.5**	**7.4**	**1.04**	**1.20**	**10.0**
15	**4.5**	**7.4**	**1.28**	**0.06**	**10.0**
16	**4.5**	**7.0**	**0.91**	**0.54**	**10.0**
17	**4.5**	**7.2**	**0.69**	**0.05**	**10.0**
18	**4.5**	**7.2**	**1.28**	**0.09**	**10.0**
19	**4.5**	**7.2**	**1.03**	**0.13**	**10.0**
20	**4.5**	**7.2**	**0.86**	**0.16**	**10.0**
21	**4.5**	**7.2**	**0.69**	**0.15**	**10.0**

3.5. Ground motion attenuation

In the current investigation, regional attenuation relations for peak horizontal ground acceleration as developed by Jonathan (1996) and Twesigomwe (1996) are used.

a) Jonathan's (1996) relation reads:

$$\ln A = 3.024 + 1.030M_s - 1.351 \ln R - 0.0008R + \varepsilon \quad (2)$$

b) Twesigomwe's (1996) relation reads:

$$\ln A = 2.832 + 0.886M_s - \ln R - 0.0025 R + \varepsilon \quad (3)$$

where M_s is surface wave magnitude, R the hypocentral distance and ε the standard deviation.

4. METHODS OF ANALYSIS

4.1. Methods

There are two main approaches for seismic hazard assessment. These are the probabilistic and the deterministic approaches.

For the probabilistic case, seismic hazard is defined as the probability that a certain level of ground motion be exceeded at a given place and within a given time period. The method results in an estimate of the likelihood of hazard at the location of interest and is mainly used when detailed mapping of active faults are not known.

On the other hand, the deterministic analysis requires as input discrete, single-valued events (maximum earthquake) and models to arrive at a description of earthquake hazard. The input parameters are seismic sources, size of damaging earthquake (controlling earthquake) and an earthquake ground motion attenuation relationship which provides estimates of ground motion such as displacement, velocity and acceleration from earthquake of a given magnitude at different distances.

In Eastern and Southern Africa detailed fault maps at a desirable scale indicating active faults are lacking to use the deterministic method. Also, one of the disadvantages of the deterministic seismic hazard analysis is that the results can easily be upset by the occurrence of new earthquakes and development of new hypotheses and understanding.

Regarding the probabilistic method, there are two approaches widely in use today. These are the extreme value method (Gumbel, 1954); and the method developed by Cornell (1968) and McGuire (1976, 1993).

The extreme value approach treats the earthquake data by considering the annual extremes of earthquakes that occur in a region. According to the theory, there are three types of asymptotic distributions from which the extremes are sampled. These distributions are called the first, second and third asymptotic distributions of Gumbel, or simply Gumbel I, II and III, respectively. The first type is not characterized by upper and lower limits (unlimited in both

directions) and thus usually used for the estimation of ground acceleration, velocity, or displacement. The second type of Gumbel's distribution is not proper for our case, because it assumes a lower limit of extreme values. The third type arises when the distribution is bounded from above (upper limit) and thus is used for maximum magnitudes which are obvious in the data. Even though the extreme value approach seems easier to use it is not the one recommended for the GSHAP purpose.

The other probabilistic approach to seismic hazard analysis most widely used is that of Cornell (1968) and McGuire (1976, 1993). Using the total probability theorem (McGuire, 1976), the probability of a given ground motion, say a (acceleration) being exceeded at a given site is expressed in the form:

$$P(A>a)=\iint P(A>a \mid m,r) f_M(m) f_R(r \mid m)\, dm\, dr \qquad (4)$$

where P (A > a) is the probability that a given acceleration will be exceeded and P (A > a| m, r) is the conditional probability given m and r. In eq. (4), m is a random variable. $f_M(m)$ is the independent probability distribution of m while $f_R(r|\ m)$ is the probability density function of r given m.

The existing scale of tectonic maps and the level of precision of the earthquake catalogue for our region imply that the location of earthquakes must be designated in terms of areal sources within which earthquake characteristics will be taken to be uniform. Thus, we employed the later probabilistic approach for the hazard results presented in this study. For the case considered here (areal seismic source zones), the probability density function, $f_R(r|\ m)$ is known in the process of numerical integration of eq.(4) from the configuration of source zones. The method is the one recommended for GSHAP.

4.2. Treating modeling uncertainty

Hazard estimates given by experts may sometimes be significantly different from each other for many reasons. One of the main reasons for the differences is due to the expert judgment on the input model parameters. The differences reflect uncertainties in modeling parameters. In practice, several possible seismic source zonation (areal source and major faults), recurrence parameters, ground motion relations, depth distribution of earthquakes can be found from literature. They may encourage one to suggest different values for the same input parameter. The most widely used method for combining these different inputs is the logic tree formalism (approach). It is a decision flow path consisting of nodes and branches, in which each branch represents a discrete choice of parameters. For example, the choice could be between two values of upper magnitudes, say M_1 = 6.5 or 7.0. In this approach a likelihood of being correct is assigned to each branch. In our case, the logic tree formalism is employed only to combine the two regional attenuation relations (both taken to be equally correct) mentioned above. All the other input parameters are fixed to the values given in Table 1. To accomplish the task of computation the FRISK88 computer program as supplied by R. K. McGuire is used.

5. RESULTS

Using the foregoing method, hazard maps for Eastern and Southern Africa for 10% probability of exceedence in 50 years, 10% probability of exceedence in 100 years, 10% probability of exceedence in 50 years(85th percentile), 10% probability of exceedence in 100 years (85th

percentile), 50 years return period, 100 years return period, 50 years return period (85th percentile), 100 years return period (85th percentile) are obtained. Figure 3 shows sample hazard maps for 10% probability of exceedence in 50 years (3a) and 10% probability of exceedence in 100 years (3b), respectively. A close look at figure 3b shows that high peak horizontal ground acceleration values (over 250 gals) are obtained for the Afar depression, the Western Gulf of Aden and the Western rift. For the same level of probability intermediate hazard values of the order of 180 gals are obtained for south western and northern Tanzania.

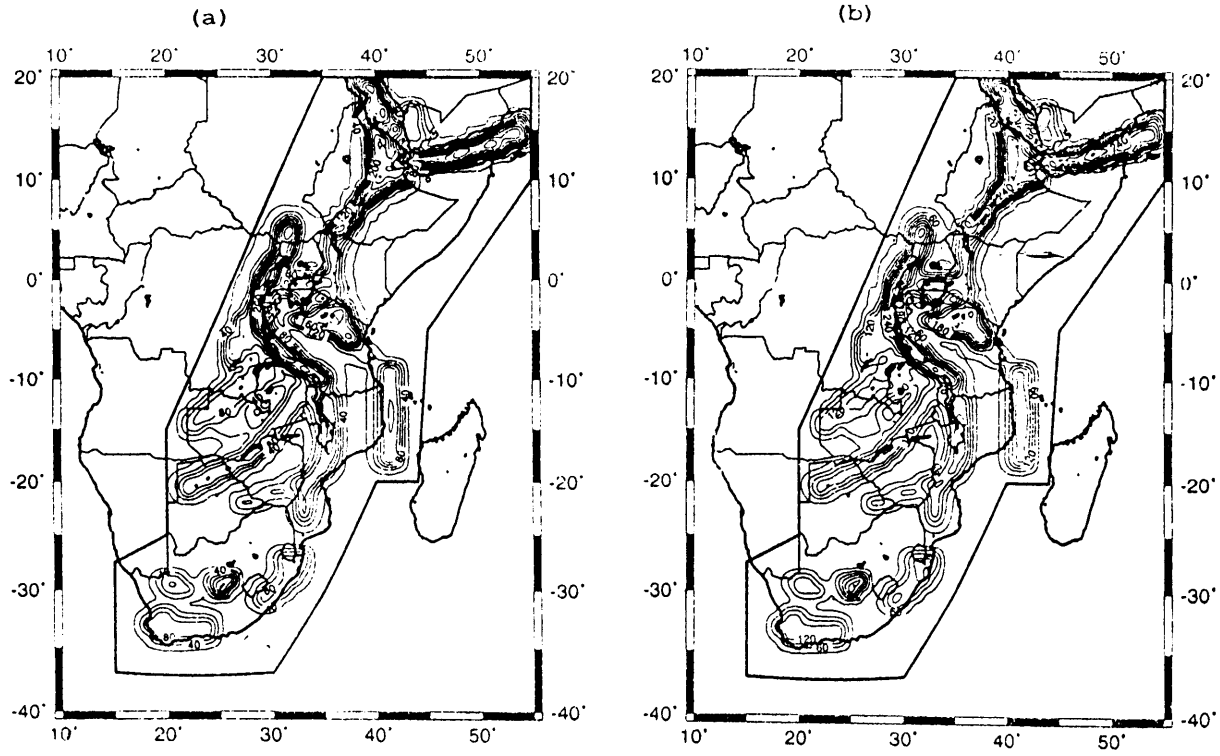

Fig. 3. Seismic hazard for the Eastern and Southern Africa. The hazards are for: a) 10% probability of exceedence in 50 years; b) 10% probability of exceedence in 100 years. The isolines give values of ground acceleration in units of gal.

Figure 4 shows hazard maps for 50 years return period (4a) and 100 years return period (4b), respectively. Comparison of Figs. 3 and 4 shows that even though the contour patterns of the two figures are similar the hazard values differ significantly.

In all the hazard maps presented in this paper, the hazard values are computed at 1.0 degrees interval both in latitude and longitude.

An attempt is also made to compute hazard at various probabilities for each capital city located in Eastern and Southern Africa. Figure 5 shows sample plot of peak horizontal ground acceleration versus annual probability of exceedence for the cieties of Asmara in the north and Harare in the south.

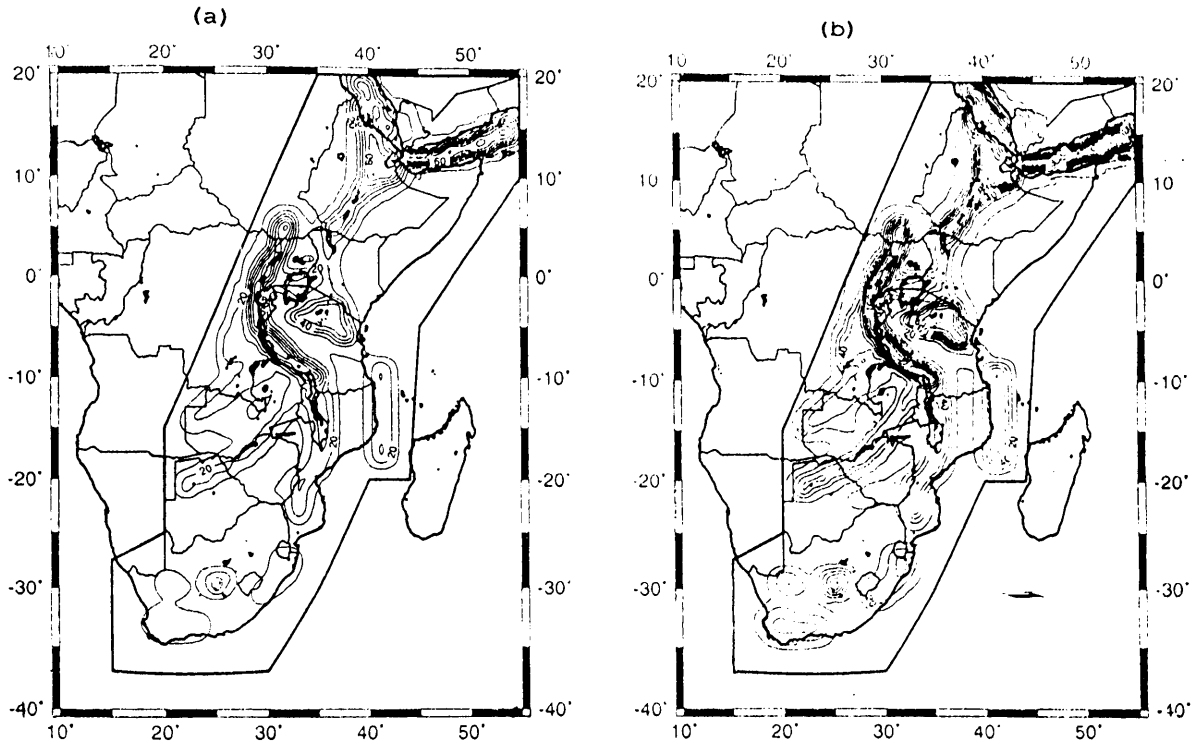

Fig. 4. Seismic hazard for the Eastern and Southern Africa. The hazards are for: a) 50 years return period ; b) 100 years return period. Other notations as in Figure 3.

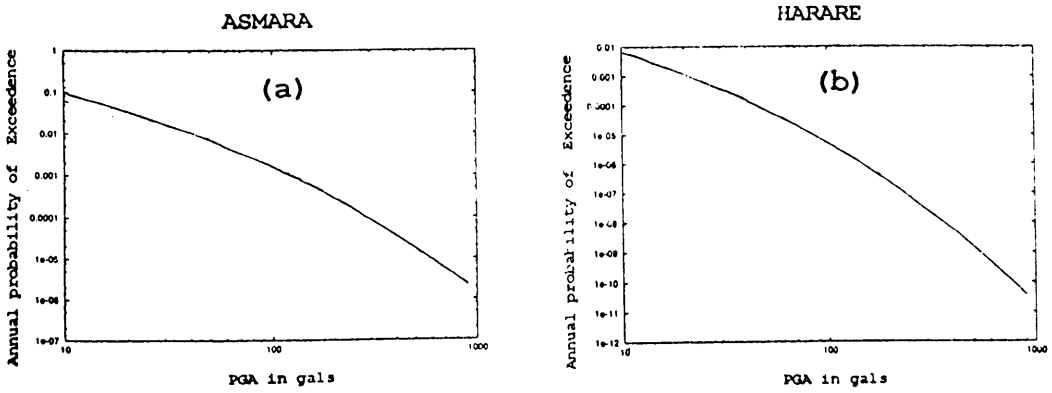

Fig. 5. Seismic hazard curves of peak horizontal ground acceleration versus annual rate of exceedence for: a) Asmara; b) Harare.

As can be seen from the figure, relatively high peak horizontal ground acceleration values are obtained for the northern cities.

6. DISCUSSION AND CONCLUDING REMARKS

The results presented in this paper (Fig. 3) show that relatively high peak horizontal ground acceleration values are obtained for Afar Depression and Djibouti area, southern Red Sea, Western rift including southern Sudan (i.e. Rwanda and Burundi, etc.) and south western and

northern Tanzania. This could be due to the high seismicity and/or the high occurrence rate of large earthquakes in the source regions mentioned above. The main contribution for the southern Sudan is attributed to the 1990 earthquake sequence (the largest magnitude being M_s=7.1).

The relatively low hazard values obtained for the southern part of the region under study may be attributed to the low seismic activity observed for this segment of the rift. Otherwise, the region has experienced the occurrence of some intermediate-size earthquakes in this century. Examples are the 1969 earthquakes in South Africa and the 1989 Salima earthquake in Malawi (M_s = 6.1).

The hazard results obtained for the nine selected sites (capital cities) also show that high hazard values are attributed to the northern cities when compared to those located in the southern part of the region.

Comparison of the results obtained here with the results of earlier works, specifically with earlier works done for the southern part of the region shows that the hazard values obtained here are lower. The discrepancy could be due to the different approaches employed (e.g. Hlatywayo, 1995) and different input parameters used (e.g. Twesgomwe, 1996; Chapola, 1997; Lombe, 1997).

The results presented in this paper are for rock type conditions. However, it is known that local soil conditions play a great role in amplifying seismic wave energy. Thus, hazard assessment which includes the effect of local geology and detail tectonics of the area of interest, especially major cities and economic centers should be carried out in the future. A thorough study based on a multi-disciplinary approach should be performed to have well defined seismic source zones for the region. Also, more work needs to be done to improve the catalogue for future improvement of the hazard results, especially for the southern part of the region.

ACKNOWLEDGEMENTS

The results presented in this paper were achieved during the 2nd, 3rd and 4th workshops on seismic hazard assessment for the Eastern and Southern Africa with the financial support of the International Program for Physical Sciences (IPPS) and the Global Seismic Hazard Assessment Program (GSHAP).

REFERENCES

Chapola, L. S. (1997). State of stress in East and Southern Africa and Seismic hazard analysis of Malawi. M.Sc. thesis, Inst. of Solid Earth Physics, Univ. of Bergen, Norway,143 pp.

Cornell, C.A. (1968). Engineering seismic risk analysis. Bull. Seism. Soc. Am. 18: 1583 - 1606.

ESARSWG Committee. (1996). Report on the seismic hazard analysisin Eastern and Southern Africa. Sixth Eastern and Southern Africa region Seismological workshop, 14 pp.

Gouin, P. (1976). Seismic zoning in Ethiopia. Bull. Geophys. Obs. (Ethiopia), 17: 1-46.

Gumbel, E. J. (1954). Statistical theory of extreme values and some practical applications, U. S. Dept. of Commerce, Applied Maths series 33, 51 pp.

Gutenberg, B. and Richter, C. F. (1954). Seismicity of the Earth and associated Phenomena. 2nd edn. Princeton University, Princeton New Jersy, 310 pp.

Hlatywayo, D. J. (1995). Seismotectonics and seismic hazard estimates in Central and Southern Africa. Ph.D. thesis, Seismology Dept., Uppsala University, Sweden.

Jonathan, E. (1996). Some aspects of seismicity in Zimbabwe and Eastern and Southern Africa. M.Sc. thesis, Inst. of Solid Earth Physics, Univ. of Bergen, Norway, 100 pp.

Kebede, F. and Asfaw, L. M. (1996). Seismic hazard assessment or the Ethiopia and the neighboring countries. SINET (Ethiopian Journal of Science), 19 (1), 73-107.

Kebede, F. and Kulhanek, O. (1994). Spatial and temporal variations of b-value along the East African rift system and the southern Red Sea. Phys. Earth Planet. Inter. 83: 249-264.

Kebede, F. and Van Eck. T. (1997). Probabilistic seismic hazard assessment for the Horn of Africa based on seismotectonic regionalization, Tectonophysics, 270 (3-4), 221-238.

Lazarov, R. and Christoskov, L. (1981). Statistical aspects of magnitude relation for Bulgaria. Proceedings of the 2nd International Symposium on the analysis of seismicity and on seismic hazard, Liblie, Czechoslovakia, 56-66.

Lombe, D. K. (1997). Seismic hazard assessment for Zambia and surrounding areas. M.Sc. thesis, Inst. of Solid Earth Physics, Univ. of Bergen, Norway, 100 pp.

McConnell, R. B. (1972). Geological development of the rift system of eastern Africa. Bull. Geol. Soc. Am., 83: 2549-2572.

McGuire, R. K. (1976). Evaluation of Earthquake risk to site. U.S. Geol. Survey Open-file Report 76 - 77.

McGuire, R. K. (1993). Computation of seismic Hazard. Ann. Di Geofisica 36 (3-4): 181-200.

Shudofsky, G. N. (1985). Source mechanisms and focal depths of East African earthquakes using Rayleigh wave inversion and body-wave modeling. Geophys. J. Astron. Soc. 83: 563-614.

Twesigomwe, E. M. (1996). Probabilistic seismic hazard assessment of Uganda, Ph.D. Thesis, Dept. of Physics, Makerere University, Uganda, 152 pp.

Weichert, D. H. (1980). Estimation of the Earthquake recurrence parameters for unequal observation periods for different magnitudes, Bull. Seism. Soc. Am. 70: 1337-1346.

SEISMIC DATA CATALOGUES AND ATTENUATION RELATIONS
- A General Review on Data Available in the Eastern and Southern Africa Region

Dumisani John Hlatywayo and Ezekiel Jonathan

Goetz Observatory, Zimbabwe Meteorological Services, Seismic Unit Section, Box Ac 65, Ascot, Bulawayo, Zimbabwe. Email: goetz@harare.iafrica.com Fax : 263 9 77811

1. INTRODUCTION

It is necessary to prepare a reliable earthquake catalogue before work on seismic hazard assessment for any given area or region can be embarked upon. This fact has been recognised as one of the basic requirements in seismic hazard assessment work (Giardini & Basham, 1993). Most catalogues that have been constructed are from seismological bulletins or lists of earthquake phases. These sources have provided a primary data base for nearly all catalogues that have recently been compiled by a number of workers in the East and Southern Africa region.

Most parts of the African continent are considered to be aseismic. Research on seismicity on the continent has been confined to areas along the East Africa rift system. The East Africa rift is one of the few rift systems found on land. It therefore offers scientists an opportunity to have an insight into the driving forces or mechanisms of a continental rift. Research work has been in progress in the active regions of the rift; for example, in the Rukwa-Malawi area, the Lake Tanganyika-Uganda-Southern Sudan region, the eastern arm of the rift system in Kenya and the Afar Depression in the Horn of Africa. Work concentrated in attempting to understand the nature of stresses along the rift, the focal mechanisms and the general seismicity. A number of earthquake catalogues for specific areas within the region have been compiled by either individuals or groups of persons. Most of these catalogues contain data that satisfied the needs and requirements of the research that was being carried out. The earliest catalogues include work by Fairhead and Girdler (1971), Sykes and Landisman (1964), Fairhead and Stuart (1982), Maasha (1975) and Båth (1975). The area covered by each catalogue was also subject to the requirements of the study at the time. These types of catalogues continue to be compiled up to the present time. More recent catalogues include those by workers like Iranga (1991), Asfaw (1992), Hlatywayo (1992), Musson (1994), Twesigomwe (1996), Turyomurugyendo (1996), Chapola (1997) and Lombe (1997). In addition, there exists data on the open files from agencies like the National Earthquake Information Centre (NEIC) and the International Seismological Centre (ISC). This paper reviews some of the more recent catalogues that have been compiled for the east and southern Africa region or portions of it. Most of these data have been compiled to form data bases from which seismic hazard estimates have been determined. The eight catalogues reviewed in this paper are believed to contain nearly all earthquake data known to exist in the region.

2. SEISMIC DATA SOURCES

Although seismic monitoring along the East Africa rift dates back more than thirty-five years, it was done mainly on "piece-meal" basis; that is, seismic stations were deployed in an area for a specific period. Few stations therefore have been in continuous operation for a long time. These include stations like Addis Ababa in Ethiopia, Nairobi in Kenya, Lwiro in the

Democratic Republic of the Congo, Bulawayo in Zimbabwe, Pretoria in South Africa and Tananarive in Madagascar. The middle of the 1980's witnessed an improvement in the overall seismic station network coverage in the region as individual countries endeavoured to set up national seismological networks. Although station coverage improved over the past ten years, individual national networks continue to experience occasional station break-downs and persistent shortages of spare parts for seismic equipment maintenance. These problems have reduced the detection capability of the network in the region; consequently, data completeness has been affected.

For this region, reliable instrumental data became available in the early 1960's when the World Wide Standard Seismograph Network (WWSSN) operated by the United States Geological Survey (USGS) was established. Data found in catalogues for the period prior to 1960 comprise mainly historical data. From 1992, nine countries from the east and southern Africa region started to come together twice annually, to prepare bulletins of events that have occurred in the region. These bulletins were prepared for six-month periods. Epicentres for regional events that were localised improved, particularly for events of magnitude ≥ 4 that were recorded by a large number of stations. For small magnitude events, local networks within the broad-based regional network, continued to provide the epicentre locations.

3. CATALOGUES

Earlier catalogues were compiled to study the seismicity of the region or portions of it. The later catalogues have been compiled to provide the necessary data base for the calculation of seismic hazard estimates. In this paper, we shall check and discuss the completeness of these catalogues with reference to event magnitude distribution with time. We believe this gives a sufficient view of the completeness of the catalogues.

3.1 Tanzania catalogue

The Tanzania catalogue (Iranga, 1991) was prepared for the period 1846 - 1988 from both macroseismic and instrumental data for the region bounded by latitude 0° - 12° S and longitude 29° - 42° E. Continuous and uninterrupted earthquake data flow only starts in 1954. The catalogue was prepared in order to study and understand the seismicity of Tanzania. Most of its data are drawn from the International Seismological Summaries (ISS) and ISC bulletins for the period 1910 - 1987, NEIC catalogue for the period 1950 - 1989, Ambraseys, for the period 1846 - 1971, Båth, for the period 1910 - 1974 and Shah, for the period 1880 - 1979. All macroseismic data in the catalogue were sourced from Ambraseys (1972).

Except for the seismic stations at Dar -es - Salaam (1906 - 1914), Dodoma (1960 -1961) and the Stigler's Gorge Seismic network (1978 - 1981), there were no permanent seismic stations operating in Tanzania until after 1990. All data for the region are drawn from teleseismic seismograph stations like Lwiro in the Democratic Republic of the Congo, Bulawayo in Zimbabwe, Tananarive in Madagascar, Nairobi in Kenya and Addis Ababa in Ethiopia. With no local seismic stations to argument teleseismic stations, epicentre accuracy for local events is often compromised.

This catalogue contains 2767 events. Macroseismic events from Ambraseys (1972) have assigned '*personal*' magnitudes. Examination of data prior to the year 1950 (these were derived from macroseismic data from Ambraseys) reveal that the bulk of events were assigned magnitudes ranging between 4.0 and 4.8 regressed from macroseismic intensities. For all data

in the catalogue, magnitude regression relations for the five agencies reporting magnitude were used to unify magnitudes in the catalogue. An analysis of the data shows its completeness in both space and time. Data in the catalogue may be considered complete for magnitude ≥ 4.5 for the period 1954 to 1988 (Fig. 1).

Few events occurred before 1900. For this period, data are all historical and dependent upon the historical information that the author could lay his hands upon. The gap occurring between 1920 and 1940 may not be easily explained if it be not due to absence of historical information. It is therefore, a manifestation of the temporal in-completeness of the data in the catalogue. After 1910, a number of events with magnitudes > 5 are on record. This scenario results from the criterion used in assigning magnitudes to events. Before one uses the data for any specific study, it may be necessary to re-examine the magnitudes that were regressed from Ambraseys' data.

There are few events of magnitude < 3.5. These events occurred during the period 1960 - 1961 when the Dodoma station was operational. Before unifying the magnitudes, these events had magnitudes < 3.0. That the bulk of the data in the catalogue has magnitudes $4.0 < m < 5.5$ may be attributed to the regression relations used in unifying magnitude in the data set. Genuine small magnitude events were therefore compromised for magnitude homogeneity.

3.2. Zimbabwe catalogue

The Zimbabwe catalogue was prepared for a period of 32 years, from 1959 to 1990 and contains 3433 events (Hlatywayo, 1992). It covers an area bounded by latitudes 14° - 24° S and longitudes 24° - 34° E. All data are instrumental. Although some agencies like NEIC and ISC contributed data to the catalogue, the bulk of data were sourced from the Zimbabwe Meteorological Services Seismological bulletins at Bulawayo, Zimbabwe. These bulletins were compiled from event epicentre locations from the Zimbabwe seismic network which operated no more than five stations at any one given period. Epicentres were determined manually and are claimed to be accurate to within 0.2° in both latitude and longitude of the epicentre.

Of the 3433 events in the catalogue, there are nearly 800 events that occurred in the Lake Kariba region that had no determined epicentres but have been assigned arbitrary epicentres. Event magnitudes were unified using magnitude regression relations to a body wave magnitude type. There is neither historical nor macroseismic data in this catalogue. Taking into account the brevity of the catalogue period, it may be considered complete in space and time for magnitudes ≥ 3.6 (Fig. 2). Although the author gives reasons for converting the Bulawayo (BUL) MbLg magnitudes to another unified magnitude, since Bulawayo provided more than 90% of magnitude data in the catalogue, it would have been more plausible and reasonable to have converted the 10% magnitude data that was not from Bulawayo, to BUL MbLg. The effect of magnitude regression was to raise the magnitudes of smaller magnitude events to slightly yet significantly noticeable larger magnitudes. However, the catalogue lists the original BUL magnitudes for whoever may be interested in them.

3.3. Malawi catalogue

The Malawi catalogue (Chapola, 1997) covers the period 1900 to 1994. It has three main sources: Turyomurugyendo (1996) for the period 627 to 1994, NEIC, for the period 627 to 1963 and the ISC bulletins, covering the period 1964 to 1993. A few additional events were

sourced from the eastern and southern African Seismological Workshop (EAF) bulletins of 1993 and 1994. The catalogue is prepared to form a prime data-base for input parameters required for seismic hazard study of Malawi. The area covered in the study is bounded by latitude 7° S to 19° S and 31° E to 38° E. There are 1692 events, 41 of which are believed to be fore- and after-shock events.

By 1972, there were two stations (Chileka and Mzuzu) in Malawi. These two stations were operated by Zimbabwe until late in the 1980's. Seismogram analysis was done at Bulawayo in Zimbabwe. Events were located using mainly the Zimbabwe national seismic network. All locations were manually done, using the "*swinging of arcs*" method. Because the Zimbabwe seismic network was not dense, small magnitude events were not recorded by all stations to sufficiently provide accurate epicentral data. There are therefore large magnitude and epicentre uncertainties in the data. However, large events of magnitude ≥ 5.5 are generally well recorded at both regional and teleseismic distances. With a larger number of recording stations, more accurate epicentres for the larger events may be determined. There are 27 such events in the catalogue.

Bulawayo gives the largest portion of magnitude data reported in the catalogue. Magnitudes in the catalogue are unified to a surface wave magnitude type using magnitude regression relations. Fig. 3 shows that there are no data with magnitude < 3.3 in the data set except for the last three years of the catalogue period. There are two possible reasons for the absence of this data in this catalogue. Firstly, as pointed out earlier, the main source of data was Bulawayo. Bulawayo used a magnitude reporting threshold of 2.8 on the MbLg magnitude scale. Secondly, the regression relations used tended to raise magnitude values to above the unified magnitude value of 3.3. That this is so may be confirmed from a comparison of data presentations in the two figures, Fig. 2 for the Zimbabwe catalogue and Fig. 3 for the Malawi data. The pattern of data in the two figures is the same for the period 1966 to 1990 except for the magnitude values which are different because the events covered in the two figures are not all the same, and the regression relations used in unifying magnitude data are different.

The period before 1955 is characterised by a scarcity of data from historical records. Data in the catalogue may be assumed complete for magnitude ≥ 4.5 from 1950 to 1995, while for the period 1966 to 1994, it is complete for magnitude ≥ 3.6. For the period 1920 to 1940, there are no events on record in the data set. That there are no earthquakes on record for this period may be attributed to the absence of historical data. It is therefore not worth the effort to attempt to determine completeness of data for the period 1900 to 1950 for this catalogue.

3.4 Uganda catalogue

The Uganda catalogue (Twesigomwe, 1996) was prepared specifically as input for seismic hazard studies in Uganda. It is for the area bounded by latitude 6° N to 4° S and 27°E to 37° E. Data sources include ISC and NEIC bulletins, Ambraseys (1991), Ambraseys & Adams (1986), Sykes & Landisman (1964), Shah (1986) and Wohlenberg (1968). Original sources for data are detailed in Twesigomwe (1996), giving originally reported earthquake magnitudes. There are 1631 events in the catalogue, spanning the period from 1850 to 1991. Magnitude data for 1561 events in the data set are unified to a surface wave magnitude type using regression relations.

The period 1850 to 1950 is characterised by a scarcity of data. Data were sourced from historical records. Continuous data flow only started after 1950. Fig. 4 shows the difficulty associated with attempting to attribute a '*blanket*' statement on data completeness for this catalogue. We may only assume data in the catalogue to be complete for magnitude > 6 for portions of the catalogue period. For this catalogue, the period 1900 to 1956 is one such example. There was an out-burst of data flow during the period 1957 to 1971. This includes the period when the station at Entebbe in Uganda was in operation. There-after, the nearest permanent seismic station was perhaps, Lwiro in the Democratic Republic of the Congo. For this period, data *may only be assumed* complete for magnitude ≥ 3.0. For the remainder of the period, data are complete for magnitude ≥ 4.0.

The pattern of magnitudes represented in Fig. 4, unlike those found in other catalogues in the region, do not show a heavy influence from regression relations used to unify magnitude data in the catalogue. The main problems with data in this catalogue are its lack of completeness. Even for the last portion of the catalogue period (1957 to 1991), it is difficult to ascribe completeness for a given magnitude to the whole period; hence, the *assumption on completeness*. This data set is a good example of an incomplete catalogue. Data analysis for calculations of b-values and activity rates required as input in seismic hazard studies should employ methods that take into account data incompleteness. The catalogue also lists original magnitudes as reported by agencies from whom data have been sourced. Any worker who wishes to use the data therefore has an option to re-examine the earthquake magnitudes and carry out his own magnitude unification.

3.5. Zambia catalogue

Zambia catalogue (Lombe, 1997) was extracted from the ECESA catalogue (Turyomurugyendo, 1996). Details of sources for the ECESA catalogue are given later in this paper. This catalogue was prepared for an area bounded by latitude 8° and 18° S and longitude 22° and 34° E. It contains a total of 5 325 events and was prepared as source for input parameters to seismic hazard calculations in Zambia. Although the unified magnitudes in this catalogue are not exactly those for the ECESA catalogue, the procedure followed in unifying magnitude was exactly the same. Body wave magnitudes were assumed to be equivalents, irrespective of reporting agency. It is well known that body wave magnitudes calculated by different agencies are not exactly equal. Magnitude regressions were however done under the assumption contrary to this fact.

Figure 5 looks much the same as Fig. 8. This is not surprising since the Zambia data is a sub-set of the ECESA catalogue. Completeness of the Zambia data therefore follows that of the ECESA catalogue. It is worth pointing out that the shape of the figure for the period 1960 to 1984 is greatly influenced by data from the Zimbabwe network which contributed the bulk of magnitude data in the ECESA catalogue for that period. What has been discussed on the Zimbabwe and Malawi data on magnitudes directly applies to this catalogue as well.

3.6. Ethiopia catalogue

The Ethiopia catalogue spans the period 800 to 1994. Magnitude data for the period 1900 to 1994 are shown in Fig. 6. Data were obtained from Ethiopia (*courtesy of Kebede from the*

Addis Ababa Geophysical Observatory). The main sources of data upon which this catalogue was built are the works of Gouin, 1979 (Kebede & van Eck, 1997). Other supplementary sources included NEIC and ISC bulletins, BGS catalogue (Musson, 1994), Ambraseys & Adams (1992), Ambraseys et. al. (1994) and the Addis Ababa Observatory seismological records. Magnitude data are unified to a surface wave magnitude type using regression relations. Details of the catalogue preparation are found in Kebede & van Eck (1997).

As with all other catalogues within the region, it is difficult to assign a precise magnitude value for catalogue completeness for the period not covered by the instrumental record. However, data in Fig. 6 may be *assumed* complete for magnitude ≥ 5.5 for the period 1900 to 1955; and thereafter, it is complete for magnitude ≥ 4.5. We could not however establish as to the cause of the gap in the record for magnitudes 3.0 to 4.0 for the period 1970 to 1994. It could have resulted from the effect of regressing magnitude data in magnitude data unification. On the other hand, if the gap is genuine, we are unable to give a reasonable explanation for its existence.

Unlike other catalogues, this catalogue contains a substantial number of events from the pre-instrumental period, 1900 to 1960. Although the data shows some elements of incompleteness for the period 1900 to 1955 for magnitudes below 6 when compared to the later period 1956 to 1994, this catalogue represents one of the best well researched historical record and well compiled data within the region.

3.7. BGS SSAEC catalogue

The British Geological Survey (BGS) Sub-Saharan African Earthquake Catalogue (SSAEC), Musson (1994) was prepared with the object of providing a primary catalogue for preliminary seismic hazard study in the Africa region, south of the Sahara Desert. It was hoped that this catalogue would form prime data for work on seismic hazard study in the Eastern and Southern Africa region during the Global Seismic Hazard Assessment Programme (GSHAP) period. It also provides a foundation upon which improved catalogues may be built in future studies on seismic hazard. The catalogue was compiled from a variety of sources with varying uncertainties and accuracy. Earthquake magnitudes in the catalogue were unified to a surface wave magnitude type. Unification of magnitudes was achieved using empirical relations from Marshall (1970) and Marrow (1992). Events with no known magnitudes were assigned an *assumed* magnitude value of 5.0 while events with only macroseismic reported intensity were estimated.

The full data set comprised over 14000 events. A minimum magnitude threshold of 4.0 was applied to all data. The SSAEC catalogue with a minimum magnitude 4.0 and containing a total of 2325 events that occurred during the period 1071 to 1993 evolved from the data set. The original data set with all events is available to any who is interested in examining it and making improvements on the SSAEC catalogue. The area covered by the catalogue is bounded by latitude 20° N and 40° S and longitude 20° W and 55°E.

The main contributors to events in the catalogue include the ISC (1517 events), NEIC Preliminary Determination of Epicentres (PDE) (193 events), Rothé (123 events) and the Bureau Centrale and International Seismologique (142 events). Details of other sources used in the data compilation may be found in Musson (1994). Fig. 7 shows a number of events,

magnitude 5.0 to have occurred between 1900 and 1960. These events originally had no reported magnitudes. The magnitude of 5.0 was arbitrarily assigned to these events by the author.

As may be seen from Fig 7 (for the period 1900 - 1993), unlike all data in the other catalogues discussed earlier in this paper, earthquake magnitude data do not show bias towards regression relations because empirical relations were used instead. Data in the catalogue may best be considered to be complete for different magnitude levels. Discarding the 5.0 assigned magnitude events that occurred before 1960, this catalogue may be considered complete for magnitude ≥ 6 for the period 1900 to 1993. The later portion of the catalogue period, 1960 to 1993, data are complete for magnitude ≥ 4.0.

3.8. ECESA catalogue

The Earthquake catalogue for eastern and southern Africa (ECESA), Turyomurugyendo (1996), was prepared specifically for on-going seismic hazard study in the region carried out jointly by nine countries, namely; Eritrea and Ethiopia to the north, Uganda, Tanzania and Kenya in the central regions and Zambia, Malawi, Zimbabwe and South Africa to the south. This catalogue covers an area that is slightly less than that covered by the SSAEC catalogue and is bounded by latitudes 25° N and 40° S and longitude 10° E and 55° E. It covers the period 627 - 1994. There are three main sources for data, namely, NEIC data-base (period, 627 to 1963), ISC bulletins (period, 1964 to 1993) and EAF, for the period 1993 to 1995. Other sources included papers by individuals like Ambraseys & Adams (1986), Båth (1975), Sykes & Landisman (1964), Iranga (1991), Asfaw (1992) and Musson (1994). There are 13836 events in the catalogue.

Magnitude data were unified to surface wave magnitude type. Too *simple assumptions* on body wave magnitudes reported by various agencies, were made. All body-wave magnitudes were assumed to be equivalent. By the same token, all reported surface wave magnitudes were assumed to be equivalent irrespective of the reporting agency. One regression relation for all Ms magnitudes against all mb magnitudes reported by all agencies was determined. The resulting regression relation was then used to unify magnitudes in the catalogue. This over simplification of magnitude types introduces gross errors in magnitude values for events in the catalogue and therefore affects the homogeneity of the catalogue.

There is a large number of events in the SSAEC catalogue that do not appear in this catalogue. A clear example is in the events to the south east of the Cape Peninsula, in the off-shore Mozambique area and east of the Davis ridge which are in the SSAEC catalogue but are absent in this catalogue. The completeness figure (Fig. 8), shows a consistent line of events of magnitude 4.0 to have occurred between 1920 and 1963. These events were arbitrarily assigned magnitude, Ms = 4.0. Musson assigned magnitude, Ms = 5.0 to these events. Magnitude, Ms = 5.0 seems more likely than Ms = 4.0 if we take cognisance of the fact that these events were obtained from historical data records. For the period 1966 to 1990, data profile in Fig. 8 shows the influence of the Zimbabwe network (see Fig. 2) which contributed a large portion of the epicentral data, and the Entebbe station in operation between 1966 and 1971.

Despite the erroneous methods used in magnitude data unification, Fig. 8 shows that data in this catalogue *may be assumed* complete for the period 1900 to 1966 for magnitude, Ms > 5.0 and complete for magnitude, Ms ≥ 2.7 for the remainder of the period. It remains though to warn any one who may want to use this data to make sure that he re-evaluates the magnitudes and carries out his own magnitude data unification.

4. ATTENUATION RELATIONS

An attenuation model expresses how ground motion parameters change with distance, for a certain magnitude. Attenuation relations are normally developed by applying statistical regression analyses to data recorded by strong motion instruments, e.g., accelerographs. Usually, the attenuation model is of a functional type. The functional model is chosen such that the variables are kept to a minimum. Variables should be those whose inclusion in the model have a physical reason (Joyner and Boore, 1988). A general form of some of the models used is (Boore and Joyner, 1982);

$$Y = \frac{b_1 e^{b_2 m} e^{b_3 D} e^{b_5 S} e^{b_6 P}}{D^{b_4}} \qquad (1)$$

where, Y is the required ground motion parameter, M the magnitude, D is the distance, S is a constant representing the local site geology (0 for rock, 1 for soil), and P is the uncertainty in the prediction (0 and 1 for 50 and 84 percentile values respectively). b_i (i = 1 - 6), are constants which have to be determined from regression analyses of the observed data. The above equation may be expressed as,

$$\ln Y = \text{constant} + b_2 M + b_3 D - b_4 \ln D + b_5 S + b_6 P \qquad (2)$$

The physical basis for this model is found in Boore and Joyner, (1982). Magnitude has been expressed as an exponential term since it is a logarithmic measure of ground motion. Dependence on distance accounts for the anelastic attenuation (b_3) and geometrical spreading (b_4). The S term accounts for the notion that site effects should be multiplicative and the uncertainty term borders on the assumption of a log-normal distribution of the observations about the regression line.

Attenuation relations of the form of equation 2, are *critical* input in seismic hazard analysis. The deterministic method and the probabilistic approach, commonly used in seismic hazard analysis, both require an attenuation relation. The aim in seismic hazard analysis is to determine the likelihood of different levels of ground motion being exceeded at a site. Attenuation of seismic waves is, in general, affected by the following factors: the earthquake source, the propagation path from source to the site, and the geologic conditions beneath the site.

As cited earlier in this paper, seismic activity in the eastern and southern Africa region, is controlled by tectonic processes associated with the east Africa rift system which is considered by many to be the best example of continental rifting (Fairhead and Stewart, 1982; Kebede, 1989). The influence of the rift is evident from the seismic activity which clearly outlines this feature on the continent. Within the region a number of studies have been and are still being carried out on seismic hazard analysis.

There is however only one attenuation relation by Jonathan (1996) that has been developed for the region. All other relations have been adopted and modified for the regions where they have been used in seismic studies. Where available, attenuation relations used by workers from within the region in estimating seismic hazard for particular areas will be described briefly in this paper.

4.1. Ethiopia

In Ethiopia three attenuation relations have been used for seismic hazard calculations (Kebede and van Eck, 1997). These relations are the Joyner and Boore (1988), the Joyner and Fumal (1986) and Asfaw (1986) attenuation relations.

(a) strong ground motion attenuation

The horizontal peak ground acceleration attenuation relation (Joyner and Boore, 1988) is given as,

$$\ln A_{\max} = 0.43 + 0.23(M_w - 6) - \ln r - 0.0027r + \varepsilon \qquad (3)$$

where $r = (R^2 + h^2)^{\frac{1}{2}}$ with R being the shortest distance in kilometres to the surface rupture; h was fixed at 8 km. A_{max} is the horizontal component of peak ground acceleration and $\varepsilon = 0.28$ is the standard deviation. M_w is the moment magnitude obtained from the magnitude - moment relation as obtained empirically by Hanks (1979) using M_s within the magnitude interval 5.0 to 7.7.

Justification for the use of this attenuation relation was based on the fact that, both California (the region for which it as developed) and the Horn of Africa regions have substantial parts of their surface area as plate boundaries running through them. Secondly, the hypocentral depths of earthquakes which significantly influence strong ground motion are, in both regions, constrained to the crust.

(b) Frequency dependent attenuation

For engineering purposes the frequency content of the strong motion is usually of more importance than the horizontal or vertical peak ground acceleration. Since for the peak ground acceleration, there are no attenuation information available for spectral amplitudes, a relation based on California data developed by Joyner and Fumal (1986) was used. This relation is given as

$$\ln a(\tau) = c_o(\tau) + c_1(\tau)(M_w - 6) + c_2(\tau)(M_w - 6)^2 + c_3(\tau)\ln r + c_4(\tau)r + \varepsilon(\tau) \qquad (4)$$

$a(\tau)$ is the amplitude of the randomly oriented component of the horizontal-pseudo velocity (cms^{-1}) at a period τ for the 5% damped spectral response. $r = (R^2 + h^2)^{\frac{1}{2}}$ is the same as in the Joyner and Boore relation.

(c) Intensity attenuation

The intensity attenuation (Asfaw, 1986), for M_L, obtained using regional data, was also used (Kebede and van Eck, 1997). The relation is given as

$$I = 4.71 - 2.43 \log R + 1.04 M_S + \varepsilon \quad (5)$$

where M_L was replaced by M_s using a regional empirical relation between M_L and M_s. ε was set to be equal to 0.43, R is the hypocentral distance in kilometres.

4.2. Zimbabwe

Attenuation relation for input into the seismic hazard study for this region was obtained from random vibration method (Hlatywayo, 1997). The relation uses a Fourier acceleration spectrum A(f) which assumes a constant-stress-drop and an ω^{-2} source model of Brune (1970). The relation is given as

$$A(f) = CG(R)S(f)D(f)F(f) \quad (6)$$

where C is a scaling factor, G(R) accounts for the geometrical spreading of the seismic waves, S(f) is the source spectrum dependent on the seismic moment, D(f) is the diminution function and F(f) is a filtering term.

The relation requires input parameters like $\Delta\sigma$ (stress drop) and Q_o (the quality factor).

$\Delta\sigma$ = 100 bars was chosen. Such a value has been used in other regions e.g. California and eastern North America which are of continental crust similar to the central southern Africa region. The value of Q_o = 600 used is an average of Q_o values obtained for the region by different workers like Chow et. al. (1980), Xie and Mitchel (1990), and Hlatywayo and Midzi (1995). In the frequency dependent relation Q(f);

$$Q(f) = Q_o f^{\eta} \quad (7)$$

η was set to 1.

4.3. Uganda

A generalised attenuation relation (Joyner and Boore, 1988) given as,

$$\ln A = c_1 + c_2 m + c_3 \ln R + c_4 R + \varepsilon \quad (8)$$

was used in Uganda (Twesigomwe, 1996). The constants, c_1, c_2 and c_3 were taken from the attenuation relation of Krinitzy et. al. (1988) developed for eastern Canada for shallow earthquakes (depths < 20 km) and for hard rock sites. The author argues that Uganda is primarily situated on Precambrian metamorphosed formation which probably exhibits attenuation to seismic waves that is similar to that of eastern Canada. The constant c_4, accounts for anelastic attenuation and / or scattering. It can be expressed as

$$c_4 = \frac{-\pi f}{v Q(f)} \quad (9)$$

Scientific Technical Report STR 98/05
DOI: 10.2312/GFZ.b103-98055

where f is the frequency, v is the seismic wave velocity and Q(f) is the seismic quality factor. Values of Q_o = 360 and η = 0.5 were used for f = 1 Hz, giving c_4 = -0.0025 used in the attenuation equation. The attenuation relation used in Uganda is therefore given as

$$\ln A = 2.832 + 0.886 M_S - \ln R - 0.0025R + \varepsilon \qquad (10)$$

with peak ground acceleration measured in cms^{-2}.

The constant term and the scaling coefficient of M_s relate to new excitation of earthquake wave motion which is considered to be more or less the same for similar tectonic conditions (Hanks and Johnston, 1992; Bungum et. al., 1992).

4.5. Zambia

Lombe (1997) used Donovan's global attenuation relation (Donavan, 1973) given by

$$\ln A = 7.19 + 0.58 M_W - 1.52 \ln(R - 25) \qquad (11)$$

for seismic hazard calculations in Zambia. In this relation, A is peak ground acceleration in cms^{-2}, R is the epicentral distance in kilometres, M_w is the moment magnitude. The standard deviation of the natural logarithm of A, σ_{lnA} is given as 0.84. There were no attempts to modify the relation to the Zambian geological and tectonic condition.

4.6. Malawi

In estimating seismic hazard for Malawi (Chapola, 1997), three attenuation relations were used.

(a) Jonathan's (1996) attenuation relation

This relation, derived in a manner similar to that used by Hlatywayo (1997), assumes a Fourier acceleration spectra of the S-wave, a(f) , given by

$$a(f) = CG(R)S(f)D(f) \qquad (12)$$

for a constant stress-drop and an ω^{-2} source model of Brune (1970). In this relation, C is a scaling factor, G(R) is the geometrical spreading term, S(f) is the source function and D(f) is the diminution function which accounts for the loss of energy due to internal friction and scattering.

This attenuation relation was derived using the theory of random vibration. The required input parameters were partially validated using some of the available digital data from the region. The results obtained are expressed mathematically as

$$\ln A = 3.024 + 1.030 M_W - 1.351 \ln R - 0.0008R + \varepsilon \qquad (13)$$

(b) Twesigomwe's (1996) attenuation relation

$$\ln A = 2.832 + 0.886 M_S - \ln R - 0.0025R + \varepsilon \quad (14)$$

(c) Atkinson's (1984) attenuation relation

$$\ln A = 5.943 + 0.373M - \ln R - 0.001R + \varepsilon \quad (15)$$

where for all the equations above, A is the peak ground acceleration (cms^{-2}), M is the moment magnitude, M_s is the surface wave magnitude, R is the focal distance and ε is the uncertainty in the attenuation. An ε value of 0.6 was used for all the three attenuation relations.

5. REMARKS

Earthquake catalogues for the eastern and southern Africa region are complete for magnitude ≥ 4.5 for the period after 1960. Data in this period are all instrumental. For any particular area within the region and for the period before 1960, data are characterised by incompleteness. Most historical data are assigned either arbitrary magnitudes or magnitudes regressed from macroseismic intensity. Catalogues have been compiled from different sources reporting a variety of earthquake magnitudes. In an attempt to create homogeneity in magnitude data, various workers have unified magnitudes using regression relations. Regression relations usually have a range of data values within which they are valid. In applying regression onto data, most workers have ignored this fact and have applied the regression to all data irrespective of whether or not data fall within the range of values for which the regression relation has been established. In doing so, gross errors in magnitude data have been introduced. These errors are apparent in the shift to higher magnitudes for small events seen in most catalogues whose data has been subjected to this practice. However, information from the original data sources is still available in most of the catalogues for anyone who may want to use the same data but with own unified magnitudes.

Although data for catalogues like the Sub-Saharan Africa and the ECESA catalogues appear to be complete for the period 1900 to 1994 for magnitude ≥ 6, when data are considered for smaller areas or regions, it becomes clear that earthquake data for the eastern and southern Africa region is far from being complete. This is apparent in the six other catalogues reviewed in this paper. Additional information in paleoseismic data will assist with valuable information on historical data.

Only one attempt is known to have been made to develop an attenuation relation for the region. A wrong attenuation relation "*breeds*" meaningless seismic hazard results. There is therefore a definite need for studies on seismic wave attenuation in the region. In Fig. 9, we show the different attenuation relation curves that were presented in this review. The accuracy of seismic hazard data derived from the use of these relations is subject to the reasons and justifications advanced by the user in adopting a particular relation for his study. There is a need to carry out research on attenuation of seismic waves in the region. Although Jonathan (1996) has done some work on such study in the region, it only constitutes preliminary work upon which improvements need to be done. However, effective studies on attenuation of seismic waves require strong motion seismic data. Despite the fact that the east and southern Africa region is a seismically active region, there are no accelerograph stations. There is a need in the region to set up accelerograph stations. Equally important is the upgrading of

existing analogue stations to digital stations. Data from such stations may be used in attenuation relation work in the absence of accelerograph data.

It is hoped that the information given in this paper on earthquakes catalogues and attenuation relations used by workers in the east and southern Africa region, will provoke debate and inspire the reader with a desire to improve upon what already exists. This data therefore is important in providing the necessary foundation upon which future studies may be advanced. Preliminary seismic hazard work has been done in a number of countries and on the region as a whole. Future work will therefore seek to improve the data bases as well as the seismic hazard maps already reported by different workers in the region.

ACKNOWLEDGEMENTS

We wish to thank Mr. Patrick Ngulube for his patience in entering on to the computer, part of the data used in the catalogue completeness figures in this paper. We will remain indebted to his service. We also wish to express our sincere gratitude and thanks to Dr. Fekadu Kebede for making available to us via electronic mail, data on Ethiopia used in this paper.

REFERENCES

Ambraseys, N. N., 1991. Earthquake hazard in the Kenya rift: the Subukia earthquake 1928, Geophy J. Int. 105, 253-269.

Ambraseys, N. N. & R. D. Adams, 1986. Seismicity of Sudan, Bull. Seism. Soc. Am. 76, 483 - 493.

Ambraseys, N. N. and Adams, R. D., 1992. Reappraisal of major African earthquakes south of 20° N, 1900-1930, Natural Hazards, 4, 389-419.

Ambraseys, N. N., Melville, C. P. and R. D. Adams, 1994. The seismicity of Egypt, Arabia and the Red Sea, a historical review, Cambridge Univ. Press.

Asfaw, L. M., 1986. Catalogue of Ethiopian Earthquakes, Earthquake Parameters, Strain Release and Seismic Risk. In: G. Woldeyes (editor), Proc. SAREC- ESTC Conference on Research Development and Current Research Activities in Ethiopia, May 1988. pp 252 - 279.

Asfaw, L., 1992. Seismic risk at a site in the East Africa rift system, Tectonophysics, 209, 301-309.

Atkinson, G. A., 1984. Attenuation of strong motion in Canada from random vibration approach. Bull. Seismo. Soc. Amer. 74, No. 6, 2629 - 2653.

Boore, D. M. and W. B. Joyner, 1982. The empirical prediction of ground motion, Bull. Seism. Soc. Am., 72, S43 - S60

Båth, M., 1975. Seismicity of the Tanzania region, Tectonophysics, 27, 353-379.

Bungum, H. A., Dahle, G. R., McGuire, R. K. and Gudmestad, O. T., 1992. Ground motions from Intraplate Earthquakes. Proceedings 10th World conference on Earthquake Engineering, Madrid.

Brune, J. N., 1970. Tectonic stress and the spectra of seismic shear waves, J. Geophys. Res., 75, 4997 - 5009.

Chapola, L. S., 1997. State of stress in east and southern Africa and seismic hazard analysis of Malawi. M. Sc. Thesis, Ist. of Solid Earth Physics, Univ. of Bergen, Norway, 143.

Chow, R. A. Fairhead, J. D. and Henderson, N. B., 1980. Magnitude and Q determination in Southern Africa using Lg-wave amplitudes. Geophys. JR. astr. Soc. 63. 735 - 745.

Donovan, N. C., 1973. Earthquake hazard for building, In building practice for disaster mitigation. Natl. Bur. Standard Building Sci. Series 46, 82 -111.

Fairhead J. D. and R. W. Girdler, 1971. The seismicity of Africa, Geophy. J. astr. Soc. 24, 271-301.

Fairhead, J. D. and Stuart, G. W., 1982. The seismicity of the east Africa rift system and comparison with other continental rifts. In: G. Palmason (editor). Continental and Oceanic Rifts. Geodynamics Ser., 8, 41 - 61.

Giardini, D. and Basham, P., 1993 (eds). Global Seismic Hazard Assessment Programme for the UN/IDNDR, Ann. Geof., 36, 3-4.

Hanks, T. C., 1979. A moment magnitude scale. J. Geophys. Res., 84, 2348 - 2350.

Hanks, T. C. and Johnston, A. C., 1992. Common Features of the Excitation and Propagation of strong ground motion for North America Earthquakes. Bull. Seismo. Soc. Amer. Vol. 82, 1 - 23.

Hlatywayo, D. J., 1992. Seismicity of Zimbabwe during the period 1959 - 1990, Seismology Dept., Uppsala Univ. Report, 3-92. 1-98.

Hlatywayo, D. J. and V. Midzi, 1995. Determination of Lg-wave attenuation using single station seismograms - *A case study for Zimbabwe*, Geophys. J. Int., 123, 291 - 296.

Hlatywayo, D. J., 1997. Seismic hazard estimates in central southern Africa, Geophy. J. Int., (*in the press*).

Iranga, M. D., 1991. An earthquake catalogue for Tanzania, 1846 - 1988, Report No. 1-91, Uppsala Univ. Sweden.

Joyner, W. B. and Boore, D. M., 1988. Measurement, characterisation, and prediction of strong motion. Proceedings of Earthquake Engineering and Soil Dynamics II, GT Div/ASCE, Park City, Utah.

Joyner, W. B. and Fumal, T. E., 1985. Predictive mapping of earthquake ground motion. In: J. I. Ziony (editor), Evaluating Earthquake Hazards in the Los Angelos Region - An Earthscience Perspective. U. S. Geol. Surv. Prof. Pap., 1360, 203 - 220.

Jonathan, E., 1996. Some aspects of seismicity in Zimbabwe and eastern and southern Africa. M. Sc. Thesis, Ist. of Solid Earth Physics, Univ. of Bergen, Norway, 100.

Kebede, F., 1989. Source parameters and tectonic implications of selected earthquakes in Afar depression of Ethiopia and neighbouring regions, PhD. D. Thesis, Uppsala University.

Kebede, F. and van Eck, T., 1997. Probabilistic seismic hazard assessment for the Horn of Africa based on seismotectonic regionalisation. Tectonophysics 270, 221 - 237.

Krinitzky, E. L., Chang, F. K. and Nutli, O. W., 1988. Magnitude-related earthquake ground motions. Bulletin of the Association of Engineers and Geologists. Vol. XXV, 399 - 423

Lombe, D. K., 1997. Seismic hazard assessment and estimation of the local crustal velocity model for Zambia and Surrounding areas. M.Sc. Thesis, Ist. of Solid Earth Physics, Univ. of Bergen, Norway, 143.

Maasha, N., 1975. The seismicity of the Ruwenzori Region in Uganda, J. Geophy. Res. 80, 1485-1495.

Marshall, P. D., 1970. Aspects of spectral difference between earthquakes and underground explosions, Geophy. J. R. astr. Soc., 20, 397 - 416.

Marrow, P. C., 1992. UK earthquake magnitudes: a comparison of methods and published results, BGS Global Seismology Report no WL/92/36.

Musson, W. M. R., 1994. The BGS sub-Saharan African Earthquake catalogue, British Geol. Techn. Rept., WL/28, 1-59

Shah, E., 1986. Seismicity of Kenya, PhD Thesis, Univ. of Nairobi, Kenya, 1-104.

Sykes, L R. & M. Landisman, 1964. Seismicity of East Africa, the Gulf of Aden and Arabian and Red Sea, Bull. Seism. Soc. Am. 54, 1927-1940.

Twesigomwe, E. M., 996. Probabilistic Seismic Hazard Assessment of Uganda. PhD. Thesis. Makerere University, Uganda.

Turyomurugyendo, G., 1996. Earthquake catalogue for eastern and southern Africa, MSc. Thesis, Univ. Bergen, Norway.

Wohlenberg, J., 1969. Remarks on the seismicity of East Africa between 4° N - 12° S and 23° E - 40° E, Tectonophysics, 8, 567-577.

Xie, J. and Mitchell, J. B., 1990. A back-projection method for imaging large-scale lateral variations of Lg coda Q with applications to continental Africa. Geophysical Journal International. Vol. 100, 161 - 181.

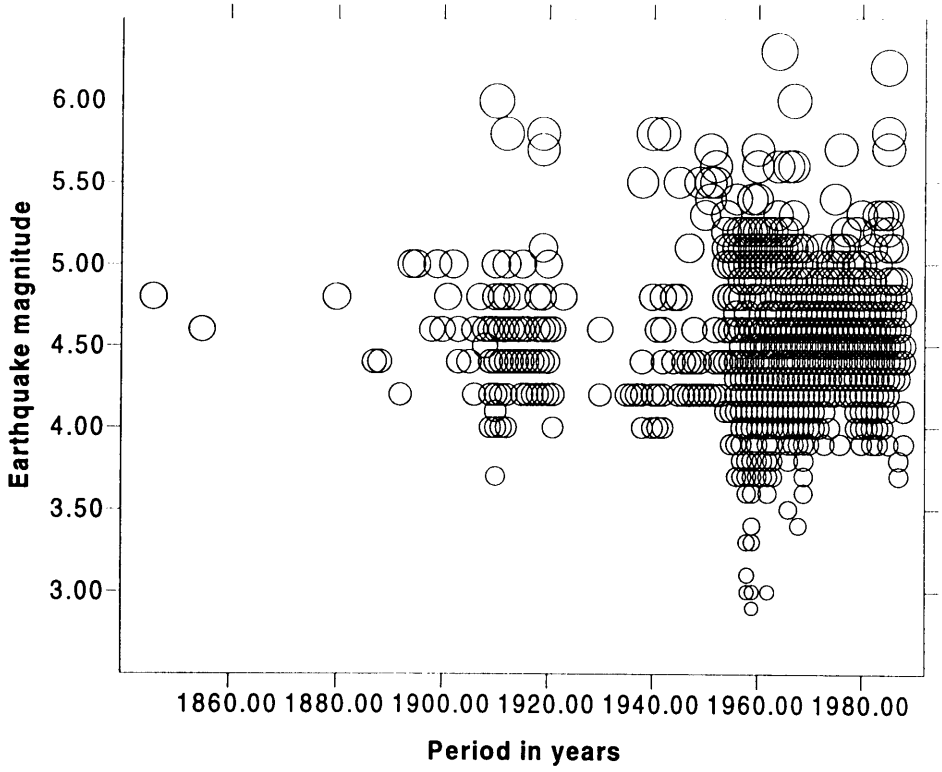

Figure 1. Tanzania catalogue (Iranga, 1991).

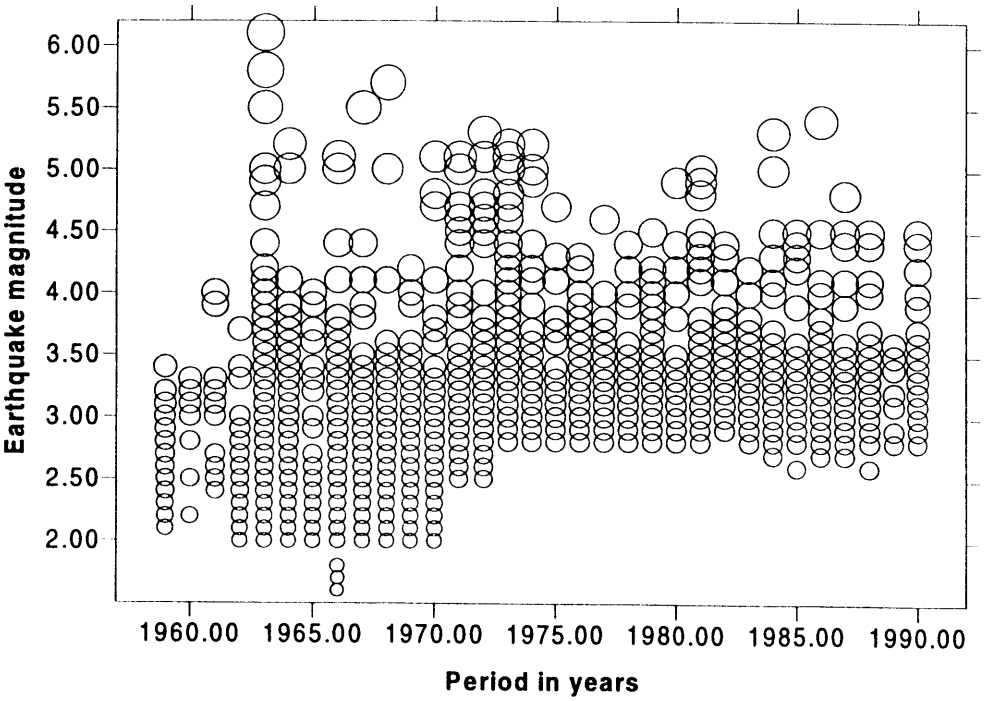

Figure 2. Zimbabwe catalogue (Hlatywayo, 1992)

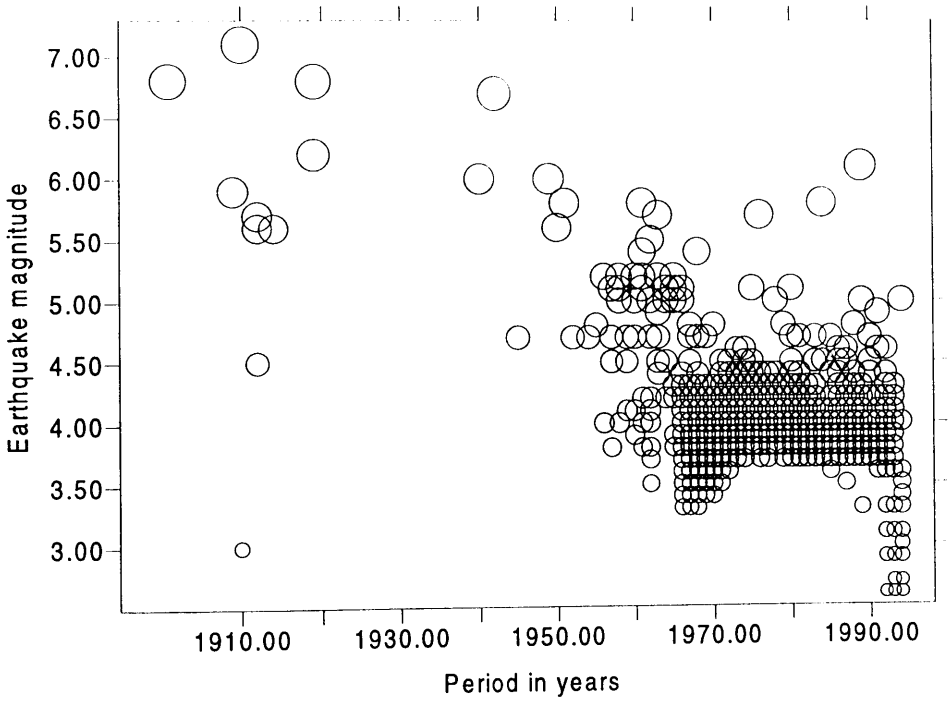

Figure 3. Malawi catalogue (Chapola, 1997)

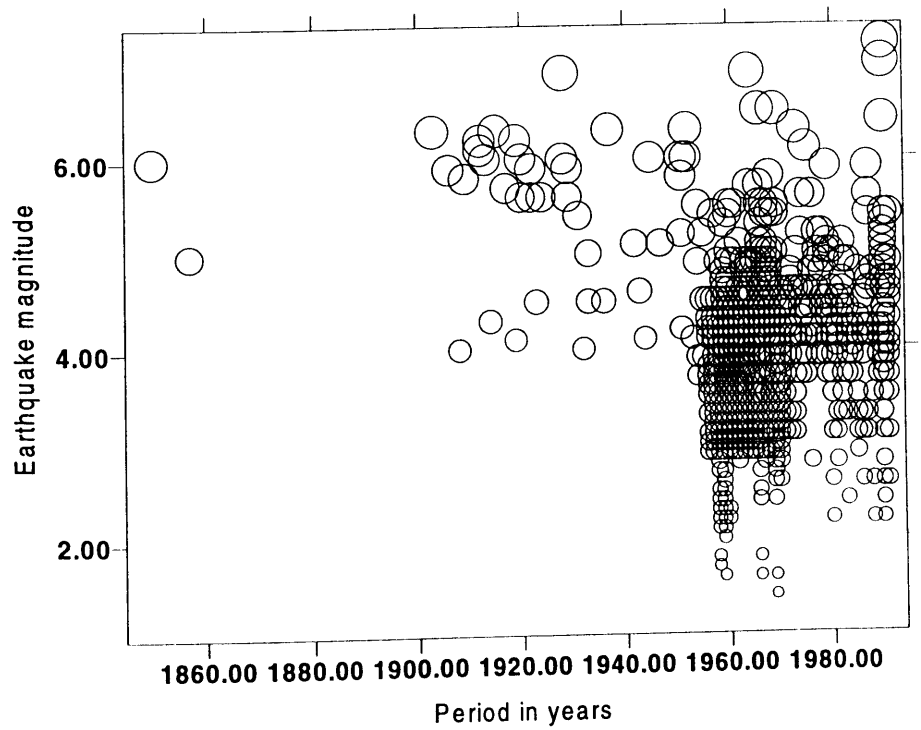

Figure 4. Uganda catalogue (Twesigomwe, 1996)

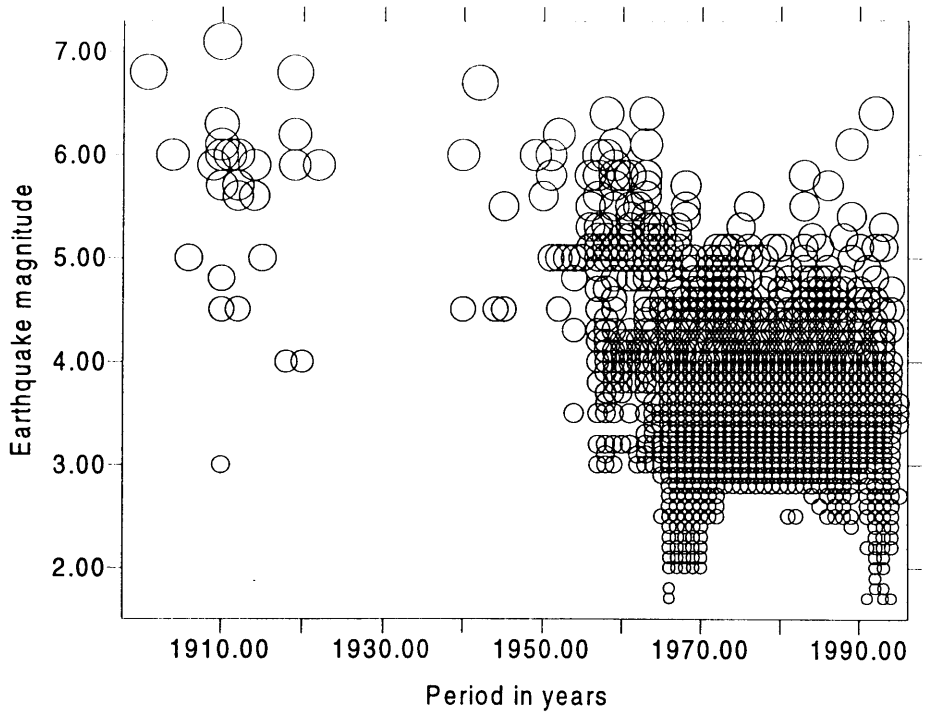

Figure 5. Zambia catalogue (Lombe, 1997)

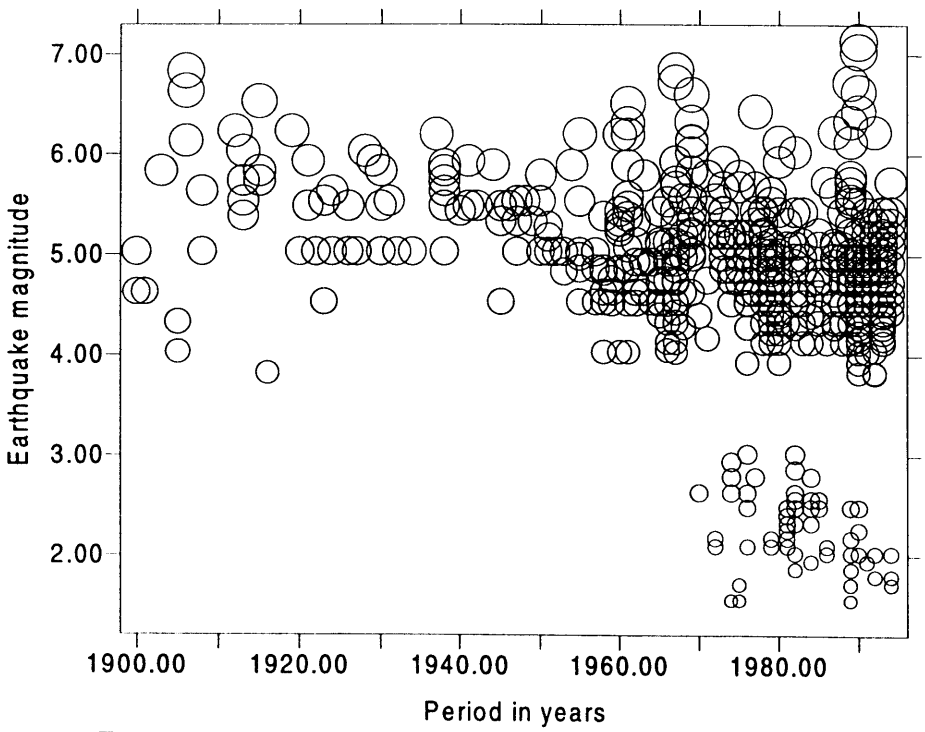

Figure 6. Ethiopia catalogue (courtesy of F. Kebede, Addis Ababa Geophysical Observatory)

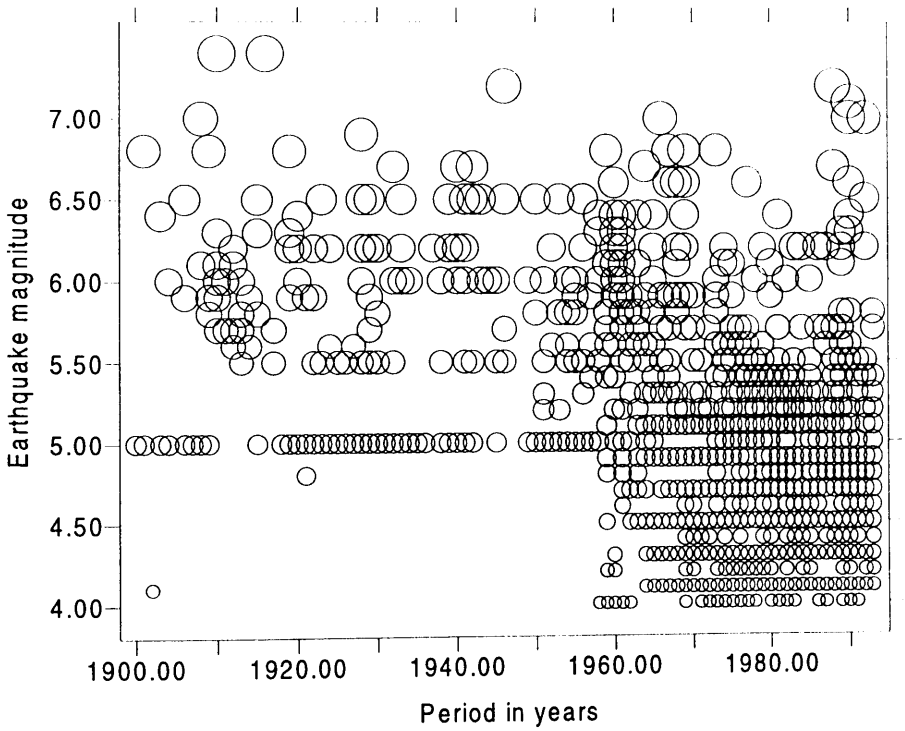

Figure 7. Sub-Saharan African earthquake catalogue (Musson, 1994)

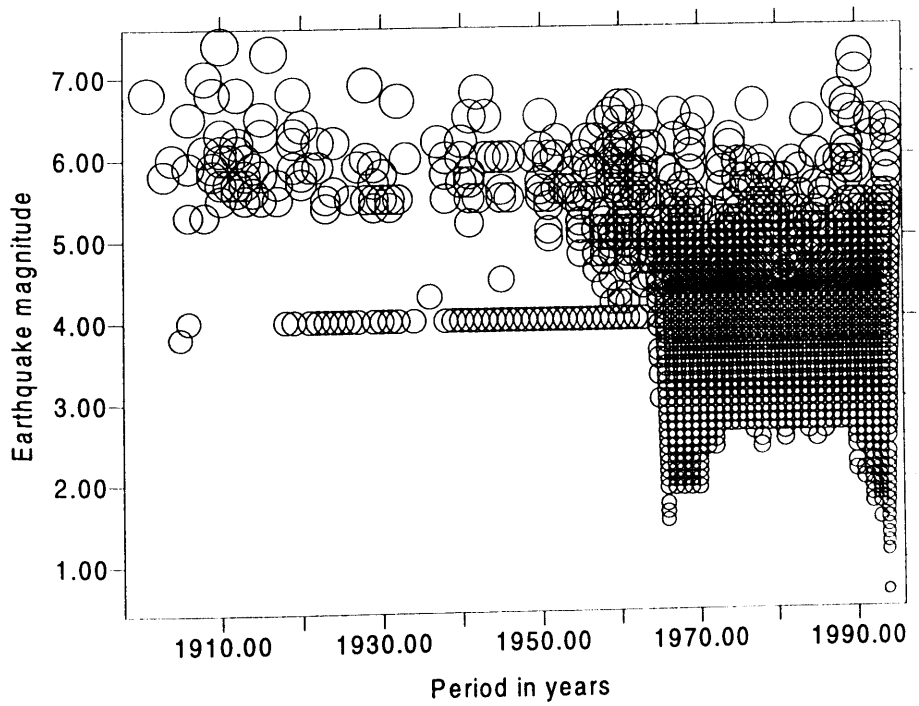

Figure 8. The ECESA catalogue (Turyomurugyendo, 1996)

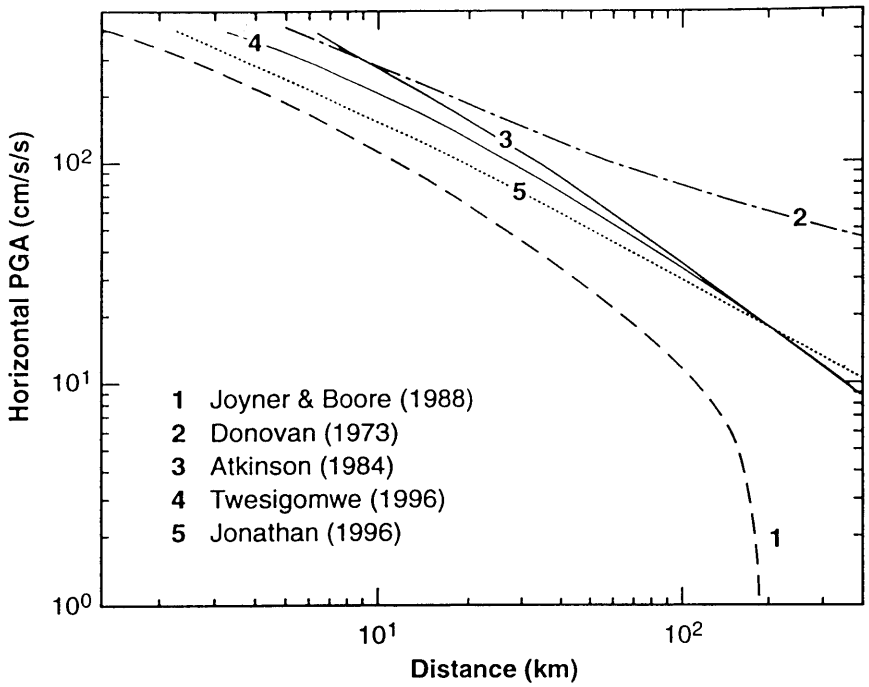

Fig. 9: Attenuation relation curves used in the eastern and southern Africa region and cited in this paper. Note that the Jonathan relation and that used by the chairman of the training course are equivalent and values obtained are nearly the same.

"PARAMETRIC - HISTORIC" PROCEDURE FOR SEISMIC HAZARD ASSESSMENT

Andrzej Kijko and Gerhard Graham

Council for Geoscience, Geological Survey of South Africa
Private Bag X112, Pretoria 0001, South Africa

1. INTRODUCTION

Following McGuire (1993), existing procedures of SHA fall into two main categories: **deductive** and **historic**[1]. The name of the first category (**deductive**) comes from the fact that by applying the procedure, we deduce what the causative sources, characteristics, and ground motions for future earthquakes are. The theoretical base for the deductive method was formulated almost 30 years ago by C.A. Cornell, (Cornell, 1968). The approach permits incorporation of geological and geophysical evidence to supplement the seismic event catalogues. Any application of the procedure includes several steps. The initial step requires definition of potential seismic sources which usually are associated with geological or tectonic features (as e.g. faults) and delineation of potentially active regions (zones) over which all available information is averaged. In the next step, for each seismogenic source zone, seismicity parameters are determined. Following the most common assumptions made in engineering seismology viz. that earthquakes are described by a Poisson process and that earthquake magnitudes follow a Gutenberg-Richter doubly truncated distribution, then for each seismogenic source zone the parameters are: mean activity rate λ (which is the parameter of the Poisson distribution), the level of completeness of the earthquake catalogue m_{min}, the maximum earthquake magnitude m_{max},

---

1 It must be noted that in addition to these two categories, alternative approaches are occasionally used. These procedures attempt to assess temporal or temporal and spatial dependence on seismicity. In order to incorporate memory of past events they use the formalism of non-Poissonian distributions or Markov chains. On this approach seismogenic zones that recently produced strong earthquakes become less hazardous than others that did not rupture in recent history. Clearly such models may result in a more realistic SHA, but they are nevertheless still only research tools and have not yet reached the level of development required by engineering applications. An excellent review of such procedures is given by Cornell and Toro (1992). Other recent treatises of the subject may be found e.g. in Muir-Wood (1993), and Boschi *et al.* (1996).

and the Gutenberg-Richter parameter b. Assessment of the above parameters requires a seismic event catalogue containing origin times, size of seismic events (in terms of magnitude or intensity) and spatial location. This allows the calculation of a distance PDF (probability density function) to the specified site. In the next step, a ground-motion relation is selected, giving the cumulative distribution function (CDF) for a required ground motion parameter such as peak ground velocity, peak ground acceleration, or response spectrum. The final step requires the integration of individual contributions from each seismogenic zone into a site-specific distribution. The procedure of integration is straightforward and is performed by application of the total probability theorem (Benjamin and Cornell, 1970). There is no doubt that deductive (or deductive-type) procedures of SHA are dominant and remain the method most commonly used all over the world.

Probably the strongest point of any deductive-type procedure of SHA is its ability to account for all sorts of deviations from the "standard" model, i.e. it accounts for phenomena such as migration of seismicity, seismic "gaps" or, in general, any non-stationary properties of seismicity. This is possible because the procedure is parametric by nature.

Unfortunately, the deductive procedure also has significant weak points. The major disadvantage stems from the requirement of specifying the seismogenic source zones. Often, a different seismogenic zone specification leads to significantly different assessments of hazard. In addition, the procedure requires, for each zone, a knowledge of the model parameters (in the simplest case the Gutenberg-Richter parameter b, the level of completeness m_{min}, the mean activity rate λ, and m_{max}), which cannot be determined reliably for areas that are small or have a very incomplete seismic history.

Following McGuire's division (McGuire, 1993), the second category of SHA consists of the so called "historic" methods (Veneziano *et al.*, 1984), which, in their original form, are non-parametric. These methods require as input data, information about past seismicity only, and do not require specification of seismogenic zones. For each historic earthquake, the empirical distribution of the required seismic hazard parameter is estimated by using its value of magnitude, distance and assumed ground motion attenuation relation. By normalizing this distribution for the duration of the seismic event catalogue, one obtains an annual rate of the exceedance of the required hazard parameter. The major advantage of the method is that specification of seismogenic source zones is not needed. Furthermore the approach does not require designation of the model, and this can be an advantage. By its nature, the historic method works well in areas of

Scientific Technical Report STR 98/05
DOI: 10.2312/GFZ.b103-98055

frequent occurrence of strong seismic events, when the record of past seismicity is "reasonably" complete (Boschi, *et al.*, 1996).

At the same time, the non-parametric historic approach has significant weak points. Its primary disadvantage is probably its poor reliability in estimating small probabilities for areas of low seismicity. The procedure is not recomended for an area where the seismic event catalogues are highly incomplete. In addition, in its present form, the procedure is not capable of making use of any additional geophysical or geological information to supplement the pure seismological data.

Bearing in mind both the weak and strong points of the above two approaches we propose an alternative procedure, which, following McGuire's scheme, could be classified as a **parametric-historic** approach. The new approach combines the best from the deductive and non-parametric historic procedures, and, in many cases, is free from the basic disadvantages characteristic of each of the procedures.

The proposed procedure is parametric and its application consists essentially of two steps. The first step is applicable to the **area** in the vicinity of the site for which a knowledge of the seismic hazard is required. In this respect the procedure is similar to the deductive approach and requires estimation of **area**-specific parameters. The parameters depend on the SHA model selected, which in our case are the **area**-specific mean seismic activity rate λ, Gutenberg-Richter parameter b and the maximum regional magnitude m_{max}. The approach is also open to any alternative parameterization.

The second step is applicable to a specified **site**, and consists of an assessment of the parameters of distribution of amplitude of the selected ground motion parameter.

Since in each step, parameters are estimated by the maximum likelihood procedure, by applying the Bayesian formalism, any additional geological or geophysical information (as well as all kinds of uncertainties) can be easily incorporated. The new procedure is consequently capable of giving a realistic assessment of seismic hazard in the areas of both low and high seismicity, including the case where the catalogues are incomplete.

In the present form, the procedure allows assessment of seismic hazard in terms of peak ground acceleration (PGA), peak ground velocity or peak ground displacement. Extension of the procedure and assessment of the whole response spectra of ground motion is straightforward.

Scientific Technical Report STR 98/05
DOI: 10.2312/GFZ.b103-98055

If the procedure is applied to all grid points of, and around, a region, then a map of seismic hazard for the whole region can be obtained.

The need for the development of the new approach to SHA was dictated by incompleteness of our seismic catalogues and by the inability to divide South Africa into reliable seismogenic source zones. The closest approach in conception that we have seen, to our approach, is that of Frankel (1995), in which seismic hazard is mapped in the central and eastern United States. The Frankel approach has been taken up by Lapajne *et al.* (1997), in modelling of seismic hazard in Slovenia.

The theoretical background of the procedure is described in the Chapter 1. *Outline of Theory*. An illustration of the procedure is given in the Chapter 2. *Example of Application*, where we present results of a typical SHA for a site of a hypothetical engineering structure.

2. OUTLINE OF THEORY

2.1. Assessment of Maximum Credible Magnitude m_{max}

At present there is no generally accepted method for estimating the value of maximum regional (credible) magnitude m_{max}. The methods for evaluating m_{max} fall into two main categories: **deterministic** and **probabilistic.**

The most often applied **deterministic** procedure is based on the empirical relationships between the magnitude and various tectonic and fault parameters. There are several papers devoted to such relationships. The relationships are variously developed for different seismic areas and different types of faults (e.g. Smith, 1976; Wyss, 1979; Singh *et al.*, 1980; Schwartz, *et al.*, 1984; Wells and Coppersmith, 1994; Anderson, *et al.*, 1996, and references therein). Another class of deterministic procedures for the assessment of maximum regional magnitude is based on extrapolating the frequency-magnitude curves. As an alternative to the two techniques above, researchers often try to relate the value of m_{max} with the strain rate or the rate of seismic-moment release (e.g. Papastamatiou, 1980; Anderson and Luco, 1983). Such an approach has also been applied by McGarr (1984) to evaluate the maximum possible magnitude of seismic events induced by mining. In most cases, unfortunately, the value of the parameter m_{max} determined by means of any deterministic procedure is very uncertain; the uncertainty can reach a value of up to one unit on the Richter scale.

Scientific Technical Report STR 98/05
DOI: 10.2312/GFZ.b103-98055

The value of m_{max} can also be estimated purely on the basis of the seismological history of the area, viz. by utilizing seismic event catalogues and appropriate **statistical** estimation procedures. The statistical techniques falling into this category form an important class of probability problems dealing with extreme values of random variables and estimation of the end-point of a distribution function. The statistical theory of extreme values was known and well-developed already in the fifties (e.g. Gumbel, 1958), and almost at the same time was applied in seismology[2]. Statistical tools required for the estimation of the end-point of distribution functions were developed later (e.g. Tate, 1959; Robson and Whitlock, 1964; Cooke, 1979) and used in the estimation of maximum regional magnitude only recently (Dargahi-Noubary, 1983; Kijko and Dessokey, 1987; Kijko and Sellevoll, 1989, 1992; Pisarenko, 1991; Pisarenko *et al.*, 1996). The available statistical tools suitable for the estimation of maximum regional magnitude vary significantly. Even if explicit functional parameterization of the magnitude distribution is not specified, they differ in:

(i) assumptions regarding the properties of functional representations of the magnitude distribution (especially in the behaviour of the tail for large values),

(ii) the criterion applied for the estimation of the end-point of the distribution.

In this chapter we present two statistical procedures which can be used for the evaluation of the maximum regional magnitude m_{max}. Broadly speaking, the first procedure is more "straightforward", while the second one is more "advanced" and requires a more detailed input and/or more complex calculations.

For both procedures the confidence limits for the estimated maximum magnitude are also derived.

2.1.1. Formulation of the problem. Assumptions

---

2 The theory of extreme statistics was probably first applied in seismology by Nordquist (1945), who demonstrated that the largest earthquakes in California are in good agreement with Gumbel's Type I asymptotic distribution of extremes. The major breakthrough in seismological applications of extreme-value statistics was made by Epstein and Lomnitz (1966), who proved that the Gumbel I asymptote can be derived directly from assumptions that seismic events are generated by a simple Poisson process and that they follow the Gutenberg-Richter frequency-magnitude distribution.

Scientific Technical Report STR 98/05
DOI: 10.2312/GFZ.b103-98055

Suppose that in the area of concern, within a specified time interval T, there are n main seismic events with magnitudes[3] M_1, M_2,..., M_n. Each magnitude $M_i \geq m_{min}$ ($i = 1,\ldots, n$), where m_{min} is a known threshold of completeness (i.e. all events having magnitude greater than or equal to m_{min} are recorded). We assume further that the seismic event magnitudes are independent, identically distributed random values with probability density function (PDF), $f_M(m|m_{max})$ and cumulative distribution function (CDF), $F_M(m|m_{max})$, respectively. Parameter m_{max} is the upper limit of the range of magnitude and thus denotes the unknown maximum regional magnitude, which is to be estimated.

For the classical Gutenberg-Richter relation, which is a frequency-magnitude relation that is **unbounded** from above (i.e. $m_{max} \longrightarrow \infty$), the PDF and CDF $f_M(m) \equiv f_M(m|\infty)$ and $F_M(m) \equiv F_M(m|\infty)$ are continuous, and equal to (Aki, 1965):

$$f_M(m) = \begin{cases} \beta\exp[-\beta(m - m_{min})], & \text{for } m \geq m_{min}, \\ 0, & \text{for } m < m_{min}, \end{cases} \tag{1}$$

$$F_M(m) = \begin{cases} 1 - \exp[-\beta(m - m_{min})], & \text{for } m \geq m_{min} \\ 0, & \text{for } m < m_{min}, \end{cases} \tag{2}$$

The respective PDF and CDF of earthquake magnitude which are bounded from above by m_{max}, are (Page, 1968; Cosentino *et al.*, 1977):

$$f_M(m|m_{max}) = \begin{cases} \dfrac{\beta\exp[-\beta(m - m_{min})]}{1 - \exp[-\beta(m_{max} - m_{min})]}, & \text{for } m_{min} \leq m \leq m_{max} \\ 0, & \text{for } m < m_{min},\ m \geq m_{max}, \end{cases} \tag{3}$$

and

---

3 It should be noted that the approach offered here is not limited to the case when the size of seismic event M, is earthquake magnitude. All the results are valid also when the size of the earthquake is described by energy, seismic moment or seismic intensity.

Scientific Technical Report STR 98/05
DOI: 10.2312/GFZ.b103-98055

$$F_M(m|m_{max}) = \begin{cases} 0 & \text{for } m < m_{min}, \\ \dfrac{1 - \exp[-\beta(m - m_{min})]}{1 - \exp[-\beta(m_{max} - m_{min})]}, & \text{for } m_{min} \le m \le m_{max}, \\ 1, & \text{for } m > m_{max}. \end{cases} \quad (4)$$

where $\beta = b\ln(10)$, and b is the b-parameter of the Gutenberg-Richter relation. Both distribution functions are obtained as a result of truncation of unbounded distributions (1)-(2) at the point m_{max}, that is

$$f_M(m|m_{max}) = \begin{cases} f_M(m)/F_M(m_{max}), & \text{for } m_{min} \le m \le m_{max} \\ 0, & \text{for } m < m_{min}, \ m > m_{max}, \end{cases} \quad (5)$$

and

$$F_M(m|m_{max}) = \begin{cases} 0, & \text{for } m < m_{min}, \\ F_M(m)/F_M(m_{max}), & \text{for } m_{min} \le m \le m_{max}, \\ 1, & \text{for } m > m_{max}. \end{cases} \quad (6)$$

where

$$F_M(m) = \int_{m_{min}}^{m} f_M(\xi)d\xi. \quad (7)$$

The above classical formulation of the problem has significant shortcomings. The main ones are:

(i) Earthquakes are often missing from the catalogues, especially lower magnitude earthquakes from older catalogues. Consequently the most suitable methods for analyzing the old and incomplete data sets are those which require knowledge of strongest events only, rather than complete data sets (e.g. Burton, 1979; Yegulalp and Kuo, 1974). If the largest events are used, then, in all the equations, the original magnitude distribution $F_M(m)$ has to be replaced by its extreme-value counterpart $F_M^{max}(m)$. Assessment of basic hazard parameters by means of extreme distributions (or mixed, extreme and complete as illustrated in Fig. 1) is discussed in Section 2.2.

(ii) The sizes of earthquakes listed in catalogues might require adjustment or

Scientific Technical Report STR 98/05
DOI: 10.2312/GFZ.b103-98055

Scientific Technical Report STR 98/05
DOI: 10.2312/GFZ.b103-98055

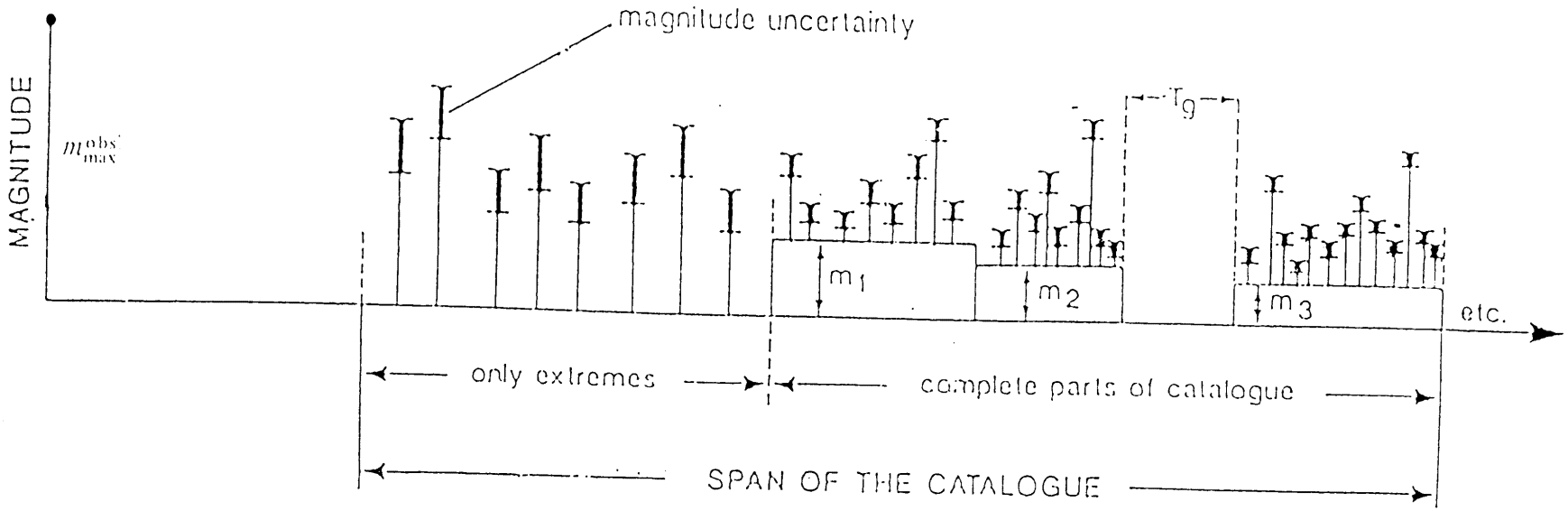

Fig. 1. An illustration of data which can be used to obtain basic seismic hazard parameters for the area in the vicinity of the selected site by the procedure used. The approach permits the combination of largest earthquake data and complete data having variable threshold magnitudes. It allows the use the largest known historical earthquake (m_{max}^{obs}) which occurred before the catalogue begins. It also accepts "gaps" (T_g) when records were missing or the seismic networks were out of operation. Uncertainty in earthquake magnitude is also taken into account in that an assumption is made that the observed magnitude is the true magnitude subjected to a random error that follows a Gaussian distribution having zero mean and a known standard deviation σ_M.

conversion to a different magnitude scale. Conversion of one type of magnitude to a single measure common to the whole span of the catalogue requires conversion by means of empirical relations. As has been pointed out many times (e.g. Chung and Berneurer, 1981; Bender, 1993; McGuire, 1993), such a procedure is not necessarily valid. In addition, a change in the characteristics of seismic sensors can cause systematic errors in the conversion of magnitudes (see, for example, the case of magnitude conversion for the eastern and western United States, Nuttli and Herrmann, 1982). Hence, a catalogue that contains earthquakes with magnitudes adjusted or converted is heterogeneous and requires appropriate techniques for dealing with it. Probably the most efficient technique for estimating the parameters in the magnitude distributions using both complete catalogues as well as catalogues containing only the largest events, and which, furthermore, takes into account the uncertainty of earthquake magnitude was that developed by Tinti and Mulargia (1985 a,b), in which they introduced the concept of "apparent magnitude". The Tinti-Mulargia approach was recently extended by Rhoades (1995), by allowing different uncertainties of magnitude for individual earthquakes. Since the presence of uncertainty of magnitude can also effect the estimation of the maximum regional magnitude m_{max}, this question will be discussed further in the following section.

(iii) The choice of the model for the distribution of earthquake magnitudes can significantly influence the results of the estimation of seismic hazard and maximum regional magnitude. Is the simplest model of all, based on the Gutenberg-Richter relation, enough? In most engineering applications, for magnitudes in the middle of the range of distribution, the choice of the model is relatively unimportant. The most important consideration is the upper tail of the distribution, which determines the value of m_{max}. Hence, for example, the taking into account of the occurrence of characteristic earthquakes (Schwartz and Coppersmith, 1984) can drastically influence the tail of the magnitude distribution, and so influences the value of the estimated m_{max}.

Even if the concept of the existence of characteristic earthquakes were not applicable, one would not be able to neglect the effect of non-linearity in frequency-magnitude relationships. There are, by way of illustration, some well-documented cases including the natural seismicity in Alaska (Devison and Scholz, 1984), Mexico (Singh *et al.*, 1983), Japan (Wesnousky *et al.*, 1983), and the New Madrid zone of the United States (Main and Burton, 1984), as well

Scientific Technical Report STR 98/05
DOI: 10.2312/GFZ.b103-98055

as mine-induced seismicity in Poland and South Africa (Gibowicz and Kijko, 1994; Finnie, 1994).

In addition, a significant shortcoming is our implicit assumption that seismicity parameters such as the *b*-value of the Gutenberg-Richter relation and the mean activity rate λ, remain constant in time. Temporal variations of seismic activity have been reported and described many times in the literature and a complete list of these reports would be very long. We will mention only a few of them, and only those that are well documented. Significant fluctuations in seismic activity have been reported in e.g. Kamchatka and the Kuril Islands (Fedotov, 1968), California, and, notably, Parkfield (Bakun and McEvilly, 1984), China (McGuire and Barnhard, 1981), the New Madrid Zone, USA (Mento *et al.*, 1986), Greece (Papadopoulos and Voidomatis, 1987) and the North Sea (Lindholm *et al.*, 1990). For other areas, the seismic activity shows temporal variations but it is not clear whether these changes are periodic, e.g. southern Italy (Bottari and Neri, 1983), New Zealand (Vere-Jones and Davis, 1966), the Alpine-Himalayan belt (Rao and Kalia, 1986), Japan (Shibutani and Oike 1989) and all subduction zones of the Circum-Pacific Belt (Lay *et al.*, 1989). Global seismicity also shows temporal variation but with no clear periodicity (e.g. Kanamori, 1981; Shimshoni, 1984).

It should be clear that neglecting the uncertainty resulting from a selection of a wrong model of magnitude distribution and/or temporal variation of seismicity can lead to significantly biased estimates of seismic hazard, and also biased estimates of $m_{\max}$.

The Bayesian approach, where the model parameters are treated as random variables, provides the most appropriate tool for handling the uncertainties considered above.

In the following two sections we will derive two procedures in which the uncertainty of seismic hazard parameters can be incorporated and in which Bayesian-based, analytical (or semi-analytical) equations can be obtained. We shall think of these as the "*Straightforward Procedure*" and the "*Advanced Procedure*", respectively. It is assumed that for each of the procedures both the analytical form and the parameters of the CDF $F_M(m|m_{\max})$ are known. In both the procedures considered the largest **observed** magnitude $m_{\max}^{obs}$ plays a crucial role.

Scientific Technical Report STR 98/05
DOI: 10.2312/GFZ.b103-98055

2.1.2. Procedure I

This procedure is very straightforward and does not require extensive calculations. It can be shown that the procedure attempts to correct the bias of the classical maximum likelihood estimator $\hat{m}_{max} = m_{max}^{obs}$, (Pisarenko *et al.*, 1996), but fails to provide an estimator having a smaller mean squared error. The same formulae can be obtained by applying at least three different approaches, namely:

(i) by using a purely intuitive criterion and employing well-known properties of the simple uniform distribution, or,

(ii) by applying a formal statistical technique of reducing the bias of the estimator, as developed e.g. by Quenouille (1956), or

(iii) by expressing parameter m_{max} by means of unknown functions in integral equations of a convolution type, and then obtaining m_{max} by an integral transform method (Tate, 1959).

In our derivation we choose the first approach, as described by Kijko (1997).

Derivation of Estimator I

In this approach we utilize the fact that the random variables Y[4], where $Y = F_M(M)$, and $F_M(M)$ is any CDF, are independently distributed, with uniform CDF over the range 0 to 1, that is

$$F_Y(y) = \begin{cases} 0, & \text{for } y < 0, \\ y, & \text{for } 0 \le y \le 1, \\ 1, & \text{for } y > 1. \end{cases} \tag{8}$$

The estimators derived here are based on the order statistics of earthquake magnitudes

4 In general we are following convention where a capital letter is used for a random variable, and the same letter, in lowercase, represents the values which it may take on.

Scientific Technical Report STR 98/05
DOI: 10.2312/GFZ.b103-98055

$M_1 \le M_2 \le \ldots \le M_{n-1} \le M_n$, where the unordered M_i are independent and identically distributed according to CDF $F_M(m|m_{max})$. In addition it is assumed that $F_M(m|m_{max})$ belongs to the class of functions which admit a Taylor Series expansion about the point m_{max}. We observe that after the transformation $Y_1 = F_M(M_1|m_{max})$, $Y_2 = F_M(M_2|m_{max}),\ldots,$ $Y_n = F_M(M_n|m_{max})$, the values $Y_1,\ldots, Y_n$ form an ordered data set $Y_1 \le Y_2 \le \ldots \le Y_{n-1} \le Y_n$, and each of them are distributed uniformly.

The CDF of the largest among $(Y_1,\ldots, Y_n)$, that is Y_n, is

$$\begin{aligned} F_{Y_n}(y) &\equiv Pr[Y_n \le y] \\ &= Pr[Y_1 \le y,\ Y_2 \le y,\ldots,\ Y_n \le y] \\ &= [F_Y(y)]^n \\ &= y^n. \end{aligned} \tag{9}$$

Then, the PDF of variable Y_n is given by

$$f_{Y_n}(y) \equiv \frac{dF_{Y_n}(y)}{dy} = \begin{cases} 0, & \text{for } y < 0, \\ ny^{n-1}, & \text{for } 0 \le y \le 1, \\ n, & \text{for } y > 1, \end{cases} \tag{10}$$

and its expected value is

$$\mathcal{E}(Y_n) = \int_{\xi=0}^{1} \xi\, f_{Y_n}(\xi)d\xi = n \int_{\xi=0}^{1} \xi^n d\xi = \frac{n}{n+1}. \tag{11}$$

A natural way to obtain the estimator $\hat{m}_{max}$ is to introduce the condition that

$$\mathcal{E}(Y_n) = y_n, \tag{12}$$

where y_n is calculated from the relation $y_n = F_M(m^{obs}_{max}|m_{max})$, and m^{obs}_{max} is the maximum **observed** magnitude.

Bearing in mind that $\mathcal{E}(Y_n) = n/(1+n)$ we obtain the equation

$$F_M(m^{obs}_{max}|\hat{m}_{max}) = \frac{n}{n+1}. \tag{13}$$

Scientific Technical Report STR 98/05
DOI: 10.2312/GFZ.b103-98055

Thus the estimator of m_{max} becomes a function of the known observations m_{max}^{obs} and n, and is obtained as a root of the equation (13).

The above result is valid for any of the magnitude CDF $F_M(m|m_{max})$, (describing the complete as well as extreme events), and does not require the fulfillment of the truncation condition (5)-(7).

It can be shown that the estimator of parameter m_{max} as defined above, belongs to the class of so-called " moment estimators" (Kendall and Stuart, 1967) and, from the formal point of view, complies with all the requirements of proper statistical estimators.

One of the simplest ways to assess the properties of the above estimator is to use the Taylor Series expansion of an inverse of CDF $F_M^{-1}(Y_n|m_{max})$. At the same time, such an expansion provides insight into the bias of the estimator. The expansion of the function $F_M^{-1}(Y_n|m_{max})$ in a Taylor series about the point $Y_n = 1$, yields

$$M_n = F_M^{-1}(1|m_{max}) - \left.\frac{\partial F_M^{-1}(Y_n,m_{max})}{\partial Y_n}\right|_{Y_n=1} (1 - Y_n) + \ldots \qquad (14)$$

Since $F_M^{-1}(1|m_{max}) = m_{max}$, $\mathcal{E}(1 - Y_n) = 1 - n/(n + 1) = 1/(n + 1)$,

$$\left.\frac{\partial F_M^{-1}(Y_n,m_{max})}{\partial Y_n}\right|_{Y_{max}=1} = \frac{1}{\left.\frac{\partial F_M(m,m_{max})}{\partial m}\right|_{m_{max}}} = \frac{1}{f_M(m_{max}|m_{max})} . \qquad (15)$$

For n large, $\mathcal{E}(1 - Y_n) \cong 1/n$, and $f_M(m_{max}|m_{max}) \cong f_M(m_{max}^{obs}|m_{max}^{obs})$. After replacing $1 - Y_n$ by its expected value, viz. 1/n, the estimator (13) takes the simple form

$$\boxed{\hat{m}_{max} = m_{max}^{obs} + \frac{1}{n\, f_M(m_{max}^{obs}|m_{max}^{obs})}.} \qquad (16)$$

The end-point estimator (16) was probably first derived by Tate (1959). It was used by Pisarenko *et al.* (1996), who quoted it without derivating it, after Kendall and Stuart

Scientific Technical Report STR 98/05
DOI: 10.2312/GFZ.b103-98055

(1967), and appllied it for estimation of maximum regional magnitude m_{max}. We have provided this formula with the simple derivation shown above, because the Tate's original derivation is very complex, and understanding it requires an advanced background in theoretical statistics.

It is easy to extend this approach and assess the approximate variance of the estimator (16). By applying the relation between the derivative of a continuous, strictly monotonic function and its inverse function (e.g. from Apostol, 1961), the approximate variance of $\hat{m}_{max}$ can be written as

$$Var(\hat{m}_{max}) = \left[\frac{dF_M(m_{max}^{obs} | m_{max})}{dm_{max}} \right]^{-2} \Bigg|_{m_{max}=\hat{m}_{max}} Var(\hat{y}_n). \quad (17)$$

Following (10) and (11) we obtain

$$\mathcal{E}(Y_n^2) = \int_{\xi=0}^{1} \xi^2 f_{Y_n}(\xi) d\xi = n \int_{\xi=0}^{1} \xi^{n+1} d\xi = \frac{n}{n+2}, \quad (18)$$

and

$$Var(Y_n) = \mathcal{E}(Y_n^2) - [\mathcal{E}(Y_n)]^2 = \frac{n}{(n+2)(n+1)^2}. \quad (19)$$

We also obtain

$$\frac{dF_M(m_{max}^{obs} | m_{max})}{dm_{max}} = -F_M(m_{max}^{obs} | m_{max}) \, f_M(m_{max} | m_{max}) \quad (20)$$

and after replacing $[F_M(m_{max}^{obs} | \hat{m}_{max})]^2$ by its expected value $\mathcal{E}(Y_n^2)$, for large n, we obtain

$$Var(\hat{m}_{max}) = \frac{1}{n^2 f_M^2(m_{max}^{obs} | m_{max}^{obs})}. \quad (21)$$

The equation above describes the variance of the truncation point $\hat{m}_{max}$, estimated according to the formula (16).

Scientific Technical Report STR 98/05
DOI: 10.2312/GFZ.b103-98055

Uncertainty in the Determination of m_{max}: *What Contributes to the Uncertainty and How ?*

Formula (21) quantifies the uncertainty of maximum magnitude determination, an uncertainty which has its source in the randomness of the earthquake generation process. This variability (known as **aleatory** variability) is inherent in natural processes and must be clearly distinguished from another type of uncertainty, which has its source in the application of the wrong mathematical model of the process [for example an inadequate CDF $F_M(m)$], or wrong values of the model parameters (as e.g. Gutenberg-Richter parameter b). Often such an uncertainty is known as **epistemic** variability (McGuire, 1993; Toro *et al.*, 1997).

It is important to distinguish between these two types of uncertainties, since often they require entirely different treatments. In this section we will take into account two facts, which have a contribution to the uncertainty in the estimation of the parameter m_{max}:

(i) The number of observed earthquakes n, within the span of the catalogue T, is a **random** number. Let as assume that n obeys the Poisson distribution having parameter λ, the mean activity rate. In this case, uncertainty in the number of earthquake occurrences belongs to the class of aleatory variability, since the random nature of the number of earthquake occurrences is inherent in the earthquake generation process.

(ii) The observed (apparent) earthquake magnitude m is a true magnitude distorted by a random observation of magnitude error, ε. The concept of apparent magnitude was introduced by Tinti and Mulargia (1985a) and the effect of uncertainty of magnitude on the assessment of seismic hazard has been studied extensively and is well understood. In practice, two distributions for the error ε are considered: normal (e.g. Tinti and Mulargia, 1985a; Bender, 1987; Kijko and Sellevoll, 1992), and uniform (Tinti and Mulargia, 1985b). Sometimes the magnitude uncertainties are expressed in terms of intervals, such as those that arise from rounded data (Kijko, 1988). An alternative treatment of the problem was given by Rhoades (1995), who provides both for normally distributed magnitude observation errors and for errors arising from round-off. Following the adopted classification, this uncertainty in earthquake magnitude determination can be classified under epistemic variability.

Scientific Technical Report STR 98/05
DOI: 10.2312/GFZ.b103-98055

The approximate contributions of both of the above uncertainties to the variance of m_{max} estimation can be easily taken into account by applying the law of propagation of errors.

Following the assumption that the number of earthquakes in unit time within a specified area obeys the Poisson distribution with parameter λ, after replacement of n by λT, Tate's (1959) estimator (16), is

$$\hat{m}_{max} = m_{max}^{obs} + \frac{1}{\lambda T \, f_M(m_{max}^{obs} | m_{max}^{obs})}. \tag{22}$$

If we take into account that, by the definition of the Poisson process, the variance of n is equal to λT, the contribution of the randomness in the number of earthquake occurrences to the variance of $\hat{m}_{max}$ is approximately equal to $(\lambda T)^{-3} f_M^2(m_{max}^{obs} | m_{max}^{obs})$. Hence, formula (21) should be extended to the form

$$Var(\hat{m}_{max}) \cong \frac{1}{(\lambda T)^2 f_M^2(m_{max}^{obs} | m_{max}^{obs})} + \frac{1}{(\lambda T)^3 f_M^2(m_{max}^{obs} | m_{max}^{obs})}. \tag{23}$$

Clearly, the second term in the equation (23) is responsible for uncertainty in the number of earthquake occurrences and is λT times less than the first one. Therefore, for an area with high mean activity rate λ, and for a long period of observations (T large), its contribution may be neglected.

Finally, let us assess the effect of uncertainty in earthquake magnitude determination. Now, the relation (14) which was used as a base and starting point for derivation of later formulas, is

$$m_{max}^{obs} = F^{-1}(1 | \hat{m}_{max}) - \left. \frac{\partial F^{-1}(y_n | \hat{m}_{max})}{\partial y_n} \right|_{y_n = 1} (1 - y_n) + \ldots + \varepsilon, \tag{24}$$

where ε is a random error in the determination of the maximum observed magnitude m_{max}^{obs}. Assuming that the variance of ε is known and equal to $Var(\varepsilon) = \sigma_M^2$, the approximate variance of $\hat{m}_{max}$ estimated according to Procedure I is

Scientific Technical Report STR 98/05
DOI: 10.2312/GFZ.b103-98055

$$Var(\hat{m}_{max}) \cong \sigma_M^2 + \frac{1}{f_M^2(m_{max}^{obs} | m_{max}^{obs})} \left[\frac{\lambda T + 1}{(\lambda T)^3} \right]. \quad (25)$$

The contribution of the new additional term to the variance of the maximum regional magnitude $\hat{m}_{max}$ can be significant, especially when the magnitude m_{max}^{obs} is recovered from historical records. In such cases the uncertainty in the determination of m_{max}^{obs} can reach a value of half a unit of earthquake magnitude ($\sigma_M = 0,5$) and even higher.

Confidence Limits for Estimator I

Knowledge of the CDF of $y_n = F_M(m_{max}^{obs} | m_{max})$, makes it possible to construct an upper confidence limit for the parameter m_{max}. For this, we select the number z_α in such a way that the probability

$$Pr[y_n < z_\alpha] = \alpha. \quad (26)$$

Following (9), one obtains $Pr[y^n < z_\alpha^n] = \alpha$, from which $z_\alpha = \alpha^{1/n}$. Hence, after simple transformations, a $100(1 - \alpha)\%$ upper confidence limit on $\hat{m}_{max}$ is given by $F_M^{-1}(m_{max}^{obs} | \alpha^{1/n})$, or equivalently

$$Pr\left[m_{max} < F_M^{-1}(m_{max}^{obs} | \alpha^{1/n}) \right] = 1 - \alpha. \quad (27)$$

Knowledge of the above equation makes it possible to construct the fiducial distribution

$$Pr[m_{max} < z] = 1 - \left[F_M(m_{max}^{obs} | z) \right]^n. \quad (28)$$

Again, after accepting the assumption that the number of seismic events n occurring within specified area obeys the Poisson distribution with parameter λ, after the replacement $n = \lambda T$, one obtains a distribution of m_{max} independent of the number of observations n. Hence, the fiducial distribution (28) takes the form

$$Pr[m_{max} < z] = 1 - \left[F_M(m_{max}^{obs} | z) \right]^{\lambda T}. \quad (29)$$

Scientific Technical Report STR 98/05
DOI: 10.2312/GFZ.b103-98055

These formulae are general and are valid for any magnitude CDF, $F_M(m^{obs}_{max}|z)$, having finite upper bound m_{max}. Alternative formulae for confidence limits for the estimator $\hat{m}_{max}$ can be obtained by means of the Gumbel Type III asymptotic distribution of the extremes.

It should be noted that our approach has several limitations. One of these is the assumption that parameters of the magnitude CDF $F_M(m|m_{max})$ are known without error. In the following section, we consider the case when in addition to the above uncertainties, uncertainties of CDF of earthquake magnitude are considered. A similar line was taken by Pisarenko *et al.* (1996). The main difference between Pisarenko's approach and ours is that the former requires numerical integration, while ours provides an analytical or semi-analytical solution.

Account of Parameter Uncertainties in the Distribution Function of Earthquake Magnitude

The treatment of uncertainties in our model can be done in different ways. Probably the most efficient is the Bayesian approach, which takes into account the uncertainty in parameters by regarding them as random variables (e.g. DeGroot, 1970). Unfortunately, a straightforward implementation of Bayesian formalism often requires numerical integration (Pisarenko *et al.*, 1996).

In our work we propose an approach which is also based on the Bayesian formalism, but does not require numerical integration. In order to consider the most general case, when uncertainties are present both in magnitude and other parameters, we have applied the formalism of compound distributions. Compound distributions arise when parameters of the distribution of a random variable are themselves treated as random variables. Let vector $\mathbf{p}$ denote the parameters of the model [as, for example, the β-value in the Gutenberg-Richter-based CDF (4)], which are known with some degree of uncertainty. In general, if a random variable M has a CDF $F_M(m)$ which depends upon continuous random parameters $\mathbf{P}$ [which might be written as $F_M(m|\mathbf{p})$[5]], then the CDF

$$F_M(m) = \int_{\mathbf{p}} F_M(m|\mathbf{p})\, f_P(\mathbf{p})\mathrm{d}\mathbf{p}, \tag{30}$$

[5] It must be noted that since the m_{max} is not included in the distribution parameters $\mathbf{P}$, it would be more correct to introduce the notation $F_M(m|\mathbf{p},m_{max})$.

Scientific Technical Report STR 98/05
DOI: 10.2312/GFZ.b103-98055

where $f_P(\mathbf{p})$ is a PDF of parameters **P**, is known as a compound (Bayesian) distribution of a random variable M. The compound CDF is therefore the weighted average of the CDF of M for each value of **P**.

An application of the above formalism to the uncertainty of the Gutenberg-Richter parameter b is shown in Section 2.1.4.

2.1.3. Procedure II

This procedure is based on an equation that compares the maximum **observed** magnitude m_{max}^{obs}, and the maximum **expected** magnitude $\varepsilon(M_n|T)$ during a specified time interval T.

It has been shown that the procedure provides an estimator of the upper end of distribution which in terms of mean squared error is **substantially** better than the respective Tate (1959) estimator given by Procedure I. The drawback of the procedure is that it requires integration, which, for some distribution functions, can be performed only numerically. Fortunately for the CDF of Gutenberg-Richter, analytical formulae are available.

Derivation of Estimator II

Let us accept the assumption previously made that the earthquake magnitudes M_1, M_2,..., M_n occurring within a specified time interval T, are independent, random variables, each with CDF $F_M(m|m_{max})$, where m belongs to the magnitude interval $[m_{min},m_{max}]$. As before, let us assume that the magnitudes are already ordered in ascending order, i.e. $M_1 \le M_2 \le \ldots \le M_n$.

Following the same technique as was used in the derivation of the CDF of the largest of the variables Y_1,..., Y_n, where $Y = F_M(M|m_{max})$, the largest magnitude M_n has a CDF

$$F_{M_n}(m|m_{max}) = \begin{cases} 0, & \text{for } m < m_{min}, \\ [F_M(m|m_{max})]^n, & \text{for } m_{min} \le m \le m_{max}, \\ 1, & \text{for } m > m_{max}. \end{cases} \tag{31}$$

After integrating by parts, the expected value of M_n, $\varepsilon(M_n)$, is

Scientific Technical Report STR 98/05
DOI: 10.2312/GFZ.b103-98055

$$\varepsilon(M_n) = \int_{m_{min}}^{m_{max}} m \, dF_{M_n}(m|m_{max}) = m_{max} - \int_{m_{min}}^{m_{max}} F_{M_n}(m|m_{max})dm. \quad (32)$$

Hence

$$m_{max} = \varepsilon(M_n) + \int_{m_{min}}^{m_{max}} \left[F_M(m|m_{max})\right]^n dm. \quad (33)$$

This expression, after replacement of the **expected** value of maximum observed magnitude $\varepsilon(M_n)$ by the maximum magnitude already observed, m_{max}^{obs}, suggests an estimator of m_{max} of the form:

$$\hat{m}_{max} = m_{max}^{obs} + \int_{m_{min}}^{m_{max}^{obs}} \left[F_M(m|m_{max}^{obs})\right]^n dm. \quad (34)$$

This equation follows from the condition $\varepsilon(M_n) = m_{max}^{obs}$, and so, again, the value of m_{max} thus obtained, belongs to the class of moment estimators mentioned above (Kendall and Stuart, 1967). This estimator is valid for each CDF $F_M(m|m_{max})$, and does not require fulfilment of the truncation condition (5)-(7). It is also important to note that since the value of the integral $\int_{m_{min}}^{m_{max}^{obs}} \left[F_M(m|m_{max}^{obs})\right]^n dm$ is never negative, it provides a value of m_{max} which is never less than the maximum magnitude m_{max}^{obs}, already observed. The drawback of the formula is that it requires integration. For some of the magnitude distribution functions, the analytical expression for the integral does not exist, or even if it does exist, it requires awkward calculations.

Cooke (1979) was probably the first to obtain the estimator (34) as above. An alternative and independent derivation was given by Kijko (1983), who applied formalism of the moment generating functions.

Further modifications of estimator (34) are straightforward. For example, following the assumption that the number of earthquakes occurring in unit time within specified area obeys the Poisson distribution with parameter λ, Cooke's estimator (34) becomes

Scientific Technical Report STR 98/05
DOI: 10.2312/GFZ.b103-98055

$$\hat{m}_{\max} = m_{\max}^{obs} + \int_{m_{\min}}^{m_{\max}^{obs}} \left[F_M(m \mid m_{\max}^{obs}) \right]^{\lambda T} dm. \qquad (35)$$

Again, different approaches can be used in the estimation of higher moments (in particular, the variance) of the estimator (35). It is clear that for catalogues that at are long enough, the main "contributor" to the uncertainty in the estimation of parameter $\hat{m}_{\max}$ comes from the uncertainty of the maximum observed magnitude $m_{\max}^{obs}$. As in Procedure I, this uncertainty has two components: aleatory and epistemic. Elementary computations show that the approximation of aleatory uncertainty is of the order of the value of the integral in formula (35), that is,

$$Var(\hat{m}_{\max}) \cong \left\{ \int_{m_{\min}}^{m_{\max}^{obs}} \left[F_M(m \mid m_{\max}^{obs}) \right]^{\lambda T} dm \right\}^2. \qquad (36)$$

The effect of randomness in the number of earthquake occurrences and the effect of random error, ε, in the determination of maximum observed magnitude $m_{\max}^{obs}$ can be calculated by the same technique as in Procedure I. Assuming that the variance of ε is known, and is equal to σ_M^2, the approximate variance of estimator of $\hat{m}_{\max}$ (35) is

$$Var(\hat{m}_{\max}) \cong \sigma_M^2 + \left\{ \int_{m_{\min}}^{m_{\max}^{obs}} \left[F_M(m \mid m_{\max}^{obs}) \right]^{\lambda T} dm \right\}^2 + \lambda T \int_{m_{\min}}^{m_{\max}^{obs}} \ln \left[F_M(m \mid m_{\max}^{obs}) \right]^2 \left[F_M(m \mid m_{\max}^{obs}) \right]^{2\lambda T} dm. \qquad (37)$$

In most cases the third term in the equation (37), which is responsible for uncertainty in the number of earthquake occurrences, is significantly less than the first two, and its contribution may be neglected.

Scientific Technical Report STR 98/05
DOI: 10.2312/GFZ.b103-98055

Confidence Limits for Estimator II

The confidence limits for the estimator II of $\hat{m}_{max}$ can be constructed in several ways. Probably the simplest approach is to employ well-known results from the asymptotic distributions of extreme values. Such an approach provides general and asymptotic equations, which are useful when the initial CDF $F_M(m|m_{max})$ is not known. Since we are assuming that the analytical form of magnitude distribution is known, we may obtain more accurate equations by deriving explicity confidence limits for the given CDF

Let z_α be such that

$$Pr[m_{max}^{obs} < z_\alpha] = \alpha. \tag{38}$$

Since any probability CDF $F_M(m|m_{max})$ is a strictly increasing function, from equation (38) we obtain

$$Pr\ [F_M(m_{max}^{obs}|m_{max}) < F_M(z_\alpha|m_{max})] = \alpha, \tag{39}$$

from which, and (31), we obtain

$$Pr\left[\ [F_M(m_{max}^{obs}|m_{max})]^n < [F_M(z_\alpha|m_{max})]^n\ \right] = \alpha. \tag{40}$$

Therefore $[F_M(z_\alpha|m_{max})]^n = \alpha$, and z_α can be regarded as the inverse of the probability transformation and equal to $F_M^{-1}(\alpha^{1/n}|m_{max})$. Hence, a $100(1 - \alpha)\%$ upper confidence limit on $\hat{m}_{max}$ can be obtained from the relation

$$Pr\left\{ F_M^{-1}(\alpha^{1/n}|m_{max}) < m_{max}^{obs} \right\} = 1 - \alpha. \tag{41}$$

An application of the above formula for the determination of the upper confidence limit for the maximum regional magnitude m_{max}, when the magnitude distribution follows the Gutenberg-Richter relation, is given in the following section.

Both the derivation of the fiducial distribution and the treatment of uncertainties in the distribution parameters **P**, can be done by applying the same technique as was done under Procedure I.

Scientific Technical Report STR 98/05
DOI: 10.2312/GFZ.b103-98055

2.1.4. Application to the Gutenberg-Richter magnitude distribution

In this Section we will demonstrate how to apply the above formalism to one of the most often used frequency-magnitude relationships - the one introduced by Gutenberg and Richter.

Application of the Estimator I to the Gutenberg-Richter Magnitude Distribution

By the original definition of this procedure, the estimation of m_{max} is obtained as a root of equation (12)

$$F_M(m_{max}^{obs} | \hat{m}_{max}) = \frac{n}{n+1} \tag{42}$$

where the Gutenberg-Richter CDF of earthquake magnitude $F_M(m|m_{max})$ is defined by equation (4). Hence

$$\frac{1 - \beta\exp[-\beta(m - m_{min})]}{1 - \beta\exp[-\beta(\hat{m}_{max} - m_{min})]} = \frac{n}{n+1}, \tag{43}$$

from which the required m_{max} is obtained as

$$\hat{m}_{max} = -\frac{1}{\beta} \ln \left\{ \exp(-\beta m_{min}) - [\exp(-\beta m_{min}) - \exp(-\beta m_{max}^{obs})] \frac{n+1}{n} \right\}. \tag{44}$$

Here, m_{max}^{obs} is the maximum observed magnitude in the catalogue, for the time span T, and n is the number of earthquakes occurring within T, having magnitude equal to or exceeding the level of completeness, m_{min}. The above estimator was first used by Gibowicz and Kijko (1994) for the assessment of the magnitude of the maximum possible seismic events in the Klerksdorp gold mining district in South Africa.

Unfortunately, such a straightforward solution as given by the formula (44) is not always possible - the RHS is not defined if the argument in braces turns out negative. It is therefore preferable to use Tate's (1959) formula (16), which, for the Gutenberg-Richter PDF takes the simple form

Scientific Technical Report STR 98/05
DOI: 10.2312/GFZ.b103-98055

$$\hat{m}_{max} = m_{max}^{obs} + \frac{1}{n} \frac{1 - \exp[-\beta(m_{max}^{obs} - m_{min})]}{\beta \exp[-\beta(m_{max}^{obs} - m_{min})]} . \quad (45)$$

Equation (45) describes Tate's (1959) estimator, as applied to the Gutenberg-Richter magnitude distribution. If the number of earthquakes n that have occurred is not known, but the mean activity rate λ of earthquake occurrence is available, equation (45) can be used after replacement of n by λT. Equation (45) is in good agreement with our intuitive expectations: for given values of β and m_{min}, the larger n is, or the larger the period of observation T, the less the estimated maximum regional magnitude $\hat{m}_{max}$ deviates from the maximum observed magnitude m_{max}^{obs}. The estimation of maximum regional magnitude m_{max} by application of Tate's (1959) formula (16) was first used by Pisarenko *et al.* (1996). We shall denote the estimator of equation (45) as the Tate-Pisarenko estimator of m_{max}, or in short as T-P.

Following (25), the approximate variance of the T-P estimator of m_{max}, for the Gutenberg-Richter CDF of earthquake magnitude is given by

$$Var(\hat{m}_{max}) \cong \sigma_M^2 + \frac{n+1}{n^3} \frac{\{1 - \exp[-\beta(m_{max}^{obs} - m_{min})]\}^2}{\beta^2 \exp[-2\beta(m_{max}^{obs} - m_{min})]} . \quad (46)$$

Finally, following (27), a $100(1 - \alpha)\%$ upper confidence limit for $\hat{m}_{max}$, estimated by the T-P equation, is given by

$$Pr\left[m_{max} < -\frac{1}{\beta} \ln \left\{ \exp(-\beta m_{min}) - \alpha^{-1/n} [\exp(-\beta m_{min}) - \exp(-\beta m_{max}^{obs})] \right\} \right] = 1 - \alpha, \quad (47)$$

while the fiducial distribution (equation 28) takes the form

$$Pr\left[m_{max} < z \right] = \left[\frac{1 - \beta \exp[-\beta(m_{max}^{obs} - m_{min})]}{1 - \beta \exp[-\beta(z - m_{min})]} \right]^n . \quad (48)$$

Again, if the number of earthquakes n is not known, equations (45)-(48) can be used after replacement of n by λT.

Scientific Technical Report STR 98/05
DOI: 10.2312/GFZ.b103-98055

Following (34), estimator II requires calculation of the integral $\int_{m_{min}}^{m_{max}^{obs}} \left[F_M(m|m_{max}^{obs})\right]^n dm$, where for the Gutenberg-Richter magnitude distribution, the CDF $F_M(m|m_{max})$ is described by equation (4). Fortunately, for n large, after substitution of n by λT, the expression $\left[F_M(m|m_{max})\right]^n$ can be replaced by its Cramér's approximation (Cramér, 1948) as:

$$\left[F_M(m|m_{max})\right]^n \cong \exp\left\{-\lambda T\left[\frac{\exp[-\beta(m - m_{min})] - \exp[-\beta(m_{max} - m_{min})]}{1 - \exp[-\beta(m_{max} - m_{min})]}\right]\right\}, \tag{49}$$

and the integral in equation (34), (Kijko and Sellevoll, 1989) is equal to

$$\int_{m_{min}}^{m_{max}^{obs}} \left[F_M(m|m_{max}^{obs})\right]^n dm = \frac{E_1(Tz_2) - E_1(Tz_1)}{\beta\exp(-Tz_2)} - m_{min}\exp(-\lambda T), \tag{50}$$

where $z_1 = -\lambda A_1/(A_2 - A_1)$, $z_2 = -\lambda A_2/(A_2 - A_1)$, $A_1 = \exp(-\beta m_{min})$, $A_2 = \exp(-\beta m_{max}^{obs})$, and $E_1(\cdot)$ denotes an exponential integral function (Abramowitz and Stegun, 1970)

$$E_1(z) = \int_z^{\infty} \exp(-\zeta)/\zeta \, d\zeta. \tag{51}$$

The function $E_1(z)$ can be conveniently approximated as

$$E_1(z) = \frac{1}{z}\exp(-z)\frac{z^2 + a_1 z + a_2}{z^2 + b_1 z + b_2}, \tag{52}$$

where $a_1 = 2.334733$, $a_2 = 0.250621$, $b_1 = 3.330657$, and $b_2 = 1.681534$. Formula (52) is an approximation of the exponential integral function with a maximum error of 5.10^{-5} over the interval $1 \le z \le \infty$.

Scientific Technical Report STR 98/05
DOI: 10.2312/GFZ.b103-98055

Hence, following a general solution (equation 34) for the Gutenberg-Richter-based magnitude CDF, the estimator of m_{max} is

$$\hat{m}_{max} = m_{max}^{obs} + \frac{E_1(Tz_2) - E_1(Tz_1)}{\beta \exp(-Tz_2)} - m_{min}\exp(-\lambda T). \qquad (53)$$

The above estimator of m_{max} for the doubly truncated Gutenberg-Richter relation was first obtained by Kijko (1983), who was inspired by discussions with Professor M. Sellevoll from Bergen University, Norway. Subsequently equation (53) has been used for estimation of the maximum regional earthquake magnitude in more than 30 seismic areas of the world. We shall denote equation (53) as the Kijko-Sellevoll estimator or, in short, K-S.

From equations (37) and (49), the approximate variance of the maximum regional magnitude $\hat{m}_{max}$, estimated according to the K-S procedure, is

$$Var(\hat{m}_{max}) = \sigma_M^2 + \left[\frac{E_1(Tz_2) - E_1(Tz_1)}{\beta \exp(-Tz_2)} - m_{min}\exp(-\lambda T) \right]^2. \qquad (54)$$

It can be shown that the upper confidence limits for m_{max} (equation 41) and for the fiducial distribution have the same form as the respective equations for Procedure I.

Treatement of Uncertainty in the b-value of Gutenberg-Richter

Let us derive the Gutenberg-Richter-based, compound CDF of earthquake magnitude. In order to do this, we have to specify the form of the PDF $f_P(\mathbf{p})$ (equation 30), which characterizes the uncertainty of the Gutenberg-Richter parameter b. One of the best candidates for such a choice is the gamma distribution, since it is flexible and can fit a large variety of shapes (e.g. DeGroot, 1970). Following (30) and by assuming that the variation of the β-value in the Gutenberg-Richter-based CDF (4) may be represented by a gamma CDF having parameters p and q, the compound CDF of earthquake magnitudes (Campbell, 1982) takes the form:

Scientific Technical Report STR 98/05
DOI: 10.2312/GFZ.b103-98055

$$F_M(m|m_{max}) = \begin{cases} 0 & \text{for } m < m_{min}, \\ C_\beta \left[1 - \left(\dfrac{p}{p + m - m_{min}} \right)^q \right], & \text{for } m_{min} \le m \le m_{max}, \\ 1, & \text{for } m > m_{max}. \end{cases} \quad (55)$$

where C_β is a normalizing coefficient. It is not difficult to show that p and q can be expressed through the mean and variance of the β-value, where $p = \bar{\beta}/(\sigma_\beta)^2$ and $q = (\bar{\beta}/\sigma_\beta)^2$. The symbol $\bar{\beta}$ denotes the mean value of the parameter β, σ_β is the known standard deviation of β and describes its uncertainty, and C_β is equal to

$$C_\beta = \left[1 - \left(\frac{p}{p + m_{max} - m_{min}} \right)^q \right]^{-1}. \quad (56)$$

Equation (55) is known as the Bayesian exponential-gamma CDF of earthquake magnitude.

This way of dealing with the uncertainty of parameter β is far from unique. For example, for the same purpose Mortgat and Shah (1979) used a combination of the Bernoulli and the beta distributions. Dong *et al.* (1984) as well as Stavrakasis and Tselentis (1987) used a combination of uniform and multinomial distributions. An excellent study on how to handle all kinds of uncertainties that are present in the parameters, the model, and the data, can be found in the paper by Rhoades *et al.* (1994).

Knowledge of equation (55) makes it possible to construct the Bayesian version of estimators T-P and K-S. Following (55), the PDF of Bayesian exponential-gamma distribution is equal to

$$f_M(m|m_{max}) = \begin{cases} pqC_\beta \left(\dfrac{p}{p + m - m_{min}} \right)^{q+1}, & \text{for } m_{min} \le m \le m_{max} \\ 0, & \text{for } m < m_{min}, \quad m \ge m_{max}. \end{cases} \quad (57)$$

Thus, following (16) and (25), the Bayesian extension of the T-P estimator and its approximate variance become,

Scientific Technical Report STR 98/05
DOI: 10.2312/GFZ.b103-98055

$$\hat{m}_{max} = m_{max}^{obs} + \frac{1}{nC_\beta\, pq}\left[\frac{p}{p + m_{max}^{obs} - m_{min}}\right]^{-(q+1)} \tag{58}$$

and

$$Var(\hat{m}_{max}) \cong \sigma_M^2 + \frac{1}{(C_\beta\, pq)^2}\left[\frac{p}{p + m_{max}^{obs} - m_{min}}\right]^{-2(q+1)}\left[\frac{n+1}{n^3}\right]. \tag{59}$$

The Bayesian version of the T-P estimator (equation 58), will be denoted as T-P-B.

Unfortunately the derivation of the Bayesian version of the K-S estimator is not so straightforward. By definition, (equation 34), it requires the calculation of the integral

$$\Delta = \int_{m_{min}}^{m_{max}^{obs}}\left[F_M(m|m_{max}^{obs})\right]^n = C_\beta^n \int_{m_{min}}^{m_{max}^{obs}}\left[1 - \left(\frac{p}{p + m - m_{min}}\right)^q\right]^n dm, \tag{60}$$

which can only be approximated. Again, one of the simplest approximations can be obtained by application of Cramér's procedure in the derivation of asymptotic extreme distributions. Following Cramér (1948), for large n, the value of $\left[F_M(m|m_{max}^{obs})\right]^n$ is approximately equal to $\exp\{-n[1-F_M(m|m_{max}^{obs})\}$, and therefore integral (60) takes the form

$$\Delta = c_1 \int_{m_{min}}^{m_{max}^{obs}} \exp\left[-nC_\beta\left(\frac{p}{p + m - m_{min}}\right)^q\right] dm, \tag{61}$$

where $c_1 = \exp[-n(1-C_\beta)]$. Further simple calculations lead to the following equation:

Scientific Technical Report STR 98/05
DOI: 10.2312/GFZ.b103-98055

$$\Delta = \frac{pc_1}{q} \frac{1}{\delta - 1/q} \sum_{i=0}^{\infty} (-1)^i \frac{\delta^{i-1/q} \left[1 - \left(\frac{p}{p + m_{max}^{obs} - m_{min}} \right)^{q^{i-1/q}} \right]}{(i - 1/q)\, i!}, \qquad (62)$$

where $\delta = nC_\beta$. This leads to the Bayesian version of the K-S estimator

$$\boxed{\hat{m}_{max} = m_{max}^{obs} + \Delta,} \qquad (63)$$

and its variance

$$\boxed{Var(\hat{m}_{max}) \cong \sigma_M^2 + \Delta^2.} \qquad (64)$$

The Bayesian version of the K-S estimator (equation 62-63) we will denote as K-S-B .

From the above relations it follows that the assessment of the maximum credible regional magnitude m_{max} requires knowledge of the seismic activity rate λ, and the Gutenberg-Richter parameter b. The maximum likelihood procedure for the assessment of these two parameters is presented in the Section 2.2.

2.1.5. Comparison of procedures I and II

One way to compare the performance of estimators based on Procedures I and II is to use an empirical approach in a simulation study.

We choose a value of $m_{max} = 6.5$, $\beta = 2$, (or equivalently $b \cong 0.87$), and $m_{min} = 3.0$, and then simulate earthquake magnitudes from a Gutenberg-Richter-based CDF as equation (4) or (55). Then we compare the two estimated magnitudes $\hat{m}_{max}^{(I)}$ and $\hat{m}_{max}^{(II)}$ computed according to the Procedure I and Procedure II respectively, with the true value of $m_{max} = 6.5$, to see which estimator performed better. This operation was repeated 1000 times in order to discern a general pattern with respect to the relative performance of the estimators.

Two properties of estimators were studied: bias and mean error. It should be realized that when an estimator is biased (i.e. it has a **systematic** error), it is often possible to find some simple correction that removes the bias altogether. Even when this cannot be done, a biased estimate can be used, provided only that we are able to show that the amount of the bias is small - which is often the case in large samples.

Scientific Technical Report STR 98/05
DOI: 10.2312/GFZ.b103-98055

On the other hand, even when an estimator is unbiased it is of little use if we do not know the extent of its dispersion about the true value. A natural measure of **dispersion** about the given point is provided by the second order moment. Accordingly, the efficiency of our two estimators for the maximum regional magnitude m_{max}, viz. $\hat{m}_{max}^{(I)}$ and $\hat{m}_{max}^{(II)}$, can be compared by means of the corresponding mean errors $\sqrt{\varepsilon(\hat{m}_{max}^{(I)} - m_{max})^2}$ and $\sqrt{\varepsilon(\hat{m}_{max}^{(II)} - m_{max})^2}$. Clearly the estimate having the smaller mean error is the more efficient one.

Comparison of Performance of Estimators T-P *and* K-S.

In this section we shall illustrate the performance of the two "standard" estimators, viz. T-P and K-S, in the case when the error in the b-value is so small that it can be neglected. We have repeated our simulations 1000 times for different numbers of earthquakes, ranging from 50 to 250.

Figure 2a show the average of 1000 solutions computed respectively by estimator T-P and K-S. The K-S solutions are significantly closer to the "true" value of $m_{min} = 6.5$ than the corresponding solutions provided by estimator T-P.

Figure 2b illustrates respective mean errors. The figure shows very clearly that in terms of mean error, the estimator K-S is indisputably more efficient than T-P. The superiority of estimator K-S is seen especially clearly when the number of earthquakes is small (say 50-100); in this case the mean error in the estimation of m_{max} by T-P is several times larger than for the corresponding estimator K-S. The large errors, (up to 2 units of earthquake magnitude), practically disqualify the use of T-P estimator in the case of a small sample of observations.

Comparison of Performance of Estimators T-P-B *and* K-S-B.

The next 3 figures show the performance of estimators T-P and K-S and their Bayesian counterparts (viz. T-P-B and K-S-B) in the presence of uncertainties in the Gutenberg-Richter parameter b.

Figures 3 and 4 show application of these estimators in two situations: when the presence of uncertainty in the Gutenberg-Richter parameter b is taken into account (m_{max}

Scientific Technical Report STR 98/05
DOI: 10.2312/GFZ.b103-98055

Scientific Technical Report STR 98/05
DOI: 10.2312/GFZ.b103-98055

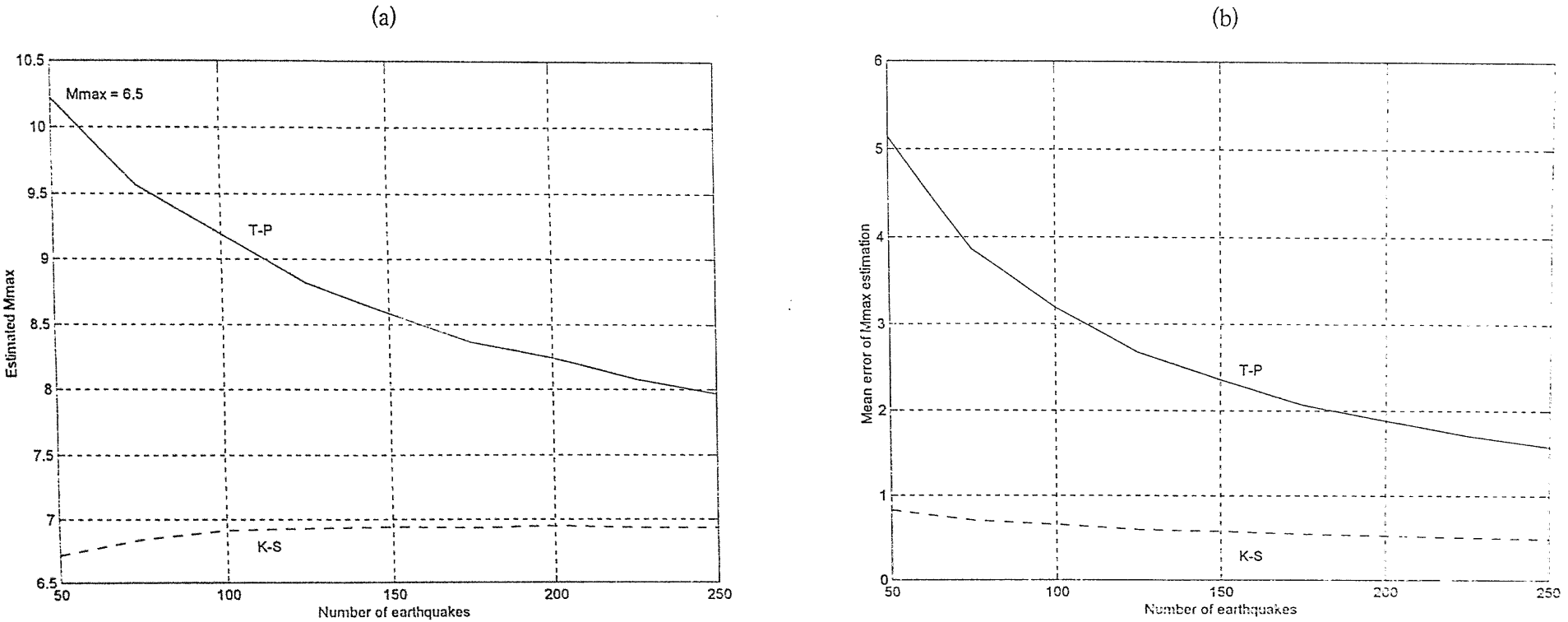

Fig. 2. Comparison of performance of estimators Tate-Pisarenko (T-P) and Kijko-Sellevoll (K-S) based on 1000 synthetic catalogues where the "true" value of m_{max} = 6.5. Superiority of estimator K-S is clearly seen, especially for small number of earthquakes. (a) Mean value of m_{max} estimation. (b) Mean error of m_{max} estimation.

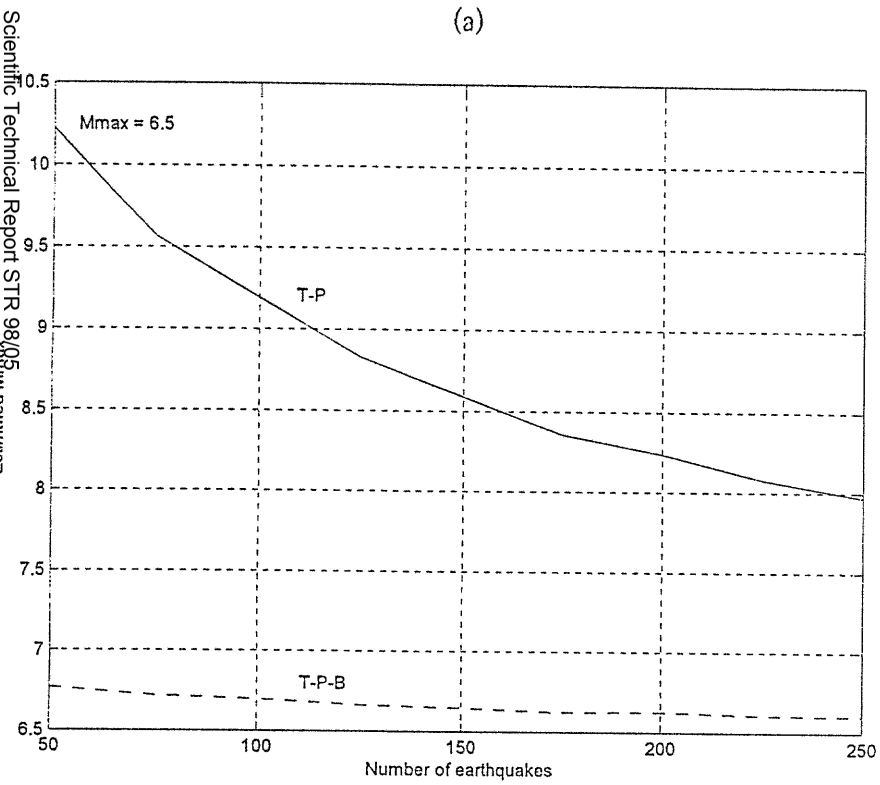

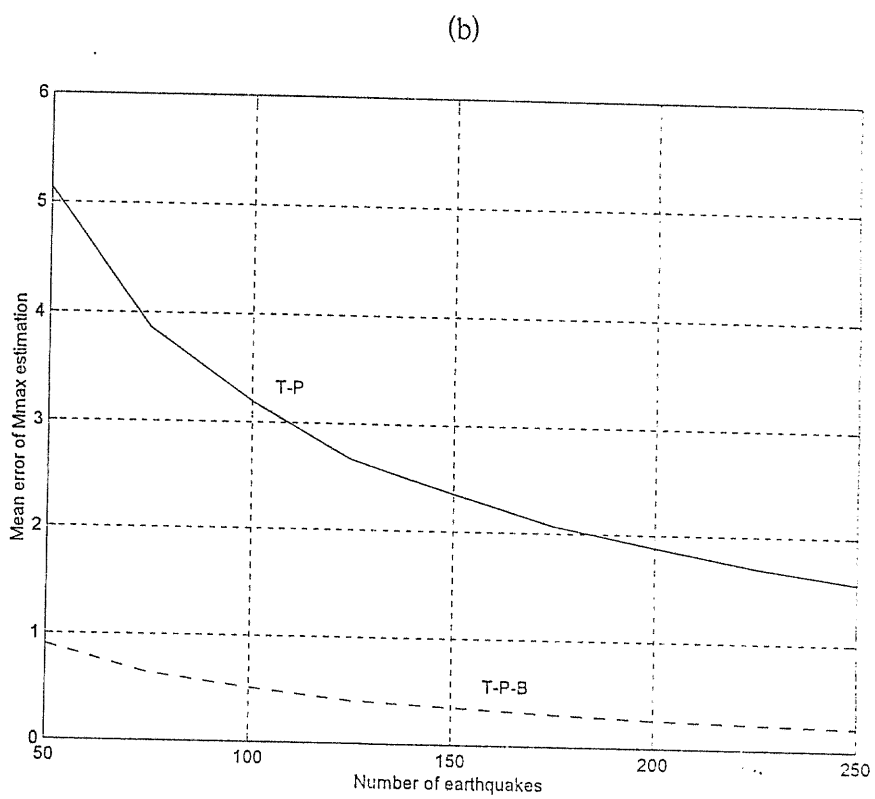

Fig. 3. Comparison of performance of estimator T-P and its Bayesian counterpart (viz. T-P-B) based on 1000 synthetic catalogues where the "true" value of $m_{\max} = 6.5$ and the b-value was subjected to random, normally distributed error with zero mean and standard deviation equal to 25% of b-value. Application of Bayesian estimator T-P-B significantly reduces the bias as well as mean error. (a) Mean value of $m_{\max}$ estimation. (b) Mean error of $m_{\max}$ estimation.

Scientific Technical Report STR 98/05
DOI: 10.2312/GFZ.b103-98055

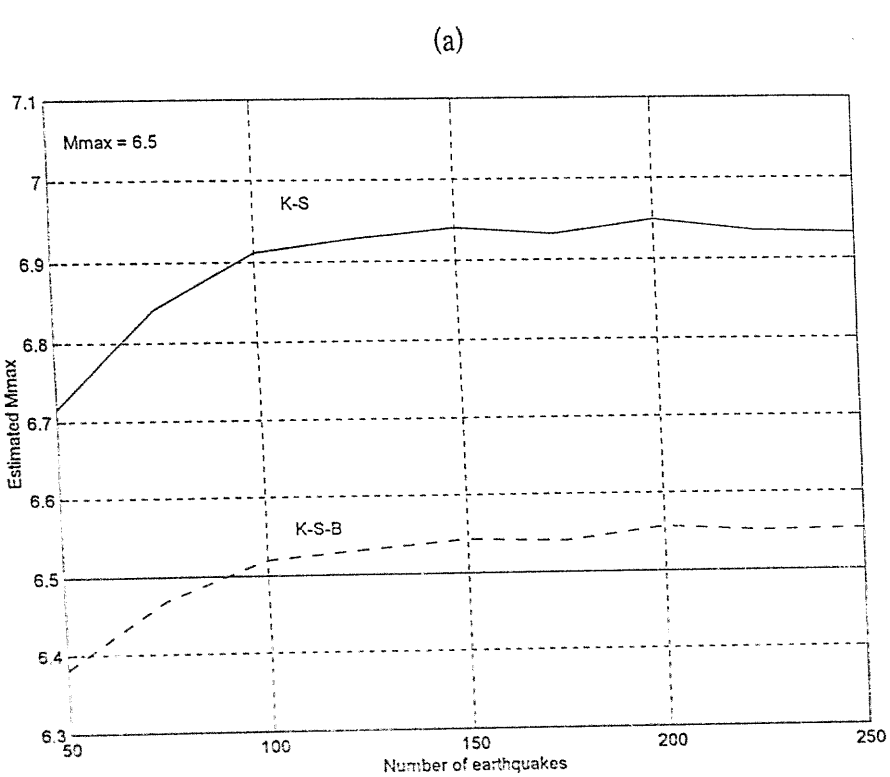

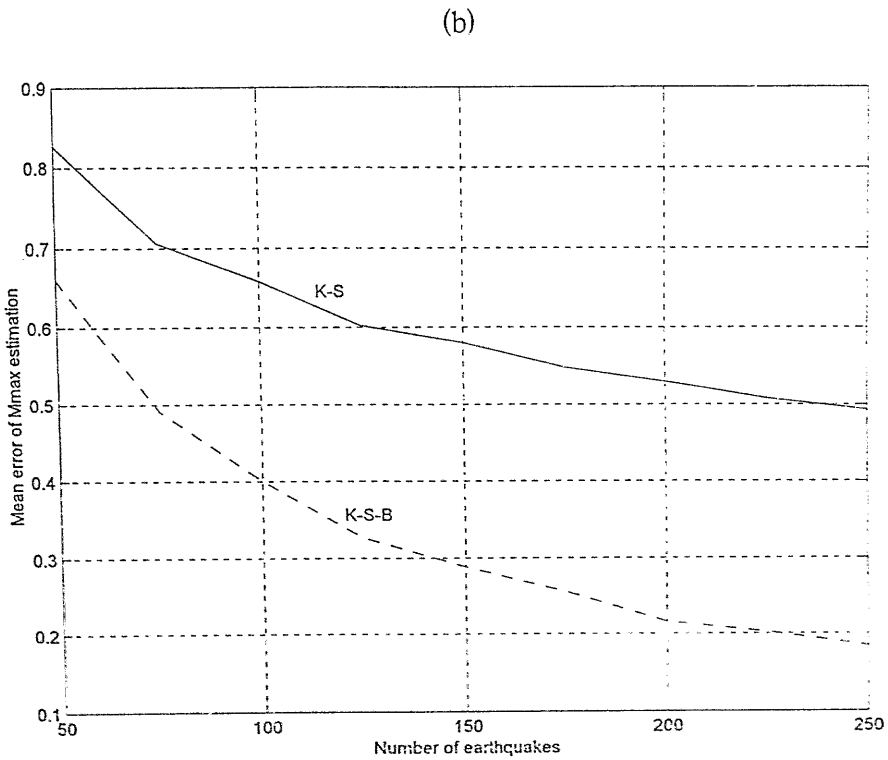

Fig. 4. Comparison of performance of estimator K-S and its Bayesian counterpart (viz. K-S-B) based on 1000 synthetic catalogues where the "true" value of m_{max} = 6.5 and the b-value was subjected to random, normally distributed error with zero mean and standard deviation equal to 25% of b-value. Application of Bayesian estimator T-P-B significantly reduces the bias as well as mean error. (a) Mean value of m_{max} estimation. (b) Mean errors of m_{max} estimation.

Scientific Technical Report STR 98/05
DOI: 10.2312/GFZ.b103-98055

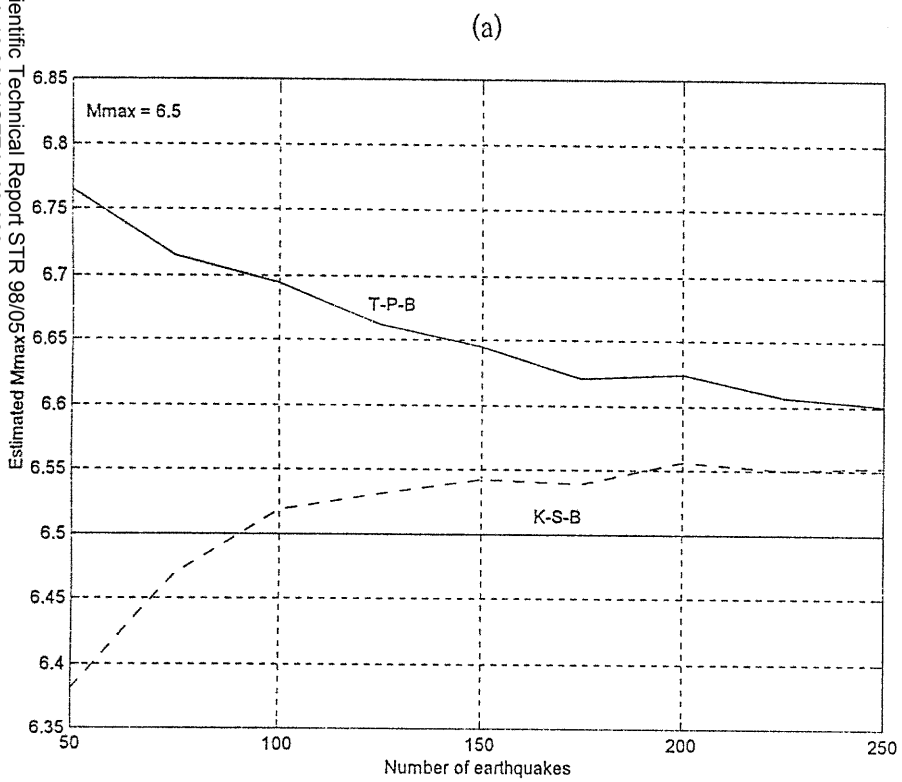

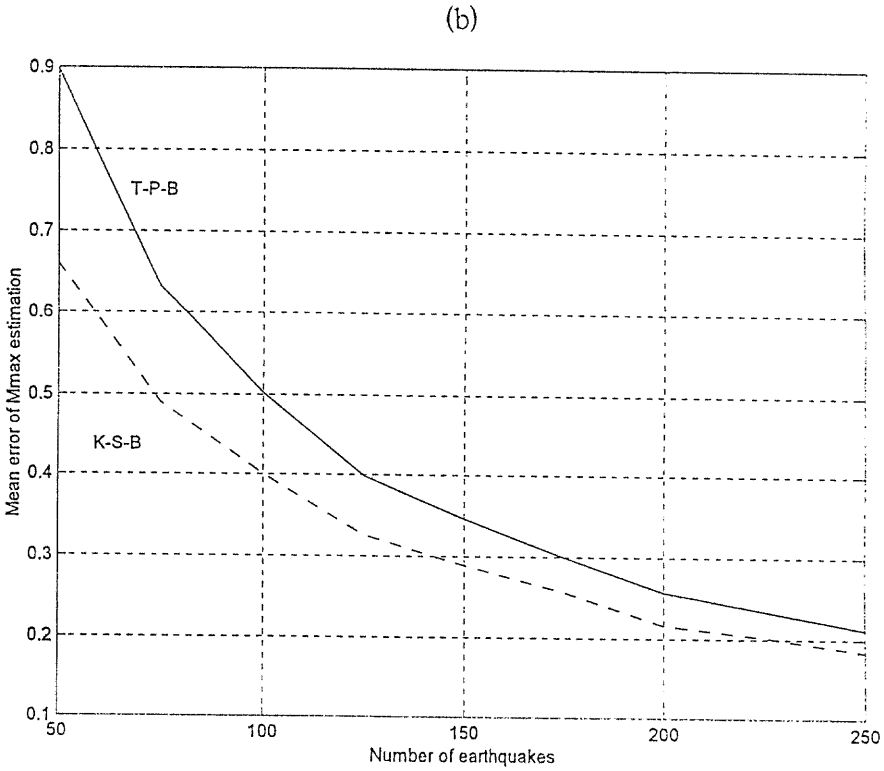

Fig. 5. Comparison of performance of estimators Tate-Pisarenko-Bayes (T-P-B) and Kijko-Sellevoll-Bayes (K-S-B) based on 1000 synthetic catalogues where the "true" value of m_{max} = 6.5 and the b-value was subjected to random, normally distributed error with zero mean and standard deviation equal to 25% of b-value. (a) Mean value of m_{max} estimation. (b) Mean error of m_{max} estimation.

is estimated by the respective Bayesian distributions), and when the uncertainty in the b-value is ignored.

Figure 3a illustrates the results of the estimation of m_{max} by 2 estimators: T-P and T-P-B, where during the data generation procedure, the b-value was subjected to a random, normally distributed error with mean zero and standard deviation σ_b equal to 25% of the b-value. This figure shows very clearly that an application of the "standard" procedure, (viz. estimator T-P), which does not take into account the presence of errors in the b-value, leads to significantly biased (overestimated) values of m_{max}. Figure 3b shows the respective mean errors. Application of the respective Bayesian procedure significantly reduces the bias as well as the mean error.

Figure 4 is analogous to Figure 3, but here the estimators of Procedure I have been replaced by the respective estimators of Procedure II, viz. K-S, and K-S-B.

Figure 5 shows the performance of estimators T-P-B and K-S-B in the presence of uncertainties in Gutenberg-Richter parameter b.

The above numerical experiments have show that both the Bayesian estimators, particularly K-S-B, tend to perform well in the presence of significant uncertainty in the b-value.

2.2. Assessment of the Activity Rate λ and the Gutenberg-Richter Parameter b

In the procedure applied here, cognisance is taken of the fact that earthquake catalogues frequently contain mixed data. In general, the extreme part of the catalogue contains information on the strongest historical events and the complete part includes more recent observations, instrumental and/or macroseismic. The complete part can be divided into several subcatalogues, each one complete above a given magnitude threshold. One or more periods of time can be omitted if seismic records are missing or uncertain (Figure 1).

2.2.1. Extreme magnitude distribution as applied to the macroseismic part of the catalogue

If we assume the Poisson occurrence of earthquakes with activity rate λ and the validity of the doubly truncated, Gutenberg-Richter-based CDF (4), then the probability that in a time interval t, either **no** earthquake occurs or **all** occurring earthquakes have magnitude

Scientific Technical Report STR 98/05
DOI: 10.2312/GFZ.b103-98055

not exceeding m, may be expressed as (e.g. Gan and Tung, 1983)

$$\exp\{-\lambda_0 t[1 - F_M(m|m_{min},m_{max})]\}, \tag{65}$$

where $\lambda_0 = \lambda[1 - F_M(m_0|m_{min},m_{max})]$[6] is the mean activity rate of earthquakes occurring within the specified area with magnitude m_0 and above; m_0 is the smaller earthquake magnitude in the extreme part of the catalogue, and $m_0 \geq m_{min}$. Magnitude m_{min} is the minimum threshold magnitude for the entire catalogue. The condition in the choice of its value is that m_{min} cannot exceed m_0, or any level of completeness of any part of the complete subcatalogue (Figure 1). Hence, the CDF of the strongest earthquake during the time interval t, is given by

$$F_M^{max}(m|m_0,m_{max},t) = \frac{\exp\{-\lambda_0 t[1-F_M(m|m_0,m_{max})]\} - \exp(-\lambda_0 t)}{1 - \exp(-\lambda_0 t)} \tag{66}$$

In most real cases we deal with a high enough activity rate λ_0 and long enough time intervals t. Hence the term $\exp(-\lambda_0 t)$ can be ignored.

2.2.2. Uncertainty in magnitude

If the error of determination of magnitude is assumed to be normally distributed with a standard deviation σ_M, the PDF and CDF of the apparent magnitude become (Kijko and Sellevoll, 1992; Gibowicz and Kijko, 1994)

$$f_M(m|m_{min},m_{max},\sigma_M) = f_M(m|m_{min},m_{max})\ C_\sigma(m), \tag{67}$$

$$F_M(m|m_{min},m_{max},\sigma_M) = F_M(m|m_{min},m_{max})\ D_\sigma(m), \tag{68}$$

respectively, where

$$C_\sigma(m) = \frac{e\chi^2}{2}\left[\mathrm{erf}\left(\frac{m_{max} - m}{\sqrt{2}\,\sigma_M} + \chi\right) + \mathrm{erf}\left(\frac{m - m_{min}}{\sqrt{2}\,\sigma_M} - \chi\right)\right], \tag{69}$$

---

6 From now on in text, notations like $f_M(m|m_{max})$, and $F_M(m|m_{max})$ are replaced by $f_M(m|m_{min},m_{max})$ and $F_M(m|m_{min},m_{max})$, respectively. Hence, in all distributions, we show both the lowel and the upper limit of the magnitude range.

Scientific Technical Report STR 98/05
DOI: 10.2312/GFZ.b103-98055

$$D_\sigma(m) = \left\{ A_1 \left[\operatorname{erf}\left(\frac{m - m_{\min}}{\sqrt{2}\,\sigma_M} \right) + 1 \right] + A_2 \left[\operatorname{erf}\left(\frac{m_{\max} - m}{\sqrt{2}\,\sigma_M} \right) - 1 \right] \right.$$

$$\left. - 2C_\sigma(m)\, A(m) \right\} \,/\, 2[A_1 - A(m)], \tag{70}$$

$A(m) = \exp(-\beta m)$, $A_1 = \exp(-\beta m_{\min})$, $A_2 = \exp(-\beta m_{\max})$, $\operatorname{erf}(\cdot)$ is the error function, $\chi = \beta\sigma_M/\sqrt{2}$, and the magnitude m is unbounded from both ends.

Further application of distributions (67)-(68) requires additional renormalizations. If m_0 is the lowest magnitude at and above which the observations are complete, then its **normalized** PDF $\tilde{f}_M(m|m_0,m_{\max},\sigma_M)$ is zero up to m_0, and is equal to $f_M(m|m_{\min},m_{\max},\sigma_M)/[1 - F_M(m_0|m_{\min},m_{\max},\sigma_M)]$ for $m \geq m_0$. In a similar way, the **normalized** CDF of apparent magnitude is

$$\tilde{F}_M(m|m_0,m_{\max},\sigma_M) = \frac{F_M(m|m_{\min},m_{\max},\sigma_M) - F_M(m_0|m_{\min},m_{\max},\sigma_M)}{1 - F_M(m_0|m_{\min},m_{\max},\sigma_M)}. \tag{71}$$

In fact, $\tilde{f}_M(m|m_0,m_{\max},\sigma_M)$ and $\tilde{F}_M(m|m_0,m_{\max},\sigma_M)$ are conditional distributions of m given that $m \geq m_0$.

Finally, assuming that the model in which the PDF of magnitude vanishes below the cut-off value of m_0 is unrealistic, (in practice the transition occurs gradually) the relation between the apparent activity rate $\tilde{\lambda}(m)$ and the "true" one takes the form

$$\tilde{\lambda}(m) = \lambda(m)\,\frac{e\chi^2}{2}\left[1 + \operatorname{erf}\left(\frac{m_{\max} - m}{\sqrt{2}\,\sigma_M} + \chi \right) \right]. \tag{72}$$

2.2.3. The likelihood function of seismicity parameters

From relation (66) it follows that $f_M^{\max}(m|m_0,m_{\max},t,\sigma_M)$, the PDF of the strongest earthquake within a period t with apparent magnitude m and standard deviation σ_M, is:

Scientific Technical Report STR 98/05
DOI: 10.2312/GFZ.b103-98055

$$f_M^{max}(m|m_0,m_{max},t,\sigma_M) = \frac{\tilde{\lambda}_0 t \tilde{f}_M(m|m_0,m_{max},t,\sigma) \cdot \exp[-\tilde{\lambda}_0 t[1 - \tilde{F}_M(m|m_0,m_{max},t,\sigma_M)]}{1 - \exp(-\tilde{\lambda}_0 t)}. \quad (73)$$

After introducing the PDF (73), the likelihood function of unknown parameters (λ,β), following from the extreme part of the catalogue, becomes

$$L_0(\lambda,\beta|\mathbf{m}_0) = const \prod_{i=1}^{n_0} f_M^{max}(m_{0i}|m_0,m_{max},t_{0i},\sigma_{M0i}). \quad (74)$$

In relation (74), the $\mathbf{m}_0 = (m_{0i},\sigma_{M0i},t_i)$, where m_{0i} is the apparent magnitude of the strongest earthquake occurring during the time interval t_i, σ_{M0i} is the value of its standard deviation, $i = 1,\ldots, n_0$, and n_0 is the number of earthquakes in the extreme part of the catalogue. The time intervals t_i are calculated according to the simple formula:

$$t_i = \begin{cases} \tau_1 - t_{01}, & \text{for } i = 1 \\ \tau_i - \tau_{i-1}, & \text{for } i = 2,\ldots, n_0 - 1 \\ t_{02} - \tau_{n_0-1}, & \text{for } i = n_0, \end{cases} \quad (75)$$

where t_{01} and t_{02} are the beginning and the end of the extreme part of the catalogue, and $\tau_1,\ldots,\tau_{n_0}$ are the earthquake origin times. *Const* is a normalization factor independent of parameters λ and β.

Let us assume that the second, complete part of the catalogue can be divided into s subcatalogues (Figure 1). Each of them has a time span T_i and is complete, starting from the known magnitude m_i. For each subcatalogue i, the $\mathbf{m}_i = (m_{ij},\sigma_{Mij})$ be the apparent magnitude together with its standard deviation where $j = 1,\ldots, n_i$, where n_i denotes the number of earthquakes in each complete subcatalogue and $i = 1,\ldots, s$.

If the size of seismic events is independent of their number, the likelihood function of (λ,β), for each complete subcatalogue i, is equal to

$$L_i(\lambda,\beta|\mathbf{m}_i) = L_\beta(\beta|\mathbf{m}_i) \cdot L_\lambda(\lambda|\mathbf{m}_i), \quad (76)$$

which is the product of the likelihood function of β, $L_\beta(\beta|\mathbf{m}_i)$, and the likelihood

Scientific Technical Report STR 98/05
DOI: 10.2312/GFZ.b103-98055

function of λ, $L_\lambda(\lambda|\mathbf{m}_i)$. The above relations generate $L_\beta(\beta|\mathbf{m}_i)$ of the following form:

$$L_\beta(\beta|\mathbf{m}_i) = \text{const} \prod_{j=1}^{n_i} \mathcal{F}_M(m_{ij}|m_i,m_{max},\sigma_{Mij}). \tag{77}$$

The assumption that the number of earthquakes per unit time is a Poisson random variable gives a form of $L_\lambda(\lambda|\mathbf{m}_i)$ equal to

$$L_\lambda(\lambda|\mathbf{m}_i) = const\ (\tilde{\lambda}_i t_i)^{n_i} \exp(-\tilde{\lambda}_i t_i), \tag{78}$$

where *const* is a normalizing factor. The apparent activity rate is defined by relation (72), and $\lambda_i = \lambda[1 - F_M(m_i|m_{min},m_{max})]$.

Relations (76)-(78), for $i = 1,\ldots s$, define the likelihood functions of the parameters sought for each complete subcatalogue. Finally, the joint likelihood function based on all data, extreme and complete, is given by:

$$L(\lambda,\beta|\mathbf{m}) = \prod_{i=0}^{n_s} L_i(\lambda,\beta|\mathbf{m}_i). \tag{79}$$

The maximum likelihood estimates λ and β are the values of $\hat{\lambda}$ and $\hat{\beta}$ that maximize the likelihood function (79). From the formal point of view, the maximum likelihood estimate of m_{max} is simply the largest observed earthquake magnitude m_{max}^{obs}. This follows from the fact that the likelihood function (79) decreases monotonically for $m_{max} \longrightarrow \infty$. Therefore by including one of the formulae for m_{max} [i.e. the T-P estimator (45), its Bayesian version (58), the K-S estimator (53), or its Bayesian version (63)], we obtain a set of equations determining the maximum likelihood estimate of $\hat{\lambda}$, $\hat{\beta}$ and $\hat{m}_{max}$. Such a set of equations can be solved by an iterative procedure (Kijko and Sellevoll, 1989).

2.3. Distribution of Accelerations Recorded at the Site

Our aim is to calculate the conditional probability that a single earthquake of random magnitude M at a distance R will cause a peak ground acceleration (PGA) equal to, or greater than, an acceleration of engineering interest a_{min}. For this purpose we use the assumption (e.g. Boore and Joyner, 1982; Ambraseys, 1995), that in the range of interest

Scientific Technical Report STR 98/05
DOI: 10.2312/GFZ.b103-98055

the attenuation curve of the peak ground acceleration a, has the following form:

$$\ln(a) = c_1 + c_2 \cdot m + \phi(r), \tag{80}$$

where c_1 and c_2 are empirical constants, m is the earthquake magnitude, and $\phi(r)$ is a function of earthquake distance r. Usually $\phi(r)$ is of the form

$$\phi(r) = c_3 \cdot \ln(r) + c_4 \cdot r, \tag{81}$$

where c_3, and c_4 are empirical constants and $\ln(\cdot)$ denotes the natural logarithm.

If an earthquake of magnitude M occurs at a distance R from the site, the probability that this earthquake will cause a PGA equal to, or greater than a, is given by

$$Pr[\text{PGA} \geq a | R=r] = P[c_1 + c_2 M + \phi(R) \geq \ln(a) \mid R=r]. \tag{82}$$

If earthquake magnitude M and distance R are statistically independent, the probability (82) may be written as (Cornell, 1968)

$$Pr[\text{PGA} \geq a | R=r] = 1 - F_M\left[\frac{\ln(a) - c_1 - \phi(r)}{c_2}\right], \tag{83}$$

where $F_M(\cdot)$ is the CDF of earthquake magnitudes.

The effect for all possible values of earthquake distances R an be calculated by integrating over the range of R:

$$Pr[\text{PGA} \geq a] = \int_{r_{min}}^{r_{max}} Pr(\text{PGA} \geq a | R=r) \cdot f_R(r) \mathrm{d}r, \tag{84}$$

where $f_R(r)$ is the PDF of R, and r_{min} and r_{max} are the minimum and maximum distances of potential earthquakes that can generate an acceleration of engineering interest at the site, respectively.

The assumption that earthquake magnitudes are distributed according to the Gutenberg-Richter-based CDF (4), implies that the probability that a random earthquake

Scientific Technical Report STR 98/05
DOI: 10.2312/GFZ.b103-98055

magnitude M in the magnitude range $m_{min} \le M \le m_{max}$ will cause a PGA at the site exceeding a is:

$$Pr[\text{PGA} \ge a] = \frac{\exp(-\beta m_{max}) - y \cdot \exp[-\beta(x - c_1)/c_2]}{\exp(-\beta m_{max}) - \exp(-\beta m_{min})}, \quad (85)$$

where $x = \ln(a)$, $y(\cdot)$ is a function of the form

$$\int_{r_{min}}^{r_{max}} \exp[\beta \cdot \phi(r)/c_2] \cdot f_R(r)\, dr. \quad (86)$$

and m_{min} is the minimum value of an earthquake magnitude capable of generating an PGA a of engineering interest i.e. PGA $\ge a_{min}$. The value of function $y(\cdot)$ is characteristic for each site. According to formula (86) its value depends on the spatial distribution of seismicity $f_R(r)$, on the functional form of the PGA vs. distance [function $\phi(r)$ in formula (81)], and on the value of $\beta = b\ln(10)$. For each site, the value of function $y(\cdot)$ is constant.

Finally, from relation (85) it follows that at any given site the logarithm of the PGA is distributed according to the same type of distribution as earthquake magnitude, i.e. negative exponential - the form of the familiar Gutenberg-Richter distribution. The two distributions differ only in the value of their parameters. If the parameter of magnitude distribution is equal to β, (equation 82), the parameter of the distribution of ln(PGA) is equal to β/c_2. Indeed, from (85), after normalization, the CDF of the logarithm of PGA is:

$$F_X(x|x_{min},x_{max}) = \frac{\exp(-\gamma x_{min}) - \exp(-\gamma x)}{\exp(-\gamma x_{min}) - \exp(-\gamma x_{max})}, \quad (86)$$

where $\gamma = \beta/c_2$, $x_{min} = \ln(a_{min})$, $x_{max} = \ln(a_{max})$, and a_{max} is the maximum possible PGA at the site.

From the fact that the CDF of earthquake magnitudes (equation 4) and the logarithm of PGA recorded at the site (formula 86) are of the same type, it follows that the value of the maximum possible PGA at the site a_{max} can be estimated according to the same procedure as m_{max}, where in formulas (3)-(4), the parameter β is replaced by γ, the

Scientific Technical Report STR 98/05
DOI: 10.2312/GFZ.b103-98055

activity rate for the **area**, λ is replaced by the activity rate at the **site** λ, and the maximum observed magnitude m_{max}^{obs} is replaced by the maximum observed PGA a_{max}^{obs}. It must be noted that the functional forom of the CDF (86) depends on the functional form of the attenuation relation formula (80). Selection of different functional forms of the attenuation relation may result in different functional forms of the CDF (86).

2.4. Distribution of the Largest Accelerations Recorded at the Site and Estimation of its Parameters

For most engineering applications, a function of particular interest is the CDF of the **maximum** PGA expected at the site during a specified time interval t. In order to estimate this function one has to make certain assumptions regarding the temporal distribution of the earthquakes recorded at the site. Let us again accept the common assumption made in engineering seismology viz. that the occurrence of events with PGA a, (where $a \geq a_{min}$) **at the site** follows a Poisson distribution, with mean activity rate $\lambda \equiv \lambda(x=x_{min})$[7]. The above assumption implies that earthquakes which cause PGA at the site equal to, or exceeding a certain value a, can be represented by a Poisson process with average occurrence rate $\lambda(x) = \lambda[1 - F_X(x|x_{min},x_{max})]$, where $x = \ln(a)$. Hence the CDF of the logarithm of the **largest** PGA recorded at the site within a period of time t, is given by

$$F_X^{max}(x|x_{min},x_{max},t) = \frac{\exp\{-\lambda t[1 - F_X(x|x_{min},x_{max})]\} - \exp(-\lambda t)}{1 - \exp(-\lambda t)}. \quad (87)$$

The CDF (87) of the logarithm of the largest PGA observed at the site is doubly truncated. The first truncation, from the bottom, $x_{min} = \ln(a_{min})$, represents the chosen threshold of acceleration of engineering interest. The second truncation, $x_{max} = \ln(a_{max})$ is an unknown parameter representing the logarithm of the maximum possible PGA at the site. Therefore, for a given a_{min}, the seismic hazard at the site is determined by three parameters: λ, γ, and a_{max}.

In order to estimate these parameters, the largest PGAs $(a_1,\ldots, a_n)$ felt at the site of

---

7 The difference between the meaning of the mean activity rate λ here, and that introduced in Section 2.1 should be noted. In Section 2.1-2.2, the parameter λ characterizes mean rate of seismicity for the whole selected **area** in the vicinity of the site for which SHA is performed. Here, the value of λ describes the mean activity rate of the selected ground motion parameter experienced at the **site**.

Scientific Technical Report STR 98/05
DOI: 10.2312/GFZ.b103-98055

interest are selected from n consecutive time intervals $(t_1,\ldots, t_n) = \mathbf{t}$, and the maximum likelihood procedure is used. For specified a_{max}, the likelihood function of the sample $\mathbf{x} = (x_1,\ldots, x_n)$, where $x_i = \ln(a_i)$ $(i = 1,\ldots, n)$, is a function of the unknown parameters λ and γ, and is given by

$$L(\lambda,\gamma|\mathbf{x},\mathbf{t}) = \prod_{i=1}^{n} f_X^{max}(x_i|x_{min},x_{max},t_i), \tag{88}$$

where $f_X^{max}(x_i|x_{min},x_{max},t_i)$ is the PDF of the logarithm of the largest PGA occurring at the site during a specified time interval t. From the definition of the PDF, and from formula (87), the PDF $f_X^{max}(x|x_{min},x_{max},t)$ is equal to

$$f_X^{max}(x|x_{min},x_{max},t) = \lambda\, t\, F_X^{max}(x|x_{min},x_{max},t)\, f_X(x|x_{min},x_{max}), \tag{89}$$

where $f_X(x|x_{min},x_{max})$ is the PDF of x and is equal to

$$f_X(x|x_{min},x_{max}) = \frac{\gamma \exp(-\gamma x)}{\exp(-\gamma x_{min}) - \exp(-\gamma x_{max})}. \tag{90}$$

The maximum likelihood estimation of parameters λ and γ, are those values (say $\hat{\lambda}$ and $\hat{\gamma}$), that for a given value of $x_{max} = \ln(a_{max})$ make the likelihood function as large as possible. If stationary values of the likelihood function exist, they are given by the roots of the equation pair $\partial\ln(L)/\partial\lambda = 0$ and $\partial\ln(L)/\partial\gamma = 0$, which, in our case, takes the form

$$\begin{cases} \dfrac{1}{\lambda} = \dfrac{<t>A_2 - <tA>}{A_2 - A_1} - \left<\dfrac{t\exp(-\lambda t)}{1 - \exp(-\lambda t)}\right>, \\ \dfrac{1}{\gamma} = <X> - \dfrac{B_2 - B_1}{A_2 - A_1} + \lambda\left[\dfrac{(<t>A_2 - <tA>)(B_2 - B_1)}{(A_2 - A_1)^2} - \dfrac{<t>B_2 - <tB>}{A_2 - A_1}\right], \end{cases} \tag{91}$$

where

$$A_1 = \exp(-\gamma x_{min}), \qquad A_2 = \exp(-\gamma x_{max}),$$

$$B_1 = x_{min}\exp(-\gamma x_{min}), \qquad B_2 = x_{max}\exp(-\gamma x_{max}),$$

Scientific Technical Report STR 98/05
DOI: 10.2312/GFZ.b103-98055

$$< \frac{t\exp(-\lambda t)}{1 - \exp(-\lambda t)} > = \frac{1}{n} \sum_{i=1}^{n} \frac{t\exp(-\lambda t_i)}{1 - \exp(-\lambda t_i)} ,$$

$$< t > = \sum_{i=1}^{n} t_i/n, \qquad < X > = \sum_{i=1}^{n} x_i/n,$$

$$< tA > = \sum_{i=1}^{n} t_i \, A(x_i)/n, \qquad < tB > = \sum_{i=1}^{n} t_i \, B(x_i)/n,$$

$A(x) = \exp(-\gamma x)$ and $B(x) = x \exp(-\gamma x)$.

Relations (91) provide two equations which, for given x_{max}, can be used for the maximum likelihood estimation of λ and γ. It should be noted that when the expression $\exp(-\lambda t)$ in the first equation of (91) is small enough, the second term may be neglected. This will be the case when the time intervals t are long enough and/or the activity rate λ is high enough. Equations (91) then take the simpler form (Kijko and Dessokey, 1987):

$$\begin{cases} \dfrac{1}{\lambda} = \dfrac{< t > A_2 - < tA >}{A_2 - A_1}, \\ \dfrac{1}{\gamma} = < X > - \dfrac{< tAX > - < t > A_2 \, x_{max}}{< tA > - < t > A_2}. \end{cases} \tag{92}$$

2.5. Inclusion of Additional Information

One of the strongest points of our procedure for SHA is the ability to account for any additional information on its parameters, coming from independent geophysical or geological sources. Such an ability is especially important when seismic event catalogues are highly incomplete (there is not enough information to assess model parameters with required accuracy) or the area for which the SHA is required has a very low level of seismicity.

Let us assume that in order to obtain more reliable estimates of the parameters γ and λ,

Scientific Technical Report STR 98/05
DOI: 10.2312/GFZ.b103-98055

we want to include information about the Gutenberg-Richter parameter b for an area in the vicinity of the given site. Let us assume that its approximate value (say b_0, or, equivalently, β_0) is known, since, for example, it is taken as the same as for another area of similar geotectonic features. Alternatively, one can use the value of $\hat{\beta}$, which was obtained (together with the mean seismic activity λ and m_{max}) by the maximization of likelihood function (79). The simplest way to include this information is to apply the Bayesian concept of estimation, which is described e.g. by Jackson and Matsu'mura (1985). Following the Bayesian formalism, the value of β_0 is understood as *a priori* information about an unknown β-value and can be written in the form

$$\beta_0 = \beta + \delta\beta, \tag{93}$$

where β is the unknown, "true" value of parameter β, which is subject to the unknown error $\delta\beta$. Let us assume that the PDF of errors $\delta\beta$ is known and equal to $p(\beta)$. From a Bayesian approach, the joint p.d.f of the model parameters is proportional to the likelihood function (88) multiplied by the *a priori* PDF $p(\beta)$. Taking into account that parameter $\gamma = \beta/c_2$, where c_2 is known constant, the joint (posterior) PDF is:

$$p(\lambda,\beta|\mathbf{x},\mathbf{t}) = const\ L(\lambda,\beta/c_2|\mathbf{x},\mathbf{t})\ p(\beta). \tag{94}$$

The parameter *const* is the normalizing factor, which ensures that the integral $p(\lambda,\beta|\mathbf{x},\mathbf{t})$ over the whole domain of the parameters (λ,β), is equal to one. According to Bayesian estimation theory, the best estimates of λ and β are those that maximize the posterior PDF (94). The same formalism can be applied in order to incorporate additional information about the activity rate λ, or in general, any unknown model parameter.

3. EXAMPLE OF APPLICATION.

3.1. SHA the for Site of a Hypothetical Engineering Structure

As an illustration, the procedure as described above was used to estimate the seismic hazard parameters at the site hypothetical engineering structure (HES) with latitude $\phi = 33^{\circ}21.7'$ S and longitude $\lambda = 19^{0}17{,}6'$ E, located in the territory of South Africa (Fig. 6). The assessment is based on the seismic events recorded by the South African National Seismological Network of the Council for Geoscience (formerly the Geological Survey of South Africa), originating in the area of interest from the begining of 1801.

Scientific Technical Report STR 98/05
DOI: 10.2312/GFZ.b103-98055

The procedure for the estimation of the maximum credible regional magnitude m_{max} was applied to seismic data limited by a distance of 450 km from the site. The compiled catalogue was divided into three parts.

The first part of the catalogue contains the largest seismic events during the period 1 January 1801 to 31 December 1970. It was assumed that for all of these events, the standard deviation of uncertainty of magnitude was 0.4.

The second part (from 1 January 1971 to 31 December 1990) includes the complete catalogue of seismic events from magnitude level $m_{min} = 3.8$ upwards. The uncertainty of magnitude was assumed to be 0.2.

The third part (from 1 January 1991 to 31 December 1995) includes the complete data from magnitude level $m_{min} = 3.5$ upwards. The uncertainty of magnitude was assumed to be 0.1.

The first part of the catalogue contains 32 of the largest seismic events. The second part of the catalogue contains 13 events with local magnitude 3.8 or larger. The third part contains 8 events with local magnitude 3.5 or larger.

The strongest known earthquake which occurred within the **area** was an event of local magnitude $m_L \cong 6.3$. We assume that the magnitude of this event is determined with standard deviation equal to 0.25.

Application of the T-P-B estimation procedure (equation 58) for the **area** surrounding the site of HES gives $\hat{m}_{max} = 6.96 \pm 0.71$, $\hat{b} = 0.93 \pm 0.11$, and $\hat{\lambda} = 9.87 \pm 3.80$ (for $m_{min} = 2.5$).

The K-S-B estimator (equations 62-63), for the estimation of the maximum credible magnitude for the same area gives $\hat{m}_{max} = 6.66 \pm 0.44$, $\hat{b} = 0.92 \pm 0.11$, and $\hat{\lambda} = 9.65 \pm 3.73$ (for $m_{min} = 2.5$). A summary of the results obtained through the application of the two methods of assessing the maximum credible magnitude is given in Table I.

In all further computations, the value of $\hat{m}_{max}$, equal to 6.66 ± 0.44, obtained from application of K-S-B technique was used.

To assess the maximum credible acceleration at the site of the HES, it was assumed that an earthquake at a depth of 10 km, having maximum credible magnitude $\hat{m}_{max} = 6.66$, can

Scientific Technical Report STR 98/05
DOI: 10.2312/GFZ.b103-98055

TABLE I

Hypothetical Engineering Structure - Assessment of seismic hazard parameters

Method	$\hat{m}_{max}$	$\hat{b}$	$\hat{\lambda}(m=2.5)$
Tate-Pisarenko (Bayesian)	6.96±0.71	0.93±0.11	9.87±3.80
Kijko-Sellevoll (Bayesian)	6.66±0.44	0.92±0.11	9.65±3.73

Table I. Seismic hazard parameters estimated by two different procedures, for the **area** within a radius of 450 km of the hypothetical engineering structure.

Scientific Technical Report STR 98/05
DOI: 10.2312/GFZ.b103-98055

Table II

Hypothetical Engineering Structure

$\hat{m}_{max}$ = 6.66 ± 0.44 (Maximum Credible Earthquake Magnitude)

a_{max} (Δ=0; Depth=10 km)	a_{max} (Δ=10; Depth=10 km)	a_{max} (Δ=25; Depth=10 km)
0.352	0.261	0.144

Table II. The expected maximum horizontal peak accelerations at epicentral distance 0, 10 and 25 km from the site of the hypothetical engineering structure generated by an earthquake with MCE magnitude equal to 6.66. All Accelerations are in units of [g].

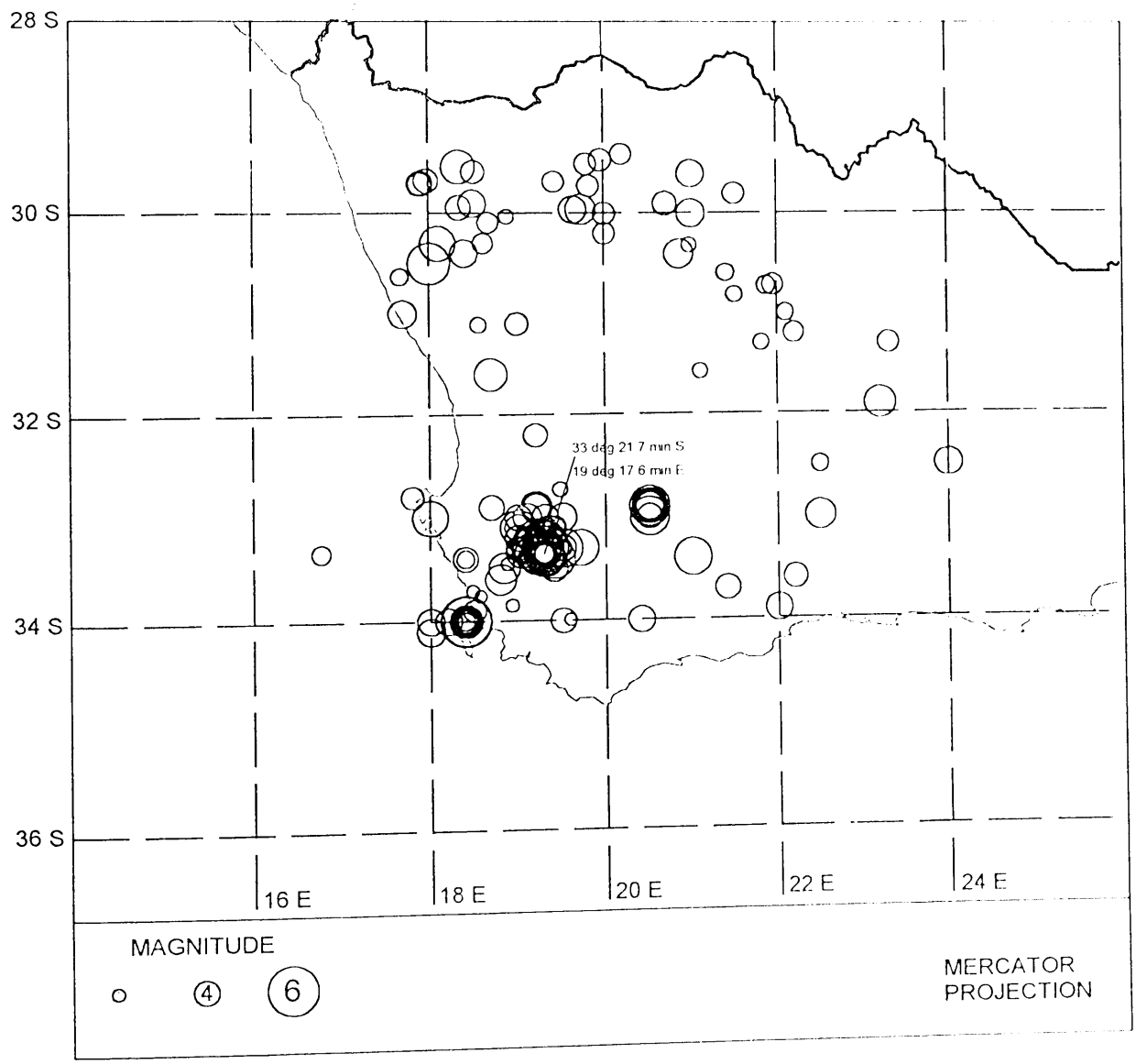

Fig. 6. Seismicity map within a distance of 450 km from the site of the hypothetical engineering structure.

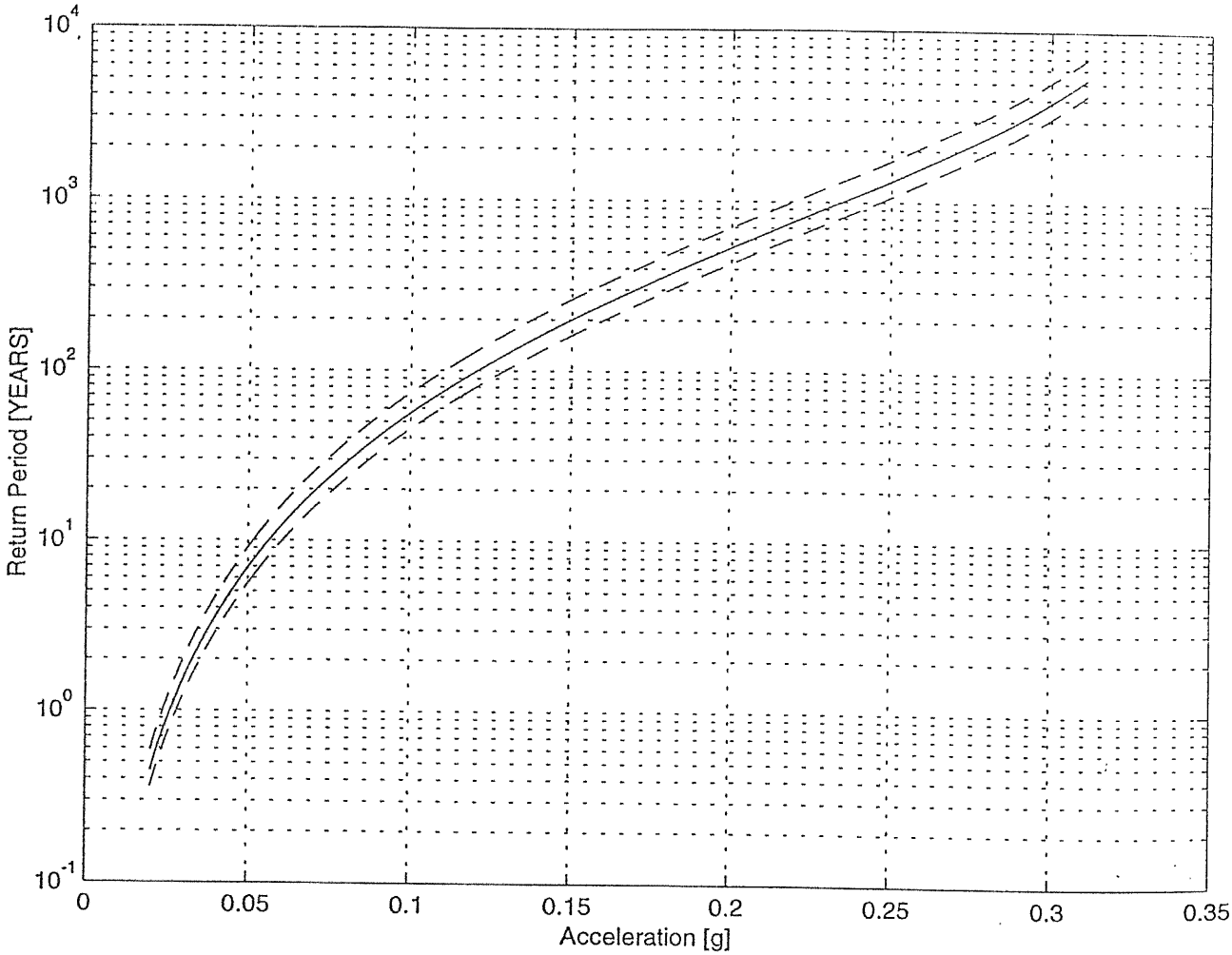

Fig. 7. Mean return periods of accelerations expected for the analyzed hypothetical engineering structure.

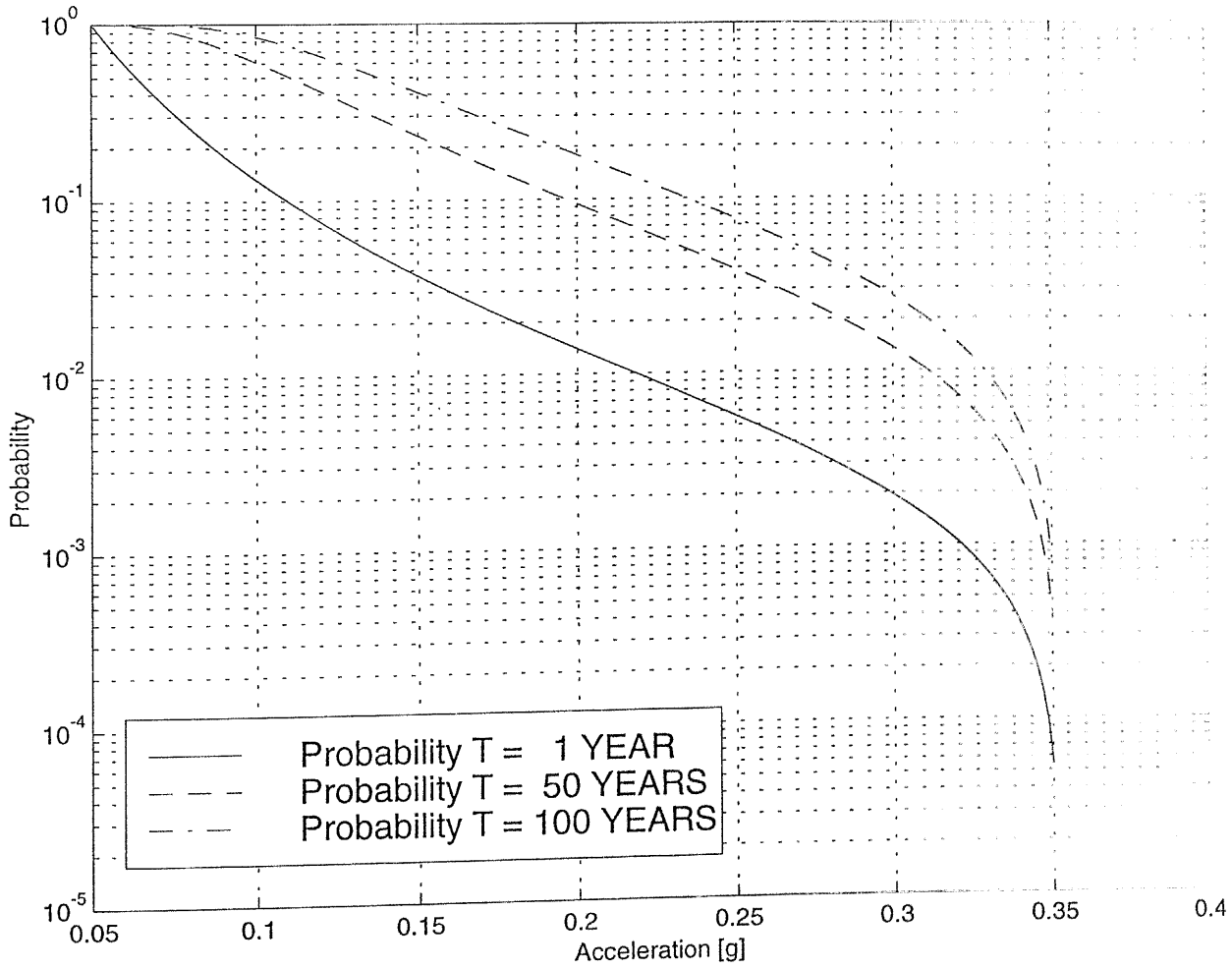

Fig. 8. Probabilities that a given peak ground acceleration will be exceeded in 1, 50 and 100 years for the site of the analyzed hypothetical engineering structure.

SUB-SAHARAN AFRICAN SEISMIC HAZARD 1071 -1996

Peak horizontal ground acceleration (g) with a 10% probability of being exeeded at least once in 50 years

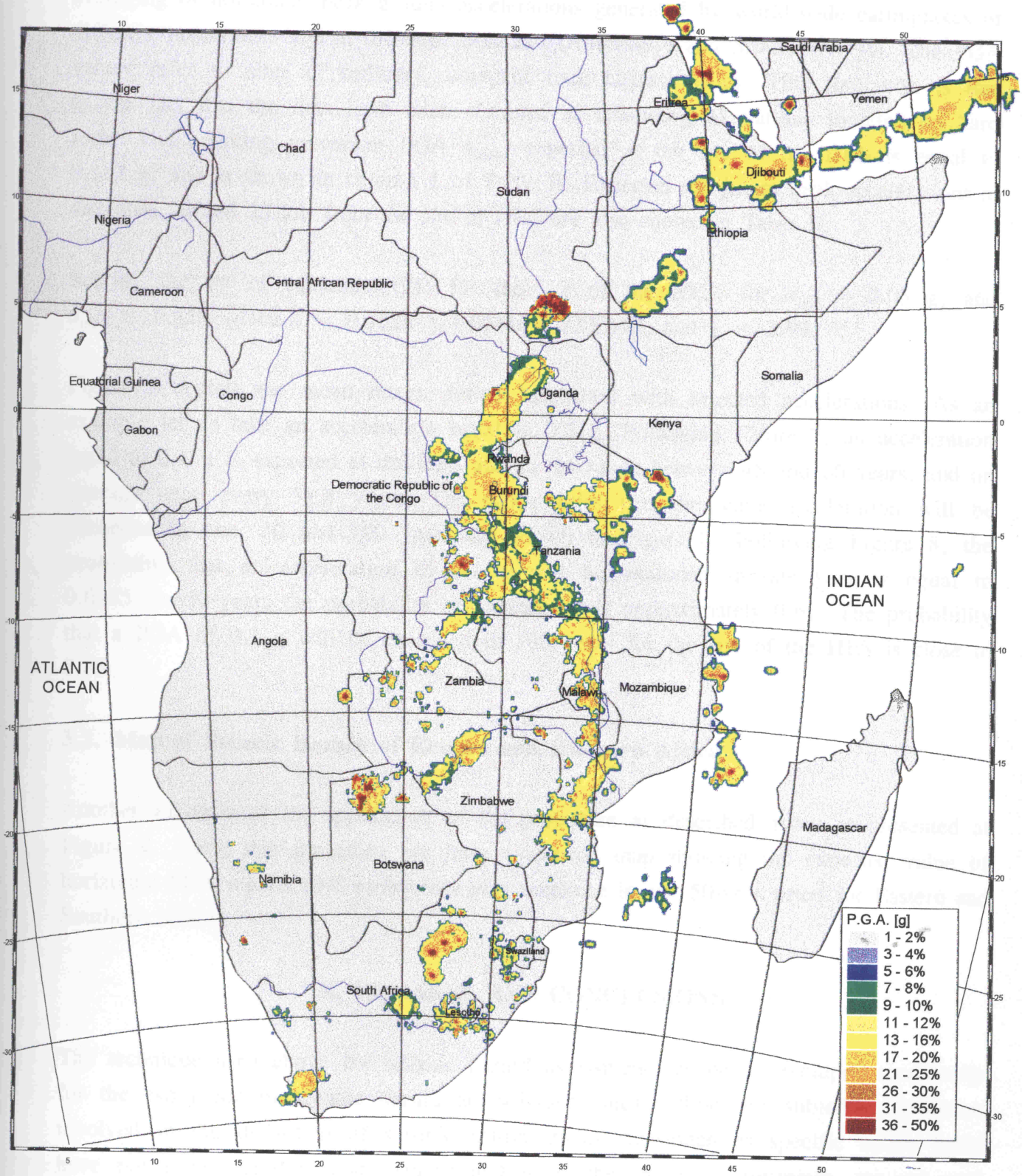

Fig. 9

Scale 1:9 000 000

Projection: Transverse Mercator
Central Meridian: 25 degrees East

Map Compiled by A. Kijko and G. Graham
Map produced by M. Kotzé and P. Cole

Acknowledgement:
Data provided by the Council for Geoscience and the Eastern and Southern African Working Group

Scientific Technical Report STR 98/05
DOI: 10.2312/GFZ.b103-98055

occur at the site of the HES. The resulting horizontal peak ground acceleration at the site of the station was calculated, using the attenuation curve obtained from the averaging of horizontal peak ground accelerations generated by world-wide earthquakes of different magnitudes and at different distances (Ambraseys and Srbulov, 1994). The PGA values refer to sites of ordinary, compent rock characteristics. This limitation is due to the fact that the data have been obtained at seismological stations founded on hard rock. The resulting maximum PGA a_{max}, expected at the site of the HES is equal to 0.352 g, and is shown in column 1 of Table II. Expected maximum peak accelerations at distances 10 and 25 km from the site of HES are also shown in Table II.

Solving the set of equations (91) for the site of the HES, for a_{min} = 0.05 g, and a_{max} = 0.352, gives $\hat{\lambda}$ = 0.1519 ± 1.05*10^{-2}[1/YEAR], and $\hat{\gamma}$ = 2.99.

Figure 7 depicts the mean return period associated with selected accelerations. As an example let us take an acceleration equal to 0.1 g. Following Figure 7, an acceleration equal to 0.1 g is expected at the HES site in the range between 48 and 60 years, and on average once every 53.5 years. The probabilities that the same acceleration will be exceeded in one, 50 and 100 years are shown in Figure 8. Following Figure 8, the probability that an acceleration of 0.1 g will be exceeded in one year is equal to 0.0185. In 50 years the probability of exceedence is approximately 0.61. The probability that a PGA of 0.1 g will be exceeded in 100 years for the site of the HES is close to 0.85.

3.2. Map of Seismic Hazard of Eastern and Southern Africa

Another example of the application of the procedure as described above is presented at Figure 9. Using this procedure we have calculated map showing the expected value of horizontal PGA with a 10% probability of exceedence in any 50-year priod for Eastern and Southern Africa.

4. REMARKS AND CONCLUSIONS

The technique used above for seismic hazard assessment has been developed specifically for the estimation of seismic hazard at individual sites without the subjective judgment involved in the definition of seismic source zones, inasmuch as specific active faults have not been identified and mapped and when the causes of seismicity are not well understood.

Scientific Technical Report STR 98/05
DOI: 10.2312/GFZ.b103-98055

This technique combines the best features of the "deductive" (Cornell, 1968) and "historic" (Veneziano *et al.*, 1984) procedures.

The procedure takes into account incompleteness of the seismic catalogues. The method accepts mixed data of two types, one type containing only the largest earthquakes and the other type containing data sets complete from different thresholds of magnitude upwards. The procedure also incorporates uncertainty in earthquake magnitude determination.

The method applies a Poisson distribution as a model of earthquake occurrence in time and a doubly-truncated, negative exponential distribution (which is equivalent to the frequency-magnitude Gutenberg-Richter relation limited by the maximum earthquake magnitude m_{max}) as a model of earthquake magnitude distribution.

If applied to a grid of points it will result in a map of seismic hazard, in which the contours of expected largest peak ground accelerations during specified time periods can be drawn.

Our approach is particularly useful for the mapping of seismic hazard in areas where both largest, historical, and also complete, recent instrumental observations are available.

REFERENCES

Abramowitz, M., and I.A. Stegun (1970). *Handbook of Mathematical Functions*, 9th ed. Dover Publ. New York.

Aki, K. (1965). Maximum likelihood estimate of b in the formula $\log N = a - bM$ and its confidence limits, *Bull. Earthquake Res. Inst., Univ. Tokyo*, **43**, 237-239.

Ambraseys, N.N. (1995). The prediction of earthquake peak ground acceleration in Europe, *Earthquake Eng. Struct. Dyn.* **24**, 467-490.

Ambraseys, N.N. and M. Srbulov (1994). Attenuation of earthquake-induced ground displacements, *Earthquake Eng. Struct. Dyn.* **23**, 467-487.

Boore, D.M. and W.B. Joyner (1982). The empirical prediction of ground motion, *Bull. Seism. Soc. Am.* **72**, S43-S60.

Anderson, J.G. and J.E. Luco (1983). Consequences of slip rate constrains on earthquake occurrence relation, *Bull. Seism. Soc. Am.* **73**, 471-496.

Anderson, J.G., S.G. Wesnousky, and M.W. Stirling (1996). Earthquake size as a function

Scientific Technical Report STR 98/05
DOI: 10.2312/GFZ.b103-98055

of slip rate, *Bull. Seism. Soc. Am.* **86**, 683-690.

Apostol, T.M. (1961). *Calculus. Introduction, with Vectors and Analytic Geometry, Vol. I*, Blaisdell Publishing Company, New York.

Bakun, W.H. and T.W. McEvilly (1984). Recurrence models and Parkfield, California earthquakes, *J. Geophys. Res.* **89**, B5, 3051-3058.

Bender, B. (1987). Effects of observational errors in relating magnitude scales and fitting the Gutenberg-Richter parameter β, *Bull. Seismol. Soc. Am.* **77**, 1400-1428.

Bender, B. (1993). Treatment of parameter uncertainty and variability for a single seismic hazard map, *Earthquake Spectra*, **9**, 165-193.

Benjamin, J.R. and C.A. Cornell (1970). *Probability, Statistics and Decidion for Civil Engineers,* McGraw-Hill, New York.

Boshi, E., D. Giardini, D. Pantosti, G. Valensise, R. Arrowsmith, P. Basham, R. Bürgmann, A.J. Crone, A. Hull, R.K. McGuire, D. Schwartz, K. Sieh, S.N. Ward, and R.S. Yeats (1996). New trends in active faulting studies for seismic hazard assessment, *Ann. Di Geofisica*, **39**, 1301-1304.

Bottari, A. and G. Neri (1983). Some statistical properties of a sequence of historical Calabro-Peroritan earthquakes, *J. Geophys. Res.* **88**, B2, 1209-1212.

Burton, P.W. (1979). Seismic risk in southern Europe through to India examined using Gumbel's third distribution of extreme values, *Geophys. J.* **59**, 249-280.

Campbell, K.W. (1982). Bayesian analysis of extreme earthquake occurrences. Part I. Probabilistic hazard model, *Bull. Seism. Soc. Am.* **72**, 1689-1705.

Chung, D.H. and D.L. Berneurer (1981). Regional relations among earthquake magnitude scales, *Rev. Geophys. Space Phys.* **19**, 649-663.

Cooke, P. (1979). Statistical inference for bounds of random variables, *Biometrika*, **66**, 367-374.

Cornell, C.A. (1968). Engineering seismic risk analysis, *Bull. Seism. Soc. Am.* **58**, 1583-1606.

Cornell, C.A. and G. Toro (1992). Seismic Hazard Assessment. In: *International Association for Mathematical Geology Studies in Mathematical Geology*, No. 4, *Techniques for Determining Probabilities of Geologic Events and Processes*. Ed. by R.L. Hunter and C.J. Mann. Oxford University Press, 147-166.

Cosentino, P., V. Ficara and D. Luzio (1977). Truncated exponential frequency-magnitude relationship in the earthquake statistics, *Bull. Seism. Am.* **67**, 1615-1623.

Cramér, H. (1948). *Mathematical Methods of Statistics*. Princeton University Press. Princeton.

Dargahi-Noubary, G.R. (1983). A procedure for estimation of the upper bound for earthquake magnitudes, *Phys. Earth Planet. Interiors*, **33**, 91-93.

DeGroot, M.H. (1970). *Optimal Statistical Decisions*, McGraw-Hill, New York.

Devison, F.C. and C.H. Scholz (1984). The test of the characteristic earthquake model

Scientific Technical Report STR 98/05
DOI: 10.2312/GFZ.b103-98055

for the Aleutian Arc (abstract), *EOS*, **65**, 242.

Dong, W.M., H.C. Shah and A.B. Bao (1984). Utilization of geophysical information in Bayesian seismic hazard model, In: *Soil Dynamics and Earthquake Engineering*, **3**, 103-111.

Epstein, B. and C. Lomnitz (1966). A model for the occurrence of large earthquakes, *Nature*, **211**, 954-956.

Fedotov, S.A. (1968). *On the seismic cycle, the possibilities for quantitative seismic zoning and long-range seismic prediction*, In: Seismic Zoning in the USSR, Moscow, Nauka, 121-150, (in Russian).

Finnie, G. (1994). A stationary model for time-dependent seismic hazard in mines. *Acta Geophys. Pol.* **42**, 111-118.

Frankel, A. (1995). Mapping seismic hazard in the central and eastern United States, *Seismological Research Letters*, **66**, 8-21.

Gan, Z.J. and C.C. Tung (1983). Extreme value distribution of earthquake magnitude, *Phys. Earth Planet. Inter.* **32**, 325-330.

Gibowicz, S.J. and A. Kijko (1994). *An Introduction to Mining Seismology*, Academic Press, San Diego.

Gumbel, E.J. (1958). *Statistics of Extremes*, Columbia University Press, New York.

Jackson, D.D., and M. Matsu'mura (1985). A Bayesian approach to nonlinear inversion, *J. Geophys. Res.* **90**, 581-591.

Kanamori, H. (1981). The nature of seismicity patterns before large earthquakes, In: *Earthquake Prediction, An International Review.* Maurice Ewing series IV, Eds: D. W. Simpson, and P.G. Richards. American Geophysical Union, Washington, D.C. 1-19.

Kendall, M. and A. Stuart (1967). *The Advanced Theory of Statistics in Inference and Relationship*, Vol. 2, Griffin, London.

Kijko, A. (1983). A modified form of the first Gumbel distribution: model for the occurrence of large earthquakes. Part II: Estimation of parameters. *Acta Geophys. Pol.*, **31**, 27-39.

Kijko, A. (1988). Maximum likelihood estimation of Gutenberg-Richter *b* parameter for uncertain magnitude values, *Pure Appl. Geophys.* **127**, 573-579.

Kijko, A. (1997). *Statistical Estimation of Maximum Earthquake Magnitude*, Council for Geoscience, Geological Survey, Pretoria, Report No. 1997-0245. pp. 52.

Kijko, A. and Dessokey, M. (1987). Application of extreme magnitude distribution to incomplete earthquake files, *Bull. Seism. Soc. Am.* **77**, 1429-1436.

Kijko, A. and M.A. Sellevoll (1989). Estimation of earthquake hazard parameters from incomplete data files. Part I. Utilization of extreme and complete catalogues with different threshold magnitudes, *Bull. Seism. Soc. Am.* **79**, 645-654.

Kijko, A. and M.A. Sellevoll (1992). Estimation of earthquake hazard parameters from incomplete data files. Part II. Incorporation of magnitude heterogeneity, *Bull. Seism. Soc. Am.* **82**, 120-134.

Scientific Technical Report STR 98/05
DOI: 10.2312/GFZ.b103-98055

Lapajne, J.K., B.S. Motnikar, B. Zabukoviec and P. Zupancic (1997). Spatiall smoothed seismicity modelling of seismic hazard in Slovenia, *Journal of Seismology*, **1**, 73-85.

Lay, T., L. Astia, H. Kanamori and D.H. Christensen (1989). Temporal variation of the large intraplate earthquakes in coupled subduction zones, *Phys. Earth Planet. Inter.* **54**, 258-312.

Lindholm, C.D., J. Havskov, and M.A. Sellevoll (1990). Periodicity in the Seismicity; Examination. of four catalogues, (manuscript).

Main, I.G. and P.W. Burton (1984). Physical links between crustal deformation, seismic moment, and seismic hazard for regions of varying seismicity, *J. R. Astr. Soc.* **79**, 469-488.

McGarr, A. (1984). Some applications of seismic source mechanism studies to assessing underground hazard, In: *Rockburst and Seismicity in Mines*, (N.C. Gay and E.H. Wainwright, eds) Symp. Ser. No. 6, 199-208. S. Afric. Inst. Min. Metal. Johannesburg.

McGuire, R.M. (1993). Computation of seismic hazard, *Ann. Di Geofisica*, **36**, 181-200.

McGuire, R.K. and T.P. Barnhard (1981). Effects of temporal variations in seismicity on seismic hazard, *Bull. Seism. Soc. Am.* **71**, 321-334.

Mento, D.J., C.P. Ervin and L.D. McGinnis (1986). Periodic energy release in the New Madrid seismic zone. *Bull. Seism. Soc. Am.* **76**, 1001-1009.

Mortgat, C.P. and H.C. Shah (1979). A Bayesian model for seismic hazard mapping, *Bull. Seism. Soc. Am.* **69**, 1237-1251.

Muir-Wood, R. (1993). From global seismotectonics to global seismic hazard, *Ann. Di Geofisica*, **36**, 153-168.

Nordquist, J.M. (1945). Theory of largest values applied to earthquake magnitudes, *Trans. Am. Geophys. Union* **26**, 29-31.

Nuttli, O.W. and R.B. Herrmann (1982). Earthquake magnitude scales. *J. Geotech. Eng. Div. ASCE* **108**, 783-786.

Page, R. (1968). Aftershocks and microaftershocks. *Bull. Seism. Soc. Am.* **58**, 1131-1168.

Papadopoulos, G.A. and Ph. Voidomatis (1987). Evidence for periodic seismicity in the inner Aegean seismic zone, *Pure Appl. Geophys.* **115**, 375-385.

Papastamatiou, D. (1980). Incorporation of crustal deformation to seismic hazard analysis, *Bull. Seism. Soc. Am.* **70**, 1321-1335.

Pisarenko, V.F. (1991). Statistical evaluation of maximum possible magnitude, *Izvestiya, Earth Physics*, **27**, 757-763.

Pisarenko, V.F., A.A. Lyubushin, V.B. Lysenko, and T.V. Golubieva (1996). Statistical Estimation of seismic hazard parameters: maximum possible magnitude and related parameters, *Bull. Seism. Soc. Am.* **86**, 691-700.

Quenouille, M.H. (1956). Notes on bias estimation, *Biometrika*, **43**, 353-360.

Scientific Technical Report STR 98/05
DOI: 10.2312/GFZ.b103-98055

Rao, N.M. and K.L. Kalia (1986). Model of earthquake-energy periodicity in the Alpine-Himalayan seismotectonic belt, *Tectonophysics*, **124**, 261-270.

Rhoades, D.A. (1995). Estimation of the Gutenberg-Richter relation allowing for individual earthquake magnitude uncertainties. *Tectonophysics*, (in print).

Rhoades, D.A., R.J. Van Dissen and D.J. Dowrick (1994). On the handling of uncertainties in estimating the hazard of rupture on a fault segment, *J. Geophys. Res.* **99**, **B7**, 13701-13712.

Robson, D.S. and Whitlock J.H. (1964). Estimation of a truncation point, *Biometrika*, **51**, 33-39.

Sauter, F. (1996). Redefining terms in the field of seismic safety and risk mitigation, *Earthquake Spectra*, **12**, 315-326.

Schwartz, D.P. and K.J. Coppersmith (1984). Fault behavior and characteristic earthquakes: examples from the Wasatch and San Andreas fault zones, *J. Geophys. Res.* **89**, 5681-5698.

Schwartz, D.P., K.J. Coppersmith and F.H. Swan (1984). Methods for estimating maximum earthquake magnitude, *Eight World Conference on Earthquake Engineering. Proceeding* **I**, 279-285.

Shibutani T. and K. Oike (1989). On features of spatial and temporal variation of seismicity before and after moderate earthquakes, *J. Phys. Earth*, **37**, 201-224.

Shimshoni, M. (1984). Possible periodicities of the annually released global seismic energy (M≥7.9) during the period 1898-1971 - discussion, *Tectonophysics*, **107**, 173-176.

Singh, S.K., E. Bazan and L. Esteva (1980). Expected earthquake magnitude from a fault, *Bull. Seism. Soc. Am.* **70**, 903-914.

Singh, S.K, M. Rodriques, and L. Esteva (1983). Statistics of small earthquakes and frequency of large earthquakes along the Mexico subduction zone, *Bull. Seism. Soc. Am.* **73**, 1779-1796.

Smith, S.W. (1976). Determination of maximum earthquake magnitude, *Geophys. Res. Lett.* **3**, 351-354.

Stavrakasis, G.N. and G.A. Tselentis (1987). Bayesian probabilistic prediction of strong earthquakes in the main seismic zones of Greece, *Boll. Geof. Teor. Appl.*, **29**, 51-63.

Tate, R.F. (1959). Unbiased estimation: Function of location and scale parameters. *Ann. Math. Statist.* **30**, 331-366.

Tinti, S. and F. Mulargia (1985a). Effects of magnitude uncertainties in the Gutenberg-Richter frequency-magnitude law, *Bull. Seism. Soc. Am.* **75**, 1681-1697.

Tinti, S. and F. Mulargia (1985b). Application of the extreme value approaches to the apparent magnitude distribution of the earthquakes, *Pure Appl. Geophys.* **123**, 199-220.

Toro, G.R., N.A. Abrahamson, and J.F. Schneider (1997). Model of strong ground motions from earthquakes in Central and Eastern North America: best estimates and uncertainties, *Seism. Res. Lett.* **68**, 41-57.

Scientific Technical Report STR 98/05
DOI: 10.2312/GFZ.b103-98055

Veneziano, D., C.A. Cornell, and T. O'Hara (1984). Historic method for seismic hazard analysis, *Elect. Power Res. Inst., Report,* **NP-3438**, Palo Alto.

Vere-Jones, D. and R.B. Davis (1966). A statistical survey of earthquakes in the main seismic region of New Zealand. 2. Time series analysis, *N.Z. J. Geol. Geophys.* **9**, 251-284.

Wells, D.L. and K.J. Coppersmith (1994). New empirical relationships among magnitude, rupture length, rupture width, rupture area, and surface displacement, *Bull. Seism. Soc. Am.* **84**, 974-1002.

Wesnousky, S.G., C.H. Scholz, K. Shimazaki, and T. Matsuda (1983). Earthquake frequency distribution and the mechanics of faulting, *J.Geophys. Res.* **88**, 9331-9340.

Wyss, M. (1979). Estimating maximum expectable magnitude of earthquake from fault dimensions, *Geology* **7**, 336-340.

Yegulalp, T.M. and J.T. Kuo (1974). Statistical prediction of occurrence of maximum magnitude earthquakes, *Bull. Seism. Soc. Am.* **64**, 393-414.

Scientific Technical Report STR 98/05
DOI: 10.2312/GFZ.b103-98055